

Canonical elastoplastic - damage modelling of reinforced concrete

Salah El-Din Mohammed Fahmy Taher

Civil Engineering

June 1995

Abstract

Reinforced concrete is per se neither elastic nor plastic material. It exhibits damage attributable to irreversible changes; i.e. slip and microcracking. Three phases of behavior exist and interact: elasticity, plasticity and damage. An extensive literature review is carried out to figure out the phenomenological aspects of damage along with the existing constitutive models.

New concepts in the framework of continuous damage mechanics are established. The notions of metaphorical generalized damage variables, generalized material degradation paths and generalized effective stress are defined. Free energy terms are derived based on the concepts of thermodynamics of irreversible changes. Incorporation with the classical theory of plasticity and micromechanics are made. A canonical elastoplastic damage model is proposed for concrete. The model is initially formulated through a rudimentary scrutiny of the uniaxial behavior. The derivation stems from recoverable energy equivalence based on the formal split of the total strain to its components; elastic damage and plastic-damage strain. On the basis of the proposed theory of dichotomy, the model is extended to handle biaxial orthotropic damage associated with cyclic behavior. Verification is carried out against a wide set of experimental data. The model is shown to properly predict strain softening, stiffness degradation, volumetric dilatancy under compression, strength increase under biaxial compressive states. Furthermore, a damage model is then proposed for the uniaxial behavior of steel.

Numerical implementation of the proposed damage model in terms of a computational framework is carried out by development of two nonlinear finite element programs; DMGTRUSS and DMGPLSTS. The first package deals with multi-dimensional trusses while the other handles two-dimensional plane stress states. Practical applications to plain and reinforced concrete structural members are shown to be in good agreement with well documented results.

INFORMATION TO USERS

This manuscript has been reproduced from the microfilm master. UMI films the text directly from the original or copy submitted. Thus, some thesis and dissertation copies are in typewriter face, while others may be from any type of computer printer.

The quality of this reproduction is dependent upon the quality of the copy submitted. Broken or indistinct print, colored or poor quality illustrations and photographs, print bleedthrough, substandard margins, and improper alignment can adversely affect reproduction.

In the unlikely event that the author did not send UMI a complete manuscript and there are missing pages, these will be noted. Also, if unauthorized copyright material had to be removed, a note will indicate the deletion.

Oversize materials (e.g., maps, drawings, charts) are reproduced by sectioning the original, beginning at the upper left-hand corner and continuing from left to right in equal sections with small overlaps. Each original is also photographed in one exposure and is included in reduced form at the back of the book.

Photographs included in the original manuscript have been reproduced xerographically in this copy. Higher quality 6" x 9" black and white photographic prints are available for any photographs or illustrations appearing in this copy for an additional charge. Contact UMI directly to order.

UMI

A Bell & Howell Information Company
300 North Zeeb Road, Ann Arbor, MI 48106-1346 USA
313:761-4700 800:521-0600



**CANONICAL ELASTOPLSTIC - DAMAGE
MODELLING OF REINFORCED CONCRETE**

BY

Salah El-Din Mohammed Fahmy Taher

A Dissertation Presented to the
FACULTY OF THE COLLEGE OF GRADUATE STUDIES
KING FAHD UNIVERSITY OF PETROLEUM & MINERALS
DHAHRAN, SAUDI ARABIA

In Partial Fulfillment of the
Requirements for the Degree of

DOCTOR OF PHILOSOPHY

In

CIVIL ENGINEERING

June, 1995

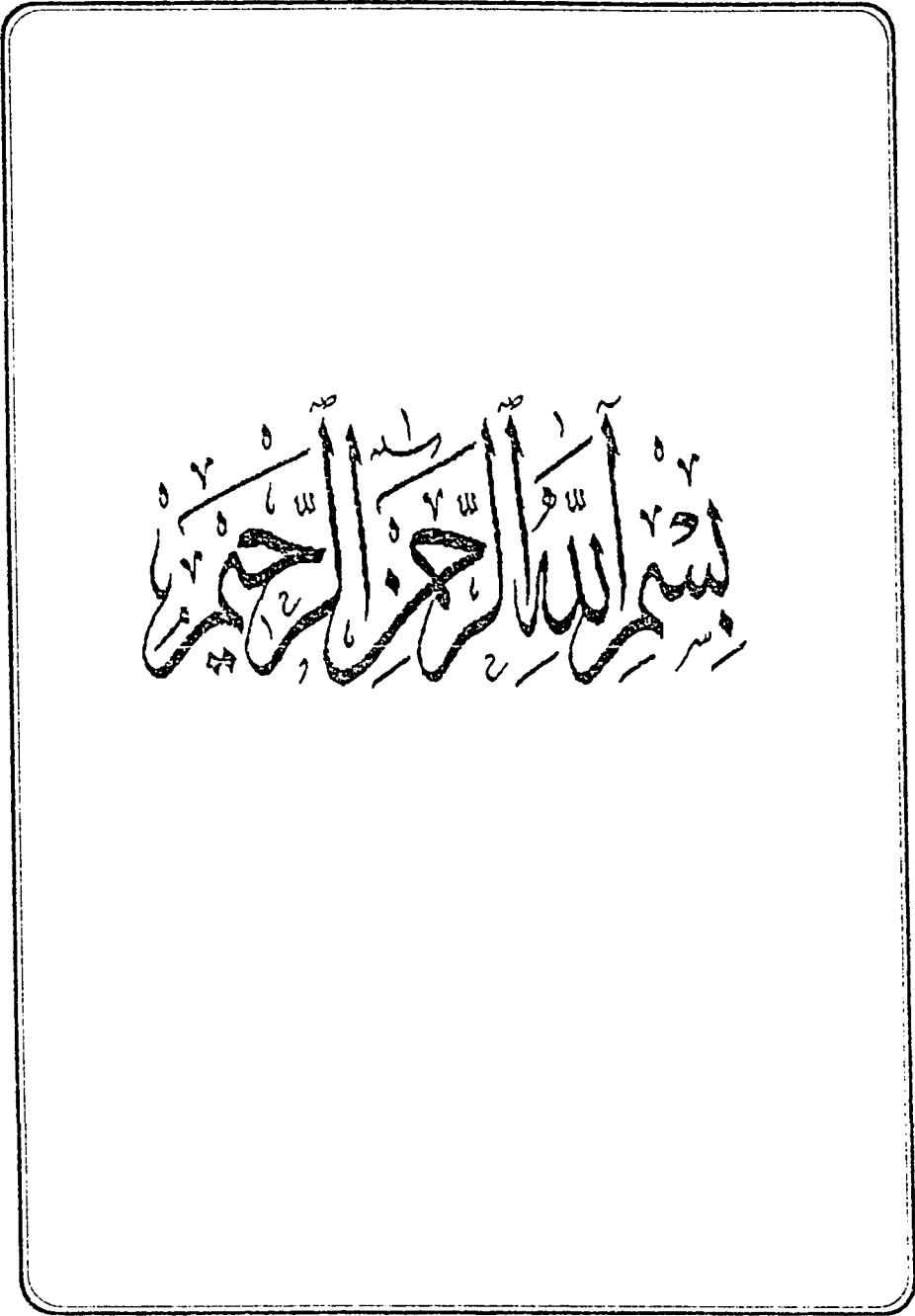
UMI Number: 9542286

UMI Microform 9542286
Copyright 1995, by UMI Company. All rights reserved.

**This microform edition is protected against unauthorized
copying under Title 17, United States Code.**

UMI

**300 North Zeeb Road
Ann Arbor, MI 48103**

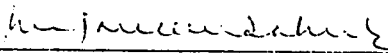



KING FAHD UNIVERSITY OF PETROLEUM AND MINERALS
DHAHRAN, SAUDI ARABIA

COLLEGE OF GRADUATE STUDIES

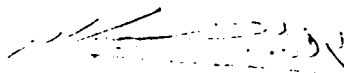
This Dissertation, written by SALAH EL-DIN MOHAMMED FAHMY MOHAMMED TAHER under the direction of his Dissertation Advisor and approved by his Dissertation Committee, has been presented to and accepted by the Dean of the College of Graduate Studies, in partial fulfillment of the requirements for the degree of DOCTOR OF PHILOSOPHY in CIVIL ENGINEERING.

Dissertation Committee

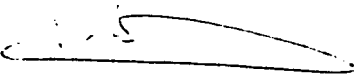

Prof. M. Baluch (Chairman)



Dr. A. Al-Gadhib (Co-Chairman)


Dr. A. AL-Khathlan (Member)


Dr. A. Al-Musallam (Member)


Dr. M. El-Gebeilly (Member)


Dr. Al-Farabi Sharif
Department Chairman


Dr. Ala H. Al-Rabeh
Dean, College of Graduate Studies

7/6/05
Date



To all Muslims

ACKNOWLEDGEMENTS

First and foremost, praise and thanks be to Almighty Allah, the Most Gracious, the Most Merciful, and peace be upon His Prophet.

Acknowledgement is due to King Fahd University of Petroleum and Minerals for support of this study through its enormous computing and laboratory facilities.

I would like to express my sincere gratitude and appreciation to Prof. Mohammed Baluch, my major advisor, for his invaluable guidance, support and encouragement through all the stages of this study. Also, I greatly appreciate the help and encouragement provided by Dr. Ali Al-Gadhib who served as a co-advisor. Thanks are also due to Dr. Al-Khathlan, Dr. Al-Musallam and Dr. Al-Gebeilly who served as committee members for their valuable suggestions and kind attention.

TABLE OF CONTENTS

Chapter	Page
ACKNOWLEDGEMENTS	v
LIST OF CONTENTS	vi
LIST OF TABLES	xv
LIST OF FIGURES	xv
THESIS ABSTRACT (English)	xxix
THESIS ABSTRACT (Arabic)	xxx
1. INTRODUCTION	1
1.1 General	1
1.2 Objectives	1
1.3 Knowledge Base	2
1.4 Procedure	3
1.5 Organization	5
2. PHENOMENOLOGICAL ASCPECTS	9
2.1 General	9
2.2 Historical Background	10
2.3 Concrete Composition	11
2.3.1 Cementitious Matrix	11
2.3.2 Aggregate Particles	13
2.3.3 Entire Composite	14
2.4 Structural Levels of Concrete	15

2.5	Cracking of Concrete	17
2.6	Behavior of Concrete	23
2.6.1	Uniaxial Compression	25
2.6.2	Uniaxial Tension	28
2.6.3	Biaxial Loading	30
2.7	Special Considerations for Concrete	34
2.7.1	Strain softening	34
2.7.2	Structural Effects	35
2.7.3	Volumetric Changes	36
2.8	Reinforcing Steel	37
2.9	Reinforced Concrete	40
3.	CONSTITUTIVE MODELLING	42
3.1	General	42
3.2	Historical Background	43
3.3	Models Classification	43
3.3.1	Classification According to Loading Conditions	45
3.3.2	Classification According to Formulation Basis	46
3.3.3	Classification According to Mathematical Form	46
3.3.4	Classification According to Compressibility	47
3.3.5	Classification According to Material Linearity	49
3.3.6	Classification According to Directional Properties .	51
3.3.7	Classification According to Structural Scale	53
3.3.8	Classification According to Material Heterogeneity ..	54
3.3.9	Classification According to Hypothetical Basis	56

3.4	Strength Based Models	58
3.4.1	Elasticity Models	58
3.4.2	Plasticity Models	59
3.4.2	Friction Models	72
3.5	Energetic Models	73
3.6	Stochastic Models	73
3.7	Numerical Simulation Models	74
3.8	Damage Models	75
3.9	Continuous Damange Mechanics	81
3.10	Definition of the Damage Variables	85
3.11	A State-of-the-Art on Damage Modelling	89
3.12	Local, Nonlocal, and Distributed Damage	137
3.13	Rational Split of State Tensors	141
3.14	Coupled Strain-Damage Scheme	148
4.	RE-CONCEPTUALIZATION OF DAMAGE MECHANICS	154
4.1	General	154
4.2	Generalized Damage Variables	154
4.3	Generalized Material Degradation Paths	156
4.4	Generalized Decomposition of Strain Tensor	159
4.5	Generalized Effective Stresses Concept	165
4.6	Demonstration on Generalized Uncoupling	167
4.6.1	Concrete	167
4.6.2	Copper 99.9%	176
4.7	On Lemaitre's Ductile Damage Model	182

4.8	Decoupled Free Energy Terms	184
4.9	Incorporation with the Theory of Plasticity	187
4.10	Incorporation with Micromechanics	191
4.10.1	Formulation Layout	191
4.10.2	Phenomenological Behavior Genera	192
4.10.3	Thermodynamical Considerations	197
4.10.4	Condition of Softening	199
4.10.5	Micromechanics of the Elastic-Damage Behavior	200
4.10.6	Applications to Concrete	206
4.11	Incorporation with Unilateral Damage Models	215
5.	CANONICAL ELASTOPLASTIC DAMAGE MODEL	218
5.1	General	218
5.2	Concrete Under Uniaxial Tension	219
5.2.1	Stress-Total Strain Relation	219
5.2.2	Strain Components	221
5.2.3	Stress-Strain Components Relationships	225
5.2.4	Uniaxial Tensile MGDV	229
5.3	Concrete Under Uniaxial Compression	235
5.3.1	Stress-Total Strain Relation	235
5.3.2	Strain Components	237
5.3.3	Stress-Strain Components Relationships	239
5.3.4	Uniaxial Compressive MGDV	244
5.4	Concrete Under Biaxial Loading	252
5.4.1	Theory of Dichotomy	253

5.4.2	Canonicalization of the Constitutive Laws	254
5.4.3	Total and Incremental Stress Components	259
5.4.4	Thermodynamical Considerations	263
5.4.5	Identification of Parameters	267
5.4.6	Biaxial Tensile MGDV	280
5.4.7	Biaxial Compressive MGDV	281
5.4.8	Pseudo Initial Moduli	289
5.4.9	Stress Free Straining	289
5.4.10	Decanonization of Constitutive Relations	293
5.5	Predictions of the Canonical Model	295
5.5.1	Uniaxial Behavior under Monotonic Loading	296
5.5.2	Biaxial Behavior under Monotonic Loading	304
5.5.3	Behavior under Cyclic Loading	327
5.6	Uniaxial Damage Model for Steel	332
6.	NUMERICAL IMPLEMENTATIONS	343
6.1	General	343
6.2	Nonlinear Finite Element	343
6.3	Computer Program DMGTRUSS	344
6.3.1	Material Nonlinearity	345
6.3.2	Displacement Model	353
6.3.3	Strain-Displacement Relationship	358
6.3.4	Tangential Modulus	359
6.3.5	Tangential Stiffness	360
6.3.6	Residual Forces	361

6.3.7	DMGTRUSS Structure	362
6.3.8	DMGTRUSS Master Program and Subroutines	365
6.3.9	Damage Models Library	370
6.3.10	Load Reversal and Hysteresis Loop	372
6.3.11	Data Communication	372
6.3.12	Thermal Loading and Thermal Degradation	372
6.3.13	DMGTRUSS Extendability to Other Applications ..	375
6.4	Computer Program DMGPLSTS	376
6.4.1	Finite Element Formulation for Concrete	376
6.4.1.1	Proportionality of Loading	376
6.4.1.2	Displacement Model	377
6.4.1.3	Strain-Displacement Relationship	379
6.4.1.4	Tangential Relations	383
6.4.1.5	Tangential Stiffness	387
6.4.1.6	Residual Forces	388
6.4.1.7	Reduction of Concrete Elements to Interface Elements	388
6.4.2	Finite Element Formulation for Reinforcement	392
6.4.2.1	Material Nonlinearity	392
6.4.2.2	Displacement Model	392
6.4.2.3	Strain-Displacement Relationship	398
6.4.2.4	Tangential Modulus	401
6.4.2.5	Tangential Stiffness	402
6.4.2.6	Residual Forces	403
6.4.3	DMGPLSTS Structure	403

6.4.4	DMGPLSTS Master Program and Subroutines	406
6.4.5	Load Reversal and Hysteresis Loop	411
6.4.6	Data Communication	411
6.4.7	DMGPLSTS Extendability to Other Applications	412
7.	APPLICATIONS	413
7.1	GENERAL	413
7.2	FEATURES CAPTURED BY DMGTRUSS	414
7.2.1	Plain Concrete Under Reversed Loading	414
7.2.2	Tension Stiffening of Plain Concrete Under Uniaxial Loading	416
7.2.3	Uniaxial Tension of Reinforcing Steel	419
7.2.4	Tensile Loading on Reinforced Concrete	421
7.2.5	Compressive Loading on Reinforced Concrete	423
7.3	FEATURES CAPTURED BY DMGPLSTS	423
7.3.1	In-Plane Loading of Plain Concrete Panels	425
7.3.2	Uniaxial Tension on Reinforced Concrete	436
7.3.3	Perfect Bond Characteristics of Reinforced Concrete	443
7.3.4	Pure Bending	448
7.4	COMPARISON WITH PREVIOUS WORK	452
7.4.1	Plain Concrete Beams	452
7.4.2	Reinforced Concrete Beams without Shear reinforcement	456
7.4.3	Reinforced Concrete Beams with Shear reinforcement	

.....	458
7.4.4 Steel/Concrete Bond Problem	462
7.5 CALIBRATION AGAINST CODE PROVISIONS	468
7.5.1 Reinforced Concrete Beams without Shear Reinforcement	468
7.5.1.1 Concrete softening	470
7.5.1.2 Nonlinearity of the response	472
7.5.1.3 Damage pattern	476
7.5.1.4 Cracking load	482
7.5.1.5 Ultimate capacity	487
7.5.2 Reinforced Concrete Beams with Shear Reinforcement	488
7.5.2.1 Effect of amount of shear reinforcement	491
7.5.2.2 Effect of spacing between stirrups	500
8. CONCLUSIONS AND RECOMMENDATIONS	506
APPENDIX I : Formulation of the Finite Element Equations .	512
APPENDIX II : Nonlinear Solution Techniques	515
APPENDIX III : Convergence Criteria	520
APPENDIX IV : DMGTRUSS Glossary	523
APPENDIX V : DMGTRUSS' Instructions	537
APPENDIX VI : DMGPLSTS Glossary	541

APPENDIX VII : DMGPLSTS' Instructions	547
REFERENCES	551

LIST OF TABLES

Table	Page
2.1 Hierarchy of structural scales of concrete (after Krajcinovic and Fanella, 1986)	16
2.2 Macro-scale of representative volume element (after Lemaitre,1986)	16
3.1 Failure theories in chronological order	62
3.2 Various CDM concepts of equivalence for uniaxial tension .	86
3.3 Comparison between two approaches for thermodynamics of damage formulation	109
4.1 Material constants from uniaxial cyclic tension test for concrete	207
5.1 Threshold and critical compressive parameters	250
5.2 Ratio of the elastic and plastic moduli to the total moduli in tension and compression	290
5.3 Strength parameters of structural steel (after Kato et al.,1990)	341
6.1 Properties of the elements developed in DMGFLSTS	380
7.1 Properties of two concrete grades	415
7.2 Ranges of total damage variable for different damage levels	477
7.3 Failure modes of reinforced concrete beams without shear reinforcement	481
7.4 Properties of uncracked transformed section of reinforced concrete beams without shear reinforcement	483
7.5 Failure modes of reinforced concrete beams with shear	

	reinforcement	493
7.6	Properties of uncracked transformed section of reinforced concrete beams with shear reinforcement	497

LIST OF FIGURES

Figure	Page
1.1 Organization of the current study	8
2.1 Modes of loading: I. opening, II. shearing and III. tearing	22
2.2 Compressive behavior of aggregate, paste and concrete ...	24
2.3 Cyclic response of concrete	27
2.4 Experimental biaxial strength envelope for concrete	32
2.5 Residual strains for uniaxial and biaxial loadings	33
2.6 General and modified Menegotto-Pinto model for steel	38
3.1 Various bases for constitutive modelling classification	44
3.2 Classification of hypothetical constitutive models	57
3.3 Different plasticity models	60
3.4 Existing phenomenological damage model	76
3.5 Various applications incorporating damage mechanics	78
3.6 Simplified damage models in tension and compression	84
3.7 Mathematical modelling according to Mazars (1980) and Loland (1981)	112
3.8 Various schemes for splitting the strain tensor	144
3.9 Various solution techniques	149
3.10 Strain-damage coupling schemes	152
4.1 Generalized material degradation paths	157
4.2 Generalized decomposition of the total strain	160

4.3	Generalized effective stress concept	164
4.4	Idealized stress-total strain relationship for concrete under uniaxial compression	168
4.5	Idealized stress-elastic strain relationship for concrete under uniaxial compression	170
4.6	Idealized stress-plastic strain relationship for concrete under uniaxial compression	172
4.7	Evolution of generalized damage variables for concrete under uniaxial compression	174
4.8	Experimental stress-total strain relationship for copper 99.9% under uniaxial tension (after J. Lemaitre,1985)	178
4.9	Stress-elastic strain for copper 99.9% under uniaxial tension	179
4.10	Stress-plastic strain for copper 99.9% under uniaxial tension	180
4.11	Evolution of generalized damage variables for copper 99.9% under uniaxial tension	181
4.12	Schematic idealization of the uniaxial cyclic response	193
4.13	Variation of Poisson's ratio with the elastic damage variable	202
4.14	Generalized damage variables based on the incorporation of micromechanics for concrete	210
4.15	Prediction of the uniaxial cyclic tensile behavior of concrete based on the incorporation of micromechanics	211
4.16	Numerical scheme for determination of the biaxial strength envelop based on the incorporation of micromechanics	212
4.17	Prediction of the biaxial strength envelope for concrete based on the incorporation of micromechanics	214
5.1	Stress-total strain relationship in uniaxial tension according to Guo and Zhang's idealization (1987) for concrete	220
5.2	Strain components in uniaxial tension for concrete	224
5.3	Stress-elastic strain relationship in uniaxial tension for	

concrete	226
5.4 Stress-plastic strain relationship in uniaxial tension for concrete	227
5.5 Total damage variable in uniaxial tension for concrete	232
5.6 Elastic damage variable in uniaxial tension for concrete ..	233
5.7 Plastic damage variable in uniaxial tension for concrete ..	234
5.8 Stress-total strain relationship in uniaxial compression according to Popovics' idealization (1973) for concrete ...	236
5.9 Strain components in uniaxial compression for concrete ...	238
5.10 Stress-elastic strain relationship in uniaxial compression for concrete	242
5.11 Stress-plastic strain relationship in uniaxial compression for concrete	243
5.12 Total damage variable in uniaxial compression for concrete	246
5.13 Elastic damage variable in uniaxial compression for concrete	247
5.14 Plastic damage variable in uniaxial compression for concrete	248
5.15 Dichotomy scheme for a material point under proportional biaxial loading	255
5.16 Schematic representation of the evolution of the peak stresses with the biaxiality ratio	261
5.17 Schematic representation of the evolution of the peak strains with the biaxiality ratio	262
5.18 Stress functions in the tension-tension quadrant	272
5.19 Stress functions in the tension-compression quadrant	273
5.20 Stress functions in the compression-compression quadrant	274
5.21 Strain functions in the tension-tension quadrant	277
5.22 Strain functions in the tension-compression quadrant	278

5.23	Strain functions in the compression-compression quadrant	279
5.24	Modified Guo and Zhang's coefficient in the direction of the major principal stress in the tension-tension quadrant ...	282
5.25	Modified Guo and Zhang's coefficient in the direction of the intermediate principal stress in the tension-tension quadrant	283
5.26	Modified Guo and Zhang's coefficient in the direction of the major principal stress in the tension-compression quadrant	284
5.27	Modified Popovics' coefficient in the direction of the minor principal stress in the tension-compression quadrant	286
5.28	Modified Popovics' coefficient in the direction of the intermediate principal stress in the compression-compression quadrant	287
5.29	Modified Popovics' coefficient in the direction of the minor principal stress in the compression-compression	288
5.30	Variation of Poisson's ratio in uniaxial compression test ..	293
5.31	Comparison of the present study with some of the existing models for uniaxial tension:(a) Scanlon;(b) Lin and Scordelis;(c) Bazant and Oh;(d) Gylltoft; (e) Owen et al. ;(f) Mazars;(g) Loland; and (h) Canonical model	298
5.32	Comparison of the present study with some of the existing models for uniaxial compression:(a) elastic-perfectly plastic;(b) elastic-work hardening;(c) Loland;(d) Hognstaad parabola;(e) Mazars; and (f) Canonical model	299
5.33	Schematic presentation of the brittle behavior in various spaces	300
5.34	Model prediction for relatively low strength concrete under monotonic uniaxial tension	302
5.35	Model prediction for relatively high strength concrete under monotonic uniaxial tension	303
5.36	Comparison of Model's prediction with experimental data of Hognstaad et al. (1955) in monotonic uniaxial compression	305
5.37	Comparison of Model's prediction with experimental data of Smith and Young (1956) in monotonic uniaxial compression	306

5.38	Comparison of the model's prediction of the peak stress envelop and experimental data for biaxial loading	308
5.39	Comparison of the model's prediction of the peak stress envelop and Kupfer's experimental data for biaxial loading	309
5.40	Comparison of the model's prediction for the relative stress-relative strains versus the experimental data of Kupfer et al. (1969) for tension-compression quadrant of stress ratio 0.204/-1.0	310
5.41	Comparison of the model's prediction for the relative stress-relative strains versus the experimental data of Kupfer et al. (1969) for tension-compression quadrant of stress ratio 0.103/-1.0	311
5.42	Comparison of the model's prediction for the relative stress-relative strains versus the experimental data of Kupfer et al. (1969) for tension-compression quadrant of stress ratio 0.052/-1.0	312
5.43	Comparison of the model's prediction for the relative stress-relative strains versus the experimental data of Tasuji et al. (1978) for tension-compression quadrant of stress ratio 0.25/-1.0	313
5.44	Comparison of the model's prediction for the relative stress-relative strains versus the experimental data of Tasuji et al. (1978) for tension-compression quadrant of stress ratio 0.10/-1.0	314
5.45	Comparison of the model's prediction for the relative stress-relative strains versus the experimental data of Tasuji et al. (1978) for tension-compression quadrant of stress ratio 0.05/-1.0	315
5.46	Comparison of the model's prediction for the relative stress-relative strains versus the experimental data of Schickert and Winkler (1977) for compression-compression quadrant of stress ratio -1/-3	316
5.47	Comparison of the model's prediction for the relative stress-relative strains versus the experimental data of Schickert and Winkler (1977) for compression-compression quadrant of stress ratio -2/-3	317
5.48	Comparison of the model's prediction for the relative stress-relative strains versus the experimental data of Schickert and Winkler (1977) for compression-compression quadrant of	

stress ratio -3/-3	318
5.49 Comparison of the model's prediction for the relative stress- relative strains versus the experimental data of Kupfer et al. (1969) for compression-compression quadrant of stress ratio -0.52/-1.00	319
5.50 Comparison of the model's prediction for the relative stress- relative strains versus the experimental data of Kupfer et al. (1969) for compression-compression quadrant of stress ratio -1.00/-1.00	320
5.51 Comparison of the model's prediction for the relative stress- relative strains versus the experimental data of Tasuji et al. (1969) for compression-compression quadrant of stress ratio -0.52/-1.00	321
5.52 Comparison of the model's prediction for the relative stress- relative strains versus the experimental data of Tasuji et al. (1969) for compression-compression quadrant of stress ratio -1.00/-1.00	322
5.53 Comparison of the model's prediction for the relative stress- relative volumetric strain versus the experimental data of Schickert and Winkler (1977) for compression-compression quadrant under different stress ratio	324
5.54 Comparison of the model's prediction for the relative stress- relative volumetric strain versus the experimental data of Kupfer et al. (1969) for compression-compression quadrant under different stress ratio	325
5.55 Comparison of the model's prediction for the relative stress- relative volumetric strain versus the experimental data of Tasuji et al. (1969) for compression-compression quadrant under different stress ratio	326
5.56 Model prediction for the cyclic behavior under uniaxial tension	329
5.57 Comparison of the model's prediction for the cyclic behavior versus the experimental data of Sinha et al. (1964) under uniaxial compression	330
5.58 Comparison of the model's prediction for partial cyclic behavior versus the experimental data of Spooner and Dougill (1976) under uniaxial compression	331
5.59 Comparison of the model's prediction for full cyclic behavior versus the experimental data of Spooner and Dougill (1976)	

	under uniaxial compression	332
5.60	Comparison of the model's prediction for cyclic behavior versus the experimental data of Buyukozturk and Tseng (1984) under uniaxial compression	334
5.61	Experimental monotonic load-deflection curve of reinforcing steel sample T1	335
5.62	Experimental cyclic load-deflection curve of reinforcing steel sample T2	336
5.63	Experimental cyclic load-deflection curve of reinforcing steel sample T3	337
5.64	Experimental cyclic load-deflection curve of reinforcing steel sample T4	338
5.65	Parameters defining general stress-strain considered in the damage model for reinforcing steel	339
5.66	Total damage variable for structural steel SS41 and SM50	342
6.1	An example for a multiple zone stress-strain curve	346
6.2	Regionalized parameters used in DMGTRUSS	347
6.3	Stress discontinuity code ISTEP	348
6.4	Sign convention for the stress discontinuity value STEP .	350
6.5	Various unloading paths allowed in DMGTRUSS	351
6.6	Different stress-strain curves which can be captured by DMGTRUSS	354
6.7	Prismatic two-noded truss element used in DMGTRUSS ...	355
6.8	Possible loading, unloading and reloading paths	363
6.9	Main calls in program DMGTRUSS	364
6.10	Nassi-Schneidermann chart for main calls from master DMGTRUSS	366
6.11	Nassi-Schneidermann chart for main calls from subroutine REFORT	369
6.12	Typical stress-strain curve exhibiting unloading with sign	

reversal in DMGTRUSS	373
6.13 Reduction of concrete element to interface element	389
6.14 Three noded isoparametric element as an example for boom element	393
6.15 Main calls in program DMGPLSTS	404
6.16 Possible forms and occurrence of moduli matrices in various planes	407
7.1 Finite element prediction for the reponse of plain concrete to reversed loading	417
7.2 Finite element prediction for the range of tension stiffening of plain concrete subjected to axial loading	418
7.3 Finite element prediction of steel behavior using two idealizations	420
7.4 Finite element prediction for the response of reinforced concrete to uniaxial tension	422
7.5 Finite element prediction for the response of reinforced concrete to uniaxial compression	424
7.6 Plain concrete panel considered in the analysis of the reponse to in-plane loading	426
7.7 Finite element prediction for the response of plain concrete panel subjected to equal biaxial tension	429
7.8 Finite element prediction for the response of plain concrete panel subjected to uniaxial tension	430
7.9 Finite element prediction for the response of plain concrete panel subjected to equal tension and compression	431
7.10 Finite element prediction for the response of plain concrete panel subjected to general tension and compression	432
7.11 Finite element prediction for the response of plain concrete panel subjected to uniaxial compression	433
7.12 Finite element prediction for the response of plain concrete panel subjected to general biaxial compression	434

7.13	Finite element prediction for the response of plain concrete panel subjected to equal biaxial compression	435
7.14	Reinforced concrete member under uniaxial tension: (a) mesh discretization of uncapped member, and (d) loading on capped member	437
7.15	Finite element prediction for the distributions of displacement and stress in both concrete and steel for the uncapped sample	439
7.16	Finite element prediction for the load-elongation diagram of reinforced concrete under uniaxial tension for various cases	440
7.17	Finite element prediction for the evolution of the load carrying capacity of both concrete and steel for the capped sample	441
7.18	Distribution of stresses in concrete and reinforcement prior to first cracking for the bond problem	446
7.19	Effect of tension stiffening of concrete on the overall behavior	44
7.20	Simplified single element discretization for the bending problem: (a) plain concrete, (b) reinforced concrete, (c) Different element types used	450
7.21	Investigating the effect of the integration rule on the cracking load: (a) 2X2 rule, (b) 3X3 rule, (c) an assumed linear stress distribution	451
7.22	Three-point loading on beams considered for comparison with Mazars' work (1984): (a) plain concrete, (b) reinforced concrete	454
7.23	Comparison of the finite element prediction for the response of plain concrete beam with Mazars' work (1984)	455
7.24	Comparison of the finite element prediction for the response of reinforced concrete beam with Mazars' work (1984)	457
7.25	Four-point loading on beams without shear reinforcement: (a) configuration, (b) finite element mesh	460
7.26	Comparison of the finite element prediction for the response of reinforced concrete beams without shear reinforcement against previous work	461

7.27	Steel/concrete bond problem considered for comparison with Mazars' work (1984): (a) Geometry, (b) Finite element mesh	464
7.28	Comparison of the finite element prediction for the load-displacement characteristics in bond problem	465
7.29	Comparison of the finite element prediction for the damage evolution in concrete: (a) current study, (b) Mazars' work (1984)	466
7.30	Comparison of the finite element prediction for the evolution of internal stresses in reinforcing steel: (a) current study, (b) Mazars' work (1984)	467
7.31	Reinforced concrete beams considered for calibration against code provisions: (a) without shear reinforcement, (b) with shear reinforcement	469
7.32	Softening characteristics of plain concrete beams	471
7.33	Effect of amount of main reinforcement on response nonlinearity for beams without shear reinforcement	473
7.34	Effect of shear span to depth ratio on response nonlinearity for lightly under-reinforced concrete beams without shear reinforcement	474
7.35	Effect of shear span to depth ratio on response nonlinearity for heavily under-reinforced concrete beams without shear reinforcement	475
7.36	Effect of shear span to depth ratio on damage pattern for lightly under-reinforced concrete beams without shear reinforcement	478
7.37	Effect of shear span to depth ratio on damage pattern for heavily under-reinforced concrete beams without shear reinforcement	479
7.38	Effect of amount of main reinforcement on cracking load for beams without shear reinforcement	484
7.39	Effect of shear span to depth ratio on cracking load for lightly under-reinforced concrete beams without shear reinforcement	485
7.40	Effect of shear span to depth ratio on cracking load for heavily under-reinforced concrete beams without shear reinforcement	486

7.41	Effect of shear span to depth ratio on ultimate capacity for lightly under-reinforced concrete beams without shear reinforcement	489
7.42	Effect of shear span to depth ratio on ultimate capacity for heavily under-reinforced concrete beams without shear reinforcement	490
7.43	Effect of amount of shear reinforcement on response nonlinearity or heavily under-reinforced concrete beams .	494
7.44	Effect of amount of shear reinforcement on damage pattern for heavily under-reinforced concrete beams	495
7.45	Effect of amount of shear reinforcement on cracking load for heavily under-reinforced concrete beams	498
7.46	Effect of amount of shear reinforcement on ultimate capacity for heavily under-reinforced concrete beams	499
7.47	Four-point loading on heavily under-reinforced concrete beams with different spacings between stirrups	501
7.48	Effect of spacing between stirrups on response nonlinearity for heavily under-reinforced concrete beams	503
7.49	Effect of spacing between stirrups on ultimate capacity for heavily under-reinforced concrete beams	504

DISSERTATION ABSTRACT

Student Name : SALAH EL-DIN MOHAMMED FAHMY MOHAMMED TAHER

Title of Study : CANONICAL ELASTOPLASTIC DAMAGE MODELLING OF REINFORCED CONCRETE

Major Field : CIVIL ENGINEERING

Date of Degree: June 1995

Reinforced concrete is per se neither elastic nor plastic material. It exhibits damage attributable to irreversible changes; i.e. slip and microcracking. Three phases of behavior exist and interact: elasticity, plasticity and damage. An extensive literature review is carried out to figure out the phenomenological aspects of damage along with the existing constitutive models.

New concepts in the framework of continuous damage mechanics are established. The notions of metaphorical generalized damage variables, generalized material degradation paths and generalized effective stress are defined. Free energy terms are derived based on the concepts of thermodynamics of irreversible changes. Incorporation with the classical theory of plasticity and micromechanics are made. A canonical elastoplastic damage model is proposed for concrete. The model is initially formulated through a rudimentary scrutiny of the uniaxial behavior. The derivation stems from recoverable energy equivalence based on the formal split of the total strain to its components; elastic damage and plastic-damage strain. On the basis of the proposed theory of dichotomy, the model is extended to handle biaxial orthotropic damage associated with cyclic behavior. Verification is carried out against a wide set of experimental data. The model is shown to properly predict strain softening, stiffness degradation, volumetric dilatancy under compression, strength increase under biaxial compressive states. Furthermore, a damage model is then proposed for the uniaxial behavior of steel.

Numerical implementation of the proposed damage model in terms of a computational framework is carried out by development of two nonlinear finite element programs; DMGTRUSS and DMGPLSTS. The first package deals with multi-dimensional trusses while the other handles two-dimensional plane stress states. Practical applications to plain and reinforced concrete structural members are shown to be in good agreement with well documented results.

DOCTOR OF PHILOSOPHY

KING FAHD UNIVERSITY OF PETROLEUM AND MINERALS
Dhahran, Saudi Arabia

1995

xxviii

خلاصة الرسالة

اسم الطالب الكامل : صلاح الدين محمد فهمي محمد طاهر
عنوان الرسالة : النمذجة المرنة اللدنة التلفية المبسطة للخرسانة المسلحة
التخصص : هندسة انشائية .
تاريخ الشهادة : يونيو ١٩٩٥ م .

تعتبر الخرسانة المسلحة مادة غير مرنة فقط وغير لدنة أيضاً ولكنها تتميز بالاضافة لذلك بتعرضها للتلف نتيجة التغيرات اللا انعكاسية كالتزلق والتشوهات . تشمل هذه الدراسة مراجعة نظرية مستفيضة لأوجه التلف المختلفة وكذلك للنماذج الدستورية لمحاكاة تصرف المواد تحت تأثير الأحمال .

عنيت هذه الأطروحة بتعريف مفاهيم جديدة لميكانيكا التلف المستمر وتشمل الاصطلاحات الآتية : متغيرات التلف المعممة الاستعارية ، المسارات المعممة لتدهور المواد ، ومفهوم الاجتهادات الفعالة المعممة . وقد استخدمت مفاهيم الديناميكا الحرارية للتغيرات اللا انعكاسية لاشتقاق معاملات الطاقة الحرة . وقد ادمجت هذه المصطلحات بنظرية اللدونة الكلاسيكية وكذلك الميكانيكا المتناهية الصغر (ميكروميكانيكا) .

تم في هذه الدراسة افتراض نموذج مبسط للتصرف المرن - اللدن التلفي للخرسانة وذلك بتقسيم الانفعال الكلي إلى قسمين : مرن تلفي ، ولدن تلفي . وقد أمكن عن طريق نظرية التقسيم المتتابع المقترحة تعميم النموذج من التصرف المحوري إلى حالات التلف المتعامد ثنائي الاتجاه الخاص بالتحميل الدوري . وقد تم التحقق من صحة النموذج بمقارنة النتائج بالقيم العملية . وقد ثبتت قدرة النموذج على التنبؤ بليونة الانفعال وتدهور الكزازة والتمدد الحجمي تحت الضغط وكذلك زيادة المقاومة بفعل حالات التحميل ثنائية الضغط . بالاضافة إلى ذلك فقد تم افتراض نموذج لتلف الصلب المحوري .

تشلت المحاكاة الرقمية لنموذج التلف المفترض في بناء برنامجين غير خطيين بطريقة الشرائح الحدية . يختص الأول بالجماليات متعددة الأبعاد بينما يقوم الآخر بالتحليل الثنائي البعد لحالات الاجتهاد المستوي . وتطبيقهما على العديد من الاعضاء الانشائية المكونة من الخرسانة العادية المسلحة ، فقد تم الحصول على نتائج جيدة وذلك بالمقارنة بالنتائج جيدة التوثيق .

درجة الدكتوراه في الفلسفة
جامعة الملك فهد للبترول والمعادن
الظهران ، المملكة العربية السعودية
التاريخ : يونيو ١٩٩٥ م .

CHAPTER 1

CHAPTER 1

INTRODUCTION

1.1 GENERAL

Reinforced concrete is the most widely used material in construction. It has been in use for more than a century but the problem of modelling the constitutive equations representing the salient notions of its behavior remains one of the most difficult tasks in structural engineering. Despite the inherent complexity of its chemical, physical and thermomechanical responses, it always proves itself as immutably universal building material. Most of its phenomenological aspects which disguised for decades were explored as a natural result of the present state of technology concerned with laboratory facilities, construction techniques and materials development. These keep modelling in the challenging track and spin with theory in a rotating orbit.

Along the lines of this chapter, the objectives of the current study are summarized, then the followed procedures are outlined. The organization of the work is featured.

1.2 OBJECTIVES

Concrete modelling is not an end by itself but the goal is the

proper prediction of the overall behavior of a reinforced concrete structure. Thousands of researches have been conducted to develop a versatile, simple and realistic model which is able to capture as many as of its features, but unfortunately such a model is still absent. Rolling from elasticity to plasticity to fracture mechanics and currently to continuous damage mechanics, knowledge is expanding and theory is refining. The main objectives of the current work are summarized hereafter:

1. Outline the main items for material behavior necessary for proper modelling.
2. Stand at the previous proposals with emphases devoted to those based on the concepts of continuous damage mechanics.
3. Develop a rigorous , yet, simple elastoplastic damage model capable of competing against existing models in its application.
4. Utilize the proposed model in one-dimensional and two-dimensional plane stress nonlinear finite element computational framework.
5. Examine the present model through practical applications.

1.3 KNOWLEDGE BASE

Engineering is very different from science in critical ways. Basically, science aims to increase understanding of the physical world

while engineering aims to solve practical problems. Informations may be of many types and qualities to engineers, for example it may be (Beeby, 1991) :

- (a) theoretical based on agreed assumptions;
- (b) empirical from experiment-quantitative;
- (c) rules of thumb; and
- (d) anecdotal information.

The engineer would be failing in his duty if he did not take account of any information which might assist him in arriving at a solution to his problem. He could not, however, use this information uncritically; he must make judgement about the relevance and quality of each piece of data available. The statistical scatter of the properties of concrete is distinctly larger than that of metals, polymers, and most other materials. Thus, it is not surprising to see a strong and certainly justified tendency to keep the mathematical models simple (Bazant, 1983). In the current study, it is aimed at utilizing almost all types of information available in order to achieve a realistic yet simple model.

1.4 PROCEDURE

The specific tasks involved in the development of the proposed model are as follows:

1. Investigate the physical and mechanical features of concrete as well as reinforcing steel. Some solicitations concerned with

reinforced concrete are discussed.

2. Classify the existing models for the sake of unbiased comparison among them.
3. Provide a state-of-the art on damage mechanics utilizing the concept of damage variable.
4. Investigate the rationality of the split of the state tensors.
5. Conceptually define some generalized terms in the frame of continuous damage mechanics.
6. Integrate the phenomenological aspects of damage to construct a uniaxial elastoplastic damage model for both concrete and steel, separately.
7. Investigate the possible elastoplastic damage uncoupling using the concepts of thermodynamics of irreversible changes.
8. Derive rigorously the tangential elastoplastic damage constitutive relations for yielding materials using the proposed generalized concepts.
9. Develop a phenomenological-micromechanical damage model for cyclic multiaxial state of stresses using the proposed generalized concepts.
10. Develop a canonical elastoplastic damage model for cyclic biaxial state of stresses which overcomes many of the drawbacks of

other models.

11. Construct a nonlinear finite element FORTRAN 77 program to examine the uniaxial model. This is handled by DMGTRUSS which is a multi-dimensional truss package.
12. Construct a nonlinear finite element FORTRAN 77 program to examine the canonical biaxial model. This is carried out through the package DMGPLSTS.
13. Derive concluding remarks on the proposed model.

1.5 ORGANIZATION

This work has four folds as shown in Fig. 1.1. The first is an extensive literature review as presented in Chapters 2 and 3. The second is re-conceptualization of continuous damage mechanics as established in Chapter 4. The third is the development of the elastoplastic damage constitutive models as formulated in Chapter 5. The final is the construction of nonlinear finite element programs in Chapter 6 to examine the model then applications in Chapter 7 are made.

In Chapter 2, the phenomenological aspects of materials are reviewed. Composition of concrete, its structural levels, cracking and mechanical properties are discussed. Mathematical formulation of the stress-strain relationship for reinforcing steel according to as far as possible up-to-date researches is highlighted. Problems associated with

reinforced concrete such as bond, tension stiffening and shear retention are presented. This background aims at providing physical insight of the most observed material characteristics required to broaden the scope of knowledge as a prerequisite to modelling.

In Chapter 3, the various models, yet developed are classified on different bases. The adopted scheme is appealing since it facilitate comparison purposes which indicates superiority of continuous damage mechanics. Light is, then, shed on models arised from this concept. The fundamental equations are reformulated. Various definitions of damage variables along with concepts of strain equivalence and effective stress are given. A state-of-the-art on damage models utilizing damage variables is presented. Advantages and limitations of phenomenological damage models are investigated.

In Chapter 4, new concepts in the framework of continuous damage mechanics are established. The notions of the concepts of metaphorical damage variables, generalized material degradation paths, generalized effective stresses are defined. Incorporation with the classical theory of plasticity is undertaken through a rigorous derivation of the tangential elastoplastic damage constitutive relations for yielding materials. Furthermore, the phenomenological and micromechanical aspects of damage are merged altogether.

In Chapter 5, uniaxial elastoplastic damage models, for concrete, in both tension and compression are formulated on the basis of the formal split of the total strain tensor. These models are extended to biaxial

loading by the proposed theory of dichotomy and the canonical elastoplastic damage model for cyclic anisotropic plane stress states for concrete is developed. Verification and validation of this model are thoroughly made. A damage model for uniaxial behavior of reinforcing steel is then suggested.

In Chapter 6, two FORTRAN nonlinear finite element programs are developed. The first is DMGTRUSS; a multi-dimensional truss software package. The second is DMGPLSTS; a two dimensional plane stress program. The formulation of these programs, the basic structure and their organization are described. This chapter represents the practical implementation of the canonical model into a computational framework.

In Chapter 7, the numerical framework of the canonical model is examined. Applications are made to investigate the behavior of plain concrete as well as reinforced concrete structures. Emphases are made to focus on the prolificacy of the canonical model.

Finally the work is crowned by conclusions and recommendations. Suggestions for future studies are also provided.

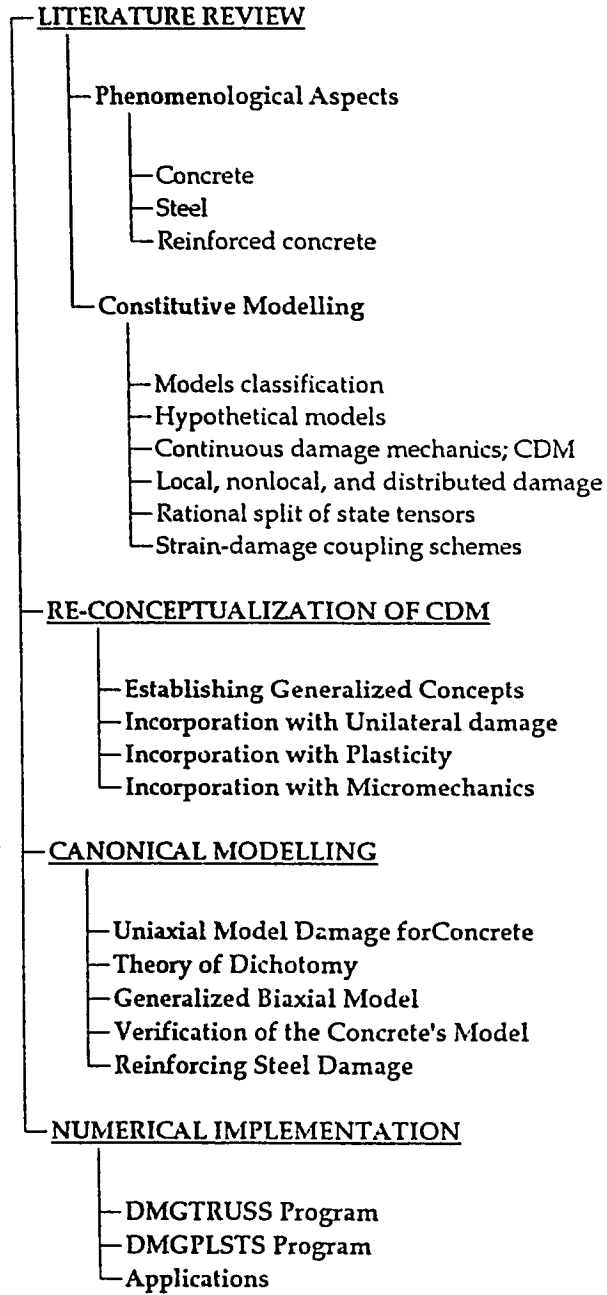


Figure 1.1 Organization of the current study

CHAPTER 2

CHAPTER 2**PHENOMENOLOGICAL ASPECTS****2.1 GENERAL**

Complexity of reinforced concrete as a building material was the real incentive of many investigators to devote a great deal of effort to physically understand its internal structure and to mathematically try to model its responses to different influences. The starting point in this manuscript is a historical background aiming at framing out the current stage of development. Describing concrete's composition, the salient notions of its structural levels and cracking criteria are highlighted in order to be able to elucidate its behavior. The various aspects of the mechanical response of concrete are then illustrated. Some special considerations, e.g. strain softening, structural effects and volumetric changes, are discussed. The mechanical properties of reinforcing steel are further investigated along with mathematical proposals to describe the stress-strain relationship. Combined concrete-steel behavior in terms of bond, tension stiffening and shear retention are finally outlined.

2.2 HISTORICAL BACKGROUND

Steel is one of the eldest materials known to humanity before Christ. Perhaps its forming returns back to profit Dawood (David) PBUH (Holy Quraan, 34-70). Steel reinforcement may consist of bars, welded wire fabric, or wires. For usual construction, deformed bars having lugs or protrusions are used.

"Concrete" originates from "concretus" which is the past participle of the latin verb "conrescere", meaning "to join together" or "to unit in growth". Thus the word concrete is a verb form that defines a process rather than a material. This is a good description as the term concrete can be constructed to include a considerable variety of products (Modeer, 1979). The main binding material in concrete is cement.

"Cement" originated from the lattin word "cementus", meaning "cut stone". The hardened cement is thus an artificial stone, usually made by a mixture of portland cement and water. Portland cement was invented in 1824 by J. Aspdin, and named portland simply because its color is the same as that of a natural rock from the island Portland. Previous trials to introduce hydraulic mortars were made by Greek and Romans by adding the lime clays to silicious constituents (pozzolanas). In 1845, Joseph Aspdin and Issac Charles, developed a better form of the portland cement by calcining a mixture of lime stone and clay at high temperatures (Elfgren, 1989). Joseph Monier introduced the reinforced concrete in 1870. In 1890, Ransome built the Leland Stanford Jr. Museum in San Francisco, a reinforced concrete building

two story high (Wang and Salmon, 1979). Eugene Freysinnet introduced the prestressed concrete in 1928. The use of dispersants and microsilica to increase density, strength and durability enjoyed a surge of interest since the late of sixties. Special types of concrete such as polymer, fiber-reinforced, and others are currently in use.

2.3 CONCRETE COMPOSITION

The usual engineering definition of concrete is expressed in the British Encyclopedia, 1963 edition, that says, "*Concrete is a building material consisting of a mixture in which a paste of portland cement and water binds inert aggregates into a rock-like mass as the paste hardens through chemical reaction of cement with water*". The main constituents of concrete are cement, water and aggregates.

2.3.1 Cementitious Matrix

Tri-calcium silicate, di-calcium silicate, tri-calcium aluminate and calcium aluminoferrite, the major constituents of cement, react with water to produce gel, calcium hydroxide and other minor products (ettringite, monosulfate, and sulfate sulfoaluminate and sulfo aluminoferrite). A freshly mixed cement paste is a dispersion of cement particles in water which has a certain structure owing to the forces of attraction and repulsion among these particles. When the reaction between cement and water takes place the products develop a structure

that originates from this dispersion structure and that is called hydrated cement.

The structure of the hydrated cement comprises a hierarchy of aggregations or gel particles, the latter being a term for particles in the submicroscopic range of the size called colloidal, i.e. from $0.001 \mu\text{m}$ to $0.1 \mu\text{m}$. These colloids have one of the three dimensions is often greater than the upper limit $0.1 \mu\text{m}$, they are thus needle-shaped. Many models were hypothesized to describe the structure of the cement gel. Among which are Powers', Ishai's and Feldman and Sereda's with differences exist mainly in the interpretation of the interlayer water (Mehta, 1986).

The most important colloidal particle of hydrated cement is an impure calcium silicate hydrate (CSH) with properties like those of a natural mineral called tobermorite. Although hydrated portland cement contains up to 25 percent of hydrated compounds other than the calcium silicate, the hardened paste has properties that justify its classification as a "tobermorite gel" (Mehta, 1986). It is also referred to as xerogel in the literature (Wittmann, 1983).

Along with the colloidal particles in the paste there is crystalline calcium hydroxide. The amount of calcium hydroxide is usually 15 percent per volume of hardened paste, a considerable proportion that must influence the behavior of the paste in a significant manner. Calcium hydroxide crystals are usually surrounded by and intergrown with colloidal material, and thus they constitute an integral part of the

solid structure (Idorn et al., 1966). The colloidal matter, together with calcium hydroxide appear as a solid structure. The porosity of the structure depends on the water to cement ratio (W/C), the rate of hydration and air-entraining. The pores occur in a wide variety of sizes and shapes. Gel pores, capillary pores and air-pores are the typical pore types (Powers and Brownyard, 1947; Verbeck, 1966).

The main constituents of hardened portland cement paste are thus unhydrated cement particles, tobermorite gel, calcium hydroxide, gel pores and entrapped air voids.

2.3.2 Aggregate Particles

Aggregates occupy about 50 percent of the volume of mortar and about 75 percent of concrete. Gradation, shape, surface texture, specific gravity and mechanical properties strongly influence the properties of the composites. Most aggregates are chemically stable rock materials. A smoother shape, such as that of river aggregates, does not raise such stress gradients as the angular shape of crushed materials. The bond between the aggregates and the paste is mainly influenced by the surface texture. Thus, river aggregates bond to the paste in a weaker way than crushed aggregates (Modeer, 1979). The influence of the aggregate grading on the properties of concrete materials has been extensively studied since the invention of portland cement and many methods have been proposed but non of them have been universally successful. Grading specifications were developed such

that on the average will give a concrete of satisfactory kind with respect to workability, strength and density.

2.3.3 Entire Composite

The complex behavior of a material can be understood only by studies of its interior structure. These structural studies can be done in different levels, from the atomic scale up to a scale where the material can be considered continuous and homogeneous.

Concrete may be considered as a two-phase material with one homogenous and one particle phase. In cement paste the particle phase is unhydrated cement particles and the homogeneous phase is cement gel, in mortar the two phases are fine aggregates with diameter equal to or less than 4 mm and cement paste, and in concrete are coarse aggregates with diameter bigger than 4 mm and mortar. However, Mehta (1986) considered concrete as a three-phase material with each phase being a multi-phase by itself. In sum, the composite nature of concrete seems to have a decisive influence on the development and propagation of microcracks (Ortiz and Popov 1982a, 1982b; Ortiz 1984).

2.4 STRUCTURAL LEVELS OF CONCRETE

The nonlinearity of mechanical response of most engineering materials can, in majority of cases, be attributed to the irreversible, energy dissipating changes in their microstructure. While the atomic lattices of constituent phases and their volume average determine the elastic properties of a composite, the geometry of its mesostructure (in terms of dispersions of the phases, specific area of weak interfaces and the size and distribution of initial defects) plays the most important role in the process which ultimately leads to the rupture of the material. For example, the relatively fragile bond at the aggregate-cement paste interface is the inherent weakness of concrete which is the dominant factor in the chain of events macroscopically observed as the nonlinearity in the stress-strain curve. According to the classification made by Wittmann (1983) there are at least three different levels (or scales) on which the physical and chemical processes can be observed. These scale levels with their representative features are presented in Table 2.1 (Krajcinovic and Fanella, 1986). A rough estimate of range of scale as suggested by Lemaitre (1986a) for various materials is listed in Table 2.2.

Table 2.1 Hierarchy of structural scales defining the mechanical response of concrete (after Krajcinovic and Fanella, 1986).

Scale	Volume element	Defect	Model
Micro	Hardened cement paste, xerogel, aggregate	Atomic voids, crystal defects	Material science models
Meso	Unit cell containing statistically valid sample of phases	Microcracking, large pores	Micromechanical models
Macro	Concrete specimen	Macrocrack	Continuum theories, fracture mechanics

Table 2.2 Macro scale of representative volume element (after Lemaitre, 1986)

Material	Scale
Metals	0.1 mm
Polymers	1.0 mm
Wood	10.0 mm
Concrete	100.0 mm

Lemaitre (1992) suggested a representative length scale of 100 mm. Modeer (1979) additively suggested that this length contain at least three aggregates., Krajinovic and Fanella (1986) suggested a cell size criterion at the meso-level for concrete to be a cube containing 30-100 aggregates. Bazant et al (1991a) advocated to representative elementary volume which is a sphere of radius equal to three times the maximum aggregate size. They considered this volume to be sufficient to include crack band formation and moreover the nonlocality effect of damage.

It is clear that the cell-size is quite arbitrary. However, it should give good representation of the behavior of the material

2.5 CRACKING OF CONCRETE

The two most prominent modes of the irreversible changes of the micro-structure are:

1. slip on the preferred crystallographic planes; and
2. nucleation and growth of microcracks and microvoids.

Slip is promoted by shear stresses available for moving and stacking dislocations (line defects) into preferential configuration. For material slips through the crystalline lattice, the number of bonds between particles remains practically unchanged (Krajinovic, 1984b). The plastic deformation is phenomenological result of the slips on all active slip systems in the solid. Concrete lack the crystalline lattice necessary

for the sustained slip deformation. This phenomenon is studied within the context of the theory of plasticity (or the slip theory). Response dominated by slip in shear planes is usually perceived as ductile as for concrete if partially or totally confined.

Ortiz (1984) pointed out that it is important to note, however, that both the cracking and plastic flow of concrete exhibit a variety of typical features that are not contained within the classical theories of fracture mechanics and plasticity. It is a well-known fact (Wastiels, 1979) that when concrete is subjected to uniaxial compression it develops cracks that are parallel to the axis of loading. In some cases, these cracks become so large to be the direct cause of failure of the specimen. This situation persists even if the specimen is laterally confined by means of a moderate compressive pressure. It is thus concluded that cracks in concrete can open against compressive stresses, which is in apparent contradiction to the second law of thermodynamics that require that cracks open only in tension (Sneddon and Lowengrub, 1969).

Whereas plastic strain does not significantly reduce the elastic moduli, micro-cracking causes both inelastic strain and a reduction of the elastic moduli (Bazant and Shieh, 1980b). Microcracking in the cleavage mode occurs in planes perpendicular to the direction in which the direct tensile strain exceeds some threshold value reflecting the cohesive and/or adhesive strength of the solid locally. Since the microcracking involves progressive loss of bonds between adjacent

particles (grains) the elastic properties of the solid are affected as well. Microcracks are actually not randomly oriented but exhibit a prevalent orientation, thus giving rise to stress-induced anisotropy of incremental elastic moduli (Bazant and Shieh, 1980b). Response characterized by microcracking in cleavage mode is typically classified as brittle as for a concrete specimen in unconfined uniaxial compression.

The extension of microcracks, for instance is known to play a decisive role in the inelasticity of concrete (Ortiz, 1984), as it results in the degradation of the elastic compliances (Hsu et al., 1963; Gardener, 1969; Karsan and Jirsa, 1969; Mills and Zimmerman, 1970, 1971; Linse, 1973; Palaniswamy and Shah, 1974; Wastiels, 1979) and interacts with the plasticity of the material (Hueckel, 1975, 1976; Hueckel and Mair, 1977; Dafalias 1977a, 1977b, 1978), an effect which is known as elastoplastic coupling.

The cracking of materials results from creation, propagation and coalescence of microcracks. For materials characterized by ductile behavior, Chaboche (1990) considered four different levels of cracking:

1. crack nucleation;
2. micro-crack initiation;
3. macro-crack initiation; and
4. breaking up.

On the other hand, one must distinguish two other types of structural materials (Bazant et al., 1991a):

1. those failing at the initiation of the macroscopic crack growth (i.e., the structure just before failure contains only macroscopic cracks or other flaws, as in typical sorts of many ceramics and fatigue-embrittled metal structures); and
2. those failing only after large stable microscopic crack growth (which is the case of reinforced concrete structures).

These considerations give rise to the brittle damage. Damage is generally termed brittle when it occurs by decohesion without any sensible plastic strain at the mesoscale. For a unified classification it is worth mentioning the two categories of brittle damage aligned by Lemaitre (1992):

1. Pure-brittle damage : in which permanent micro strains (plastic strains) may be neglected.
2. Quasi-brittle damage : in which the behavior is brittle at the mesoscale but localized damage growth occurs at the microscale.

For concrete, the heterogeneity of its microstructure associated with great porosity of the binding material and with the presence of granulates, is an essential factor of the phenomenological aspect of the behavior. From experimental observations and from micromechanical models which were proposed by several authors (cf. Lino, 1980; Modeer, 1979; Buyukozturk et al., 1971 and others), the following points can be described for concrete schematically:

1. a state of initial degradation (defects of compactness, microcracks

- in the paste created by dilation and shrinkage);
2. a propagation of the microcracks around the biggest grains under load; and
 3. a dependence of the microporous structure of the cement paste on the hydrostatic pressure.

A salient aspect of the material behavior of concrete that can be deduced in the process of damage undergone by its elastic properties as a consequence of microcrack growth (Gardener, 1969; Karsan and Jirsa, 1969; Palaniswamy and Shah, 1974; Wastiels, 1979; Ortiz, 1984). It has been experimentally shown through crack surveys that crack textures quickly become highly anisotropic (Kranz, 1979). This endows the elasticity of concrete with a strong induced anisotropy (Ortiz, 1984).

The other main characteristics deriving from these phenomenological considerations are (Mazars and Lemaitre, 1984b):

1. damage is the principal aspect of the behavior of the material;
2. damage only appears beyond a certain threshold of solicitation but this point is in contradiction with other investigators. Lorrain and Loland (1983) showed that damage takes place as early as loading starts;
3. damage influences the macroscopic mechanical characteristic of the material; and
4. damage modes differ according to the type of solicitation corresponding to:

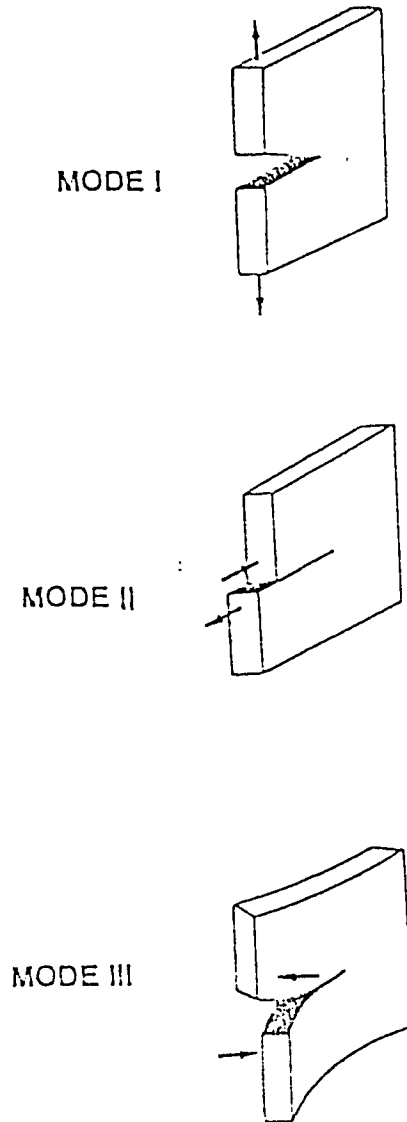


Figure 2.1 Modes of loading: I. opening, II. shearing and III. tearing

type A: the solicitation applied allows extensions in one main direction at least, the formation of microcracks in mode I (shown in Fig. 2.1) is then possible and the behavior of the material shows an instability. This type leads to cracking of concrete.

type B: the solicitation applied allows no extension, the strong hydrostatic pressure associated leads to the local initiation of microcracks in modes II and III (shown in Fig. 2.1), the friction between the lips yields a ductile macroscopic behavior;

type C: the solicitation is a hydrostatic pressure, the essential phenomenon is then the collapse of the microporous structure which leads to a consolidation of the material.

2.6 BEHAVIOR OF CONCRETE

The material properties (i.e., its response to mechanical, physical or chemical influences) are linked to its structure and the changes that may occur within this structure. With reference to the three structural levels adopted by Wittmann (1983): the macro-level, the meso-level and the micro-level, most models are usually confined to properties or phenomena observed at the macro-level. The matrix, which can be regarded as a continuum at the meso-level, consists of smaller aggregates embedded in a hardened cement paste. The ratio between matrix and inclusion stiffness, the matrix composition, the type of

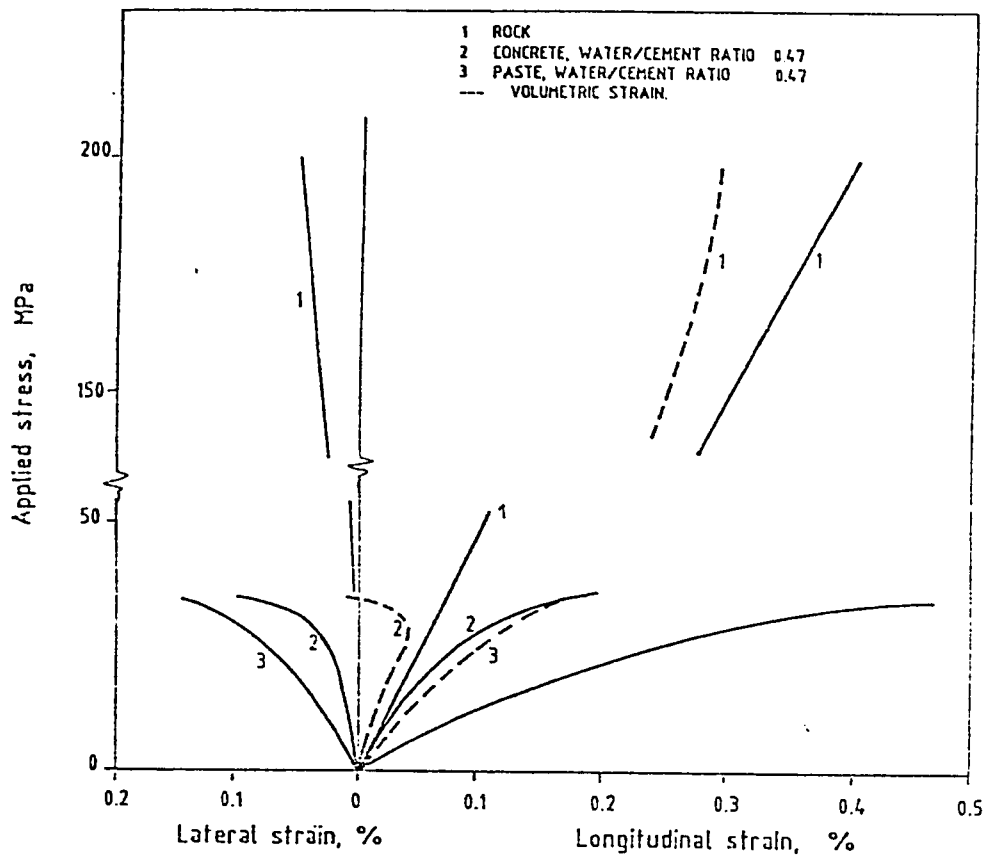


Figure 2.2 Compressive behavior of aggregate, paste and concrete

aggregates as well as the size distribution are examples of parameters influencing the material structure and the response on the material under load (Hobbs, 1977).

2.6.1 Uniaxial Compression

For most concretes, the aggregate volume concentration ranges between 0.55 and 0.80 and as a result the elastic properties of the aggregates have a very significant effect upon the deformation. Stress-strain curves for rock, paste and concrete loaded in uniaxial compression are illustrated in Fig. 2.2 (Hobbs, 1983). Rocks that are used as the aggregate in concrete generally exhibit an approximately linear relationship between stress and longitudinal strain up to failure, whereas both paste and concrete exhibit markedly non-linear behavior. The stress-volumetric strain curves for aggregate, paste and concrete are generally non-linear. For pastes there is a continuous reduction in volume as the applied stress decreases. The behavior of concrete is of similar form except that, at a stress of about 70 to 90 percent of the peak stress sustained, the volumetric strain increases. The salient notions of concrete behavior under uniaxial compression can be summarized as follows:

1. Unlike uniaxial tension, in uniaxial compression several longitudinal cracks (Campbell, 1962; Guo and Zhang, 1981) and diagonal shear type fracture plane develop (Hordijk et al., 1989). However, Shah and Sankar (1987) traced the internal crack pattern and observed

no shear band type of failure.

2. There is a non-linear trend in the stress-strain diagram with strain softening in the post-peak and it is still not clear whether this is a material phenomenon, an artifact of the method of testing and strain measurement technique, a result of localized shear band formation, or a result of distributed cracking (Read and Hegemier, 1984; Sandler, 1984; Wu and Freund, 1984; Van Mier, 1984; Frantziskonis, 1986; Kotsovos and Cheong, 1984).
3. A reduction in the unloading slope during the first loading cycles takes place at very low strains (Spooner and Dougill, 1975). Early onset of permanent deformations are also observed (Karsan and Jirsa, 1969).
4. During the strain-softening regime, the apparent Poisson's ratio can be greater than one, indicating a substantial lateral expansion (Case, 1984; Shah and Sankar, 1987).

It is apparent that the damage in concrete occurs at applied stress well below the maximum stress supported by the concrete. Some investigators (Hsu et al., 1963) have deduced that small cracks are formed in concrete before loading these cracks propagate and grow. A number of investigators (K. Newman, 1965; Kotsovos and J. Newman, 1979) took the view that the fracture process can be divided into a number of discrete stages and have suggested that critical or discontinuity stress levels exist. This is not supported by the work of Spooner and Dougill (1975). To assess damage, concrete specimens were subjected to series of cycles of loading and unloading (Fig. 2.3)

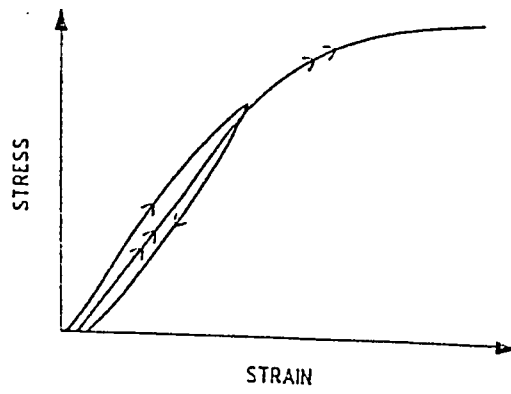
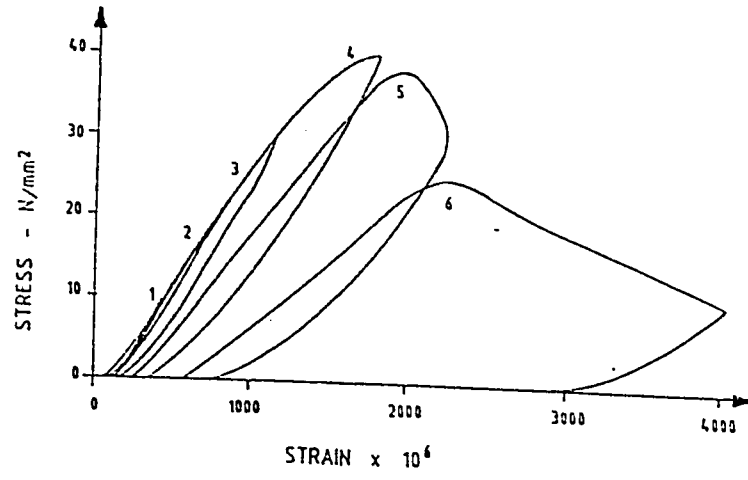


Figure 2.3 Cyclic response of concrete

and it was assumed that the reduction in the initial slope of the reloading curve is related to structural degradation of the material. Spooner and Dougill (1975) found that damage during the first loading cycle occurs in concrete at very low strains, about 200 micro-strains, and that once started the process is continuous. For the concretes tested, no evidence to support the existence of any "critical" or "discontinuity" stress was found. Spooner and Dougill (1975) and others used such results for quantifying the various energy components that were contributing to the fracture process of concrete as such. Similar load-paths were followed by others (for example Sinha et al., 1964; Karsan and Jirsa, 1969) and discussions evolved regarding the uniqueness of the descending branch with respect to different load-paths. However, in experiments by Hughes and Ash (1970), a considerable influence of the initial stress on the uniaxial compressive and tensile strength was reported and explanation of non-uniformity of deformation in the softening regime was made by Van Mier (1984).

2.6.2 Uniaxial Tension

The tensile behavior of concrete has long been considered to be of minor importance to failure analysis (Hordijk et al., 1989). This is due to the fact that concrete is a material most suitable to withstand compressive stresses rather than tensile stresses. With the introduction of fracture mechanics, however, it became clear that the tensile properties play even a dominant role in the failure of concrete

structures. This is reflected by the fact that the basic input for fracture mechanics models is the complete stress-deformation relation for discrete crack or stress-strain for crack band models for concrete under tensile loading. Fracture mechanics proposed the following quantifiers (Hordijk et al., 1989): (1) the fracture energy G_F , (2) the maximum crack opening w_o , (3) the characteristic length l_{ch} , and (4) the band width. The salient notions of concrete behavior in tension can be summarized as follows:

1. Cracking process starts at low level of stresses (Yankelevsky and Reinhardt, 1987). A localized fracture plane develops perpendicular to the tensile direction (Hordijk et al., 1989; Hordijk, 1992).
2. The initial tangent modulus for concrete in tension is mostly taken to be equal to that for compression (Neville, 1963; Hobbs, 1983; Gopalaratnam and Shah, 1985).
3. The Poisson's ratio ranges between 0.15 and 0.25 in the pre-peak region, and varies considerably in the post peak or descending branch prior to failure (Guo and Zhang, 1987).
4. Experiments show non-linearity in the stress-strain relation up to peak load (Evans and Marathe, 1968). Gustafsson (1985) claimed that this nonlinearity is due to experiment conditions and produced by any type of initial stress or undesired eccentric loading. However, this nonlinearity should be taken into consideration regardless of its source.
5. A softening post-peak behavior, in which large strains are involved,

is exhibited (Reinhardt, 1985; Shah, 1985; Wittmann, 1983; Carpinteri and Ingrassia, 1984).

6. The descending branch of the stress-strain curve is due to the reduction of the effective area (Guo and Zhang, 1987).
7. The stress-strain curve can neither be classified as elastic-perfectly brittle, nor as elastic-perfectly plastic (Rots and de Borst, 1989).
8. The cyclic response has received scant attention with some authors proposing idealized branches of unloading and reloading (Gopalaratnam and Shah, 1985; Rots et al., 1985; Rots, 1985; Yankelevsky and Reinhardt, 1987).
9. Snap-back behavior was reported by many investigators (de Borst, 1986; Carpinteri et al., 1986; Crisfield, 1986; Rots and de Borst, 1989).

2.6.3 Biaxial Loading

Investigations on the concrete behavior under biaxial stress states showed a considerable scatter in the results (Linse et al., 1975; Linse and Aschl, 1976; Kupfer et al., 1969; Kupfer and Gerstle, 1973; Buyukozturk et al., 1971; Buyukozturk and Tseng, 1984; Lino, 1975; Wastiels, 1979; Liu, 1971, 1972a,b; Van Mier, 1984; Kotsovos, 1974, 1979; Kotsovos and Newman, 1977; Vile, 1968). Some of the strength envelopes determined experimentally are ; Grestle, 1981; Akroyd, 1961; Anson, 1962; Bellamy, 1961; Karni and McHenry, 1958; Launay and Gachon, 1970). Some of the strength envelopes are shown in Fig.

2.4. This fact is mainly due to the type of end restraint. Loading through solid platens, loading through brush platens, loading by fluid pressure and loading and stressing hollow cylinders were some of the techniques attempted to determine the strength (Hobbs, 1983). Brush platens were claimed to completely eliminate friction at the interface (Kupfer et al., 1969). The salient notions of the behavior are summarized as follows:

1. Failure occurs by tensile splitting, with the fracture surface(s) orthogonal to the direction of the maximum tensile strain (Tasuji et al., 1978). However, another mechanism was given by Hordijk et al. (1989) for multi-axial states of stresses.
2. The strength in biaxial compression is higher than the uniaxial compression.
3. Compressive stress at failure decreases as the simultaneously acting tensile stress is increased.
4. No significant change in strength was reported under biaxial tension (Kupfer et al., 1969).
5. Similar to uniaxial loading, the residual strain in biaxial load combinations depends only on the corresponding strain on the loading curve at which unloading commences as shown in Fig. 2.5.

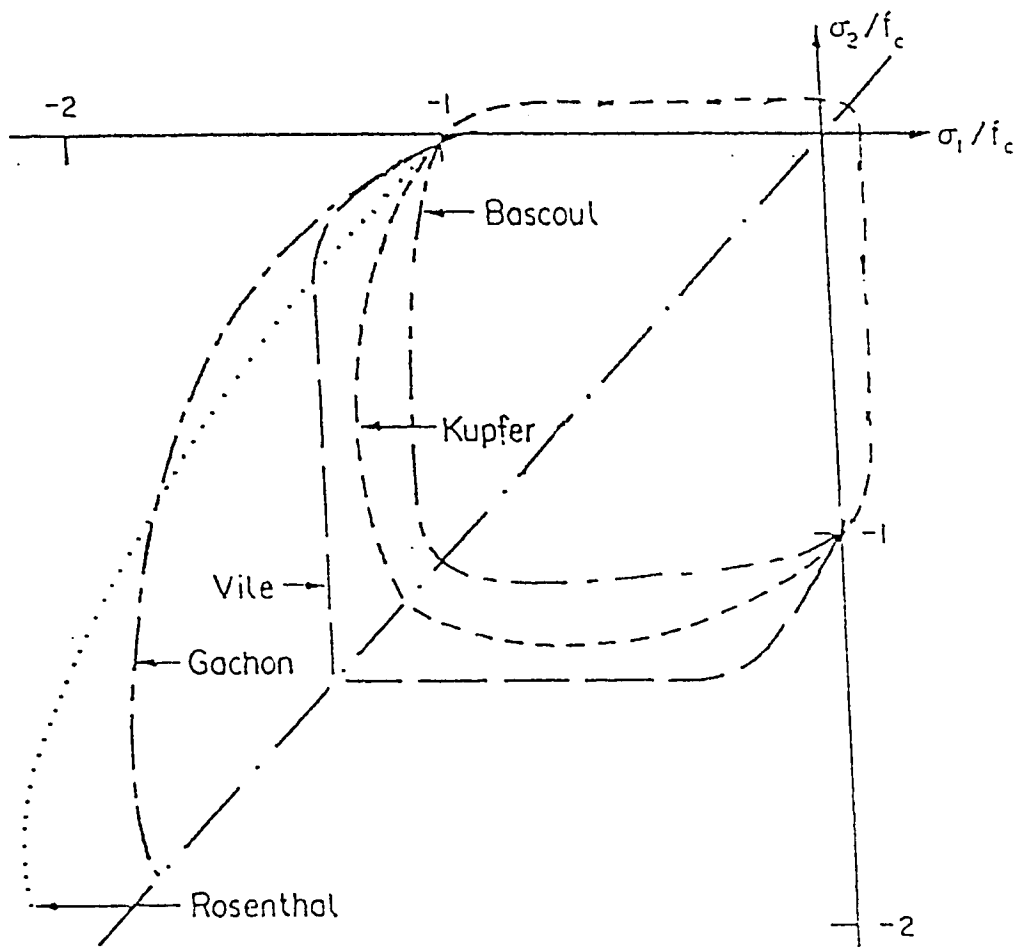


Figure 2.4 Experimental biaxial strength envelope for concrete

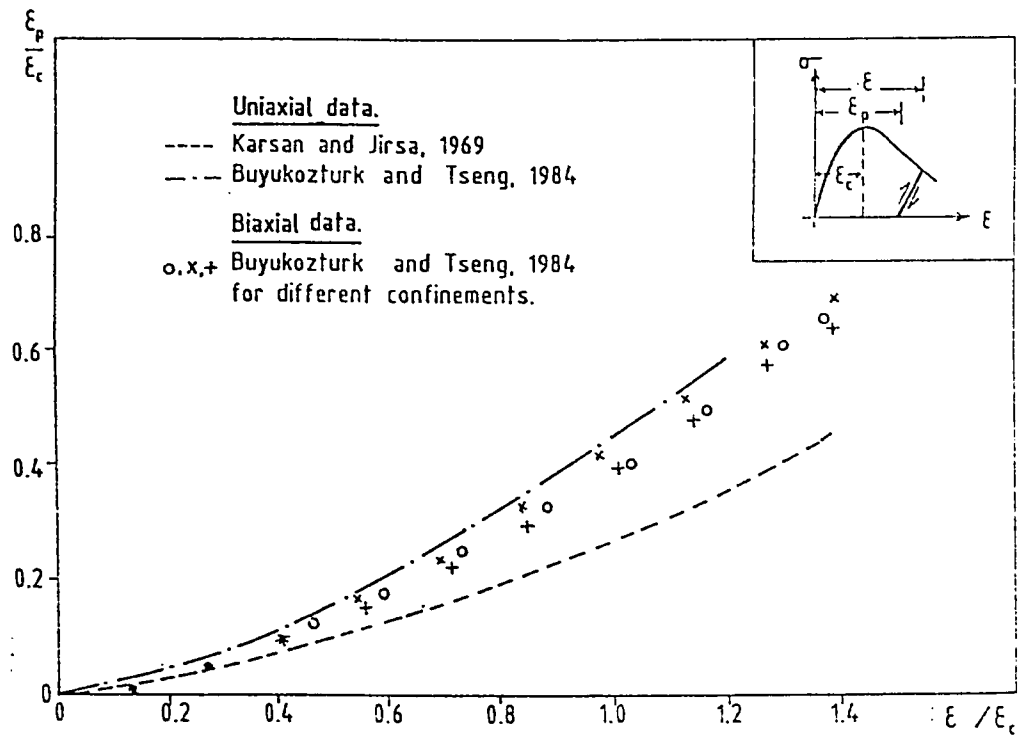


Figure 2.5 Residual strains for uniaxial and biaxial loadings

2.7 SPECIAL CONSIDERATIONS FOR CONCRETE

2.7.1 Strain softening

A number of materials, such as concrete, rock and dense soils, show a decrease in strength during progressive straining after the peak strength is reached. This phenomenon is termed strain softening (c.f. Bazant and coworkers, 1983g,m). Softening behavior of concrete is still under tremendous arguments whether it is a material property or a structural effect (Discussions, 1989). From experimental observations of strain softening, it has been found that strain softening may not be a material property of concrete, rock or soil treated as a continua, but rather the performance of a structure (finite size specimen) composed of microcracks, joints and interface that result in an overall loss of strength (Bazant, 1976a; Frantziskonis and Desai, 1987a, 1987b). A review on this subject is given by Sandler (1984) and Read and Hegemier (1984). If strain softening is assumed to be a true (continuum) material property, various anomalous conditions may arise with respect to the solution of boundary and initial value problems. As shown by Valanis (1985), these anomalies can lead to loss of uniqueness in the softening part of the stress-strain response. Subsequently, loss of uniqueness leads to numerical instabilities. This is illustrated by the high sensitivity of the numerical solution to the finite element mesh size (Sandler, 1984; Pietruszczak and Mroz, 1984).

The softening effect of damage in the overall material response has several potentially far-reaching consequences concerning the nature of the associated boundary value problem (Ortiz, 1984). Foremost among these is the loss of ellipticity with the ensuing possibility of localization of the inelastic deformation. While the theory of localization is presently well developed (Rice, 1976), it has mainly been applied to the study of shear band formation in metals and soils. The case of concrete presents an interesting variant of the process of localization, namely, the localization of diffuse microcracking into discrete cracks. Such extended cracks are observed to develop in reinforced flexural members.

2.7.2 Structural effects

Regardless of the strain softening of concrete, three well-established structural effects were reported (Bazant, 1983e; Bazant and Kim, 1984c; Saouridis and Mazars, 1989):

1. the volume effect;
2. the strain gradient effect; and
3. the structural size effect.

The volume effect is caused by the heterogeneous character as well as the initial microcracking of the material structure. That is there is a random distribution of the local defects, and by consequence a large volume will exhibit smallest macroscopic strength. The strain gradient effect is observed when structures of identical dimensions are loaded in

different ways. If the existence of microcracks are considered, the presence of strain gradient is beneficial for the local strength since compression applied in a direction lateral to that in which the crack will propagate delays microcrack growth. The structural size effect concerns with the variation of the fracture parameters which are assumed to be material constants when geometrically similar structures are tested.

2.7.3 Volumetric changes

The inelastic volume dilatancy and compaction are the salient characteristics of the inelastic behavior of concrete. Little attention has, yet, been given to them in the literature. Care was given to this phenomenon in few models; e.g. endochronic theories by Bazant and coworkers (1976b,c,d,e, 1978a,b,c, 1980b), damage models by Krajcinovic and coworkers (1981, 1983a,b, 1985, 1989), and Resende (1987). However, three elements were observed to contribute to volume changes in concrete:

1. dilatancy due to shear;
2. Shear compaction which occurs at the start of shear straining in the presence of triaxial compression; and
3. hydrostatic compaction for which its significance can be observed only at very high hydrostatic loading.

Unlike the first two elements, the latter is not a cross-effect due to shear deformation and does not result from microcracking. Rather it is

caused by a collapse of pore walls due to hydrostatic pressure or volumetric compression.

2.8 REINFORCING STEEL

It is now well recognized that the mechanical properties of steel beyond the yield strength are of prime interest. In terms of strain the ductility capacities are required for static plastic design and for seismic design. In terms of strength, the ultimate strength is the main parameter for determination of structural capacity. Elastoplastic idealizations give poor approximation since the post-yield region is assumed linear.

Between the yield strength and the ultimate strength it is important to know the behavior with enough accuracy where the rate of strain hardening is a determinant parameter, or simply where the level of stress is between these two values which is the customary case for reinforced concrete. RILEM Technical Committee 83 (1990) has proposed a tension testing method and some standardized mathematical expressions for idealization. Ramborg-Osgood and Menegotto-Pinto models were suggested. The latter seems to be more appealing for the so-called "round house" type of which the stress-strain diagram has no yield point. However, modifications of the general Menegotto-Pinto model were made to properly idealize the stress-strain curves for steel (Colson and Boulabiza, 1992). Fig. 2.6 shows the general model, the modified one, as well as the ranges of experimental data for parameter identification.

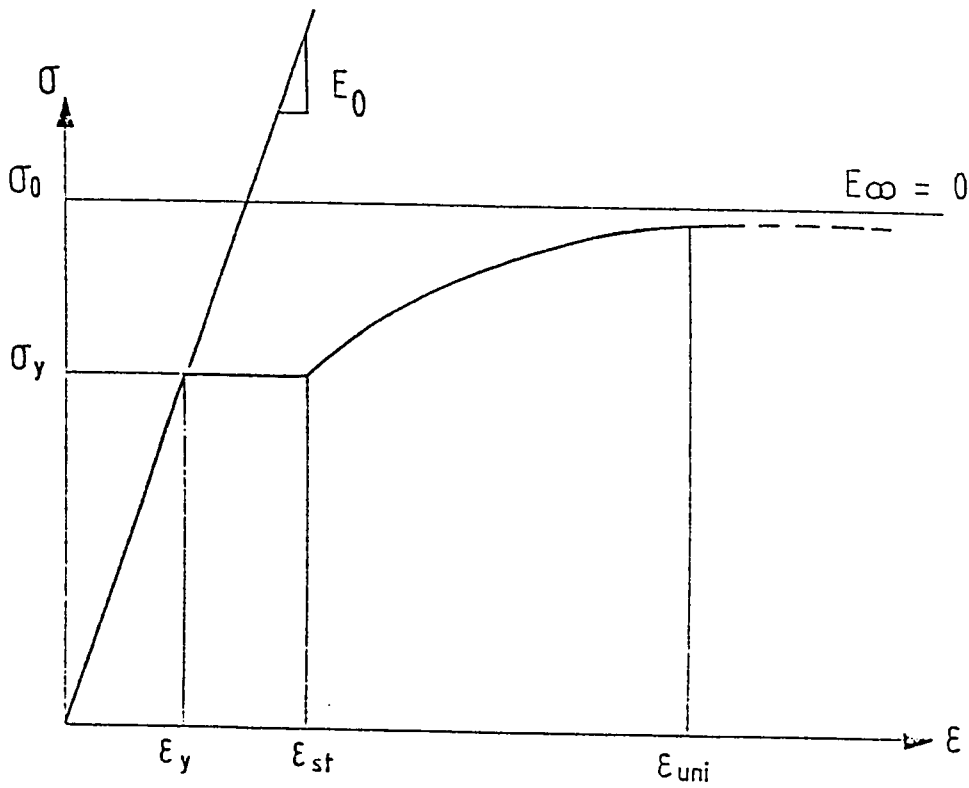


Figure 2.6 General and modified Menegotto-Pinto model for steel

Mathematical equations for the idealization are given as (Colson and Boulabiza, 1992):

$$0 < \varepsilon \leq \varepsilon_y \quad \sigma = E \varepsilon \quad (2.1)$$

$$\varepsilon_y < \varepsilon < \varepsilon_{st} \quad \sigma = f_y \quad (2.2)$$

$$\varepsilon \geq \varepsilon_{st} \quad \sigma = \frac{E \varepsilon}{[1 + (\varepsilon/\varepsilon_0)^R]^{1/R}} \quad (2.3)$$

in which σ is the stress, ε is the strain, ε_y is the yield strain, ε_{st} is the hardening strain, $\varepsilon_0 = \sigma_0/E$, E is Young's modulus, f_y is the yield strength, σ_0 is the ultimate strength and R is a material parameter. It has to be noted that the curve (Equation 2.3) is tangential to the initial stiffness (Equation 2.1). From experimental investigations (Colson and Boulabiza, 1992) using the modified least-squares method proposed earlier by Pilvin (1983), the following remarks were deduced :

1. The yield strength is directly dependent on the thickness (diameter) of the specimen.
2. Other parameters, E, R , and σ_0 , are independent on the thickness and could be considered as constant.

This emphasizes the idea of the existence of a skeleton curve for a given grade of steel depending only on the chemical composition, the skeleton curve is being governed by E, R , and σ_0 . On the other hand the well known yield strength would be dependent only on the

manufacturing process and to get the final shape of the product. With such an understanding the main strength parameter would be σ_0 . This idea fits quite well with the concepts of the ultimate limit states that are widely used and in nonlinear modelling.

2.9 REINFORCED CONCRETE

Reinforced concrete is unique in that two materials, reinforcing steel and concrete, are used together; thus the principles governing the structural design in reinforced concrete differ in many ways from those involving design in one material. Steel and concrete work readily of combination for several reasons (Wang and Salmon, 1979):

1. bond (interaction between bars and surrounding hardened concrete) prevents slip of the bars relative to the concrete;
2. proper concrete mixes provide adequate impermeability of the concrete against bar corrosion; and
3. sufficiently similar rates of thermal expansion albeit other thermal properties (conductivity, specific heat, ...etc) are different.

The feature of concrete cracking enhances three main issues; bond, tension stiffening and shear retention.

The transfer of stress across the interface between concrete and steel reinforcement by bond is of fundamental importance to most aspects of localized reinforced concrete behavior. Substantial difficulties

in pull-out/anchorage and transfer tests resulted in a widespread variation of results (Abd Al-Rahman, 1984).

Tension carried by microcracked concrete in zones adjacent to macrocracks is usually referred to as tension stiffening. The effect of tension stiffening is of major importance in under-reinforced concrete members. Factors affecting tension stiffening are the bond characteristics, tensile properties of concrete, macrocrack spacing and the bar sizes and arrangements (Clark and Cranston, 1979).

The surface of cracks that develop due to excess tensile stresses in concrete are usually rough and irregular. The mechanism of shear transfer in cracked concrete is called the "interface shear transfer" mechanism (Bazant and Gambarov, 1984b). Apparently the initial crack width is the primary variable affecting this mechanism. Smaller crack widths correspond to greater shear stiffness and strength. Aggregate size, reinforcement ratio, bar size and concrete strength are less important factors. Another important mechanism of shear transfer in cracked concrete is caused by "dowel action" of reinforcing steel. In sum, cracked concrete can still transfer shear through aggregate interlocking, friction and tension and/or dowel action in the reinforcement.

CHAPTER 3

CHAPTER 3

CONSTITUTIVE MODELING

3.1 GENERAL

Modelling of any physical phenomenon constitute an immortal challenge to researchers. With the help of fast computers the number of assumptions encountered with material idealization has been reduced considerably. Moreover, laboratory facilities have highly developed and experimental techniques declared several characteristics were not previously known and thus the challenge is continuous. Many models were proposed in various directions with no single trial to organize their dispersion. In this chapter, different categories of existing models are classified. Comparisons among the models themselves to distinguish the most promising modelling technique is made. It is revealed that continuous damage mechanics possesses superiority over others in many aspects. The advantages and limitations of this concept, after brief demonstration of its notions, are summarized. A state-of-the-art on continuous damage mechanics utilizing the concept of damage variable for concrete is presented. Finally, the local, the nonlocal, and the distributed natures of damage are discussed and the strain-damage coupling schemes are outlined.

3.2 HISTORICAL BACKGROUND

Design aspects started with empirical rules, then linear elastic theory was developed using the concept of allowable stresses at the end of the nineteenth century. Ultimate strength design using the ultimate capacity and elastic structural analysis (e.g. ACI-code) and limit state design using the ultimate capacity and the theory of plasticity (e.g. CEB-FIP code) were developed and are currently in use. Many other approaches were further proposed to replace the latter methods aiming at more realistic presentation of materials behavior. It was 1961 (Kaplan, 1961) that the concepts of fracture mechanics were applied to concrete. Numerous researchers came up with the conclusion that linear elastic fracture mechanics is not the proper way to model concrete, thus shedding the light on nonlinear fracture mechanics techniques augmented by the availability of fast electronic computers. Damage mechanics is still under the development phase and great effort was devoted to this area since the previous two decades. Other attempts which were made to model concrete on the basis of numerical simulation, stochastic theories, and homogenization gave good understanding of some physical aspects of material response.

3.3 MODELS CLASSIFICATION

Many models have been proposed to capture the main features of material responses and to predict its behavior (Bazant, 1981, 1982b). Experiments are liable to many sources of errors due to several influences. A proper model can replace with confidence the costly

CONSTITUTIVE MODELS CLASSIFICATION BASES

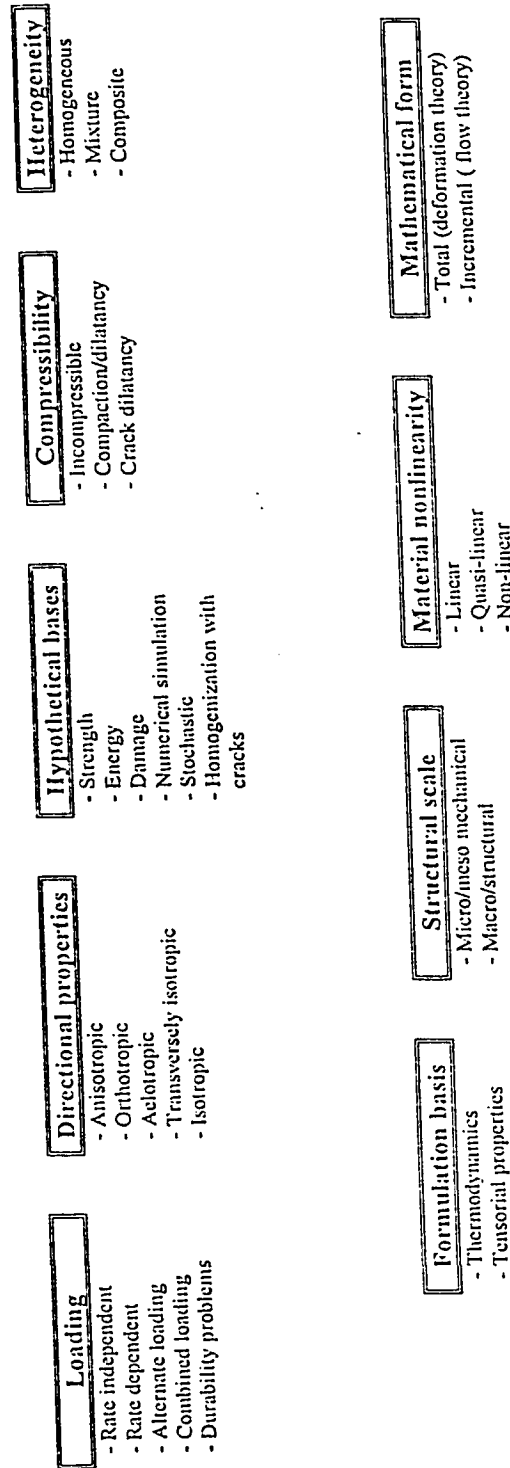


Fig. 3.1 Various bases of constitutive modelling classification

testing. Classification of models is not an easy task since it is mainly arbitrary and depends on many factors. For the sake of objectivity, the following herd of categories can be schematically described (Fig. 3.1):

3.3.1 Classification According to Loading Conditions

- a. *Rate independent models* : includes models adopted to predict response attribute to static, quasi static and cyclic loading conditions.
- b. *Rate dependent models* : include rheological models for dynamic and long term sustained loadings. Examples of this type are viscoelastic, viscoplastic, and elastic-viscoplastic models to predict behavior due to creep, relaxation and shrinkage.
- c. *Alternate loading models* : include models for low-cycle fatigue and high-cycle fatigue due to alternate loading associated with or without sign reversal.
- d. *Combined loading models* : include models concerned with interaction between two or more of the previous models; e.g. creep-fatigue interaction models.
- e. *Durability problems models* : this category became necessary after realization of the scientific community that durability problems should obtain the proper consideration in modelling. Currently, many researches are devoted to numerical modelling of corrosion, alkali silica reactivity and sulfate attack induced

structural deterioration.

3.3.2 Classification According to Formulation Basis

- a. *Thermodynamics based models* : include models emerging from the free energy function (whether the Helmholtz's or the Gibb's function). They utilize a group of state and internal variables and consider a dissipation function or a yield surface provided by Clausius-Duhem inequality (Lubliner, 1972, 1980).
- b. *Tensorial properties based models* : In this type of formulation the material's constitutive relations are often derived from the fundamental tensorial partitioning of the stress or strain to the deviatoric and spherical components. Bazant (1978a) recommended such models since the information furnished by thermodynamics is quite limited. Kachanov (1985) derived similar conclusions.

3.3.3 Classification According to Mathematical Form

- a. *Total models* : have the form of algebraic equations; relating the total stress to the total strain
- b. *Incremental models* : have the form of differential or integral equations; relating the strain increment to the stress increment.

Similar classification was suggested in the early history of plasticity and was termed: (a) *deformation theory*; and (b) *flow theory*. The former is based on a paper by Hencky (1926) which

relates the plastic strains themselves to the actual stresses. The flow theory follows the line of St. Venant (1870)-Levy (1870)-Von Mises (1913)-Prandtl (1924)- Prandtl and Reuss (1950) which relates the increments of the plastic strain to the actual stresses.

Lebmann (1982) gave the view that the deformation theory is physically unsatisfactory based on the classical experiments reported by Hohenemser and Prager (1932) and on the other hand, flow theory failed in bifurcation problems (Hohenemser, 1931; Rice, 1976, Christoffersen and Hutchinson, 1979; Sewell, 1974).

3.3.4 Classification According to Compressibility

- a. *Incompressible models* : old plasticity models assume no volume changes (Prandtl and Reuss, 1950). This, however, applicable for metals and some alloys in certain strain range but this is usually accompanied by change in density (Dufailly, 1980; Lemaitre, 1992). The density change is always neglected except in few ductile damage or material science models.
- b. *Compressible/Dilant models* : Concrete, rock and dense soils whether totally or partially confined when subjected to distortional compressive stress show compressibility then dilatancy can be obviously observed. The reason for such behavior is the evolution of microcracks. Many models were adopted with main target to model this phenomenon (e.g. Resende and Martin, 1984; Resende, 1987; Bazant and Tsubaki, 1980e).

c. *Crack dilatancy models* : the fact that cracked concrete structures still have a considerable load carrying capacity is attributable to such phenomena as bond slip, dowel action in reinforced concrete in addition to tension-softening behavior and aggregate interlock. The last phenomenon in particular, is often assumed to contribute significantly to the load-carrying capacity of concrete structures that show large cracks (greater than 0.1 mm) (Feenstra et al., 1991). Indeed, a large amount of research has been conducted in the past two decades either experimentally (Walraven et al., 1979; Walraven, 1980; Walraven and Reinhardt, 1981) or analytically (e.g. Bazant and Gambarova, 1980d; Gambarova and Karakoc, 1983; Li et al., 1989; Walraven, 1980, Walraven and Reinhardt, 1981). The mathematical models for crack dilatancy can be classified into two categories (Feenstra et al., 1991):

1. Empirical crack models

- Rough crack models (Bazant and Gambarova, 1980d; Gambarova and Karakoc, 1983).
- Aggregate-interlock relation (Walraven and Reinhardt, 1981).

2. Physical crack models

- Two-phase model (Walraven, 1980).
- Contact density model (Li et al., 1989).

3.3.5 Classification According to Material Linearity

- a. *Linear models* : include linear stress elasticity and linear elastic fracture mechanics.
- b. *Quasilinear models* : include models approximating the nonlinear material behavior to piece-wise linear segments or models which are incrementally linear (Hodge, 1956).
- c. *Nonlinear models* : include models accounting for material nonlinearity even though the behavior is not elastic.

Linear elastic models based on either a strength criterion or linear elastic fracture mechanics failed to distinguish the three structural effects aforementioned in clause 2.7.2. These three structural effects cannot be predicted if the damage zone is neglected. Nonlinear elastic models can be helpful for zones stressed at low levels (Saouridis and Mazars, 1989).

For materials exhibiting inelastic behavior such as concrete, the stress increment $d\sigma_{ij}$ ($i, j = 1, 2, 3$), which is corresponding to a strain increment $d\varepsilon_{ij}$, is composed of two parts. The first is (an elastic) stress increment assuming the intact material $d\sigma_{ij}^0 = C_{ijkl}^0 d\varepsilon_{kl}$, where C_{ijkl}^0 is the initial fourth order modulus tensor of the material. The second is an inelastic stress decrement $-d\sigma_{ij}^{in}$, the expression of which distinguishes among various models. Dougill (1975, 1976) assumed, for instance, a fracture surface which yields the fracture stress increment

$d\sigma_{ij}^{fr}$ by normality condition, then assumed that $d\sigma_{ij}^{in} = d\sigma_{ij}^{fr}$. On the other hand, in the plastic fracturing model, Bazant and Kim (1979) considered the inelastic stress to consist of plastic and fracturing components, $d\sigma_{ij}^p$ and $d\sigma_{ij}^{fr}$, respectively. These stress increments are determined by two interacting loading surfaces. In the endochronic models developed for concrete by Bazant and co-workers (Bazant and Baht, 1976; Bazant and Shieh, 1980) used similar decomposition but each component was expressed by proper intrinsic time increment which was never negative.

Recently continuous damage mechanics emerged in various forms to provide a simple and realistic understanding of the material behavior. The inelastic behavior of concrete was characterized utilizing several forms of the damage variable. The easiest approach is to consider a scalar damage variable D through which the inelastic stress is expressed as $d\sigma_{ij}^{in} = C_{ijk}^0 d(Dr_{km}) + f_{ij}$, f_{ij} is a tensorial function which depends on the damage model and reduces to zero for brittle behavior. Ju (1990) showed that such scalar type formulation need not represent isotropic behavior. Moreover, he claimed, in another study (Ju, 1989), that the damage process is associated to both the elastic and plastic phases of concrete behavior. Following different approaches, the damage variable was defined on the basis of either: (1) an assumed potential of dissipation function (Lemaitre, 1985), (2) a kinematic damage surface (Krajcinovic and Fonseka, 1981), (3) a phenomenological consideration (Mazars, 1984), (4) an energy based (Simo and Ju, 1987), (5) an exponentially decaying form (Desai and Frantziskonis, 1987), (6)

micromechanically (Budiansky and O'Connell, 1976), (7) intuitively suggested form in terms of strain rate and hydrostatic pressure (Resende, 1987), or (8) bounding surface (Suaris et al., 1990; Taher and Voyiadjis, 1993; Voyiadjis and Taher, 1993).

3.3.6 Classification According to Directional Properties

- a. *Anisotropic models* : include models where there are no material symmetry at all (Lekhnitskii, 1963).
- b. *Orthotropic models* : include models for material for which three orthogonal planes of symmetry exist (Bazant, 1983n).
- c. *Aelotropic models* : mainly developed for crystals of symmetry group less than the full orthotropic group (Smith and Rivlin, 1958; Smith, 1962). In this case there exists a finite group of symmetries, while isotropy and transverse isotropy are characterized by continuous group (Malvern, 1969, Spencer and Rivlin, 1959a,b).
- d. *Transversely isotropic models* : include models for materials possessing a rotational symmetry with respect to one of the coordinate axes and if moreover every plane containing this axis is a plane of reflection symmetry (Spencer and Rivlin, 1959a,b, 1961).
- e. *Isotropic models* : mechanical behavior is identical in all directions

For linear elastic material obeying Hook's law, the number of material constants are reduced from 21 to 9 to 5 and to 2 for anisotropic, orthotropic, transversely isotropic and isotropic, respectively. For aelotropic materials, the number of material parameters depend on the number of symmetry planes and is intermediate between the orthotropic and transversely isotropic materials.

A salient aspect of the material behavior of concrete is the process of damage undergone by its elastic properties as a consequence of microcrack growth (Gardener, 1969; Karsan and Jirsa, 1969; Linse, 1973; Mills and Zimmerman, 1970, 1971; Palanswamy and Shah, 1974; Wastiels, 1979). It has been experimentally shown through crack surveys that crack textures quickly become highly anisotropic (Kranz, 1979). This endows the elasticity of concrete with a strong induced anisotropy. Despite this fact, most models were isotropic (Kupfer and Gerstle, 1973; Budiansky and O'Connell, 1976; Cedolin et al., 1977; Bazant and Kim, 1979a; Resende and Martin, 1982; Resende, 1984; Mazars, 1980, 1983, 1986a; Lemaitre, 1992) or orthotropic (Liu et al., 1972a, 1972b, Romstad and Taylor, 1974; Darwin and Pecknold 1977a, 1977b; Elwi and Murray, 1979, 1980; Bashur and Darwin, 1979). This clearly restricts the validity of such models to certain loading conditions. Few theories are available that do account for induced anisotropy (Dougill, 1976; Dougill et al., 1977; Costin, 1983; Ortiz and Popov, 1982b; Ortiz, 1984,1985). These theories have invariably characterized microcrack textures by controlling microcrack along selected directions.

3.3.7 Classification According to Structural Scale

- a. *Nano-/micro-/meso-mechanical models* : include models emphasizing the dominant mode of irreversible changes of the mesostructure embedded, via an appropriate homogenization algorithm, into a constitutive relation mapping macrostresses on macrostrains in a homogenized solid (Krajcinovic and Summarac, 1989). Elasticity takes place at the level of atoms while plasticity is governed by slips at the level of crystals or molecules through dislocations. Damage is debonding from the level of atoms to the mesolevel for crack initiation (Lemaitre, 1986b).
- b. *Phenomenological models* : include models describing phenomena only at macro and structural scales (Lemaitre, 1986a, 1986b). The major weakness of all phenomenological models resides in the arbitrariness of the choice of the kinetic equations which at the very best only vaguely, if at all, reflect underlying processes on the mesoscale (Krajcinovic, 1984a, 1984b).

In the micromechanical type of models, the microscopic mechanisms are the primary object and the macroscopic response is then deduced. This is the case of micro-plane models (Bazant, 1983c), models using homogenization technique, as well as statistical models. This kind of approaches must be better seen as very useful tools for material modelling rather than tools for structural analysis.

In the phenomenological type of models, two approaches available are the global and the local. Global approaches such as nonlinear fracture

mechanics models were established in such a manner that fracture properties were forced to remain size-independent. Local approaches such as the continuum damage mechanics models which introduce for damage a continuum variable generally affecting the elastic properties. However, the criteria guiding the model's choice is the capability to simulate or predict the localized as well as the non-localized failure modes. Continuous damage mechanics is then convenient since nonlinear fracture mechanics models could simulate only the localized failure modes (Lemaitre, 1986b). It can be concluded that continuous damage mechanics should gain more research considerations as a promising tool to properly model the material behavior of concrete under various loading conditions.

3.3.8 Classification According to Material Heterogeneity

- a. *Homogenization models* : most of the existing concrete models postulate perfect homogeneity. However, this is a crude assumption since strain softening never takes place in a homogeneous continuum (Bazant, 1976a). Also, splitting failure in uniaxial compression could not be justified if homogenization is assumed (Ortiz, 1984).
- b. *Homogeneous medium with cracks* : many models assumes a homogenization for the cracks in the matrix either using Taylor model (1938) or self-consistent model (Budiansky and O'Connell, 1976). In models assuming isotropy and homogeneity of the paste-aggregate matrix, the complete geometry of the mesostructure is defined by (Kanaun, 1983) :

- Three random vectors describing the Bravais lattice formed by the centers of cracks as nodes.
- Two scalars approximating the shape of the crack by an ellipse.
- Three normals to the crack surface.

c. *Composite models* : Include models dealing with materials of various phases. The complete description of each phase at the considered structural scale should be specified assuming known behavior. The most widely accepted models for composite materials considers elasticity with load transfer between the phases (e.g. unidirectional and angle ply composites). Orthotropic properties of prime importance to utilize the composite action for intentionally oriented reinforced elements.

d. *Mixture models* : These models are based on the theory of interacting continua, or the theory of mixtures. The averaging may be obtained using Hill, Voigt, Reuss approaches or combination of them all (Zimmerman, 1991). For concrete, as a two phase material, the constituents can be regarded as mortar and aggregate. Foremost among the advantages of the theory of interacting continua is the notion of phase stresses, i.e., that the externally applied stress distribute unevenly between mortar and aggregate. These phase stresses jointly equilibrate the external ones, but are in general vastly different from each other. A detailed study of concrete as a mixture has been presented by Ortiz and Popov (1982a). The

aggregate phase stresses does not represent the stresses within the aggregate particles but rather it accounts for the contact forces that develop between them. The absence of diffusion between mortar and aggregate results in strain compatibility between mortar and aggregates. Such strains refer to the macroscopic deformation of the phase and are not in any way intended as measures of deformation processes that take place at the microstructural level. In other words, the compatibility which is meant takes a completely different meaning and serves a completely different purpose than the similar one which is postulated in Taylor's method for composite materials (Taylor, 1938). In this latter case, compatibility of deformations between the matrix and the inclusions is postulated at the microstructural level. This is a rather restrictive assumption that has been relaxed in various ways in subsequent refinements of the theory.

3.3.9 Classification According to Hypothetical Basis

- a. *Strength based models* : include elasticity, plasticity and frictional models.
- b. *Energy based models* : include linear elastic fracture mechanics and nonlinear fracture mechanics.
- c. *Stochastic models* : include models utilizing statistical distributions to predict failure.
- d. *Numerical simulation models* : include techniques simulating the

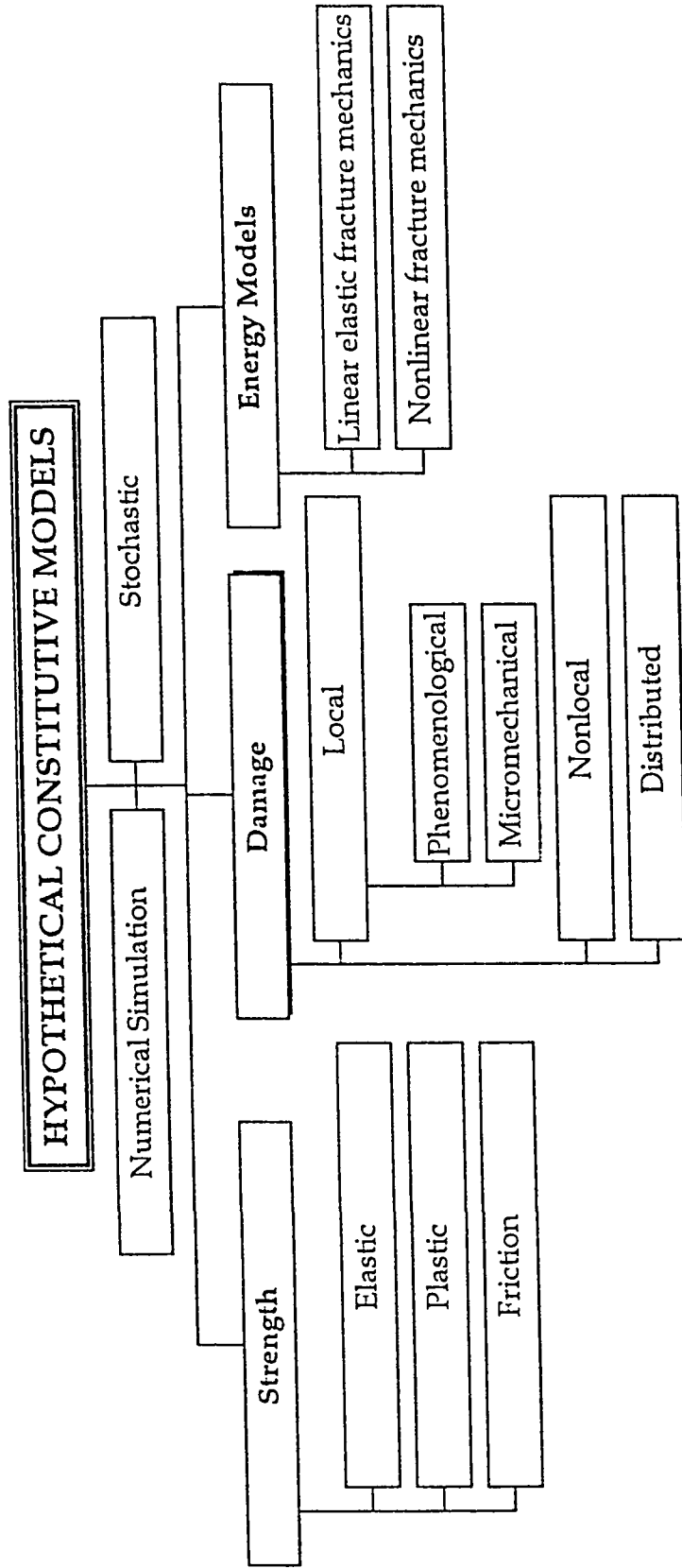


Fig. 3.2 Classification of hypothetical constitutive models

composition and behavior of concrete as a random process by computer.

e. *Damage models* : include models featuring the material degradation with the course of straining or loading the material.

This classification is the most general and cover a broad set of models as illustrated in Fig. 3.2. Each category will be discussed separately hereafter.

3.4 STRENGTH BASED MODELS

Many models were proposed to describe the behavior of concrete under various loading conditions. These models may be categorized on the following basis:

3.4.1 Elasticity Models

Elasticity is full recovery upon load removal. Linear elasticity is the simplest form of elasticity (Hook's law). The stress can be related to the strain through an elastic response function. The relationship should be reversible and path independent. The actual behavior of geotechnical materials is nonlinear. A bevy of models were adopted to simplify such a behavior including a bilinear, multilinear or piecewise linear, hyperbolic (Christian and Desai, 1979), Rambor-Osgood (1943), and similar models (Desai and Wu, 1976) and using other functions such as spline functions (Desai, 1971; Ahlberg et al., 1967) or polynomials.

Cauchy elastic material may generate energy under certain loading-unloading cycles which violate thermodynamics (Eringen, 1962; Malvern, 1969). Restricted to the existence of an elastic strain energy function, hypoelastic or Green elastic material is limited (Fung, 1965; Eringen, 1962; Green and coworkers, 1957, 1959; Malvern, 1969). Hypoelasticity is used to describe the incremental elastic relations (Malvern, 1969; Truesdell, 1955; Green, 1956).

3.4.2 Plasticity Models

A sheaf of models based on plasticity were developed merely for metals then were applied to concrete and soils. These models can be reasonably grouped under conventional and unconventional plasticity as shown in Fig. 3.3.

a. *Conventional Plasticity*

The theory of plasticity is a branch of the strength of materials that can be traced back at least to Galiles (Braestrup and Nielsen, 1983).

Any deformational response to applied loads, or to environmental changes, that does not obey the constitutive laws of classical elasticity may be spoken of as an inelastic deformation. In particular, irreversible deformations which result from the mechanism of slip, or from dislocations at the atomic level, and which thereby lead to permanent dimensional changes are known as plastic deformations. In the theory of plasticity, the primary concerns are with the mathematical formulation

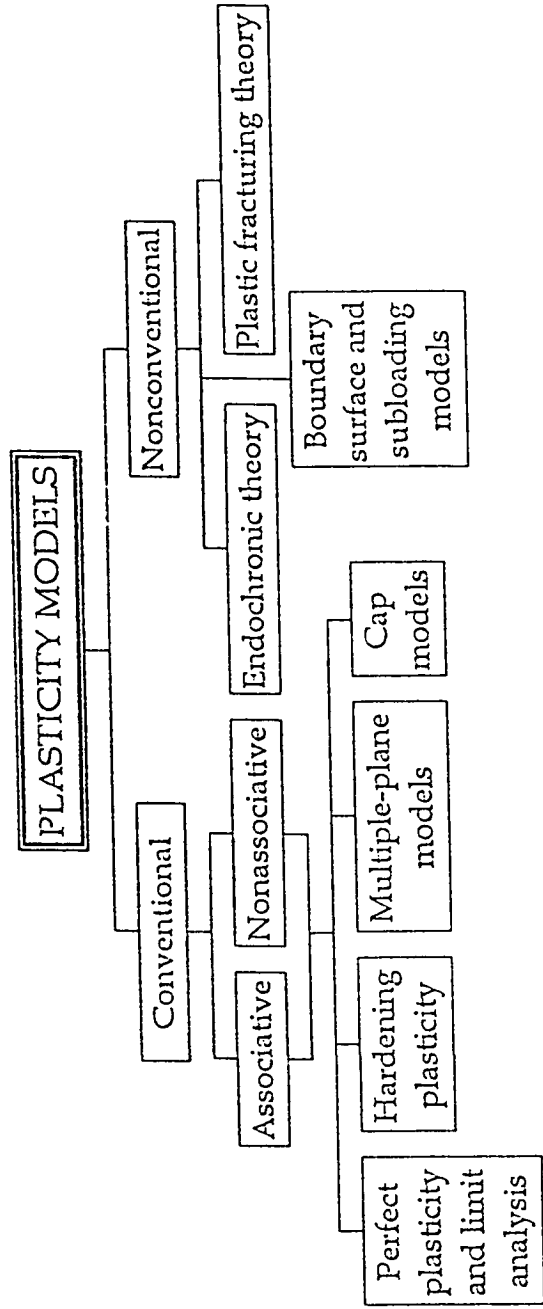


Fig.3.3 Different plasticity based models

of the stress-strain relationship suitable for the phenomenological description of the plastic deformation and often with establishment of approximate yield criterion for predicting the onset of plastic behavior. A tremendous amount of models were suggested in the literature, most of which are listed in Table 3.1.

i. Associative plasticity

The phrase plastic flow is essentially a generalization to multi-dimensional states of the concept of the yield stress in one-dimensional loading. Continued loading after initial yield leads to plastic deformations which may be accompanied by changes in the yield surface. For an assumed perfectly plastic material the yield does not change during plastic deformations and the initial yield condition remains valid. The alternative for strain hardening material is hardening plasticity. It is accounted for by either strain or work hardening. Three hardening rules were adopted: isotropic, kinematic and mixed hardening. Bazant and Kim (1979a) introduced the jump-kinematic hardening rule for unloading, reloading and cyclic loading. In addition, anisotropic hardening (Mroz, 1979) and nonuniform hardening (cf. Han and Chen, 1985) were proposed.

To sum up, the ingredients of the traditional elasto-plastic theory can be summarized as follows:

1. A constant, symmetric, positive definite tensor of elastic moduli;
2. A "yield function" of the stress tensor which defines (as the

Table 3.1 Failure theories in chronological order

Reference	Criterion
Coulomb, 1774 Rankine, 1850 St. Venant, 1855 Tresca, 1864	Two-parameter shear friction failure. Maximum principal stress. Maximum principal strain. Maximum tangential (shear) stress. Also known as Coulomb and as Guest's theories.
Beltrami, 1892 Von Mises, 1913a,b	Maximum strain energy density. Maximum distortional strain energy density. Also known as Maxwell's theory.
Mohr, 1914 Griffith, 1921	Modified Coulomb criterion. Failure Criterion for brittle material containing elliptical minute flaws.
Hencky & Nadai, 1924	Maximum octahedral shear stress criterion. Also known as Hencky-Mises criterion.
Leon, 1934 Kojic & Cheatham, 1947 Hill, 1948 Lame, 1950; Ciaperym, 1950	Parabolic Mohr envelop. Modified Mohr -Coulomb. Maximum principal deviatoric stress. Extended maximum principal stress criterion.
Drucker & Prager, 1952 a	Smooth approximation to the Mohr-Coulomb surface by a simple modification of the Von Mises criterion.
Cowan, 1953	Combination of Mohr-Coulomb with maximum strength cut-off.
Bresler & Pister, 1958a,b McClintock and Walsh, 1962	Modified octahedral shear stress criterion. Modified Griffith's theory for compressive stress.
Norris, 1963	Failure due to yielding or fracture of orthotropic materials.
Murrell, 1963	Three-dimensional extension of Griffith's theory.
Reimann, 1965	Four-parameter model; meridians are parabolic and the deviatoric sections are non circular.
Baker, 1967	Failure criterion accounting for cracking due to differential stiffness between the aggregate matrix and interface; failure surface is a tetrahedron.

Table 3.1 (continued)

Reference	Criterion
Suh, 1969	Modified Mohr-Coulomb accounting for dilatancy and compaction.
Schimmelpfenning, 1971	Modified Reimann criterion.
Sandhu, 1972	Review of theories of failure for isotropic and anisotropic materials.
Hobbs, 1974	Empirical criterion for concrete.
William & Warnke, 1974	Three-parameter failure surface expressed in terms of the average normal and shear stresses.
Argyris et al., 1974a	Three-parameter model involving all three stress invariants; straight meridians and non circular deviatoric sections.
William & Warnke, 1974b	Five-parameter criterion of elliptic deviatoric sections and parabolic meridians.
Wu, 1974	Dual failure criterion for plain concrete.
Chen and Chen, 1975	Modified Mohr-Coulomb.
Ottosen, 1977 a, 1977 b, 1979	Four parameter model; Meridians are parabolic and the deviatoric sections are non circular.
Lowe, 1978	Modified maximum tensile strain criterion.
Chen, 1979	Dual representation of fracture criterion in terms of stress and strain.
Yang, 1980a, b	Generalized Von Mises criterion for yield and fracture.
Hsieh et al., 1979	Four-parameter failure criterion which contain several earlier criteria as special cases (e.g., Von Mises, Drucker-Prager and maximum tensile cut-off).
Bangash, 1982	Simplified two-parameter model .
Zienkiewicz and Pande, 1983	Hyperbolic and parabolic approximations of the Mohr-Coulomb criterion with an added strain dependent elliptical surface.
Lade, 1982	Three-parameter failure criterion for concrete.
Braestrup, 1983	Parabolic failure envelop with circular tension cut-off.

locus where is negative) the current elastic domain in the space of the stress components,

3. A plastic flow rule which relates plastic strain rates to stress states which is assumed to be associated; and
4. A hardening rule according to which some parameters contained in the yield function depend on on some measures of the 'irreversible' deformation process (such as volumetric plastic strain or, more generally, "internal variables").

ii. Non-associative plasticity

For rock-like materials, the following significant phenomenological aspects were not captured in the framework of associative-plasticity theories:

1. The plastic strain rate vector has a direction, still independent from stress rates, but different from the outward normal to the yield surface in the stress point and related to the plastic dilatancy (non-normality);
2. The elastic moduli change as inelastic deformations develop (elastic-plastic coupling); and
3. In an incremental yielding process, the yield surface may either locally expand (hardening behavior), shrink (softening behavior), or remain unaltered (perfectly plastic or critical states).

Generalization was effected by the introduction of the loading function. Strains are assumed to be perpendicular to the loading function by

normality condition, thus giving non-associative flow rule. If the yield surface replaced the loading function associated flow rule is recovered. Hagemann et al. (1970, 1971) developed the stiffness relations for an elastic, perfectly plastic material using a nonassociative flow rule based on the assumption that all the plastic dilatational strains predicted by the Mohr-Coulomb criterion with the associated flow rule are removed. Such a derivation resulted in unsymmetrical stiffness relation which implied that the material was unstable in Drucker's (1950) sense. Lade and Duncan (1975) proposed a theory which incorporates special failure and yield criteria, a non-associative flow rule, and an empirical work-hardening law for cohesionless soils. The latter represented an improvement in the non-associative plasticity. Investigating the material stability, Maier and Hueckel (1979) outlined the possible ranges of hardening modulus. Mechanical stability was considered as the tendency to preserve the equilibrium configuration despite disturbances. It was shown that the stability of time-independent materials in given state under dead loading can be connected with the non-negativeness of the second order work density performed by an external agency over any infinitesimal path leading from considered actual situation to any neighbouring (virtual) configuration. Hill's stability condition for stability (1948) was utilized which turns out to be implied by the Drucker's stability criterion (1964) in the small [non-negativeness of the second work density performed along any proportional path]. It can be concluded from the stability consideration that the limits of the hardening modulus are rather restrictive.

iii. Limit Analysis

In the current century, the (upper, lower and uniqueness) theorems of limit analysis were formulated by Gvozdev (1938) but his work was not widely known till much later. The commonly used version was developed after the Second World War by Prager (1955), Drucker (1950), Hodge and Prager (1948), Hill (1950), Koiter (1953). Modern accounts of the theory of plasticity in many languages may be found (Braestrup and Nielsen, 1983) in the monographs by Martin (English, 1975), Kachanov (Russian, 1969), Massonet and Save (French, 1963), and Reckling (German, 1967). Whereas Gvozdev (1938) formulated the theory with explicit reference to structural concrete, the western schools (e.g. Hill, 1950, 1964, 1967) was mostly concerned with metallic bodies. Concrete was regarded as a brittle material, generally unfit for plastic analysis, an exception being formed by cases where the strength is mainly governed by flexural reinforcement. A prominent example is the yield line theory for slabs, developed by Johansen (1962) before the limit analysis theorems were formulated, i.e. The connection with the theory of plasticity was not firmly established till the 1960s, mainly through the work of Neilsen (1964). The implications of applying limit analysis to reinforced concrete structures were discussed by Drucker (1952, 1961), Chen and Drucker (1969) considered a problem of plain concrete, using modified Coulomb criterion with a nonzero cut-off. The same constitutive model has since been applied by Nielsen et al. (1978) and Braestrup et al. (1978) to treat a number of cases, mainly shear in plain and reinforced concrete. Similar research has been carried out by Muller (1978) and Mart (1980). In May 1979, a colloquium on

plasticity in reinforced concrete was organized in Copenhagen, sponsored by the International Association for Bridge and Structural Engineering. Most of the results obtained so far were collected in the conference reports (1978, 1979). A necessary condition for the validity of the limit analysis theorems is that the internal forces can be redistributed within the structure during loading to collapse. Thus a certain ductility of the material is essential. It is an open question whether concrete can be said to satisfy this requirement (Nielsen, 1984).

iv. Capped yield models

Conventional plasticity models developed for geotechnical materials such as concrete, frictional soils and rocks (e.g. Mohr-Coulomb, 1914; and Drucker-Prager, 1951, 1952a) were limited in accounting for certain characteristics. Of the latter are: (a) volume changes, (b) stress path dependence, and (c) nonassociative characteristics (Desai and Farouque, 1984). To overcome these deficiencies, Drucker et al. (1957) introduced a second yield function which hardens and, in the case of a soil, softens; this is the cap, so called because it closes the cone shaped yield surface of Drucker-Prager's in the principal stress space (Resende and Martin, 1985). Therefore, from a general point of view, a cap model falls within the the framework of the classical incremental theory of plasticity (Sandler et al., 1976). The development at Cambridge University (Schofield and Wroth, 1968), known as the critical state soil mechanics concept, provided a rational basis for modelling

volume change behavior and continuous yielding of materials (Desai and Sirdardane, 1983). Detailed exposition are found in DiMaggio and Sandler (1971), Rosco et al. (1958, 1963), Isenberg and Bagge (1972), Schofield and Wroth (1968), in the Rosco Memorial volume (Parry, 1971), Farouque (1983a,b , 1987) and in many other publications. The shape of the cap was chosen in various ways; models developed by Sandler and coworkers (1976, 1979) use an elliptically shaped cap, whereas Bathe et al. (1979) allow only for a plane cap. Isotropic hardening cap models were proved not to be suitable for cyclic stress-strain responses (Farouque, 1987). Some cap models were developed to account for the directional properties as suggested by Humphrey and Gondhalekar (1990) for materials with transversely isotropic elastic parameters.

Several question have, however, recurred in the development of the theory of capped yield criteria (Christian and Desai, 1979); some of the most significant are as follows:

1. What is the shape of the cap ?
2. Does the theory apply to tests other than the triaxial ?
3. How should one account for anisotropy of yielding ?

In addition, some other points can be questioned with no satisfactory answers, of which are:

4. Is the cap surface associative ?
5. Is the general yield surface fully coupled with the cap (Resende and Martin, 1984) ?
6. Does the accuracy obtained deserve the determination of

28-parameters and using 7-functions subjected to 6-constraints as required by the generalized cap model suggested by Sandler et al. (1976) ?

a. *Unconventional Plasticity*

Viscoplasticity with strain-rate dependent viscosity (Schapery, 1968, 1969) has been crystallized as the endochronic theory (Valanis, 1971). It consists of characterizing the inelastic strain accumulation by a certain parameter called intrinsic time whose increment is a function of strain increment (Bazant, 1974, 1976, 1978a, b, c, 1980a). In other words, it uses the principal that the history of deformation is defined in terms of a 'time scale' which is not the real time, but is in itself a property of the material. No use of the classical yield surface concept is required in the theory. Moreover, the intrinsic time replaces the real time in the viscoplastic constitutive equations. A great deal of interest was given to refine the theory (c.f. Valanis and coworkers, 1975a, b, 1976, 1977, 1979, 1980, 1982a, b, c, 1983, 1984) and to implement it in a numerical framework (c.f. Watanabe and Alturi, 1985; Bangash, 1987). However, Sandler (1978) pointed out that the use of a simple endochronic model implies the material to be unstable and, hence, nonuniqueness of problem solutions can result. Hsien (1978, 1980) found out that the simplest form of the theory does show some 'material instability' in the sense it does not satisfy Drucker's postulate when subjected to certain conditions. Furthermore, it was shown that the endochronic solution is at least as unique as that of the elastoplastic theory and no numerical difficulties were reported.

Incremental plasticity and fracturing (microcracking) material theory are combined to obtain a nonlinear triaxial constitutive relation that is incrementally linear. The plastic-fracturing theory combines the plastic stress decrements with fracturing stress decrements, which reflect microcracking and accounts for internal friction, pressure sensitivity, inelastic dilatancy due to microcracking and strain softening degradation of elastic moduli due to microcracking and the hydrostatic nonlinearity due to pore collapse. Failure envelopes are obtained from the constitutive law as a collection of the peak points of the stress-strain response curves. Six scalar material functions are needed to fully define the monotonic response.

Dafalias (1975) and Krieg (1975) developed, independently, the concept of Bounding surface. This concept was used to develop the bounding/yield surface model, radial mapping model, the vanishing elastic range model (Dafalias, 1981) and subloading surface model (Hashiguchi, 1989). The main feature of the model is that the material exhibits both a memory of past loading history and a projected foresight of how far the current state is from a bounding state. Cyclic behavior is efficiently captured.

The theory of plasticity was developed to deal with the phenomena characterized by slip which is dominant for metals. Since microcracking is the main prominent mode of irreversible changes in concrete rather than slip especially if unconfined, it is, therefore, unrealistic to expect that plasticity alone, irrespective of its incarnation, could account for the behavior caused by the interaction of both modes of microstructural

change. A recent surge in the interest in the continuum damage mechanics raises a hope that it will be possible to analyze the behavior of solids dominated by the nucleation and growth of microcracks (Krajcinovic, 1984a).

In more details, the plastic response of concrete, or the development of plastic or irrecoverable strains exhibits a number of features which are foreign to the classical theory of plasticity (Ortiz, 1984). For instance, lack of concrete with the normality rule has been shown experimentally. On the other hand, the characteristic descending branch of the uniaxial stress-strain diagram of concrete has been commonly viewed as a violation of Drucker's second postulate. Considerable effort has been devoted in the past to extending the classical theory of plasticity to a framework suitable for the study of such materials as concrete, rocks and granular media. Weak stability criteria have been proposed that relieve the requirements of Drucker's postulate and allow for unstable behavior (Bazant, 1980a). However, this work is mostly speculative and does not address the issue of why concrete appears to violate the classical stability postulates (Ortiz, 1984). A further complication arises from the unloading hysteretic loops that develop when concrete is subjected to cyclic loading (Karsan and Jirsa, 1969; Grestle and Tulin, 1964; Spooner and Dougill, 1975). These unloading loops have heretofore defied explanation. Furthermore, their numerical modelling in the context of plasticity has frequently involved questionable artifices such as internal variables which experience sudden jumps in time (Bazant and Kim, 1979).

3.4.3 Friction Models

A commonly accepted theory which accounts for the frictional behavior of sliding surfaces of material (Hobbs, 1983) is the cohesion theory of friction. In the theory, contact between two nominally flat surfaces is assumed to occur at the tips of widely spaced irregularities or asperities, even when the two surfaces are apparently smooth. It is further assumed that at the areas of contact there is such intimate contact between the two surface materials that molecular adhesion occurs.

A number of models of increasing complexity, all of which have been considered by Archard (1958). In all but the simplest model, the number of contact areas is a function of the normal load.

The progressive damage in concrete leads to oriented anisotropies near the ultimate failure zone. In order to account for this, the so-called crack friction theory was proposed (Bazant and Tsubaki, 1980e). This theory is based on internal friction, but it differs from the classical Mohr-Coulomb friction theory in that the friction is considered on one particular plane, the crack plane, rather than as isotropic frictional behavior as in the Mohr-Coulomb criterion. It is further assumed that the crack plane can have any orientation, which contrasts with the Mohr-Coulomb friction theory for which the frictional slip planes can have only one orientation as determined by the limiting stress. A more detailed survey is given by Jaeger and Cook (1969).

3.5 ENERGETIC MODELS

These models considers that crack initiation and propagation is governed by the amount of energy release rate. These concepts are covered by the concepts of fracture mechanics including linear elastic fracture mechanics and nonlinear facture mechanics (Elices and Planas, 1989). The second got more attention because of the limitations on applicability of the first to concrete and four sub-groups were proposed to simulate the nonlinearity imposed in the fracture process zone: 1. crack models including cohesive crack models without and with bulk dissipation (Hillerborg's fictitious crack model, 1979; RILEM method, 1985; and Rice's J-integral method, 1968); 2. band models (c.f. Bazant, 1982a, 1983b) including the smeared crack band model, band models with bulk dissipation, and general band models using nonlocal approach (scalar or directed models); 3. two-parameter model proposed by Jenq and Shah (1985); and 4. the highly stressed volume model (Torrent and Brooks, 1985).

3.6 STOCHASTIC MODELS

These are the models inspired by statistical distributions. The eldest well known models were the two and three parameter Weibull's (1939). In this model, which is widely known as the 'the weakest link model', a local strength distribution function was introduced from which the probability of fracture was introduced. Freudenthal (1968) linked this model to Griffith crack instability criterion to deduce the scatter of fracture phenomena of brittle materials. Jayatilaka and Trustum (1979)

developed a general expression for the failure probability of a brittle material based on the flaw size distribution and the stress necessary to propagate from an inclined crack. Mihashi and Izumi (1977) considered four levels of sources for fracture (paste, paste-aggregate bond, initial defects, aggregates) and was incorporated in a stochastic process. Burt and Dougill (1977) modelled concrete heterogeneity by means of a bar structure in which the bars have a random scattering in space. Mazars (1984) used a Weibull distribution to find the threshold strain of damage. Rossi and Richer (1985) introduced the stochastic process into local scale of the material, considering that cracks are created within the concrete with different energy dissipation depending on the spatial distribution of the constituents and initial defects. Sentler (1985) proposed a stochastic model in which the volume of the structure, the loading intensity and loading time (also accounted for fatigue) intervene in the brittle fracture of this structure. Fafitis and Shah (1984) represented the behavior of concrete by an infinite number of rheological elastic-plastic type of parallel elements, the properties of which are statistically assumed. More recently, Fafitis and Won (1992) developed a statistical model for concrete which was based on a space truss analogy to construct the constitutive equations in hypoelastic form. Bazant and coworkers (1991a, b) presented a modified form of the Weibull model to consider nonlocality of damage in multiaxial space. In addition, a tremendous amount of reliability models were proposed to predict the life time of structural elements.

3.7 NUMERICAL SIMULATION MODELS

Numerical simulation models include Semean's (1985) and Roelfastra and Sadouki's models (1986). Generally speaking, this technique is based on a numerical simulation with a computer. For example, the shapes and location of aggregates can be simulated by a random process based on statistical modelling of concrete cross section. The physical, chemical and mechanical behavior of these computer generated structures can be analysed with the help of suitable programs (Elices and Planas, 1989).

3.8 DAMAGE MODELS

Damage models, presented in Fig. 3.4, include scalar damage (cf. Mazars' (1981), Resende's (1987), and Loland's (1981) models), directed damage (based on first (Krajcinovic and Fonseka, 1981), second (Chow and Wang, 1987), fourth (Chaboche, 1977), or eighth (Chaboche, 1979) order damage tensors), unilateral (Ladevez, 1983; Mazars, 1985) damage, mixture (Ortiz, 1985), micro-plane (Bazant and coworkers, 1983c, i, k), highly stressed volume-continuous damage (Brooks and Al-Samarie, 1990), damage with permanent strain and induced anisotropy (Collombet, 1985), damage of high compressive loading (Pijaudier-Cabot, 1985), softening with snapback (Nielsen et al., 1990), combined fracture-damage (Janson and Hult, 1977; Janson, 1977, 1978a, b; Lorrain, 1979; Loland and Gjorv, 1980a; Loland, 1980b, 1981a, b), and coupled damage-elasto-plastic models (Simo and Ju, 1986, 1987a,b; Simo, 1989; Ju, 1989a; Frantziskonis and Desai, 1987; Voyiadjis and Kattan, 1990, 1991; Niu, 1989).

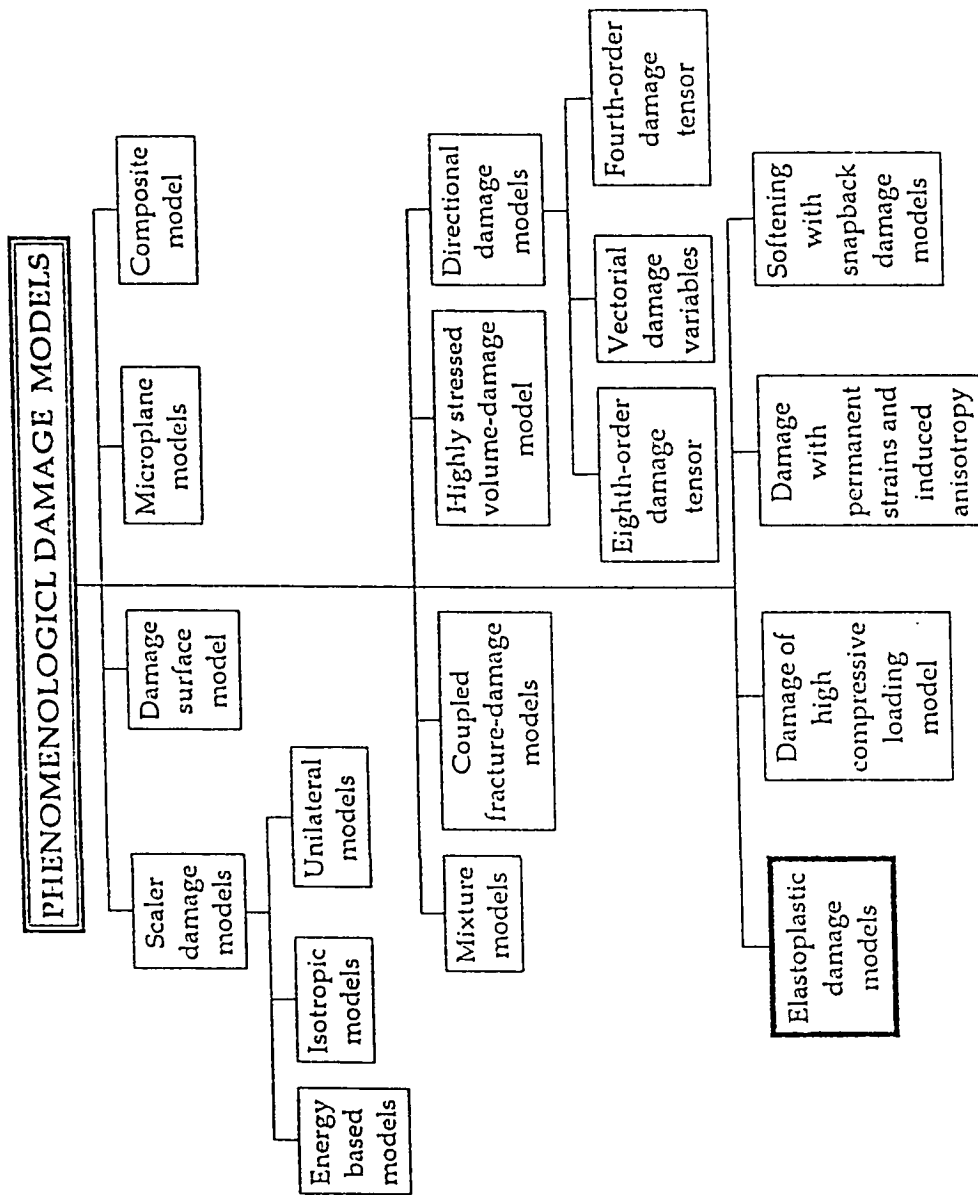


Fig. 3.4 Some of the existing phenomenological damage models

In the past two decades, the damage mechanics approach has emerged as a viable framework for the description of distributed material damage including material stiffness degradation, microcrack initiation, growth and coalescence, as well as damage-induced anisotropy, etc. Damage mechanics has been applied, as shown in Fig. 3.5, to model creep damage (Hult, 1974; Kachanov, 1958, 1980a, 1984, 1987; Krajcinovic, 1983a; Leckie and Hayhurst, 1974; Leckie, 1978; Lemaitre, 1984; Murakami, 1978, 1981a; Murakami and Ohno, 1981b, Rabotnov, 1963, 1968), fatigue damage (Chaboche, 1974; Lemaitre, 1971, 1984; Marigo, 1985), creep-fatigue (Lemaitre, 1979a, 1984, Lemaitre and Chaboche, 1974; Lemaitre and Plumtree, 1979c), elasticity coupled with damage (Cordebois and Sidoroff, 1979; Ju et al, 1989a; Kachanov, 1980b, 1985, 1987; Krajcinovic and Fonseka, 1981; Lemaitre et al., 1979b, 1981, 1982a, b; Ortiz, 1985; Wu, 1985), and ductile plastic damage (Cordebois and Sidoroff, 1982; Dragon, 1985a; Dragon and Chihab, 1985b; Lemaitre and Dufailly, 1977; Lemaitre, 1984a, b, c, 1985a, b, 1986; Simo and Ju, 1986 1987a, 1987b). In addition damage mechanics has been introduced to describe the inelastic behavior of brittle materials such as concrete and rock (Francois, 1984; Hankamban and Krajcinovic, 1987; Kachanov, 1972, 1982; Krajcinovic, 1983b; Krajcinovic and Fonseka, 1981; Loland, 1980b, 1981a, 1981b; Lorrain and Loland, 1983; Mazars, 1983, 1984a, 1986a, c; Mazars and Lemaitre, 1984b; Mazars and Legendre, 1984c; Mazars and Pijaudier-Cabot, 1986b; Mazars and Borderie, 1987; Resende and Martin, 1984; Resende, 1987; Simo and Ju, 1987, 1987b).

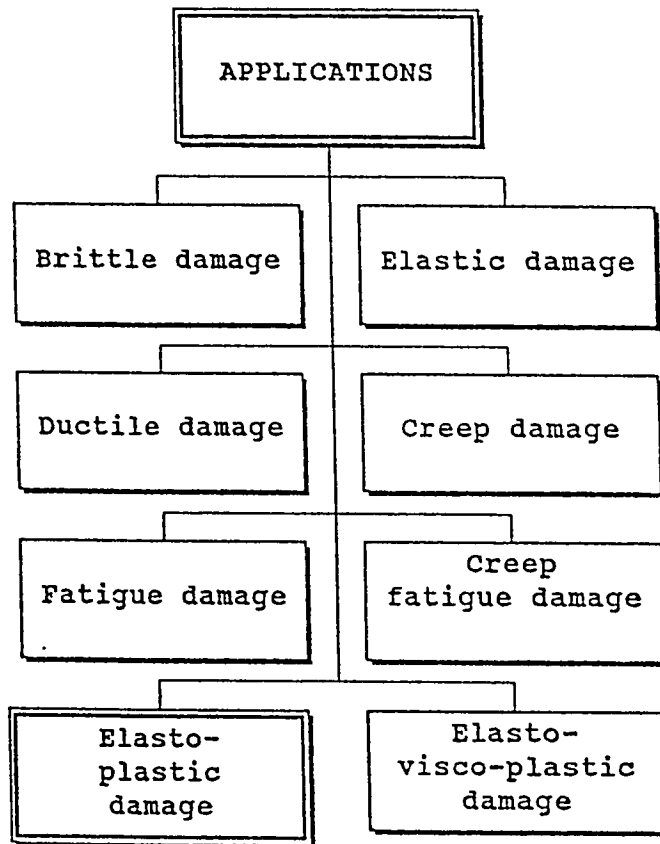


Figure 3.5 Various applications incorporating damage mechanics

Recently, micromechanical damage theories are proposed in the literature to model non-interacting microcrack growth in an originally isotropic linear elastic brittle solid; see, e.g. Wu (1985), Krajcinovic and Fanella (1986), Krajcinovic (1987), Summarac (1987) (which extends the work of Horii and Nemat-Nasser (1983) to a process model). In the case of nonlinear elastoplasticity coupled with many distributed interface microcracks, nevertheless, such micromechanical derivation of microcrack Kinetic laws showed tremendous difficulties and challenges, and is an objective for future research. Further, as was remarked, as was remarked by Krajcinovic (1985), a purely micromechanical theory may never replace a properly formulated phenomenological theory as a design tool.

Continuum damage mechanics is based on the thermodynamics of irreversible changes of irreversible processes, the internal state variable theory and relevant physical considerations (e.g., micromechanical damage variable, kinetic law of damage growth, nonlocal damage characterization and plasticity-damage coupling mechanism, etc.). A scalar damage variable may be suitable for characterization of (homogenized) isotropic damage processes. Nevertheless, a tensor-valued damage variable (fourth order) is necessary in order to account for anisotropic damage effects.

Many researchers in damage mechanics focused on the linear "elastic-damage" mechanics for brittle materials; i.e. Linear elastic solids with distributed microcracks. For nonlinear elastic solids and elastoplastic solids, nonetheless, their methods are not applicable in

general. By contrast, some elastoplastic damage theories have been proposed (e.g., Lemaitre, 1984, 1985a, 1986b; Dragon, 1985; Simo and Ju, 1987a, 1987b). However, it appears that the thermodynamic free energy function and the "damage energy release rate" proposed by Lemaitre (1985a) may not be physically appropriate. In fact, the theory advocated by Lemaitre implies that the thermodynamic force conjugate to elastoplastic microcrack evolution is simply the elastic strain energy, i.e. plastic strains do not contribute to the microcrack growth process. On the other hand, the theory proposed by Dragon (1985) does not offer thermodynamic damage energy damage criteria, nor provide tangent moduli or numerical simulations or experimental validations. Hence, coupled elastoplastic damage mechanics warrants further study.

It is important to clarify the term "damage" employed in the literature . As was pointed out by Krajcinovic (1985) there are at least three different levels of scale of "damage" in the material mechanical responses:

- (a) atomic voids and crystal lattice defects, which require the use of non-continuum mechanics model at the atomic scale;
- (b) microcracks and microvoids, which require micromechanical damage models (to model microstructural changes and individual microcracks growth) or phenomenological continuum damage models (to model distributed microcracks); and
- (c) macrocracks, which warrant fracture mechanics models to model the growth of discrete macrocracks.

Different combinations of continuum damage and plasticity theories have been proposed aiming progressively at reducing the number of assumptions and thus giving great promise (Bazant and Kim 1979a; Lemaitre 1984, 1985a, 1986b; Frantziskonis, 1986; Frantziskonis and Desai 1987a,b; Dragon and Mroz 1979; Ju 1989; Ortiz 1985; Simo and Ju 1987a,b; Stevens and Krauthammer, 1989; Yazdani and Schreyer, 1990; Simo, 1989; Schreyer, 1987; Cordebois and Sidoroff, 1982; Dragon 1985; Dragon and Chihab, 1985; Lemaitre and Dufailly, 1977; Chow and Wang, 1987a,b). Tracing previous work on energy-based coupled elasto-plastic damage theories, Ju (1989a) showed, effectively, the appeal of the "strain split" elasto-plastic damage formulation and, severely, criticized the work of pioneering colleagues in this field. He developed sound thermodynamic constitutive model, but unfortunately was based on an incorrect uncoupling assumption as will be shown later.

3.9 CONTINUOUS DAMAGE MECHANICS

Originally introduced by Kachanov (1958), the damage theory has been used to describe the progressive deterioration of materials. Janson and Hult (1977) suggested the term "Continuous Damage Mechanics" to designate methods of rupture analysis involving damage concept. The main characteristic of this method is that a mathematical parameter replaces other physical functions. Rabotnov (1968), Lemaitre (1971), Broberg (1974a, b, 1975), Hult (1974), Chaboche (1974), Janson and Hult (1977), Lemaitre and Chaboche (1974, 1978) made the first trials to extend Kachanov's idea and applied the damage concept to some

practical problems. In the previous decade many mathematical models were proposed seeking for the best idealization of the material behavior.

Damage corresponds to irreversible degradation of the cohesion of the material under internal and/or external straining (Lorrain and Loland 1983). This leads to failure of an elementary volume. In damage mechanics, the strength of a loaded structure is determined by the deterioration (damage) of the material caused by loading in terms of a continuous defect field. On the other hand, in fracture mechanics the strength of a loaded structure is determined by the severity of a single defect such as a sharp crack and the medium around the crack is assumed to be intact. Janson and Hult (1977), Loland and Gjørv (1980a), Loland (1981a,b), and Mazars and Lemaitre (1985) proposed combining these two approaches for a more realistic assessment of the behavior of a loaded structure.

At this stage a conceptual review of the basic Kachanov's damage model will be helpful to understand the notions of the framework of this theory. Consider a damaged body in which a volume element at the macroscale level has been isolated. Let A be the overall sectional area of that element defined by its normal \bar{n} . In this section the microcracks and cavities have intersections of different shapes of total area A_D . Let A^* be the effective resisting (net) area taking into account this area A_D , the microstress concentrations in the vicinity of discontinuities and the interactions between closed defects such that

$$\Lambda^* \leq \Lambda - \Lambda_D \quad (3.1)$$

The concept of effective stress associated to the hypothesis of strain equivalence avoids the calculation of Λ^* , by definition, the damage variable D associated with the normal \bar{n} is given by (Lemaitre 1985):

$$D_n = \frac{\Lambda - \Lambda^*}{\Lambda} \quad (3.2)$$

From a physical point of view the variable D_n is the corrected area of cracks and cavities per unit surface cut by a plane perpendicular to \bar{n} . From a mathematical point of view, as Λ approaches zero then D_n is the corrected surface density of discontinuities in the body relative to the normal \bar{n} . For isotropic damage, the cracks and voids being equally distributed in all directions, D_n does not depend upon \bar{n} and the intrinsic damage variable is the scalar D . Under uniaxial states of stress, the damage theory can be characterized by the same scalar parameter, D , which denotes the concentration of microcracks (microvoids, microdefects) existing in the elementary volume of the material (Lorrain and Loland, 1983) where,

$D = 0$ corresponds to undamaged state

$D = 1$ corresponds to failure of an elementary volume of the material.

However, rupture or failure takes place earlier at a critical damage and

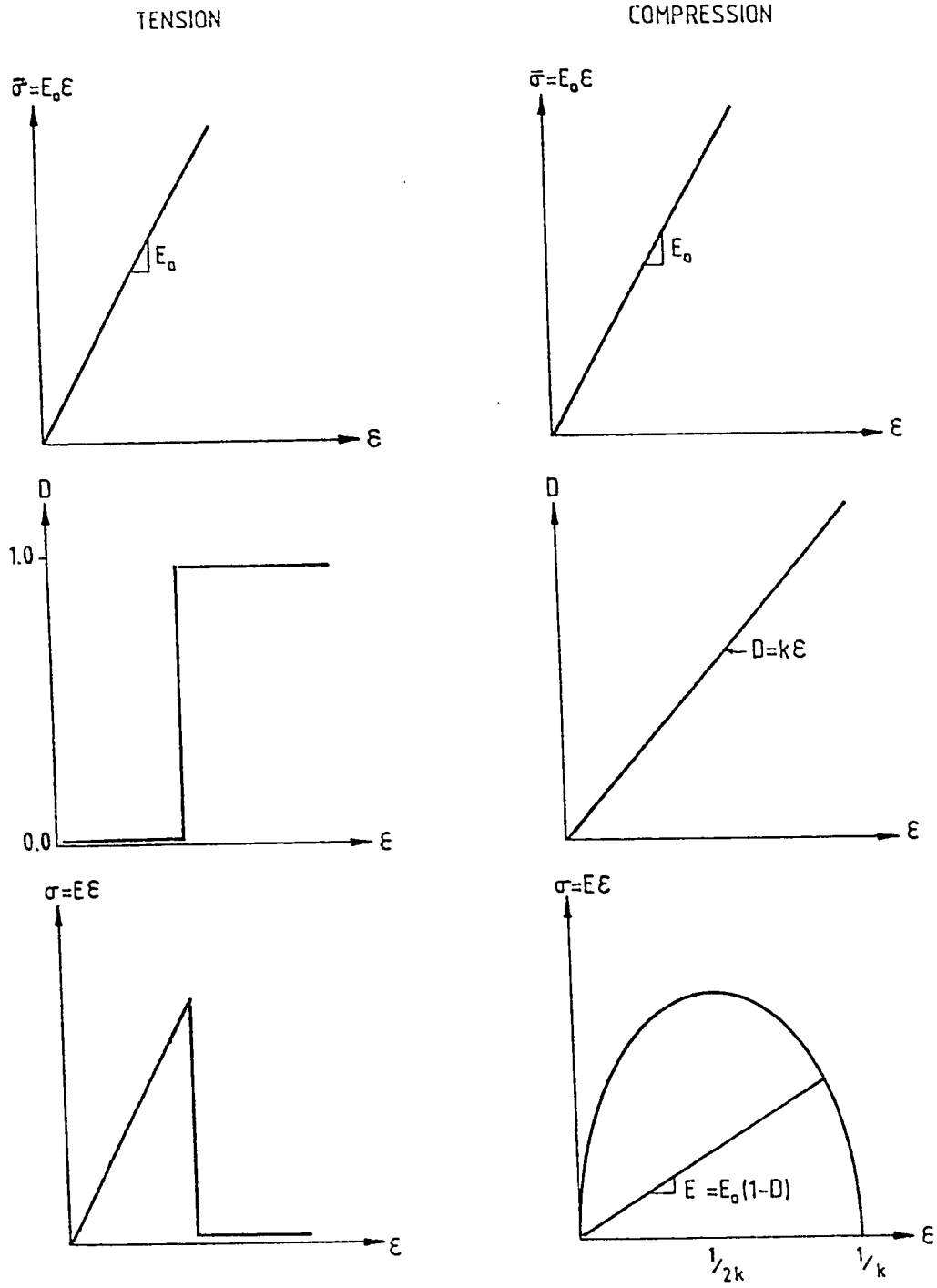


Figure 3.6 Simplified damage models in tension and compression

also starts after certain threshold limit of the state variables. In such a case, the effective stress tensor $\bar{\sigma}$ replaces the stress tensor σ in the constitutive relations. The two stress terms are related by

$$\bar{\sigma} = \frac{\sigma}{1 - D} \quad (3.3)$$

Associating this concept of effective stress with linear elasticity using simplified description of the damage variable yields nonlinear presentation of the tensile and compressive behavior of brittle materials as shown in Fig. 3.6. The introduction of similar terms allowed the definition of various equivalence concepts which are summarized in Table 3.2.

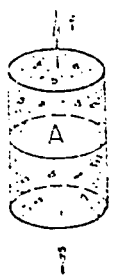
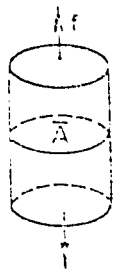
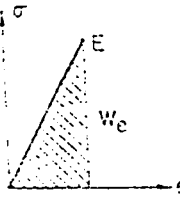
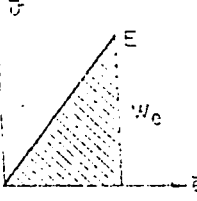
3.10 DEFINITION OF THE DAMAGE VARIABLE

Damage is defined in the literature in many ways. One of the broad definition was the one cited by Talreja (1985) as:

"A collection of permanent microstructural changes concerning material thermomechanical properties (e.g. stiffness, strength, anisotropy, etc.) brought about in a material by a set of irreversible physical microcracking process resulting from the application of thermomechanical loadings".

The description of damage often requires employing a damage variable. Some of the definitions were summarized by Ju (1989a) as follows:

Table 3.2 Various CDM concepts of equivalence.

	Damaged material	Fictitious undamaged material	Relation
Concept			$E = E_0(1-D)$
Strain equivalence	σ, ϵ, E	$\bar{\sigma}, \bar{\epsilon}, E_0$	$\bar{\lambda} = A(1-D)$ $\bar{\sigma} = \sigma(1-D)^{-1}$
Stress equivalence	σ, ϵ, E $\sigma = \epsilon E$	$\sigma, \bar{\epsilon}, E_0$ $\sigma = \bar{\epsilon} E_0$	$\bar{A} = A$ $\bar{\epsilon} = \epsilon(1-D)$
Energy equivalence	σ, ϵ, E  $W_e = \frac{1}{2} \sigma \epsilon$ $\sigma = E \epsilon$	$\bar{\sigma}, \bar{\epsilon}, E_0$  $W_e = \frac{1}{2} \bar{\sigma} \bar{\epsilon}$ $\bar{\sigma} = E_0 \bar{\epsilon}$	$\bar{A} = A(1-D)$ $\bar{\epsilon} = \epsilon(1-D)^{-2}$ $\bar{\sigma} = \sigma(1-D)^{-1/2}$

1) Define the second order damage tensor, D , as a spatial average

$$D = \frac{1}{2V} \sum_k \int_{S^k} (\boldsymbol{\pi} \times \bar{\boldsymbol{\pi}} + \bar{\boldsymbol{\pi}} \times \boldsymbol{\pi})^k dS^k \quad (3.4)$$

where

V statistically representative volume;

\boldsymbol{u} the displacement discontinuity vector;

$\bar{\boldsymbol{\pi}}$ the unit normal vector across the surface of the k^{th} crack;
and

S^k the k^{th} microcrack surface

This definition was proved to be thermodynamically incorrect since it leads to energy dissipation during unloading (Krajcinovic, 1985).

2) Define the damage measure, d , of single microcrack

$$d = \frac{a^3}{V} \quad (3.5)$$

where

a radius of an assumed single spherical microcrack; and

V the volume of the representative unit cell in the mesostructure.

This definition is related to microcrack porosity and leads to a

fourth order damage tensor representation (Ju, 1989).

3) Define the damage variable, d_n , in the normal direction as

$$d_n = \frac{A_d}{A_T} \quad (3.6)$$

where

A_d damaged surface area

A_T total cross-sectional area of a unit cell along a normal
direction \bar{n} .

This definition is the most widely used since it may be utilized in micromechanical as well as phenomenological models. Many other versions of damage models emerged from this definition such as those relating damage to the degradation of material parameters. Lemaitre (1992) summarized the measurements of damage based on this definition as follows:

i. Experimentally

The results are usually averages of nonuniform quantities over a mesovolume since mechanical experiments at the microscale are difficult to perform.

1. Direct measurements by observing micrographic picture.

2. Variation of the elasticity modulus using either the ultrapulse velocity and/or strain gages to monitor the unloading slope.
3. Variation of the microhardness using a process of very small indentation.
4. Variation of the electrical resistance.
5. Other methods such as variation of density and variation of the cyclic plasticity response (stress amplitude drop). However, these methods are recommended not to be tried for concrete.

ii. Analytically

Using micromechanics concepts (c.f. Budiansky and O'Connell, 1976).

3.11 A STATE OF THE ART ON CONCRETE DAMAGE MODELS

Bazant and Gambarova (1984b) and Bazant and Oh (1985b) developed the 'microplane model' which was extended latter to the 'microphone model'. The model uses a continuous distribution of internal variables which are kinematically linked. The essence of the model is the consideration that, at a microlevel, cracking occurs at random orientations rather than in parallel array. For normal concrete, the cracks occur through mortar surrounding the aggregates. The model relies only on a scalar microplane stress-strain relation and on two scalar constants. Elices and Planas (1989) comment on the model that it is, rather than a single model, a whole family of models

displaying anisotropic general damage in a quite natural way.

Bazant (1984d) and Bazant and Belytschko (1987c) have proposed nonlocal constitutive equations with a long-range interaction among material particles. This was made to avoid the ellipticity of the equilibrium equations of rate-independent form of softening laws. Valanis (1991) criticized this approach that little physical evidence of such interactions has been found in the materials considered when these materials are in the undamaged state.

Bazant (1990b) used simplified micromechanical analysis to demonstrate the nonlocality of damage. He claimed that continuum damage due to microcracking must be nonlocal since the fracturing strain due to damage is the result of the release of stored energy from the microcrack neighbourhood, the size of which is not zero but finite. Thus if the nonlocality is expressed as a function of the spatially averaged (nonlocal) strain in a certain neighborhood of the given continuum to the given point, a size effect which is intermediate between plasticity (no size effect) and linear elastic fracture mechanics (largest size effect) will be captured.

Bazant and Cabot (1988b) studied the nonlocalization instability and convergence using a nonlocal scalar damage variable and assumed strain locality such that

$$\sigma_{ij} = (1 - \bar{\omega}) C_{ijkl} \epsilon_{kl} \quad (3.7)$$

The nonlocal damage variable $\bar{\omega}$ was related to the local damage variable

ω by the following relation:

$$\bar{\omega} = \frac{1}{V_r(\mathbf{x})} \int_V \omega(\mathbf{s} - \mathbf{x}) \omega(\mathbf{s}) dV(\mathbf{s}) \quad (3.8)$$

in which

$$V_r(\mathbf{x}) = \int_V \omega(\mathbf{s} - \mathbf{x}) dV(\mathbf{s}) \quad (3.9)$$

where \mathbf{s} and \mathbf{x} are coordinate vectors of the neighborhood and of the point considered. The weighting function $\omega(\mathbf{x})$ is proposed to be

$$\omega(\mathbf{x}) = \exp[-(k|\mathbf{x}|/l_c)^2] \quad (3.10)$$

in which l_c is the characteristic length which was found experimentally to be three times the maximum aggregate size (Bazant and Cabot, 1987b), while $|\mathbf{x}|$ is the norm of the vector \mathbf{x} with k is given as $\sqrt{\pi}$, 2 and $(6\sqrt{\pi})^{1/3}$ for 1-D, 2-D and 3-D, respectively. This formulation arrived at nonsymmetrical tangential stiffness matrix and the finite element analysis appeared to exhibit power-type convergence which was almost quadratic. This model was latter criticized by Valanis (1991) that the idea of an 'imbricate' continuum seemed to have been supplanted because the theory was proposed in terms of an evolution equation of nonlocal character but local elastic constitutive response.

Bazant (1991b) extended further previous micromechanical arguments (Bazant, 1987a) on the nonlocality of damage that :

1. Fracturing strain caused by damage is the result of the release

of stored energy from a microcrack neighborhood, the size of which is not negligible.

2. Existence of the interaction among microcracks.
3. Local and nonlocal damage do not have analogous physical meanings; i.e. nonlocal spatial integral is not averaging.
4. Inhomogeneities.

It was stated that the two factors affecting the weighting function were:

1. Weighting functions for nonlocal spatial integration is a fixed material property, independent of stresses, only if the stress is hydrostatic and damage is small
2. Weighting functions for nonlocal spatial integration evolves a function of the size and configuration of the microcracks, proximity of the boundary and its shape.

Benallal et al. (1991) defined four numerical algorithms: (1) uncoupled; (2) fully coupled; (3) semi-coupled and (4) locally coupled. Implementation to elastic-perfectly-viscoplastic creep damageable materials was carried out using time dependent finite element by Wilson θ method with 8-noded element by 2X2 integration numerical integration rule. The critical damage variable $D_c = 0.9$ was postulated. The constitutive equations were mathematically expressed as follows:

- (1) the observed variables:

$$\dot{\epsilon}^e = [(1-D)A^e]^{-1} : \sigma \quad (3.11)$$

and

$$\dot{\epsilon}^p = f(\sigma, \alpha, D) \quad (3.12)$$

(2) the internal variables:

$$\dot{\alpha} = G(\sigma, \alpha, D) \quad (3.13)$$

and

$$\dot{D} = H(\sigma, \alpha, D) \quad (3.14)$$

in which α are a set of internal variables representing isotropic and kinematic hardening. These equations were applied to investigate the behavior of a sphere under external pressure and a cylindrical notched bar. The uncoupled approach, which is of the lowest cost, was recommended to be used when the redistribution of the stresses can be neglected. This situation takes place when the dissipated damage energy is small or when damage zone is either small or large and approximately uniform.

Billardon and Doghri (1989) conducted a localization bifurcation analysis for damage softening elastoplastic materials. Fully coupled elastic-damage plastic with kinematic and isotropic hardening was used. Biaxial application on perforated plates loaded in plane stress conditions was considered. It was proposed that the ultimate stage of diffuse damage process was the onset of dramatic strain and damage localization

which can be detected by a general material bifurcation analysis carried out at each step of the loading process at each integration point of the finite element mesh. The specific free energy ψ was chosen as

$$\psi = (1/\rho) (1/2) (\epsilon - \epsilon^P) : (1-D)E_0 : (\epsilon - \epsilon^P) + \psi^P(V) \quad (3.15)$$

where E_0 denoted the usual Hookean operator which is a function of Young's modulus and Poisson's ratio. The set of the internal variables V incorporated the plastic strain tensor ϵ^P , the hardening variables a and r , and the damage variable D associated with the corresponding thermodynamical forces $A = -\rho \partial \psi / \partial V$, viz. the stress tensor σ , the kinematic hardening tensor X , the isotropic hardening scalar R and the damage energy release rate Y . The yield function f was given in the form

$$f = \frac{J_2(S-X)}{1-D} - R - \sigma_y \quad (3.16)$$

and the plastic potential F was particularized such that

$$F = f + \frac{b}{2a} X : X + \frac{S_0}{s_0 + 1} \left(\frac{Y}{S_0} \right)^{s_0 + 1} \frac{1}{1-D} H((r - r_D)^+) \quad (3.17)$$

where $J_2(S-X) = \sqrt{3/2 \text{tr}(S-X)^2}$, S is the deviatoric stress, σ_y is the initial stress and a, b, S_0, s_0 and r_D are other material dependent parameters.

Brooks and Al-Samaraie (1990) modified previous work of Torrent (1983) and Torrent and Brooks (1985) to improve the performance of the highly stressed volume HSV approach. This concept was combined with continuous damage mechanics to model the tensile failure of concrete. The HSV was defined as the volume V in which the tensile stress lies between the maximum stress σ_m and $0.95\sigma_m$, so that

$$\sigma_m = B V^a \quad (3.18)$$

where a and B are concrete parameters. The damage variable ω defined in terms of the effective area reduction as a ratio to the original area was further expressed as

$$\omega = \left(\frac{\langle \epsilon - \epsilon_o \rangle}{\kappa} \right)^n \quad (3.19)$$

where n and κ are material parameters expressed as

$$n = \frac{\sigma_d}{\epsilon_d} \left(\frac{\epsilon_d - \epsilon_o}{E_o \epsilon_d - \sigma_d} \right) \quad (3.20)$$

and

$$\kappa = (\epsilon_d - \epsilon_o) \left(1 - \frac{\sigma_d}{E_o \epsilon_d} \right)^{1/n} \quad (3.21)$$

The subscripts o and d denote the threshold and direct tension strength limits. The model assumed that the threshold strain ϵ_o is

dependent on the HSV of the member so that the threshold strain $\bar{\epsilon}_0$ of a specimen having an HSV, \bar{V} , is given by

$$\bar{\epsilon}_0 = \epsilon_0 + \frac{\sigma_d}{bE_0} \left[\left(\frac{\bar{V}}{V} \right)^a - 1 \right] \quad (3.22)$$

in which b which depended on n , was the slope of the approximate straight line relation between the threshold and direct tensile strength. In the finite element scheme the damage factor was used as

$$\omega = \left(\frac{\sigma_1 - E_0 \epsilon_0}{\kappa E_0} \right)^n \quad (3.23)$$

where σ_1 was the maximum principal stress in each element.

Chen and Tzou (1990) utilized the results of Budiansky and O'Connell (1976) for penny shaped cracks to develop an isotropic continuum damage theory. They assumed that the cracks are activated by the maximum principal tensile strain $\epsilon_{p_{max}}$ and the density of activated cracks C_d to be described by a Weibull statistical distribution as

$$C_d = \kappa \epsilon_{p_{max}}^n \quad (3.24)$$

The required material constants (E , ν , κ , n) were determined from uniaxial tensile test data. The effective moduli were expressed as (Budiansky and O'Connell, 1976)

$$\frac{\bar{K}}{K} = 1 - \frac{16(1-\nu^2)}{9(1-2\nu)} C_d \quad (3.25)$$

and

$$\frac{\bar{G}}{G} = 1 - \frac{32(1-\nu)(5-\nu)}{45(2-\nu)} C_d \quad (3.26)$$

Thus the constitutive relation can be written as

$$\sigma_{ij} = 2\bar{G}e_{ij} + 3\bar{K}\epsilon_{ii}\delta_{ij} \quad (3.27)$$

in which e_{ij} is the deviatoric part of the strain tensor. The model was implemented in a finite element scheme and was applied to concrete in biaxial tension and showed good agreement.

Chow and Wang (1987a,b) developed an anisotropic elastic damage theory by deriving a damage effect tensor $M(D)$. With the help of the effective stress concept ($\bar{\sigma} = M(D) : \sigma$), the hypothesis of elastic energy equivalence (Sidoroff, 1981) was used to find the effective compliance C^{-1} and was shown to have the form

$$C^{-1} = M_T : C_0^{-1} : M \quad (3.28)$$

The theory was illustrated in uniaxial tension and torsion tests. It was further extended to include ductile damage and implemented in a finite element scheme (Chow and Wang, 1988).

Collombet (1985) developed a damage model which exhibit permanent strains and induced anisotropy. The Helmholtz total free energy was

expressed as follows

$$\rho\Psi = \frac{1}{2} [A_D : \varepsilon^e] : (\varepsilon^e + \varepsilon^p) \quad (3.29)$$

where the elastic strain tensor was given by the tensorial product

$$\varepsilon^e = A_D^{-1} : \sigma = A_0^{-1} : [L_D : \sigma] \quad (3.30)$$

where L_D is a fourth order damage tensor. The moduli A_0 and A_D are the undamaged and damaged fourth order material tensors. For orthotropic materials, the following tensorial relation was derived :

$$L_D : \sigma = \begin{vmatrix} l_1 & l_{12} & l_{13} \\ l_{12} & l_2 & l_{23} \\ l_{13} & l_{23} & l_3 \end{vmatrix} \quad (3.31)$$

Specific equations for particular tests were given for directional properties, i.e. Young's moduli and Poisson's ratios $E_i, \nu_{ij} (i, j=1, 2, 3)$. For instance, results on cubes and cylinders initially isotropic ($i=3$ represents the axis of loading)

$$E_3 = E_0 \frac{AB(\bar{\varepsilon} - K_0) + 1}{B(\bar{\varepsilon} - K_0) + 1}, \quad E_1 = E_2 = E_0 \quad (3.32)$$

and

$$\nu_{12} = \nu_{23} = \frac{B[1 - (1 - \nu_0)A](\bar{\varepsilon} - K_0) + \nu_0}{B(\bar{\varepsilon} - K_0) + 1} \quad (3.33)$$

in which A, B are additional material parameters to the conventional

Young's modulus E_0 of the undamaged material and the corresponding Poisson's ratio ν_0 . The threshold damage strain is K_0 and the effective strain is $\bar{\epsilon} = \sqrt{|\epsilon|_i^2}$, $|\cdot|$ denotes the positive eigenvalues.

Costin (1985) developed a continuum damage model for brittle materials including the effect of interaction among neighboring microcracks on the evolution of damage. The model included a limited region of homogeneous softening beyond the peak. For only those cracks that were currently open under tension participating in the damage process were accounted for, the damage variable was expressed as

$$D_i = \frac{1}{a_0} \int_V n_i (a^{(0,\varphi)} - a_0) H[K_I^{(0,\varphi)}] dV \quad (3.34)$$

where a is the crack function defined over a unit hemisphere ($dV = \sin\theta d\theta d\varphi$) and a_0 was the initial crack length. The Heaviside function H is unity for stress intensity factor K_I greater than zero while was null otherwise. The study considered time independent compressive loading and allowed for time dependent damage under subcritical conditions ($K_I < K_{Ic}$). The constitutive relation was expressed as

$$\epsilon_{ij} = S_{ijkl} \sigma_{kl} \quad (3.35)$$

where

$$\begin{aligned}
S_{ijkl} = & \frac{1+\nu}{E_0} \delta_{ij} \delta_{kl} - \frac{\nu}{E_0} \delta_{ij} \delta_{kl} \\
& + C_1 \delta_{ij} (D_i D_l \delta_{jk} + D_j D_k \delta_{il}) - C_2 \delta_{ij} (D_i D_j \delta_{kl}) \quad (3.36)
\end{aligned}$$

in which C_m ($m=1,2$) were material parameters. The evolution of damage was viewed, in this study, as a stress driven microcracking-process. In many other damage models (Grady and Kipp, 1980; Krajcinovic and Fonseka, 1981; Sauris and Shah, 1983; Ortiz, 1984), the damage was computed from an evolutionary equation (or damage potential) which usually involves the strain-rate and current state of damage.

Frantziskonis and Desai (1986, 1987a,b) decomposed the total behavior into topical (elastoplastic) and stress-relieved behaviors as suggested by Van Mier (1984). The damage was shown to be caused from deviatoric stress component; thus the topical and average stress lied on the same deviatoric plane. Therefore,

$$\sqrt{J_2} = \sqrt{J_2^t} (1 - d) \quad (3.37)$$

where $J_2 = (1/2 S_{ij} S_{ij})^{1/2}$ was the second invariant of the deviatoric stress S_{ij} and the superscript t denoted the topical behavior. The stress tensor was, thus, expressed as

$$\sigma_{ij} = (1 - d) \sigma_{ij}^t + \frac{d}{3} \sigma_{kk}^t \delta_{ij} \quad (3.38)$$

the damage variable d was expressed as an exponentially decaying

function in the form

$$d = d_c (1 - e^{-\kappa \bar{\epsilon}_p^R}) \quad (3.39)$$

in which κ and R are material constants and d_c was the critical damage and $\bar{\epsilon}_p = \int d\bar{\epsilon}_p$, $d\bar{\epsilon}_p$ was the norm of the incremental deviatoric plastic strain. Consequently, it was shown that the damage was responsible for the observed degradation of strength and unloading shear modulus, as well as induced anisotropy. The incremental stress-strain relationships were finalized as

$$\sigma_{ij}^t = C_{ijkl}^{ep} \epsilon_{kl} \quad (3.40)$$

for loading and

$$\sigma_{ij}^t = C_{ijkl}^e \epsilon_{kl} \quad (3.41)$$

for unloading. The average stress increment was

$$\sigma_{ij} = (1-d)C_{ijkl}^{ep} \epsilon_{kl} + \frac{d}{3} \delta_{ij} C_{ppkl}^{ep} \epsilon_{kl} - d S_{ij}^t \quad (3.42)$$

The elastoplastic tensors were expressed using conventional associative plasticity and the modulus tensor was derived to be

$$C_{ijkl}^{ep} = C_{ijkl}^e - \frac{C_{ijpq} \frac{\partial F}{\partial \sigma_{pq}} \frac{\partial F}{\partial \sigma_{mn}} C_{mnkl}^e}{\frac{\partial F}{\partial \sigma_{uv}} C_{uvrs}^e \frac{\partial F}{\partial \sigma_{rs}} - \frac{\partial F}{\partial \bar{\epsilon}_p} \left(\frac{\partial F}{\partial \sigma_{kl}} \frac{\partial F}{\partial \sigma_{kl}} \right)^{1/2}}$$

(3.43)

in which the yield surface $F = F(I_1^t, J_2^t, J_3^t)$, I_1^t was the first invariant of the topical stress tensor, J_3^t was the third invariant of the deviatoric stress tensor of the topical behavior and $\bar{\epsilon}_p = \int d\bar{\epsilon}_p$ and $d\bar{\epsilon}_p$ was the norm of the plastic strain tensor. The model required a total of eleven parameters (3 for damage, 6 for plasticity, 2 for elasticity). Numerical investigations of the model showed that unique solutions for rate independent as well as rate dependent cases. Moreover, the finite element analysis showed mesh insensitivity.

Herrmann and Kestin (1989) in an attempt to lay down the fundamental elements of an exact thermodynamic theory of damage in an elastic solids, considered one-dimensional problem. The total energy was assumed to consist of elastic energy, loss of energy due to formation and growth of microcracks and microvoids and additional recoverable energy due to diffusion (transfer) of material from microcracks and microvoids. The expression for the total energy was reduced to

$$\rho \psi = E_0 (1 - \gamma d) \frac{\epsilon^2}{2} + E_0 (1 - \beta d) \frac{d^2}{2} \quad (3.44)$$

in which ρ, γ and β were material parameters. The damage variable d was described, for small straining and slow loading (i.e. conjugate thermodynamic force to damage, Y , was zero), as

$$d = \frac{1}{2} \gamma \epsilon^2 \quad (3.45)$$

The stress was obtained by differentiating the total energy equation with respect to the strain and was simplified to

$$\sigma = E_0 (\epsilon - \gamma \epsilon^3 / 2 - \beta \gamma^2 \epsilon^4 / 8) \quad (3.46)$$

Having expressed the stress for unloading ($Y \neq 0$) and equated it to zero, the residual strain was given as

$$\epsilon_p = \beta \frac{\epsilon_g^2}{2} \quad (3.47)$$

where the subscript g denoted the greatest ever reached value.

Janson and Hult (1977) in one of the earliest investigations on the applicability of the damage mechanics to concrete provided a fracture mechanics viewpoint. A concrete cylinder with a damage zone of height $4b$ and a cross sectional area A was used to equate the external energy W with the internal energy U at the critical condition of fracture to calculate the critical damage parameter D_c as follows

$$W = 2 \mu A \quad (3.48)$$

in which μ is the specific surfacic energy

$$U = 4 b A \frac{f_t^2}{2 E_0 (1 - D_c)} \quad (3.49)$$

where f_t and E_0 are the tensile strength and Young's modulus of the concrete specimen as found from uniaxial experiment.

Ju (1989a) considered energy-based coupled elastoplastic damage. Additive strain split was assumed and the total energy ψ which corresponded to undamaged total energy ψ^0 was expressed as

$$\psi(\varepsilon_e, \mathbf{q}, d) = (1-d) \psi^0(\varepsilon_e, \mathbf{q}) = (1-d) [\psi_e^0(\varepsilon_e) + \psi_q^0(\mathbf{q})] \quad (3.50)$$

in which \mathbf{q} is a set of plastic variables and $\psi_m^0(m=e, \mathbf{q})$ was the energy associated with the behavior m of the undamaged material. The damage energy was energy based and the plasticity equations were expressed in terms of the effective stress tensor. The formulation was extended to handle rate dependent models and to consider microcrack opening and closing. On formulating an anisotropic elastoplastic damage model, the total energy was expressed as

$$\psi(\varepsilon_e, \mathbf{q}, C) = \psi_{ed}(\varepsilon_e, C) + \psi_{pd}(\mathbf{q}, C) \quad (3.51)$$

in which equivalently $C=M(D)$ C_0 was defined as the anisotropic damage variable instead of D . The subscripts ed and pd denoted elastic damage and plastic damage, respectively. Computational algorithm using the operator split method (Chorin et al., 1978) was shown to be efficient for numerical implementation of the models.

Ju (1990) pointed out that scalar damage variable need not mean isotropic damage. It was also shown, by micromechanical arguments, that even for isotropic damage one should employ an isotropic fourth order damage tensor to characterize the state of damage in materials, in accordance with the effective stress concept.

Krajcinovic (1979) developed a theory for distributed damage for beams in pure bending. The damage variable ω was assumed to be linear with the effective tensile stress with slope $1/D$, D was the damage modulus. The compressive behavior was assumed linear, i.e. the damage variable is zero. Consequently, the assumption that plane section before bending remained plane after bending (linear strain distribution along the depth of the beam) was equivalent to linear effective stress distribution. The derivation showed a ratio of the maximum tensile strength at rupture in bending to that in tension of 1.42.

Krajcinovic and Fonseka (1981) developed a damage model for brittle materials consisting of a multitude of flat, penny-shaped voids. The damage variable was assumed in vectorial form, i.e. $D^{(n)}, \kappa$ denoted damage fields. The Helmholtz free energy was expressed as

$$\begin{aligned} \rho\psi = & \frac{1}{2} (\lambda + 2\mu) \varepsilon_{kk} \varepsilon_{ll} - \nu (\varepsilon_{kk} \varepsilon_{ll} - \varepsilon_{kl} \varepsilon_{lk}) \\ & + C_1 D_k^{(n)} \varepsilon_{kl} D_l^{(m)} \varepsilon_{mm} + C_2 D_k^{(n)} \varepsilon_{kl} \varepsilon_{lm} D_m^{(n)} \end{aligned} \quad (3.52)$$

where ρ, C_1, C_2, λ and ν are material parameters. The associated affinities with damage and strain were obtained from normality conditions

$$R_i^{(n)} = - \rho \frac{\partial \psi}{\partial D_i^{(n)}} \quad (3.53)$$

and

$$\sigma_{ij} = \rho \frac{\partial \psi}{\partial \varepsilon_{ij}} \quad (3.54)$$

Kinematics of voids growth was considered by a second order tensor $d\Omega_{ij}$ describing the change in the void geometry whose components accounted for both slip $d\Omega_{NT}$ and cleavage $d\Omega_{NN}$. The damage law was obtained by assuming a damage surface f (as in Dragon and Mroz, 1979; Kachanov, 1980a; Paul, 1961) and the damage rate $d\Omega_{NM}$ was expressed as

$$d\Omega_{NM} = \zeta G(\varepsilon, D) \left[\frac{\partial f}{\partial \varepsilon_{NN}} d\varepsilon_{NN} + \frac{\partial f}{\partial \varepsilon_{NT}} d\varepsilon_{NT} \right] \frac{\partial f}{\partial \varepsilon_{NM}}, \quad M = N, T \quad (3.55)$$

in which ζ was a constant and G was a positive scalar-valued function which was termed the softening parameter. The model was applied to uniaxial tension and compression and plane strain loading of concrete.

Krajcinovic (1983a) slightly modified the energy equation in the form

$$\begin{aligned} \rho \psi = & \frac{1}{2} (\lambda + 2\mu) \varepsilon_{kk} \varepsilon_{ll} - \nu (\varepsilon_{kk} \varepsilon_{ll} - \varepsilon_{kl} \varepsilon_{lk}) \\ & + C_1 (\omega_p \omega_p)^{1/2} \varepsilon_{kl} \varepsilon_{mm} \omega_k \omega_l + C_2 (\omega_p \omega_p)^{1/2} \varepsilon_{kl} \varepsilon_{lm} \omega_k \omega_m \\ & + C_3 (\omega_p \omega_p)^{3/2} (\varepsilon_{kl} \omega_k \omega_l) \end{aligned} \quad (3.56)$$

in which $\omega_n = D_n^2$ and C_3 is an additional material parameter. Another modification was to generalize the theory to ductile and brittle

behaviors. Also, the damage law was derived directly from normal dissipative mechanism in conjunction with orthogonality property. However, the theory in either form was criticized by Kachanov (1985) for: (1) the undetermined coefficients (for one scalar damage variable of Kachanov (1958) two parameters and of Mazars (1981) three parameters were used), (2) linearity of potential in damage was not insured, (3) Difficulty in forming combined invariants of strain tensor and the damage vector due to the vectorial rather than tensorial representation of damage and (4) difficulty in establishing a link between the model and literature on effective elastic properties of solids with many cracks.

It is remarkable to phrase a paragraph in which Kachanov (1985) stated

"Although the framework of irreversible thermodynamics may provide a general structure of constitutive equations, one cannot obtain sufficient concretization of these equations on the basis of thermodynamics alone. Such attempts results in the introduction of undetermined constants playing, essentially, the role of adjustable coefficients, their number depends on the complexity of the damage parameters used in the model."

Ladevez (1983) assumed different deviatoric and hydrostatic damage modes in tension and in compression. Consequently, the model was based on stress split into its tensile and compressive components and the choice of four scalar damage variables, d_t, δ_t, d_c and δ_c . The energy is determined from the relation

$$\varepsilon = \frac{\partial \Psi}{\partial \sigma} = \frac{\partial \Psi}{\partial \sigma'} + \frac{\partial \Psi}{\partial \sigma} \quad (3.57)$$

Therefore, the stress-strain tensorial relation is written as

$$\begin{aligned} \varepsilon = & \frac{1}{3E_0} \left\{ \left[\frac{(1+\nu_0)}{(1-d_t)} (3\sigma' - |\text{tr}\sigma'| \mathbf{I}) + \frac{(1-2\nu_0)}{(1-\delta_t)} |\text{tr}\sigma'| \mathbf{I} \right] \right. \\ & \left. + \frac{1}{3E_0} \left\{ \left[\frac{(1+\nu_0)}{(1-d_c)} (3\sigma - |\text{tr}\sigma| \mathbf{I}) + \frac{(1-2\nu_0)}{(1-\delta_c)} |\text{tr}\sigma| \mathbf{I} \right] \right\} \right\} \quad (3.58) \end{aligned}$$

in which the brackets [] used denotes the function

$$|\mathbf{x}|^+ = \frac{\mathbf{x} + |\mathbf{x}|}{2}, \quad |\mathbf{x}|^- = \frac{\mathbf{x} - |\mathbf{x}|}{2} \quad (3.59)$$

Lemaitre (1985a) developed a continuous damage model for isotropic fracture. In this model, it was assumed that the damage process contributes only to the elastic process and hence the total free energy was expressed as

$$\Psi = \Psi_e(\varepsilon^e, T, D) + \Psi_p(T, p) \quad (3.60)$$

in which T is the absolute temperature and p is the effective plastic strain which is given as

$$p = \int p \, dt, \quad p = \sqrt{(3/2) \varepsilon^p : \varepsilon^p} \quad (3.61)$$

For isothermal process, a comparison of the basic thermodynamic equation with those of Ju's (1989a) is presented in Table 3.3.

Table 3.3 Comparison between two approaches for thermodynamics of damage formulation.

	Lemaitre, 1985	Ju, 1989
Thermodynamic Potential	$\begin{aligned} & \Psi(\epsilon, p, d, T) - \Psi(\epsilon, d, T) + \\ & \Psi_p(p, T) - (1-d)\Psi^o(\epsilon, T) \\ & + \Psi_p(p, T) \end{aligned}$	$\begin{aligned} & \Psi(\epsilon, p, d, T) - \Psi(\epsilon, d, T) + \\ & \Psi_p(p, d, T) - (1-d)\Psi^o(\epsilon, p, T) \\ & - (1-d) [\Psi^o(\epsilon, T) - \Psi^o(p, T)] \end{aligned}$
Stress Tensor	$\begin{aligned} \sigma &= \rho \frac{\partial \Psi}{\partial \epsilon} - (1-d)\rho \frac{\partial \Psi^o}{\partial \epsilon} \\ & - (1-d)A_o \epsilon - (1-d)\bar{\sigma} \end{aligned}$	$\begin{aligned} \sigma &= \rho \frac{\partial \Psi}{\partial \epsilon} - (1-d)\rho \frac{\partial \Psi^o}{\partial \epsilon} \\ & - (1-d)\bar{\sigma} \end{aligned}$
Damage Energy Strain Rate	$\begin{aligned} -\dot{Y} - \rho \frac{\partial \Psi}{\partial d} - \rho \Psi^o(\epsilon, T) \\ - \frac{1}{2} A_o \epsilon : \epsilon - \frac{W_c}{1-d} \end{aligned}$	$-\dot{Y} - \rho \frac{\partial \Psi}{\partial d} - \rho \Psi^o(\epsilon, p, T)$
Clausius-Duhem Inequality	$\begin{aligned} -\dot{Y} + \sigma : \dot{\epsilon} &\geq 0 \quad \rightarrow \\ -Y\dot{d} &\geq 0 \quad \rightarrow \quad \dot{d} \geq 0 \\ &\& \\ \sigma : \dot{\epsilon}_p - R\dot{p} &\geq 0 \end{aligned}$	$\begin{aligned} -\dot{Y} + \sigma : \dot{\epsilon} &\geq 0 \quad \rightarrow \\ -Y\dot{d} &\geq 0 \quad \rightarrow \quad \dot{d} \geq 0 \\ &\& \\ \frac{\partial \Psi^o}{\partial \epsilon} : \dot{\epsilon}_p - \frac{\partial \Psi^o}{\partial p} \cdot \dot{p} &\geq 0 \end{aligned}$

The damage evolution was derived from the transformed potential of dissipation φ^* , which was obtained by Fenchel-Legendre rule, by the normality rule as follows

$$D = - \frac{\partial \varphi^*}{\partial y} \quad (3.62)$$

the potential of dissipation was further postulated as power function

$$\varphi^* = \frac{S_0}{(s_0 + 1)} \left(\frac{-y}{S_0} \right)^{s_0 + 1} p \quad (3.63)$$

Lemaitre (1984b) outlined the coupled and uncoupled framework for constitutive equations. Elasticity coupled with damage was applied to brittle failure and to high cycle fatigue. Elastoplasticity coupled with damage was applied to ductile damage and to low cycle fatigue. Elasto-visco-plasticity coupled with damage was also reviewed.

Lemaitre (1986a) summarized the limitations of classical fracture mechanics and provided a precise summary for local approaches. Different forms of the damage variable and the corresponding constitutive equations as related to elasticity, elastoplasticity and elasto-visco-plasticity were briefed. Various failure criteria postulated in the literature were discussed. Finally applications with results were provided.

Lemaitre (1984c) gave a background to ductile damage and fatigue damage. Calculations of macrocrack initiation by coupled and uncoupled

algorithms were discussed and conclusions were conducted that the coupled algorithms are recommended for better accuracy. Fracture limits of metal forming, initial value of damage, creep-fatigue damage and bifurcation of cracks were the specific applications of the theory made in this study.

Lorrain and Loland (1983) conducted a literature review and formulated the basic equations using a scalar damage variable. Applications to concrete by Mazars' scalar model (1980) and Loland's scalar model in tension (1980b, 1981) are compared in Fig. 3.7. Also, Loland's model for behavior of concrete in compression (1981), Benounich's model (1979) for multiaxial generalization and for the specific application to uniaxial compression, Janson's and Hult's damage-fracture (1977) were summarized. In addition to the uniaxial applications, the flexural response of reinforced concrete beams using Mazars' model (1980) were shown to be in good agreement with experiments. Models of Zaitsev and Scerbakov (1977) for sustained loading on concrete were briefly outlined.

Maier et al. (1990) derived four models to simulate the damage behavior of masonry as a composite material, namely α , β , γ , and delta models. The first was suggested for general rate independent applications and the moduli matrix $|K| = |K(E_b, E_m, D)|$, E_b and E_m are the Young's moduli of the brick and mortar, was given. The bricks were assumed to be linear elastic and to follow the maximum principal stress criterion while the mortar was postulated to exhibit an elastic damage behavior. The other three models were proposed to model, in sequence

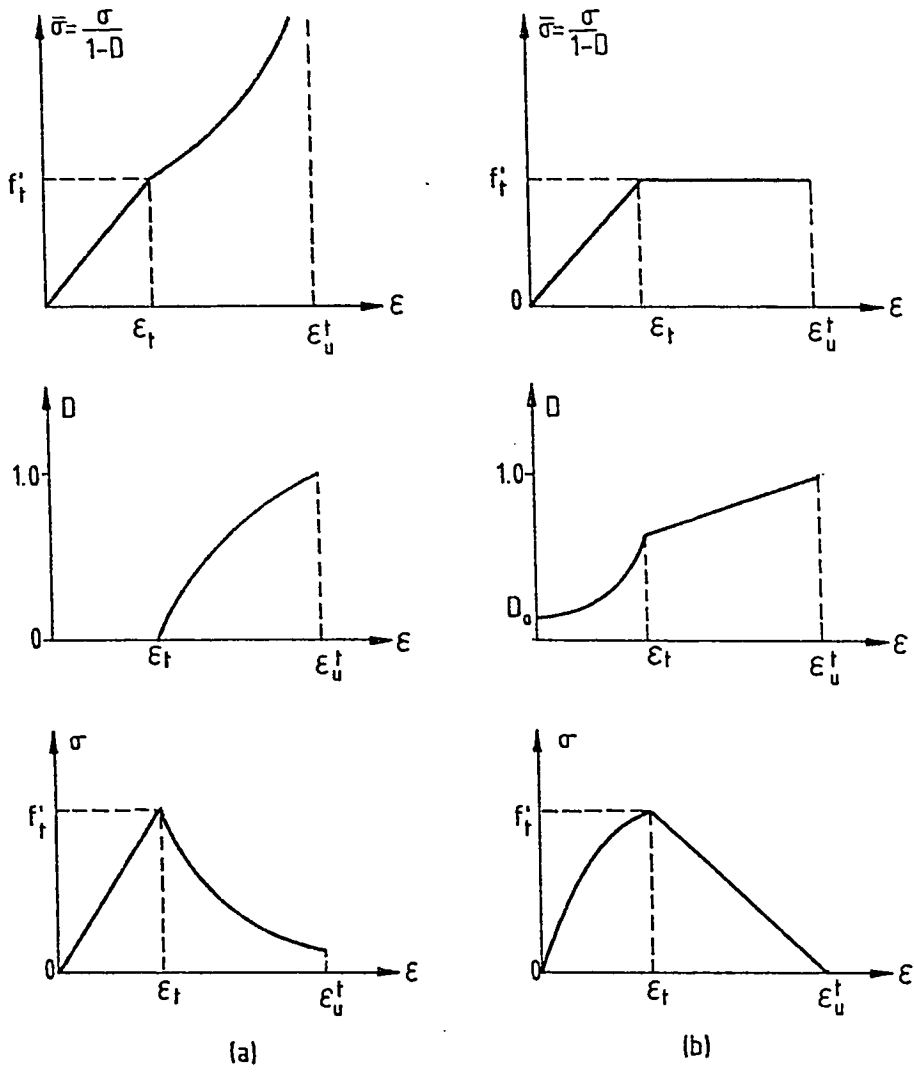


Figure 3.7 Mathematical modelling according to Mazars (1980) and Loland (1981)

the unilateral, fatigue and damage plasticity responses.

Mazars and Lemaitre (1984) discussed the aspects of the behavior of concrete in an attempt to elaborate the nature of damage process encountered with material loading. Both damage mechanics and fracture mechanics were pointed out to be applicable to material which is elastic-damageable and material which is perfectly brittle. Energy equivalence of the two approaches for notched specimen loaded under constant load yielded the following relation for the crack length extension δA

$$\delta A = \frac{\int_V - Y \delta D \, dV}{G_c} \quad (3.64)$$

in which G_c is the critical fracture energy. Probabilistic aspects of damage using Weibull distribution was discussed and applications to C-T plate were carried out.

Mazars (1986a) showed that there are two types of structural damage: (1) surfacic and (2) volumetric. Extending Ladevez's (1983) model, in either tension or compression a single damage parameter was assumed to be sufficient to describe both the volumetric and surfacic damage. But with the help of the splitting the stress tensor into its positive and negative components, i.e

$$\sigma = \sigma' + \sigma \quad (3.65)$$

therefore the total energy could be expressed as

$$\psi(\sigma) = \psi(\sigma') + \psi(\sigma) \quad (3.66)$$

the the strain tensor is expressed as

$$\epsilon = \frac{\partial \psi}{\partial \sigma} = \frac{\partial \psi}{\partial \sigma'} + \frac{\partial \psi}{\partial \sigma''} \quad (3.67)$$

in other words the constitutive relation is written as

$$\begin{aligned} \epsilon = & \frac{1}{3E_0(1-D_t)} \{ |(1+\nu_0)(3\sigma' - |\text{tr}\sigma|' I)| + (1-2\nu_0)|\text{tr}\sigma|' I \} \\ & + \frac{1}{3E_0(1-D_c)} \{ |(1+\nu_0)(3\sigma'' - |\text{tr}\sigma|'' I)| + (1-2\nu_0)|\text{tr}\sigma|'' I \} \end{aligned} \quad (3.68)$$

With reference to Ladevez's (1983) model, the damage variables of Mazars' are special case because

$$d_t = \delta_t = D_t \quad , \quad d_c = \delta_c = D_c \quad (3.69)$$

Two damage surfaces $F_t(Y_t)$ and $F_c(Y_c)$ were defined in terms of the damage energy release rates Y_t and Y_c for tensile and compressive parts, respectively. Moreover the model was linked with fracture mechanics by the relation defining the fracture energy G at failure (denoted by the subscript f) as follows

$$G_f = \int_{Y_t}^{Y_f} Y_t F_t(Y_t) dY_t \quad (3.70)$$

Mazars (1986c) reviewed the micromechanical studies devoted for concrete by Barnes (1978) , Modeer (1979) and Lino (1973). Based on

the previous stress split the damage variable D was obtained by weighting the tensile and compressive damage variables D_t and D_c by the functions α_t and α_c for the tensile and compressive components, respectively. This was mathematically expressed as

$$D = \alpha_t D_t + \alpha_c D_c \quad (3.71)$$

where the damage variables are obtained by the relation

$$D_t(\bar{\epsilon}) = 1.0 - \frac{\epsilon_{D_0} (1 - A_t)}{\bar{\epsilon}} - \frac{A_t}{\exp[B_t(\bar{\epsilon} - \epsilon_{D_0})]} \quad (3.72)$$

and

$$D_c(\bar{\epsilon}) = 1.0 - \frac{\epsilon_{D_0} (1 - A_c)}{\bar{\epsilon}} - \frac{A_c}{\exp[B_c(\bar{\epsilon} - \epsilon_{D_0})]} \quad (3.73)$$

where A_t, A_c, B_t and B_c are additional material parameters while ϵ_{D_0} was the threshold damage strain. The weighting functions were given by

$$\alpha_t = \sum_i \left\{ H_i \frac{(\epsilon_{t_i} + \epsilon_{c_i})}{\bar{\epsilon}^2} \epsilon_{t_i} \right\}^{\beta-1} \quad (3.74)$$

and

$$\alpha_c = \sum_i \left\{ H_i \frac{(\epsilon_{c_i} + \epsilon_{t_i})}{\bar{\epsilon}^2} \epsilon_{t_i} \right\}^{\beta-1} \quad (3.75)$$

where $\bar{\epsilon}$ is the effective strain defined from the positive strain eigen values as follows

$$\bar{\epsilon} = \sqrt{\sum_1 |\epsilon_i|^2} \quad (3.76)$$

in which $|\epsilon_i|$ are the principal tensile strains. The function H_i is the Heaviside function defines as

$$\begin{aligned} H_i &= 1 && \text{if} && \epsilon_i \geq 0 \\ &= 0 && \text{if} && \epsilon_i < 0 \end{aligned} \quad (3.77)$$

the loading function $f(D)$ is defined by the surface

$$f(D) = \bar{\epsilon} - K(D) \quad (3.78)$$

where $K(D)$ is a hardening parameter whose initial value is $K(0) = K_0 = \epsilon_{D_0}$

Mazars et al. (1992) studied the behavior of the steel-concrete bond. It was claimed that simulating smooth bars needs interface elements to represent the frictional mechanism. On the other hand, consideration that concrete is progressively damaging around the ribbed bar is strictly equivalent to using interface elements if the bar represents surface deformation. The same model as Mazars' (1986c) was used but the β factor used in the weighting functions was introduced for the first time. This was suggested in analogy to the shear retention factor in the smeared crack model. Values greater than unity

were recommended. Nonlocal approach using Cabot's and Bazant's (1988) model was used in association. Two possible mechanisms were captured, each including the size effect. The first was the splitting failure by radial pressure applied by lugs, while the other is shear failure. For large concrete cover, concrete crushes in a shear band form. A numerical conclusion was derived on the importance of simulating the boundary conditions.

Mazars and Cabot (1986b) reviewed the models developed by french colleagues; Mazars' model (1984a), Mazars' unilateral model (1985), Collombet's damage model with permanent strains and induced anisotropy (1985), Cabot's model for high compressive loading (1985). Analytical solution for composite columns and finite element results for reinforced concrete members were demonstrated.

Murakami (1989) developed a systematic theory to describe the anisotropic damage states of a material. Two second order damage tensors, which can be related, were introduced for loaded, D , and elastically unloaded, \bar{D} , configurations. The latter was shown to have the following characteristics:

1. $(I - \bar{D})$ is a positive tensor.
2. can be partitioned into symmetric and anti-symmetric tensors. The antisymmetric component is physically irrelevant as a transformation which represents the net area reduction due to damage.

3. \bar{D} has always three orthogonal principal directions $\bar{n}_i (i=1,2,3)$ and the corresponding principal values \bar{D}_i such that \bar{D} can be expressed in a canonical form

$$\bar{D} = \sum_{i=1}^3 \bar{D}_i \bar{n}_i \otimes \bar{n}_i \quad (3.79)$$

4. \bar{D} and D cannot describe the damage states which have more complicated symmetry than orthotropy.
5. The effective stress σ^* which is related to the stress tensor σ by the relation

$$\sigma^* = (I-D)^{-1} \sigma \quad (3.80)$$

is asymmetric. Symmetrization is achieved by the following averaging technique

$$\sigma^* = \frac{1}{2} [(I-D)^{-1} \sigma + \sigma (I-D)^{-1}] \quad (3.81)$$

An alternative symmetrization was adopted by Cordebois and Sidoroff (1982) as

$$\sigma^* = (I-D)^{-1/2} \sigma (I-D)^{-1/2} \quad (3.82)$$

6. The effective stress and traction are fictitious stresses that represent the magnified effect of stress due to damage and do not satisfy the equilibrium condition in the relevant

configuration.

7. The unilateral Effect due to crack closure is taken into account by stress split. In this case the symmetric effective stress tensor will be given by

$$\begin{aligned} \sigma^* &= \frac{1}{2} \{ (I-D)^{-1} |\sigma| + |\sigma| (I-D)^{-1} \} \\ &- \frac{1}{2} \{ (I-CD)^{-1} |\sigma| + |\sigma| (I-CD)^{-1} \} \end{aligned} \quad (3.83)$$

in which C is a scalar quantity whose value is less than unity.

Najar (1989) extended previous work (Najar, 1987) to study the transition from continuous damage to failure in uniaxial loading of elastic-brittle behavior in both tension and compression. Three characteristic values of the damage parameter were related. These were the initial damage D_0 , the damage at the maximum stress D_m and the failure damage D_f . The interrelating equations were

$$1 - D_m = D_m \ln \left(\frac{D_m}{D_0} \right)^2 \quad (3.84)$$

and

$$D_f^{1-\kappa} - D_0^{1-\kappa} = (1-D_f) \ln \frac{D_f}{D_0} \quad (3.85)$$

in which κ is a material parameter. Young's modulus at any stage of loading can be related to that of the undamaged material. Therefore,

$$E_i = E (1 - D_i) \quad , \quad i = o, m, f \quad (3.86)$$

The strain was related to the damage variable and the nominal damage energy W^* by the relation

$$\epsilon = \sqrt{\frac{W^*}{E} \ln\left(\frac{D}{D_0}\right)^2} \quad (3.87)$$

The young's modulus for unloading E_u was further given as

$$E_u = E \frac{1 - D}{\frac{D^{1-\kappa} - D_0^{1-\kappa}}{1 - \frac{D}{D_0}}} \quad (3.88)$$

and the stress was related to the strain through the relation

$$\sigma = E (1 - D) \epsilon \quad (3.89)$$

An algorithm was depicted for calculation purposed and it was shown that the model was in good agreement with the experimental results for cyclic behavior of Terrien (1980) and Spooner and Dougill (1975). It was stated that:

"Since the fundamental Kachanov's idea (1958), the main thrust of the research went towards 3-D generalization, as well as applications to various types of solids and processes, ranging from creep in metals to dynamic rupture in rock (Shockey et al., 1974). It left behind, however, certain basic notions lacking clarity even in the simplest case of uniaxial processes in elastic materials with internal

damage (Dougill, 1983). Here belongs : (a) lack of an instrumental definition of damage parameter, experimentally verifiable and independent of modelling assumptions, (b) misinterpretations of the nature of the residual strain at damage, identified sometimes with plastic strain, (Lemaitre and Chaboche, 1985b), or simply neglected, (Grady and Kipp, 1980), despite ample evidence to the contrary, (Hult, 1987); (c) little interest with respect to unloading process and energy distribution considerations, despite observations of the relatively high losses on damage accompanying phenomena, like acoustic emission and heat production, (Davison and Stevens, 1976), etc."

Neilsen et al. (1990) developed a structural constitutive algorithm which was based on continuous damage mechanics for softening and snapback. In uniaxial states, if the softening zone whose length is s of a bar of length a had a damage variable ω , then the structural damage variable $\bar{\omega}$ could be derived in the form

$$\bar{\omega} = s \frac{\omega}{a(1-\omega) + s\omega} \quad (3.90)$$

and the stress was related to the average strain through the relation

$$\sigma = (1-\bar{\omega}) E_0 \varepsilon \quad (3.91)$$

This idea was generalized to two and three dimensional situations based on the assumption that damage increases the compliance of the material only in a direction perpendicular to the softening zone as postulated by Bazant and Oh (1985b). The model was used in a finite element

algorithm which was developed by Chen and Schreyer (1990) in which a constraint that limited the amount of damage generated during each step is introduced. The output results showed no mesh sensitivity.

Ofoegbu and Curran (1990) decomposed the total deformation into elastic, brittle and ductile components. Assuming that the damage process was due to cracking (no damage is associated to the bulk modulus) then the effective shear modulus could be expressed as:

$$\bar{G} = (1-d) G \quad (3.92)$$

and therefore the stress tensor σ_{ij} was expressed in terms of the latent (or topical as marked by Frantziskonis and Desai, 1987) stress σ_{ij}^t by the relation

$$\sigma_{ij} = (1-d) \sigma_{ij}^t + \frac{d}{3} \delta_{ij} \sigma_{kk} \quad (3.93)$$

Then the yield function and the plastic potential in nonassociative plasticity were expressed in terms of the effective first and second stress invariants. The model was in good agreement with experiments.

Patino (1989) studied the stability and energy minimization in elasticity with damage. Free energy with penalization term was compatible with Clausius-Duhem inequality. Free energies with and without penalization indicated that minimizers of the total free energy must be stated where damage evolution vanish. In this study the dissipation inequality was expressed as

$$\rho \dot{\psi} + \rho S \dot{T} - \sigma : \dot{\epsilon} + \frac{1}{T} \text{grad } T \cdot q \leq 0 \quad (3.94)$$

in which T is the temperature, S is the entropy and q is the heat flux. Coleman and Noll's (1963) relations were written in the form

$$\frac{\partial \psi}{\partial T} = -S \quad , \quad \rho \frac{\partial \psi}{\partial \epsilon} = \sigma \quad , \quad \frac{\partial \psi}{\partial \text{grad } T} = 0 \quad ,$$

$$\rho \frac{\partial \psi}{\partial D} \leq \sigma \quad \& \quad \text{grad } T \cdot q \leq 0 \quad (3.95)$$

Pijauder-Cabot (1985) developed a damage model for high compressive loading of concrete. The elastic free energy ψ^e is expressed in terms of the deviatoric stress tensor S and the stress tensor σ by using two damage variables. The first is a scalar δ while the other is a vector d . The energy is expressed as

$$\rho \psi^e = \frac{1}{2E_0} \left\{ (\alpha : S) : S + \frac{(1-2\nu_0)}{4(1-\delta)} |\text{tr}(\sigma)^2 - \sigma : \sigma| \right\} \quad (3.96)$$

where the scalar damage variable is given by

$$\delta = \frac{1}{1 - A(\frac{1}{3} \text{tr} \sigma - k_0)} \quad (3.97)$$

and α is given by

$$\alpha = 3(I-d)^{-1} I - \frac{1}{2} I \{ \text{tr}[(I-d)^{-1}] \} \quad (3.98)$$

PLEASE NOTE

**Page(s) not included with original material
and unavailable from author or university.
Filmed as received.**

UMI

shown to depend only on damage process. The tensorial relations were not uniquely derived since seven modes of behavior could take place (three in tension and four in compression). The resulting constitutive equation lacked symmetry in some cases. Also the shear damage variable increment was allowed to be negative which was in contradiction with thermodynamics. The constitutive relations were not in general unconditionally stable. The model was calibrated and implemented into finite element framework.

Ortiz (1985, 1987a) developed the mixture model which considered concrete to be composed of mortar (m) and aggregates (a). and The latter was assumed to exhibit non-associative plasticity following Drucker-Prager loading criterion. The mortar was assumed to be brittle material undergoing damage process. The strain of the two components was the same and equal to the macroscopic strain since diffusion was assumed to be prevented; i.e. $\epsilon = \epsilon_m = \epsilon_a$. The macroscopic stress was given as the volume average of the partial stresses of the two components as

$$\sigma = \alpha_m \sigma_m + \alpha_a \sigma_a \quad (3.102)$$

where $\alpha_i (i=m,a)$ were the volume fractions. For the damage behavior of the mortar, a novel view point was to consider the compliance S_d as an internal variable. In the recent paper, another internal variable was considered which was a plastic second order of the strain tensor ϵ_m^P such that the partial stress strain relation was given as

$$\epsilon_m = (S_o + S_d) \sigma_m + \epsilon_m^P \quad (3.103)$$

Interdependent flow rules were given for ϵ_m^P and S_d :

$$d\epsilon_m^P = \alpha (|\sigma_m| + c |\sigma_m|) d\mu \quad (3.104)$$

and

$$dS_d = (1-\alpha) \{ (|\sigma_m| + c |\sigma_m|)^{-1} |\sigma_m| \times |\sigma_m| + c (|\sigma_m| + |\sigma_m|)^{-1} |\sigma_m| \times |\sigma_m| \} d\mu \quad (3.105)$$

where α, c and μ were two material constants and the damage evolution multiplier, respectively. The model displayed hystretic behavior in unloading-reloading cycles due to the coupling of mortar and aggregate behavior.

Saouridis and Mazars (1989) used the so-called multiscale approach which was a modified version of Mazars' (1984a) model taking into account nonlocality of damage using Cabot' and Bazant's (1987a, b) spatial integral. The model was implemented in a finite element scheme and was applied to simulate the splitting test, the size effect of 3-point loading on centrally notched beams and the structural size and gradient effects on concrete beams in bending. The results were in good agreement with experiments and the damage zone seemed to be wider than that predicted by local approaches.

Saouridis and Mazars (1992) used a Weibull based theory to determine, in a statistical sense, the value of the initial damage threshold. The damage probability function was given as

(1) for uniform loading

$$P_d(\bar{\epsilon}, V) = 1 - \exp(-\kappa \bar{\epsilon}^m V) \quad (3.106)$$

(2) for non-uniform loading

$$P_d(\bar{\epsilon}, V) = 1 - \exp\left(-\kappa \bar{\epsilon}^m \int_V h^m dV\right) \quad (3.107)$$

in which $\bar{\epsilon}$ is the equivalent strain defined earlier by Mazars (1984a), the subscript g denotes the greatest value, V is the volume and κ, h , and m are material parameters.

In this study, the different localization limiters were summarized as follows:

1. Limiting the finite element size (Bazant and Oh, 1983b).
2. Using stress-displacement relation rather than stress-strain law (Hillerberg et al., 1979 : Fictitious crack model; Willam et al., 1986; Pietruszczak and Mroz, 1981 : Composite models).
3. Introducing some viscosity or strain-rate formulation (Needleman, 1987).
4. Including in the definition of the strain tensor the gradients of higher order (Belytschko and Lasry, 1989).

5. Taking into account in the constitutive law the influence of strain gradient (Triantafyllidis and Aifantis, 1986).
6. Using a nonlocal formulation of the constitutive law for both damage and strain (Bazant, 1984a).
7. Using a nonlocal formulation of the damage evolution (Cabot and Bazant, 1987a, b).
8. Introducing a localization shape function added to the finite element formulation (Ortiz, 1987b).

Sidoroff (1981) on a study on the description of anisotropic damage to elasticity assumed that the effective stress tensor $\bar{\sigma}$ is related to the stress tensor σ by the relation

$$\bar{\sigma} = M(d) \sigma \quad (3.108)$$

in which M is a linear operator on second order symmetric tensor, i. e. 4th order tensor. However, it was shown that the inverse tensor of $M(d)$ is not insured to be symmetric unless it is symmetrical and represents isotropic damage. This situation was encountered in the work of Chaboche (1979) when used a fourth order damage tensor and earlier (1978) when used eighth order damage tensor. Symmetry is obtained when the effective stress is expressed in the form

$$\bar{\sigma} = \frac{1}{2} \{ (I-D)^{-1} \sigma + \sigma (I-D)^{-1} \} + \frac{\nu}{1-2\nu} \text{tr}(\sigma D (I-D)^{-1}) I \quad (3.109)$$

This approach keeps symmetry condition to be satisfied under axes transformation. Unfortunately, it was pointed out that this description of damage is rather complicated and essentially relies on elasticity which may not be an essential phenomenon.

Simo and Ju (1987a, b) considered the strain and stress based continuum damage models. For the strain based model the free energy potential ψ was expressed as

$$\psi(\varepsilon, \sigma^P, \mathbf{q}, d) = (1-d)\psi^0(\varepsilon) - \varepsilon : \sigma^P + \Xi(\mathbf{q}, \sigma^P) \quad (3.110)$$

in which ψ^0 is the initial elastic stored energy which is a convex function, σ^P is the plastic relaxation stress tensor, Ξ is the plastic potential function, and \mathbf{q} represents a set of plastic variables. Clausius-Duhem inequality, which is written for isothermal process in the form

$$-\dot{\psi} + \sigma : \dot{\varepsilon} \geq 0 \quad (3.111)$$

yields the following inequalities

$$\psi^0(\varepsilon) d \geq 0 \quad \& \quad - \frac{\partial \Xi}{\partial \mathbf{q}} \cdot \dot{\mathbf{q}} - \left\{ \frac{\partial \Xi}{\partial \sigma^P} \right\} : \dot{\sigma}^P \geq 0 \quad (3.112)$$

In this type of formulation the stress tensor was derived to take the form

$$\sigma = \frac{\partial \psi}{\partial \varepsilon} = (1-d) \frac{\partial \psi^0}{\partial \varepsilon} - \sigma^P \quad (3.113)$$

The plastic strain ϵ^P is formulated in terms of local unloading corresponding to zero stress, i. e.

$$\epsilon^P = \Gamma^{-1}\left(\frac{\sigma^P}{1-d}\right) \quad , \quad \Gamma(\epsilon) = \frac{\partial \psi^0(\epsilon)}{\partial \epsilon} \quad (3.114)$$

The damage was characterized by an energetic criterion which led to symmetric formulation contrary to Lemaitre and Mazars (1982b) who used the strain second invariant norm. The plasticity formulation which was extended further to include viscous behavior was expressed in terms of the effective stress in Rabotnov's (1968) sense. On the other hand, the stress based formulation also considered a scalar damage variable and the complementary free energy Λ was expressed as

$$\Lambda(\sigma, \epsilon^P, \mathbf{q}, d) = d_\epsilon \Lambda^0(\sigma) - \sigma : \epsilon^P - \Xi(\mathbf{q}, \epsilon^P) \quad (3.115)$$

where Λ^0 is the complementary energy of the virgin material, d_ϵ is the reciprocal of $(1-d)$ The formulation was quite similar to that of the strain based model and was given in a systematic way. Variational formulation and subsequent numerical implementation of these models were further discussed and a a three-step operator split algorithm was proposed.

Stevens and Liu (1992) proposed a strain based constitutive model with mixed evolution rules for concrete. Combined damage and plasticity was considered and two second order damage tensors were adopted for tensile and compressive behavior. Same surfaces for damage and inelastic deformation was used. Kinematic evolution rule and shifted

elastic strain were used for the tensile surface g' while isotropic evolution law was used in compression for which the surface is g . The surfaces were mathematically described by

$$g' = \tau' - r_0' \quad , \quad \tau' = \sqrt{(\varepsilon_e' - \alpha') : C^0 : (\varepsilon_e' - \alpha')} \quad (3.116)$$

and

$$g^- = \tau^- - r_0^- \quad , \quad \tau^- = \sqrt{(\varepsilon_e^-) : C^0 : (\varepsilon_e^-)} \quad (3.117)$$

in which r_0', r_0^- and α are the radius of the unshifted tensile surface, the radius of the compressive surface and the shift of the tensile surface. The 4th order tensor C^0 represents the virgin moduli tensor of the material. The incremental moduli C_t^+ and C_t^- for tensile and compressive loading were obtained by

$$C_t^+ = \mu' \frac{\partial g'}{\partial \varepsilon_e \text{ x } \partial \varepsilon_e} \quad (3.118)$$

and

$$C_t^- = \mu^- \hat{H}(\text{tr} \varepsilon_e^-) \frac{\partial g^-}{\partial \varepsilon_e \text{ x } \partial \varepsilon_e} \quad (3.119)$$

where μ' are the consistence parameters in tension and compression. The heaviside function $\hat{H}(\text{tr} \varepsilon_e^-)$ was suggested by Yazdani and Schreyer (1990) to accommodate pressure effect. The plastic stress evolution was

given by

$$\sigma^p = \mu' \frac{\partial \mathbf{g}'}{\partial \mathbf{v}_e} + \mu \frac{\partial \mathbf{g}}{\partial \mathbf{v}_e} \quad (3.120)$$

Suaris et al. (1990) developed a damage model using the concepts of the bounding surface for monotonic and cyclic behavior of concrete. An elastic potential Λ was introduced in terms of the principal stresses and a compliance tensor dependent on the accumulated damage and used circular loading and bounding surfaces defined in terms of the thermodynamic forces R_j conjugate with the damage variables ω_j . The model is a stress based one and the plastic strain was assumed to be coaxial with the damage strain. An experimental scheme was adopted to detect microcrack growth and hence evaluate the damage variables with ultrasonic technique. The model was expressed mathematically by the following set of equations:

$$\epsilon_{ij} = \rho \frac{\partial \Lambda}{\partial \sigma_{ij}} (\sigma_{ij}, t, \omega_i) \quad (3.121)$$

and

$$R_i = \rho \frac{\partial \Lambda}{\partial \omega_i} (\sigma_{ij}, t, \omega_i) \quad (3.122)$$

The damage variables were obtained from the normality rule to the loading surface f as

$$\omega_i = L \left(\frac{\partial f}{\partial R_i} \right) \quad (3.123)$$

where L is given by

$$L = \frac{c}{H} \left(\frac{\partial f}{\partial R_i} \right) R_i \quad (3.124)$$

in which

$$H = \frac{\kappa \delta}{\langle \delta, \text{in} - \delta \rangle} \quad (3.125)$$

and

$$C = \begin{cases} 1 & , f = 0 \quad \& \quad f > 0 \\ 0 & , \text{ otherwise} \end{cases} \quad (3.126)$$

where κ is a constant, δ is the normalized distance between the loading and bounding surfaces. The complementary energy was expressed as

$$\rho \Lambda = \frac{1}{2} |\sigma' C_I \sigma' + \sigma C_{II} \sigma| \quad (3.127)$$

where

$$C_I = \frac{1}{E_0} \begin{vmatrix} 1 & -\nu & -\nu \\ \frac{1}{1-\alpha\omega_1} & 1 & -\nu \\ -\nu & \frac{1}{1-\alpha\omega_2} & 1 \\ -\nu & -\nu & \frac{1}{1-\alpha\omega_3} \end{vmatrix} \quad (3.128)$$

and

$$C_{II} = \frac{1}{E_0} \begin{vmatrix} \frac{1}{(1-\beta\omega_2)(1-\beta\omega_3)} & \frac{-\nu}{(1-\omega_1)(1-\omega_2)} & \frac{-\nu}{(1-\omega_1)(1-\omega_3)} \\ \frac{-\nu}{(1-\omega_1)(1-\omega_2)} & \frac{1}{(1-\beta\omega_1)(1-\beta\omega_3)} & \frac{-\nu}{(1-\omega_2)(1-\omega_3)} \\ \frac{-\nu}{(1-\omega_1)(1-\omega_3)} & \frac{-\nu}{(1-\omega_1)(1-\omega_3)} & \frac{1}{(1-\beta\omega_1)(1-\beta\omega_2)} \end{vmatrix} \quad (3.129)$$

It was stated that :

"The scalar damage variable used by Krajcinovic (1979), Loland (1981) and Mazars (1984a) is sufficient to model isotropic damage. However, the cracks that occur in concrete under loading are highly oriented and a vectorial - or tensorial - valued damage variable would be required to model this crack-induced anisotropy (Krajcinovic and Fonseka, 1981; Suaris and Shah, 1984; Kachonov, 1980b; Cordebois and Sidoroff, 1982)."

Voyiadjis and Taher (1993) considered a bounding surface approach for damage formulation. The initial fracture, loading and the bounding surfaces were modelled using a modified Ottoson (1977a) surface including the Lode angle, damage variable (maximum accumulated damage) using a scaling factor according to the nonuniform hardening rule (Han and Chen, 1985). Similar equations as those of Suaris et al. (1990) were used and their incremental form was derived. Different moduli for loading, unloading and reloading were allowed, thus the hysteresis loop was captured.

This model was merged with plasticity with the help of two bounding

surfaces by Taher and Voyiadjis (1993). The hardening behavior was claimed to be controlled by both damage and plasticity while the strain-softening regime to be controlled by the damage process only. The damage surface was shown to dominate at low confinements while the plasticity surface dominate at large confinement. However, the damage contribution to the plastic behavior was neglected. For plasticity, a modified Ottoson (1977a) including the Lode angle θ and a strain parameter which was chosen as the maximum principal compressive strain ϵ_{\max} , and the ratio $d = \frac{\delta}{\delta'}$, δ is measured along the tensile meridian for unloading whereas on the compressive meridian for reloading. The plastic strain increment was expressed as

$$d\epsilon_{ij}^p = \frac{S_{kl}}{3H_p \tau_0} \left| \frac{S_{ij}}{\tau_0} + \delta_{ij} \frac{\beta}{3} \right| d\sigma_{kl} + \delta_{ij} \frac{1}{9K_t} d\sigma_{kk} \quad (3.130)$$

where H_p is the plastic modulus, K_t is the tangent bulk modulus, β is the shear compaction-dilatancy factor and τ_0 is the octahedral shear stress. The material parameters were in good agreement with experiments.

Willam et al. (1984) considered a series model similar to that suggested by Bazant (1976a) of an intact elastic zone and a localized damage zone. The dimension of the damage zone was assumed $h \times d_{\xi, \xi}^t = t$, s for tension and shear respectively. Considering a tangential damage variable, the constitutive relations were written as (1) in tension

$$\sigma = E_S \epsilon \quad , \quad E_S = \frac{E}{\frac{\lambda_t}{h} - 1} \quad , \quad \lambda_t = d_t \frac{E}{E_{S,d}} \quad (3.131)$$

(2) in shear:

$$\tau = G_S \gamma \quad , \quad G_S = \frac{G}{\frac{\lambda_s}{h} - 1} \quad , \quad \lambda_s = d_s \frac{G}{G_{S,d}} \quad (3.132)$$

where $C_S, C_{S,d}, C=E, G$ are the undamaged, composite, and localized damage zone and λ_t, λ_s are the damage variables in tension and shear, respectively. Implementation of this procedure in finite element scheme showed how the mesh sensitivity was eliminated.

Yazdani and Schreyer (1990) combined plasticity with damage mechanics for concrete. The damage surface was a consequence of a damage evolution law based on the physical aspects associated with two modes of cracking; thus displaying softening and hardening modes. The plasticity surface was the classical von Mises with strain hardening but not softening. The model gave accommodation for anisotropy and showed that dilatancy arised from microcracking not from plasticity as reported by Tapponnier and Brace (1976). The uncoupling relation between plasticity and damage was derived from thermodynamic formulation by expressing the Gibb's function as follow

$$G(\sigma, q) = \frac{1}{2} \sigma : C^0 : \sigma + \frac{1}{2} \sigma : C^C(\kappa) : \sigma + \epsilon^i(q) : \sigma - \Lambda^i(q) \quad (3.133)$$

in which C_0 is the undamaged compliance, C_c is the added flexibility, Λ^i is the free energy to form microcracks (surface energy), κ is a set of damage variables, $q = \kappa, \gamma$ and γ is a set of plastic variables. The internal dissipation inequality was expressed as

$$\Phi \dot{\gamma} + \Psi \dot{\kappa} \geq 0, \quad \Phi = \frac{\partial G}{\partial \gamma}, \quad \Psi = \frac{\partial G}{\partial \kappa} \quad (3.134)$$

3.12 LOCAL, NONLOCAL, AND DISTRIBUTED DAMAGE

A continuum with nonlocal damage has recently been shown to be an effective approach for the analysis of strain softening structures (Bazant, 1987a). The basic idea of the nonlocal continuum model is that only the damage is nonlocal, being a function of the strain average from a certain neighbourhood of a given point, while all the other variables, especially the elastic strain is local. By contrast, in the original nonlocal continuum models for elastic models for elastic materials (Kroner, 1968; Krumhansl, 1968; Kunin, 1968; Levin, 1971; Eringen and Edelen, 1972; Eringen and Ari, 1983; etc.), as well as in the first nonlocal model for strain softening continuum (Bazant, 1984a), the elastic strain and total strain were nonlocal. This led to certain numerical difficulties (Bazant and Pijaudier-Cabot, 1987b), for example the existence of spurious zero-energy instability modes (which had to be suppressed artificially by overlay with local continuum), the presence of spatial integrals or higher-order derivatives in the differential equations of equilibrium or motion and in boundary and

interface conditions, and an imbricate structures of the finite element approximation which however proved cumbersome for programming.

These difficulties were later shown to be a consequence of imposing symmetry on the integral or differential operators involved. The symmetry is lost with the nonlocal damage concept, which means that the tangential (but not the elastic) structural stiffness matrix of the finite element approximations is nonsymmetric (Bazant and Pijaudier-Cabot, 1987b).

The nonlocal damage characterization is physically very appealing at the microscale. However, experimental determination of the characteristic length l_c may be major problems. Nevertheless, Bazant and Pijaudier-Cabot (1987b) proposed an interesting method to determine the characteristic length from experimental data. Further, nonlocal computation is to some extent incompatible with local finite element calculation and further enhancement in consistence and accuracy is needed. On the other hand, the viscous damage model proposed by Ju (1989a) is not suitable for accommodating dynamic rate effect but also offers a possibility for controlling loss of ellipticity. This model satisfies the positiveness condition in Valanis (1985) and leads to well posed initial boundary value problems.

In the recent years, the applicability and limitations of distributed damage model to brittle materials such as concrete have been questioned by some researchers (e.g. Read and Hegemier, 1984). The fundamental question is to what extent the softening that is observed experimentally

(for a boundary value type sufficiently large specimen) is a manifestation of local material behavior or, on the contrary, a global structure (boundary-value) effect brought about by fracture (macrocracks) and strain localization (such as shear band formation). Ju (1989b) answered this question by separating the issue into two parts. The first part concerns the boundary value type experimental testing of specimens. The second part focuses on the local constitutive behavior (not boundary-value problem) within the framework of the unit-cell-based mesomechanics, the concept of characteristic length, together with the self-consistent method or homogenization technique. It is noted in the case of concrete, the characteristic length is approximately three times the maximum aggregate size.

For a sufficiently large (bigger than unit cell) experimental specimen , the observed force-displacement curve indeed represents the global boundary value type response, rather than the local stress-strain behavior of a material element. In fact in this boundary-value problem, there are factors contributing to the apparent softening which is observed experimentally. These factors include:

- a. the nucleation and growth of of many distributed microcracks in the specimen, leading to local material softening in the sense of the unit cell based meso-mechanics;
- b. the strain localization phenomenon, resulting from the loss of ellipticity and stability of materials (e.g. Ortiz and Simo, 1986; Ortiz, 1987a, 1987b, 1987c); and

- c. the formation and propagation of global boundary-value-type macrocracks which are the direct products of microcrack coalescence in the specimen.

Based on the alluded statements, it is concluded that the true material softening is less than the global softening observed in experiments. Therefore, the global force displacement curve should not be directly interpreted as the local stress-strain curve of a material element.

On the other hand, within a statistically representative unit cell (meso-mechanics), distributed microcracks and strain softening (at the meso-scale) do make sense since distributed microcracks (within the unit cell) do influence stiffness degradation and strain and strain softening. One can apply the self-consistent method or the homogenization technique to compute the degradation of elastic and plastic material properties of a unit cell. These computations are, of course, related to the scale of the characteristic length of a material. Further, the so-called size effects (e.g., Bazant, 1984a, 1984d 1985a; Bazant and Kim, 1984c) are also closely related to the scale of characteristic length.

In summary, distributed damage models are suitable for modeling distributed (many) microcracks and material responses (not necessary softening) in structural members before macrocracks, one can switch to fracture mechanics approaches provided that one takes into account:

- a. the damage process zones in front of macrocracks (i.e. the macrocrack-macrocrack interactions); and

- b. the damage induced stiffness degradation and anisotropy in many (distributed) unit cells.

Without these accounts, the resulting fracture calculations are not realistic nor meaningful. Conversely, direct application of a distributed damage model to solve a problem involving a single dominant macrocrack (in a boundary-value setting) is not likely to yield accurate results regarding macrocrack geometry and macrocrack opening displacement. Finally, distributed damage models are not directly suitable for predicting localization instability in materials.

3.13 RATIONAL SPLIT OF STATE TENSORS

The basic step in constructing a sound nonlinear constitutive model is in the accounting of the inelastic deformations. Different investigators partition the state tensors in various ways. Two fundamental approaches have been followed in the past to account for the inelastic response of purely mechanical process. The first considers stress split to introduce the conventional elastoplastic behavior in addition to a complementary response which provides particular characteristics such as strain softening and stiffness degradation. For example, Bazant and Kim (1979a) assumed the total stress to consist of interaction between plastic and fracturing components. Frantziskonis and Desai (1987a) used a concept introduced by Van Mier (1984) to decompose the total behavior into topical (elastoplastic) and stress relieved behavior. Another split was proposed by Dougill and Rida (1980) in which the stress tensor was

decomposed into elastic and fracturing components. On the other hand, the second approach embarks with strain split which produces anomalies if not properly used. The latter will be considered in more details along this study, since it is more appealing in formulation (Ju, 1989a). Also, it elaborates the characteristic ingredients of general nonlinear material response.

In addition to the conventional elastoplastic partitioning of the strain tensor, other possible combinations between elasticity, plasticity and damage have been proposed in the literature: (i) elastic and damage components, (ii) elastic-damage component, (iii) elastic-damage and plastic components, (iv) elastic, damage and factorized damage components, (v) elastic, damage and plastic components and (vi) elastic-damage and plastic-damage components. The implications of using each of these partitioning techniques is investigated hereafter.

The split of the strain tensor is proposed according to the experimental findings for the material response under possible load combinations. For example, in the case of uniaxial loading of rigid perfectly plastic materials for which the initial slope is almost vertical the total strain is almost plastic, i.e. $\epsilon = \epsilon^P$ and all the energy is irrecoverable. The other extreme occurs for linear elastic materials ($\epsilon = \epsilon^e$) in which all the energy is recoverable. Such idealizations can, of course, never be found in reality. More practically the strain tensor is partitioned into elastic and plastic components, thus characterizing the elastoplastic behavior as shown in Fig. 3.8a. The material is initially elastic and unloads parallel to the initial slope, E_0 . The total

strain, in this case, is $\epsilon = \epsilon^e + \epsilon^p$. The plastic strain was the subject for extensive research for more than eight decades. Conventional plasticity expresses ϵ_{ij}^p through the following relationships

$$\dot{\epsilon}_{ij}^p = \dot{\lambda} \frac{\partial Q(\sigma_{ij}, q_i)}{\partial \sigma_{ij}} \quad (\text{nonassociative flow rule}) \quad (3.135)$$

$$\dot{q}_i = \dot{\lambda} h_i(\sigma_{ij}, q_i) \quad (\text{plastic hardening law}) \quad (3.136)$$

$$f(\sigma_{ij}, q_i) \leq 0 \quad (\text{yield criterion}) \quad (3.137)$$

where $\dot{(\)}$ is the time derivative, Q is the plastic potential function, σ_{ij} is the stress tensor, q_i is a suitable set of plastic variables, f is the yield surface, h_i is the vectorial hardening function and $\dot{\lambda}$ denotes the plastic consistency parameter.

As the concepts of damage mechanics evolved and came into practice, different techniques were followed for partitioning the strain tensor as shown in Fig. 3.8. Of these are:

- (1) Elastic and damage components: as usually followed by models based on micromechanics where the strain tensor is expressed as

$$\epsilon_{ij} = S_{ijkl}^0 \sigma_{kl} + S_{ijkl}^* \sigma_{kl} \quad (3.138-a)$$

$$= \epsilon_{ij}^e + \epsilon_{ij}^d \quad (3.138-b)$$

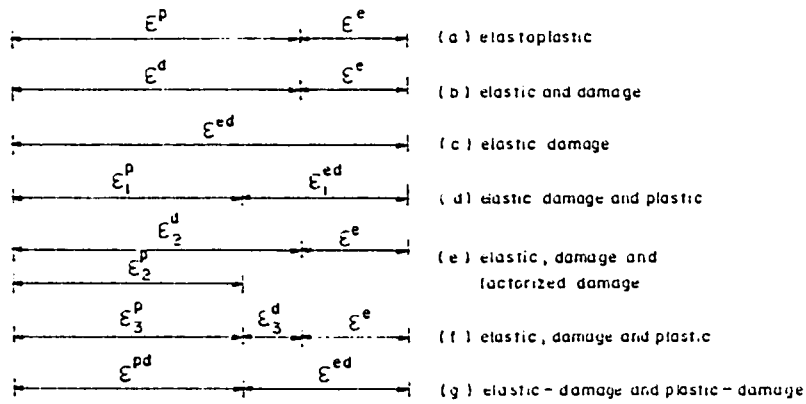
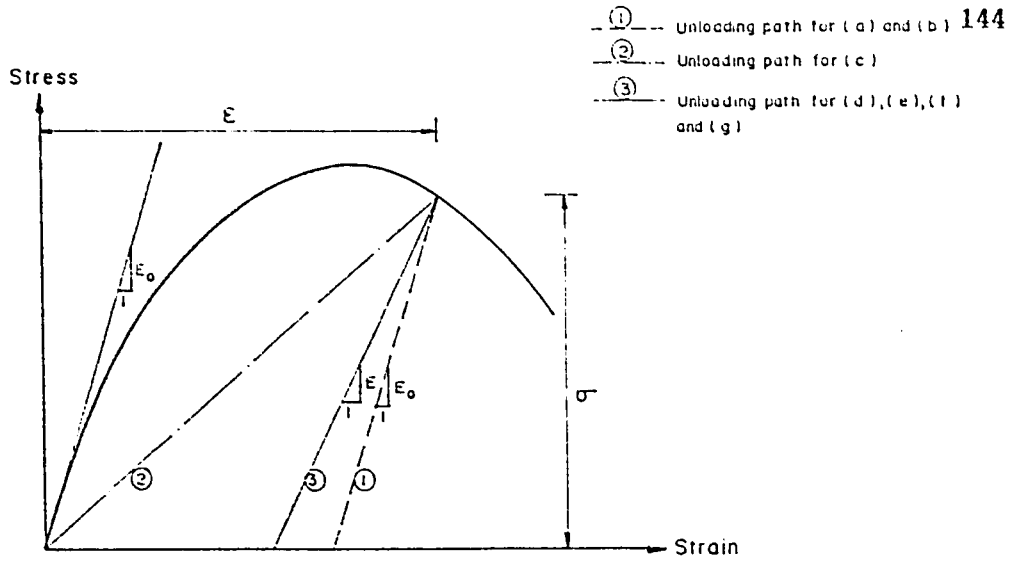


Figure 3.8 Various schemes for splitting the strain tensor

in which the elastic strain tensor $\epsilon_{ij}^e = S_{ijkl}^0 \sigma_{kL}$ and the damage strain tensor $\epsilon_{ij}^d = S_{ijkl}^* \sigma_{kL}$ where S_{ijkl}^0 is the undamaged compliance and S_{ijkl}^* gives the damage induced added flexibility (additional inelastic compliance). Such an approach is conceptually sound but following unloading slope parallel to the initial tangent (Fig. 3.8b) which is not the case for a general elastoplastic material. In some cases, the unloading slope is assumed to pass through the origin (Horri and Nemat-Nasser, 1983; Krajcinovic et al., 1991).

- (2) Elastic-damage component: This approach is also followed by micromechanics based models idealizing microcrack weakened brittle solids. The elastic moduli are changed continuously, thus yielding effective moduli based on either no-interaction (Taylor), differential (Kuster-Toksoz, Norris) or self-consistent approaches (Zimmerman, 1992). The well-known model developed by Budiansky and O'Connell (1976) falls in this category. In addition, the early proposed models for rate independent response using the concepts of continuous damage mechanics assumed unloading to the origin (Fig. 3.8c, path 2) and a stress-strain relation in the general form (ju, 1990)

$$\sigma_{ij} = M_{ijuv}(D) C_{uvkL}^0 \epsilon_{kL}^{ed} \quad (3.139)$$

where $M(D)$ is a fourth order tensorial function of the fourth order damage tensor. Examples of these models are those of Loland

(1981), Krajcinovic and Fonseka (1981a), and Mazars (1984a). It is obvious, of course, that idealization of concrete, which represents a general elastoplastic damage material, in this manner is not proper. It is more suitable for modeling brittle matrix fiber or particle composites as well as ceramics rather than concrete.

- (3) Elastic-damage and plastic components: This partitioning associates damage with the elastic process (Fig. 3.8d) only by postulating that the total strain energy $\psi = \psi_e(\epsilon_{ij}^e, D, T) + \psi_p(\epsilon_{ij}^p, T)$, where ψ_e is the elastic damage energy, ψ_p is the plastic energy, D is scalar damage variable and T is the temperature. A typical approach was followed, among others, by Lemaitre (1985) This hypothetical assumption was criticized by Ju (1989a) since it is not physically appropriate to decouple the plastic mechanism from microcrack growth process. In this case, for uniaxial loading shown in Fig. 3.8d, it has to be emphasized that the determination of the plastic strain ϵ_1^p should be different from its evaluation in elastoplastic type models where no damage is taking place. The variance between the two components ϵ^p (determined from eqns. (1) and which is shown in Fig. 3.8a) and ϵ_1^p (shown in Fig. 3.8b) should be crystallized in considering the plastic mechanism inclusive damage. Therefore, it can be concluded that if the unloading path is neither elastoplastic (path 1 in Fig. 3.8) nor brittle (path 2 in Fig. 3.8) then the plastic strain contains a certain damage fraction in it.

- (4) Elastic, damage and factorized damage components: In this approach the total strain is decomposed into elastic and damage component, i.e. $\epsilon = \epsilon^e + \epsilon_2^d$. To account for the inelastic behavior, however, the plastic strain associated with crack growth is assumed to be coaxial with the inelastic strain due to fracturing, i.e. $\epsilon_2^p = \alpha \epsilon_2^d$, α is a constant (Fig. 3.8e). This assumption was used by Ortiz (1985) to model mortar in his mixture model. It is evident that the simplified idealization for the plastic behavior is too restrictive to be considered as rigorous for generalization. Another aspect is that damage behavior is dominant for low confinement while the behavior of rock like materials is ductile at large confinements (Yazdani and Schreyer (1990)). Therefore, the ratio of the plastic strain to damage strain is not the same for all stress paths.
- (5) Elastic, damage and plastic components: To achieve more generalization this partitioning ($\epsilon = \epsilon^e + \epsilon_3^d + \epsilon_3^p$), as shown in Fig. 3.8f, was used by Yazdani and Schreyer (1990). In their formulation, Taher and Voyiadjis (1993) used this strain split but the plastic strain ϵ_3^p was determined independently from the damage process. Again this assumption, to be distinguished from elastoplastic partitioning, is physically incorrect unless ϵ_3^p includes damage effect (as originally proposed by Yazdani and Schreyer, 1990). Another important aspect is that the material may not be

initially elastic and therefore Yazdani and Schreyer's proposed partitioning (1990) is not general.

- (6) Elastic-damage and plastic-damage components: This approach was followed by Ju (1989) to characterize the elastoplastic damage behavior of concrete (Fig. 3.8g). This policy of partitioning is quite logical since the damage process, in comparison with the elastoplastic behavior, adds some flexibility to ϵ^e and decreases the plastic strain ϵ^p as defined in the classical sense (shown in Fig. 3.8a). This means that the damage does have real contribution to both the elastic and plastic behaviors.

3.14 COUPLED STRAIN-DAMAGE SCHEME

Solution techniques bifurcated into two directions; analytically and numerically (Fig. 3.9). Analytical methods of calculation were used to investigate elastic strain coupled with brittle damage (Bazant and Cedolin, 1979b; Bui et al., 1983; Ehlers, 1985; Krajcinovic, 1984a, 1984b; Krajcinovic and Fonseka, 1981), elastoplasticity coupled with ductile damage (Broberg, 1975; Chitaley and McClintock, 1971; Koning, 1977; Dougill, 1976; Norris et al., 1978; Shih et al., 1978), and elastovisco-plasticity coupled with creep damage (Broberg, 1974a, 1974b; Bui et al., 1984; Chrzanowski and Dusza, 1980; De Langre, 1984; De Langre et al., 1983; Hayhurst et al., 1983; Janson and Hult, 1977; Janson, 1985; Kachanov, 1958, 1980a; Krajcinovic, 1983f; Kubo et al.,

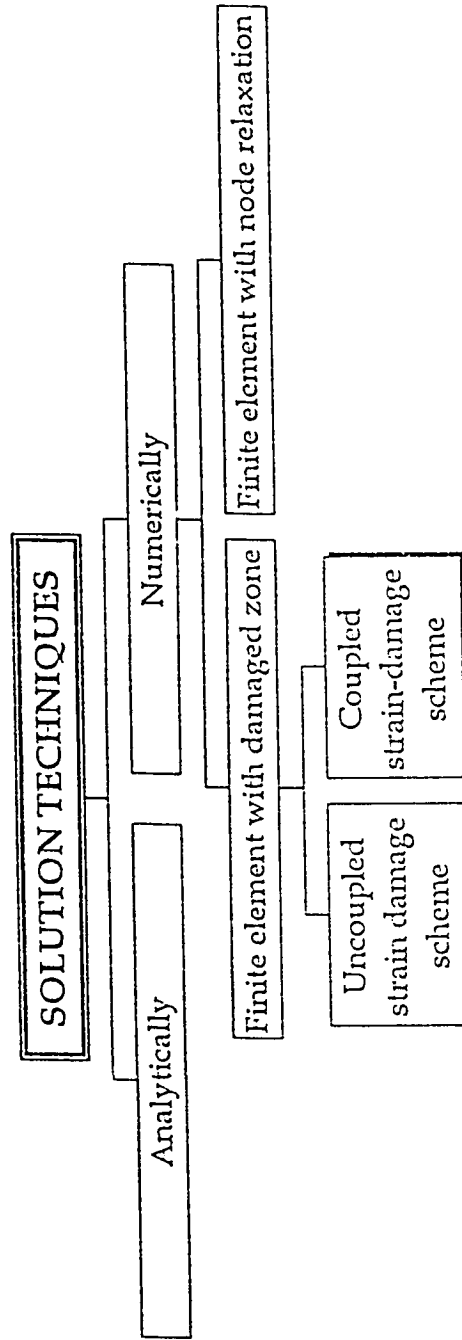


FIG. 3 : Various solution techniques for damage problems

1984; Makik, 1982; Murakami, 1981a; Murakami and Ohno, 1978, 1981b; Riedel, 1984; Riedel and Wagner, 1981).

Numerically, finite element method is widely used. Two algorithms were utilized. The first uses relaxation of nodes whereas the other uses damaged zone. Following the nodes relaxation, elasticity-brittle damage (De Borst and Nanta, 1985; Grootenboer, 1979; Hillerberg et al., 1976; Kobayashi, 1979; Petersson, 1981; Ramakrishnan, 1985; Suidan and Schnobrich, 1973), elasticity-fatigue damage (Lemaitre et al., 1981; Newman, 1982), elastoplasticity-ductile damage (Abdouli, 1982; Andersson, 1973; Devaux and D'Escatha, 1979, Devaux et al., 1985; Geegstra, 1976; Light et al., 1976; Varanasi, 1977), elastoplasticity-fatigue damage (Anquez, 1981; Lemaitre, 1984; Miller and kfour, 1974; Newman, 1977) and elasto-viscoplasticity-creep damage (Ehlers and Riedel, 1980; Ellison and Musicco, 1981; Gonclaves ana Owen , 1983) were investigated.

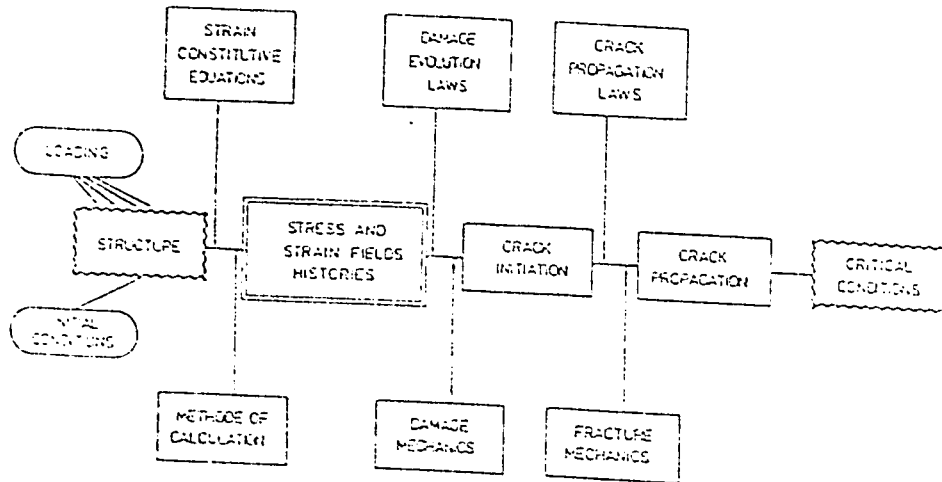
On the other hand, uncoupled strain-damage using damaged zone algorithm was employed in elasticity-brittle damage (Bazant and Cedolin, 1979b; Bazant and Cedolin, 1983c; Cedolin and Bazant, 1980; Marchertas et al., 1982), elastoplasticity-ductile damage (D'Escatha and Devaux, 1979; Rousselier, 1977, 1978) and elasto-viscoplasticity-creep damage (Benallal, 1985; Bensoussan et al., 1985, Cailletaud and Chaboche, 1982; Chaboche, 1982; Dyson and Loveday, 1981; Hayhurst, 1975; Hayhurst et al., 1981; Leckie and Hayhurst, 1974, Murakami, 1982; Policella and Culie, 1981;

Saanouni, 1984).

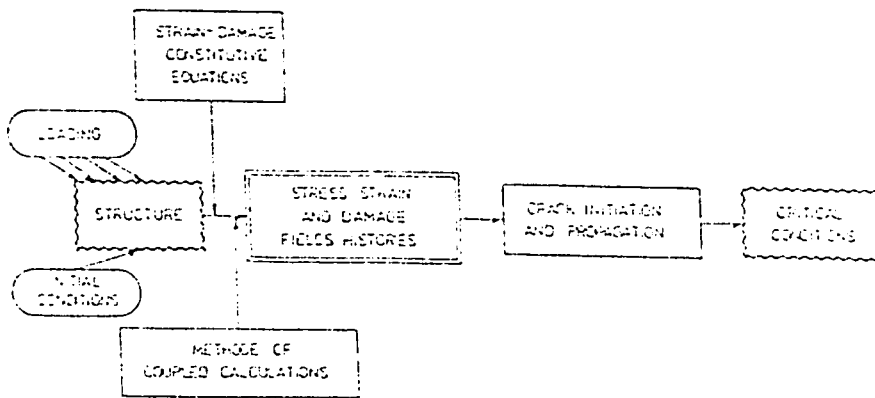
Finally, coupled strain-damage using damaged zone algorithm helped investigating elasticity-brittle damage (Legendre and Mazars, 1984; Lemaitre and Mazars, 1982b; Mazars, 1981; Mazars and Lemaitre, 1984b; Saouridis and Samake, 1985), elasticity-fatigue damage (Beremin, 1983; Billardon and Lemaitre, 1983), elastoplasticity-ductile damage (Benallal et al., 1984a, 1984b, Beremin, 1981a, 1981b, 1981c; Rousselier et al., 1985), elastoplasticity-fatigue damage (Billardon and Lemaitre, 1981), and elastoviscoplasticity-creep damage (Benallal, 1984; Saanouni and Chaboche, 1985).

The classical way to calculate the critical (rupture) conditions of a component (Fig. 3.10) is to operate in three steps (Lemaitre, 1984):

- (1) The geometry of the structure being known, together with the history of loading and initial conditions, the fields of stress and strain are first calculated by means of strain constitutive equations and a numerical procedure (finite element method).
- (2) Then, by means of a damage criterion, the most critical point(s) with regard to fracture is (are) determined and, the load, or the time, for rate dependent models, or number of cycles, for alternate loading models, corresponding to a macro-crack initiation at that point is calculated, by integration of damage constitutive equation if rate function is used, for the history of local stress or strain.



(a) Uncoupled algorithm.



(b) Coupled algorithm.

Figure 3.10 Strain-damage coupling schemes

- (3) In a third step the fracture mechanics concepts may be applied in order to calculate the evolution of the macro-crack up to the final rupture of the whole structure.

In the local approach using continuous concepts, the crack tip is a process zone in which damage increases until the rigidity and strength vanish. This gives rise to a continuous definition of a crack (at the structure scale):

"A crack is a flat zone of high gradients of rigidity and strength in which the critical conditions of damage have been reached".

This means that the third step of the previous scheme may be avoided considering that the crack evolution is the that of the damaged zone as calculated element by element (for constant strain elements) or Gauss points with recalculation of stresses. The geometry of the damaged zone is taken into account but not the possible coupling between damage and strain (Fig. 3.10a).

A further step is to take into account the coupling between strain and damage due to the fact that damage decreases the rigidity and the strength of materials. Then, by means of coupled constitutive equations, strain and damage fields are calculated in one step and the crack as a damaged zone is obtained at the same time as the strain (Fig. 3.10b).

CHAPTER 4

CHAPTER 4**RE-CONCEPTUALIZATION OF DAMAGE MECHANICS****4.1 GENERAL**

In this Chapter, fundamental aspects of elastoplastic-damage are deliberately outlined. The concepts of generalized damage variables, generalized material degradation paths and generalized effective stresses based on the hypothesis of strain equivalence are defined. For more insight of generalized elastoplastic damage uncoupling, a demonstration is made by investigations of uniaxial compressive behavior of concrete and copper 99.9% as well. Then, the Lemaitre's ductile damage model (1985) is revised. The decoupled free energy terms are derived bases on the concepts of thermodynamics of irreversible changes. Subsequently, the tangential tensorial moduli are formulated for the case of yielding materials. Phenomenological and micromechanical aspects of rate-independent isotropic elastoplastic-damage are merged to construct the constitutive relations of strain softening materials.

4.2 GENERALIZED DAMAGE VARIABLES

Damage can be defined as a collection of permanent microstructural changes concerning material thermomechanical properties (e.g. stiffness, strength, anisotropy, etc.) brought about in a material by a set of irreversible physical microcracking processes resulting from

the application of thermomechanical loadings (Talreja, 1985). Among the various definitions of the damage variable is the ratio of damaged surface area over total (nominal) surface area at a local material point (Janson and Hult, 1977; Loland, 1981; Lorrain and Loland, 1983). This definition gave guidance to alternative forms as the change in the elastic compliances (stiffnesses) (Mazars, 1982, 1984a, 1986a; Lorrain and Loland, 1983; Resende and Martin 1984; Resende, 1987; Lemaitre, 1984a, 1985, 1986a; Frantziskonis and Desai, 1987a,b; Ladeveze, 1983; Mazars and Lemaitre, 1985a). Therefore a broad definition of the generalized damage variables can be adopted as follows:

"If a material has n generalized degrading properties, $z_i, i = 1, n$, then at any time, t , the damage variable associated with any property z_i , $d_{z_i}(t)$, is given by

$$d_{z_i}(t) = 1 - \frac{z_i(t)}{z_i(t_{d_{z_i}})} \quad (4.1)$$

in which $z_i(t_{d_{z_i}})$ is the value of the i th property at its threshold time $t_{d_{z_i}}$ at which its degradation takes place".

The generalized damage variables have the following properties:

1. Non-decreasing variables in the process of thermomechanical loading.

2. Zero values correspond to undamaged state at time $t_{d_{z_i}}$.
3. Critical values $d_{c_{z_i}}$ are maximal values taking place at times $t_{c_{z_i}}$ need not define rupture as in Kachanov's sense (1958).
Rupture criterion is required to interrelate the generalized damage variables.
4. $d_{c_{z_i}} \in [-\infty, 1]^*$, $d_{z_i} \in [0, d_{c_{z_i}}]$
5. Rate values, \dot{d}_{z_i} , are equal to zero through unloadings (i.e., unloading is an elastic process).

4.3 GENERALIZED MATERIAL DEGRADATION PATHS

Rock-like materials exhibit all sorts of irreversible changes. Response of such materials is characterized by strain softening in the post peak region. Irrespective to its incarnation, this behavior is still in argument whether it is a material or structural property (Read and Hegemier, 1984; Sandler, 1984; Wu and Freund, 1984; Van Mier, 1984; Frantziskonis, 1986; Discussions at the France-US Workshop, 1988). However, a typical stress strain relation is shown in Fig. 4.1 for which five unloading paths can be described schematically, if initially assumed

* An illustration is made in Art. 4.3.

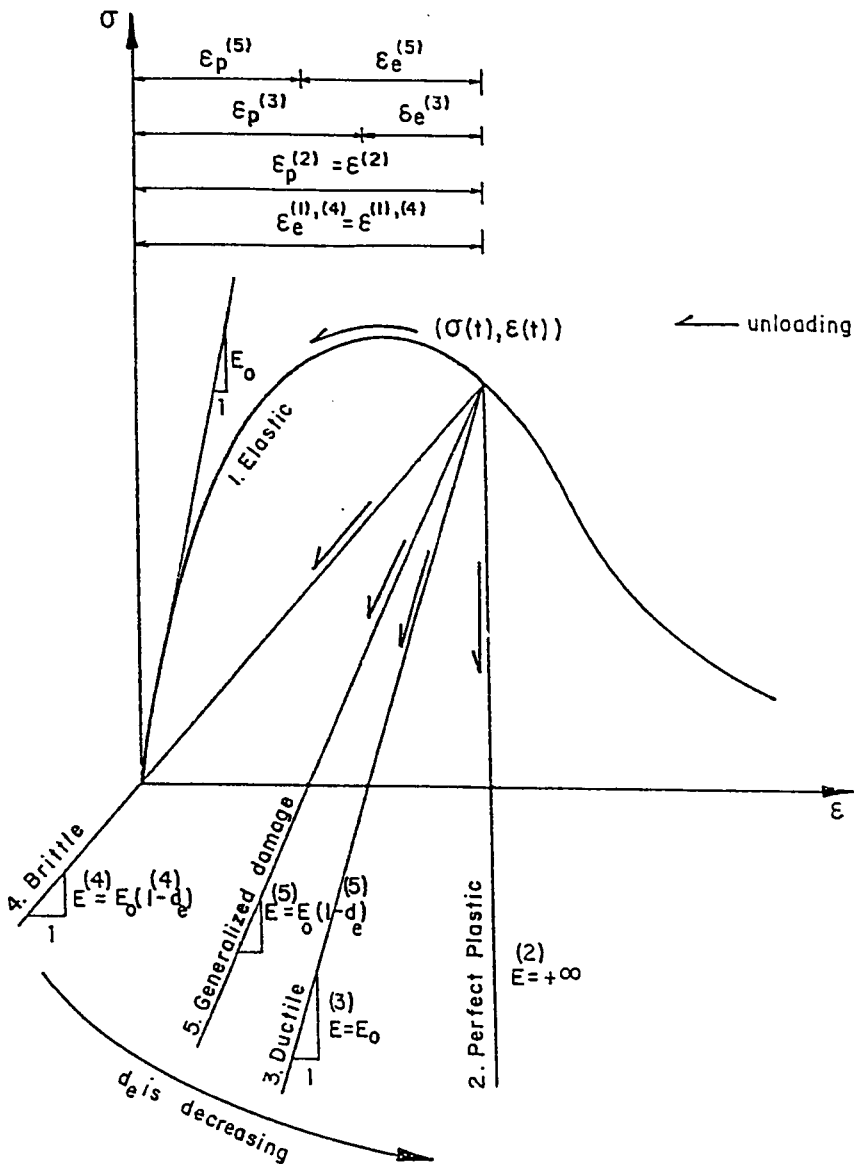


Figure 4.1 Generalized material degradation paths

elastic, based on the recovered energy density ω_r (all notations are shown in Fig. 4.1):

Path 1: Elastic unloading with no permanent deformation and full energy recovery. It represents a typical form of nonlinear elasticity and damage concept is trivial;

$$\omega_r = \int_0^{\epsilon} \sigma : d\epsilon_e^{(1)} \quad , \quad \epsilon = \epsilon_e^{(1)} \quad , \quad \epsilon_p^{(1)} = 0 \quad (4.2-a)$$

Path 2: Perfect plastic unloading with neither deformation nor energy recovery (as that used in the "Bounding surface theory" (Dafalias, 1981) and in the "Sub-loading surface" models (Hashiguchi, 1989));

$$\omega_r = 0 \quad , \quad \epsilon = \epsilon_p^{(2)} \quad , \quad \epsilon_e^{(2)} = 0 \quad (4.2-b)$$

Path 3: Ductile unloading with flow stress degradation (Elices and Palanias, 1989). It represents a typical form of elastoplasticity

$$\omega_r = \frac{1}{2} \sigma : \epsilon_e^{(3)} = \frac{1}{2} \epsilon_e^{(3)} : E_o : \epsilon_o^{(3)} \quad , \quad \epsilon = \epsilon_e^{(3)} + \epsilon_p^{(3)} \quad ,$$

$$\epsilon_e^{(3)} = E_o^{-1} : \sigma \quad (4.2-c)$$

Path 4: Brittle unloading with stiffness degradation. All microcracks are assumed to close upon unloading and permanent deformation is zero. It represents a typical form of secant type model

$$\omega_r = \frac{1}{2} \sigma : \epsilon_e^{(4)} = \frac{1}{2} \epsilon_e^{(4)} : (1 - d_e^{(4)}) E_o : \epsilon_o^{(4)} \quad ,$$

$$\begin{aligned}\varepsilon &= \varepsilon_e^{(4)} = E^{-1}(t) : \sigma, \quad \varepsilon_p^{(4)} = 0, \\ d_e^{(4)} &= 1 - E_0^{-1} : E(t)\end{aligned}\quad (4.2-d)$$

Path 5: Generalized damage (Elices and Palanas, 1989) giving energy recovery intermediate between the previous two cases. It represents damage-elasto-plastic coupling

$$\begin{aligned}\omega_r &= \frac{1}{2} \sigma : \varepsilon_e^{(5)} = \frac{1}{2} \varepsilon_e^{(5)} : (1 - d_e^{(5)}) E_0 : \varepsilon_e^{(5)}, \\ \varepsilon &= \varepsilon_e^{(5)} + \varepsilon_p^{(5)}, \quad \varepsilon_e = E^{-1}(t) : \sigma, \\ d_e^{(5)} &= 1 - E_0^{-1} : E(t)\end{aligned}\quad (4.2-e)$$

Strictly speaking, path (5) is capable of capturing the features of path (2) if $d_e^{(5)}$ approaches $-\infty$. In this case $E(t) = (1 - d_e^{(5)}) E_0 = +\infty$, which is consistent to Fig. 4.1. Paths (3) and (4) are captured, as well, if $d_e^{(5)} = 0$ and $1 - E_0^{-1} : \sigma = \varepsilon^{-1}$, respectively. After all, it is important to underline that a particular solid is per se neither brittle nor ductile (contrary to the numerous models developed on these bases).

4.4 GENERALIZED DECOMPOSITION OF STRAIN TENSOR

The format split of the total strain tensor, ε , in the case of generalized damage for isothermal process into the "elastic-damage" and "plastic-damage" components is assumed at the outset (Ju, 1989a), i.e., (Fig. 4.2.a).

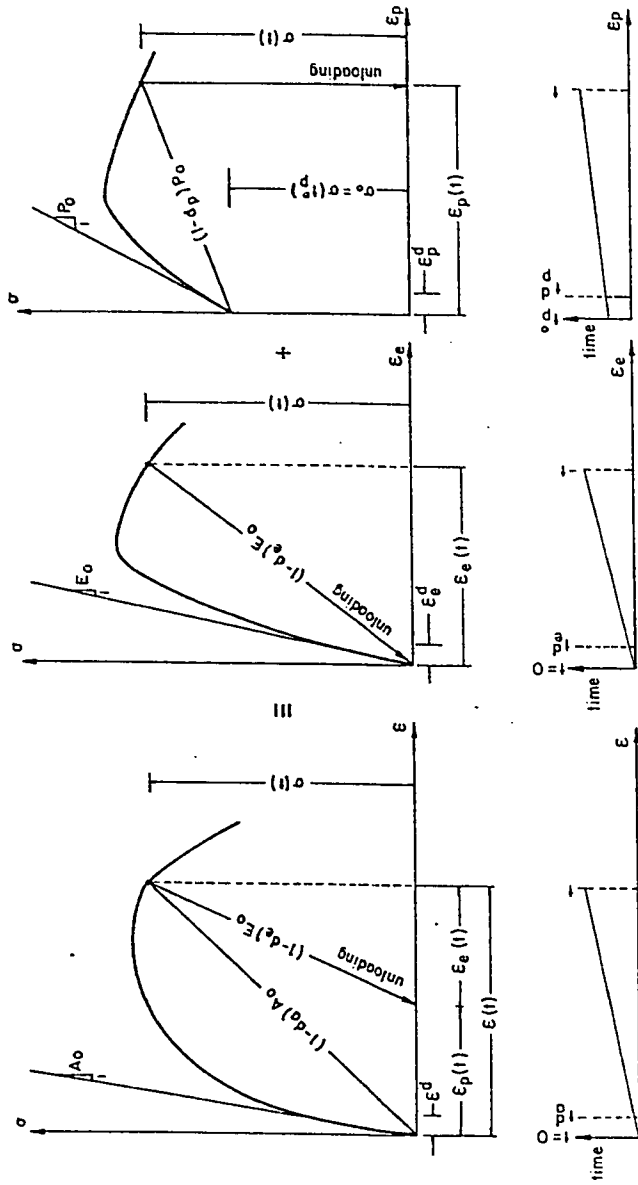


Figure 4.2 Generalized decomposition of the total strain

$$\varepsilon(t) = \varepsilon_e + \varepsilon_p \quad (4.3)$$

For this decomposition the stress tensor σ may be correlated to the total strain tensor and its components as follows:

$$\sigma(t) = A(t) : \varepsilon(t) = A(t) : (\varepsilon_e + \varepsilon_p) ; \quad (4.4-a)$$

$$\sigma(t) = E(t) : \varepsilon_e(t) , \text{ and} \quad (4.4-b)$$

$$\sigma(t) = \sigma_0 + P(t) : \varepsilon_p(t) \quad (4.4-c)$$

where A, E and P are fourth order tensors whose initial tangents are A_0 , E_0 and P_0 , respectively and σ_0 is the stress tensor at the onset of plastic deformations at time t_p^0 . Plots of Eqns. 4.4 are sketched in Fig. 4.2 in which A(t), E(t) and P(t) can be implemented as secant moduli that can be easily expressed in terms of their conjugate generalized, namely total elastic and plastic damage variables d_a , d_e and d_p , respectively given in (4.1), i.e.

$$A(t) = (1-d_a(t)) A_0 \quad (4.5-a)$$

$$E(t) = (1-d_e(t)) E_0 \quad (4.5-b)$$

$$P(t) = (1-d_p(t)) P_0 \quad (4.5-c)$$

Unloading in Fig. 4.2.a follows the generalized damaged path (path 5) with slope E(t), while in Figs. 4.2.b and 4.2.c follows "quasi sub-brittle" (path 4) and "quasi sub-perfect plastic" (path 2) schemes, respectively. For a general behavior, attention should be paid to some solicitations:

1. Elastic damage may only appear beyond a certain threshold limit; i.e. time t_e^d associated with $d_e, t_e^d \geq 0$. The elastic damage threshold was reported by many investigators (Lemaitre, 1984a, 1985, 1986a; Mazars, 1980, 1984a, 1986a; Simo and Ju, 1987a,b; Ju, 1989). Ju (1989) used the term "energy barrier" before any loading is applied for this threshold. By contrast, Krajcinovic and Fonseka (1981) and Loland (1981) took the notion, for concrete, of initial damage due to inherent flaws or cracks due to nonhomogeneous shrinkage during curing.
2. Initiation of plastic deformation may take place simultaneously with loading application, i.e., $t_p^0 \geq 0$. Thus, existence of σ_0 , which represents a yield limit, is doubtful and in this case $\sigma_0 = 0$ for $t_p^0 = 0$, hence $A_0 \neq E_0$. This can be observed from the behavior of many materials (e.g., concrete). This is contradictory to Newman's (1964) discontinuity postulate and the computational models on this basis (for example Owen et al., 1983).
3. Plastic damage may start as early as plastic deformation takes place, i.e. $t_p^d \geq t_p^0$. Lack of experimental evidence, till now, leads further to unreliability of any assumption that plastic deformation onset follows elastic damage ($t_p^0 \geq t_e^d$). However, Simo and Ju (1987a,b), Ju (1989a) used effective stress-quantities based on elastic damage variable in their formulations assuming that plastic deformation is subsequent to damage.

4. Elastic and plastic damage variables are independent in the sense that they need not evolve at the same time or by the same rate. Therefore, the Helmholtz (total) free energy, ψ , cannot be simply partitioned using a single damage parameter, i.e.

$$\psi(\epsilon^e, q, d) \neq (1-d)\psi^0(\epsilon^e, q) \neq (1-d)(\psi_e^0(\epsilon^e) + \psi_p^0(q)) \quad (4.6)$$

as postulated by Ju (1989a); in Eqn. (4.6) q, d denote a suitable set of plastic variables and damage variable. $\psi(\epsilon^e, q, d)$ is a locally averaged (homogenized) free energy function of damaged material, $\psi^0(\epsilon^e, q)$ signifies the total potential energy function of an undamaged (virgin) material. $\psi_e^0(\epsilon^e)$ and $\psi_p^0(q)$ are the uncoupled elastic and plastic potential energy functions, respectively. Partitioning of this sort is valid only if ϵ^e and q are related to the stress vector, σ , by the same modulus as given in Eqn. (4.4-a). The proper expression of the Helmholtz functional as a weighted function should be

$$\psi(\epsilon^e, q, d_e, d_p) \equiv (1-d_e)\psi_e^0(\epsilon^e) + (1-d_q)\psi_p^0(q) \quad (4.7)$$

in which d_q is the conjugate damage variable to q .

5. $d_p = 0$ for linear hardening and $d_e = 0$ for linear elasticity.
6. The alternative to consideration of damage in formulations is to use a pre-defined law accounting for nonlinearity, e.g., Ramberg-Osgood law replaces plastic damage (Eqn. 4.4.b).

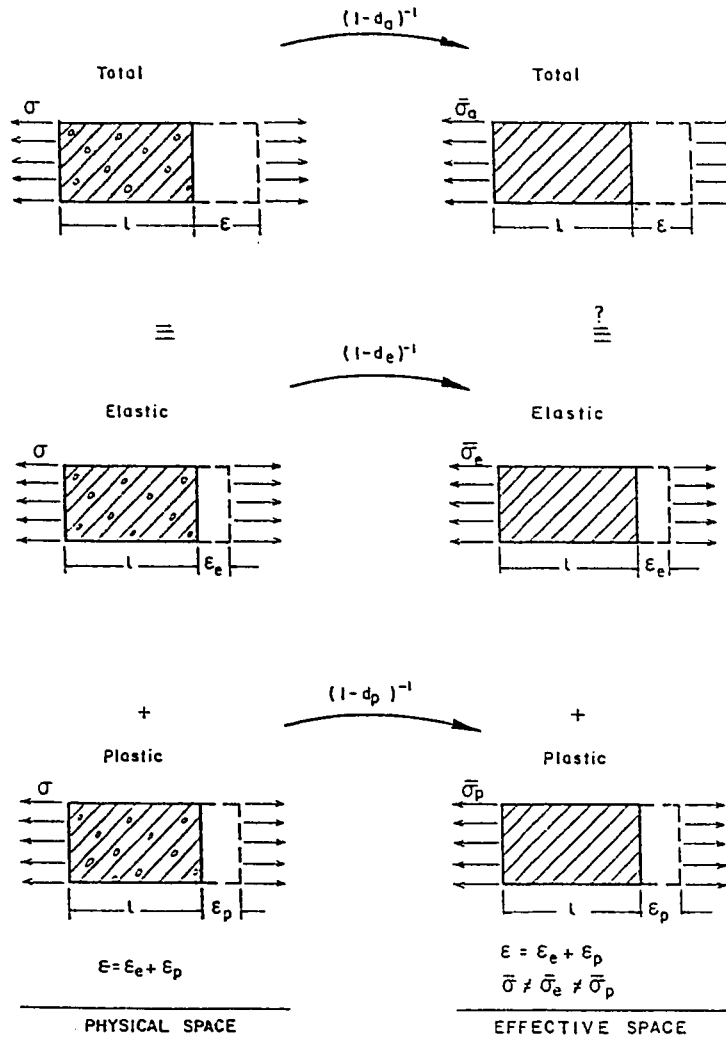


Figure 4.3 Generalized effective stress concept

4.5 GENERALIZED EFFECTIVE STRESSES CONCEPT

Based on the hypothesis of strain equivalence introduced by Lemaitre (1971): "The strain associated with a damage state under the applied stress is equivalent to the strain associated with its undamaged state under the applied the effective stress". Thus, substituting from Eqns. (4.5) to Eqns. (4.4) the strain equivalence can be expressed as follows:

$$\epsilon = A_0^{-1} : \frac{\sigma}{1-d_a} = A_0^{-1} : \bar{\sigma} \quad , \quad \bar{\sigma} = \frac{\sigma}{1-d_a} \quad (4.8-a)$$

$$\epsilon_o = E_0^{-1} : \frac{\sigma}{1-d_e} = E_0^{-1} : \bar{\sigma}_e \quad , \quad \bar{\sigma}_e = \frac{\sigma}{1-d_e} \quad (4.8-b)$$

$$\epsilon_p = P_0^{-1} : \frac{\sigma - \sigma_o}{1-d_p} = P_0^{-1} : (\bar{\sigma}_p - \bar{\sigma}_o) \quad , \quad \bar{\sigma}_p = \frac{\sigma}{1-d_p} \quad , \quad \bar{\sigma}_o = \frac{\sigma_o}{1-d_p} \quad (4.8-c)$$

in which $\bar{\sigma}$, $\bar{\sigma}_e$, $\bar{\sigma}_p$ and $\bar{\sigma}_o$ are the total, elastic, plastic and initial plastic effective stresses, respectively. Fig. 4.3 shows the equivalence of total strain and its components. It has to be figured out that for an element, of normal n subjected to force F , its effective area, \bar{S} , can be expressed in terms of the total area, S , through the total damage variable, d_a , i.e.,

$$\bar{S} = S(1-d_a) \quad (4.9)$$

and the effective traction vector \bar{T} ($\bar{T} = \bar{\sigma} \cdot n$) is related to the total traction vector T ($T = \sigma \cdot n$) by the same damage variable

$$\bar{T} = \frac{F}{\bar{S}} = \frac{F}{S(1-d_a)} = \frac{T}{1-d_a} \quad (4.10)$$

Eqns. 4.9 and 4.10 are reconciled with the effective stress concept originated by Rabotnov (1968). Consequently, Eqn. (8-a) is sufficient for constitutive relations formulation. On the other hand, for ductile unloading path; $d_e = 0$; $\sigma = \sigma_e = \bar{\sigma}_e \neq \bar{\sigma}$; A_o need not be equal to E_o , uniqueness is lost. If $A_o = E_o$, then $\epsilon_p = \epsilon - \epsilon_e = A_o^{-1} : \sigma(1/(1-d_a)-1) = A_o^{-1} : \sigma(d_a/(1-d_a)) = d_a A_o^{-1} : \bar{\sigma}$, thus $\bar{\sigma} = A_o (p_o^{-1} : \bar{\sigma}_p)/d_a = \sigma/(1-d_a)$; therefore uniqueness is achieved since $\bar{\sigma}$ is related to $\bar{\sigma}_p$. A very important special case arises when $d_a = d_e = d_p = d$, thus leading definitely to a unique effective stress $\bar{\sigma} = \bar{\sigma}_e = \bar{\sigma}_p = \sigma/(1-d)$ and Ju's formulation (1989a) is recovered. However, for full representation of both the stress and strain histories, only two relations out of Eqns. (4.8) are sufficient. This is achieved by using Eqns. (4.8) in (4.3), yields requirement of at least two damage variables, say, d_e and d_a , since

$$\begin{aligned} \bar{\sigma} &= \frac{\sigma}{1-d_a} = A_o : \left[\left[\frac{E_o^{-1}}{1-d_e} + \frac{p_o^{-1}}{1-d_p} \right] : \sigma \right] - A_o : \left[\frac{p_o^{-1}}{1-d_p} : \sigma_o \right] \\ &= A_o : \left[E_o^{-1} : \bar{\sigma}_e + p_o^{-1} : (\bar{\sigma}_p - \bar{\sigma}_o) \right] \end{aligned} \quad (4.11)$$

In other words, elasto-plastic damage follows constraint uncoupling.

4.6 DEMONSTRATION OF ELASTO-PLASTIC DAMAGE UNCOUPLING

Inasmuch as concrete experiences all kinds of irreversible changes, its behavior in uniaxial compression will be investigated in addition to Copper 99.9% as a ductile material. This demonstration will elucidate the adopted generalized concepts and link theory to practice.

4.6.1 Concrete

Two well established correlative equations were proposed in the past from experimental evidences:

1. A stress-total strain (σ - ϵ) relation by Popovics (1973)

$$\left(\frac{\sigma}{f'_c} \right) = \frac{n_o \left(\frac{\epsilon}{\epsilon_c} \right)}{n_o - 1 + \left(\frac{\epsilon}{\epsilon_c} \right)^2} \quad (4.12)$$

where n_o is a material property depending on the peak stress f'_c and ϵ_c is peak strain. Adopting a value of $n = 2$ for $f'_c = 17.2$ MPa (2500 psi), Eqn. (4.12) becomes (Fig. 4.4),

$$\left(\frac{\sigma}{f'_c} \right) = \frac{2 \left(\frac{\epsilon}{\epsilon_c} \right)}{1 + \left(\frac{\epsilon}{\epsilon_c} \right)^2} \quad (4.13)$$

2. A plastic-total strain (ϵ_p - ϵ) relation by Karsan & Jirsa (1969)

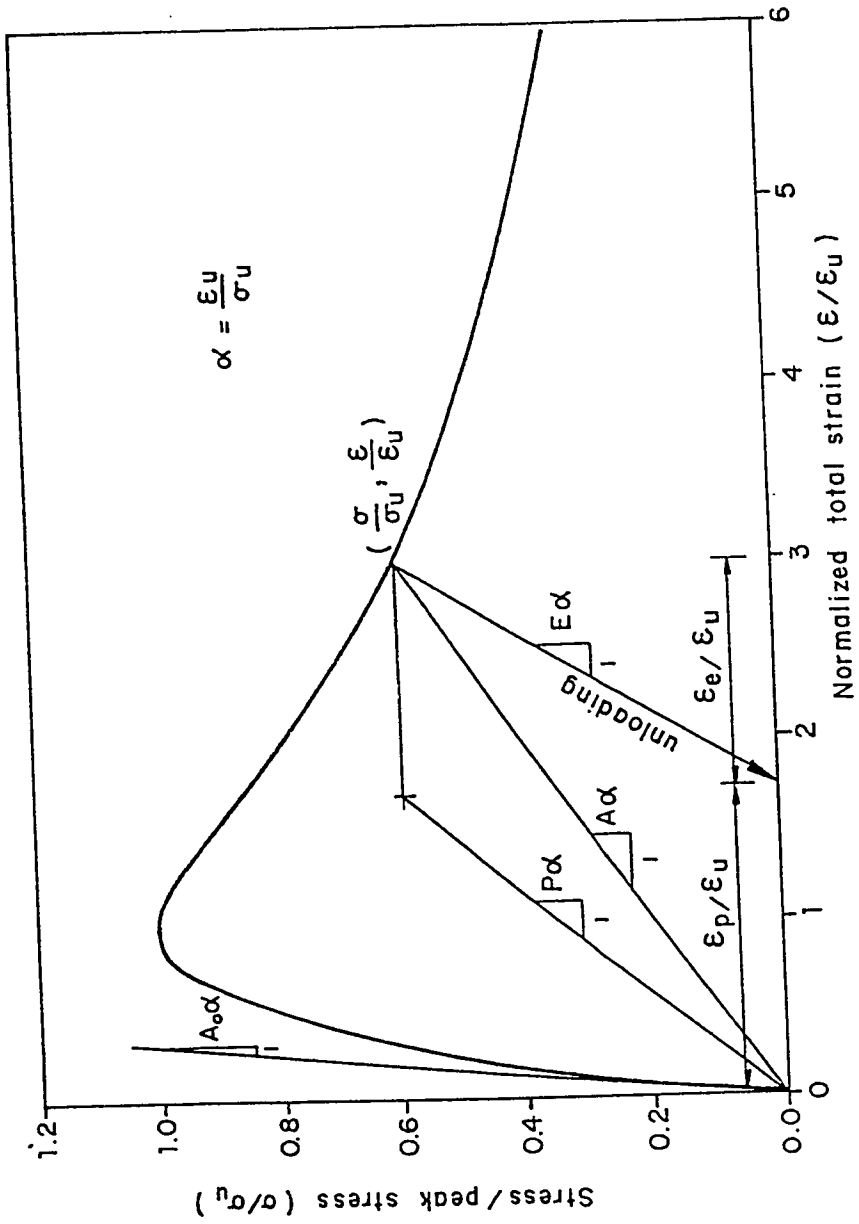


Figure 4.4 Idealized stress-total strain relationship for concrete under uniaxial compression

$$\left(\frac{\epsilon_p}{\epsilon_c}\right) = 0.145 \left(\frac{\epsilon}{\epsilon_c}\right)^2 + 0.127 \left(\frac{\epsilon}{\epsilon_c}\right) \quad (4.14)$$

Exploiting the same notations aforementioned in arts. 4.5 and 4.6, the moduli and damage variable conjugate to the total strain are

$$A_0 = \left(\frac{d\sigma}{d\epsilon}\right)_{\epsilon=0} = \left(\frac{\partial \left(\frac{\sigma}{f_c'}\right)}{\partial \left(\frac{\epsilon}{\epsilon_c}\right)}\right)_{\epsilon=0} \frac{f_c'}{\epsilon_c} = \frac{2f_c'}{\epsilon_c} \quad (4.15-a)$$

$$\begin{aligned} A(\epsilon) &= \frac{\sigma}{\epsilon} = A_0 \frac{\sigma}{\epsilon} * \frac{\epsilon_c}{2f_c'} = \frac{1}{2} A_0 \frac{\left(\frac{\sigma}{f_c'}\right)}{\left(\frac{\epsilon}{\epsilon_c}\right)} \\ &= \frac{1}{2} A_0 \frac{2}{1 + \left(\frac{\epsilon}{\epsilon_c}\right)^2} = \frac{A_0}{1 + \left(\frac{\epsilon}{\epsilon_c}\right)^2} \end{aligned} \quad (4.15-b)$$

and

$$d_a = 1 - \frac{A(\epsilon)}{A_0} = 1 - \frac{1}{A_0} \frac{A_0}{1 + \left(\frac{\epsilon}{\epsilon_c}\right)^2} = \frac{\left(\frac{\epsilon}{\epsilon_c}\right)^2}{1 + \left(\frac{\epsilon}{\epsilon_c}\right)^2} = \frac{1}{2} \left(\frac{\sigma}{f_c'}\right) \left(\frac{\epsilon}{\epsilon_c}\right) \quad (4.15-c)$$

The elastic strain component can be calculated using Eqns. (4.3) and (4.14), thus gives (Fig. 4.5)

$$\left(\frac{\epsilon_e}{\epsilon_c}\right) = \left(\frac{\epsilon}{\epsilon_c}\right) - \left(\frac{\epsilon_p}{\epsilon_c}\right) = 0.87 \left(\frac{\epsilon}{\epsilon_c}\right) - 0.145 \left(\frac{\epsilon}{\epsilon_c}\right)^2 \quad (4.16)$$

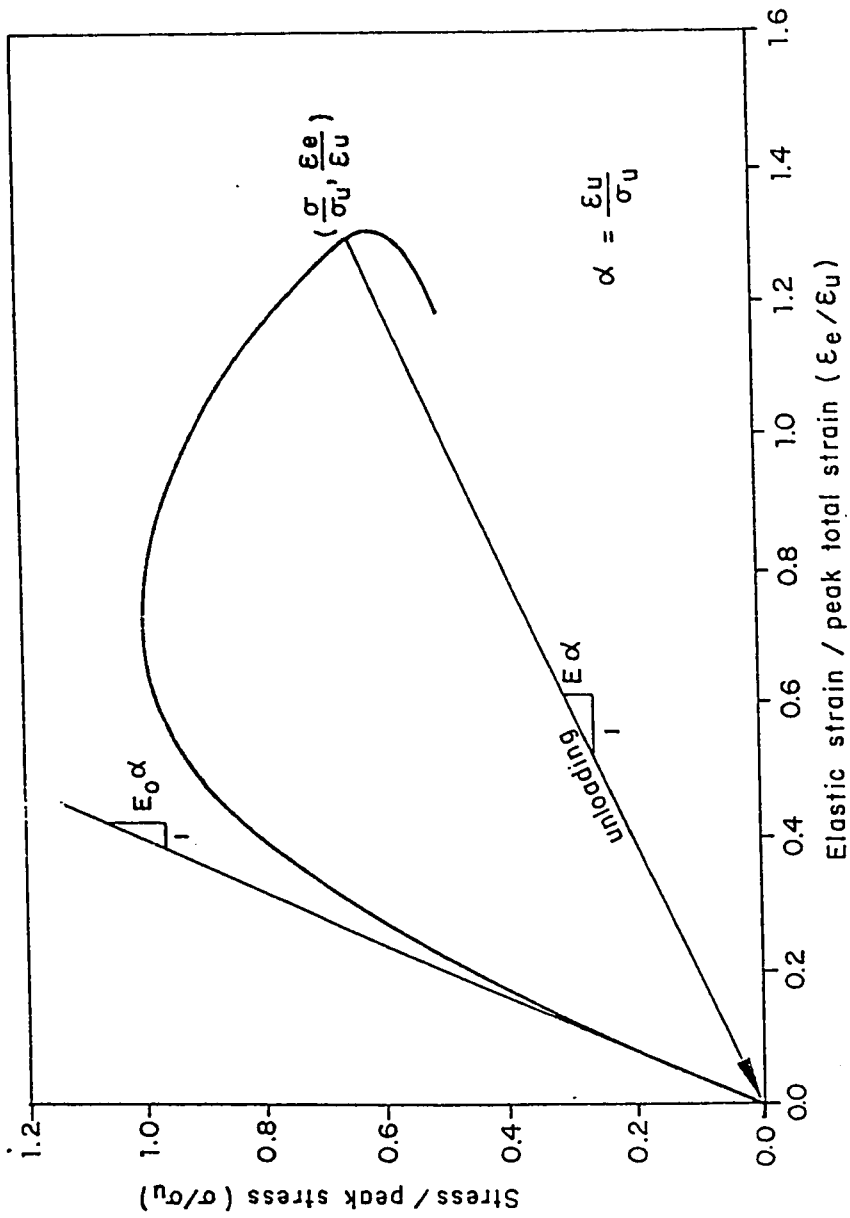


Figure 4.5 Idealized stress-elastic strain relationship for concrete under uniaxial compression

The moduli and damage variable conjugate to the elastic strain component are

$$E_0 = \left(\frac{d\sigma}{d\varepsilon_e} \right)_{\varepsilon_e=0} = \frac{\left(\frac{\partial \left(\frac{\sigma}{f_c'} \right) / \partial \left(\frac{\varepsilon}{\varepsilon_c} \right) \right)}{\left(\frac{\partial \left(\frac{\varepsilon_e}{\varepsilon_c} \right) / \partial \left(\frac{\varepsilon}{\varepsilon_c} \right) \right)_{\varepsilon=\varepsilon_e=0}} * \frac{f_c'}{\varepsilon_c}$$

$$= \frac{2}{0.873} * \frac{A_0}{2} = 1.15 A_0 \quad (4.17-a)$$

$$E(\varepsilon) = \frac{\sigma}{\varepsilon_e} = \frac{2}{\left[1 + \left(\frac{\varepsilon}{\varepsilon_c} \right)^2 \right] \left[0.873 - 0.145 \left(\frac{\varepsilon}{\varepsilon_c} \right) \right]} * \frac{f_c'}{\varepsilon_c}$$

$$= \frac{A_0}{\left[1 + \left(\frac{\varepsilon}{\varepsilon_c} \right)^2 \right] \left[0.873 - 0.145 \left(\frac{\varepsilon}{\varepsilon_c} \right) \right]} \quad (4.17-b)$$

and

$$d_e = 1 - \frac{E(\varepsilon)}{E_0} = 1 - \frac{0.873}{\left[1 + \left(\frac{\varepsilon}{\varepsilon_c} \right)^2 \right] \left[0.873 - 0.145 \left(\frac{\varepsilon}{\varepsilon_c} \right) \right]} \quad (4.17-c)$$

Eqn. (4.17-a) remarks the important evidence that $E_0 \neq A_0$. The assumption of their equality is common in the literature where A_0 is considered as the elastic (Young's) modulus (even in its nomenclature, A_0 is termed, incorrectly, E_0 in the literature). However, based on some assumptions it will be shown later that this is not completely wrong for $n_0 = 2$.

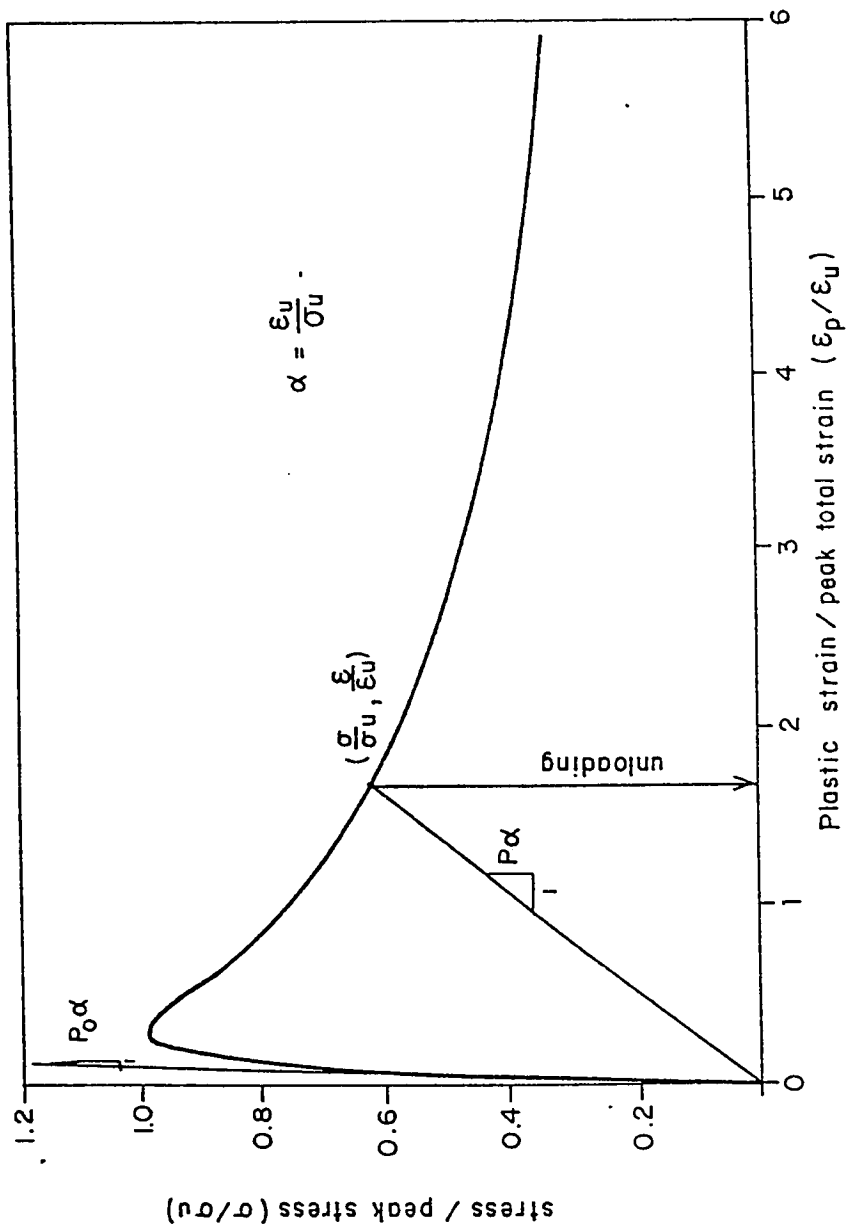


Figure 4.6 Idealized stress-plastic strain relationship for concrete under uniaxial compression

Similarly, the moduli and damage variable conjugate to the plastic strain component (Fig. 4.6) are

$$P_o = \left(\frac{d\sigma}{d\varepsilon_p} \right)_{\varepsilon_p=0} = \left(\frac{\partial \left(\frac{\sigma}{f_c'} \right) / \partial \left(\frac{\varepsilon}{\varepsilon_c} \right)}{\partial \left(\frac{\varepsilon_p}{\varepsilon_c} \right) / \partial \left(\frac{\varepsilon}{\varepsilon_c} \right)} \right)_{\varepsilon=\varepsilon_e=0} * \frac{f_c'}{\varepsilon_c}$$

$$= \frac{2}{0.127} * \frac{A_o}{2} = 7.87 A_o \quad (4.18-a)$$

$$P(\varepsilon) = \frac{\sigma}{\varepsilon_p} = \frac{A_o}{\left[1 + \left(\frac{\varepsilon}{\varepsilon_c} \right)^2 \right] \left[0.127 + 0.145 \left(\frac{\varepsilon}{\varepsilon_c} \right) \right]} \quad (4.18-b)$$

and

$$d_p = 1 - \frac{P(\varepsilon)}{P_o} = 1 - \frac{0.127}{\left[1 + \left(\frac{\varepsilon}{\varepsilon_c} \right)^2 \right] \left[0.127 - 0.145 \left(\frac{\varepsilon}{\varepsilon_c} \right) \right]} \quad (4.18-c)$$

Examination of the pre-derived relations reveals the following:

1. Onset of plastic deformations starts simultaneously with load application. This conclusion is in accord with, for instance, Spooner and Dougill (1975).
2. Elastic strain contribution to the total strain starts at a higher rate than the plastic strain. Equal share takes place at a total strain ratio $(\varepsilon/\varepsilon_c)$ equal to 2.552 corresponding to stress ratio (σ/f_c') of 0.679, after which the plastic strain contribution gets higher than the elastic strain. The maximum elastic strain ratio

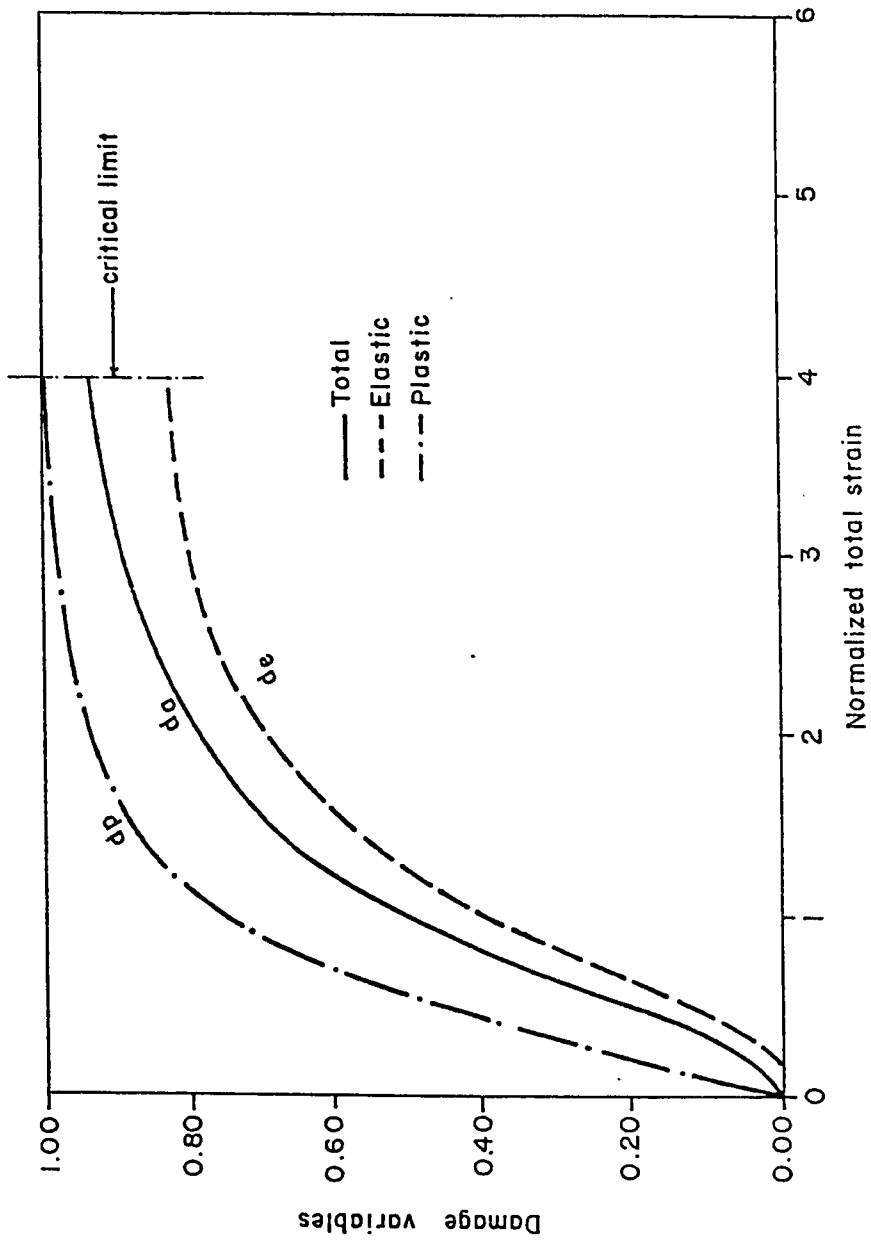


Figure 4.7 Evolution of generalized damage variables for concrete under uniaxial compression

(ϵ_c/ϵ_c) is 1.305 at which $(\epsilon/\epsilon_c) = 3$ and $(\sigma/f_c') = 0.6$. After this value of strain ratio the elastic strain decreases. This is the reason for the retrogression appearing in Fig. 4.5. In contrast, the plastic strain keeps on increasing until the total strain is irrecoverable. Mathematically speaking, this occurs at $\epsilon/\epsilon_c = 6$, $\sigma/f_c' = 0.324$ but physically damage will be considered at lower value as will be shown later.

3. The total damage variable, d_a , is a continuous function and its limit as $(\epsilon/\epsilon_c \rightarrow \infty)$ yields unity while its value @ $\epsilon/\epsilon_c = 6$ is 0.973. The trend of d_a along with d_e and d_p is shown in Fig. 4.7.
4. The elastic damage variable, d_e , is a singular function at $\epsilon/\epsilon_c = 6$, but it is continuous in the domain $\epsilon/\epsilon_c \in [0,6]$ though it has an inflection point at $(\epsilon/\epsilon_c) = 3.915$. At this value of the strain ratio, the elastic damage parameter is critical since it should be a nondecreasing and its value d_{e_c} is 0.824. The corresponding other parameters are: $\epsilon_e/\epsilon_c = 1.184$, $\epsilon_p/\epsilon_c = 2.731$, $\sigma/f_c' = 0.048$, $d_a = 0.939$ and $d_p = 0.989$. Practically, these values may be considered critical values for complete damage. Moreover, a threshold total strain ratio $\epsilon/\epsilon_c = 0.175$ is associated with d_e at which $\sigma/f_c' = 0.34$; $\epsilon_e/\epsilon_c = 0.148$, $\epsilon_p/\epsilon_c = 0.03$, $d_a = 0.03$ and $d_p = 0.188$. At this stress level the plastic strain is negligible and the total damage variable as well. This gives physical reasoning to the good results obtained, in this region, from elastoplastic

computational models assuming linear elastic for stress ratios less than 0.3 (e.g. Owen et al., 1983). In this case, E_0 may be reduced to A_0 . However, this will not violate the aforedefined generalized concepts. It has to be pointed out that elastic damage threshold is much less than the peak and is more closer to the origin.

5. The plastic damage variable, d_p , is a continuous function and follows asymptotic trend; $\lim_{\epsilon \rightarrow \infty} d_p = 1.0$. It grows at much higher rate than both d_a and d_e . This indicates that: a) damage causes more degradation in the plastic stiffness than both the elastic and overall stiffness of concrete; b) onset of plastic damage commences prior to elastic damage and c) linear hardening or perfect plasticity are inappropriate approximations for elasto-plasticity as applied to concrete.
6. Intuitively postulating the damage variables' evolution as exponentially growing functions in modelling lacks confidence concerning threshold and critical values. Also the trends may deviate from the correct ones.

4.6.2 Copper 99.9%

Complete set of experimental data was provided by Lemaitre (1984a, 1985, 1992). It is very ductile material and shows elongation almost equal to its original length at rupture. The elastic strain is negligible when compared to the plastic or total strain. Fig. 4.8 shows the stress-total strain relationship which can be decomposed to stress-

elastic and stress-plastic strain relationships as shown in Figs. 4.9 and 4.10. Original data fitting using Ramberg Osgood hardening law of the form $\sigma = k\epsilon_p^{1/M}$ (where k and M are coefficients) gives poor correlation and blurs any computational modelling. But if the law used in the form $\sigma = \sigma_0 + k\epsilon_p^{1/M}$ it will give good fitting but not better than a cubic polynomial. This note on regression is appreciated when revising Lemaitre's model (1985). Fig. 4.11 shows the evolution of the three damage variables d_a , d_e and d_p associated with the total, elastic and plastic stiffness degradation, respectively. The following implications can be conducted:

1. The total damage variable is zero up to yield (very small domain) then abruptly increase then evolve asymptotically to unity.
2. The plastic damage variable threshold is intermediate between thresholds of other damage variables.
3. The elastic damage variable evolution may be approximated by linear relation as given by Lemaitre (1985, 1986a, 1992).
4. At high values of strain, near rupture, the elastic stiffness degrades more than the plastic stiffness. This is signed by the higher evolution of the elastic damage variable at later stages.
5. Unlike concrete, the total damage variable is not intermediate to other damage variables. This is attributed to the fact that the initial total slope A_0 is very high compared with E_0

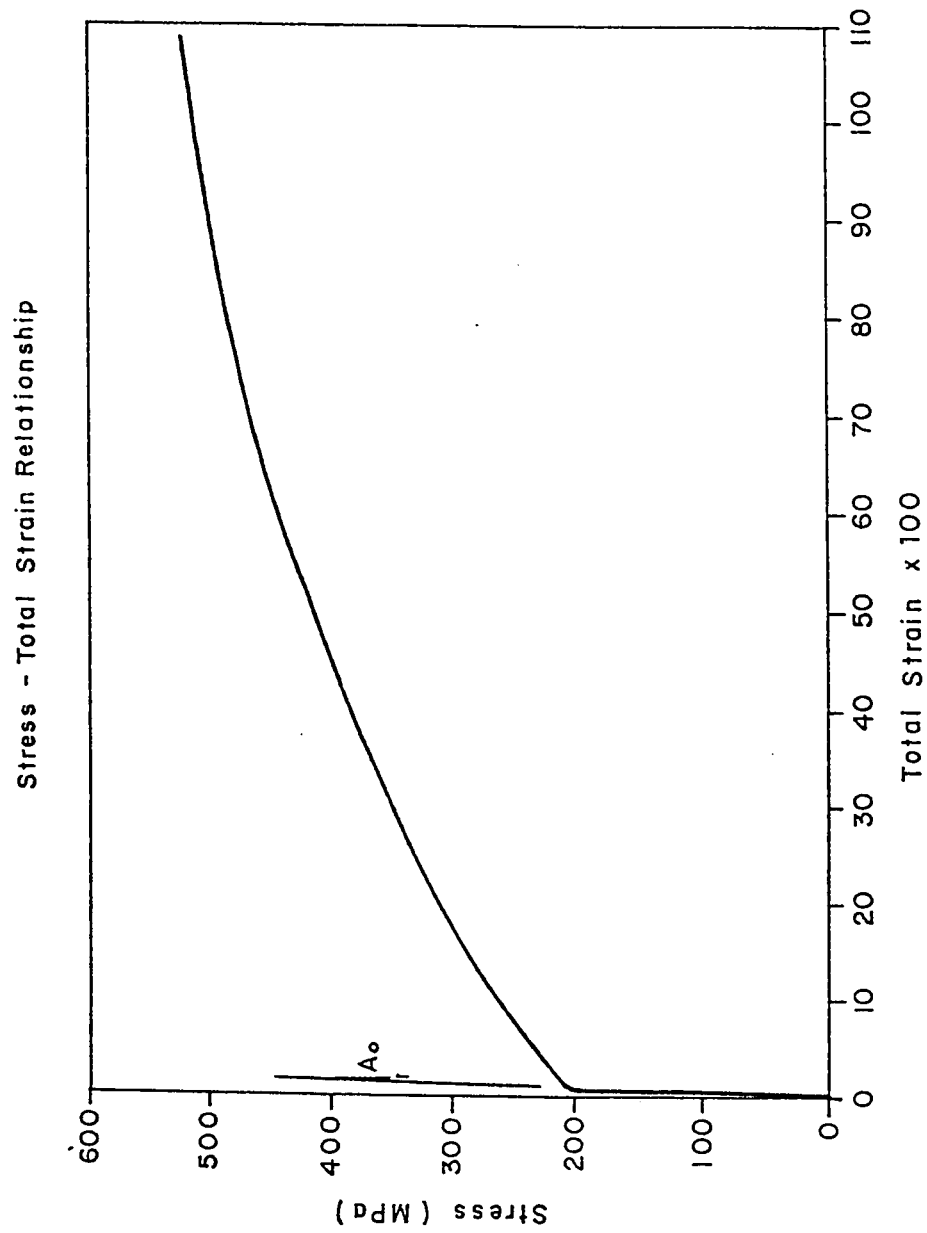


Figure 4.8 Experimental stress-total strain relationship for copper 99.9% under uniaxial tension (after J. Lemaitre, 1985)

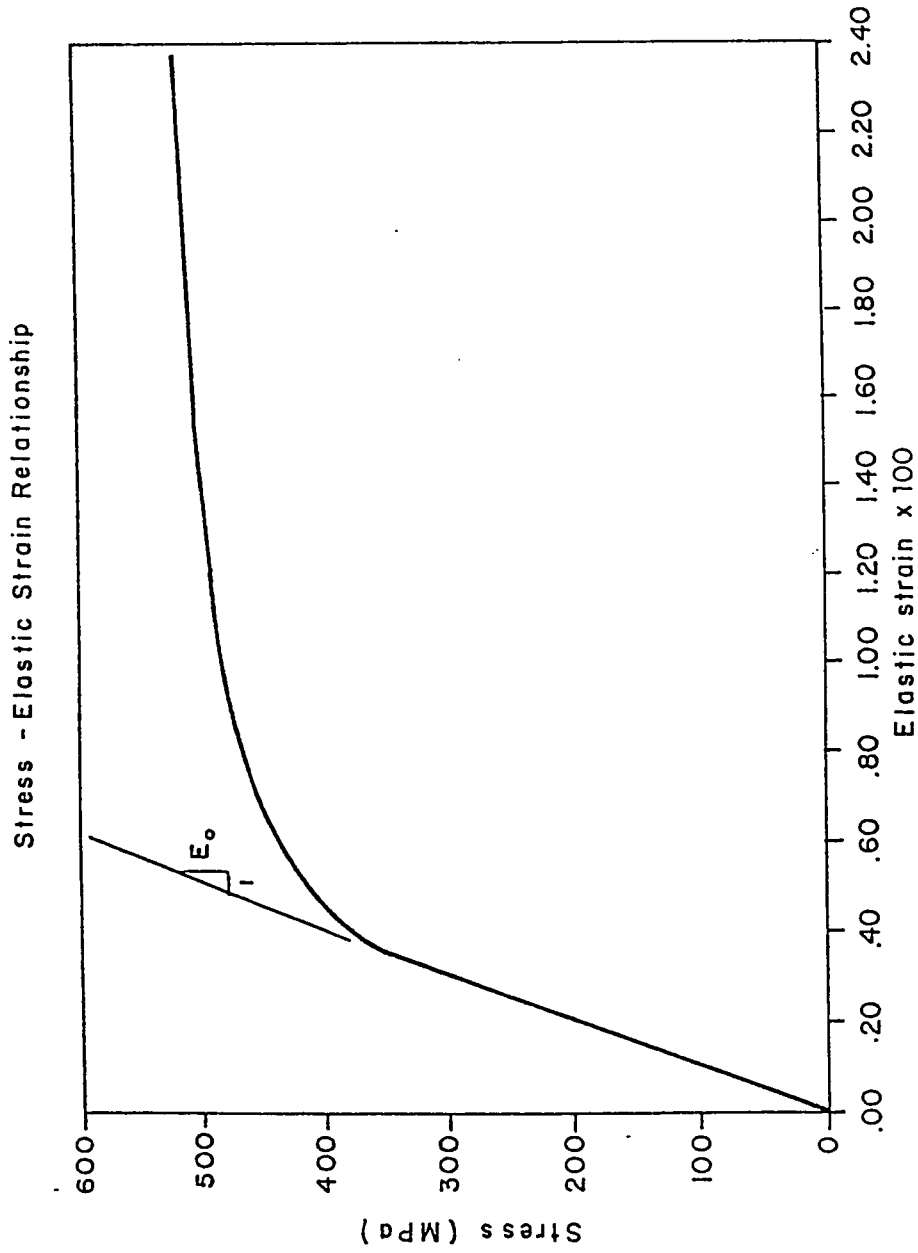


Figure 4.9 Stress-elastic strain for copper 99.9% under uniaxial tension

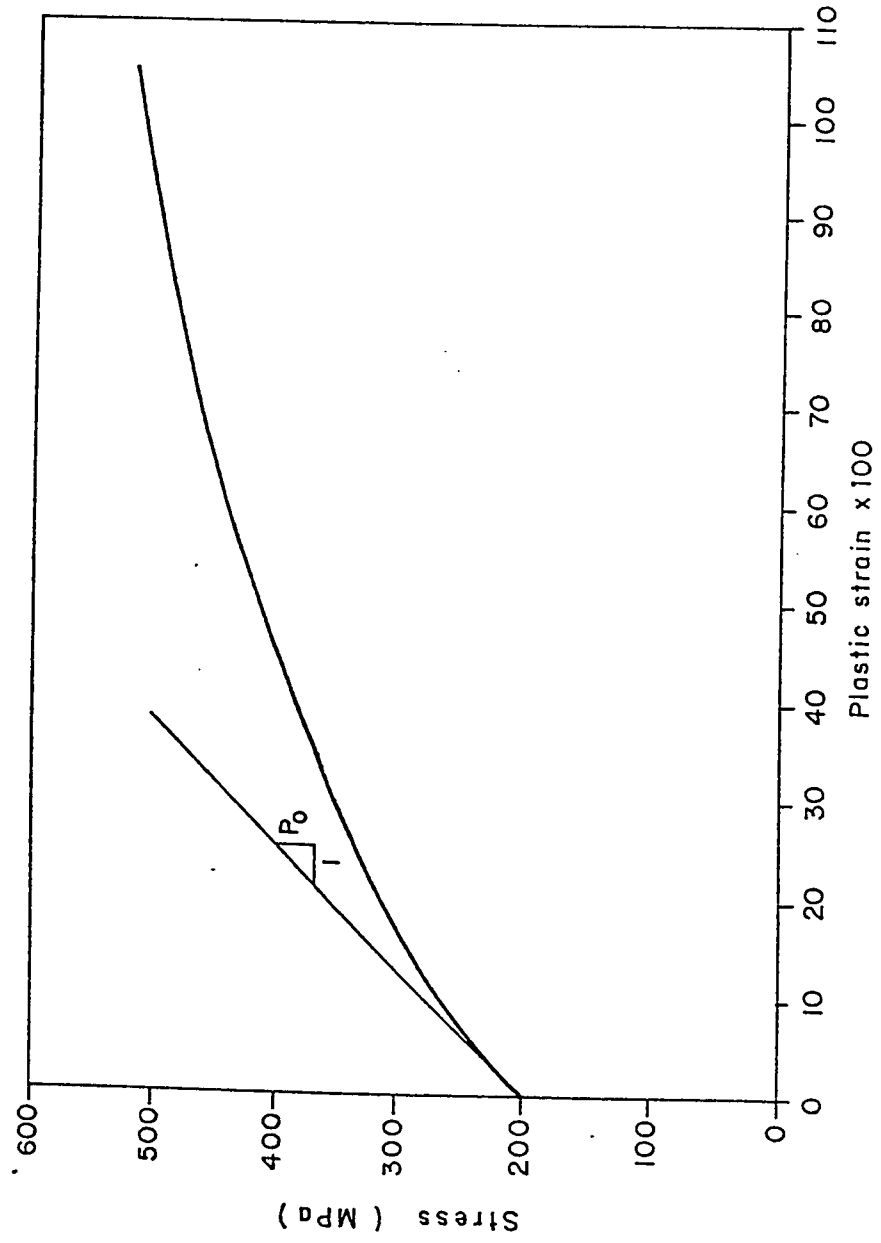


Figure 4.10 Stress-plastic strain for copper 99.9% under uniaxial tension

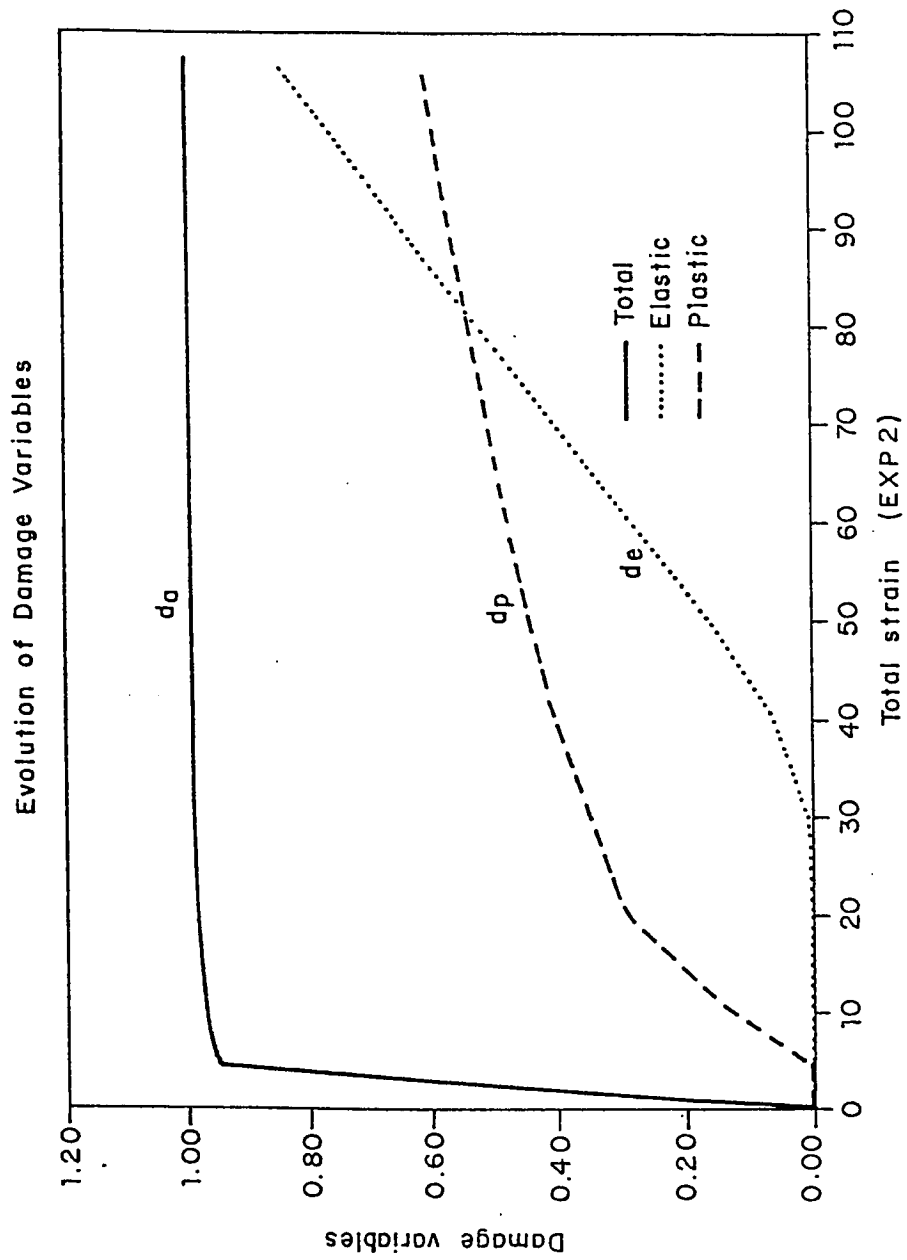


Figure 4.11 Evolution of generalized damage variables for copper 99.9% under uniaxial tension

and P_0 (almost vertical). This is observed in Fig. 4.8 in comparison with Figs. 4.9 and 4.10.

4.7 ON LEMAITRE'S DUCTILE DAMAGE MODEL

Ju (1989a) criticized Lemaitre's ductile damage model and stated: "The fundamental problem of the ductile plastic damage formulation advocated by Lemaitre (1985) is the non-optional choice of the locally averaged free energy potential. In particular, damage is associated only with elastic strains and the damage energy release rate is shown to be the elastic strain energy in Lemaitre (1985). This treatment amounts to uncoupled plasticity and damage processes, thus in a sense contradicting experimental evidence that plastic variables also contribute to the initiation and growth of microcracks".

In Lemaitre's (1985) formulation, he did consider the following:

1. The Von Mises equivalent stress for plasticity $\sigma_{eq} = \left(\frac{3}{2} S:S\right)^{1/2}$; S is the deviatoric stress tensor.
2. Ramberg-Osgood hardening law $\sigma_{eq} = kp^{1/M}$, $p = \left(\frac{2}{3} \epsilon^P:\epsilon^P\right)^{1/2}$; k and M being material parameters; p the equivalent strain and ϵ^P is the Euler-Almansi plastic strain tensor in large deformation theory.
3. Postulated a potential of dissipation φ^* .
4. Took into account only the elastic damage as the degradation in the elastic (Young's) modulus E , i.e. D in Lemaitre's (1985) is simply d_e in this study. Therefore it contributes only to elastic

behavior.

5. Only one damage process, which is the elastic damage.

He 'correctly' derived the following rate equation

$$\dot{d}_e = \dot{p} \left\{ \frac{\sigma_{eq}^2}{2ES_0(1-d_e)^2} \left[\frac{2}{3}(1+\nu) + 3(1-2\nu) \left(\frac{\sigma_H}{\sigma_{eq}} \right)^2 \right] \right\}^{s_0} \quad (4.19)$$

where ν is Poisson's ratio, σ_H is the mean hydrostatic pressure; $\sigma_H = \frac{1}{3}\text{tr}(\sigma)$. S_0 and s_0 are temperature and material dependent parameters.

($\dot{}$) implies derivative with respect to time.

Now, the hardening law should be used in its form as written before in the Ramberg-Osgood law. WHY?! The elastic damage parameter, d_e , is: a) conjugated to the elastic processes and appears only in the elastic free energy, b) it is found experimentally from degradation of Young's modulus, c) effective stress is not unique in elastic-damage plastic as declared previously. This leads that damage evolution is given by

$$\dot{d}_e = \dot{p} \left\{ \frac{k^2}{2ES_0(1-d_e)^2} \left[\frac{2}{3}(1+\nu) + 3(1-2\nu) \left(\frac{\sigma_H}{\sigma_{eq}} \right)^2 \right] p^{2/M} \right\}^{s_0} \quad (4.20)$$

Equation (4.20) is different from that of Lemaitre by the term $(1-d_e)^2$

appearing in the denominator on the right hand side. Integration of Eqn. (4.20) for proportional loading or even uniaxial cases will yield nonlinear expression for d_e which should be linear as shown by Lemaitre (1985) from experiments. This proves that his assumed potential of dissipation ϕ^* is questionable.

4.8 DECOUPLED FREE ENERGY TERMS

Based on the generalized decomposition, the stress tensor can be related to the total strain and the strain components by three alternative equations in analogy to the generalized Hooke's law as follows

$$\sigma_{ij} = A_{ijkl} \epsilon_{kl} \quad (4.21)$$

$$= E_{ijkl} \epsilon_{kl}^e \quad (4.22)$$

$$= P_{ijkl} \epsilon_{kl}^p \quad (4.23)$$

in which A_{ijkl} , E_{ijkl} and P_{ijkl} are fourth order moduli tensors representing total, elastic-damage and plastic-damage behaviors whose initial values are A_{ijkl}^0 , E_{ijkl}^0 and P_{ijkl}^0 , respectively. The degradation of these moduli can be expressed in terms of three distinct fourth order damage tensors D_{ijkl}^a , D_{ijkl}^e and D_{ijkl}^p in association with the total, elastic-damage and plastic-damage moduli;

$$D_{ijkl}^a = I_{ijkl} - A_{ijuv} A_{o_{uvkm}}^{-1} \quad (4.24)$$

$$D_{ijkl}^e = I_{ijkl} - E_{ijuv} E_{o_{uvkm}}^{-1} \quad (4.25)$$

$$D_{ijkl}^p = I_{ijkl} - P_{ijuv} P_{o_{uvkm}}^{-1} \quad (4.26)$$

in which I_{ijkl} is the fourth order unit tensor. Symmetry, invertibility and the other properties of the damage effect tensor discussed by Cordebois and Sidoroff (1979) and Murakami (1989) are assumed to be satisfied. The free energy density U^d that incorporates damage, can be expressed as

$$U^d = \frac{1}{2} \sigma_{ij} \epsilon_{ij} \quad (4.27-a)$$

$$= \frac{1}{2} \sigma_{ij} (\epsilon_{ij}^e + \epsilon_{ij}^p) \quad (4.27-b)$$

$$= \frac{1}{2} \sigma_{ij} \epsilon_{ij}^e + \frac{1}{2} \sigma_{ij} \epsilon_{ij}^p \quad (4.27-c)$$

Thus the Helmholtz total free energy is, excluding the temperature-entropy and cracks surface energy terms, $\psi = \psi^d + \psi^p$. Apart from the damage independent plastic energy ψ^p , eqn. (4.27-a) can be expanded to provide the damage energy $\psi^d(x, d_a)$ as

$$\rho \psi^d = \frac{1}{2} (I_{ijuv} - D_{ijuv}^a) A_{o_{uvkm}} \epsilon_{km} \epsilon_{ij} \quad (4.28)$$

in which ρ is the mass density. Substituting for the total strain in terms of the generalized strain split, Eqn. (4.28) reduces to

$$\rho \psi^d = \frac{1}{2} (I_{ijkl} - D_{ijkl}^a) A_{0uvkm} \left[\epsilon_{km}^e \epsilon_{ij}^e + 2\epsilon_{km}^e \epsilon_{ij}^p + \epsilon_{km}^p \epsilon_{ij}^p \right] \quad (4.29)$$

The middle term in the last bracket on the right-hand side shows the interaction between the elastic damage and the plastic damage energies, which would be ignored if only one set of damage variables (D_{ijkl}^a) is used (which may be a scalar in its simplest form). In Ju's model (1989a) the three initial moduli were implicitly considered the same and only one scalar damage variable was chosen and was equally applied to both the elastic-damage and plastic-damage components by simply replacing the stress tensor by the effective stress tensor. This assumption is not correct in view of the previous argument. In other words, if the energy equation is expressed using scalar damage variable d_a as

$$\rho \psi^d = \rho (1 - d_a) \psi_0(\epsilon_{ij}^e, \epsilon_{ij}^p) \quad (4.30)$$

where $\psi_0(\epsilon_{ij}^e, \epsilon_{ij}^p)$ is the total free energy of the undamaged material, then ψ_0 cannot be decoupled by simple averaging as

$$\psi_0(\epsilon_{ij}^e, \epsilon_{ij}^p) \neq \psi_0^e(\epsilon_{ij}^e) + \psi_0^p(\epsilon_{ij}^p) \quad (4.31)$$

where ψ_0^e and ψ_0^p are the elastic and plastic energy of the undamaged material.

The form given in Eqn. (4.27-c) provides the possible uncoupling for the elastic and plastic damage energies. By substituting for σ_{ij} from Eqns. (4.22) and (4.23), then the Helmholtz free energy associated with damage $\psi^d = \psi^d(\epsilon_{ij}^e, \epsilon_{ij}^p)$ is expressed as

$$\rho\psi^d = \frac{1}{2} (I_{ijuv} - D_{ijuv}^e) E_{o_{uvkm}} \epsilon_{km}^e \epsilon_{ij}^e + \frac{1}{2} (I_{ijuv} - D_{ijuv}^p) P_{o_{uvkm}} \epsilon_{km}^p \epsilon_{ij}^p \quad (4.32)$$

In this case, in terms of two scalar damage variables d_e and d_p for elastic-damage and plastic-damage, the damage energy can be expressed as

$$\psi^d = (1 - d_e) \psi_o^e + (1 - d_p) \psi_o^p \quad (4.33)$$

where $\rho\psi_o^e(\epsilon_{ij}^e) = \frac{1}{2} E_{o_{ijkm}} \epsilon_{km}^e \epsilon_{ij}^e$ and $\rho\psi_o^p(\epsilon_{ij}^p) = \frac{1}{2} P_{o_{ijkm}} \epsilon_{km}^p \epsilon_{ij}^p$ are the undamaged elastic energy and plastic energy. It can be concluded that to decouple the energy terms, two sets of damage variables must be used.

4.9 INCORPORATION WITH THE THEORY OF PLASTICITY

In order to simplify the formulation, scalar damage variables are chosen and Eqns. (4.21,22,23) will have the form

$$\sigma_{ij} = (1 - d_a) A_{o_{ijkm}} \epsilon_{km} \quad (4.34)$$

$$= (1-d_e) E_{o_{ijkl}} \epsilon_{km}^e \quad (4.35)$$

$$= (1-d_p) P_{o_{ijkl}} \epsilon_{km}^p \quad (4.36)$$

The tensor $E_{o_{ijkl}}$ is the conventional moduli tensor in linear elasticity.

Differentiating Eqn. (4.35) with respect to time t yields

$$\begin{aligned} \dot{\sigma}_{ij} &= (1-d_e) E_{o_{ijkl}} \dot{\epsilon}_{km}^e - \dot{d}_e E_{o_{ijkl}} \epsilon_{km}^e \\ &= (1-d_e) E_{o_{ijkl}} \dot{\epsilon}_{km}^e - \frac{\partial d_e}{\partial \epsilon_{km}^e} \epsilon_{km}^e E_{o_{ijrs}} \dot{\epsilon}_{rs}^e \end{aligned} \quad (4.36)$$

where for unloading, $\dot{d}_e = 0$. The elastic damage variable can be assumed to be a function of the elastic damage strain. In this case Eqn. (4.36) can be expressed as

$$\dot{\sigma}_{ij} = \bar{E}_{o_{ijkl}} \dot{\epsilon}_{km}^e \quad (4.37)$$

in which the tangential fourth order elastic moduli tensor

$$\bar{E}_{o_{ijkl}} = (1-d_e) E_{o_{ijrs}} f_{rskm}, \quad f_{rskm} = I_{rskm} - (\partial d_e / \partial \epsilon_{km}^e) \epsilon_{rs}^e / (1-d_e)$$

The incremental total strain ϵ_{ij} can be written as

$$\begin{aligned} \dot{\epsilon}_{ij} &= \dot{\epsilon}_{ij}^e + \dot{\epsilon}_{ij}^p \\ &= \bar{E}_{o_{ijkl}}^{-1} \dot{\sigma}_{km} + \dot{\epsilon}_{ij}^p \end{aligned} \quad (4.38)$$

With reference to the conventional associative plasticity flow rule but with the yield surface now expressed in terms of effective plastic stresses (so called because it is conjugate to the plastic damage variable d_p)

$$\bar{\sigma}_{ij}^P = \sigma_{ij}/(1-d_p) \quad (4.39)$$

then the yield function can be written as

$$F(\bar{\sigma}_{ij}^P, q_i) = 0 \quad (4.40)$$

The idea of expressing the yield surface in terms of effective values was used previously by Simo and Ju (1987a, b) and Ju (1989a). However, the overall concept herein is somewhat different.

By differentiating (4.40), one has the consistency condition

$$\dot{F} = \frac{\partial F}{\partial \bar{\sigma}_{ij}^P} \dot{\bar{\sigma}}_{ij}^P + \frac{\partial F}{\partial q_i} \dot{q}_i = 0 \quad (4.41)$$

with the flow rule in the form

$$\dot{\bar{\sigma}}_{ij}^P = \dot{\lambda} \frac{\partial F}{\partial \bar{\sigma}_{ij}^P} \quad (4.42)$$

The rate form for the effective plastic stress can be obtained from (4.39) as

$$\dot{\bar{\sigma}}_{ij}^P = \varepsilon_{rj} \dot{\sigma}_{ir} \quad (4.43)$$

where the tensorial second order function $g_{rj} =$

$$\left(\delta_{rj} + \frac{\dot{\sigma}_{rs}^{-1} \dot{\sigma}_{sj}^p}{\dot{d}_p} \right) / (1 - d_p), \quad \delta_{rj} \text{ is the Kronecker delta.}$$

Having expressed suitable hardening rules in terms of effective plastic stress using (4.42) and (4.43), Eqn. (4.41) becomes

$$\frac{\partial F}{\partial \bar{\sigma}_{ij}^p} g_{rj} \dot{\sigma}_{ir} + \dot{\lambda} \frac{\partial F}{\partial q_s} h_s = 0 \quad (4.44)$$

i.e.,

$$\dot{\lambda} = - \frac{\partial F}{\partial \bar{\sigma}_{ij}^p} g_{rj} \dot{\sigma}_{ir} / \frac{\partial F}{\partial q_s} h_s \quad (4.45)$$

Now it is possible to express an incremental stress-strain relation as

$$\dot{\epsilon}_{ij} = S_{ijklm} \dot{\sigma}_{km} \quad (4.46)$$

where the tangential elastoplastic damage compliance S_{ijklm} is defined, by using (4.45) in (4.42) and then substituting the result in (4.38), as

$$S_{ijklm} = \bar{E}_{ijklm}^{-1} - \frac{\frac{\partial F}{\partial \bar{\sigma}_{ij}^p} \frac{\partial F}{\partial \bar{\sigma}_{kr}^p} g_{mr}}{\frac{\partial F}{\partial q_s} h_s} \quad (4.47)$$

By contrast to Ju's formulation (1989a) in which a single damage variable was used, the present form of the degraded tangential

compliance employs two damage variables: the elastic damage and plastic damage variables.

4.10 INCORPORATION WITH MICROMECHANICS

4.10.1 Formulation Layout

A trial to convene the dispersion of phenomenological and micromechanical aspects of damage is presented in this investigation. Some of previous models based on this approach were developed by Krajcinovic et al. (1991) and Chen and Tzou (1990). However, a completely different approach is suggested in the current study.

Considering the uniaxial tensile response of a rock-like material, three phenomenological behavior genera are distinguished as suggested earlier in this chapter. The formal split of the total strain into elastic-damage and plastic-damage strain is used. For each phase a congruous damage variable is derived. Second law of thermodynamics is used to determine the threshold and critical limits. The tangential relation for loading is derived. Micromechanical concepts through the self-consistent method after the work of Budiansky and O'Connell (1976) are then applied to the elastic-damage phase of behavior. Such consideration allows deriving damage variables conjugate to both the bulk and shear moduli. Generalization to multiaxial states is carried out in a similar manner to the one suggested by Mazars (1984). Finally, the tensorial stress-strain relationships for loading and unloading are formulated for multiaxial loading. The model is then particularized to

concrete and the results are shown to yield good predictions.

4.10.2 Phenomenological Behavior Genera

Assuming an idealized stress-strain relationship for a rock-like material under cyclic uniaxial tension, shown in Fig. 4.12, of the following for

$$\sigma = \sigma(\epsilon) = f(\epsilon) * \epsilon \quad (4.48)$$

in which σ is the stress, ϵ is the total strain and f is a scalar function. Eqn. (4.48) is assumed to satisfy the condition of strain free corresponding to stress-free state with respect to the loaded direction.

The inelastic strain, ϵ_p , can be related to the total strain through a polynomial, i.e.

$$\epsilon_p = \epsilon_p(\epsilon) = \alpha_0 \epsilon + \alpha_1 \epsilon^2 + \alpha_2 \epsilon^3 + \dots \quad (4.49)$$

where $\alpha_0, \alpha_1, \alpha_2, \dots$ are polynomial coefficients. These coefficients can be obtained experimentally by regression analysis utilizing the residual strains in cyclic loading. Consequently, the elastic component, ϵ_e , is

$$\epsilon_e = \epsilon_e(\epsilon) = (1 - \alpha_0) \epsilon - \alpha_1 \epsilon^2 - \alpha_2 \epsilon^3 - \dots \quad (4.50)$$

The initial modulus A_0 is defined as the initial slope of the stress-total strain diagram i.e.

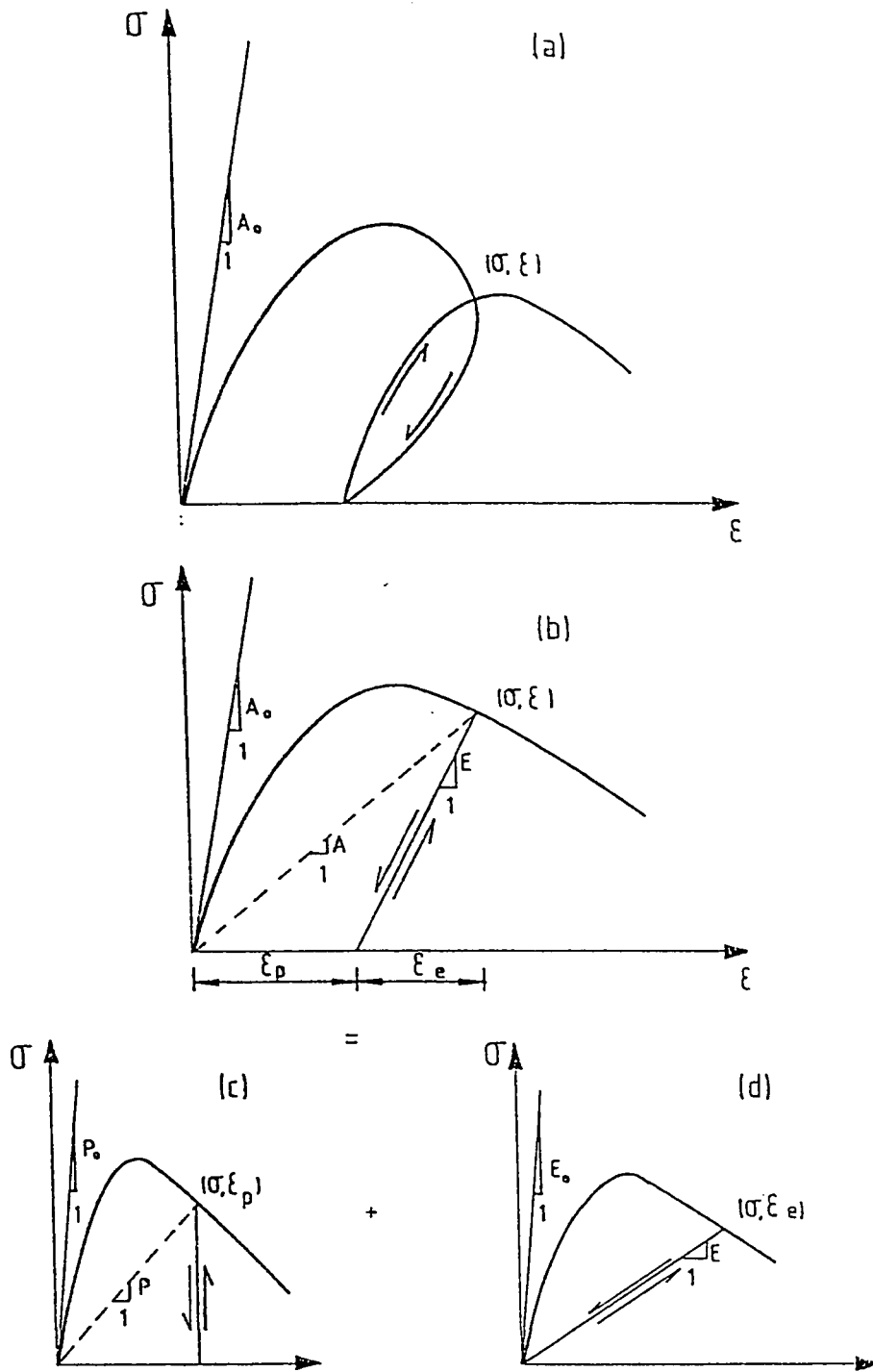


Figure 4.12 Schematic idealization of the uniaxial cyclic response

$$A_o = \left. \frac{\partial \sigma}{\partial \epsilon} \right|_{\epsilon = 0} = \left(\frac{\partial f}{\partial \epsilon} * \epsilon \right)_{\epsilon = 0} + f(0) = f(0) \quad (4.51)$$

On the other hand, the initial modulus, E_o , is the initial slope of the $\sigma - \epsilon_e$ relationship and is achieved by the following simple differentiation

$$E_o = \left. \frac{\partial \sigma}{\partial \epsilon_e} \right|_{\epsilon_e = 0} = \left. \frac{\partial \sigma / \partial \epsilon}{\partial \epsilon_e / \partial \epsilon} \right|_{\epsilon_e = 0} \quad (4.52)$$

Using (4.51) and the derivative of (4.50) in (4.52) we get

$$\begin{aligned} E_o &= \frac{f(0)}{(1 - \alpha_o) - 2\alpha_1 \epsilon - 3\alpha_2 \epsilon^2 - \dots} \Big|_{\epsilon = 0} \\ &= \frac{f(0)}{1 - \alpha_o} = \frac{A_o}{1 - \alpha_o} \end{aligned} \quad (4.53)$$

It is interesting to notice that E_o is greater than A_o by the fraction $1/(1 - \alpha_o)$ for positive values of α_o less than unity. Therefore, the initial total tangent modulus is different from the initial elastic modulus. This conclusion is valid for all materials which exhibit nonlinear behavior and unload linearly or in general whose behavior anticipates early inelastic deformation.

The initial plastic modulus, P_o , for the $\sigma - \epsilon_p$ relationship can be obtained in a similar manner by the differentiation

$$P_o = \left. \frac{\partial \sigma}{\partial \epsilon_p} \right|_{\epsilon_p = 0} = \left. \frac{\partial \sigma / \partial \epsilon}{\partial \epsilon_p / \partial \epsilon} \right|_{\epsilon_p = 0} \quad (4.54)$$

Using (4.51) and the derivative of (4.49) with respect to the total strain ϵ , yields

$$P_0 = \frac{f(0)}{\alpha_0} = \frac{A_0}{\alpha_0} \quad (4.55)$$

Again the initial plastic modulus is greater than the initial total modulus for positive values of α_0 less than unity, i.e. $\alpha_0 \in]0,1[$. The ratio of the initial elastic to initial plastic moduli is obtained by dividing (4.53) to (4.55) which leads to

$$E_0 = \frac{\alpha_0}{1-\alpha_0} P_0 \quad (4.56)$$

The value of P_0 will be greater than E_0 provided that

$$\frac{1-\alpha_0}{\alpha_0} > 1 \quad (4.57)$$

which means

$$\alpha_0 < 0.5 \quad (4.58)$$

In this case, the initial rate of plastic deformation is of less significance than the elastic one.

Equations (4.53) and (4.55) elucidate the importance of the conceptual distinction of the behavior genera, i.e., total, elastic and plastic phases of behavior from the first instant of loading. This is in complete contradiction to the concept of yielding subsequent to an initial

linear elastic response of the material.

The secant moduli for the total, elastic and plastic components, A, E, and P, respectively, at any stress level can be derived as follows:

$$A = \frac{\sigma}{\epsilon} = f(\epsilon) \quad , \quad (4.59)$$

$$\begin{aligned} E &= \frac{\sigma}{\epsilon_e} = \frac{\sigma/\epsilon}{\epsilon_e/\epsilon} = \frac{f(\epsilon)}{(1-\alpha_0) - \alpha_1\epsilon - \alpha_2\epsilon^2 - \dots} \\ &= \frac{A}{(1-\alpha_0) - \alpha_1\epsilon - \alpha_2\epsilon^2 - \dots} \end{aligned} \quad (4.60)$$

and

$$\begin{aligned} P &= \frac{\sigma}{\epsilon_p} = \frac{\sigma/\epsilon}{\epsilon_p/\epsilon} = \frac{f(\epsilon)}{\alpha_0 + \alpha_1\epsilon + \alpha_2\epsilon^2 + \dots} \\ &= \frac{A}{\alpha_0 + \alpha_1\epsilon + \alpha_2\epsilon^2 + \dots} \end{aligned} \quad (4.61)$$

Defining scalar damage variables, namely total, elastic and plastic damage variables, conjugate to the degradation of the moduli A, E and P as d_a , d_e and d_p , respectively, yields,

$$d_a = 1 - \frac{A}{A_0} \quad , \quad (4.62)$$

Using (4.60) and (4.51) in (4.64) we get

$$d_a = 1 - \frac{f(\epsilon)}{f(0)} \quad (4.63)$$

and similarly

$$d_e = 1 - \frac{E}{E_0} \quad (4.64)$$

Using (4.60) and (4.51) in (4.62) we obtain

$$d_e = \frac{(1-\alpha_0) d_a - [\alpha_1 \varepsilon + \alpha_2 \varepsilon^2 + \dots]}{(1-\alpha_0) - [\alpha_1 \varepsilon + \alpha_2 \varepsilon^2 + \dots]} \quad (4.65)$$

Similarly,

$$d_p = 1 - \frac{P}{P_0} \quad (4.66)$$

Using (4.62) and (4.55) in (4.66), we arrive at

$$d_p = \frac{\alpha_0 d_a + [\alpha_1 \varepsilon + \alpha_2 \varepsilon^2 + \dots]}{\alpha_0 + [\alpha_1 \varepsilon + \alpha_2 \varepsilon^2 + \dots]} \quad (4.67)$$

4.10.3 Thermodynamical Considerations

On the common assumption that unloading is an elastic process and on the basis of the work of Patino (1989), the elastic damage variable is, according to the second law of thermodynamics, non-negative, non-decreasing quantity. Furthermore, postulating linear unloading, its increment is zero.

The condition to obtain a non-negative d_e , as provided by Clausius-Duhem inequality, is to satisfy

$$d_e \geq 0 \quad (4.68)$$

Substituting from (4.65) in (4.69) we get

$$(1-\alpha_0) d_a - \left[\alpha_1 \varepsilon + \alpha_2 \varepsilon^2 + \dots \right] \geq 0 \quad (4.70)$$

provided that

$$(1-\alpha_0) - \left[\alpha_1 \varepsilon + \alpha_2 \varepsilon^2 + \dots \right] \geq 0 \quad (4.71)$$

Eqn. (4.71) implicitly requires that $\varepsilon_e/\varepsilon \geq 0$ which limits the plastic-damage strain to be, on the large, equal to the total strain. Substituting from (4.50) and (4.63) in (4.70), it can be easily shown that the inequality corresponds to

$$\frac{\sigma}{\varepsilon_p} \leq \frac{f(0)}{1-\alpha_0} = \frac{A_0}{1-\alpha_0} \quad (4.72)$$

or

$$P \leq E_0 \rightarrow d_p \geq \frac{1-2\alpha_0}{1-\alpha_0} \quad (4.73)$$

The equality in Eqn. (4.73) gives the threshold limit for the damage evolution which never coincides with the origin as far as Eqn. (4.58) is fulfilled.

The condition to establish a non-decreasing elastic damage parameter is to locate the strain level for the critical state at which d_e is maximum. Differentiating (4.65) with respect to ε and using (4.50), we get

$$\frac{d}{d\varepsilon} \left[\frac{1 - (1 - \sigma_0)(1 - d_a)}{\varepsilon_e/\varepsilon} \right] = 0 \quad (4.74)$$

Simple mathematical manipulation leads to the condition that

$$\frac{\partial f}{\partial \varepsilon} * \frac{\varepsilon_e}{\varepsilon} = f \frac{\partial(\varepsilon_e/\varepsilon)}{\partial \varepsilon} \quad (4.75)$$

Positive and increasing characteristic for the total damage variable are satisfied for all cases if $A_0 > A$ and also unconditionally for the plastic damage variable if polynomial coefficients σ_i ($i = 1, 2, 3, \dots$) are all positive.

4.10.4 Condition of Softening

The stress-total strain relationship as inferred from Eqns. (4.59) and (4.62) can be expressed as

$$\sigma = (1 - d_a) A_0 \varepsilon \quad (4.62)$$

The tangential modulus, A_t , is derived as

$$A_t = \frac{\partial \sigma}{\partial \varepsilon} = \left[(1 - d_a) - \frac{\partial d_a}{\partial \varepsilon} \varepsilon \right] A_0 \quad (4.77)$$

Using (4.51) and (4.63) in (4.77)

$$A_t = \left[f(\varepsilon) + \frac{\partial f}{\partial \varepsilon} \varepsilon \right] \quad (4.78)$$

Zero or negative slope in the descending branch takes place if $\Lambda_t \leq 0$,

i.e.,

$$f(\epsilon) \leq - \frac{\partial f}{\partial \epsilon} \epsilon \quad (4.79)$$

Similar procedures can be followed to derive the tangential elastic and plastic moduli. However, Λ_t is sufficient to determine the tangent to the loading path for incremental formulation while E gives the unloading slope.

4.10.5 Micromechanics of the Elastic-Damage Behavior

Having established the stress-elastic-damage strain ($\sigma - \epsilon_e$) relationship using Eqns. (4.60) and (4.64) in the form

$$\sigma = (1 - d_e) E_0 \epsilon_e \quad (4.80)$$

It can be shown that the behavior is quasi sub-brittle and always unloads to the origin. Application of self-consistent method to this phase of behavior is more plausible rather than to its application to the total behavior. Utilizing the work of Budiansky and O'Connell (1976) for long narrow elliptic cracks (Eqns. 39 and 42 of the cited reference) along with Eqn. (4.64), we get

$$d_e = \frac{2(\bar{v}_0 - \nu)(5 - 4\nu)}{10\bar{v}_0 - \nu (1 + 8\bar{v}_0)} \quad (4.81)$$

in which \bar{v}_0 is the crack free value of the effective Poisson's ratio v at any strain level. It follows from (4.81) that

$$v = \frac{9 + (1 - d_e)(1 + 8\bar{v}_0) - \sqrt{[9 + (1 - d_e)(1 + 8\bar{v}_0)]^2 - 320\bar{v}_0(1 - d_e)}}{16} \quad (4.82-a)$$

A plot of Eqn. (4.82-a) is shown in Fig. 4.13. It is clear that a straight line approximation for the relationship between effective Poisson's ratio and the elastic damage variable is still rigorous and can be expressed as

$$v = \bar{v}_0 (1 - d_e) \quad (4.82-b)$$

However, the trend by which Poisson's ratio is evolving is not unique in tension and compression (Ju, 1990). Also, the initial Poisson's ratio itself is dependent on the state of stress (Tasuji et al., 1978). Therefore, it is suggested to modify Eqn. (4.82-b) to have the form

$$v = \bar{v}_0 (1 - d_e) h \quad (4.82-c)$$

in which h is a modification function and to keep formulation as simple as possible it is advantageous to postulate it as a function of the hydrostatic pressure at the peak strength σ_m^P , i.e., expressed as

$$h = h(\sigma_m^P) \quad (4.82-d)$$

and Eqn. (4.82-c) can be rewritten as

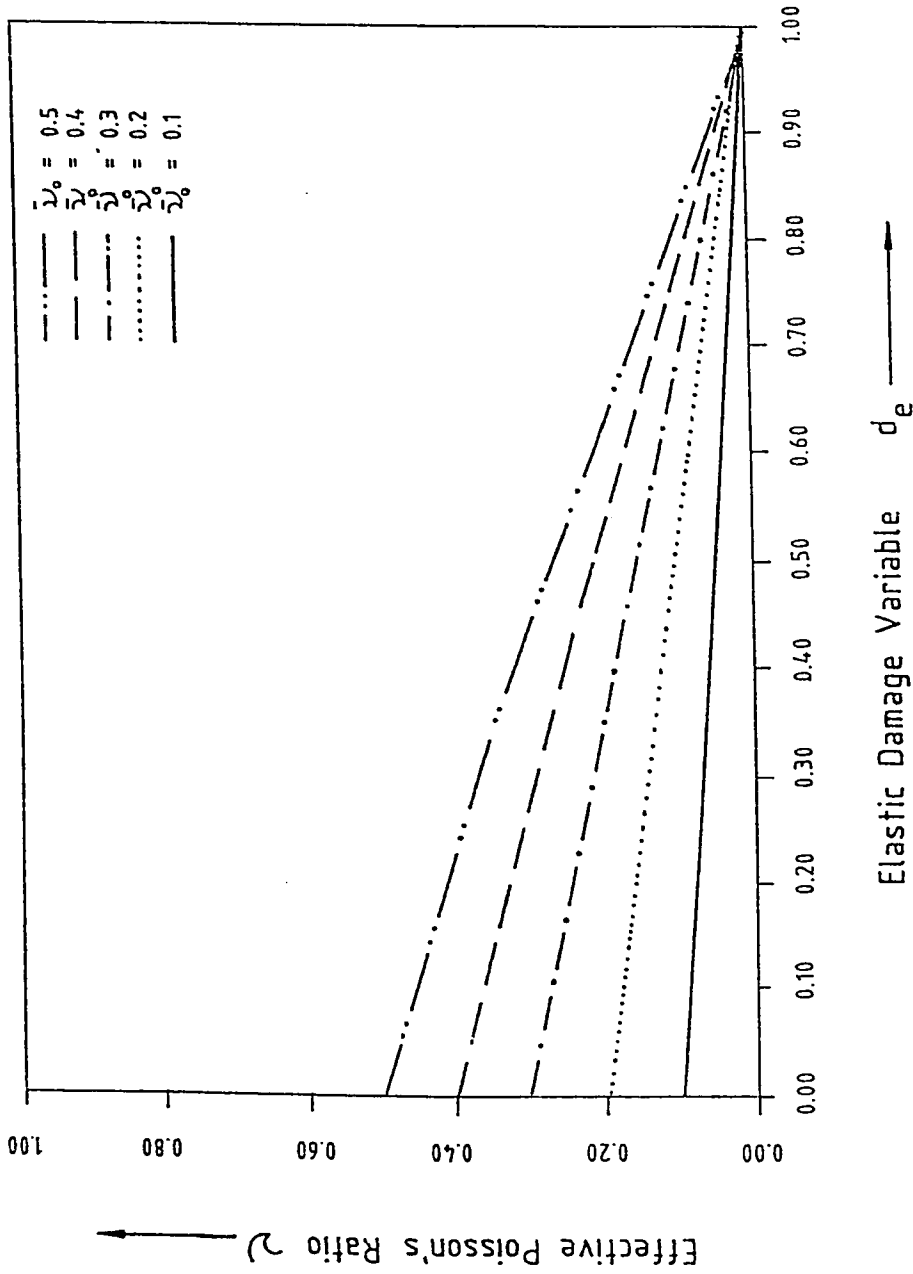


Figure 4.13 Variation of Poisson's ratio with the elastic damage variable

$$v = v_0 (1 - d_e) \quad (4.82-e)$$

in which $v_0 = \bar{v}_0 h$ is a modified undergraded Poisson's ratio.

The degraded elastic-damage bulk and shear moduli K_e and G_e whose initial values are G_{e_0} and K_{e_0} are also obtained from the work of Budiansky and O'Connell (1976). Using Eqns. (36) and (44) of Budiansky and O'Connell (1976) besides consideration of Eqn. (4.82) in the current study, one obtains

$$d_{K_e} = 1 - \frac{K_e}{K_{e_0}} = \frac{10(1-v)(v_0-v)}{(1-2v)[10v_0-v(1+8v_0)]} \quad (4.83)$$

and

$$d_{G_e} = 1 - \frac{G_e}{G_{e_0}} = \frac{(10-7v)(v_0-v)}{(1+v)[10v_0-v(1+8v_0)]} \quad (4.84)$$

in which d_{K_e} and d_{G_e} are the elastic damage parameters associated with the degradation of K and G , respectively. The original values can be found from conventional elastic relations together with Eqn. (4.53)

$$K_{e_0} = \frac{3E_0}{1-2v_0} = \frac{3A_0}{(1-\sigma_0)(1-2v_0)} \quad (4.85)$$

and

$$G_{e_0} = \frac{E_0}{2(1+v_0)} = \frac{A_0}{(1-\sigma_0)(1+v_0)} \quad (4.86)$$

Assuming that the degraded moduli for the total behavior K_a and

G_a are related to A by

$$K_a = \frac{3A}{1-2\nu} = \frac{3(1-d_a) A_o}{1-2\nu} \quad (4.87)$$

and

$$G_a = \frac{A}{2(1+\nu)} = \frac{(1-d_a) A_o}{2(1+\nu)} \quad (4.88)$$

Eqn. (4.62) has been used to arrive at (4.87) and (4.88). The value of ν given by (4.81) is assumed to hold in these two equations. The initial values of both the bulk and shear moduli are recovered by using $d_a = 0$ and $\nu = \nu_o$ in (4.87) and (4.88), respectively, and expressed as the conventional bulk and shear moduli K_{a_o} and G_{a_o}

$$K_{a_o} = \frac{3A_o}{1-2\nu_o} \quad (4.89)$$

and

$$G_{a_o} = \frac{A_o}{2(1+\nu_o)} \quad (4.90)$$

The conjugate damage variables to K_a and G_a which are d_{K_a} and d_{G_a} are obtained as

$$d_{K_a} = 1 - \frac{K_a}{K_{a_o}} = 1 - \frac{1-2\nu_o}{1-2\nu} (1-d_a) \quad (4.91)$$

and

$$d_{G_a} = 1 - \frac{G_a}{G_{a_0}} = 1 - \frac{1+\nu_0}{1+\nu} (1-d_a) \quad (4.92)$$

At this stage, it has to be pointed out that the role of micromechanics is crystallized by finding the change of Poisson's ratio due to the presence of cracks induced by the damage process through loading. Another salient feature can be observed by comparing Eqns. (4.83) and (4.84) with (4.91) and (4.92). It demonstrates the clear distinction between loading and unloading stiffnesses by the total and elastic damage variables.

To predict the cyclic behavior under multiaxial loading, the constitutive equations are expressed as follows:

(a) Loading:

$$\sigma_{ij} = 2(1-d_{G_a}) G_{a_0} e_{ij} + (1-d_{K_a}) K_{a_0} \frac{\epsilon_{kk}}{3} \delta_{ij} \quad (4.93)$$

(b) Unloading:

$$\sigma_{ij} = 2(1-d_{G_e}) G_{e_0} e_{ij}^e + (1-d_{K_e}) K_{e_0} \frac{\epsilon_{kk}^e}{3} \delta_{ij} \quad (4.94)$$

where σ_{ij} is the stress tensor, $e_{ij} = \epsilon_{ij} - 1/3 \epsilon_{kk} \delta_{ij}$ is the deviatoric strain tensor, ϵ_{ij} is the strain tensor and δ_{ij} is the Kronecker delta.

The superscript e denotes the elastic part. The values of the elastic damage variables used in Eqn. (4.94) are calculated on the unloading point of the loading path, i.e., the maximum ever reached strain level. For numerical framework, algorithms for materials with memory are to be

adopted. Inasmuch as isotropic damage is caused by microcracking in the cleavage mode, the damage variables are scalar quantities which should be calculated by considering the tensile portion of the strain tensor, hence

$$\epsilon^* = \sqrt{\langle \epsilon_1 \rangle^2 + \langle \epsilon_2 \rangle^2 + \langle \epsilon_3 \rangle^2} \quad (4.95)$$

in which $\langle \rangle$ is the McAulay bracket and ϵ_i ($i = 1,2,3$) are the principal strain values. Similar procedures based on this effective strain ϵ^* were followed by other investigators (c.f. Mazars, 1984).

4.10.6 Applications to Concrete

Behavior of concrete is neither brittle nor ductile. Tensile cracking in the cleavage mode (mode I) is observed to be the dominant phenomenological aspect in the concrete damage process (Mazars, 1984; Simo and Ju, 1987). An investigation on the capability of the present model to correctly predict the response of concrete under uniaxial and biaxial states of stress is carried out hereafter.

Although many formulae were adopted to describe the uniaxial tensile behavior of concrete, Ortiz (1984) employed successfully in the mixture model Smith and Young's formula (1955). This formula was originally developed for uniaxial compression and is used herein. Accordingly, the f -function alluded in Eqn. (4.48) is taken as

Table 4.1 Material constants from uniaxial cyclic tension test for concrete.

Polynomial coefficients	Initial moduli
$\alpha_0 = 0.474$	$A_0 = 2.718 \frac{\sigma_t}{\epsilon_t}$
$\alpha_1 = 0.253$	$E_0 = 5.167 \frac{\sigma_t}{\epsilon_t}$
$\alpha_2 = -0.050$	$P_0 = 5.734 \frac{\sigma_t}{\epsilon_t}$
$\alpha_3 = 0.0034$	

$$f = \frac{f_t'}{\varepsilon_t} e^{(1 - \frac{\varepsilon}{\varepsilon_t})^*} \quad (4.96)$$

in which f_t' , ε_t are the peak stress and total peak strain in uniaxial tension, respectively. The effective strain ε^* as given by Eqn. (4.95) reduces to the total strain for the pure tension test. With reference to the prediction of the permanent (inelastic, plastic-damage) strain upon full unloading in uniaxial tension test as expressed by Gopalaratnam and Shah (1985), a regression analysis, with the help of Eqn. (4.96), is carried out. The objective of this operation is to express the plastic-damage strain as a continuous function instead of two discrete relations for pre- and post-peak as proposed by Gopalaratnam and Shah (1985). In view of Eqns. (4.49), (4.51), (4.53) and (4.55), the material constants are listed in Table 4.1. It can be noted that $P_0 > E_0$ and, of course, $P_0 > A_0$ because α_0 is less than 0.5 as deduced from Eqn. (4.57).

Plots of the three damage parameters are drawn in Fig. 4.14. The threshold elastic damage strain is calculated from Eqn. (4.75) to be 0.1 the peak strain. The critical state takes place at 6.4 times the peak strain as obtained from Eqn. (4.70). Fig. 4.15 shows the uniaxial tensile cyclic response of concrete as predicted by the model and it is in good agreement with the experimental data.

In general, the range of Poisson's ratio for concrete ranges between 0.14 and 0.24 (Branson, 1977). A value of $\bar{\nu}_0 = 0.16$ is chosen

for the following investigation on the biaxial strength. A simple form of the function h defined in Eqn. (4.82) is postulated for the given Poisson's ratio to have the form

$$h = \begin{cases} 1 & \text{for } \left| \frac{\sigma_m^p}{\sigma_c} \right| \leq \frac{1}{3} \\ 2.75 \frac{\sigma_m^p}{\sigma_c} & \text{for } \left| \frac{\sigma_m^p}{\sigma_c} \right| > \frac{1}{3} \end{cases} \quad (4.97)$$

in which σ_c is the uniaxial compressive strength.

For biaxial state of stress ($\sigma_3 = 0$), if ϵ_1 , ϵ_2 and ϵ_3 are the total strain corresponding to the Euclidean principal space, then it can be easily shown that

$$\epsilon_2 = \epsilon_1 \frac{\beta - \nu_o (1 - d_e)}{1 - \nu_o \beta (1 - d_e)} \quad ; \quad (4.98)$$

and

$$\epsilon_3 = -\epsilon_1 \frac{\nu_o (1 - d_e)(1 + \beta)}{1 - \nu_o \beta (1 - d_e)} \quad (4.99)$$

in which β is the principal stress ratio; i.e. $\beta = \sigma_2/\sigma_1$, where σ_1 and σ_2 are the principal stresses. The value of the maximum principal stress is related to the corresponding strain through

$$\sigma_1 = \epsilon_1 \frac{A_o (1 - d_a)}{1 - \nu_o \beta (1 - d_e)} \quad (4.100)$$

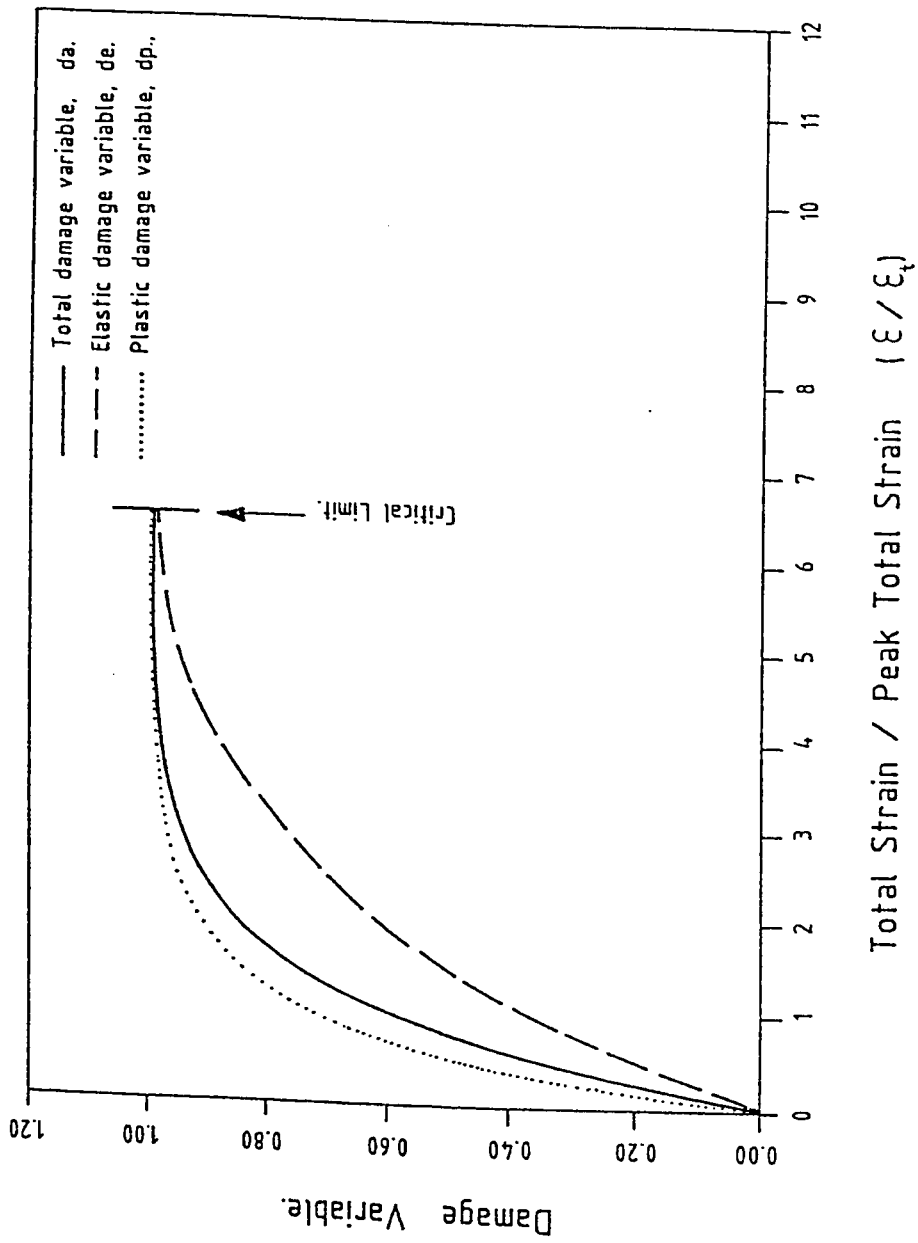


Figure 4.14 Generalized damage variables based on the incorporation of micromechanics for concrete

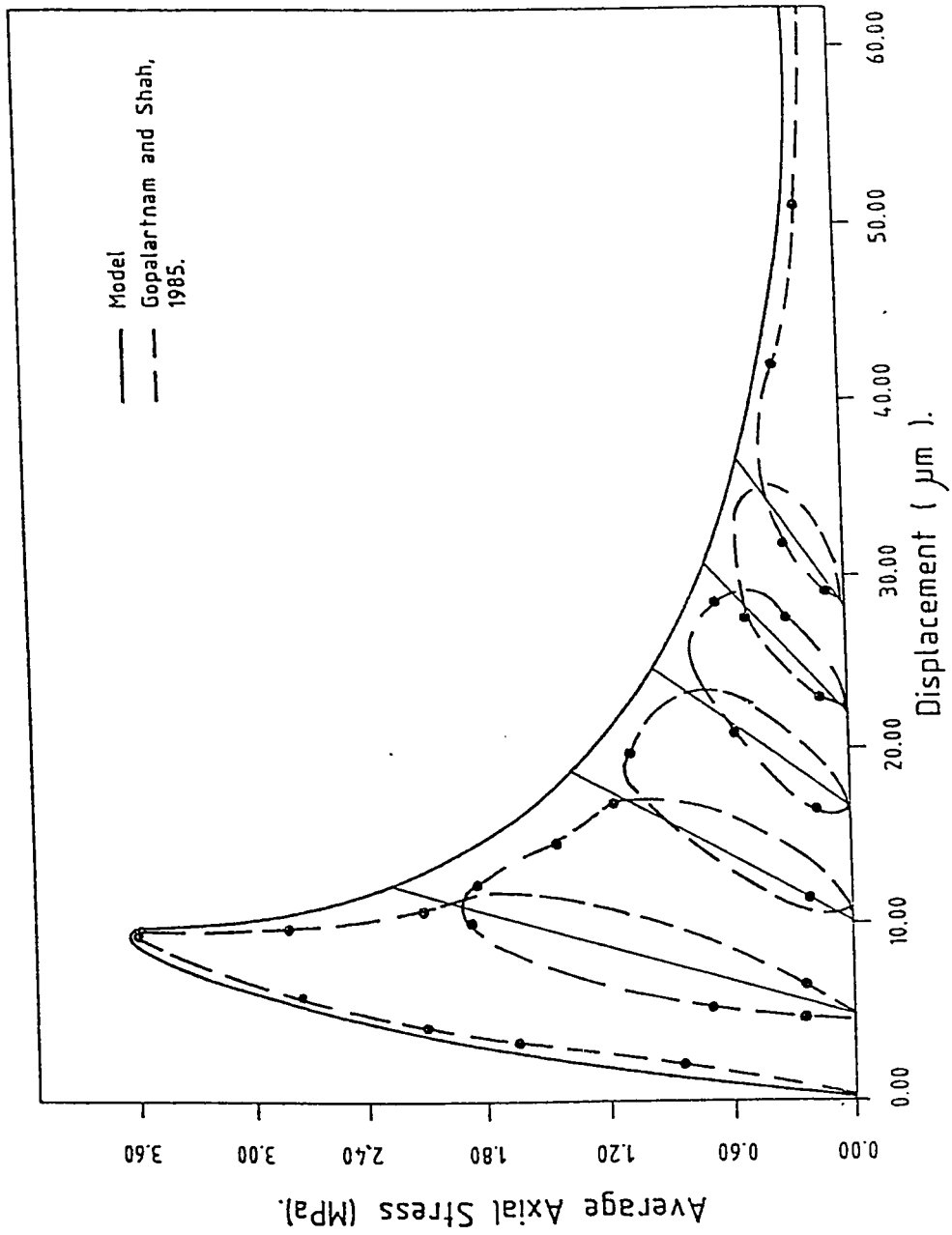


Figure 4.15 Prediction of the uniaxial cyclic tensile behavior of concrete based on the incorporation of micromechanics

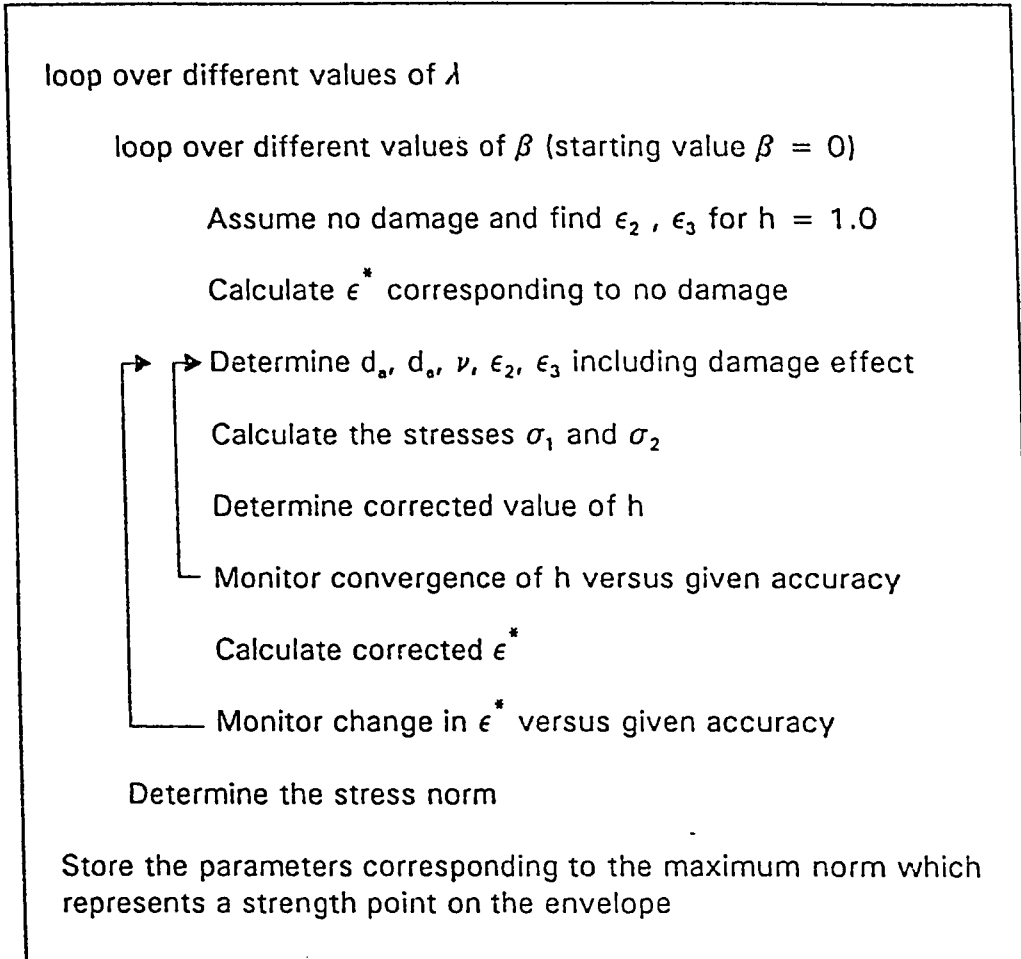


Figure 4.16 Numerical scheme for determination of the biaxial strength envelop based on the incorporation of micromechanics

Substituting for A_0 from Table 4.1 and expressing ϵ_1 as a multiple of the peak uniaxial tensile strain ϵ_t , i.e., $\epsilon_1 = \lambda \epsilon_t$, then Eqn. (4.100) reduces to

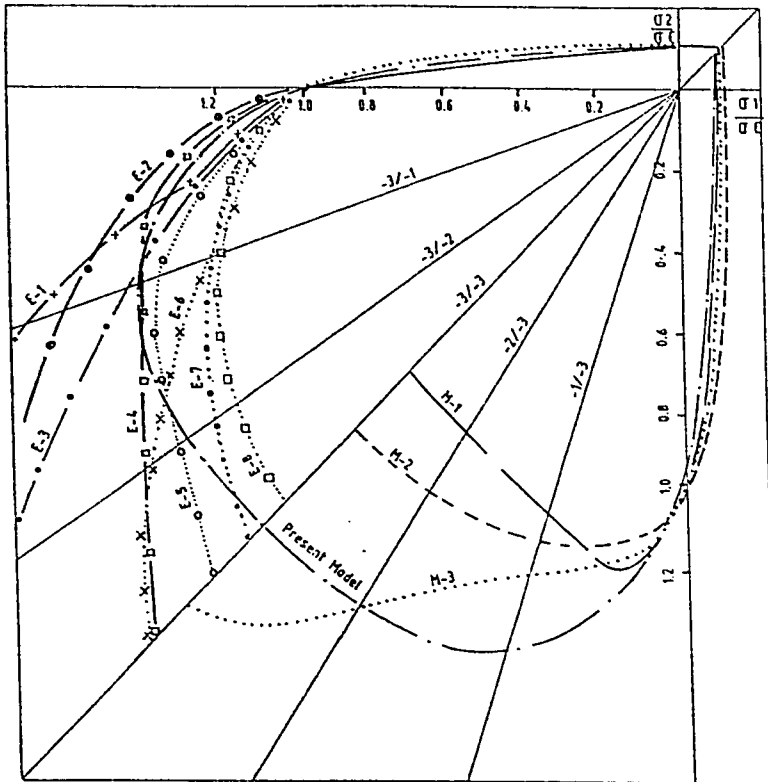
$$\frac{\sigma_1}{f_t'} = \frac{2.718 \lambda (1-d_a)}{1 - \nu_0 \beta (1-d_e)} \quad (4.101)$$

For the tensile-associate response, λ is positive and in general the effective strain in Eqn. (4.95) reduces to

$$\epsilon^* = \lambda \epsilon_t \sqrt{1 + \left(\frac{\langle \epsilon_2 \rangle}{\lambda}\right)^2 + \left(\frac{\langle \epsilon_3 \rangle}{\lambda}\right)^2} \quad (4.102)$$

The dependence of the elastic strain as well as the damage variables on the effective strain value, which is not known in advance, necessitates the construction of an iterative technique. For every value of λ a certain damage surface exists in the stress plane. This envelope, in reality, represents the failure envelope for load/stress controlled tests giving the maximal stress norm. To this end, the algorithm shown in Fig. 4.16 is employed in a FORTRAN 77 computer code. Comparison of the predictions of the model with other experimental data and existing damage models is shown in Fig. 4.17.

It is remarkable that the model predicted reasonably the uniaxial compressive strength; $\sigma_c/f_t' = 9.025$. It may be emphasized that this was attained without any input of uniaxial compressive parameters. In addition, the function h allowed for improved strength prediction in the compression-compression quadrant which is the main disadvantage of



Experimental Data :

- E-1 : Rosenthal (1970).
- E-2 : Gachon (1972).
- E-3 : Schickert & Winkler (1977) for rough platten.
- E-4 : Vile (1965).
- E-5 : Schickert & Winkler (1977) for flexible platten.
- E-6 : Andeneas et al (1977).
- E-7 : Tasuji et al (1978).
- E-8 : Kupfer et al (1968).

Damage Models :

- M-1 : Mazars (1984).
- M-2 : Suaris et al (1990).
- M-3 : Ortiz (1984).

Figure 4.17 Prediction of the biaxial strength envelope for concrete based on the incorporation of micromechanics

damage models utilizing a single damage variable as pointed out by Suaris et al. (1990). The ratio of biaxial strength to the uniaxial compressive strength is equal to 1.23 which is in very good agreement with the experimental findings. Better behavior could be obtained if a more sophisticated form of the h-function is chosen and probably in a similar form to the shape factor used by Han and Chen (1985).

It is worth mentioning that although the presented phenomenological-micromechanical model captures many features of the behavior, it is limited to low levels of confinement where extensional modes of deformation do exist.

4.11 INCORPORATION WITH UNILATERAL DAMAGE MODELS

In many situations the damage can be reasonably characterized by adopting the generalized damage variables for the uniaxial behavior in both tension and compression. Generalization to multi-axial behavior can be attained by using the notion of equivalent strain employed in the unilateral damage model proposed by Mazars (1984) as follows:

$$\varepsilon_j = \sqrt{\sum_{i=1}^3 \langle \varepsilon_i \rangle_j^2} \quad (4.103)$$

where $j = t, c$ for tension and compression, respectively and $\langle x \rangle_j = (x + \beta(j) |x|)/2$ and $\beta(j) = 1, -1$ for $j = t, c$, respectively. ε_i ($i = 1, 2, 3$) are the principal strains. The generalized damage variables d_k^j ($k =$

a, e, p for the total, elastic and plastic responses) can be determined using formulae for uniaxial tensile and compressive components and then replacing the uniaxial strain ϵ (as derived in Chapter 5 for MGDV) by the appropriate ϵ_j . The coupling for multi-axial loading conditions is given by the following relation:

$$d_k = \sum_j W_j d_k^j \quad (4.104)$$

where the weighting parameters W_j depend on the state of stress with $W_t = 1$ and $W_c = 0$ in pure tension whereas $W_t = 0$ and $W_c = 1$ in pure compression. For the general case, the sum of W_c and W_t must always be unity.

Inasmuch as the initial moduli for the elastic and plastic behaviors are not equal in tension and compression, the weighted moduli are defined as

$$E_o = \sum_j W_j E_o^j \quad (4.105)$$

and

$$P_o = \sum_j W_j P_o^j \quad (4.106)$$

Finally, the tensorial constitutive equations can be expressed by modifying Hooke's law for the three phase of behavior as follows:

$$\sigma = C_k : \epsilon_k$$

$$= C_{o_k} (1-d_k) : \epsilon_k \quad (4.107)$$

where C_{o_k} is the conventional initial stress-strain matrix but employing the initial moduli A_o , E_o and P_o for $k = a, e$ and P , respectively.

CHAPTER 5

CHAPTER 5

CANONICAL ELASTOPLASTIC DAMAGE MODEL

5.1 GENERAL

Concrete is neither elastic, plastic, elastic-perfectly brittle, nor elastic-perfectly plastic. Hence, a prudent start towards modelling is to consider uniaxial elasto-plastic damage behavior of concrete. Decomposing the total response into elastic-damage and plastic-damage requires the derivation of the metaphorical generalized damage variables (MGDV). Along with the concepts established in Chapter 4, MGDV are the generalized damage variables associated with the decomposition processes in both tension and compression. Metaphorical bears in its meaning that the generalized damage variables adopted, herein, are of the lineage of, but not exactly the same as, Kachanov's (1958). For generalization to biaxial states, the theory of dichotomy is proposed. The theory allows the reduction of the constitutive equation to a conical tensorial form. As it is customary in concrete practice, the 28 day compressive strength, f'_c , and Poisson's ratio, ν_0 , are regarded as the major material parameters, due to ease in their experimental determination. Verification of the model is investigated against a wide set of experiments.

5.2. DAMAGE VARIABLES FOR CONCRETE IN TENSION

5.2.1 Stress-Total Strain Relationship

The simplest relation describing the tensile behavior of concrete, among the numerous proposals, is as suggested by Guo and Zhang (1987) (Fig. 5.1). A gage length of 35 mm was used in their experiments (note that a gage length effect was reported by, among other investigators, Yankelevsky and Reinhardt (1987) and they advocated a reference gage length of 40 mm). The steeply rising branch is given by

$$\frac{\sigma}{f_t'} = 1.2 \left(\frac{\varepsilon}{\varepsilon_t} \right) - 0.2 \left(\frac{\varepsilon}{\varepsilon_t} \right)^6 \quad \frac{\varepsilon}{\varepsilon_t} \leq 1.0 \quad (5.1)$$

The descending branch is expressed by

$$\frac{\sigma}{f_t'} = \frac{\left(\frac{\varepsilon}{\varepsilon_t} \right)}{\alpha \left[\left(\frac{\varepsilon}{\varepsilon_t} \right) - 1 \right]^{1.7} + \left(\frac{\varepsilon}{\varepsilon_t} \right)} \quad \frac{\varepsilon}{\varepsilon_t} \geq 1.0 \quad (5.2-a)$$

where α is a parameter dependent on the tensile strength, f_t' (MPa),

which is given as

$$\alpha = 0.312 f_t'^2 \quad (5.2-b)$$

The superiority of this regression model over others stems from:

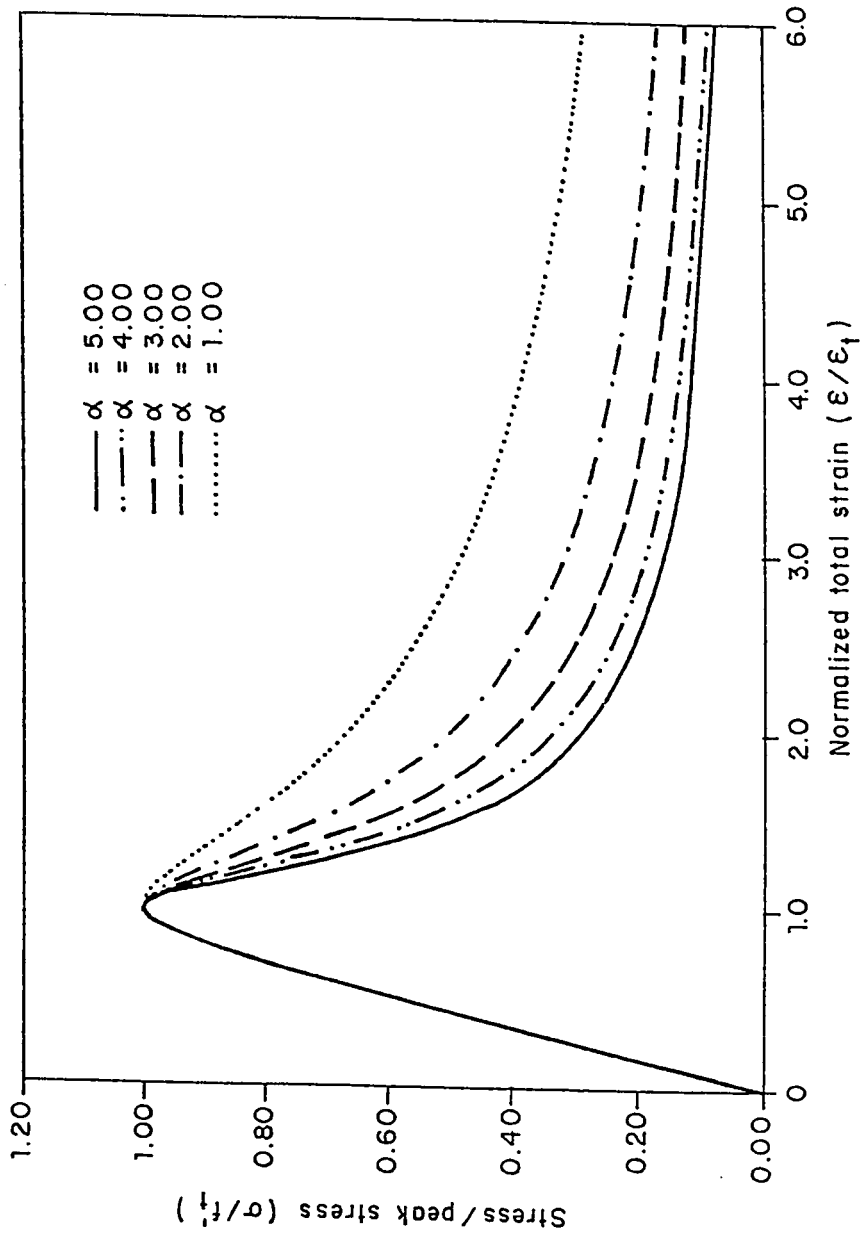


Figure 5.1 Stress-total strain relationship in uniaxial tension according to Guo and Zhang's idealization (1987) for concrete

1. Its explicit description of the $\sigma-\epsilon$ relation contrary to models relating stress to crack width (see for example Gopalaratnam and Shah, 1985).
2. Use of reduced number of material parameters and yet providing good correlation with experimental results.
3. Continuity of both value and slope between the ascending and descending branches at peak. By contrast, models adopting linear relation up to the peak fail to provide such a continuity (Petersson, 1981; Scanlon, 1971; Lin and Scordelis, 1975; Bazant and Oh, 1983; Gylltoft, 1983; Mazars, 1981).
4. The asymptotic nature of the regression model simulates experimental findings of other investigators (see for example Yankelevsky and Reinhardt, 1987). It is remarkable that Hughes and Chapman (1966) recorded, with old facilities, axial strains of magnitude 30 times the strain corresponding to the peak stress.

Several other attempts have been made to represent the post-peak softening branch, including a straight line (Bazant and Oh, 1983), a piecewise linear curve (Gustafsson, 1985; Gylltoft, 1983; Rots et al., 1985), stepped branch (Scanlon, 1971), exponential (Petersson, 1981; Gopalaratnam and Shah, 1985), polynomial (Lin and Scordelis, 1975) and combined expressions (Yankelevsky and Reinhardt, 1987).

5.2.2 Strain Components

The formal split of the total strain, ϵ , for isothermal time-

independent mechanical process into the elastic-damage (ϵ_e) and plastic-damage (ϵ_p) components expressed in a scalar form (as discussed in Chapter 4) is assumed at the outset (Ju, 1989a), i.e. (Fig. 4.2)

$$\epsilon = \epsilon_e + \epsilon_p \quad (5.3)$$

Distinction between this split and the conventional elasto-plasticity split (Malvern, 1969) should be noted, inasmuch as each component of strain contains contributions of damage effects in addition to elastic and plastic effects.

Test data of uniaxial cyclic behavior of concrete in tension is rather limited. Many of the existing models consider the monotonic loading curve only, with some proposing a simplified unloading-reloading option (Gopalaratnam and Shah, 1985; Rots, 1985; Yankelevsky and Reinhardt, 1987). Gopalaratnam and Shah (1985) gave two equations relating the residual displacement to the total displacement at point of unloading and which can be expressed in terms of permanent strains as follows:

$$\left(\frac{\epsilon_p}{\epsilon_t} \right) = \begin{cases} \frac{1}{b^*} \left(\frac{\epsilon}{\epsilon_t} \right) & \frac{\epsilon}{\epsilon_t} \leq 1 \\ \left(\frac{\epsilon}{\epsilon_t} \right) - a^* & \frac{\epsilon}{\epsilon_t} \geq 1 \end{cases}$$

(5.4-a,b)

$$a^* = \frac{A_t(1)}{A_{0t}} \quad ; \quad b^* = \frac{1}{1-a^*} \quad (5.4-c,d)$$

where a^* and b^* are constants related to the initial tangent modulus of $\sigma-\varepsilon$ curve, A_{o_t} , and the secant modulus of the peak, $A_t(1) = f_t'/\varepsilon_t$. In Eqn. (5.4-c) unloading slope for pre-peak region is assumed to be A_{o_t} . Guo and Zhang (1987) reported the ratio A_{o_t}/A_t to vary from 1.04 to 1.61 with an average value of 1.202 and a standard deviation of 0.0791. Using this in (5.4-c,d) and then in Eqns. (5.4-a) and (5.4-b), yields

$$\left(\frac{\varepsilon_p}{\varepsilon_t}\right) = \begin{cases} 0.166 \left(\frac{\varepsilon}{\varepsilon_t}\right) & \frac{\varepsilon}{\varepsilon_t} \leq 1 \\ \left(\frac{\varepsilon}{\varepsilon_t}\right) - 0.834 & \frac{\varepsilon}{\varepsilon_t} \geq 1 \end{cases} \quad (5.5)$$

Interpreting the permanent strain as the plastic damage strain, the elastic damage strain ratio $\varepsilon_e/\varepsilon_t$ can be obtained by using Eqn. (5.5) in Eqn. (5.3), yielding

$$\left(\frac{\varepsilon_e}{\varepsilon_t}\right) = \begin{cases} 0.834 \left(\frac{\varepsilon}{\varepsilon_t}\right) & \frac{\varepsilon}{\varepsilon_t} \leq 1 \\ 0.834 - & \frac{\varepsilon}{\varepsilon_t} \geq 1 \end{cases} \quad (5.6)$$

Fig. 5.2 shows plots of Eqns. (5.3), (5.5) and (5.6) in which the post-peak value of the elastic damage strain component appears as a constant while the plastic damage component is continuously growing parallel to the total strain. An equal contribution of the elastic and plastic components to the total strain takes place at a strain equal to $1.664 \varepsilon_t$.

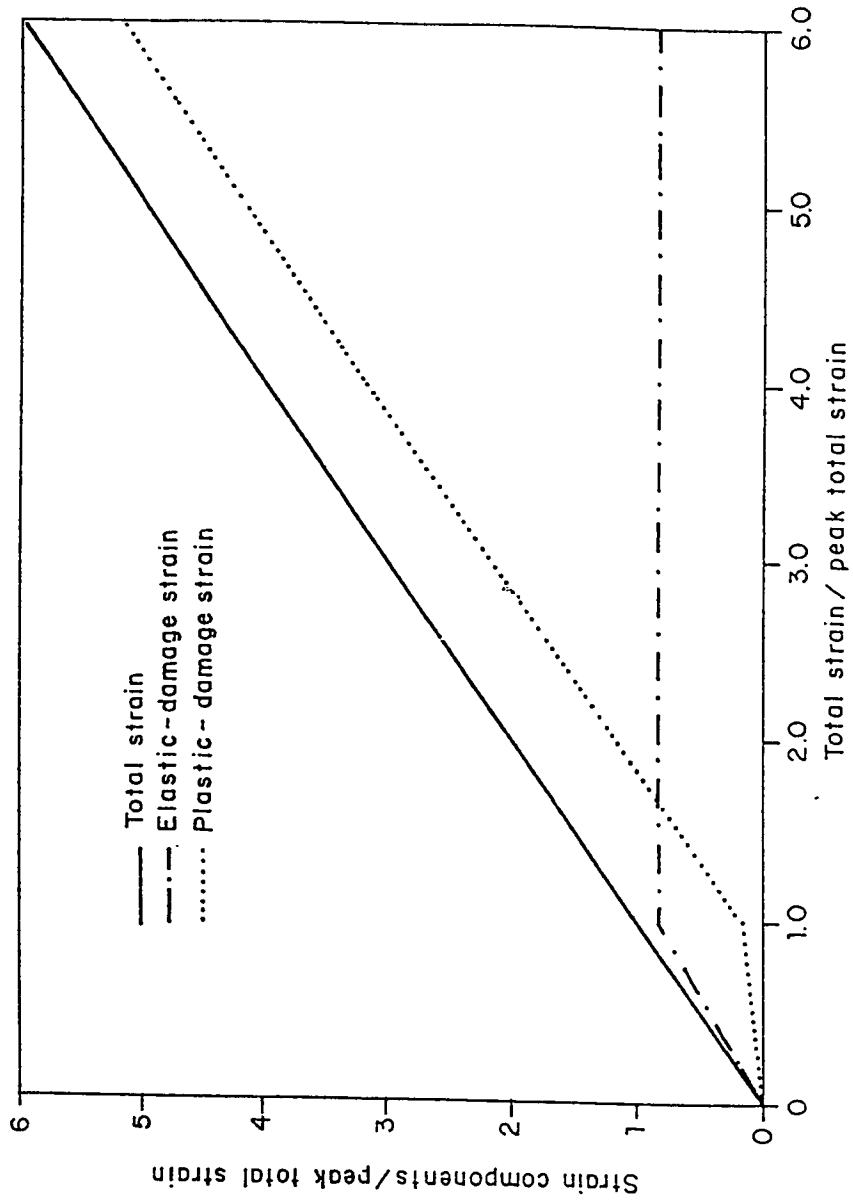


Figure 5.2 Strain components in uniaxial tension for concrete

5.2.3 Stress-Strain Components Relationships

With the relationships between $\sigma/f_t' - \epsilon/\epsilon_t$, $\epsilon_e/\epsilon_t - \epsilon/\epsilon_t$ and $\epsilon_p/\epsilon_t - \epsilon/\epsilon_t$ established, data points of $\sigma/f_t' - \epsilon_e/\epsilon_t$ and $\sigma/f_t' - \epsilon_p/\epsilon_t$ are plotted in Figs. 5.3 and 5.4, respectively. Following relevant relations between stress and appropriate strain variable may be written in terms of secant moduli as:

$$\sigma(\epsilon) = A^t_{(\epsilon)} * \epsilon \quad (5.7-a)$$

$$= E^t_{(\epsilon)} * \epsilon_e \quad (5.7-b)$$

$$= P^t_{(\epsilon)} * \epsilon_p \quad (5.7-c)$$

where $A^t_{(\epsilon)}$, $E^t_{(\epsilon)}$ and $P^t_{(\epsilon)}$ are the total, elastic and plastic secant moduli at any strain level whose initial values are A^t_0 , E^t_0 and P^t_0 , respectively. It is interesting to note that Young's modulus is defined as the elastic modulus of longitudinal deformation (Timoshenko and Goodier, 1951; Neville, 1963; Rygol, 1983; Bangash, 1989), i.e., relating the stress to the elastic strain, and not the total strain. Precisely, E^t_0 rather than A^t_0 is the initial modulus of elasticity. Misapprehension of this abecedarian concept is commonly encountered in the literature where A^t_0 is considered synonymously with E^t_0 .

The initial total tangent modulus is calculated using Eqn. (5.1) as follows

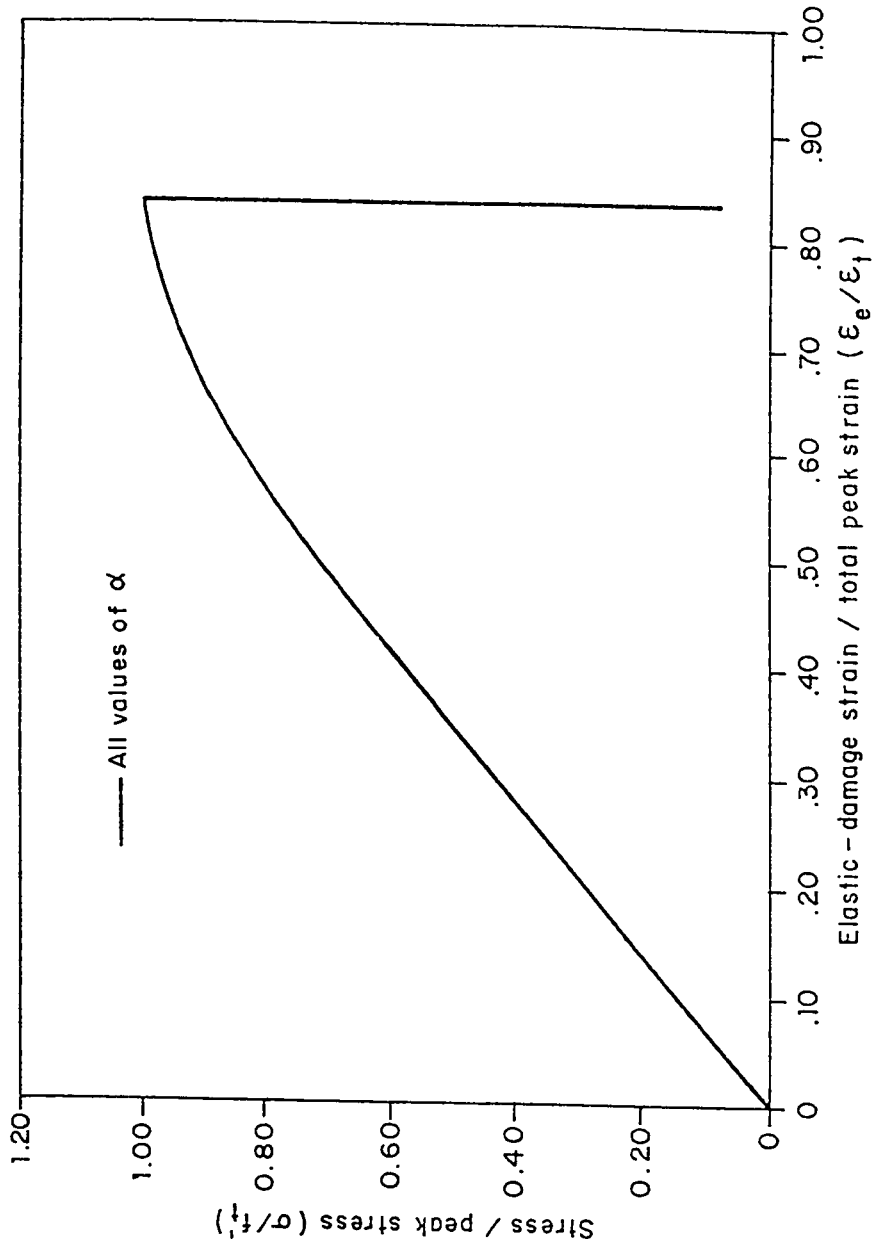


Figure 5.3 Stress-elastic strain relationship in uniaxial tension for concrete

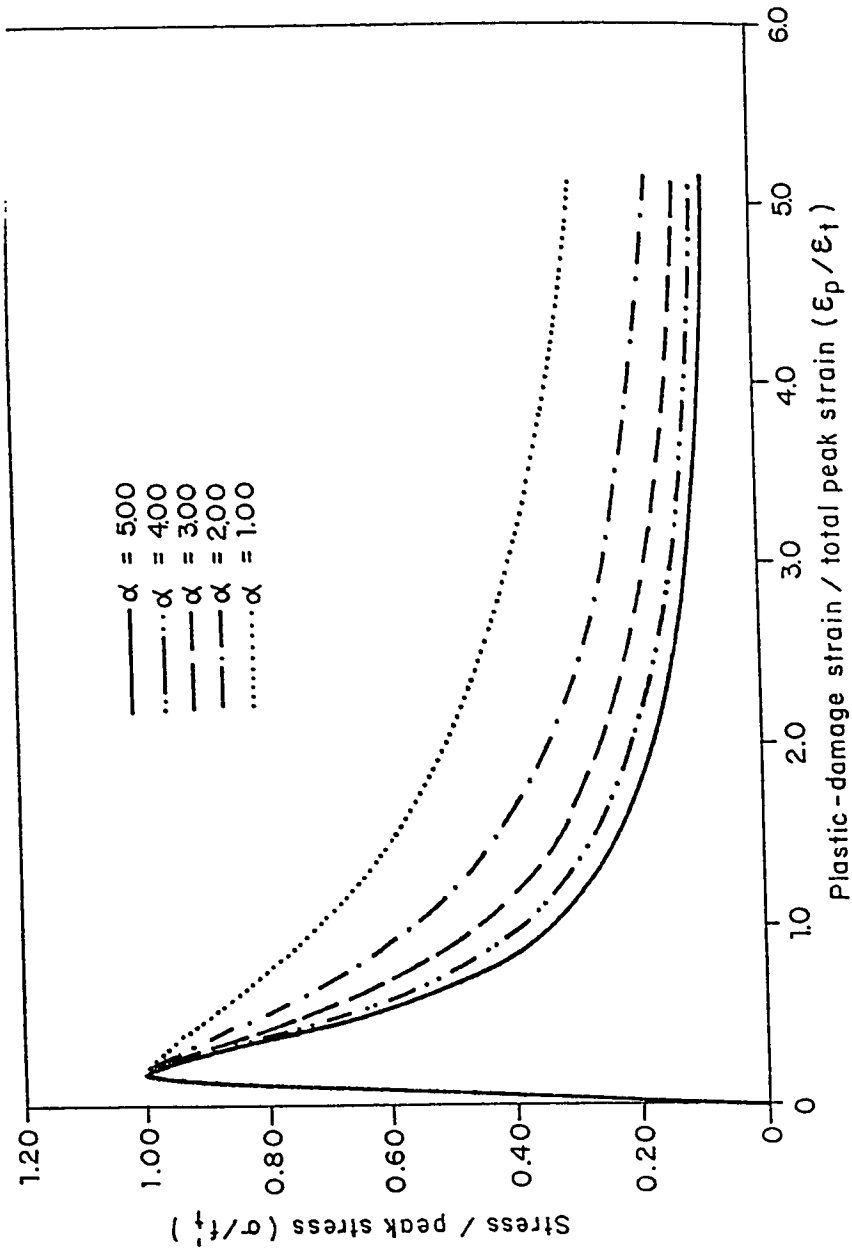


Figure 5.4 Stress-plastic strain relationship in uniaxial tension for concrete

$$A_o^t = \left(\frac{d\sigma}{dr} \right)_{\epsilon=0} = \left(\frac{\partial \left(\frac{\sigma}{f_t'} \right)}{\partial \left(\frac{\epsilon}{\epsilon_t} \right)} \right)_{\epsilon=0} \frac{f_t'}{\epsilon_t} = 1.2 \frac{f_t'}{\epsilon_t} \quad (5.8)$$

Similarly, the initial elastic damage and plastic damage moduli, E_o^t and P_o^t , can be shown to be

$$\begin{aligned} E_o^t &= \left(\frac{d\sigma}{dr_e} \right)_{\epsilon_e=0} = \left(\frac{\partial \left(\frac{\sigma}{f_t'} \right) / \partial \left(\frac{\epsilon}{\epsilon_t} \right)}{\partial \left(\frac{\epsilon_e}{\epsilon_t} \right) / \partial \left(\frac{\epsilon}{\epsilon_t} \right)} \right)_{\epsilon_e=\epsilon_e=0} * \frac{f_t'}{\epsilon_t} \\ &= \frac{1.2}{0.834} * \frac{f_t'}{\epsilon_t} = 1.44 \frac{f_t'}{\epsilon_t} = 1.2 A_o^t \end{aligned} \quad (5.9)$$

and

$$\begin{aligned} P_o^t &= \left(\frac{d\sigma}{dr_p} \right)_{\epsilon_p=0} = \left(\frac{\partial \left(\frac{\sigma}{f_t'} \right) / \partial \left(\frac{\epsilon}{\epsilon_t} \right)}{\partial \left(\frac{\epsilon_p}{\epsilon_t} \right) / \partial \left(\frac{\epsilon}{\epsilon_t} \right)} \right)_{\epsilon_p=\epsilon_p=0} * \frac{f_t'}{\epsilon_t} \\ &= \frac{1.2}{0.166} * \frac{f_t'}{\epsilon_t} = 7.2 \frac{f_t'}{\epsilon_t} = 6 A_o^t \end{aligned} \quad (5.10)$$

From the stress-strain components curves the following can be deduced:

1. The stress-elastic damage strain curve (Fig. 5.3) has the shape of an elastic perfectly-brittle response but has a distinct

characteristic. This is attributed to the fact that the stress level reduces gradually and not abruptly at $\varepsilon_e/\varepsilon_t = 0.83$. This means that every point on the locus $\varepsilon_e/\varepsilon_t = 0.83$ represents a certain degraded stiffness and which unloads to the origin (refer to Fig. 4.2b). The relation is independent of the strength factor α , i.e. valid for all concretes. Such a behavior can be termed "quasi subperfectly brittle".

2. The stress-plastic damage strain curve (Fig. 5.4) exhibits softening behavior. The characteristic of the plastic strain is different from that for metals. It incorporates microcracks cleavage as well as the localized macrocrack opening. There is apparent degradation of the plastic stiffness and unloading proceeds vertically (Fig. 4.2c). Such a behavior, based on the unloading path, may be classified as being "quasi subperfectly plastic".

5.2.4 Uniaxial Tensile MGDV

The essential feature of Kachanov's model (1958) resides in the introduction of a special internal (hidden) variable defining the state of damage locally and recording its accumulation. Krajcinovic and Silva (1982) pointed out that the most sensitive aspect of a realistic damage model consists of the establishment of a rational damage law (i.e. the response function defining the rate of the damage accumulation in terms of the current values of other state and internal variables). As long as uniaxial behavior is concerned, each stress-strain component includes a single damage variable representing the state of degradation. With

reference to Eqn. (5.3) which can be looked upon as an uncoupling constraint, only two (of the three) damage variables are sufficient to give a clear picture of the state (stress and strain constituents). These two damage variables are, therefore, generalized. Apart from the existing variability in literature in assigning a unique definition to the damage variable, emphasis is placed on the degradation of stiffness (Mazars, 1982, 1984, 1986; Resende and Martin, 1984; Ladeveze, 1983; Lorrain and Loland, 1983; Resende, 1987; Mazars and Lemaitre, 1984; Frantziskonis and Desai, 1987a,b,c; Frantziskonis, 1986).

The damage variables d_a^t , d_e^t and d_p^t conjugate to ϵ , ϵ_e and ϵ_p , respectively, may be expressed as

$$d_a^t = 1 - \frac{A^t}{A_0^t} \quad (5.11-a)$$

$$d_e^t = 1 - \frac{E^t}{E_0^t} \quad (5.11-b)$$

$$d_p^t = 1 - \frac{P^t}{P_0^t} \quad (5.11-c)$$

Using Eqns. (5.1), (5.2), (5.5) and (5.6) in Eqns. (5.7) and then substituting the results in Eqns. (5.11), the damage variables can be expressed as

$$d_a^t = \begin{cases} 0.167 \left(\frac{\epsilon}{\epsilon_t} \right)^5 & \frac{\epsilon}{\epsilon_t} \leq 1 \\ 1 - \frac{1}{1.2 \left\{ \alpha \left[\left(\frac{\epsilon}{\epsilon_t} \right) - 1 \right]^{1.7} + \frac{\epsilon}{\epsilon_t} \right\}} & \frac{\epsilon}{\epsilon_t} \geq 1 \end{cases} \quad (5.12)$$

$$d_e^t = \begin{cases} 0.167 \left(\frac{\epsilon}{\epsilon_t} \right)^5 & \frac{\epsilon}{\epsilon_t} \leq 1 \\ 1 - \frac{\epsilon/\epsilon_t}{1.2 \left\{ \alpha \left[\left(\frac{\epsilon}{\epsilon_t} \right) - 1 \right]^{1.7} + \frac{\epsilon}{\epsilon_t} \right\}} & \frac{\epsilon}{\epsilon_t} \geq 1 \end{cases} \quad (5.13)$$

$$d_p^t = \begin{cases} 0.167 \left(\frac{\epsilon}{\epsilon_t} \right)^5 & \frac{\epsilon}{\epsilon_t} \leq 1 \\ 1 - \frac{\epsilon/\epsilon_t}{7.2 \left\{ \alpha \left[\left(\frac{\epsilon}{\epsilon_t} \right) - 1 \right]^{1.7} + \frac{\epsilon}{\epsilon_t} \right\} \left\{ \frac{\epsilon}{\epsilon_t} - 0.834 \right\}} & \frac{\epsilon}{\epsilon_t} \geq 1 \end{cases} \quad (5.14)$$

Figs. 5.5, 5.6 and 5.7 show the evolution of total, elastic and plastic damage, respectively, as given by Eqns. (5.12-14). In the prepeak region all of the MGDV evolve in similar patterns while only d_a^t possesses smooth transition for both value and slope at the peak strain ϵ_t . In the post-peak region, d_p^t increases more rapidly than d_a^t and d_e^t , and with the least sensitivity to the value of α . This is attributed to the steep descent gradient in $\sigma/\epsilon_t' - \epsilon_p/\epsilon_t$ curve in the proximity to the

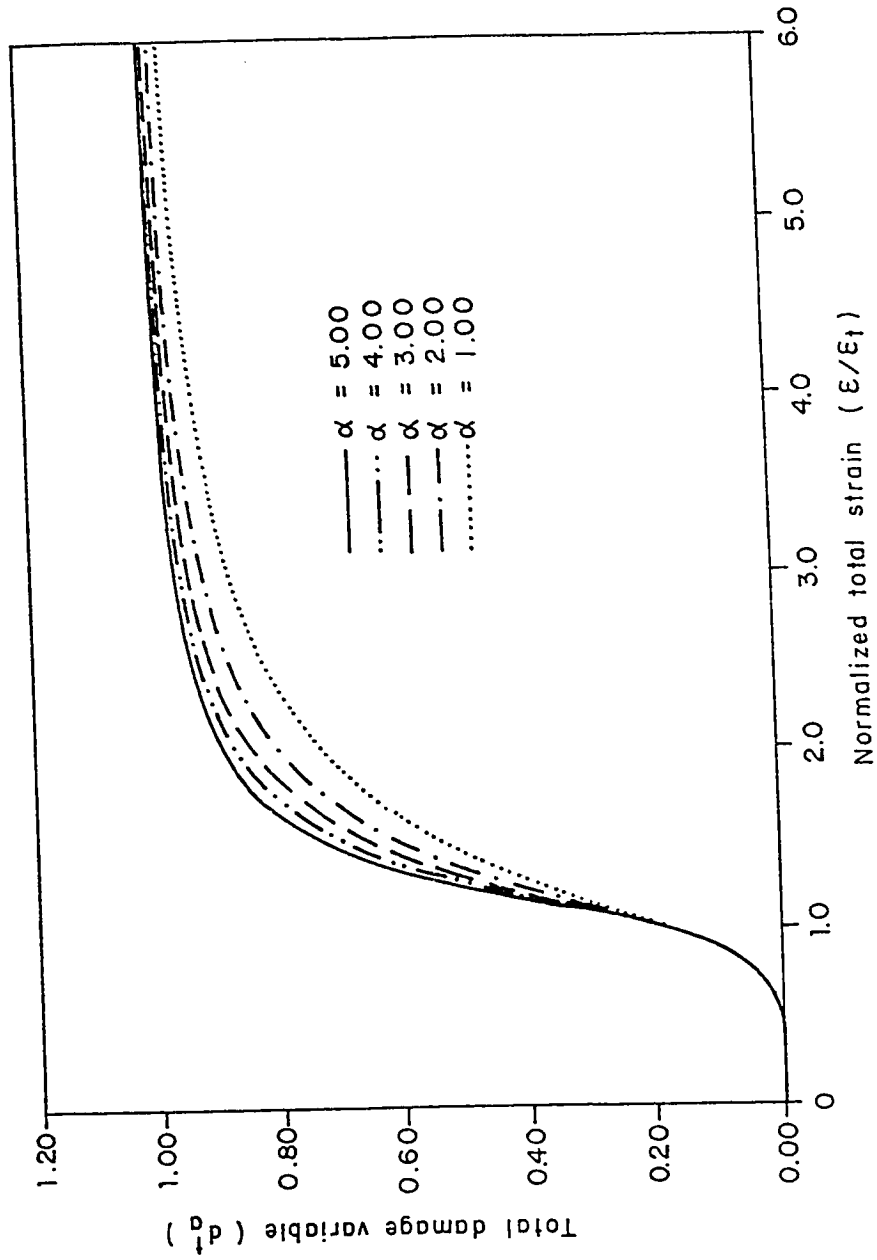


Figure 5.5 Total damage variable in uniaxial tension for concrete

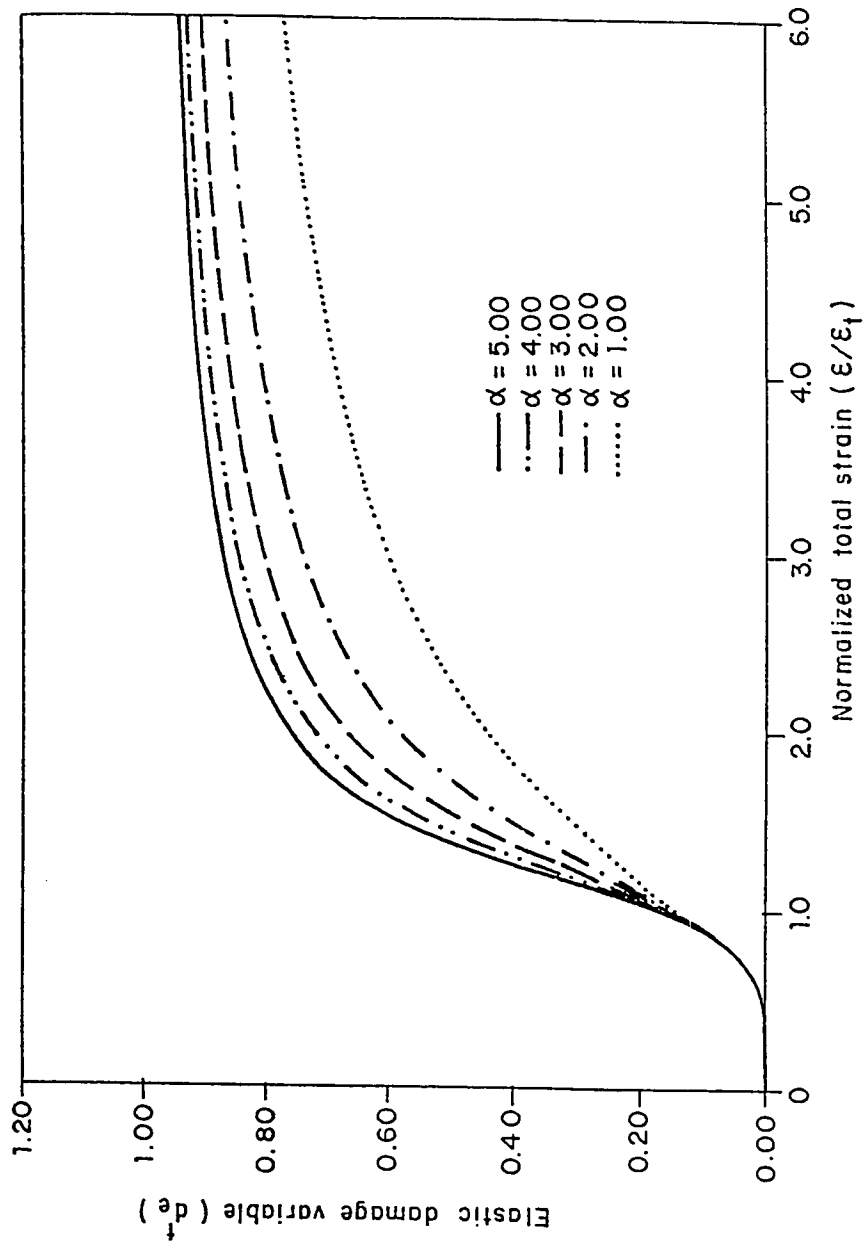


Figure 5.6 Elastic damage variable in uniaxial tension for concrete

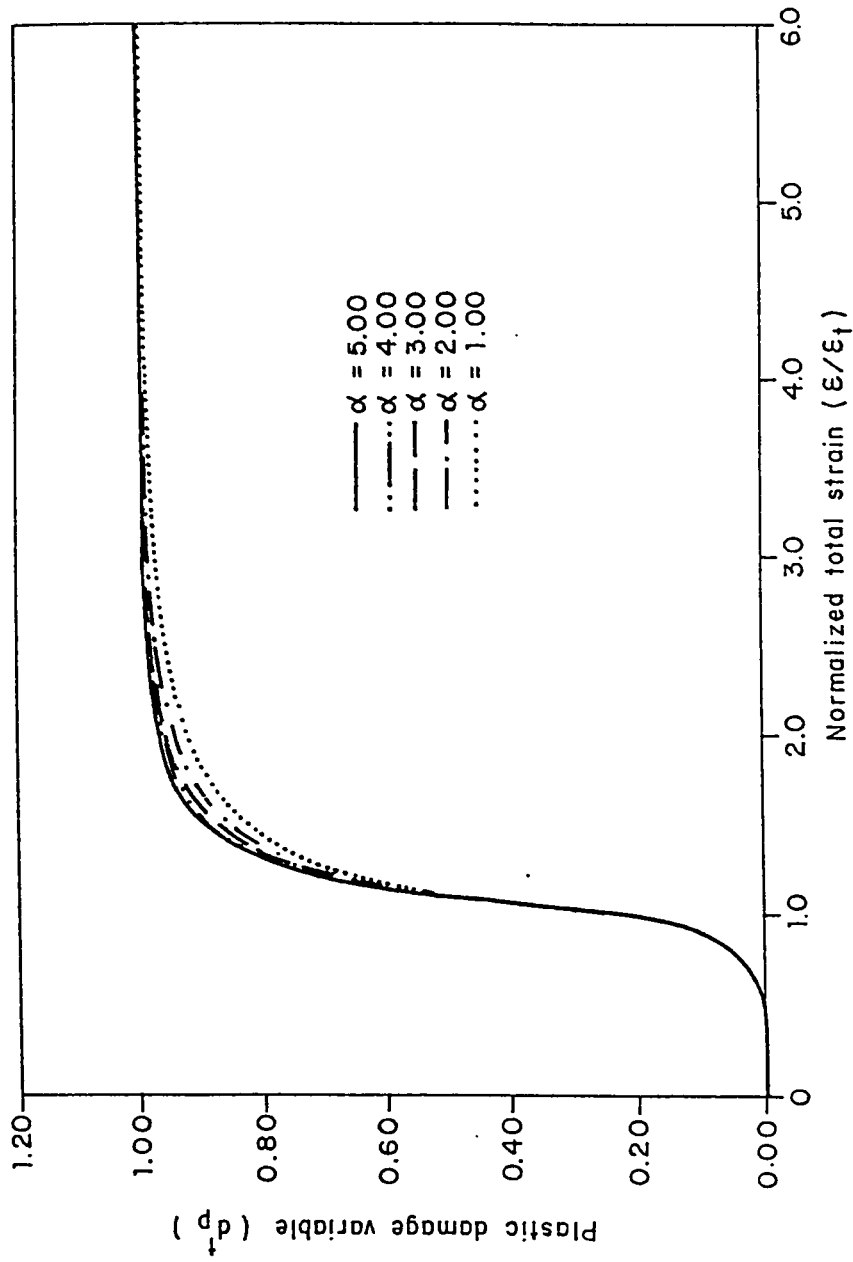


Figure 5.7 Plastic damage variable in uniaxial tension for concrete

peak. The elastic damage variable, d_e^t , shows the greatest sensitivity to α and the least damage rate. The total damage variable, d_a^t , represents an intermediate trend with respect to the other MGDV.

5.3. DAMAGE VARIABLES FOR CONCRETE IN COMPRESSION

5.3.1 Stress-Total Strain Relationship

The overall monotonic loading behavior can be described by Popovics' formula (1973) which is given as (Fig. 5.8)

$$\frac{\sigma}{f_c'} = \frac{n_o \left(\frac{\epsilon}{\epsilon_c} \right)^{n_o}}{n_o - 1 + \left(\frac{\epsilon}{\epsilon_c} \right)^{n_o}} \quad (5.15)$$

in which ϵ_c is the peak strain and n_o is a material parameter dependent on f_c' (e.g. for $f_c' = 17.25$ MPa (2500 psi) $n_o = 2$ and $f_c' = 34.5$ MPa (5000 psi); $n_o = 3$). For $n_o = 2$, it reduces to Saenz's formula (1964) and to Desayi and Krishnan's formula (1964) provided that the initial tangent modulus (A_0^c) is equal to twice the peak secant modulus (f_c'/ϵ_c). Other existing formulae for uniaxial compression are Madrid parabola, Hognestad formula (1951) and Smith and Young's formula (1955). Popovics' formula was used previously in many studies (see for

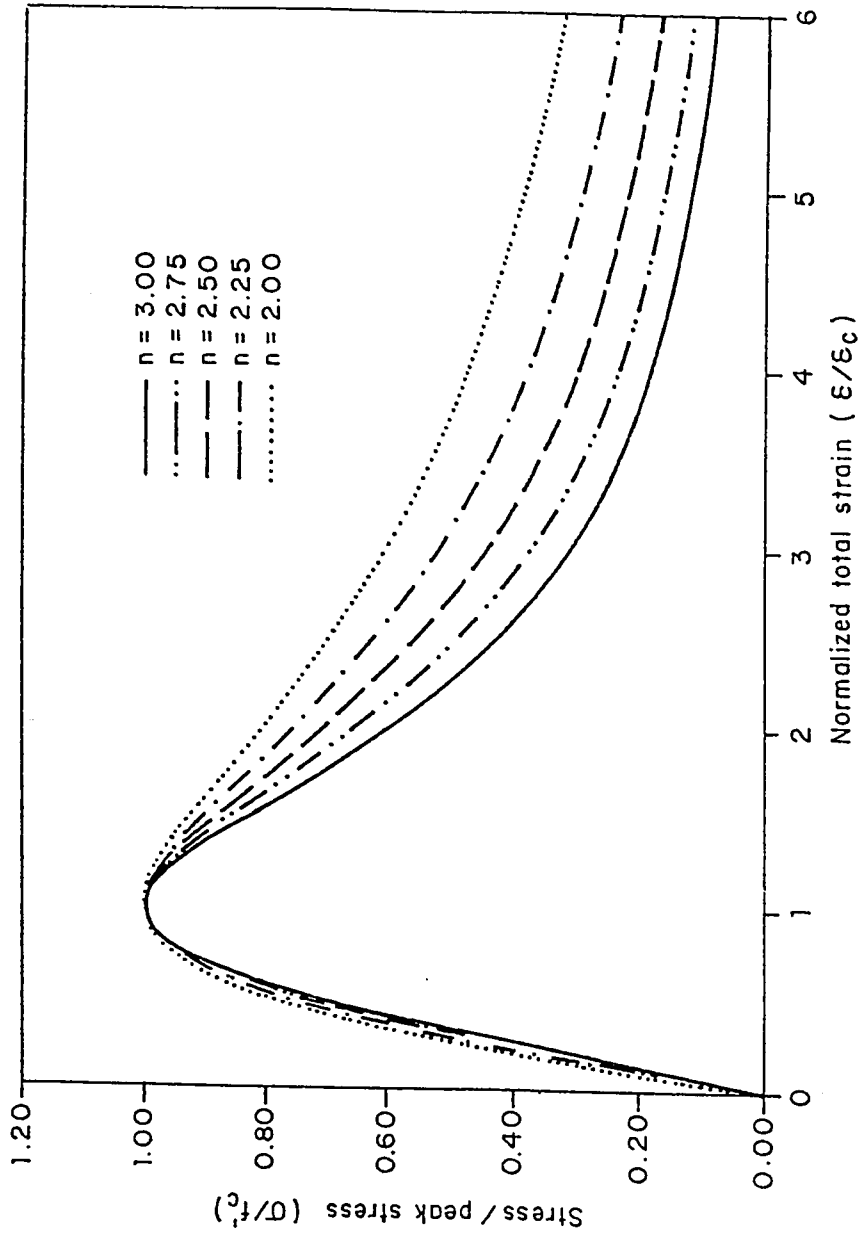


Figure 5.8 Stress-total strain relationship in uniaxial compression according to Popovics' idealization (1973) for concrete

example Bazant, 1976; Bazant and Kim, 1979; Bazant and Tsubaki, 1980; Buyukozturk and Tseng, 1984).

5.3.2 Strain Components

Data available about compressive cyclic loading of concrete are more than those related to tensile cyclic loading (see for example Karsan and Jirsa, 1969; Sinha et al., 1964; Shah and Chandra, 1970; Spooner and Dougill, 1975; Shah and Winter, 1966; Buyukozturk and Tseng, 1984). The subsequent analysis makes use of the work of Karsan and Jirsa (1969) in which a series of 46 short rectangular test specimens were subjected to repetitions of compressive stress to various levels. They developed an analytical expression relating the permanent strain to the total strain at unloading ϵ , and given as a continuous function in the form

$$\left(\frac{\epsilon_p}{\epsilon_c} \right) = 0.145 \left(\frac{\epsilon}{\epsilon_c} \right)^2 + 0.127 \left(\frac{\epsilon}{\epsilon_c} \right) \quad (5.16)$$

This expression was used by Darwin and Pecknold (1974, 1977) in concrete modelling and yielded satisfactory results. Interpreting the permanent strain as the plastic-damage strain, and using Eqns. (5.3) and (5.16), the normalized elastic-damage strain may be shown to be given by

$$\left(\frac{\epsilon_e}{\epsilon_c} \right) = 0.873 \left(\frac{\epsilon}{\epsilon_c} \right) - 0.145 \left(\frac{\epsilon}{\epsilon_c} \right)^2 \quad (5.17)$$

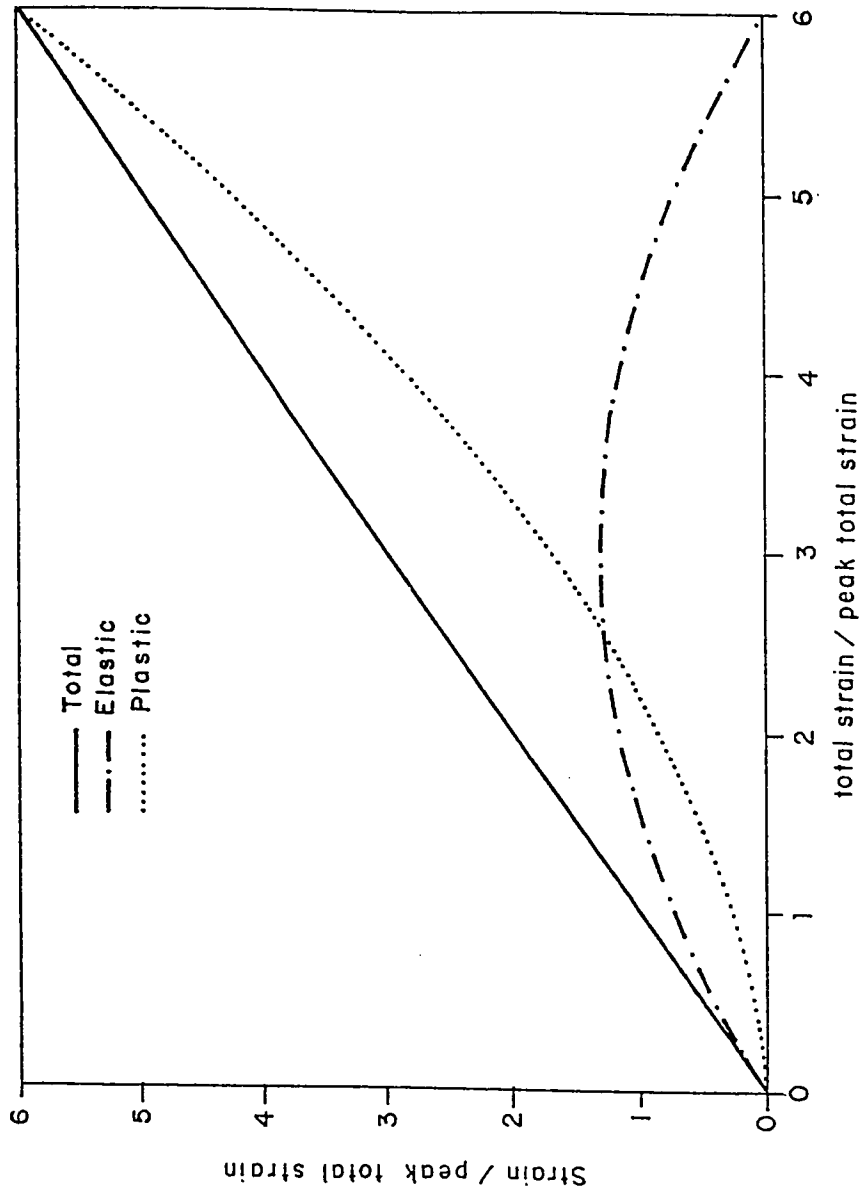


Figure 5.9 Strain components in uniaxial compression for concrete

Unlike Eqns. (5.4) used in tension, the strain components in compression exhibit nonlinearity. Fig. 5.9 shows plots of the total strain and its components. The following can be noted:

1. For $\epsilon < 2.55 \epsilon_c$, the contribution of the elastic damage strain to the total strain is larger than that of the plastic damage strain.
2. While the elastic damage strain has an inflection point, the plastic strain grows continuously.
3. The maximum elastic-damage strain is 1.3 times the peak total strain occurring at normalized total strain of 3 and then decreases.
4. All strain is supposed to be unrecoverable at normalized total strain of 6. However, this is a very high strain ratio in compression, and failure usually occurs before this value.

It is apparent here as in the case of uniaxial tension that the plastic-damage behavior is of the same, if not of more, importance as the elastic-damage behavior. This illustrates the amount of approximation associated with postulating either completely plastic or brittle behavior.

5.3.3 Stress-Strain Components Relationships

Similar to the procedures carried out in tension, the following secant relations are adopted

$$\sigma(\epsilon) = A^c(\epsilon) * \epsilon \quad (5.18-a)$$

$$= E^c(\epsilon) * \epsilon_e \quad (5.18-b)$$

$$= P^c(\epsilon) * \epsilon_p \quad (5.18-c)$$

where $A^c(\epsilon)$, $E^c(\epsilon)$ and $P^c(\epsilon)$ are the total, elastic and plastic damage moduli at any strain level, ϵ , whose initial values are A_0^c , E_0^c and P_0^c , respectively. The initial total tangent moduli is

$$A_0^c = \left(\frac{d\sigma}{d\epsilon} \right)_{\epsilon=0} = \left(\frac{\partial \left(\frac{\sigma}{f_c'} \right)}{\partial \left(\frac{\epsilon}{\epsilon_c} \right)} \right)_{\epsilon=0} \frac{f_c'}{\epsilon_c} = \frac{n_0}{n_0 - 1} * \frac{f_c'}{\epsilon_c} \quad (5.19)$$

For $n_0 = 2$, Eqn. (5.19) and the initial tangent modulus obtained from Hognestad's ascending parabola (1951) are reconciled. Since the initial tangents in tension and compression are almost equal, the peak total secant modulus in tension, $A_p^t = f_t'/\epsilon_t$, can be expressed in terms of that in compression $A_p^c = f_c'/\epsilon_c$ by using Eqns. (5.8) and (5.19) yielding

$$A_p^t = \frac{n_0}{1.2(n_0 - 1)} A_p^c \quad (5.20-a)$$

In addition, the peak strains can be correlated to the peak stresses in both tension and compression (Guo and Zhang, 1981; Popovics, 1973), leaving the characteristic strength f_c' as the only material parameter, since

$$\epsilon_c = \frac{f_c'}{f_t'} \epsilon_t \frac{n_0}{1.2(n_0-1)} \quad (5.20-b)$$

The initial elastic modulus, E_0^c , can be shown to equal

$$\begin{aligned} E_0^c &= \left(\frac{d\sigma}{d\epsilon_e} \right)_{\epsilon_e=0} = \left(\frac{\partial \left(\frac{\sigma}{f_c'} \right) / \partial \left(\frac{\epsilon}{\epsilon_c} \right)}{\partial \left(\frac{\epsilon_e}{\epsilon_c} \right) / \partial \left(\frac{\epsilon}{\epsilon_c} \right)} \right)_{\epsilon_e=\epsilon=0} * \frac{f_c'}{\epsilon_c} \\ &= \frac{n_0}{0.873(n_0-1)} \frac{f_c'}{\epsilon_c} = 1.15 A_0^c \end{aligned} \quad (5.21)$$

Again, $E_0^c \neq A_0^c$, but in comparing with the equivalent in tension, indicates the faster growth of elastic-damage strains, with respect to the total and hence the plastic-damage strains. The initial plastic modulus, P_0^c , is derived as follows

$$\begin{aligned} P_0^c &= \left(\frac{d\sigma}{d\epsilon_p} \right)_{\epsilon_p=0} = \left(\frac{\partial \left(\frac{\sigma}{f_c'} \right) / \partial \left(\frac{\epsilon}{\epsilon_c} \right)}{\partial \left(\frac{\epsilon_p}{\epsilon_c} \right) / \partial \left(\frac{\epsilon}{\epsilon_c} \right)} \right)_{\epsilon_p=\epsilon=0} * \frac{f_c'}{\epsilon_c} \\ &= \frac{n_0}{0.127(n_0-1)} \frac{f_c'}{\epsilon_c} = 7.87 A_0^c \end{aligned} \quad (5.22)$$

Fig. 5.10 shows a helmet-shaped knot in the elastic-damage behavior. The post-peak response consists of strain-softening followed by retrogression (in both stress and strain). The pattern features

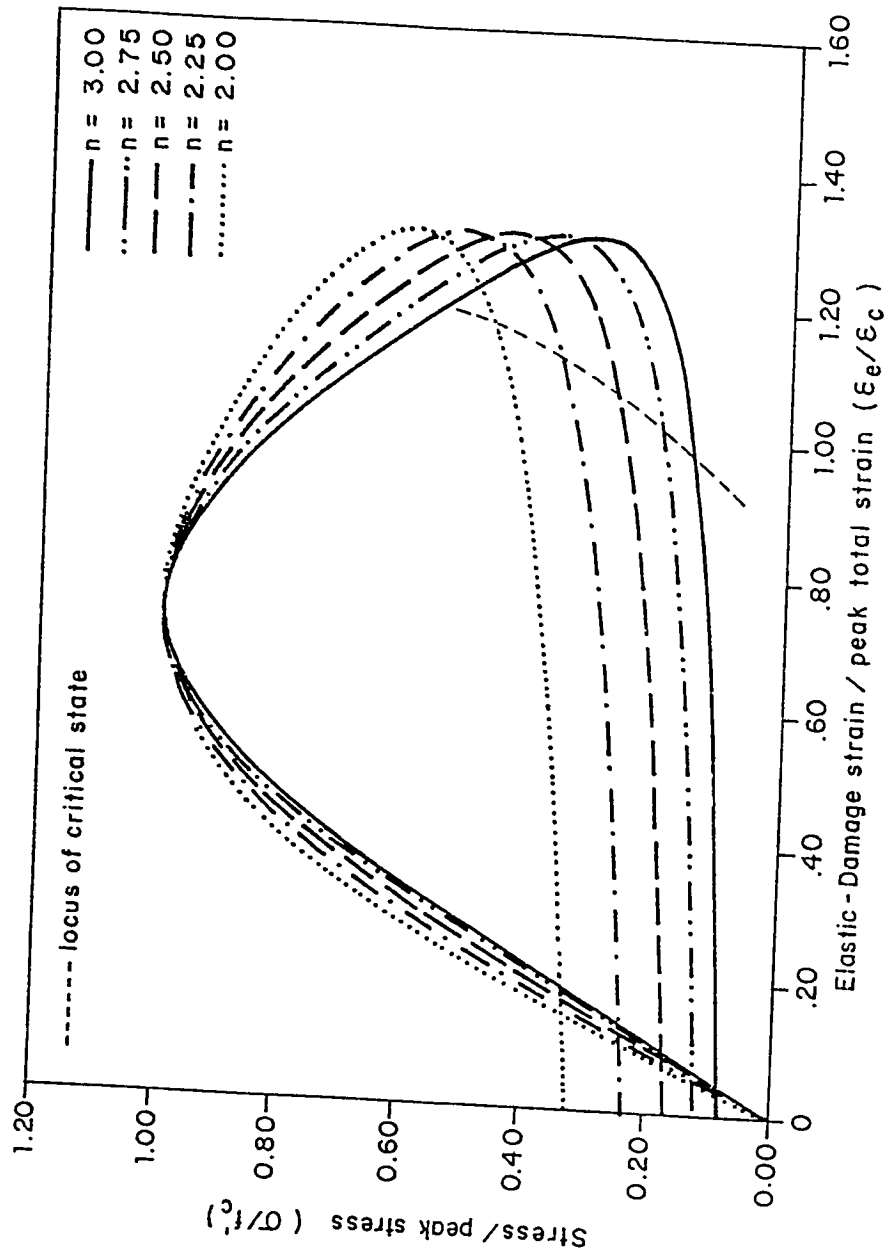


Figure 5.10 Stress-elastic strain relationship in uniaxial compression for concrete

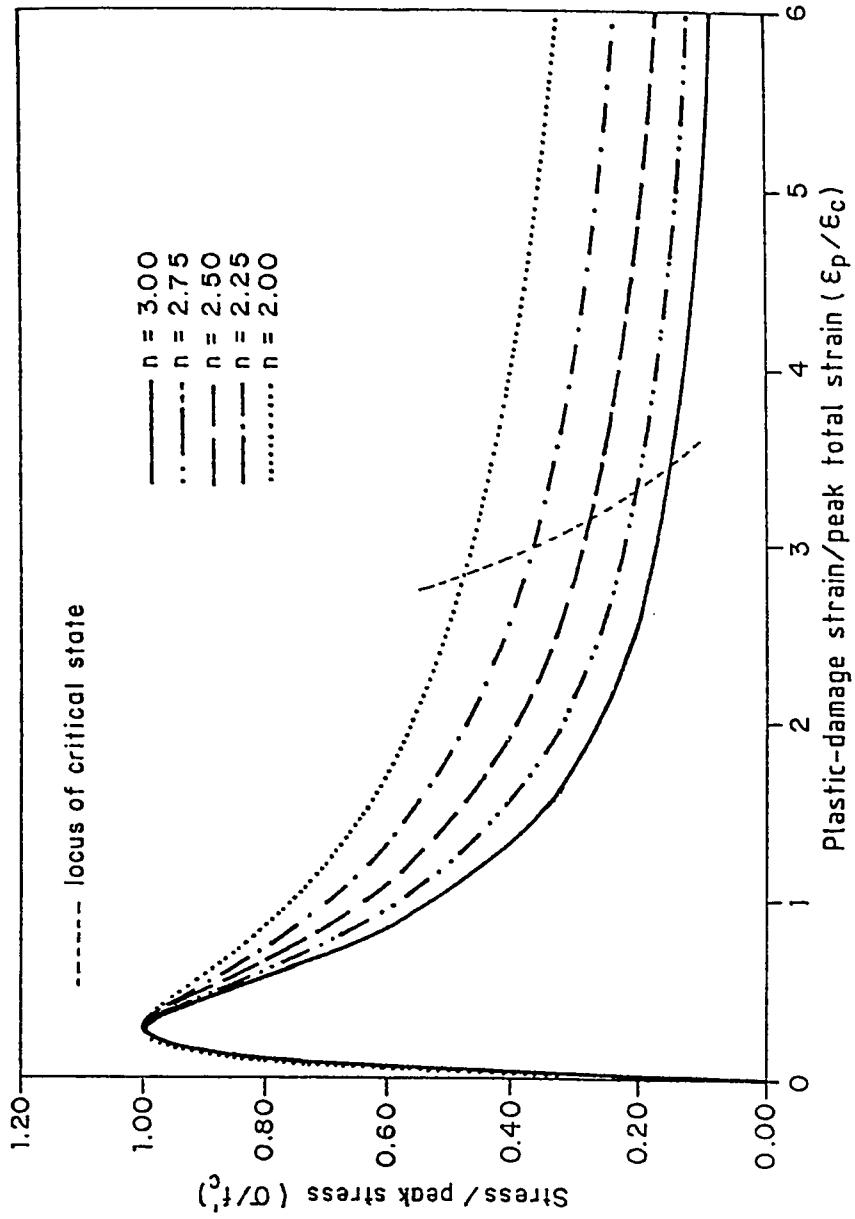


Figure 5.11 Stress-plastic strain relationship in uniaxial compression for concrete

a new characteristic countenance concealed in the concrete's uniaxial total response from which it cannot be directly grasped. In contrast, the plastic post-peak behavior (Fig. 5.11) shows only strain softening.

Similar unloading paths are followed as in tension, i.e. generalized damage for total behavior, quasi sub-perfect plastic for plastic-damage behavior while quasi sub-brittle for elastic-damage behavior.

5.3.4 Uniaxial Compressive MGDV

The damage variable, d_a^c , d_e^c and d_p^c conjugate to ϵ , ϵ_e and ϵ_p , respectively, are simply expressed as

$$d_a^c = 1 - \frac{A^c}{A_o^c} \quad (5.23-a)$$

$$d_e^c = 1 - \frac{E^c}{E_o^c} \quad (5.23-b)$$

and

$$d_p^c = 1 - \frac{P^c}{P_o^c} \quad (5.23-c)$$

Using Eqn. (5.15) in Eqns. (5.18) to find A^c , E^c and P^c , then substituting in Eqns. (5.23) with the help of Eqns. (5.19), (21) and (22), the MGDV can be reduced to the following form:

$$d_a^c = \frac{\left(\frac{\varepsilon}{\varepsilon_c}\right)^{n_0}}{n_0 - 1 + \left(\frac{\varepsilon}{\varepsilon_c}\right)^{n_0}} \quad (5.24)$$

$$d_e^c = \frac{d_a^c - 0.166 \left(\frac{\varepsilon}{\varepsilon_c}\right)}{1 - 0.166 \left(\frac{\varepsilon}{\varepsilon_c}\right)} \quad (5.25)$$

and

$$d_p^c = \frac{d_a^c + 1.142 \left(\frac{\varepsilon}{\varepsilon_c}\right)}{1 + 1.142 \left(\frac{\varepsilon}{\varepsilon_c}\right)} \quad (5.26)$$

Figs. (5.12-14) illustrate the evolution of the MGDV for different values of n_0 ($n_0 = 2, 2.25, 2.5, 2.75$ and 3). Total and plastic damage starts with the first load application but this is not the case for the elastic damage. The threshold elastic damage is delayed slightly (Fig. 5.13) and depends on the value of n_0 . The corresponding total strain is evaluated as follows:

The initial behavior of the compressive elastic damage variable, d_e^c , shows a small reduction followed by an increase in its value. According to Clausius-Duhem inequality

$$d_e^c \geq 0 \quad (5.27)$$

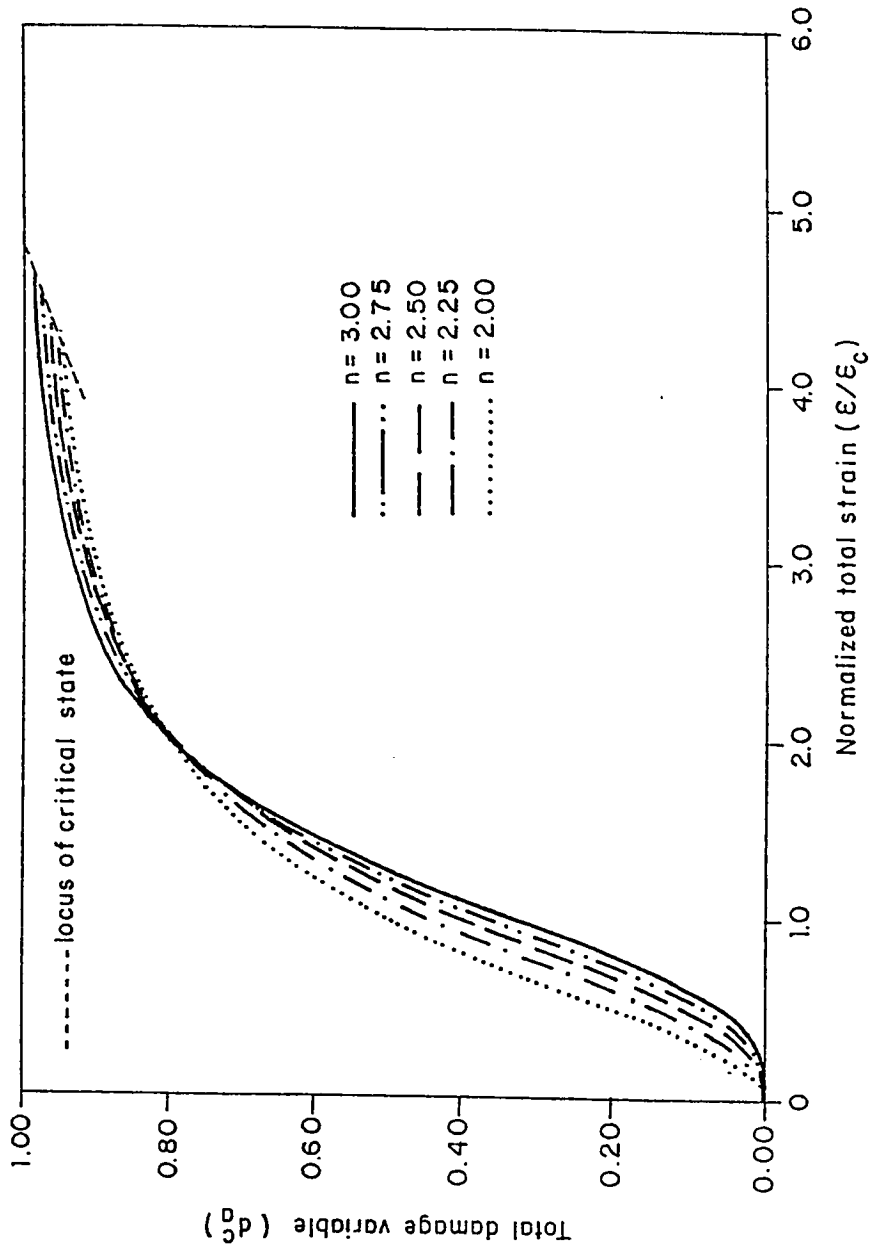


Figure 5.12 Total damage variable in uniaxial compression for concrete

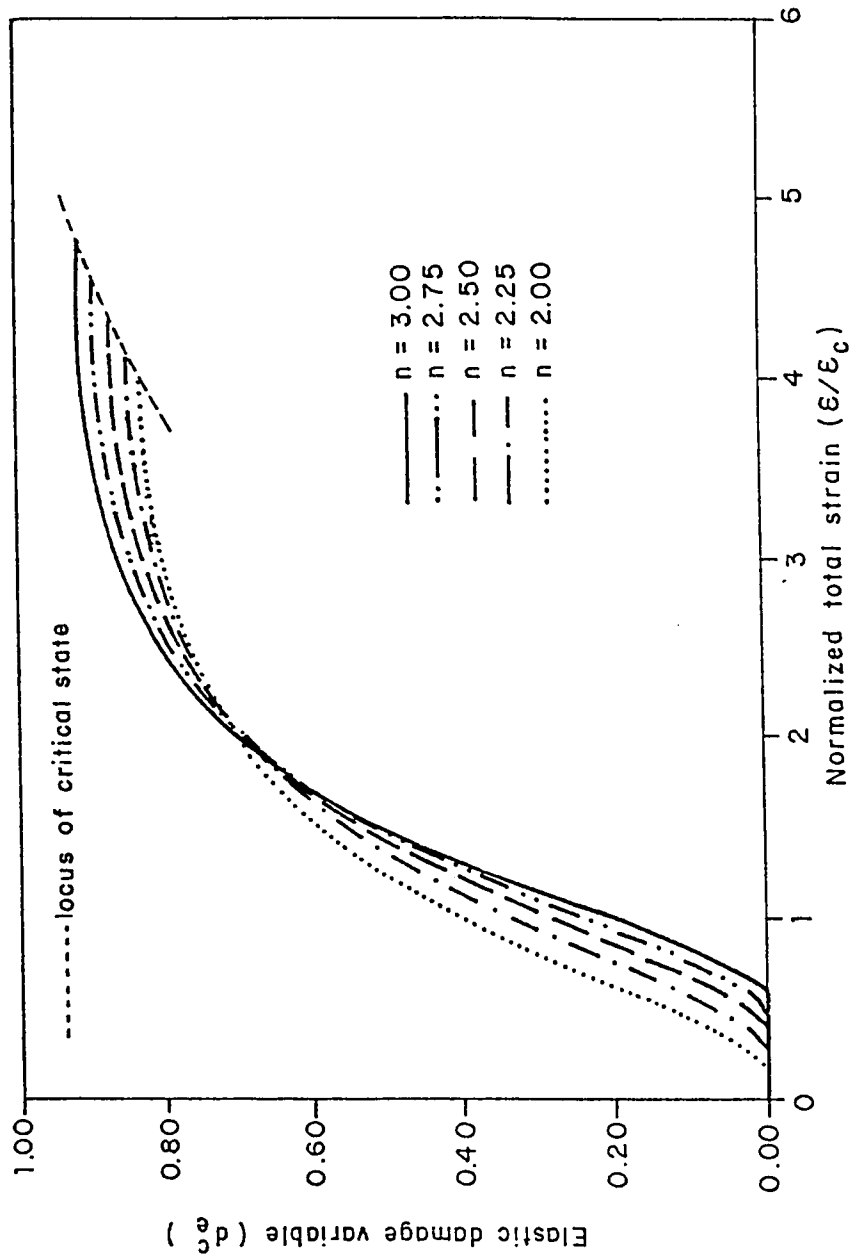


Figure 5.13 Elastic damage variable in uniaxial compression for concrete

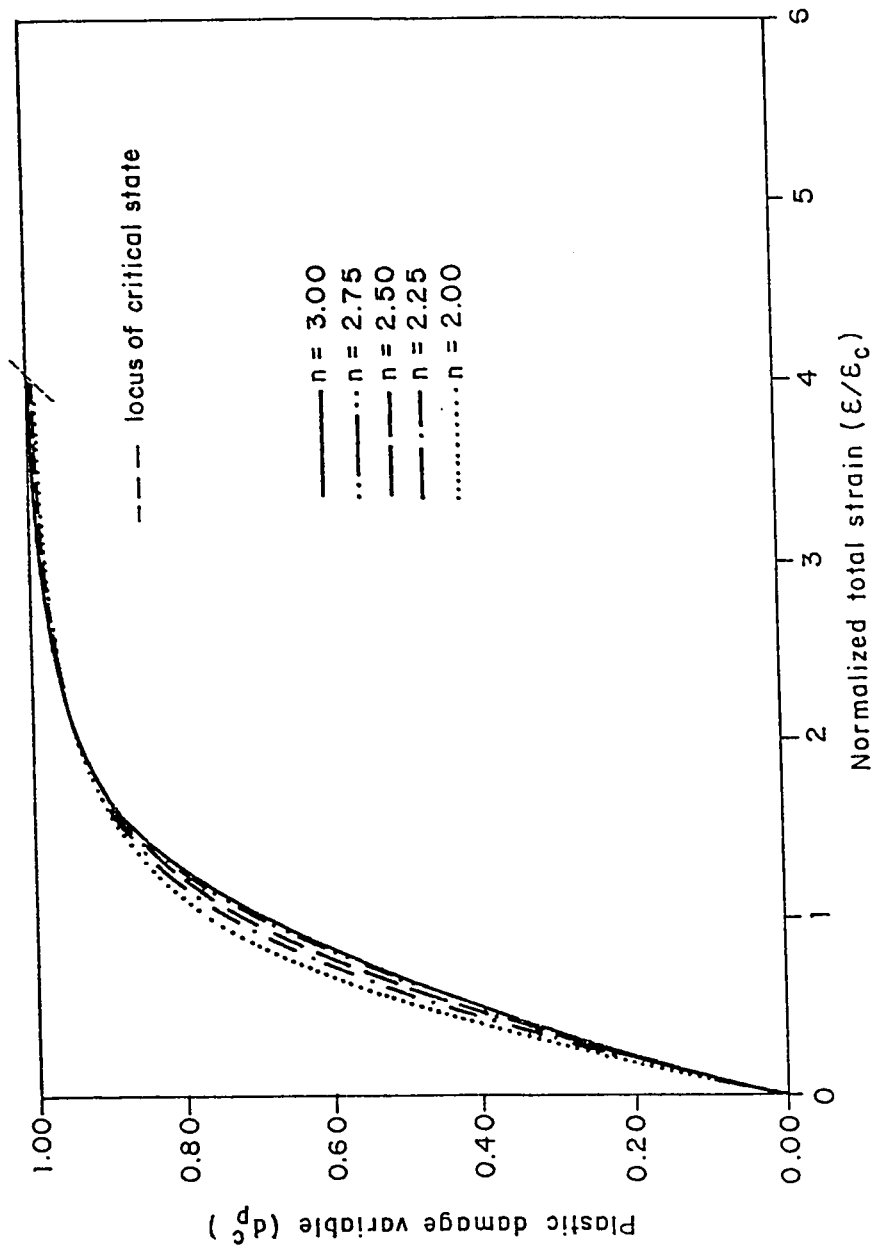


Figure 5.14 Plastic damage variable in uniaxial compression for concrete

Therefore it is advisable to discard any negative values of d_e^c . In order for $d_e^c > 0$, one notes from Eqn. (5.25) that

$$(d_a^c)_{ed} \geq 0.166 \left(\frac{\epsilon}{\epsilon_c} \right)_{ed} \quad (5.28)$$

in which subscript "ed" denotes elastic damage threshold. Using Eqn. (5.24) to eliminate $(d_a^c)_{ed}$ from (5.28), the following equation is obtained

$$\left(\frac{\epsilon}{\epsilon_c} \right)_{ed}^{n_0} - 6 \left(\frac{\epsilon}{\epsilon_c} \right)_{ed}^{(n_0-1)} + (n_0 - 1) = 0 \quad (5.29)$$

Closed form solution of Eqn. (5.29) is mathematically formidable. Solving for specific values of n_0 , getting the correct threshold total strain ratio, then fitting using quadratic regression by least square technique (values are listed in Table 5.1), the approximate strain ratio is found to be

$$\left(\frac{\epsilon}{\epsilon_c} \right)_{ed} = -1.3274 + 0.9572 n_0 - 0.1039 n_0^2 \quad (5.30)$$

Growth of plastic damage rates is faster than the total damage. Asymptotic behavior of d_a^c and d_p^c ($\lim_{\epsilon \rightarrow \infty} d_a^c = 1.0$, $\lim_{\epsilon \rightarrow \infty} d_p^c = 1.0$) can be proved from their functional behavior (Eqns. 5.24, 5.26). By contrast, behavior of d_e^c described by Eqn. (5.25) depicts not only singularity at

Table 5.1 Threshold and critical compressive parameters.

n	d ^c	Threshold				Critical				
		$\frac{\epsilon}{\epsilon_c}$	$\frac{\epsilon_r}{\epsilon_c}$	$\frac{\epsilon_p}{\epsilon_c}$	$\frac{\sigma}{f'_c}$	$\frac{\epsilon}{\epsilon_c}$	$\frac{\epsilon_r}{\epsilon_c}$	$\frac{\epsilon_p}{\epsilon_c}$	$\frac{\sigma}{f'_c}$	value
2.00	a	-	-	-	-	3.915	1.184	2.731	0.480	0.939
	e	0.175	0.148	0.027	0.340	3.915	1.184	2.731	0.480	0.824
	p	-	-	-	-	3.915	1.184	2.731	0.480	0.989
2.25	a	-	-	-	-	4.088	1.133	2.955	0.368	0.948
	e	0.297	0.246	0.051	0.508	4.088	1.133	2.955	0.368	0.843
	p	-	-	-	-	4.088	1.133	2.955	0.368	0.990
2.50	a	-	-	-	-	4.237	1.083	3.154	0.275	0.961
	e	0.417	0.338	0.079	0.647	4.237	1.083	3.154	0.275	0.867
	p	-	-	-	-	4.237	1.083	3.154	0.275	0.993
2.75	a	-	-	-	-	4.368	1.034	3.335	0.202	0.970
	e	0.519	0.412	0.107	0.745	4.368	1.034	3.335	0.202	0.892
	p	-	-	-	-	4.368	1.034	3.335	0.202	0.995
3.00	a	-	-	-	-	4.475	0.990	3.485	0.147	0.975
	e	0.610	0.477	0.133	0.822	4.475	0.990	3.485	0.147	0.914
	p	-	-	-	-	4.475	0.990	3.485	0.147	0.996

exhibiting sign reversal, thus violating the second law of thermodynamics. These can be alleviated by using Clausius-Duhem inequality (Patino, 1989) to establish the critical MGDV as follows:

Considering Eqn. (5.27), the onset of the maximum compressive elastic damage variable is required to determine the critical strain state. Differentiating Eqn. (5.25), substituting for d_a^c from Eqn. (5.24) then equating the product to zero, the total strain ratio corresponding to the critical d_e^c and therefore other damage variables can be determined from the following equation:

$$(n_o + 1) \left(\frac{\epsilon}{\epsilon_c} \right)_c^{n_o} - 6n_o \left(\frac{\epsilon}{\epsilon_c} \right)_c^{(n_o - 1)} + (n_o - 1) = 0 \quad (5.31)$$

in which the subscript "c" denotes critical state. Similar fitting treatment to that done for the threshold values to obtain reasonably an approximate feasible solution $\left[\left(\frac{\epsilon}{\epsilon_c} \right)_c \in [0, 6] \right]$ yields

$$\left(\frac{\epsilon}{\epsilon_c} \right)_c = 1.7925 + 1.395 n_o - 0.167 n_o^2 \quad (5.32)$$

Using the value of $(\epsilon/\epsilon_c)_c$ obtained from the previous equation in the compressive MGDV (Eqns. 5.24-26) yields the critical MGDV. (The correct values are listed in Table 5.1 for comparison).

Although the procedure presented seems to fully uncouple the total, elastic and plastic damage behavior, a cursory inspection of Eqns. (5.25) and (5.26) indicates that the three damage variables are interrelated. Table 5.1 lists the threshold and critical values of the damage variables along with the corresponding normalized stress, total strain and its components.

At this stage, the following features can be elucidated for both tensile and compressive behaviors:

1. The higher is the concrete strength, the higher is the critical MGDV in compression or their post peak values in tension (for a given ϵ).
2. In all cases the threshold MGDV takes place before the peak.
3. The plastic damage variable shows the least sensitivity to concrete grade and the fastest growth rate.

5.4 CONCRETE UNDER BIAXIAL LOADING

In several practical situations, biaxial states of stress do exist in many structural elements and the proper modeling is necessary for accurate analysis. Unfortunately, many of the existing damage models (c.f. Krajcinovic and Fonseka, 1981; Mazars, 1986; Simo and Ju, 1987; Suaris et al., 1990) failed to predict the strength increase due to biaxiality as reported experimentally (c.f. Kupfer, 1972; Tasuji, 1978; Aschle et al., 1973). Another set of models idealized concrete as brittle material (c.f. Loland, 1981; Krajcinovic and Fonseka, 1981; Mazars, 1984). Thus, the residual deformation upon complete unloading

can never be determined.

In the following, an orthotropic model which accounts for the inelastic behavior of concrete elements loaded biaxially is developed using the theory of dichotomy. The proposed theory replaces the continuum by a system of orthogonal springs. The behavior of concrete is idealized as elastoplastic-damage through splitting the strain tensor into two main components. Consequently, three possible forms of constitutive relation are presented which associate the stress tensor to the total strain, the elastic-damage strain and the plastic damage strain, respectively. These relations are adopted in diagonal tensorial form in the principal space using proper damage variables. The interdependence between the stress components are taken into account using the biaxiality ratio for all possible combinations of the principal stresses, i.e. compression-compression, compression-tension and tension-tension. Thermodynamical considerations in view of the proposed theory are discussed. The model is shown to be simple and in close agreement with a wide set of the well documented existing experimental data where the salient features of concrete behavior - such as strain softening, stiffness degradation, volumetric dilatation - are captured.

5.4.1 Theory of dichotomy

To predict the overall behavior of any material point under various load combinations, the following theory is postulated:

"For an element of a deformeable material, the continuum can be equivalently replaced by an orthogonal nonlinear spring system whose stiffness depends on the ratio of the principal stresses. For each principal direction, the total strain is decomposed into elastic-damage and plastic-damage components. The comprehensive loading history can be deduced using the appropriate stress-strain spaces."

The proposed dichotomy scheme for a material point loaded under proportional biaxial stress states is depicted in Fig. 5.15. For the considered case, six stress-strain spaces are deduced.

5.4.2 Canonicalization of Constitutive Equations

The incremental strain tensor dr_{ij} is composed of two main components: (1) incremental elastic-damage strain dr_{ij}^e and (2) incremental plastic-damage strain dr_{ij}^p . The relationship between the incremental stress tensor $d\sigma_{ij}$ and each of the strain components is highly nonlinear and depends on the stress path. The total quantities $\chi_{ij} = \sigma_{ij}, \epsilon_{ij}, \epsilon_{ij}^e$ or ϵ_{ij}^p are obtained by accumulation over the loading increments l i.e. $\chi_{ij} = \int d\chi_{ij} = \sum_l d\chi_{ij}^l$. Motivated by incremental formulation based on variable secant moduli (Chen and Saleeb, 1981), the total quantities at any load increment can be interrelated in a similar fashion to that of the generalized Hooke's law as follows:

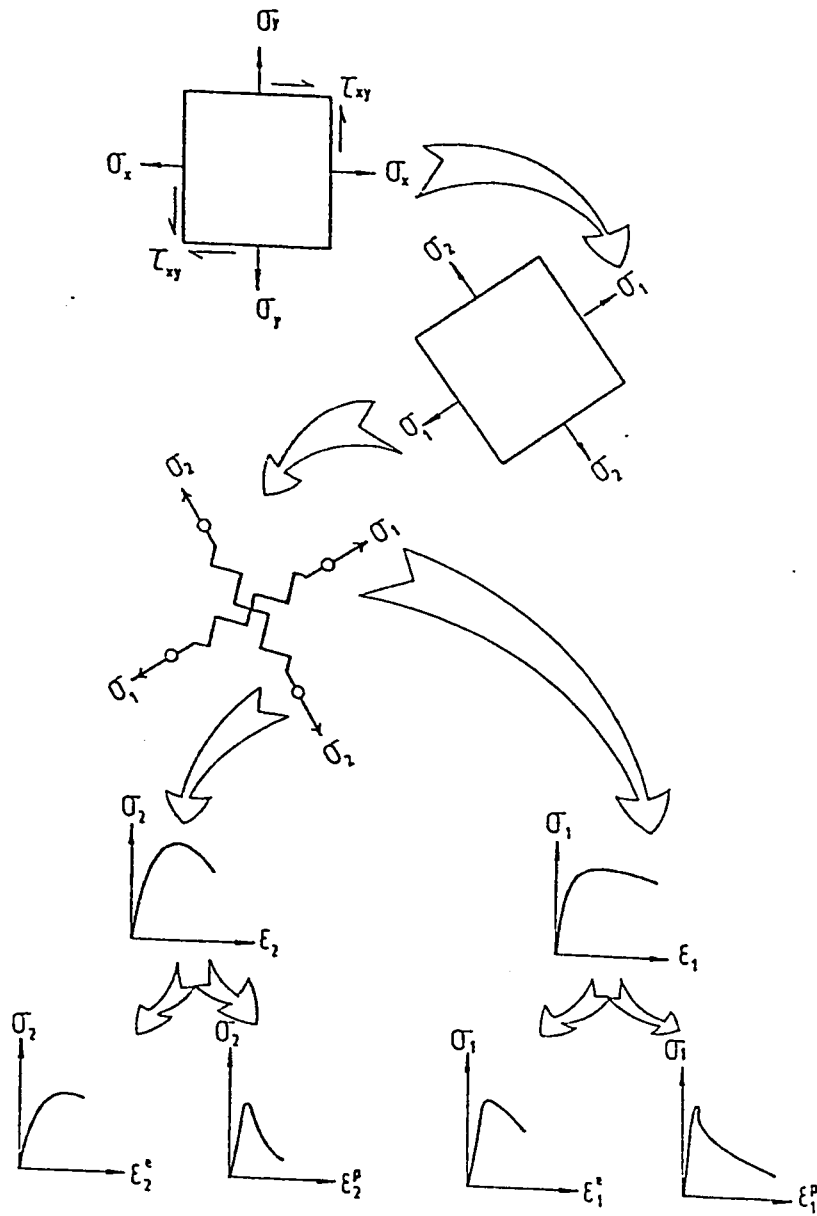


Figure 5.15 Dichotomy scheme for a material point under proportional biaxial loading

$$\sigma_{ij} = A_{ijkl} \epsilon_{kl} \quad (5.33-a)$$

$$= E_{ijkl} \epsilon_{kl}^e \quad (5.34-a)$$

$$= P_{ijkl} \epsilon_{kl}^p \quad (5.35-a)$$

in which A_{ijkl} , E_{ijkl} and P_{ijkl} are fourth order moduli tensors.

Using Von Karman (Voigt) notations, these relations can be reduced to

$$\sigma_i = A_{ij} \epsilon_j \quad (5.33-b)$$

$$= E_{ij} \epsilon_j^e \quad (5.34-b)$$

$$= P_{ij} \epsilon_j^p \quad (5.35-b)$$

Further reduction of these equations can be obtained if the principal space is considered for a material point which is loaded biaxially ($\sigma_1 \geq \sigma_2$, $\sigma_3 = 0$) and the relations are written in a canonical form.

The matrix format of the constitutive relations reduces to

$$\begin{Bmatrix} \sigma_1 \\ \sigma_2 \end{Bmatrix} = \begin{bmatrix} A_1 & 0 \\ 0 & A_2 \end{bmatrix} \begin{Bmatrix} \epsilon_1 \\ \epsilon_2 \end{Bmatrix} \quad (5.33-c)$$

$$= \begin{bmatrix} E_1 & 0 \\ 0 & E_2 \end{bmatrix} \begin{Bmatrix} \epsilon_1^e \\ \epsilon_2^e \end{Bmatrix} \quad (5.34-c)$$

$$= \begin{bmatrix} P_1 & 0 \\ 0 & P_2 \end{bmatrix} \begin{Bmatrix} \epsilon_1^p \\ \epsilon_2^p \end{Bmatrix} \quad (5.35-c)$$

An example for reducing the conventional Hook's law for biaxial states of stresses to the canonical form is formulated hereafter.

The general form of the linear stress-strain relationship expressed in the principal space, for plane stress states, can be written in the following matrix form in the principal strain space

$$\begin{Bmatrix} \sigma_1 \\ \sigma_2 \end{Bmatrix} = \begin{bmatrix} C_{11} & C_{12} \\ C_{21} & C_{22} \end{bmatrix} \begin{Bmatrix} \epsilon_1 \\ \epsilon_2 \end{Bmatrix} \quad (5.36)$$

where for an isotropic material obeying Hooke's law (as an example)

$$C_{12} = C_{21} = \frac{\nu_0 A_0}{1 - \nu_0^2} \quad (5.37a)$$

and

$$C_{11} = C_{22} = \frac{A_0}{1 - \nu_0^2} \quad (5.37b)$$

in which A_0 and ν_0 are the initial Young's modulus and Poisson's ratio, respectively. For linear elastic materials the initial moduli for the total and elastic behaviors are the same, i.e. $A_0 = E_0$.

These relations can be reduced to the following canonical form

$$\begin{Bmatrix} \sigma_1 \\ \sigma_2 \end{Bmatrix} = \begin{bmatrix} C_{01} & 0 \\ 0 & C_{02} \end{bmatrix} \begin{Bmatrix} \epsilon_1 \\ \epsilon_2 \end{Bmatrix} \quad (5.38)$$

in which

$$C_{o_1} = C_{11} \left(1 + \frac{C_{12}}{C_{11}} \frac{\epsilon_2}{\epsilon_1} \right) \quad (5.39)$$

and

$$C_{o_2} = C_{22} \left(1 + \frac{C_{21}}{C_{22}} \frac{\epsilon_1}{\epsilon_2} \right) \quad (5.40)$$

and the principal strain ratio ϵ_1/ϵ_2 can be easily shown to be expressed as a function of the biaxiality ratio $\beta_1 = \sigma_1/\sigma_2$, i.e.

$$\frac{\epsilon_1}{\epsilon_2} = \frac{\epsilon_1}{\epsilon_2} (\beta_1) = \xi(\beta_1) = \frac{\beta_1 C_{22} - C_{12}}{C_{11} - \beta_1 C_{21}} \quad (5.41)$$

Substituting (5.41) in (5.39) and (5.40), gets

in which

$$C_{o_1} = \zeta_1 A_o, \quad \zeta_1 = \frac{C_{11}}{A_o} \left(1 + \frac{C_{12}}{\xi C_{11}} \right) \quad (5.42)$$

and

$$C_{o_2} = \zeta_2 A_o, \quad \zeta_2 = \frac{C_{22}}{A_o} \left(1 + \frac{\xi C_{21}}{C_{22}} \right) \quad (5.43)$$

Using index notation with the exception that summation is not implied over the repeated index, Eqns. (5.33,34,35-c) can be alternatively rewritten as

$$\sigma_i = A_i \epsilon_i \quad (5.33-d)$$

$$= E_i \epsilon_i^e \quad (5.34-d)$$

$$= P_i \epsilon_i^P \quad (5.35-d)$$

The manner in which the above set of equations are expressed indicates that the stress components are independent. This suits the postulated spring system but apparently differs from the conventional constitutive equations that compensate for the cross effect of the stress components through Poisson's ratio. However, the existence of the process of damage makes the stress components interrelated indirectly. Another aspect is that the canonical form is preserved as far as the material point is loaded proportionally. Otherwise, this diagonal form is held only in an incremental sense.

5.4.3 Total and Incremental Stress Components

As far as for each stress components three moduli are presented in Eqns. (5.33-35), three scalar damage variables are introduced in association. The damage process is described through monitoring the degradation of these moduli. Therefore, the constitutive equations can be expressed as

$$\sigma_i = (1-d_{a_i}) A_{o_i} \epsilon_i \quad (5.33-e)$$

$$= (1-d_{e_i}) E_{o_i} \epsilon_i^e \quad (5.34-e)$$

$$= (1-d_{p_i}) P_{o_i} \epsilon_i^p \quad (5.35-e)$$

in which d_{c_i} ($c = a, e, p$) are the damage variables associated with the

pseudo initial moduli C_{o_i} ($C = A, E, P$) in the i th direction ($i = 1, 2$). In order that the constitutive equations account for the path dependence as prevalent in concrete and other rock-like materials, the forms of the pseudo initial moduli and the damage variables as well, and consequently the secant moduli, have to be selected carefully. The pseudo initial moduli are chosen to be dependent on the biaxiality ratio $\beta_1 = \sigma_1/\sigma_2$, and the current state of strain in the i th direction, i.e. The pseudo initial moduli are chosen to be dependent on the biaxiality ratio $\beta_1 = \sigma_1/\sigma_2$, and the current of state of strain in the i th direction, i.e.

$$C_{o_i} = C_{o_i}(\beta_1, \epsilon_i) \quad (5.44)$$

In a similar manner, the damage variables are chosen to be dependent on the same quantities, thus,

$$d_{c_i} = d_{c_i}(\beta_1, \epsilon_i, \dot{\epsilon}_i) \quad (5.45)$$

It is intended to utilize the damage variables derived previously for uniaxial behavior of concrete in both tension and compression. For the generalization to biaxial situations, the peak values are to be modified using the functions η_{σ_i} and η_{ϵ_i} for the peak stresses and strains, respectively. These functions are schematically sketched in Fig. 5.16 and 5.17 and their mathematical form is given later. However, it is

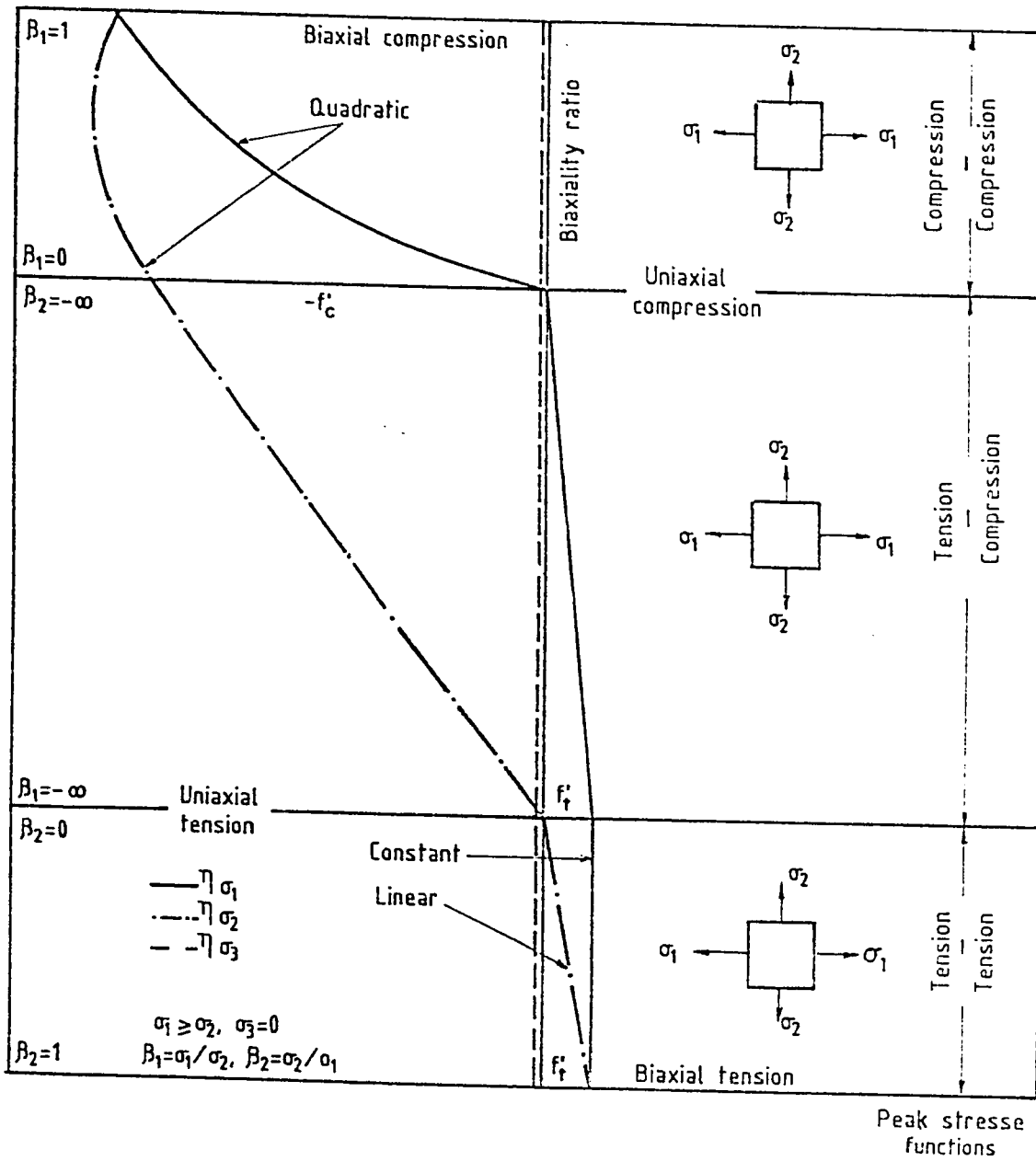


Figure 5.16 Schematic representation of the evolution of the peak stresses with the biaxiality ratio

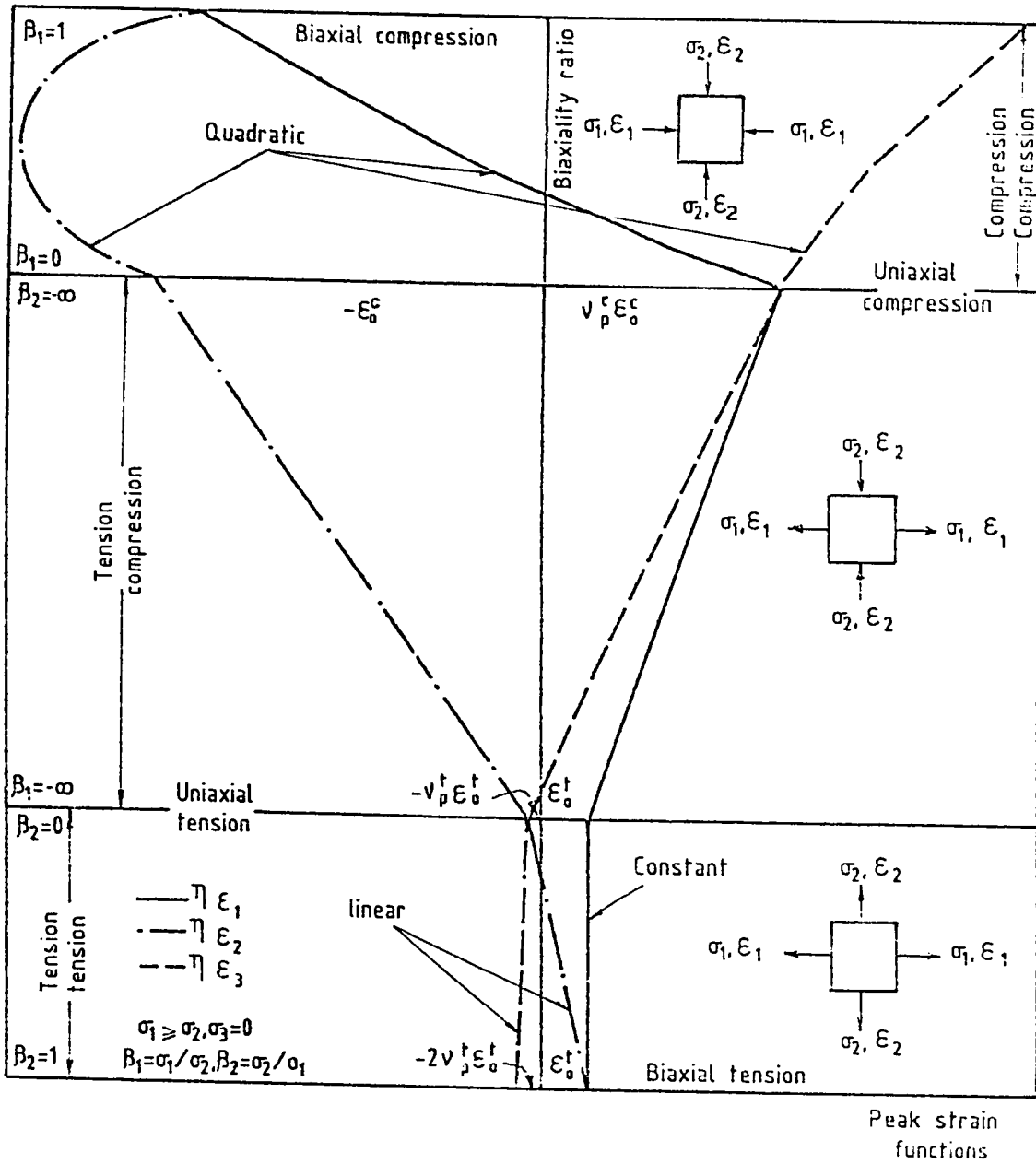


Figure 5.17 Schematic representation of the evolution of the peak strains with the biaxiality ratio

worth mentioning that η_{ϵ_i} and η_{σ_i} are functions of the biaxiality ratio

β_1 . As a result, the stress increment can be expressed in the form

$$\begin{aligned}\dot{\sigma}_i &= (1-d_{c_i}) C_{o_i} \dot{\epsilon}_i^c - C_{o_i} \epsilon_i^c \dot{d}_{c_i} \\ &= C_{o_i} \left[1 - d_{c_i} - \frac{\partial d_{c_i}}{\partial \epsilon_i^c} \epsilon_i^c \right] \dot{\epsilon}_i^c\end{aligned}\quad (5.46)$$

where $(\dot{\quad})$ is the time derivative while $\epsilon_i, \dot{\epsilon}_i$ are meant for $c = a$ in ϵ_i^c and $\dot{\epsilon}_i^c$, respectively. Additionally, for unloading in the j th direction $\dot{d}_{e_j} = 0$, since the process is purely elastic. Equation (5.46) represents the canonical form of the incremental stress-strain components relationships.

5.4.4 Thermodynamical Considerations

Using the concepts of thermodynamics of irreversible changes, the Helmholtz total free energy function ψ can be expressed as

$$\psi = \psi_1 + \psi_2 \quad (5.47-a)$$

where

$$\rho \psi_i = \frac{1}{2} (1-d_{a_i}) A_{o_i} \epsilon_i^2 \quad (5.47-b)$$

where ρ is the mass density. If the total strain is replaced by its components, Eqn. (5.47-b) can be written as

$$\begin{aligned}
\rho\psi_i &= \frac{1}{2} (1-d_{a_i}) A_{o_i} (\varepsilon_i^e + \varepsilon_i^p)^2 \\
&= \frac{1}{2} (1-d_{a_i}) A_{o_i} \left[\varepsilon_i^{e^2} + 2\varepsilon_i^e \varepsilon_i^p + \varepsilon_i^{p^2} \right] \\
&= \frac{1}{2} (1-d_{a_i}) A_{o_i} \varepsilon_i^{e^2} + \frac{1}{2} (1-d_{a_i}) A_{o_i} \varepsilon_i^{p^2} + (1-d_{a_i}) A_{o_i} \varepsilon_i^e \varepsilon_i^p
\end{aligned} \tag{5.48}$$

It is clear that if just one single set of damage variables are to be used, one set of moduli is used in association. In the case given above are the parameters associated with the total strain. Another implication of using one set of damage variables is the existence of a coupling term between the elastic and plastic components (the 3rd term in Eqn. (5.48)). In other words, if the damage process is to be separated from both the elastic and plastic behaviors, the total energy can be expressed as

$$\psi_i \left(\varepsilon_i^e, \varepsilon_i^p, d_{a_i} \right) = (1-d_{a_i}) \psi_i^o \left(\varepsilon_i^e, \varepsilon_i^p \right) \tag{5.49}$$

where $\psi_i^o \left(\varepsilon_i^e, \varepsilon_i^p \right) = \frac{1}{2} A_{o_i} \left[\varepsilon_i^{e^2} + \varepsilon_i^{p^2} + 2\varepsilon_i^e \varepsilon_i^p \right]$ denotes the total potential energy function of an undamaged (virgin) material and therefore the assumption that the elastic and plastic potential energy functions can be uncoupled (as postulated by Ju, 1989a), i.e. $\psi_i^o \left(\varepsilon_i^e, \varepsilon_i^p \right) = \psi_{e_i}^o \left(\varepsilon_i^e \right) + \psi_{p_i}^o \left(\varepsilon_i^p \right)$ is incorrect. This leads to the result that

$$\psi_i \left(\epsilon_i^e, \epsilon_i^p, d_{a_i} \right) = (1 - d_{a_i}) \left[\psi_{e_i}^0(\epsilon_{e_i}) + \psi_{p_i}^0(\epsilon_{p_i}) \right] \quad (5.50)$$

This conclusion is in contradiction with Ju's energy based model (1989).

With reference to Eqn. (5.47), the constitutive relation and the generalized thermodynamic forces of the i th damage components Y_{a_i}

derived subject to thermodynamic restrictions are given by

$$\sigma_i = \rho \frac{\partial \psi}{\partial \epsilon_i} = (1 - d_{a_i}) A_{o_i} \epsilon_i \quad (5.51)$$

Obviously, Eqn. (5.51) is reconciled with (5.33-c), and

$$-Y_{a_i} = -\rho \frac{\partial \psi}{\partial d_{a_i}} = \frac{1}{2} A_{o_i} \epsilon_i^2 = \psi_i^0(\epsilon_i^e, \epsilon_i^p) \quad (5.52)$$

It is obvious that the damage energy release rate defined in (5.52) which is conjugate to the total damage variable, is the undamaged energy function.

In general Eqns. (5.51) and (5.47) can be combined to arrive at

$$\begin{aligned} \rho \psi_i &= \frac{1}{2} \sigma_i \epsilon_i \\ &= \frac{1}{2} \sigma_i (\epsilon_i^e + \epsilon_i^p) \\ &= \frac{1}{2} \sigma_i \epsilon_i^e + \frac{1}{2} \sigma_i \epsilon_i^p \end{aligned} \quad (5.53)$$

Substituting for σ_i in the first and second terms of Eqn. (5.53) from

Eqns. (5.34-d) and (5.35-d), the total energy is reduced to

$$\rho\psi_i = \frac{1}{2} (1-d_{e_i}) E_{o_i} \epsilon_i^e{}^2 + \frac{1}{2} (1-d_{p_i}) P_{o_i} \epsilon_i^p{}^2 \quad (5.54)$$

The above equation gives the correct form of the uncoupled energy terms by weighted components of the energy of the undamaged material.

This can be easily concluded if Eqn. (5.54) is expressed as

$$\psi_i \left(\epsilon_i^e, \epsilon_i^p, d_{e_i}, d_{p_i} \right) = (1-d_{e_i}) \psi_{e_i}^o(\epsilon_i^e) + (1-d_{p_i}) \psi_{p_i}^o(\epsilon_i^p) \quad (5.55)$$

It can be concluded that at least two sets of damage variables are required to provide complete elastoplastic damage uncoupling.

As a consequence of introducing the damage variables d_{c_i} , $c = e, p$, the following thermodynamic forces Y_{c_i} ; $c = e, p$ are defined as follows

$$-Y_{e_i} = -\rho \frac{\partial \psi}{\partial d_{e_i}} = \frac{1}{2} E_{o_i} \epsilon_i^e{}^2 = \psi_e^o(\epsilon_e) \quad (5.56)$$

for the elastic-damage behavior, and

$$-Y_{p_i} = -\rho \frac{\partial \psi}{\partial d_{p_i}} = \frac{1}{2} P_{o_i} \epsilon_i^p{}^2 = \psi_p^o(\epsilon_p) \quad (5.57)$$

for the plastic-damage behavior.

The damage energy determined from Eqn. (5.56) is the same elastic energy considered by Lemaitre (1984).

The entropy production rate $\dot{\eta}$, as given by the Clausius-Duhem,

is inequality

$$\rho \dot{\eta} = -\rho \dot{\psi} + \sum_{i=1}^2 \sigma_i \dot{\epsilon}_i \geq 0 \quad (5.58)$$

Consideration of Eqns. (5.49) and (5.55) once in a time with (5.58), the following dissipative inequalities are obtained

$$\psi_i^o(\epsilon_i^e, \epsilon_i^p) \dot{d}_{a_i} \geq 0 \quad ; \quad \psi_{e_i}^o(\epsilon_i^e) \dot{d}_{e_i} + \psi_{p_i}^o(\epsilon_i^p) \dot{d}_{p_i} \geq 0 \quad (5.59)$$

which leads further to non-negative rate of the damage variables, i.e.

$$\dot{d}_{c_i} \geq 0 \quad , \quad c = a, e, p \quad (5.60)$$

It has to be pointed out that the damage variables d_{a_i} are sufficient to describe the loading process while d_{e_i} are needed for the idealized linear unloading or reloading and hence determination of d_{p_i} becomes of minor importance.

5.4.5 Identification of Parameters

As long as biaxial states of stress are concerned three possibilities can be thought of in terms of stress combinations: (1) compression-compression, (2) compression-tension and (3) tension-tension. In the current study, the initial moduli as well as the damage variables are phenomenologically determined by fitting the available monotonic and

cyclic experimental data and exploiting some of the existing regression formulas. These data include those of Andenaes et al. (1977), Kupfer et al.(1969), Nelissen (1972), Tasuji et al. (1978), Van Mier (1985), Aschl et al. (1972), Schickert and Winkler (1977),; Karsan and Jirsa (1969), Popovics (1973), Guo and Zhang (1987), and Gopalaratnam and Shah (1985).

In order to keep the mathematical form of the incremental expressions of the biaxial MGDV as simple as possible it is advantageous to introduce the following functions:

(1) *The functions $f_{1..10}$ to be used in defining the incremental damage variables:*

$$f_1 = \varepsilon c_i^{n_i - 1} \quad (5.61)$$

$$f_2 = \varepsilon c_i^{n_i} \quad (5.62)$$

$$f_3 = n_i(n_i - 1) f_1 \quad (5.63)$$

$$f_4 = (n_i - 1 + f_2)^2 \quad (5.64)$$

$$f_5 = 1 - k_1 \varepsilon c_i \quad (5.65)$$

$$f_6 = -k_1 \varepsilon c_i \quad (5.66)$$

$$f_7 = k_1 f_2 \quad (5.67)$$

$$f_8 = 5k_1 \varepsilon_{t_i} \quad (5.68)$$

$$f_9 = \varepsilon_{t_i} + \alpha_i (\varepsilon_{t_i} - 1)^{k_2} \quad (5.69)$$

$$f_{10} = k_2 \alpha_i (\varepsilon_{t_i} - 1)^{k_2 - 1} \quad (5.70)$$

and k_1, k_2 are constants whose values are

$$k_1 = 0.166 \quad (5.71)$$

$$k_2 = 1.7 \quad (5.72)$$

where ε_{j_i} is the normalized i th strain components in the biaxial space for $j=t,c$ corresponding to tension and compression, respectively. The strength parameters α_i and n_i are the modified Guo and Zhang's and Popovics parameters taking into account the effect of biaxiality.

(2) The functions g_{1-5} to be used in the expressions of the incremental damage variables

$$g_1 = f_3/f_4 \quad (5.73)$$

$$g_2 = (f_3 f_5 + f_4 f_6 + f_7)/(f_4 f_5)^2 \quad (5.74)$$

$$g_3 = f_8 \quad (5.75)$$

$$g_4 = -(1+f_{10})/f_9^2 \quad (5.76)$$

$$g_5 = g_4 \epsilon_{t_i}^{-1}/f_9 \quad (5.77)$$

(3) The function f_{ζ_i} to be used in evaluate the pseudo initial moduli:

$$f_{\zeta_i} = Z_i + H(y_i) y_i^m (Z_i - \zeta_i) \quad (5.78)$$

where m is a material parameter and the functions y_i are given as

$$y_i = y_i(\epsilon_{j_i}) = 1 - \epsilon_{j_i} \quad (5.79)$$

in which $j = t, c$ for tension and compression, respectively. The Heaviside function $H(y_i) = y_i$ for positive values of y_i and is zero otherwise. The functions Z_i depend on the peak stress and strain multiplied functions defined ahead and are given as

$$Z_i = \begin{cases} \left| \frac{\eta_{\sigma_i}}{\eta_{\epsilon_i}} \right| & \text{in tension} \\ \left| \frac{\eta_{\sigma_i}}{\eta_{\epsilon_i}} \right| \frac{n_i - 1}{n_0 - 1} & \text{in compression} \end{cases} \quad (5.80)$$

in which n_0 is the value of n_i for $|\eta_{\sigma_i}| = 1.0$.

(4) *The peak stress multiplied functions η_{σ_i} for each of the three stress quadrants*

i. Tension-Tension

$$\eta_{\sigma_1} = 1 \quad (5.81)$$

$$\eta_{\sigma_2} = \eta_{\sigma_1} \beta_2 \quad (5.82)$$

in which β_2 is the reciprocal of the stress ratio β_1 . The trend of the functions is illustrated in Fig. 5.18.

ii. Tension-Compression

$$\eta_{\sigma_1} = \beta_1 \eta_{\sigma_2} / \kappa_1 \quad (5.83)$$

$$\eta_{\sigma_2} = \frac{1}{3 \beta_1 (f_c)^{1/3} - 0.8} \quad (5.84)$$

in which κ_1 is the ratio of the peak strength in uniaxial tension to that in compression. The trend of the functions is illustrated in Fig. 5.19.

iii. Compression-Compression

$$\eta_{\sigma_1} = \beta_1 \eta_{\sigma_2} \quad (5.85)$$

$$\eta_{\sigma_2} = -1.0 - 0.7952 \beta_1 + 0.6244 \beta_1^2 \quad (5.86)$$

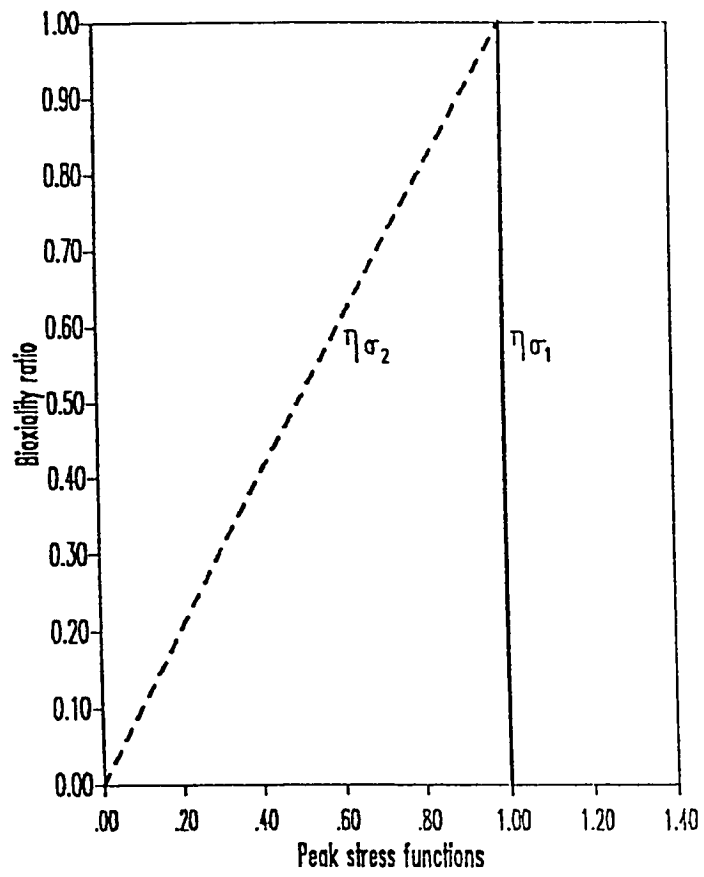


Figure 5.18 Stress functions in the tension-tension quadrant

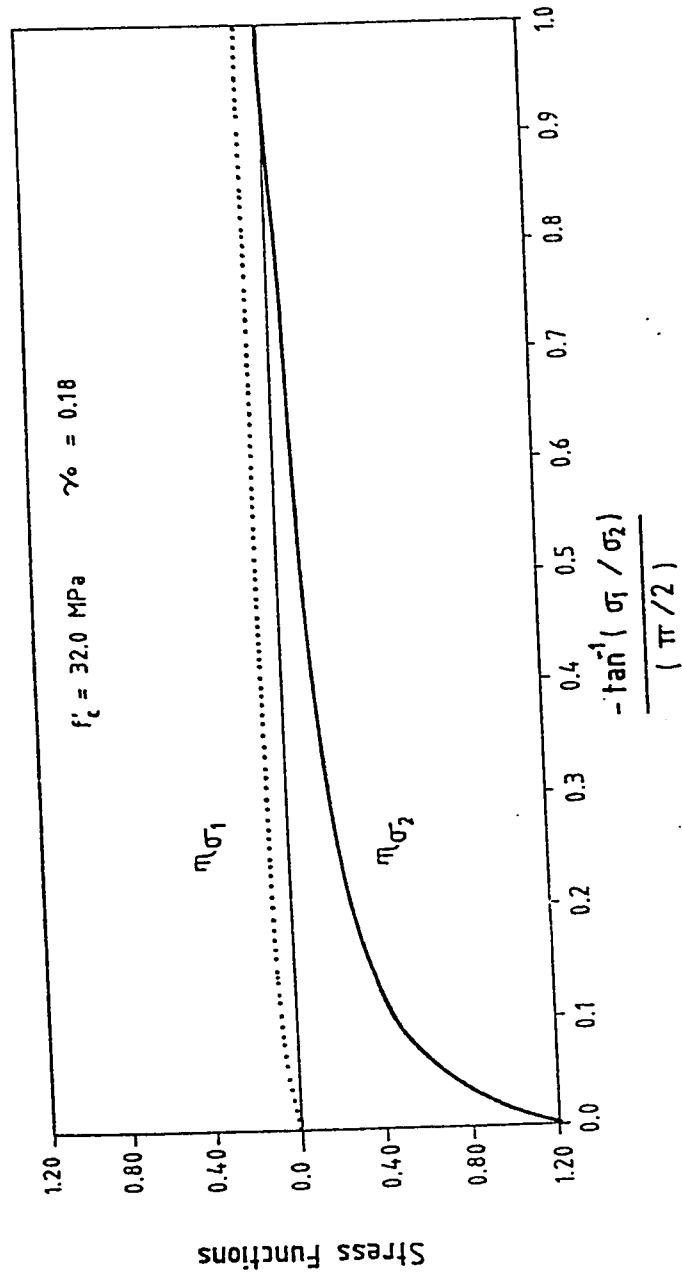


Figure 5.19 Stress functions in the tension-compression quadrant

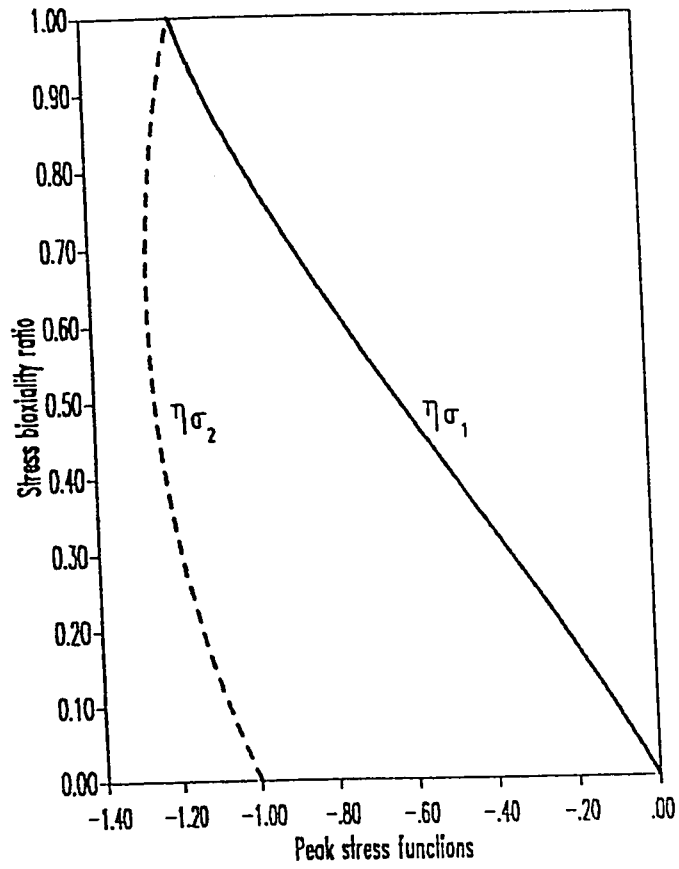


Figure 5.20 Stress functions in the compression-compression quadrant

The trend of the functions is illustrated in Fig. 5.20.

In all cases $\eta_{\sigma_3} = 0.0$ since only biaxial states of stress are of concern in the present study.

(5) *The peak strain multiplied functions η_{ϵ_i} for each of the three stress quadrants*

i. Tension-Tension

$$\eta_{\epsilon_1} = 1 \quad (5.87)$$

$$\eta_{\epsilon_2} = -\nu_0 + (1 + \nu_0) \beta_2 \quad (5.88)$$

$$\eta_{\epsilon_3} = -\kappa_2(1 + \beta_2) \nu_0 \quad (5.89)$$

The trend of the functions is illustrated in Fig. 5.21.

ii. Tension-Compression

Expressing η_{ϵ_i} in terms of $\beta = \tan^{-1} \beta_1$, gets

$$\eta_{\epsilon_1} = \begin{cases} |0.6 + 3.795\beta + 6.49132\beta^2|/\kappa_2 & \beta \geq -0.2 \\ |(0.11395 + 0.14925\kappa_2) + (0.0903 + 0.92167\kappa_2) \beta \\ + (0.0113093 + 0.93155\kappa_2) \beta^2| / \kappa_2 & \beta < -0.2 \end{cases} \quad (5.90)$$

$$\eta_{\epsilon_2} = \begin{cases} -1 - 2.0667\beta + 8.684\beta^2 & \beta \geq -0.2 \\ (-0.3018 - 0.14925v_0\kappa_2) + (-0.4491 - 0.92167v_0\kappa_2)\beta \\ \quad + (-0.16357 - 0.93155v_0\kappa_2)\beta^2 & \beta < -0.2 \end{cases} \quad (5.91)$$

$$\eta_{\epsilon_3} = \begin{cases} 0.6 + 6.1406\beta + 16.16425\beta^2 & \beta \geq -0.2 \\ (0.03105 - 0.14925v_0\kappa_2) + (0.0593 - 0.92167v_0\kappa_2)\beta \\ \quad + (0.02517 - 0.93155v_0\kappa_2)\beta^2 & \beta < -0.2 \end{cases} \quad (5.92)$$

where v_0 is the initial Poisson's ratio and κ_2 is the ratio of peak strain in uniaxial tension to that in uniaxial compression. The trend of the functions is illustrated in Fig. 5.22.

iii. Compression-Compression

$$\eta_{\epsilon_1} = 0.6 - 1.8645\beta_1 + 0.36068\beta_1^2 \quad (5.93)$$

$$\eta_{\epsilon_2} = -1.0 - 1.53225\beta_1 + 1.62847\beta_1^2 \quad (5.94)$$

$$\eta_{\epsilon_3} = 0.6 + 0.758023\beta_1 - 0.10891\beta_1^2 \quad (5.95)$$

The trend of the functions is illustrated in Fig. 5.23.

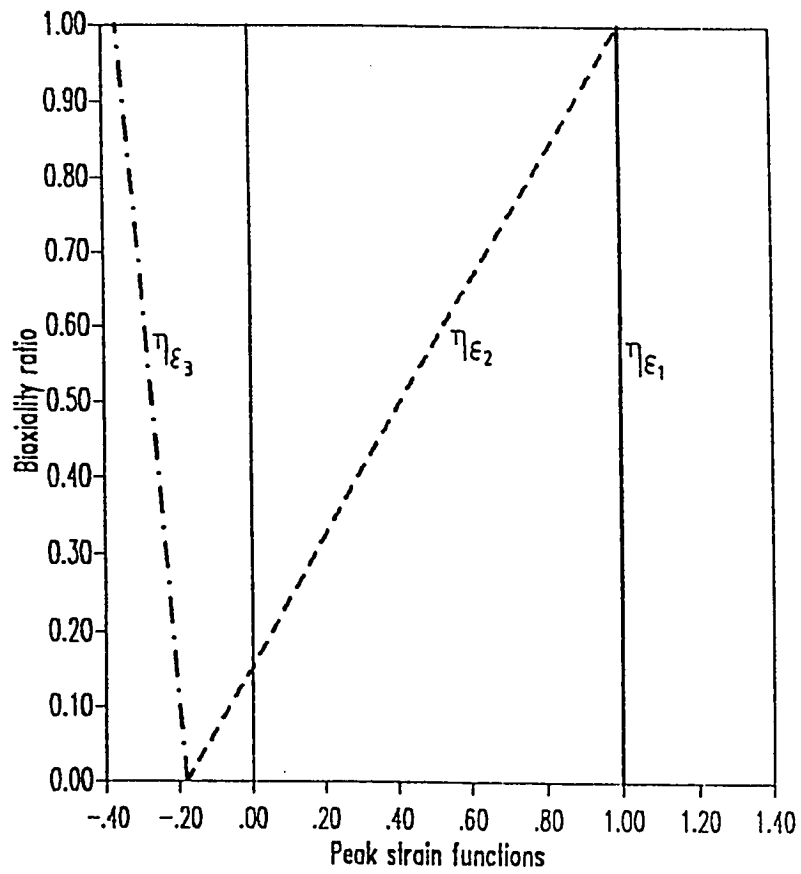


Figure 5.21 Strain functions in the tension-tension quadrant

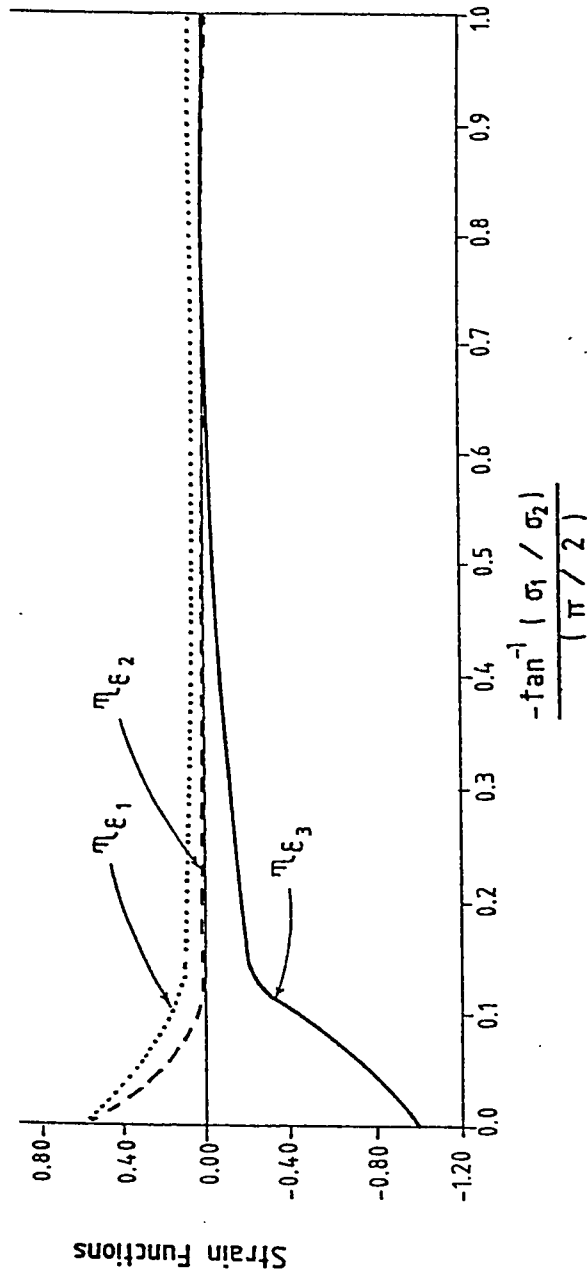


Figure 5.22 Strain functions in the tension-compression quadrant

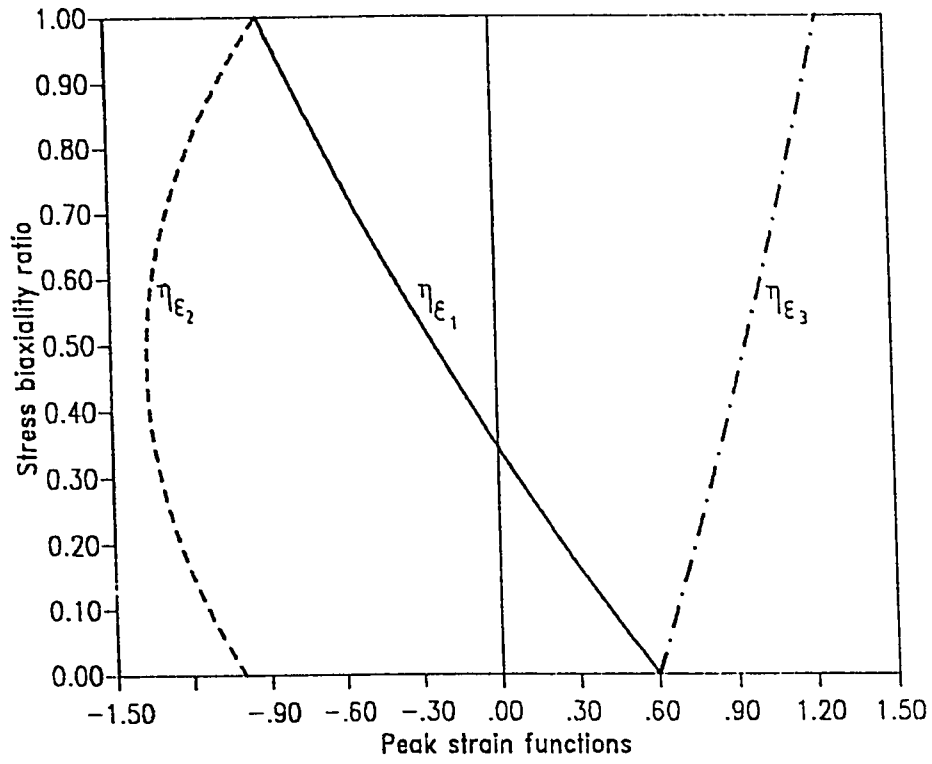


Figure 5.23 Strain functions in the compression-compression quadrant

5.4.6 Biaxial Tensile MGDV

The incremental damage variables associated with any tensile component are chosen to be linear with the strain increment and can be determined from the relations

$$d_{a_i}^t = \begin{cases} g_3 \varepsilon_{t_i} & \varepsilon_{t_i} \leq 1 \\ g_4 \varepsilon_{t_i} & \varepsilon_{t_i} > 1 \end{cases} \quad (5.96)$$

for the total damage variable, and

$$d_{e_i}^t = \begin{cases} g_3 \varepsilon_{t_i} & \varepsilon_{t_i} \leq 1 \\ g_5 \varepsilon_{t_i} & \varepsilon_{t_i} > 1 \end{cases} \quad (5.97)$$

for the elastic damage variable. The functions g_3 , g_4 and g_5 are given by Eqns 5.75-77. For proportional loading these relations are integrable to yield the following simple expressions

$$d_{a_i}^t = \begin{cases} 0.166 \varepsilon_{t_i}^5 & \varepsilon_{t_i} \leq 1 \\ 1 - \frac{1}{\alpha_i (\varepsilon_{t_i} - 1)^{1.7} + \varepsilon_{t_i}} & \varepsilon_{t_i} > 1 \end{cases} \quad (5.98)$$

$$d_{e_i}^t = \begin{cases} d_{a_i}^t & \varepsilon_{t_i} \leq 1 \\ 1 - \varepsilon_{t_i} \left(1 - d_{a_i}^t \right) & \varepsilon_{t_i} > 1 \end{cases} \quad (5.99)$$

In the current case the superscript t signifies the tensile component,

and the modified Guo and Zhang's strength parameters α_i are determined from the relation

$$\alpha_i = 0.312 \left(f_t' \eta_{\sigma_i} \right)^2 \quad (5.100)$$

The introduction of the peak stress multiplied functions in Eqn. 5.100 causes the strength parameters to be implicitly functions of the biaxiality ratios. Such dependence is plotted in Figs. 5.24-26 for all possible tensile stress components. The term ε_{t_i} is the current strain in the i th direction as a ratio to peak strain in the same direction and is defined as

$$\varepsilon_{t_i} = \frac{\varepsilon_i}{\varepsilon_t |\eta_{\varepsilon_i}|} \quad (5.101)$$

5.4.7 Biaxial Compressive MGDV

The incremental damage variables associated with any compressive component are chosen to be linear with the strain increment and can be determined from the relations

$$\dot{d}_{a_i}^c = g_1 \dot{\varepsilon}_{c_i} \quad (5.102)$$

for the total damage variable, and

$$\dot{d}_{e_i}^c = g_2 \dot{\varepsilon}_{c_i} \quad (5.103)$$

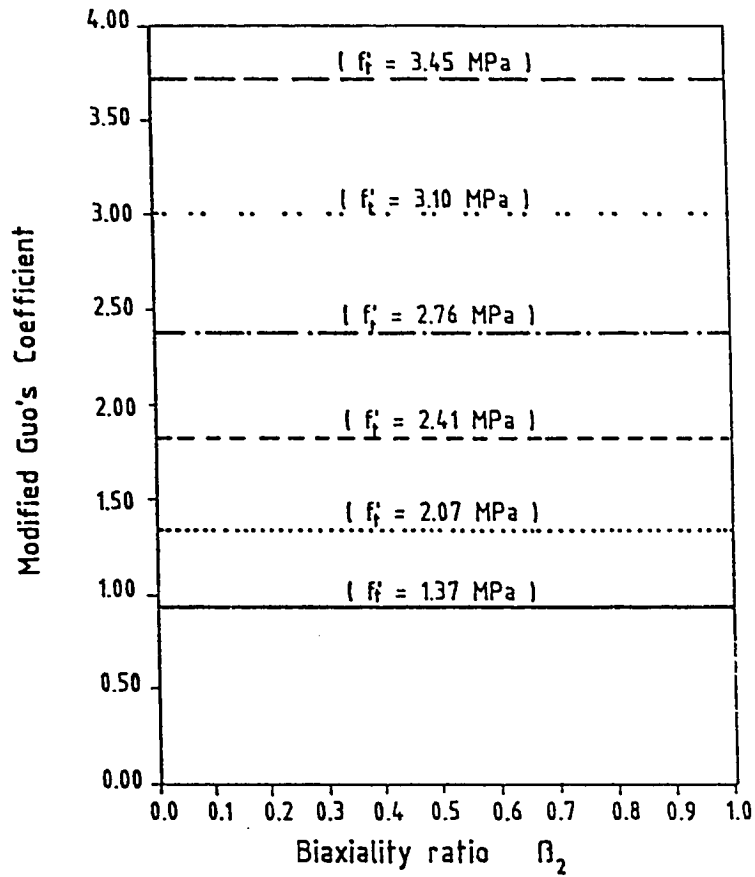


Figure 5.24 Modified Guo and Zhang's coefficient in the direction of the major principal stress in the tension-tension quadrant

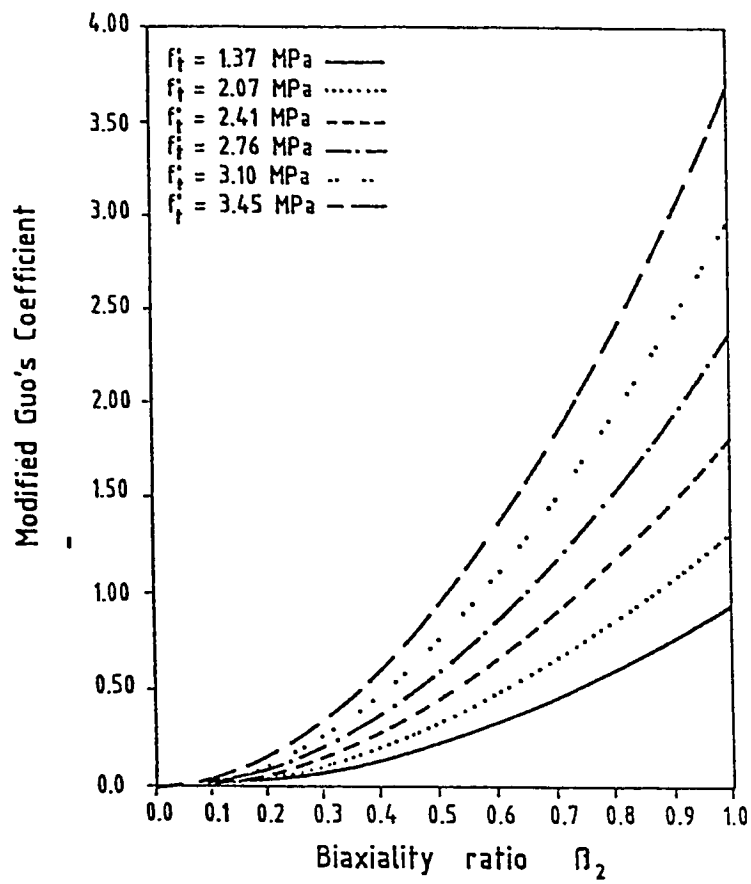


Figure 5.25 Modified Guo and Zhang's coefficient in the direction of the intermediate principal stress in the tension-tension quadrant

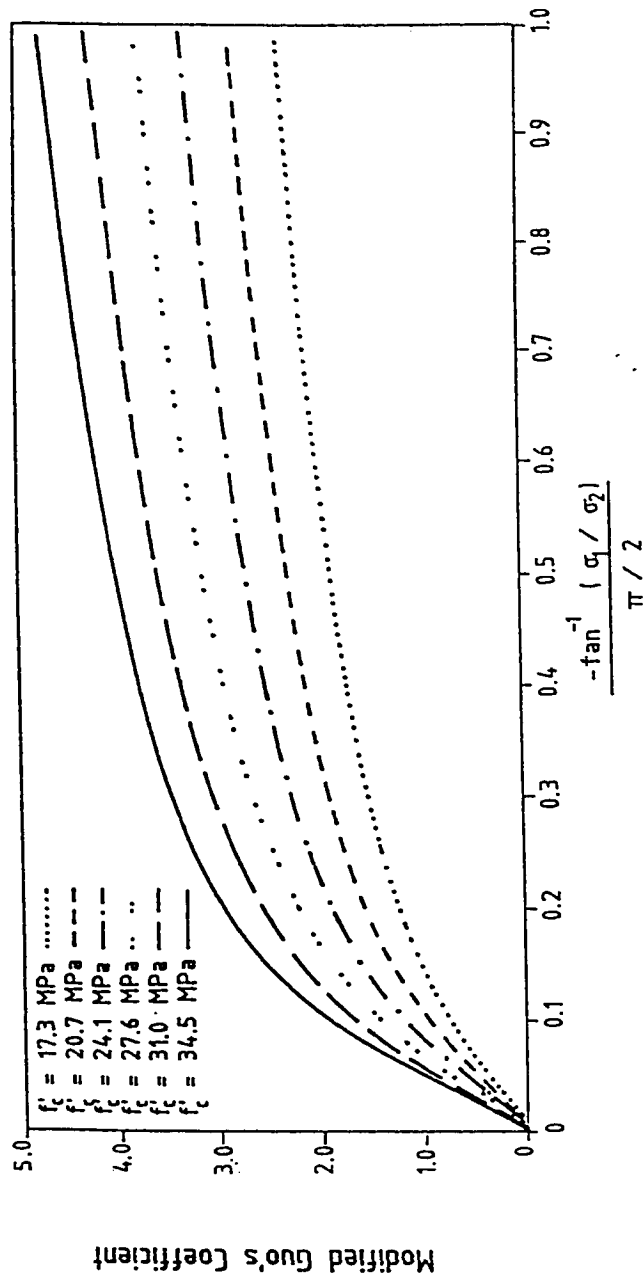


Figure 5.26 Modified Guo and Zhang's coefficient in the direction of the major principal stress in the tension-compression quadrant

for the elastic damage variable. The functions g_1 and g_2 are defined by Eqns (5.73,74). For proportional loading these relations are integrable to yield the following simple forms,

$$d_{a_i}^c = \frac{\epsilon_{c_i}^{n_i}}{n_i - 1 + \epsilon_{c_i}^{n_i}}, \quad (5.104)$$

$$d_{e_i}^c = \frac{d_{a_i}^c - 0.166 \epsilon_{c_i}}{1 - 0.166 \epsilon_{c_i}} \quad (5.105)$$

where the superscript c signifies the compressive component and the modified Popovics' strength parameters n_i are defined as

$$n_i = 0.058 f_c' \eta_{\sigma_i} + 1 \quad (5.106)$$

The introduction of the peak stress multiplied functions in Eqn. (5.106) causes the strength parameters to be implicitly functions of the biaxiality ratios. Such dependence is plotted in Figs. 5.27-29 for all possible compressive stress components. The term ϵ_{c_i} is similar to ϵ_{t_i} but ϵ_t is replaced by ϵ_c which is the peak strain in the uniaxial compression test; i.e.

$$\epsilon_{c_i} = \frac{\epsilon_i}{\epsilon_c |\eta_{\epsilon_i}|} \quad (5.107)$$

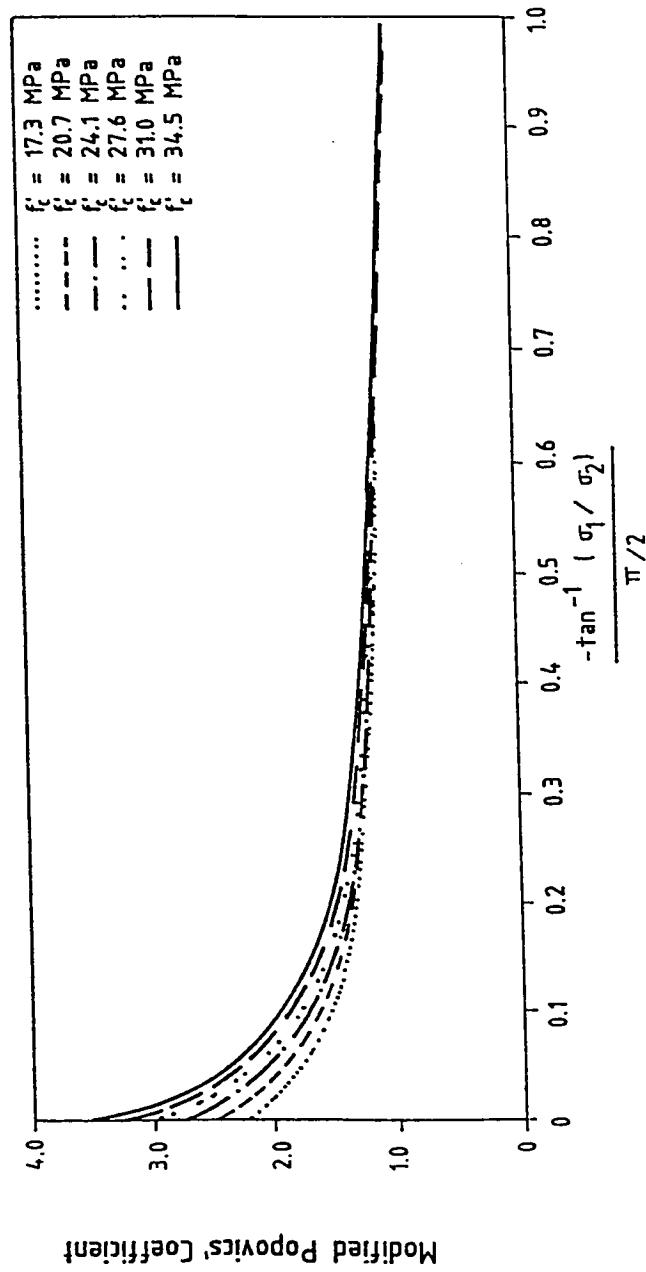


Figure 5.27 Modified Popovics' coefficient in the direction of the minor principal stress in the tension-compression quadrant

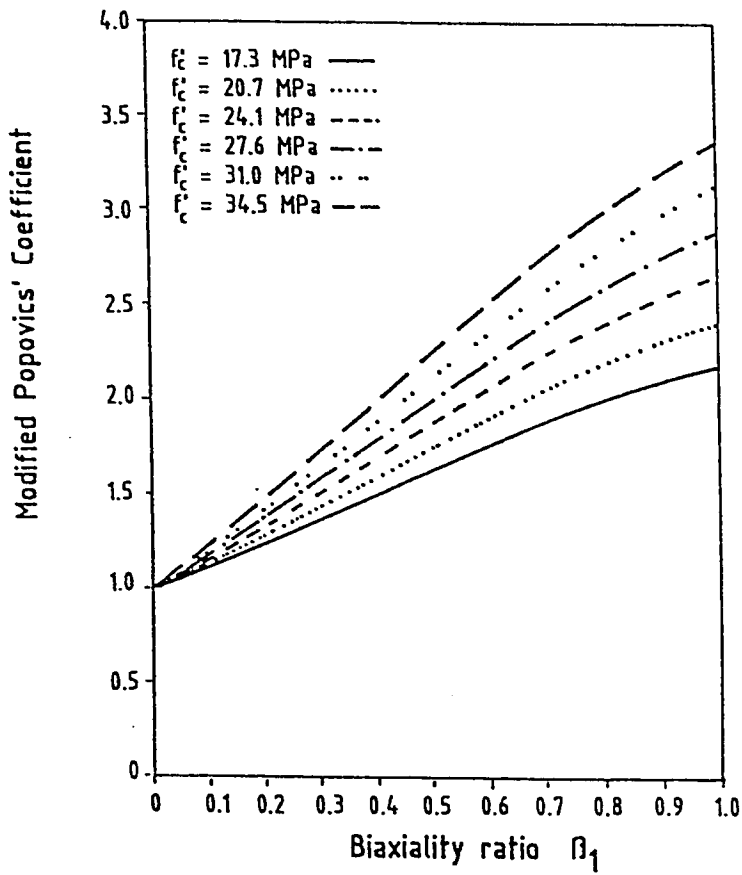


Figure 5.28 Modified Popovics' coefficient in the direction of the intermediate principal stress in the compression-compression quadrant

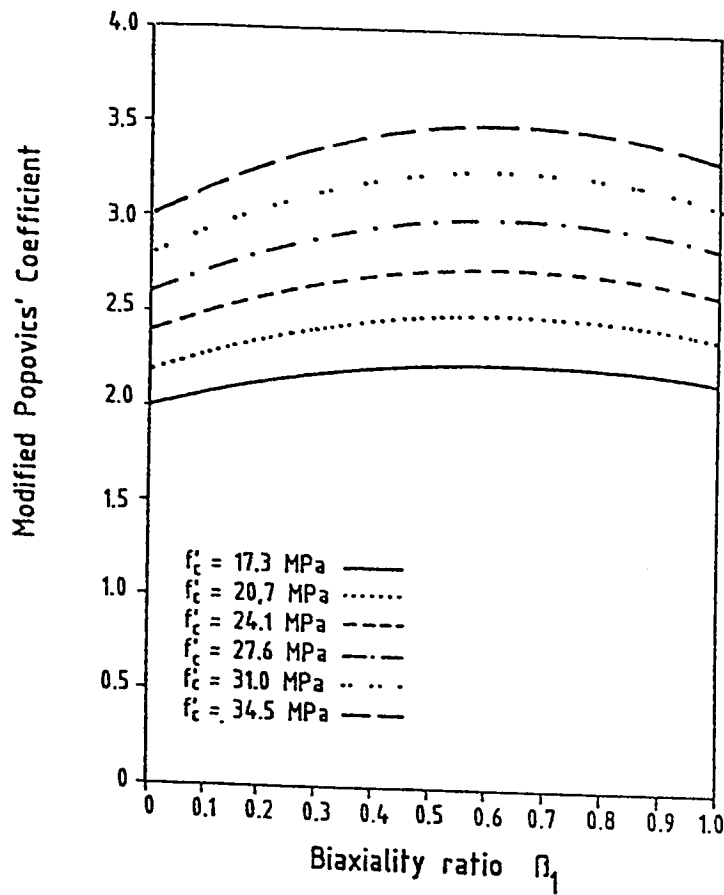


Figure 5.29 Modified Popovics' coefficient in the direction of the minor principal stress in the compression-compression

5.4.8 Pseudo Initial Moduli

The pseudo initial moduli conjugate to the total behavior are obtained by slight modification to the diagonal terms of the canonical matrix, derived for linear elastic Hookean material, as follows

$$A_{o_i} = A_o f_{\zeta_i} \quad (5.108)$$

in which the functions f_{ζ_i} depend on the current strain state and on the biaxiality ratio as shown earlier. The material parameter $m=2$ is found to yield good correlation with the experimental results for almost all biaxiality ratios. However, it can be easily shown that the peak quantities are not sensitive to the value of m except for its null value which reduces A_{o_i} to D_{o_i} for linear elastic materials. It may be noted that the moduli A_{o_i} change through the course of loading due to path dependence with the material initially (at $\epsilon_i=0.0$) possessing linear elastic isotropic properties then followed by stress induced orthotropy. The ratios of the elastic and plastic moduli to the total moduli in both tension and compression are given in Table 5.2.

5.4.9 Stress Free Straining

The principal strain ϵ_3 or any strain component corresponding to the stress free direction is of minor importance in attacking real boundary value problems using numerical technique. However, for

Table 5.2 Ratio of the elastic and plastic moduli to the total moduli in tension and compression.

Initial moduli ratio	Tension $j = t$	Compression $j = c$	Remarks
$(E_j/A_0)_i^j$	1.2	1.15	The ratio is independent of the value of β_1
$(P_j/A_0)_i^j$	6.0	7.69	

completeness and to illustrate the volumetric changes taking place through loading, a special treatment will be considered hereafter apart from the damage framework

For $\sigma_1 > |\sigma_2|$

$$\frac{\varepsilon_i}{\varepsilon_t} = \begin{cases} \eta_{\varepsilon_i} * \frac{\varepsilon_1}{\varepsilon_t} / \kappa_2 & \text{if } \sigma_2 < 0 \\ \eta_{\varepsilon_i} * \frac{\varepsilon_1}{\varepsilon_t} & \text{if } \sigma_2 \geq 0 \end{cases} \quad (5.109)$$

where i corresponds to the considered stress free strain component and κ_2 is the ratio of the peak strain in uniaxial tension to uniaxial compression, and

For $|\sigma_2| \geq |\sigma_1|$

$$\frac{\varepsilon_j}{\varepsilon_c'} = v_0 \eta_{\varepsilon_j} \left| \frac{\varepsilon_2}{\varepsilon_c'} \right| * \begin{cases} 4.55 \left| \frac{\varepsilon_2}{\eta_{\varepsilon_2} \varepsilon_c'} \right|^{3.4} - 5.55 v_0 + 2.0 & \left| \frac{\varepsilon_2}{\eta_{\varepsilon_2} \varepsilon_c'} \right| = 0 \sim 1.5 \\ -4.55 \left(3 - \left| \frac{\varepsilon_2}{\eta_{\varepsilon_2} \varepsilon_c'} \right| \right)^{3.4} - 5.55 v_0 + 38.25 & \left| \frac{\varepsilon_2}{\eta_{\varepsilon_2} \varepsilon_c'} \right| = 1.5 \sim 3 \\ 38.25 - 5.55 v_0 & \left| \frac{\varepsilon_2}{\eta_{\varepsilon_2} \varepsilon_c'} \right| > 3 \end{cases} \quad (5.110)$$

Eqn. (5.110) is mainly derived by modifying Poisson's equation

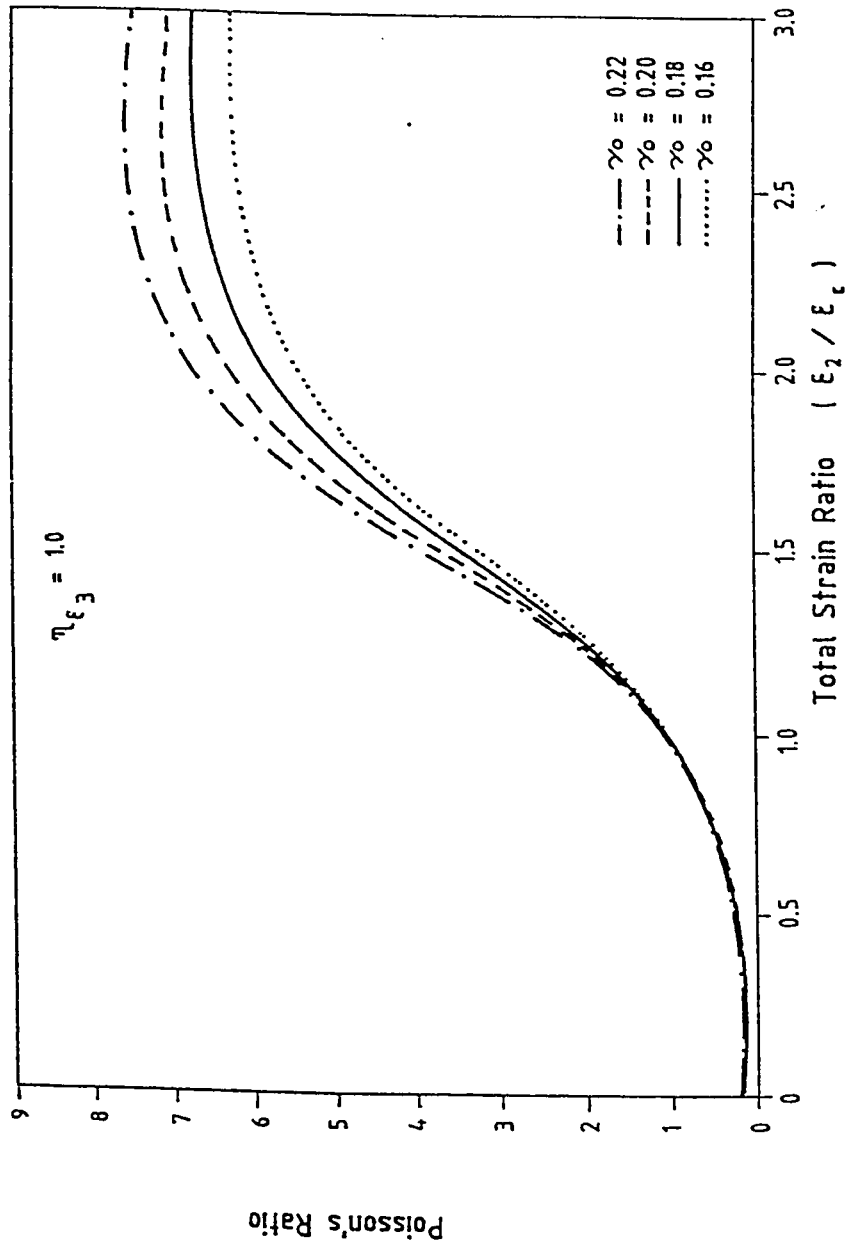


Figure 5.30 Variation of Poisson's ratio in uniaxial compression test

adopted by Fafitis and Won (1992). It allows the use of assigned value of the initial Poisson's ratio ν_0 rather than a fixed value of 0.18 and facilitates the general use for any peak value of the stress free strain other than unity. Using Eqn 5.110 the variation of Poisson's ratio in uniaxial compression is illustrated in Fig. 5.30.

5.4.10 Decanonalization of Constitutive Relations

The proposed theory of dichotomy facilitated establishing the damage model in the principal space in a canonical form which yielded the degraded moduli C_1 and C_2 corresponding to the strains ϵ^c , where the superscript $c = a, e, p$ for the total, elastic and plastic genera, respectively. Although this form is ample to get the stress components in terms of the strains, for completeness an inverse process is presented in order to obtain the conventional form of the constitutive laws. It is convenient to postulate on-axis orthotropic directional properties in the principal space for which the moduli matrix can be expressed as (Darwin and Pecknold; 1976, Tsai and Hahn; 1980)

$$[C] = \begin{vmatrix} D_{11} & D_{12} & 0.0 \\ D_{12} & D_{22} & 0.0 \\ 0.0 & 0.0 & D_{33} \end{vmatrix} \quad (5.111)$$

where

$$D_{12} = \nu \sqrt{D_{11} D_{22}} \quad (5.112)$$

and

$$D_{33} = \frac{1}{4} (D_{11} + D_{22} - 2 D_{12}) \quad (5.113)$$

in which ν is Poisson's ratio. Having equated the stress components obtained using both of the canonical and conventional forms, the following relations are arrived at

$$C_1 = D_{11} + \frac{1}{\xi_1^c} D_{12} \quad (5.114)$$

and

$$C_2 = \xi_1^c D_{12} + D_{22} \quad (5.115)$$

where $\xi_1^c = \epsilon_1^c / \epsilon_2^c$ is the principal strain biaxiality ratio which is related to the stress biaxiality ratio β_1 by the relation

$$\xi_1^c = \frac{C_2}{C_1} \beta_1 \quad (5.116)$$

Substituting from (5.112) in (5.114) and (5.115) a quadratic equation is obtained which has the form

$$a D_{11}^2 - b D_{11} + c = 0.0 \quad (5.117)$$

in which the coefficients a , b and c are

$$a = 1 - \nu^2, \quad (5.117a)$$

$$b = 2 C_1 - \nu^2 C_1 + \frac{\nu^2}{\xi_1^2} C_2 \quad , \quad (5.117b)$$

$$c = \frac{C_1^2}{\xi_1^2} + C_2 \quad (5.117c)$$

The second diagonal term is obtained by eliminating D_{12} from (5.114) and (5.115).

5.5 PREDICTIONS OF THE CANONICAL MODEL

The canonical model is utilized to predict strength characteristics in uniaxial and biaxial load combinations. The results are checked against a large set of experimental data. This verification is carried out in the following scheme:

1. Comparison of model predictions for uniaxial loading under monotonic loading.
2. Comparison of model predictions for biaxial loading under monotonic loading.
3. Comparison of model predictions for cyclic behavior.

The verification of the uniaxial behavior includes tensile as well as compressive loading. On the other hand, in biaxial load combinations the strength envelop, stress-strain curves and volumetric strain predictions are investigated. In most of the studied cases including compressive components, stress free straining is provided to show the

apparent Poisson's ratio.

5.5.1 Uniaxial Behavior under Monotonic Loading

In order to distinguish the salient features of the canonical model, it is advantageous to carry out a schematic comparison with some of existing models. Conceptually, the present formulation alluded to three damage variables for each loading condition i.e. tension and compression and a single material parameter, f'_c , is required as far as uniaxial behavior is concerned and where other peak parameters are not provided. Additionally Poisson's ratio is needed for biaxial states of stresses. In order to conduct a comparison with existing uniaxial damage variables as defined by other authors, the present variables are recapitulated in that

- d_a^j represents the damage variable associated with loading
- d_e^j represents the damage variable associated with unloading

where $j = t, c$. The existence of the plastic-damage variable d_p^j in concrete behavior can be ignored due to the redundancy inherited by virtue of split of strain tensor. However, for ductile metals d_p^j may replace d_a^j in loading since the elastic strains are rather small. The novel notion of the present formulation is its ability to predict cyclic behavior, albeit approximately, on a conceptually sound basis and in

terms of one material constant. In addition the stress-strain curves are more realistic than many of the existing analytical models in both tension and compression as shown in Figs. 5.31 and 5.32.

Inasmuch as a large number of damage models have been proposed in the last decade, comparison is limited to three of the early models: 1. Mazars' model (1984), 2. Loland's model (1981), and 3. Krajcinovic and Fonseka's model (1981). Mazars' model predicted brittle behavior and was originally adopted for tensile behavior and then extended to compression. Two damage variables were adopted for these loading conditions. Each required two material parameters (a,b) in conjunction to the peak strain. The model proposed by Loland also predicted brittle tensile behavior and was extended to compression. For each loading condition, the corresponding damage variable required two material parameters (λ_t, ϵ_u) in addition to the peak stress and the initial damage. Krajcinovic and Fonseka's model (1981) was applied to uniaxial conditions as a reduction from general tensorial equations. It also predicts brittle behavior and requires three material parameters ($C_1, C_2, B_1 - B_3$) in addition to threshold damage strain (ϵ^0), initial damage (w^0) and the conventional parameters (f_c', E, ν). This comparison indicates:

1. The parameters for the three models are unrelated although they describe the same behavior (brittle) for the same material (concrete).
2. Identification of each of the parameters is not a simple job and

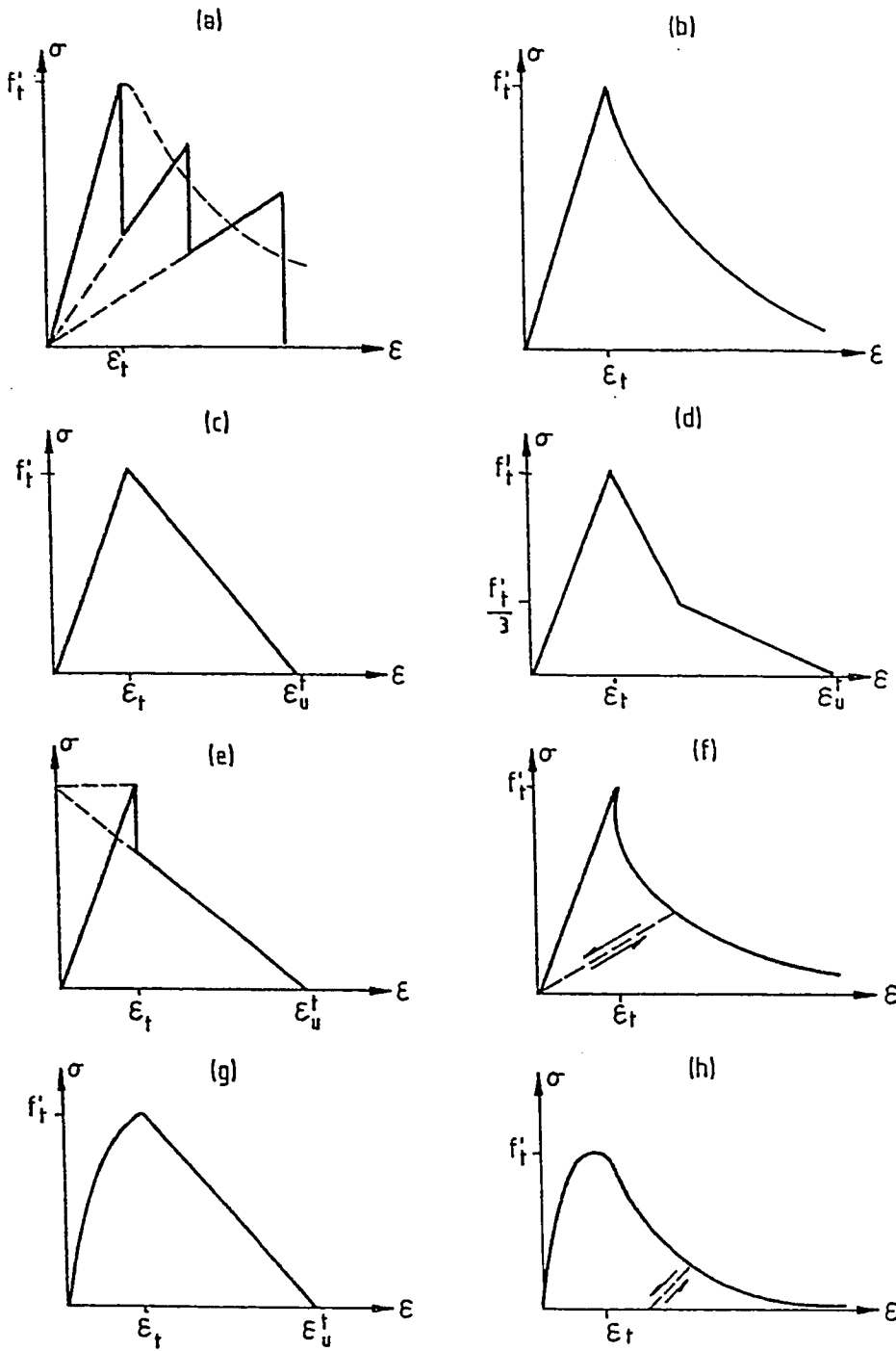


Figure 5.31 Comparison of the present study with some of the existing models for uniaxial tension:(a) Scanlon;(b) Lin and Scordelis;(c) Bazant and Oh;(d) Gylltoft; (e) Owen et al.;(f) Mazars;(g) Loland; and (h) Canonical model

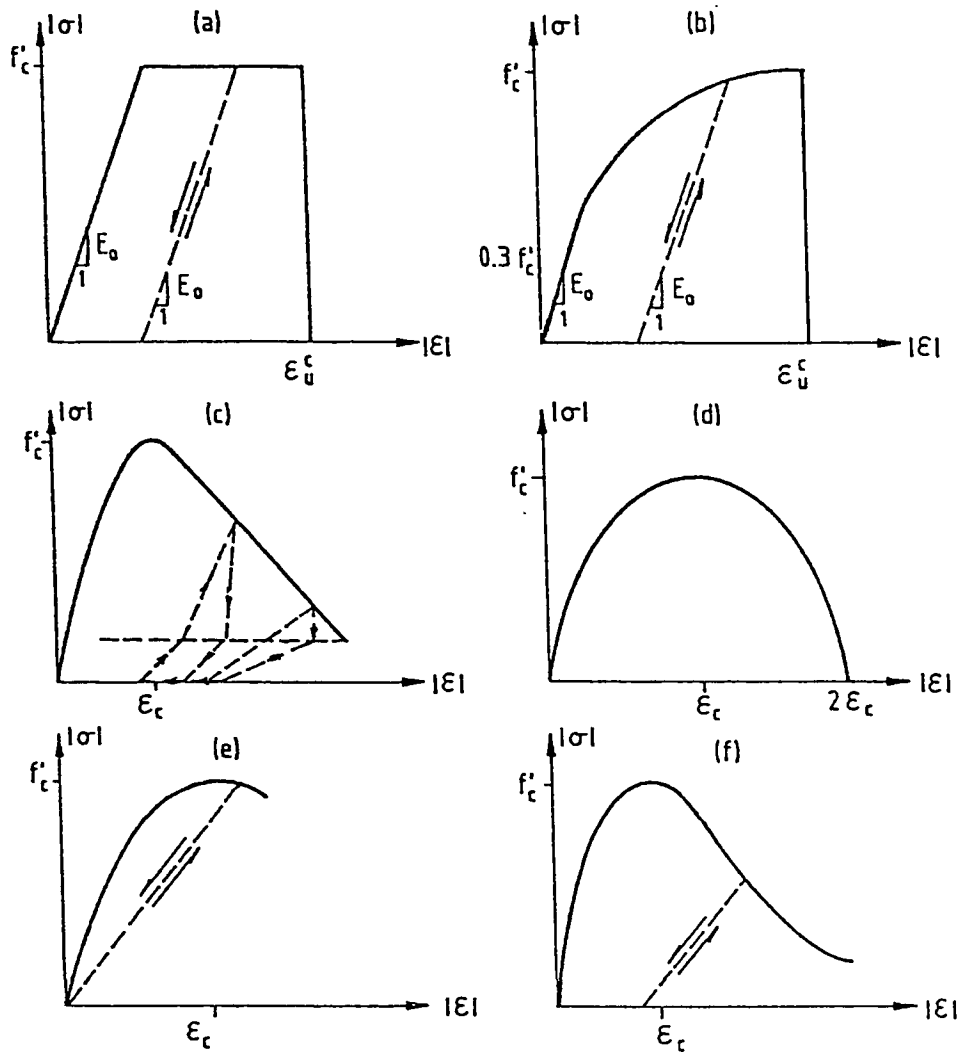


Figure 5.32

Comparison of the present study with some of the existing models for uniaxial compression: (a) elastic-perfectly plastic; (b) elastic-work hardening; (c) Loland; (d) Hognstaad parabola; (e) Mazars; and (f) Canonical model

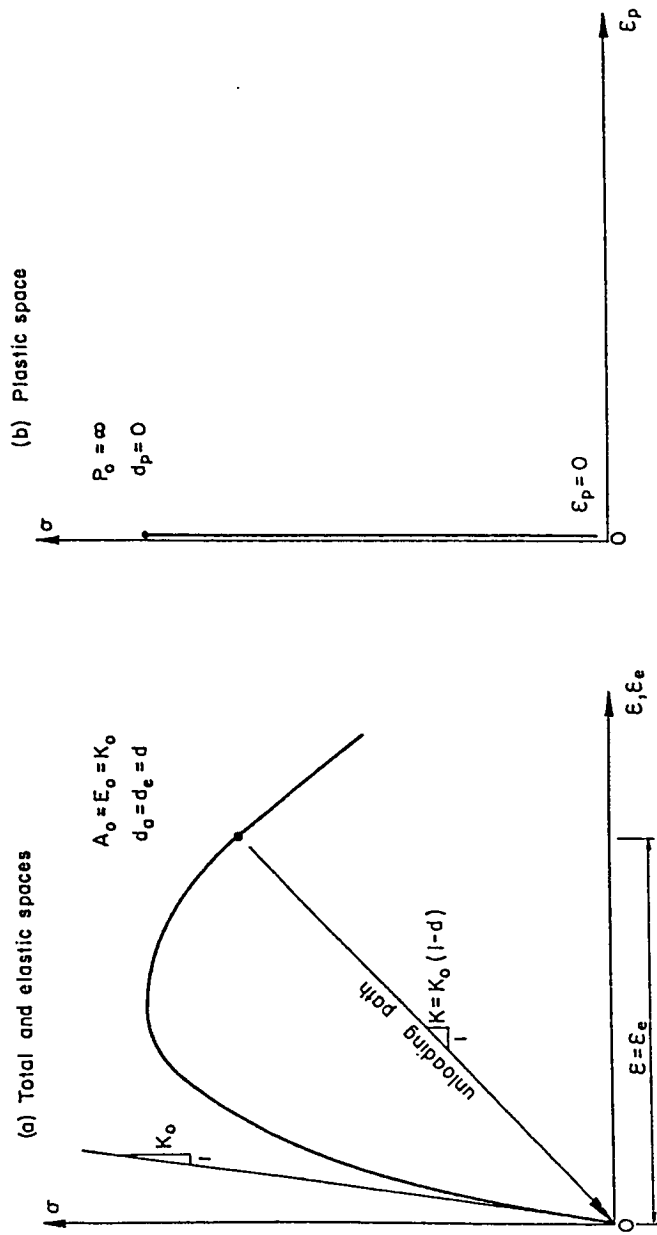


Figure 5.33 Schematic presentation of the brittle behavior in various spaces

may require automatic identification procedures as remarked by Saouridis and Mazars (1989).

3. Most of the parameters lack a simple physical interpretation. Rather, they can be looked upon as mathematical coefficients.
4. Since the behavior is assumed to be brittle for the aforementioned models, the plot of the material response in various strain spaces is reduced merely to a single graph as shown in Fig. 5.33a. Therefore, the space of the plastic-damage strain becomes trivial but for completeness, however, the stress plot is illustrated in Fig. 5.33b. In this case, one damage variable is ample for either tension or compression.

Predictions of the canonical model is performed for two sets in each of tension or compression. In tension the available experimental data are relatively limited when compared with those in compression. For uniaxial tension, The predictions are compared with two analytical models and experimental data corrected for the reference gauge length as suggested by Yankelevsky and Reinhardt (1987). The analytical models considered are those of Gopalaratnam and Shah (1985) and Yankelevsky and Reinhardt (1987). The model is first used to predict the stress-strain curve of concrete of relatively low tensile strength as shown in Fig. 5.34. The experimental data were reported by Hilsdorf et al. (1969). For relatively high tensile strength concrete, the stress-strain curve is illustrated in Fig. 5.35 against the experimental data of Gopalaratnam and Shah (1985). The model is shown to be in close agreement with other curves and to be able to predict strain softening characteristics.

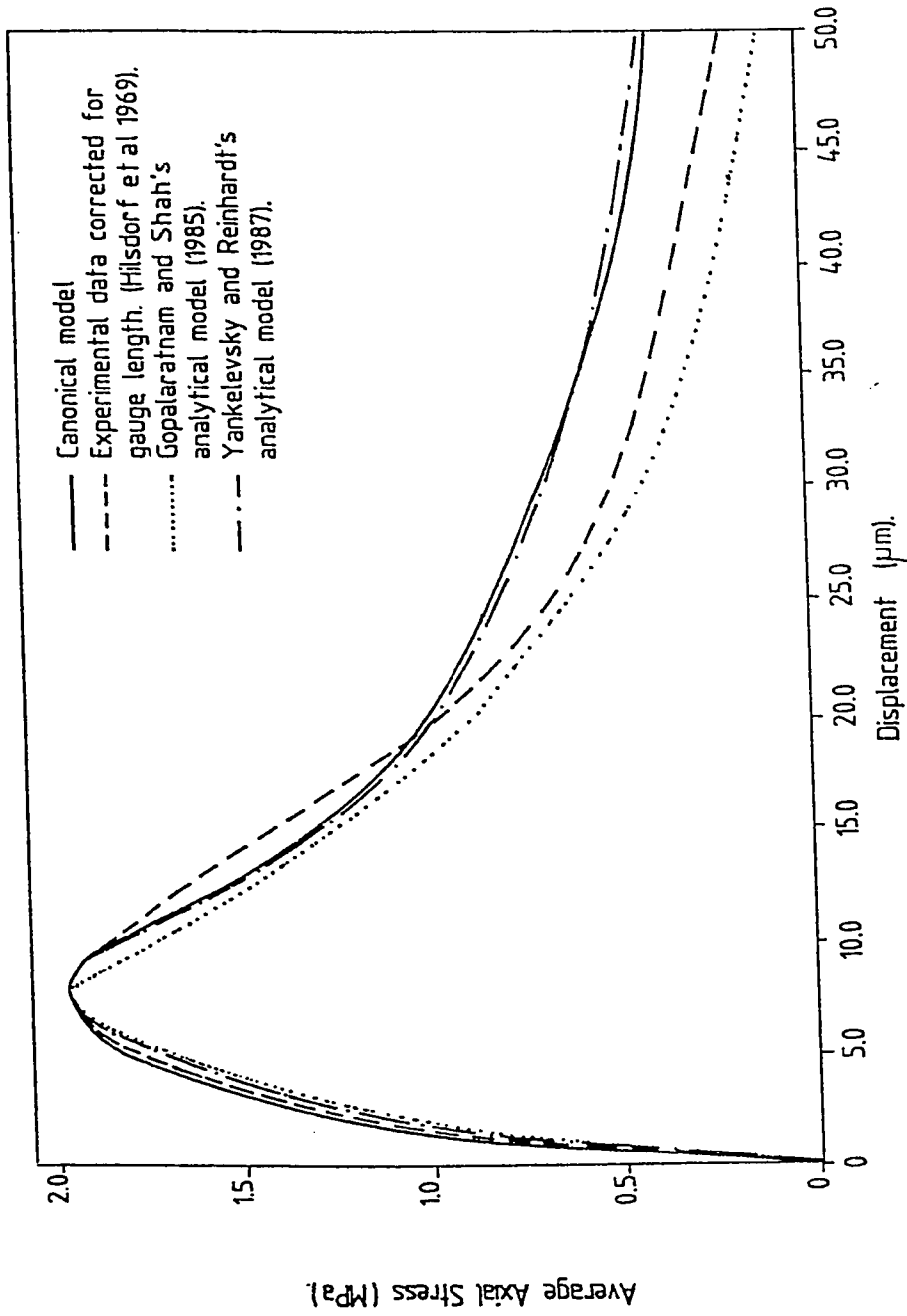


Figure 5.34 Model prediction for relatively low strength concrete under monotonic uniaxial tension

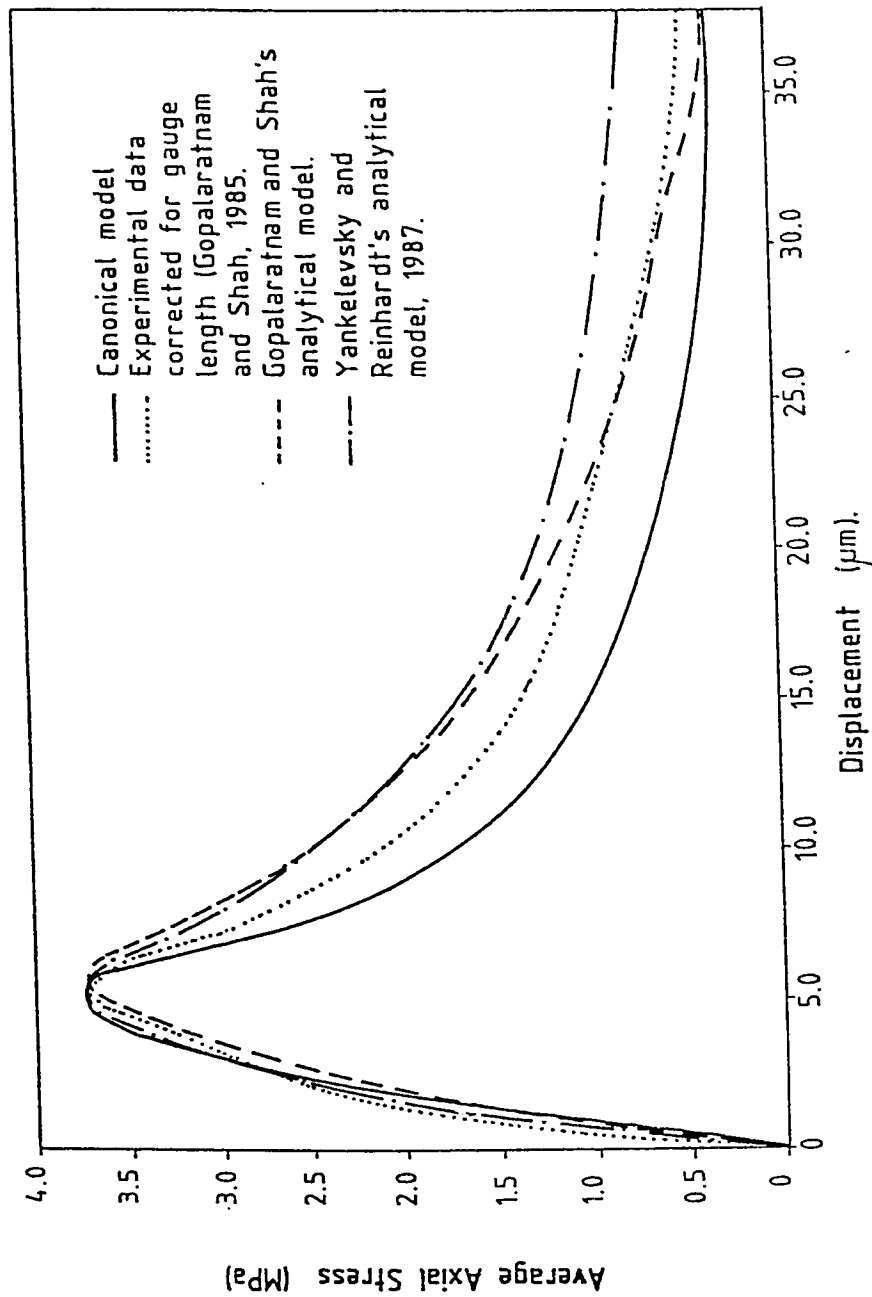


Figure 5.35 Model prediction for relatively high strength concrete under monotonic uniaxial tension

For uniaxial compression, the predictions of the model are shown for concretes of different strength. Fig. 5.36 depicts a comparison with experimental data of Hognstaad et al. (1955) for strengths ranging from 8.79 MPa to 49.52 MPa while Fig. 5.37 undertakes a range between 20.70 MPa and 42.75 MPa following experimental data of Smith and Young (1956). The model is shown to be in close agreement with experimental data which covers a broad range of concrete grades. It can be noted that strain softening is captured reasonably.

To sum up, based on the previous verification for uniaxial behavior under monotonic loading, the canonical model has the following advantages:

1. Unilateral nature since behavior in tension and compression are quite different.
2. Realistic description of the stress strain curve in both of the pre-peak and post-peak regions in both tension and compression.
3. reduced number of material parameters which are of physical sense.

5.5.2 Biaxial Behavior under Monotonic Loading

Accurate determination of the strength envelop is one of the major limitations of many of the existing models as discussed elsewhere. The canonical model has the ability of predicting this envelop as shown in Fig. 5.38. The model is compared with numerous experimental data

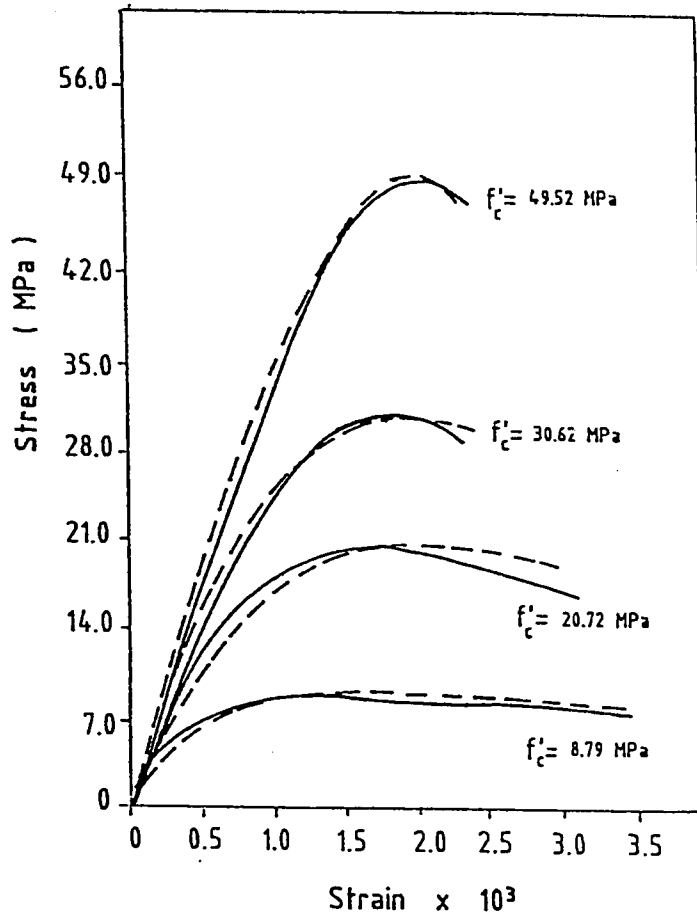


Figure 5.36 Comparison of Model's prediction with experimental data of Hognstaad et al. (1955) in monotonic uniaxial compression

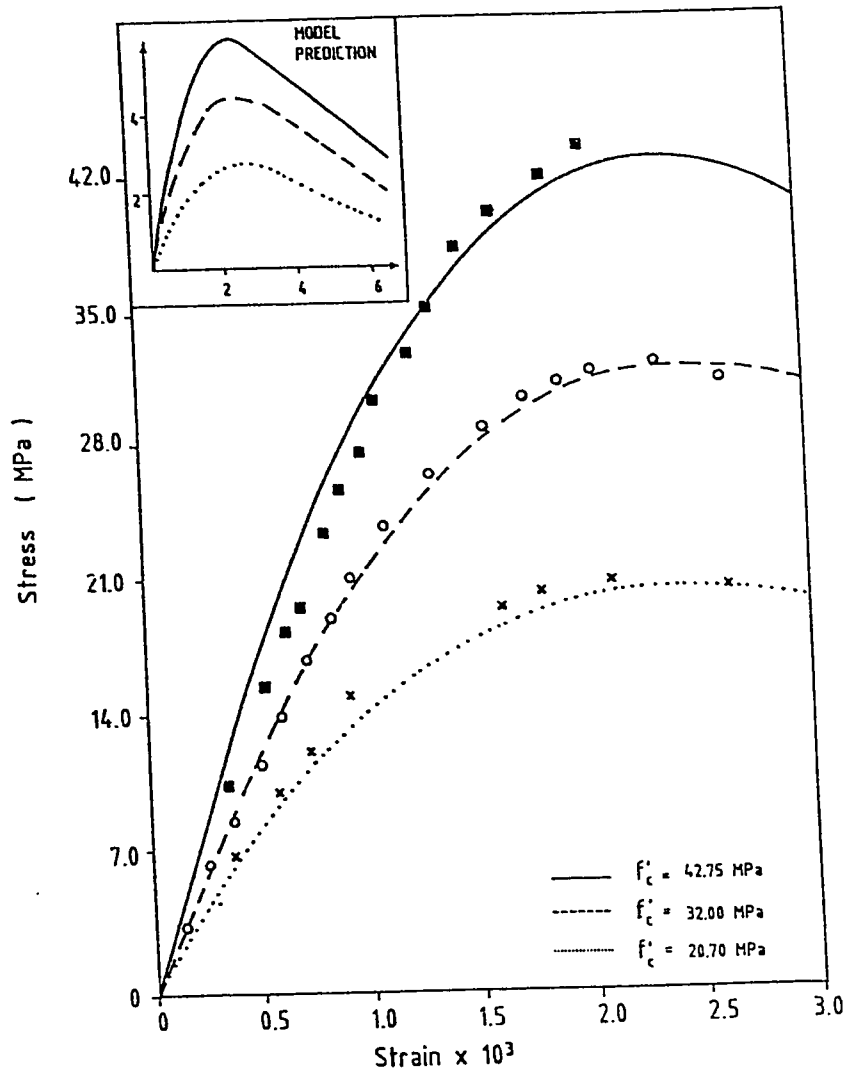


Figure 5.37 Comparison of Model's prediction with experimental data of Smith and Young (1956) in monotonic uniaxial compression

points collected from the literature. This includes those of Kupfer et al. (1969), Aschl et al. (1972), Andenaes et al. (1977), Liu et al. (1977), Schickert and Winkler (1977), Tasuji et al. (1978) and Van Mier (1985). Moreover, the model is then compared with the analytical model of Kupfer and Grestel (1973) as shown in Fig. 5.39. The envelop shows the strength increase in biaxial compressive combinations and the reduction of the tensile strength in the tension-compression quadrant. The tensile strength is kept unaltered for tension-tension stress combinations

To have a more global picture about the predictions of the model the stress-strain curves are compared against the experimental data of Kupfer et al. (1969), Tasuji et al. (1978) in the tension-compression and in the compression-compression quadrants. Additional set of experimental data were selected in the compression-compression quadrant after Schickert and Winkler (1977). These data are selected because they are well documented and also reflects the possible boundary effect and specimen size on the stress-strain trends. Volumetric changes in the compression-compression quadrant are also shown. Kupfer et al. (1969) used 200X200X50 mm concrete specimens and brush platens to avoid frictional end effects. Tasuji et al. (1978) subjected 127X127X13 mm thin concrete plates to biaxial load combinations using comb-like platens. Schickert and Winkler (1977) reported for BAM testing program results on 100 mm concrete cube subjected to biaxial loading using rigid (rough/unlubricated) and flexible platens.

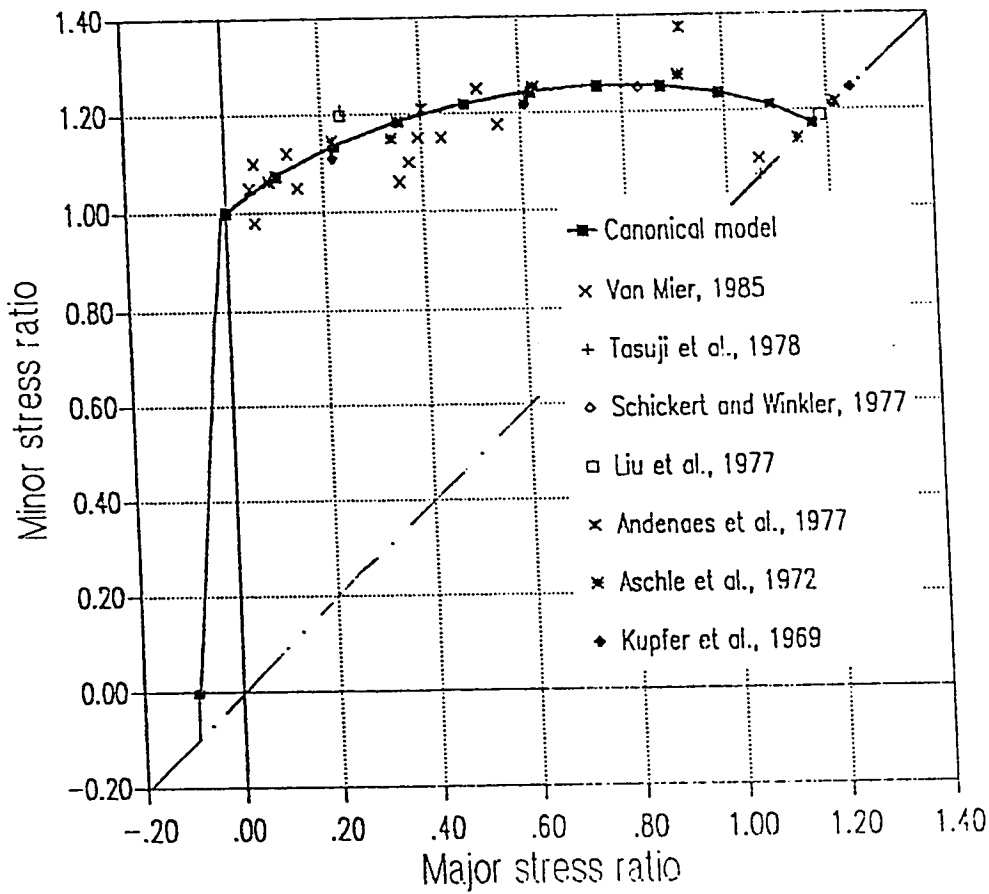


Figure 5.38 Comparison of the model's prediction of the peak stress envelop and experimental data for biaxial loading

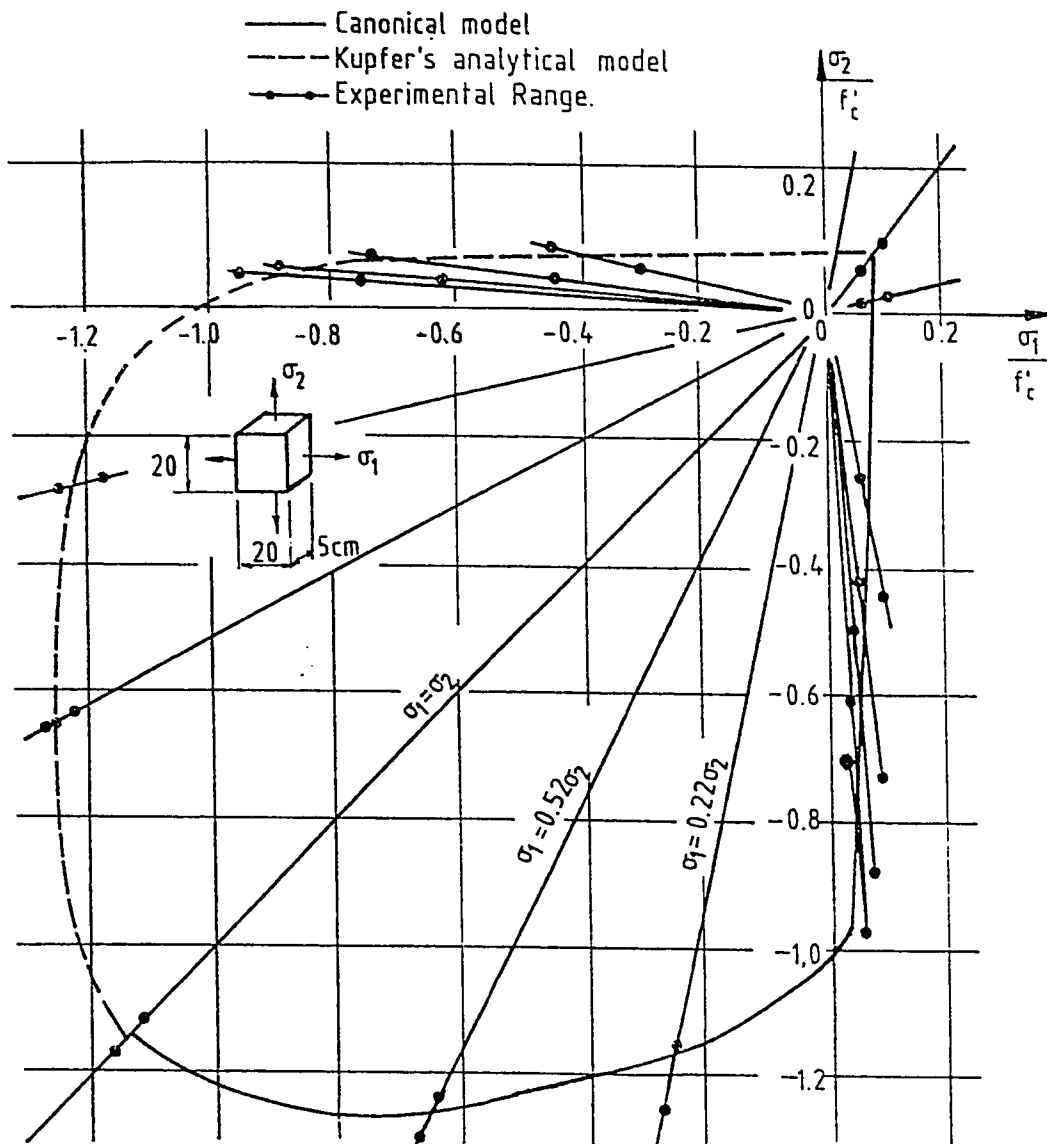


Figure 5.39 Comparison of the model's prediction of the peak stress envelop and Kupfer's experimental data for biaxial loading

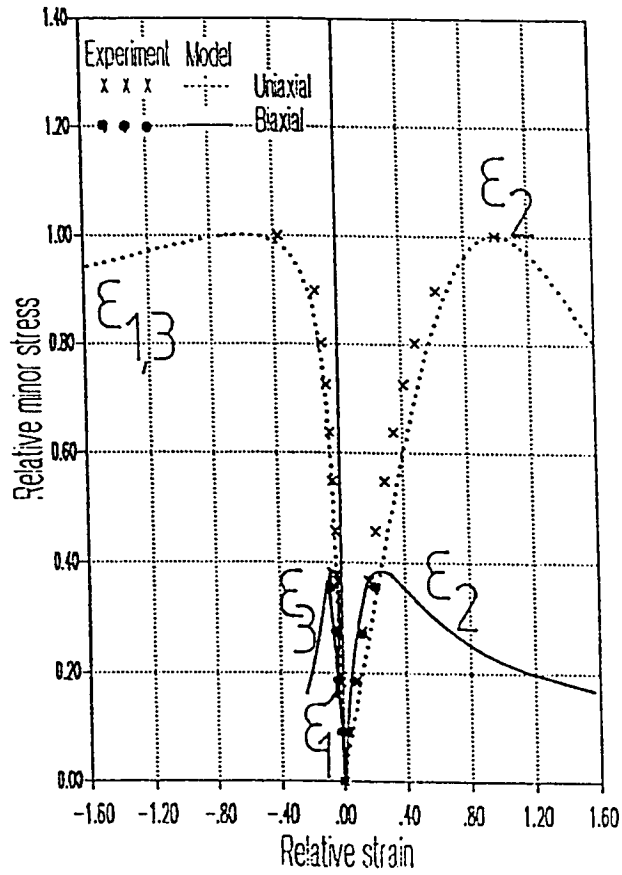


Figure 5.40 Comparison of the model's prediction for the relative stress-relative strains versus the experimental data of Kupfer et al. (1969) for tension-compression quadrant of stress ratio 0.204/-1.0

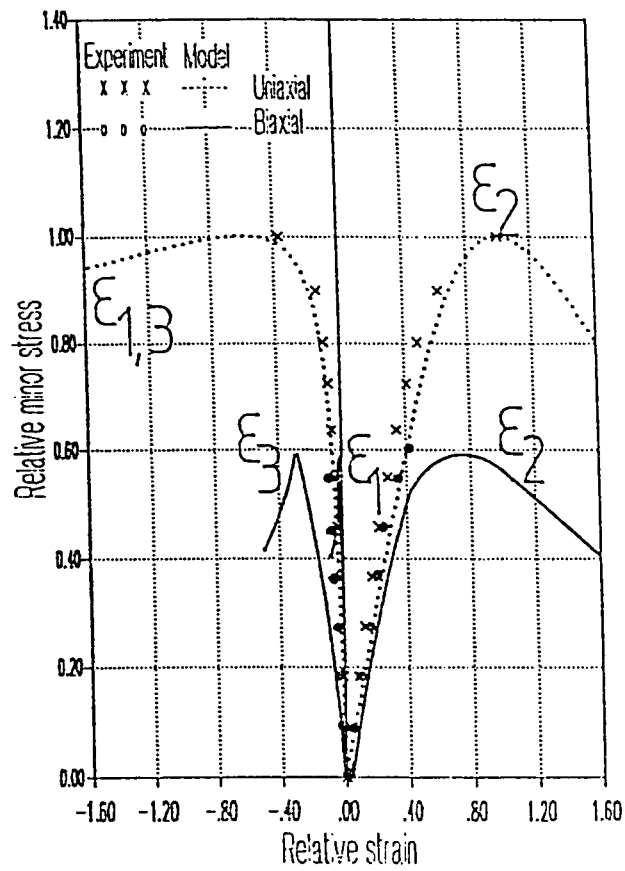


Figure 5.41 Comparison of the model's prediction for the relative stress-relative strains versus the experimental data of Kupfer et al. (1969) for tension-compression quadrant of stress ratio 0.103/-1.0

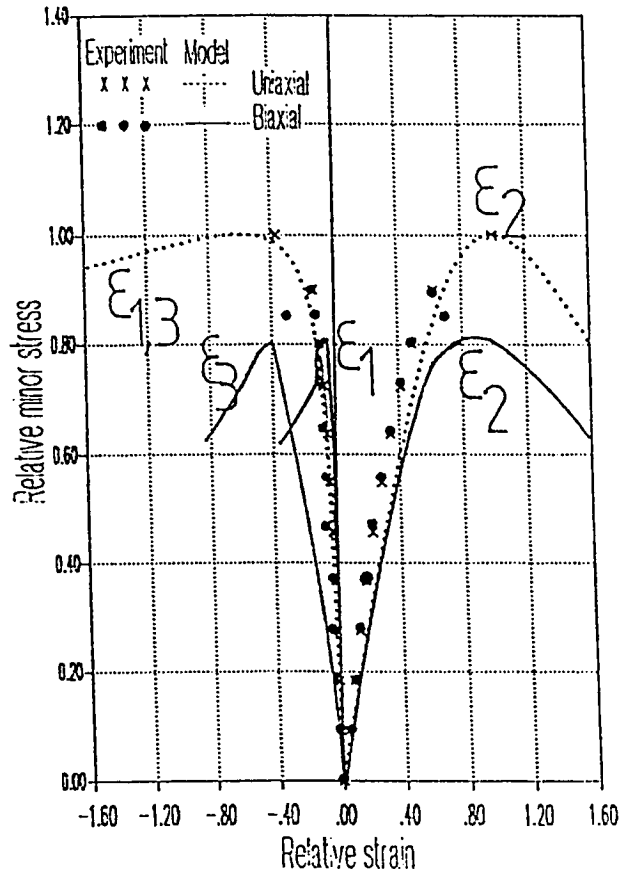


Figure 5.42 Comparison of the model's prediction for the relative stress-relative strains versus the experimental data of Kupfer et al. (1969) for tension-compression quadrant of stress ratio 0.052/-1.0

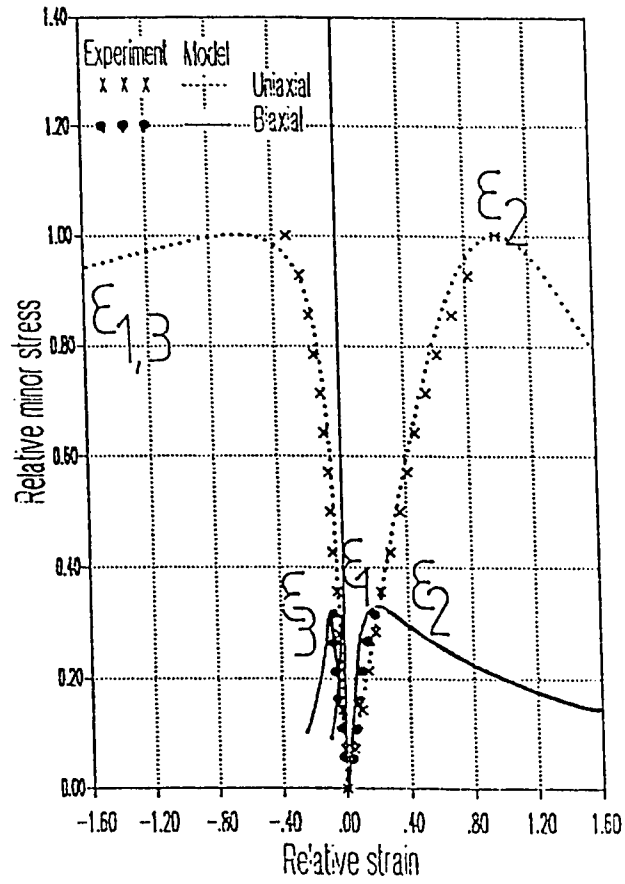


Figure 5.43 Comparison of the model's prediction for the relative stress-relative strains versus the experimental data of Tasuji et al. (1978) for tension-compression quadrant of stress ratio 0.25/-1.0

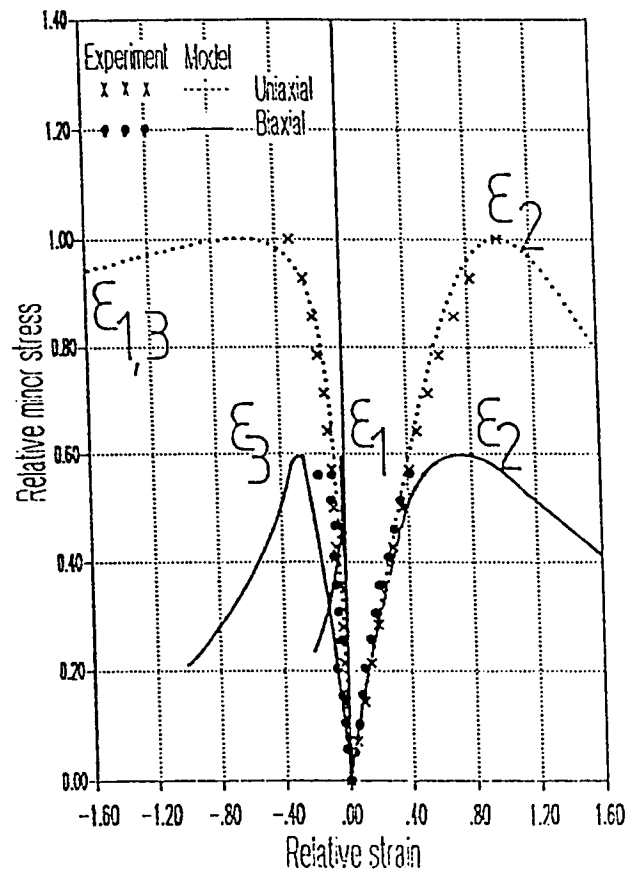


Figure 5.44 Comparison of the model's prediction for the relative stress-relative strains versus the experimental data of Tasuji et al. (1978) for tension-compression quadrant of stress ratio 0.10/-1.0

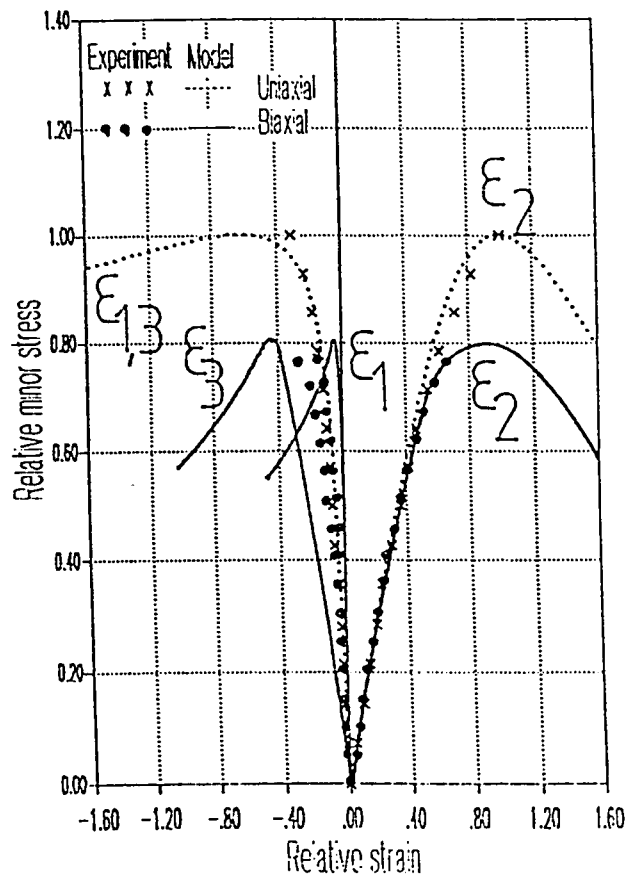


Figure 5.45 Comparison of the model's prediction for the relative stress-relative strains versus the experimental data of Tasuji et al. (1978) for tension-compression quadrant of stress ratio 0.05/-1.0

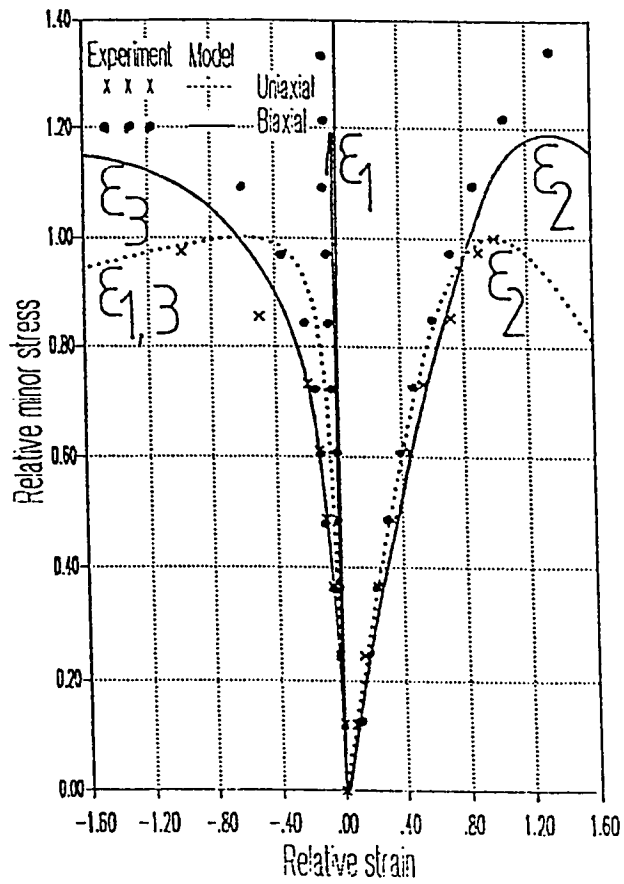


Figure 5.46 Comparison of the model's prediction for the relative stress-relative strains versus the experimental data of Schickert and Winkler (1977) for compression-compression quadrant of stress ratio $-1/-3$

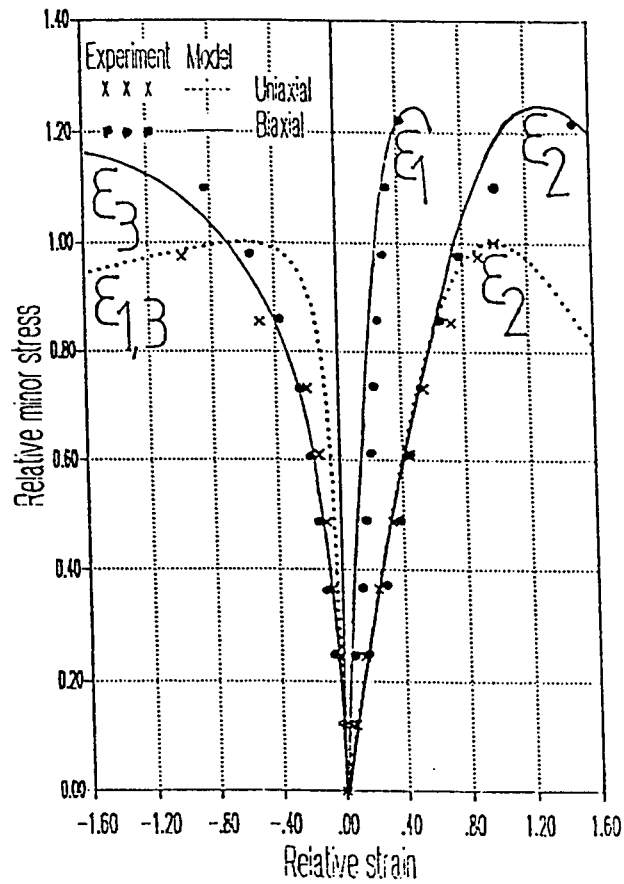


Figure 5.47 Comparison of the model's prediction for the relative stress-relative strains versus the experimental data of Schickert and Winkler (1977) for compression-compression quadrant of stress ratio $-2/-3$

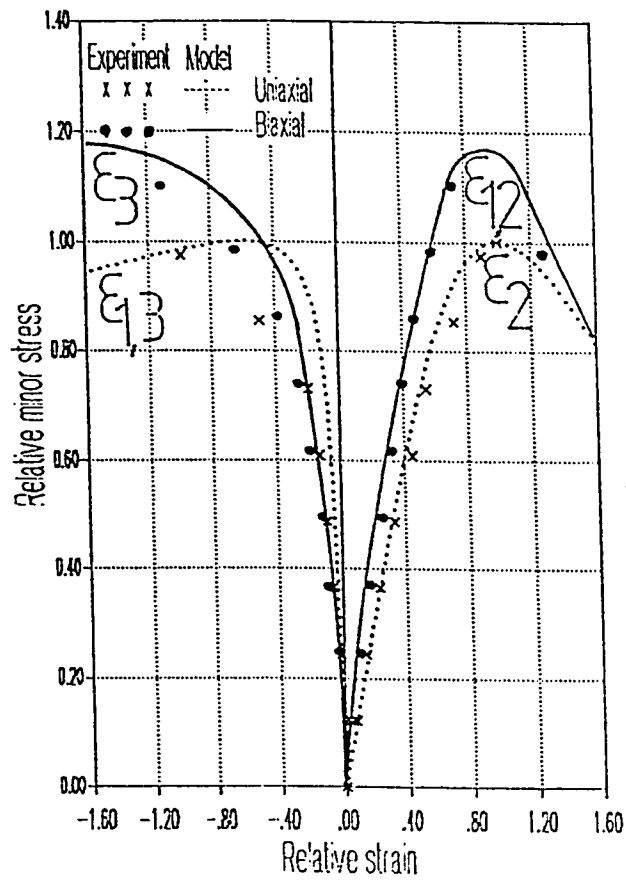


Figure 5.48 Comparison of the model's prediction for the relative stress-relative strains versus the experimental data of Schickert and Winkler (1977) for compression-compression quadrant of stress ratio -3/-3

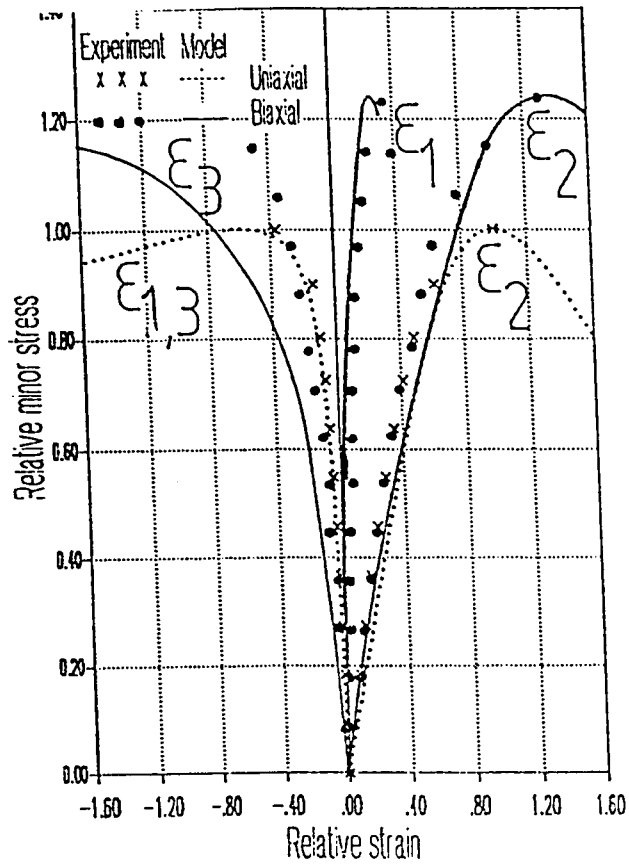


Figure 5.49 Comparison of the model's prediction for the relative stress-relative strains versus the experimental data of Kupfer et al. (1969) for compression-compression quadrant of stress ratio $-0.52/-1.00$

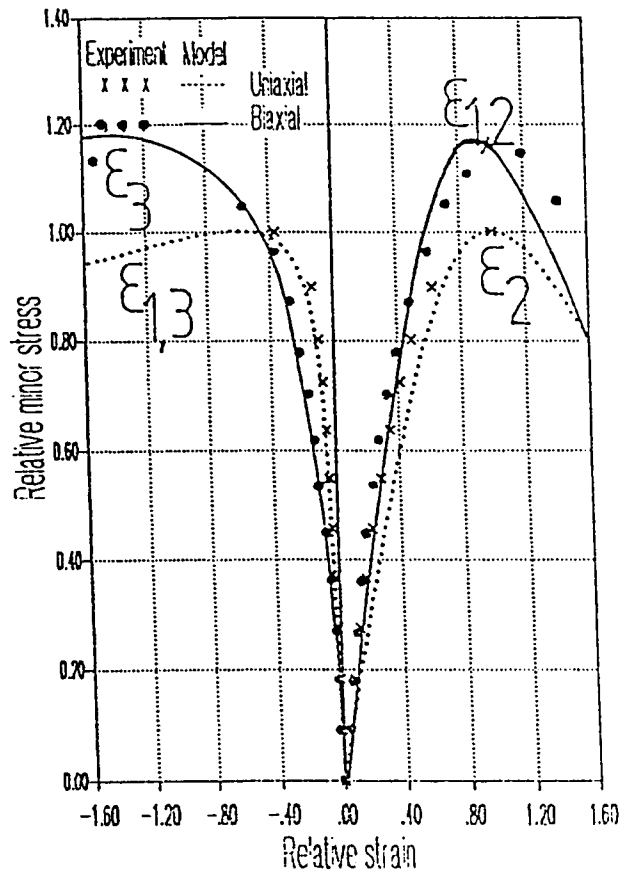


Figure 5.50 Comparison of the model's prediction for the relative stress-relative strains versus the experimental data of Kupfer et al. (1969) for compression-compression quadrant of stress ratio -1.00/-1.00

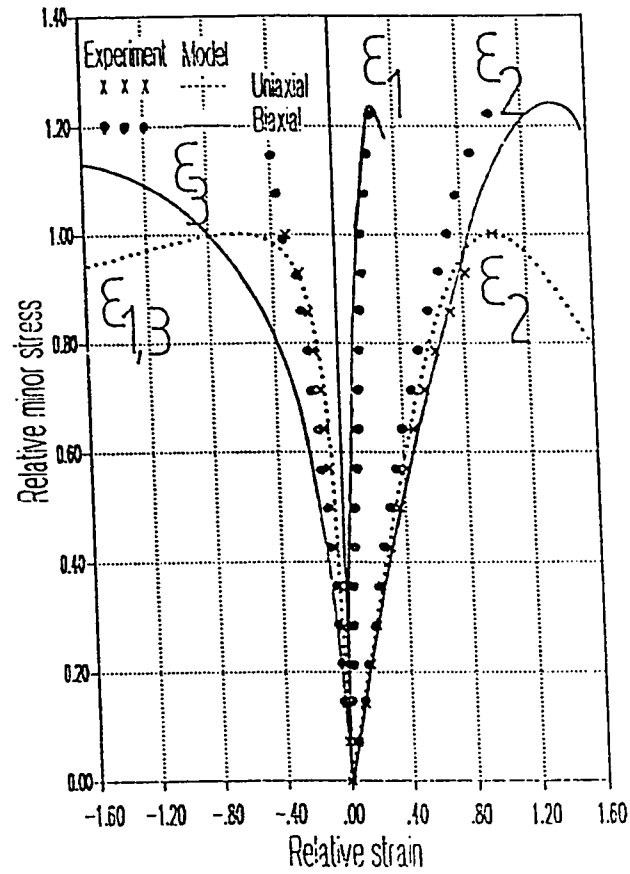


Figure 5.51 Comparison of the model's prediction for the relative stress-relative strains versus the experimental data of Tasuji et al. (1969) for compression-compression quadrant of stress ratio $-0.52/-1.00$

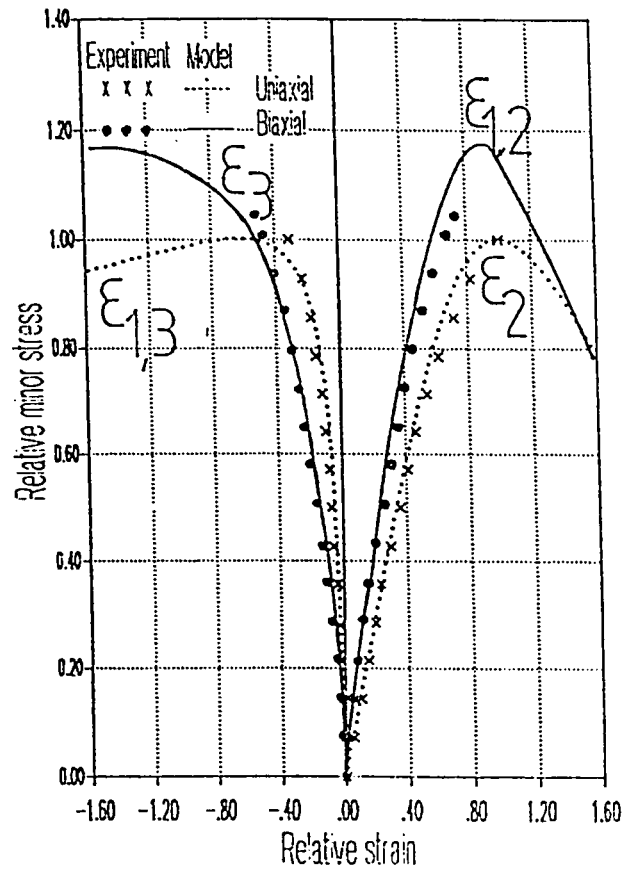


Figure 5.52 Comparison of the model's prediction for the relative stress-relative strains versus the experimental data of Tasuji et al. (1969) for compression-compression quadrant of stress ratio -1.00/-1.00

In the tension-compression quadrant, the predictions of the model are firstly plotted versus the experimental data of Kupfer et al. (1969) for biaxiality ratios of 0.204/-1.0, 0.103/-1.0 and 0.052/-1.0 as shown in Figs. 5.40-42. A comparison with the experimental data of Tasuji et al. (1978) for biaxiality ratios of 0.25/-1.0, 0.10/-1.0 and 0.05/-1.0 are illustrated in Figs. 5.43-45. In each case the three strain components of the biaxial curves are drawn altogether with those of uniaxial compression. It can be noted that strain softening is predicted for all stress combinations and for all of the three strain components. The peak stress and strains are dependant on the biaxiality ratio and are not kept constant in this quadrant as postulated in many of the existing models. The peak values decrease with the increase of the tensile stress components.

In the compression-compression quadrant, the following biaxiality ratios are used for (1) Schickert and Winkler (1977): -1.0/-3.0, -2.0/-3.0, and -3.0/-3.0 as shown in Figs. 5.46-48, (2) Kupfer et al. (1969): -0.52/-1.0 and -1.0/-1.0 as shown in Figs. 5.49-50 and (3) Tasuji et al. (1978): -0.50/-1.0 and -1.0/-1.0 as shown in Figs. 5.51-52. The trend of the predicted curves is seen to resemble that of the experimental data. The variation of the peak stress and strain values are reasonably predicted. The strain corresponding to the minor stress ratio is noted to correctly reverse sign from small biaxiality ratios to large ratios (compare for example Fig. 5.46, 47 and 5.48).

The volumetric changes as predicted by the model are compared with the experimental data in the compression-compression quadrant as shown

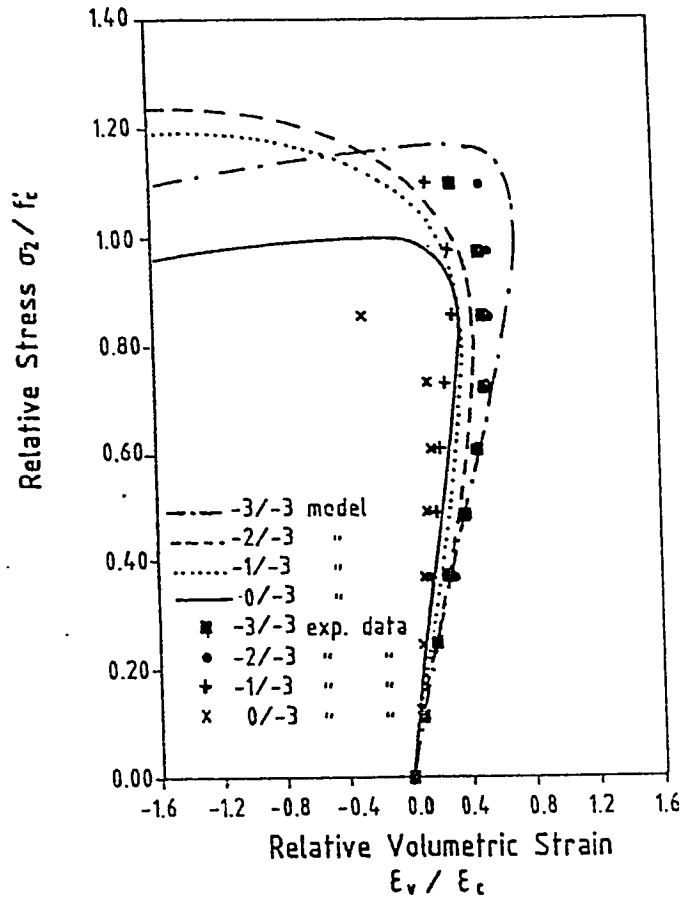


Figure 5.53 Comparison of the model's prediction for the relative stress-relative volumetric strain versus the experimental data of Schickert and Winkler (1977) for compression-compression quadrant under different stress ratio

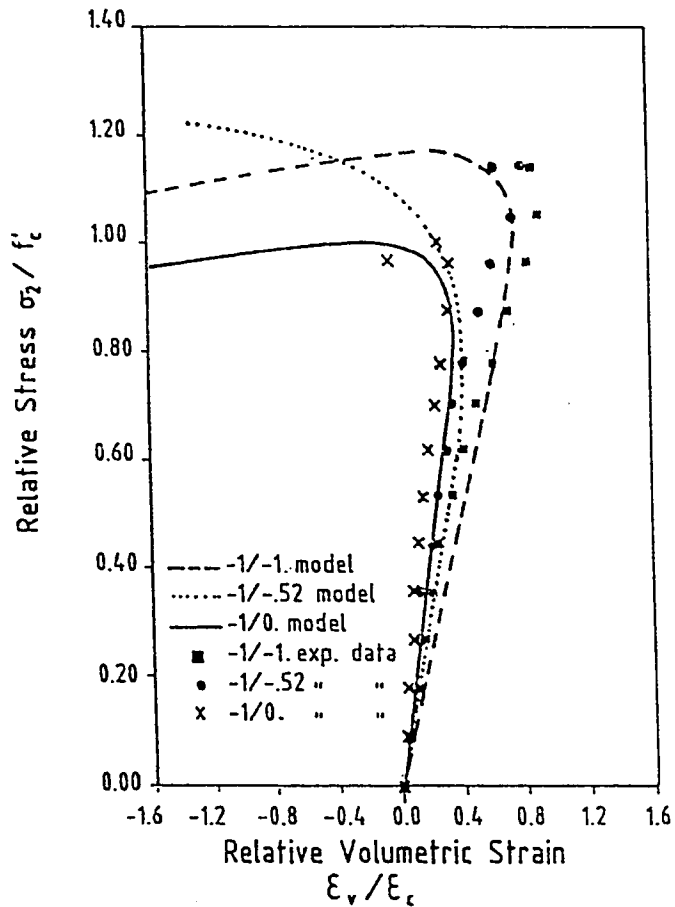


Figure 5.54 Comparison of the model's prediction for the relative stress-relative volumetric strain versus the experimental data of Kupfer et al. (1969) for compression-compression quadrant under different stress ratio

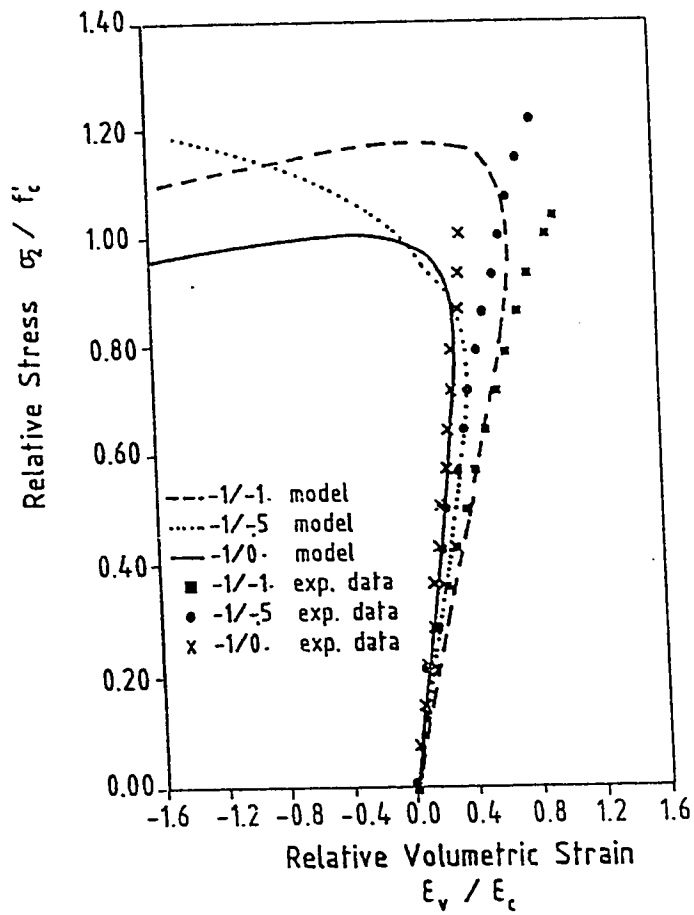


Figure 5.55 Comparison of the model's prediction for the relative stress-relative volumetric strain versus the experimental data of Tasuji et al. (1969) for compression-compression quadrant under different stress ratio

in Figs. 5.53-55. Compression (compaction) takes place in the early stages of loading and then starts to decrease such that dilation can be eventually observed for all the biaxiality ratios. Such a phenomenon represents a characteristic feature of rock like materials and granular cohesionless soils. However, limited number of models provided such volumetric changes (cf. endochronic theory for concrete).

5.5.3 Behavior under Cyclic Loading

The introduction of the elastic-damage variable in the formulation enables the determination of the degradation of the unloading slope (stiffness degradation). Alternatively, the plastic-damage variable may be utilized for the same purpose. Of course the idealization of the hysteresis loop as a straight line is a reasonable postulation as declared before. This feature is employed for the prediction of the cyclic behavior in both tension and compression.

For relatively high strength concrete subjected to cyclic tensile loading the loading envelop as well as the unloading paths are shown in Fig. 5.56. The predictions of the model are compared with the experimental data of Gopalaratnam and Shah (1985) and with the predictions of the analytical model of Yankelevsky and Reinhardt (1987). It is illustrated that both of the strain softening and the stiffness degradation are reasonably captured. In uniaxial compression more experimental data concerning cyclic loading are available. The loading and unloading schemes as predicted by the model are compared versus: (1) the experimental data of Sinha et al. (1964) as shown in

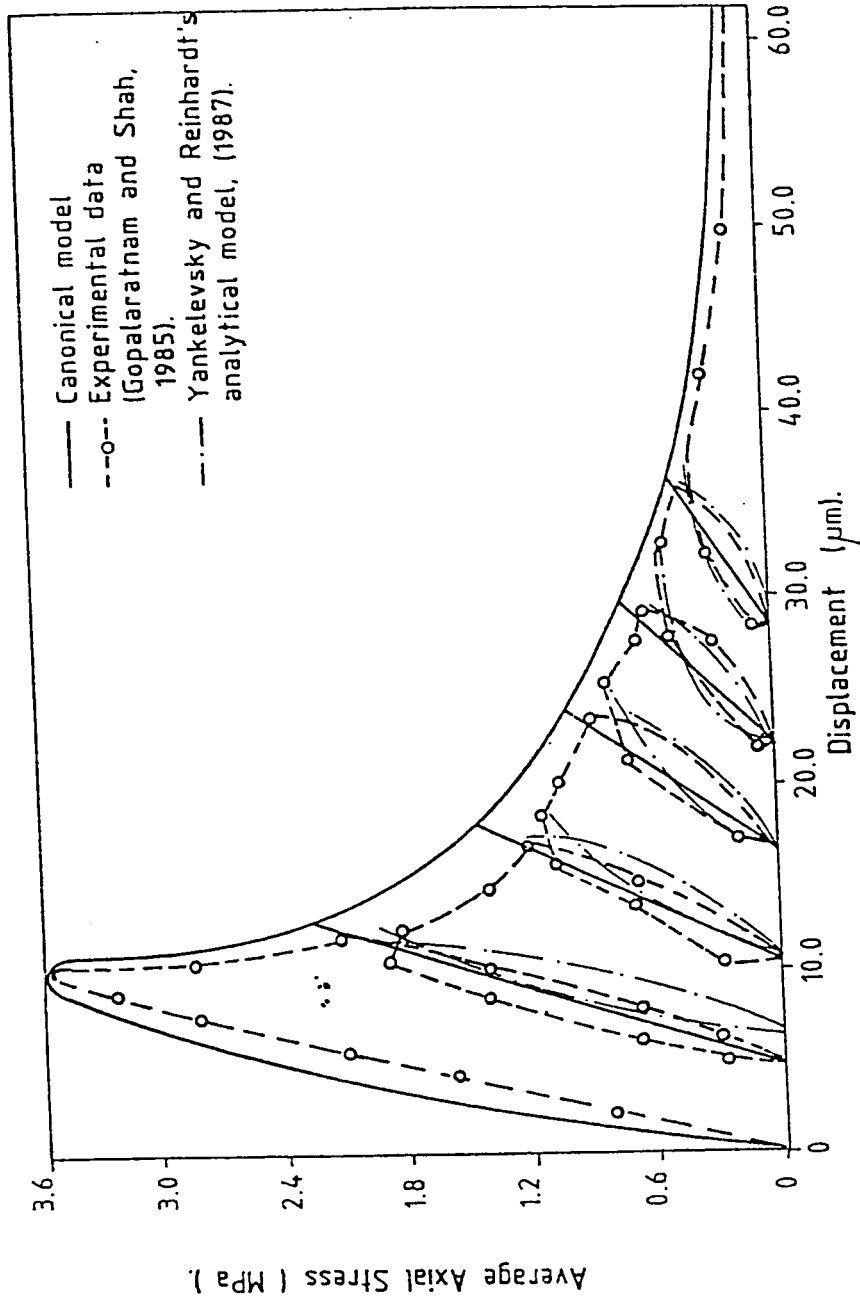


Figure 5.56 Model prediction for the cyclic behavior under uniaxial tension

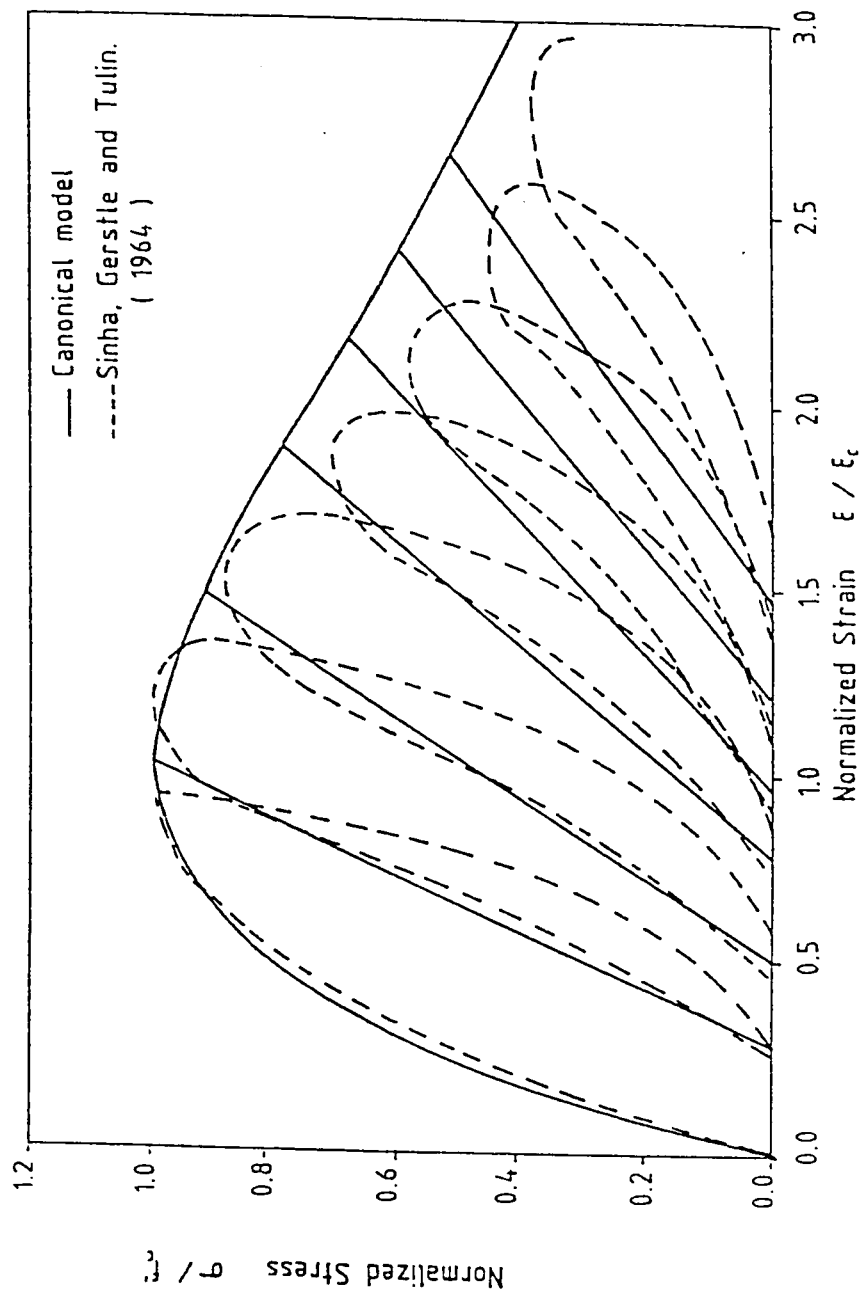


Figure 5.57 Comparison of the model's prediction for the cyclic behavior versus the experimental data of Sinha et al. (1964) under uniaxial compression

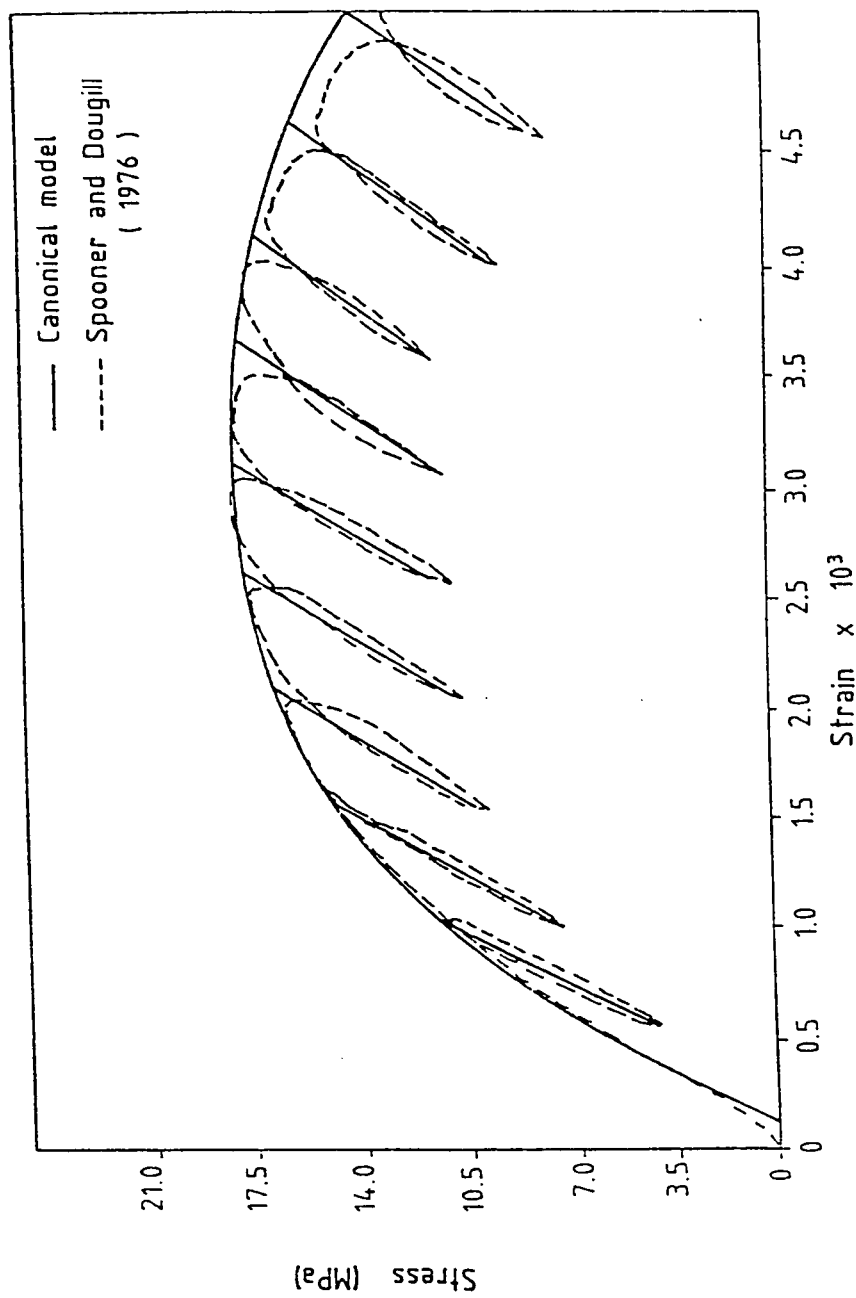


Figure 5.58 Comparison of the model's prediction for partial cyclic behavior versus the experimental data of Spooner and Dougill (1976) under uniaxial compression

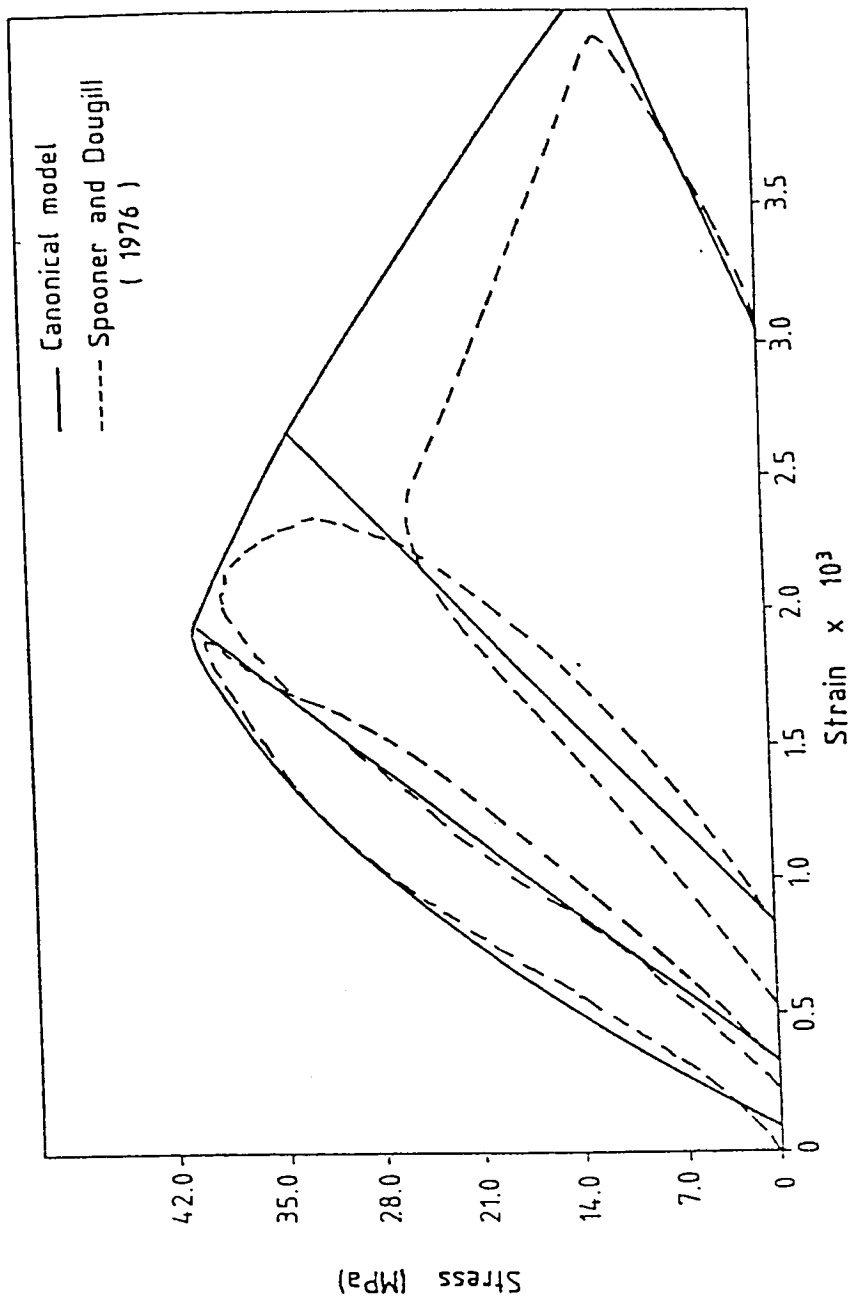


Figure 5.59 Comparison of the model's prediction for full cyclic behavior versus the experimental data of Spooner and Dougill (1976) under uniaxial compression

Fig. 5.57, (2) the experimental data for partial cycling after Spooner and Dougill (1976) as shown in Fig. 5.58, (3) the experimental data for full cycling after Spooner and Dougill (1976) as shown in Fig. 5.59 and (4) the experimental data of Buyukozturk and Tseng (1984) as shown in Fig. 5.59. The uniaxial compressive stress is plotted against the uniaxial compressive strain. The loading and unloading patterns are shown to be in good agreement with the experiment curves. For the data of Buyukozturk and Tseng (1984) the transverse strains are also given as shown in Fig. 5.59. This indicates that the free stress straining can be reasonably predicted in cyclic behavior using the proposed canonical model for concrete.

5.6 UNIAXIAL DAMAGE MODEL FOR REINFORCING STEEL

Behavior of steel in tension is almost typical to that in compression. In many situations stress-strain characteristics are of concern up to the peak. Unfortunately, experimental data on stiffness degradation of local reinforcing steel is not available. A series of uniaxial tension tests using strain controlled machine (INSTRON) was carried out and a bevy of results is shown in Figs. 5.60-63.

Deformed reinforcing steel bars of 680 mm length and 16 mm diameters were used. The deformations were measured by 20 mm length LVDT. Additionally strain gages were mounted to the steel samples. A control sample labelled T_1 was subjected to monotonic loading, as shown in Fig. 5.60, such that effects of load cycling on the loading envelop

could be observed. Three other samples labelled T_2 , T_3 and T_4 were subjected to cyclic loading as shown in Figs. 5.61-64. For all samples, necking occurred after the peak in the usual form of cup and cone. The final minimum diameter at the ruptured section was 11.5 mm.

The results demonstrated that load cycling did not affect the pre-peak stress and strain parameters where as tended to increase the strain at rupture. The delay of the necking process to the post-peak region indicated the reliability of the damage exploration in the pre-peak where damage may be considered to be distributed. No stiffness degradation was noted since the unloading slope was nearly unchanged or at most negligible in all unloading paths. This appeared to be similar to that of the experimental paths shown by Dafalias (1981). Therefore, the presence of elastic damage is absent and the enhancement of damage variables other than the elastic one is a must. The concept of skeleton curve seemed to be plausible as suggested by Colson and Boulabiza (1992).

Based on the such an understanding, the total damage variables can be derived using the modified Menegotto-Pinto relations that were reviewed in Chapter 2. However, minor changes have been carried out in order to distinguish between the lower yield stress $\sigma_{y1} = \sigma_y$ and the upper yield stress $\sigma_{yu} = \alpha\sigma_y$ as shown in Fig. 5.65. The mathematical form can be easily shown to be expressed as

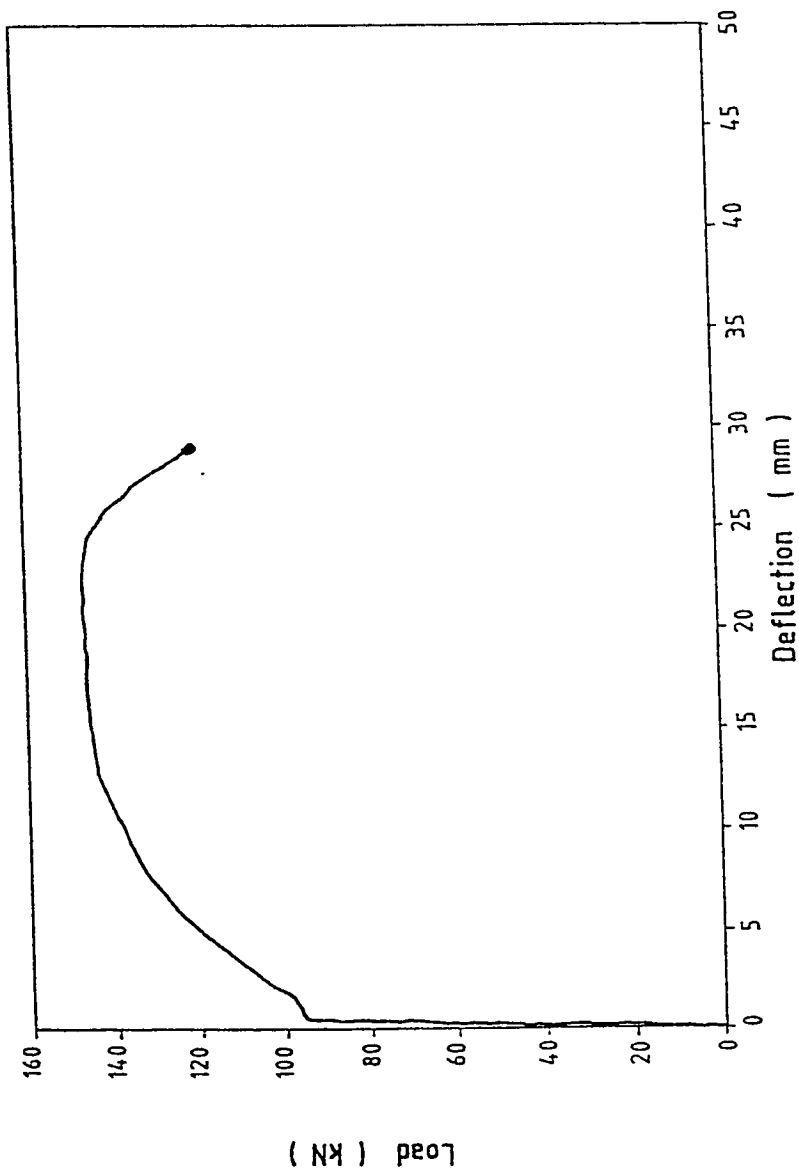


Figure 5.61 Experimental monotonic load-deflection curve of reinforcing steel sample T_1

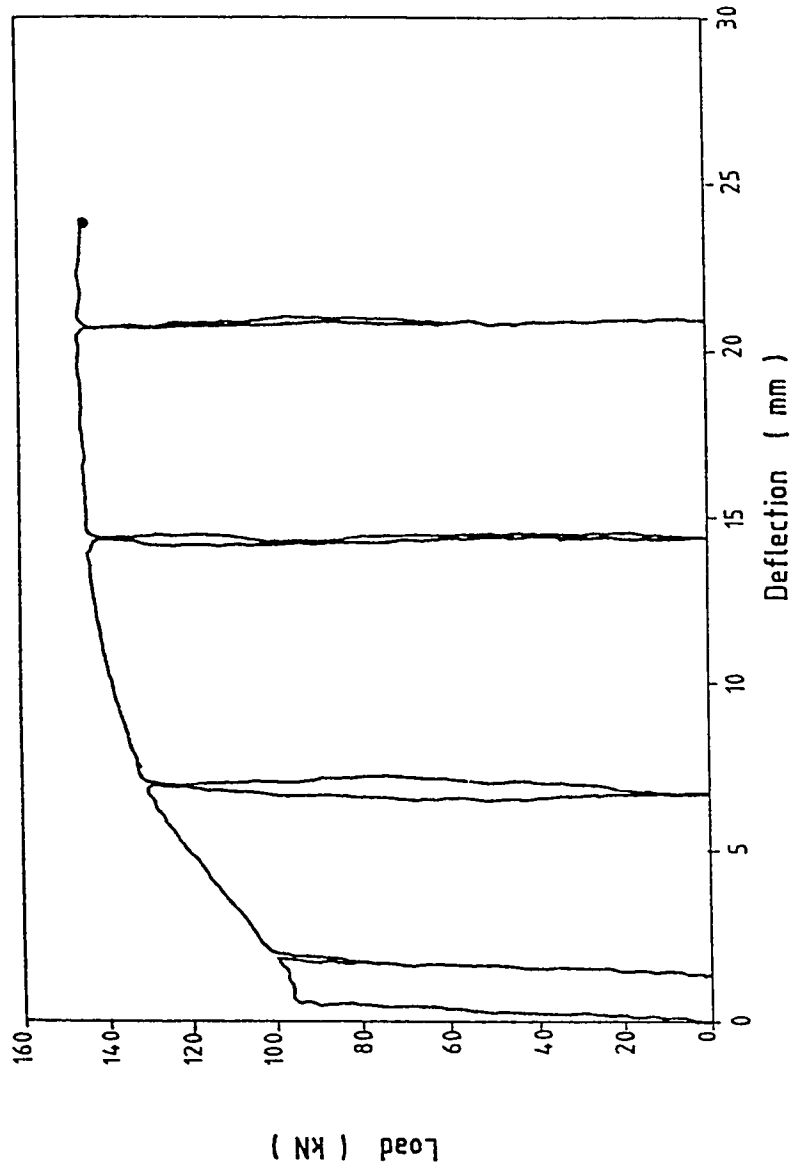


Figure 5.62 Experimental cyclic load-deflection curve of reinforcing steel sample T_2

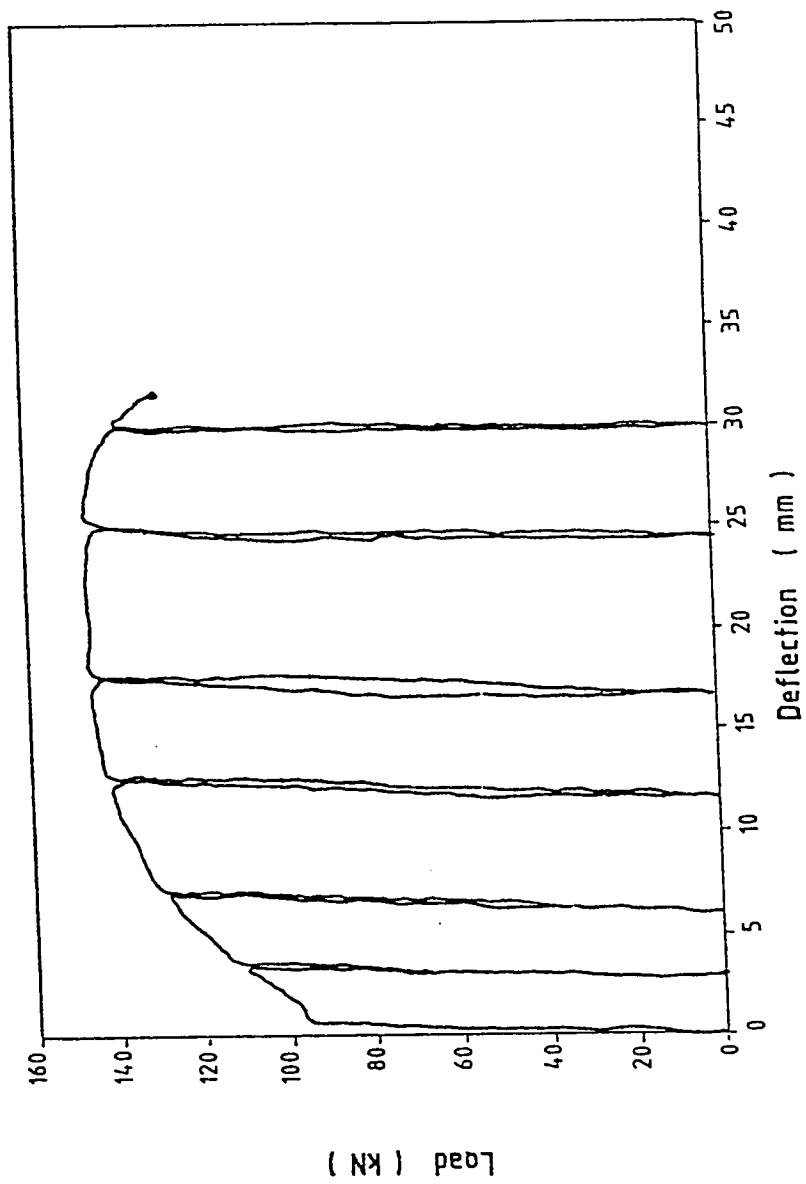


Figure 5.63 Experimental cyclic load-deflection curve of reinforcing steel sample T_3

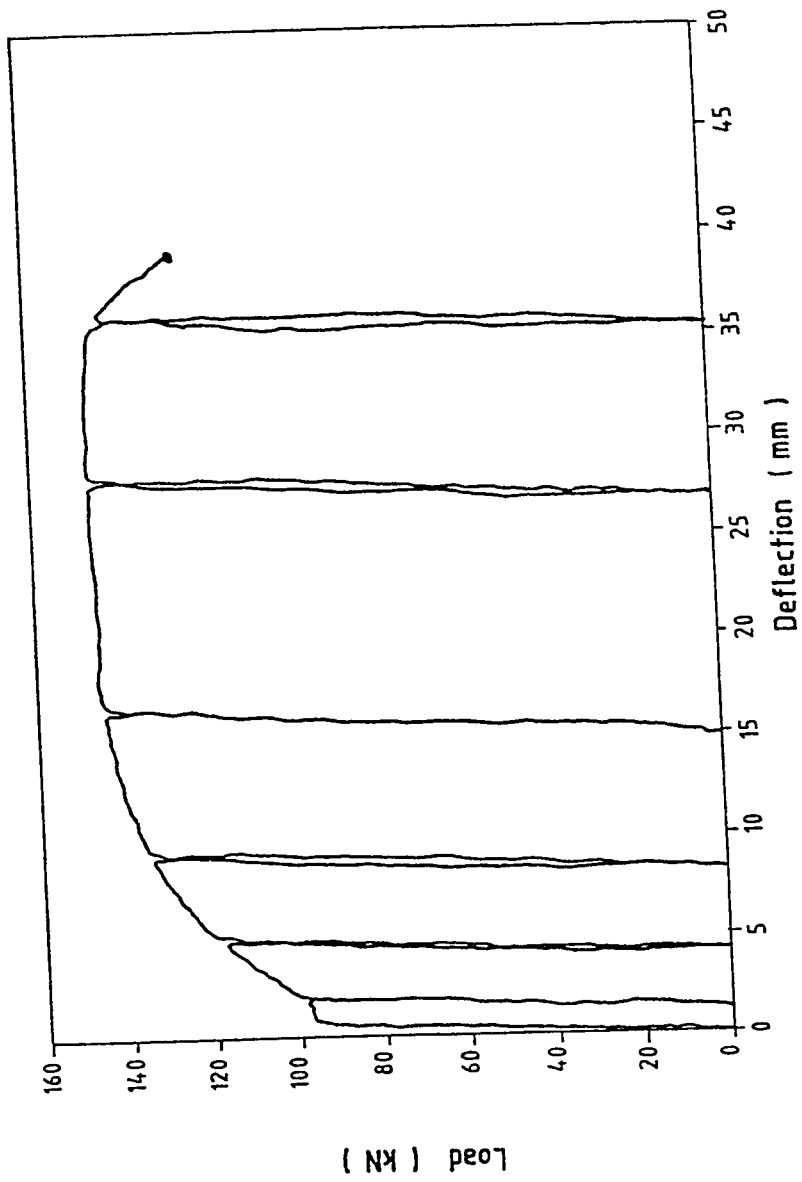


Figure 5.64 Experimental cyclic load-deflection curve of T₄

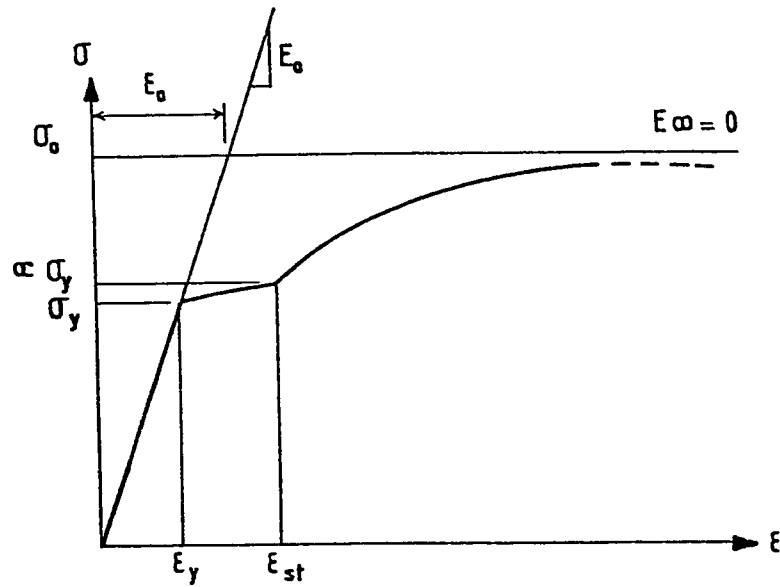


Figure 5.65 Parameters defining general stress-strain considered in the damage model for reinforcing steel

$$d_a = \begin{cases} 0 & \varepsilon \leq \varepsilon_y \\ 1 - \frac{\varepsilon_y}{\varepsilon} \left[1 + (\alpha - 1) \frac{\varepsilon - \varepsilon_y}{\varepsilon_{st} - \varepsilon_y} \right] & \varepsilon_y < \varepsilon \leq \varepsilon_{st} \\ 1 - \frac{1}{\left[1 + \left(\frac{\varepsilon}{\varepsilon_0} \right)^R \right]^R} & \varepsilon_{st} < \varepsilon \end{cases} \quad (5.118)$$

where ε_{st} is the strain corresponding to the upper yield stress at which strain hardening takes place which can be calculated from the relation

$$\varepsilon_{st} = \left[\left(\frac{\alpha}{\varepsilon_y} \right)^R - \left(\frac{1}{\varepsilon_0} \right)^R \right]^{1/R} \quad (5.119)$$

On the other hand, the elastic damage variable is given as

$$d_e = 0 \quad (5.120)$$

Applying the previous relations to the data provided by Kato and others (1990) for which the strength parameters of structural steels SS41 and SM50 are listed in Table 5.3, the total damage variable is calculated for $\alpha=1.0$ and drawn in Fig. 5.66. The trend is highly nonlinear and the steel of lower ultimate strength shows higher damage rate than the higher strength steel. However, the final values are eventually the same.

Table 5.3 Strength parameters of structural steel (after Kato et al., 1990).

Steel type	Thickness mm	Young's modulus MPa	Yield stress MPa	Peak stress MPa	Parameter R
Steel SS41	6-12	212 910	300.5	574.7	0.49
	19-25	211 600	269	550.9	0.498
Steel SM50	6-12	203 720	388.8	637.8	0.595
	19-25	213 620	388.6	590.0	0.600

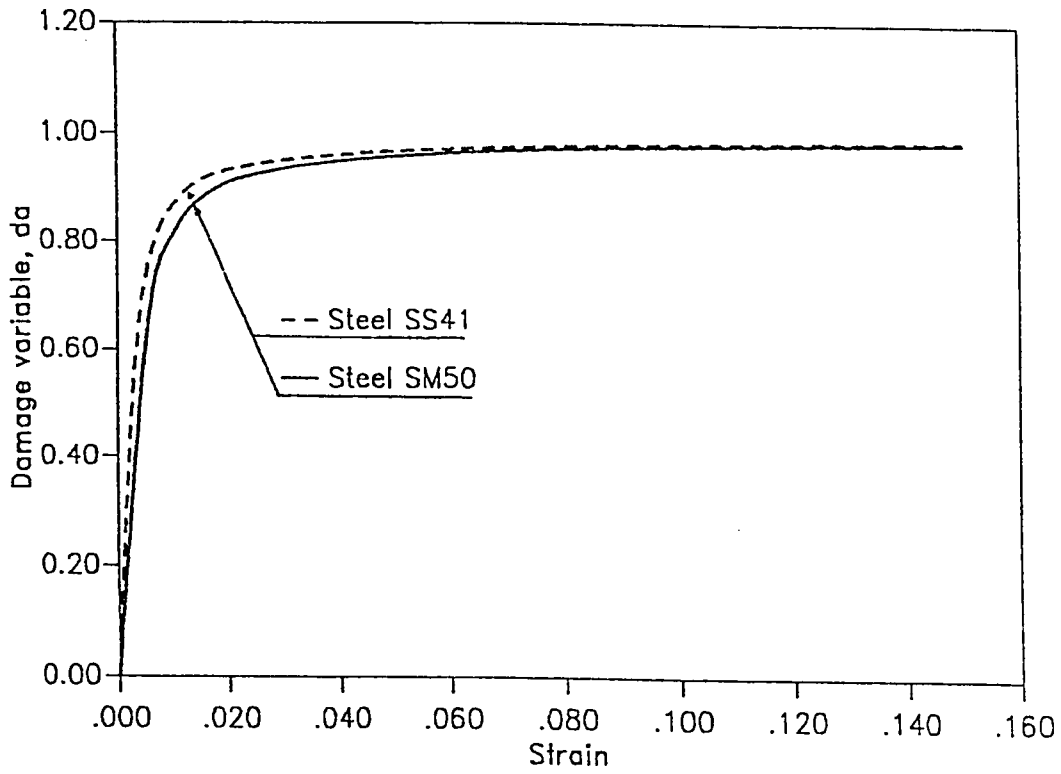


Figure 5.66 Total damage variable for structural steel SS41 and SM50

CHAPTER 6

CHAPTER 6**NUMERICAL IMPLEMENTATION****6.1 GENERAL**

The most general strain-damage coupling algorithm is used for the numerical implementation of the elastoplastic damage constitutive relations developed in this study. Considering time independent quasi-static loading, two FORTRAN 77 finite element programs are constructed. The first is DMGTRUSS for multi-dimensional trusses used to explore uniaxial behavior. The second is DMGPLSTS for plane stress formulation to investigate the applicability of the damage models derived in Chapter 5 for plain as well as reinforced concrete. Main features of both software packages besides with the basic structure, data flow and communication requirements are illustrated.

6.2 NONLINEAR FINITE ELEMENT

Nonlinear finite element proved its superiority over other numerical methods, e.g. boundary element and finite difference method. This is due to the fact that the concerned domain is fully analysed by updating changes caused by any source of nonlinearity in both the bulk and damaged zones. Nonlinear schemes reached a stabilized stage of development and its use is fairly reasonable. Inasmuch the procedures are systematic with respect to the incremental formulation of element

and overall equations, well-established nonlinear solution techniques, and convergence criteria, Appendices I, II and III provide general review of these topics in order. The latter will be frequently waved to through the next sections.

The two programs developed during the course of this study are coded in the FORTRAN 77 language and are tested against the available compilers on the IBM 370 and AMDAH, 580 machines by VM operating system. Minor changes are required to handle these programs on PC FORTRAN compilers, mainly in file communication.

6.3 COMPUTER PROGRAM "DMGTRUSS"

DMGTRUSS is a nonlinear finite element, FORTRAN 77 software package of multidimensional trusses; i.e. bar system (one-dimensional truss), plane truss (two-dimensional truss) and space truss (three-dimensional truss). It accounts mainly for material nonlinearity through the concepts of damage mechanics. The structural geometry is updated in the end of every load/displacement increment (if required). Thus, the geometric nonlinearity is not considered neither in the Lagrangian nor the Eulerian sense. A two noded truss element is used which is suitable for prismatic members. The package has the capability of analysing:

1. linear elastic materials;
2. hyperelastic materials;
3. elastic perfectly-plastic materials;

4. elastic hardening materials;
5. rigid perfectly-plastic materials;
6. rigid hardening materials; and
7. general nonlinear materials with and without stress discontinuity.

DMGTRUSS can handle materials following some of the well-known damage models. These models form a library which can be easily expanded. Description of the main features of DMGTRUSS are summarized hereafter.

6.3.1 General Material Nonlinearity

For each material, different behaviors in tension and compression can be separately described. The most general stress-strain curve for a given material can be subdivided into five zones (Fig. 6.1). Each zone is characterized by (Fig. 6.2):

1. *Initial strain*: the absolute value of the strain in the beginning of each zone, ϵ_{0i} (Fig. 6.2).
2. *Initial stress discontinuity*; three codes can be used to specify the initial stress discontinuity in each zone through ISTEP (Fig. 6.3),

ISTEP =	0	initial discontinuity is zero
	1	perfectly brittle material and stress drops to zero
	2	initial discontinuity has a prescribed value,

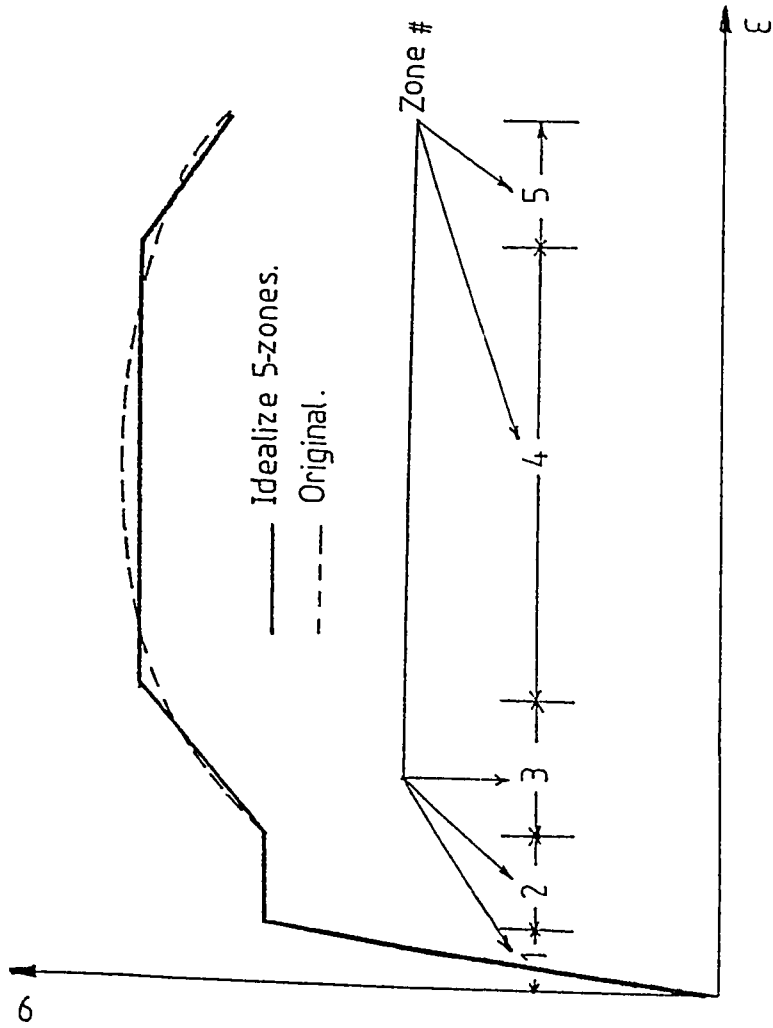


Figure 6.1 An example for a multiple zone stress-strain curve

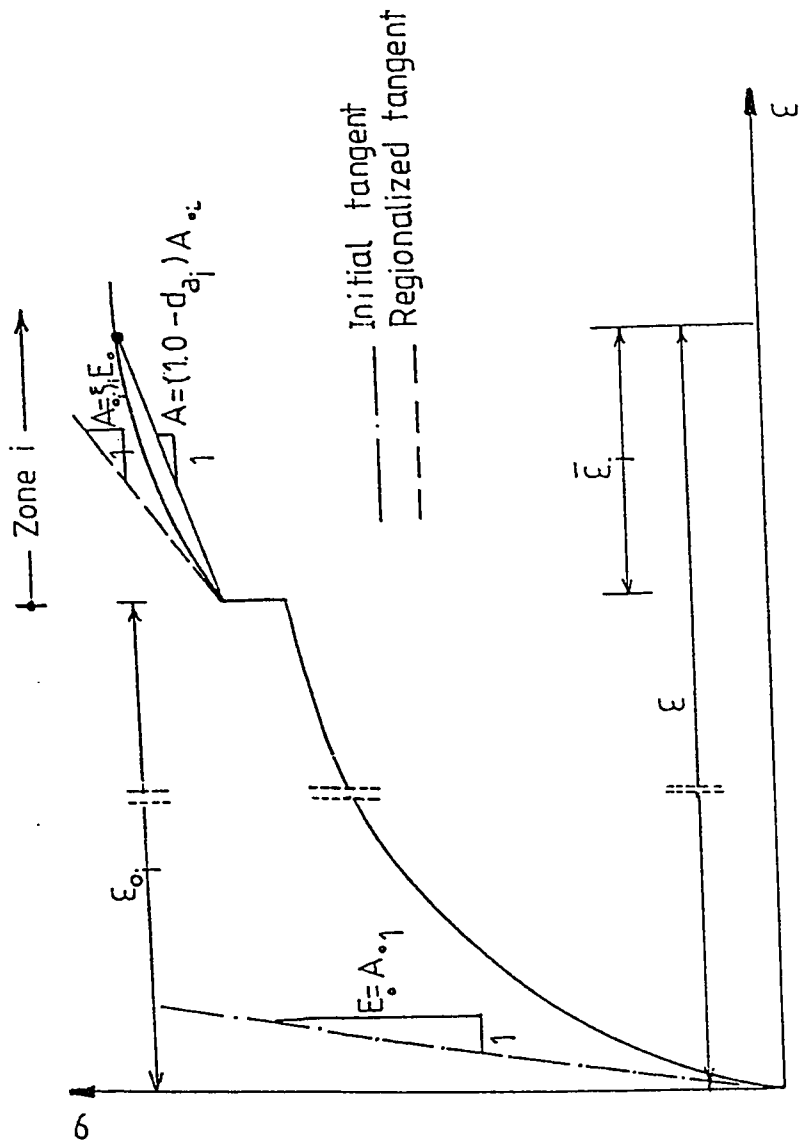


Figure 6.2 Regionalized parameters used in DMGTRUSS

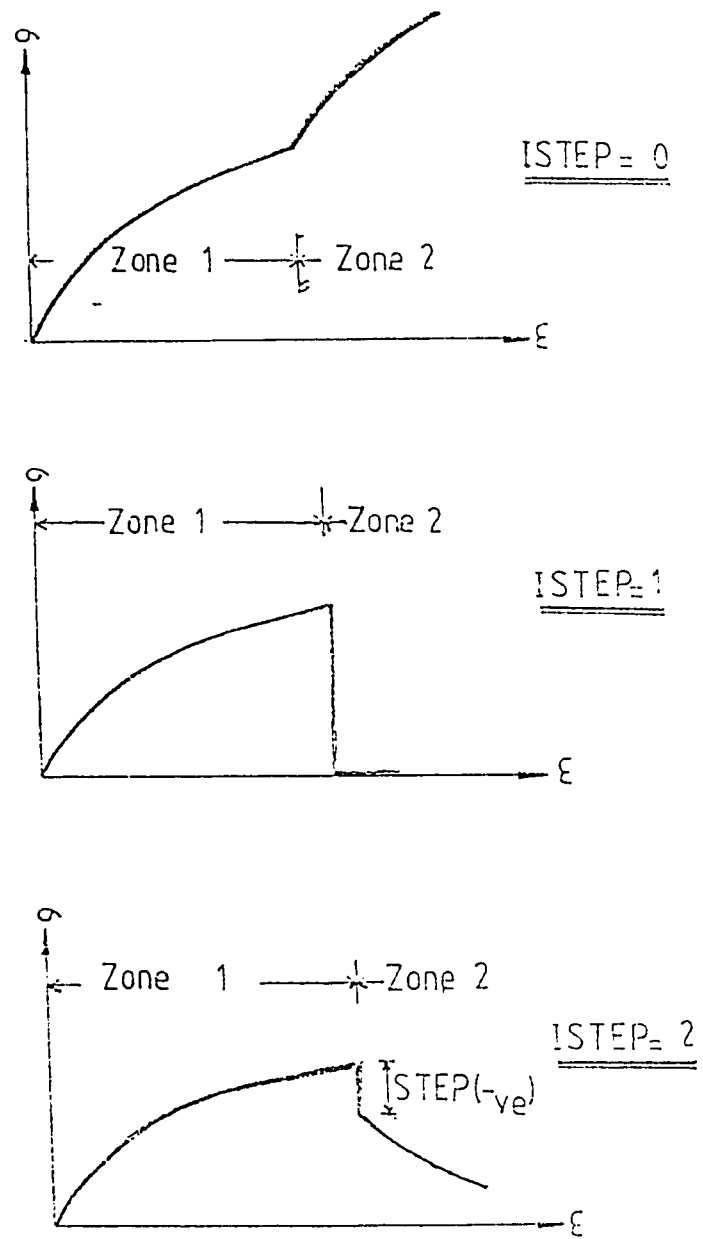


Figure 6.3 Stress discontinuity code ISTEP

$\delta\sigma_{o_i}$, that is called STEP in the program. Sign convention for the STEP value is illustrated in Fig. 6.4.

3. *Unloading path*: five unloading paths are considered in DMGTRUSS following the code KUNLC (Fig. 6.5),

- KUNLC = 0 elastic unloading (typical for hyperelastic materials)
- 1 ductile unloading
- 2 regionalized ductile unloading
- 3 brittle unloading
- 4 generalized damage unloading.

For KUNLC = 4, degradation of the initial modulus, E_o , is considered in a general polynomial form for materials originally elastic,

$$\sigma = E \epsilon,$$

$$E = E_o (1.0 - d_e) \quad (6.1)$$

$$d_e = \alpha_o + \alpha_1 \epsilon + \alpha_2 \epsilon^2, \quad \epsilon \geq \epsilon_{e_d} \quad (6.2)$$

where,

E the unloading modulus at any strain level,

E_o the initial modulus,

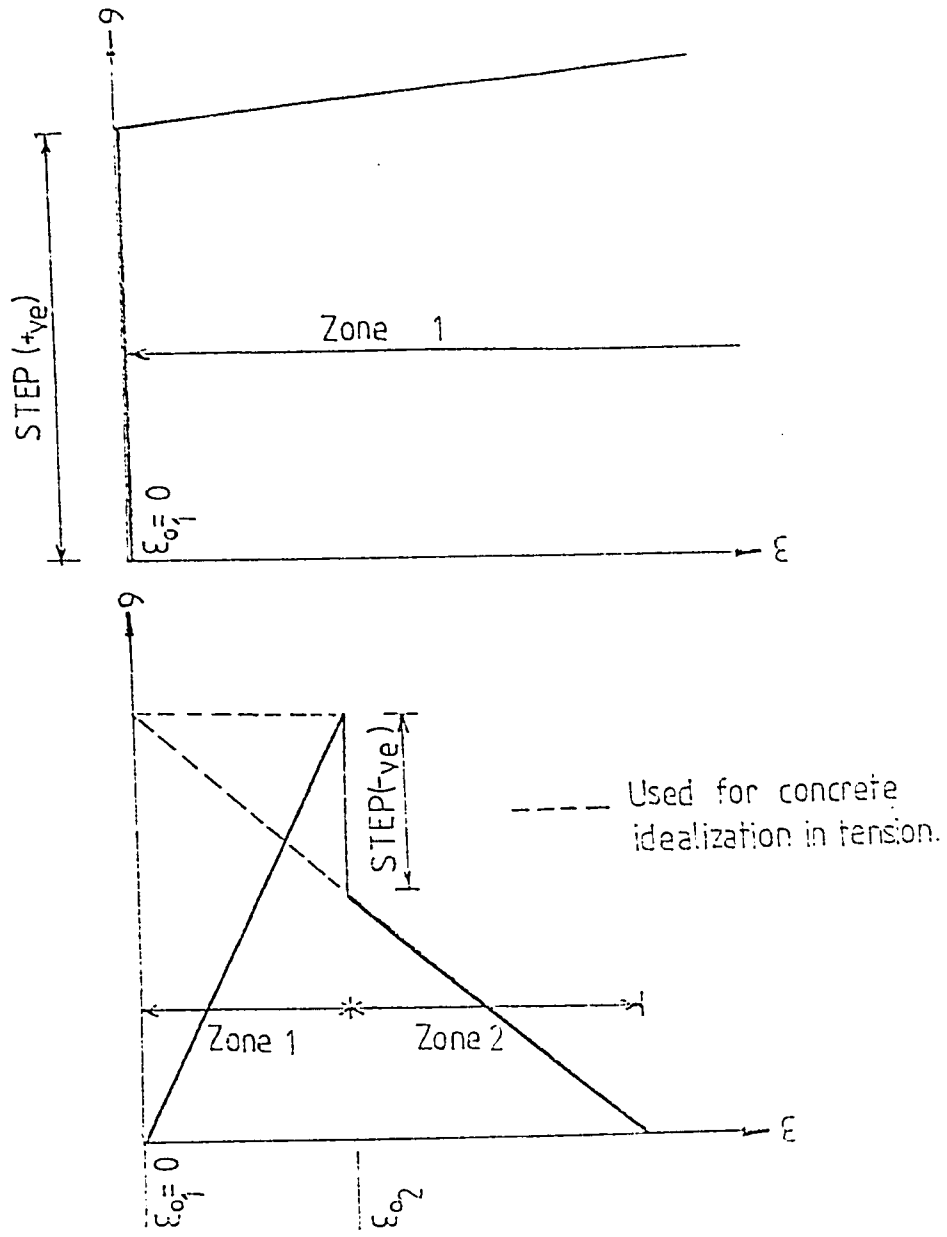


Figure 6.4 Sign convention for the stress discontinuity value STEP

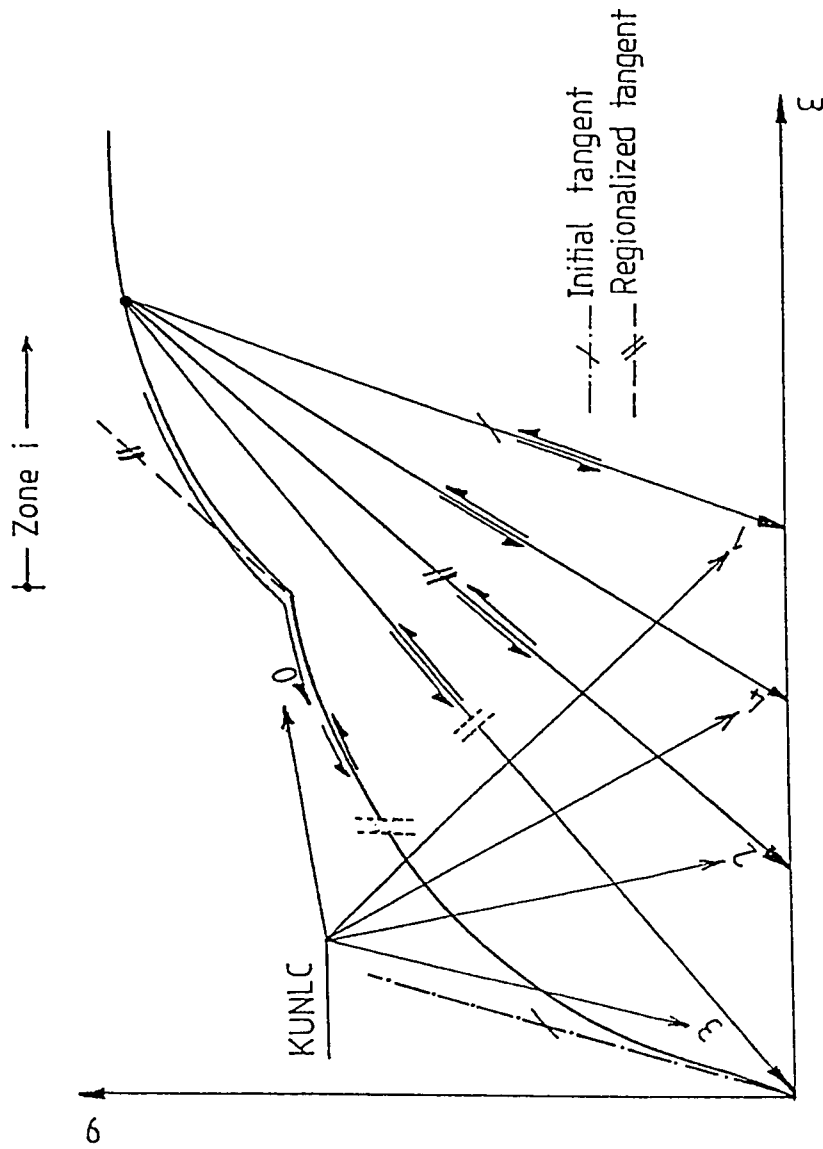


Figure 6.5 Various unloading paths allowed in DMGTRUSS

- d_e the damage variable associate with, E,
- α_i real coefficients generalized for the material response
in both tension and compression ($i=0,1,2$),
- ϵ the strain level,
- ϵ_{ed} the threshold damage strain.

4. the loading pattern:

The stress-strain relationship for each zone is considered within the context of damage theory as follows (Fig. 6.2),

$$\sigma = (1.0 - d_a) A_{o_i} \bar{\epsilon}_i \quad (6.3)$$

$$d_a = \beta_{0_i} \bar{\epsilon}_i + \beta_{1_i} \bar{\epsilon}_i^2 + \beta_{2_i} \bar{\epsilon}_i^3 \quad (6.4)$$

$$A_{o_i} = \xi_i E_o \quad (6.5)$$

where,

A_{o_i} the initial modulus of zone, i related to the initial tangent of the first zone E_o through the regional multiplier ξ_i ,

d_a the damage variable associate with regional secant modulus, A,

β_{ji} real regional coefficients described for each zone in tension and and compression, separately ($j=0,1,2$),

ξ_i initial tangent multiplier to provide the regional initial tangent modulus,

$\bar{\epsilon}_i$ the strain level with respect to each zone i , i.e.

$$\bar{\epsilon}_i = \epsilon - \epsilon_{0i}.$$

It is remarkable that the alluded loading scheme makes it possible to easily utilize a tremendous amount of idealized stress-strain relationships found in the literature. For example, linear, bilinear, trilinear, combination of multilinear and nonlinear, hardening and softening behaviors with or without stress discontinuity can be successfully employed as shown in Fig. 6.6.

6.3.2 Displacement Model

Two noded element is chosen. The element is straight, prismatic, and its geometry and displacement are culled to be linear, i.e. isoparametric element. Fig. 6.7 illustrates the considered uniaxial one dimensional element, of length L , orientation in both the local and the global systems of axes, and the nodal degrees of freedom. The local system is that for which the axis S coincides with the element's center of gravity and the nodal displacements in the local system d_1 and d_2 , by definition of a truss element, are in the S - direction. In this local

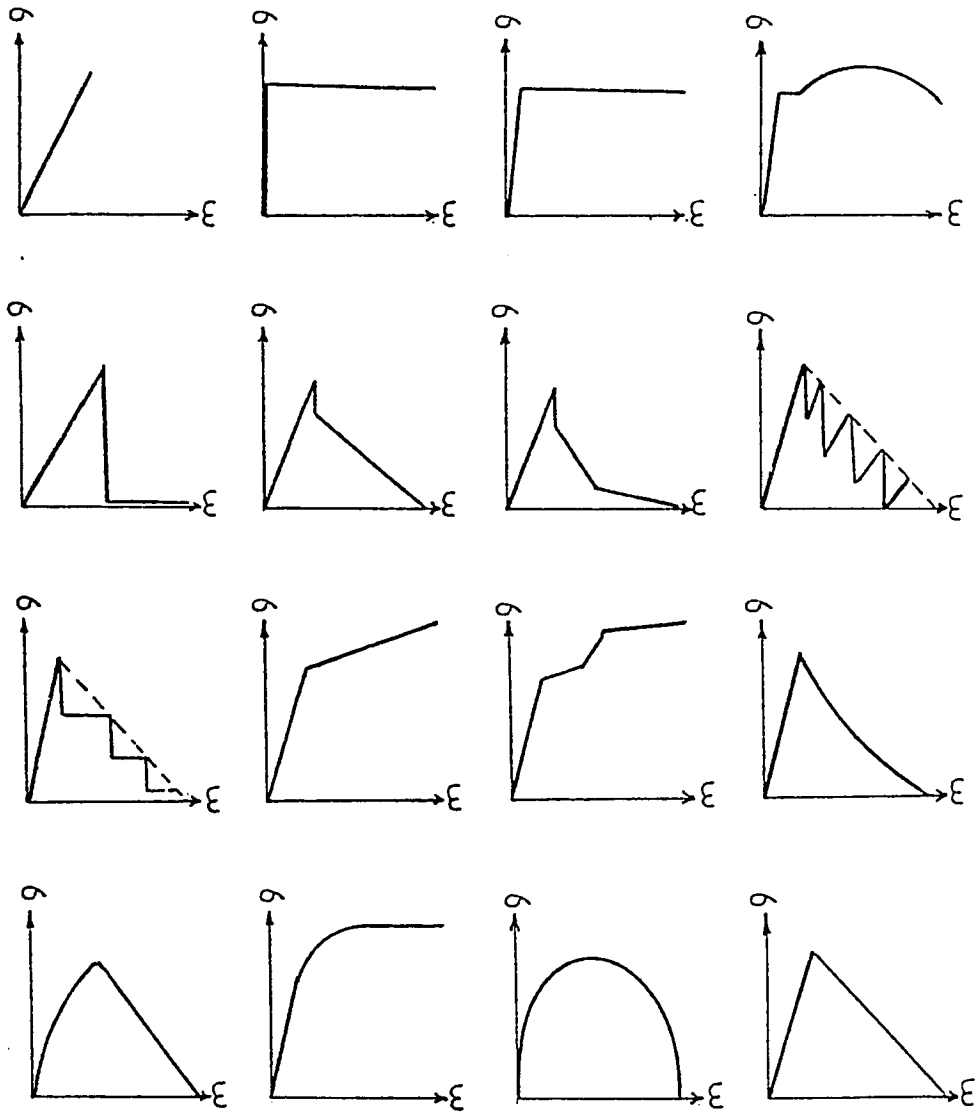


Figure 6.6 Different stress-strain curves which can be captured by DMGTRUSS

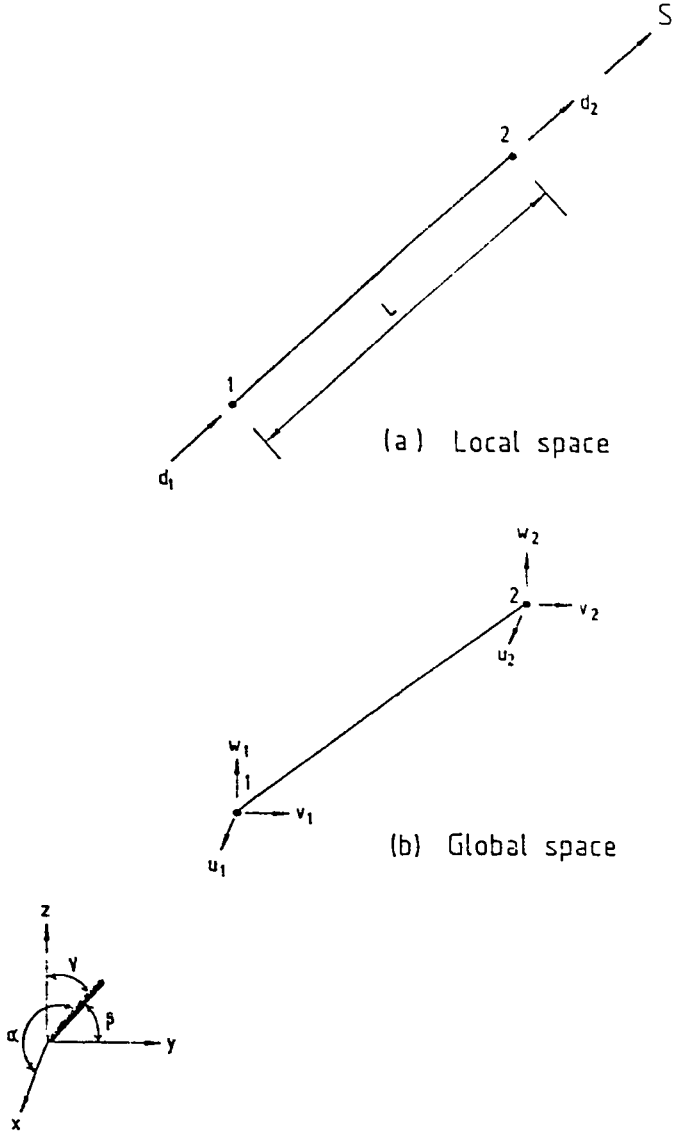


Figure 6.7 Prismatic two-noded truss element used in DMGTRUSS

system the displacement, d , at any distance s from the nodal point 1, is given by the following matrix equation:

$$\{d\} = [\bar{N}] \{\bar{d}\} , \quad (6.6)$$

$$[\bar{N}] = \begin{bmatrix} \bar{N}_1 & \bar{N}_2 \end{bmatrix} , \quad (6.7)$$

$$\bar{N}_1 = 1.0 - \frac{s}{L} , \quad (6.8)$$

$$\bar{N}_2 = \frac{s}{L} , \quad (6.8)$$

$$\{\bar{d}\} = \begin{bmatrix} d_1 & d_2 \end{bmatrix}^T \quad (6.9)$$

where,

$[\bar{N}]$ the interpolation matrix in the local system,

$\{\bar{d}\}$ the local nodal displacement vector,

\bar{N}_i the interpolation functions in the local system conjugate to the nodal point i , $i= 1, 2$.

The interpolation functions are, of course, generalized functions whose value is unity at the conjugate node and zero at all other nodes. In this case the interpolation functions and the natural coordinates are the same. The global system is the structural Euclidean system $X-Y-Z$ at which the nodal displacements are given by the global matrix $\{\bar{\varphi}\}$, where,

$$\{\bar{\varphi}\} = \begin{bmatrix} u_1 & v_1 & w_1 & u_2 & v_2 & w_2 \end{bmatrix}^T \quad (6.10)$$

in which u_i, v_i and $w_i, (i=1,2)$ are the nodal displacements in the X, Y and Z- directions, respectively. The relationship between the two (local and global) systems of axes is

$$\{S\} = \begin{bmatrix} C_x & C_y & C_z \end{bmatrix} \begin{Bmatrix} X \\ Y \\ Z \end{Bmatrix} \quad (6.11)$$

in which C_x, C_y and C_z are the direction cosines of the S axis with respect to the global system. In the same manner the nodal displacements in both systems are related by

$$\{\bar{d}\} = [T] \{\bar{\varphi}\} \quad (6.12)$$

in which $[T]$ is a transformation matrix given by

$$[T] = \begin{bmatrix} C_x & C_y & C_z & 0 & 0 & 0 \\ 0 & 0 & 0 & C_x & C_y & C_z \end{bmatrix} \quad (6.13)$$

Substituting Eqn. (6.12) in (6.13) yields

$$\{d\} = [N] \{\bar{\varphi}\} , \quad (6.14)$$

$$[N] = [\bar{N}] [T] \quad (6.15)$$

where $[N]$ is the interpolation matrix in the global system of axes.

6.3.3 Strain-Displacement Relationship

The infinitesimal strain, $\{\epsilon\}$, for the chosen element is constant along the length and can be expressed as

$$\{\epsilon\} = \left\{ \frac{\partial d}{\partial S} \right\} \quad (6.16)$$

Substituting Eqn. (6.13) into (6.14), yields

$$\{\epsilon\} = [B] \{\bar{q}\} \quad (6.17)$$

in which $[B]$ is the strain displacement matrix which may be easily proved to be equal to

$$\begin{aligned} [B] &= \left[\frac{\partial N}{\partial S} \right] [T] \\ &= \left[\begin{array}{cc} -\frac{1}{L} & \frac{1}{L} \end{array} \right] \left[\begin{array}{cccccc} C_x & C_y & C_z & 0 & 0 & 0 \\ 0 & 0 & 0 & C_x & C_y & C_z \end{array} \right] \\ &= \frac{1}{L} \left[\begin{array}{cccccc} -C_x & -C_y & -C_z & C_x & C_y & C_z \end{array} \right] \quad (6.18) \end{aligned}$$

The $[B]$ is constant and consequently the incremental strain-nodal displacement is

$$\{d\epsilon\} = [B] \{d\bar{q}\} \quad (6.19)$$

where,

$\{d\epsilon\}$ the incremental strain vector,

$\{d\bar{q}\}$ the incremental nodal displacement.

6.3.4 Tangential Modulus

The stress-strain relation in an incremental form can be expressed as

$$\{d\sigma\} = [C_t] \{d\varepsilon\} \quad (6.20)$$

where,

$\{d\sigma\}$ the incremental stress vector,

$[C_t]$ the tangential modulus matrix.

The tangential modulus matrix depends on the stress path, i.e. loading unloading and reloading paths. With reference to the proposed canonical uniaxial model, $[C_t]$ can be easily derived as follows

1. *for loading*: $[C_t]$ can be obtained by differentiating Eqn. (6.3)

with respect to $\{\varepsilon\}$ and utilizing the relation $\bar{\varepsilon}_i = \varepsilon - \varepsilon_{0i}$, i. e.

$\partial/\partial\varepsilon = \partial/\partial\bar{\varepsilon}_i$, the following equation is arrived at

$$\begin{aligned} [C_t] &= \frac{\{\partial\sigma\}}{\{\partial\varepsilon\}} \\ &= \left[(1.0 - d_a) A_0 - A_0 \bar{\varepsilon}_i \frac{\partial d_a}{\partial \bar{\varepsilon}_i} \right] \end{aligned} \quad (6.21)$$

2. *for unloading/reloading*: In DMGTRUSS, several unloading paths are allowed. For elastic unloading/reloading, the tangential modulus is the same as for loading equal to E_0 . For generalized

damage unloading path given by Eqn. (6.1), $[C_t]$ can be obtained in a similar way to that of Eqn. (6.21) by differentiation of Eqn. (6.1) with respect to $\{\epsilon\} = \{\epsilon_e\}$, which leads to

$$\begin{aligned} [C_t] &= \frac{\{\partial\sigma\}}{\{\partial\epsilon\}} \\ &= E_0 (1.0 - d_e) \end{aligned} \quad (6.22)$$

For other unloading reloading paths, $[C_t]$ is given by the path slope which can be easily obtained since the other paths are straight lines. In DMGTRUSS the maximum ever reached strain is stored in the memory.

6.3.5 Tangential Stiffness

The tangential element stiffness matrix is evaluated according to the relation derived in Appendix I as

$$[K_t] = \int_V [B]^T [C_t] [B] dV \quad (6.23)$$

Since the element is prismatic and both the strain-displacement matrix and the tangential stress-strain in the current local approach are independent of the position, then Eqn. (6.23) reduces to

$$[K_t] = A L [B]^T [C_t] [B] \quad (6.24)$$

where,

$|K_t|$ the tangential stiffness matrix.

A the cross sectional area of the element.

6.3.6 Residual Forces

In DMGTRUSS, the idea in calculating the element's stress is completely different from that of elastoplastic behavior which was described by Owen and Hinton (1980). As a matter of fact, there are two main differences from the elastoplastic procedures. The first comes from coupling the strain-damage scheme utilized in DMGTRUSS. That is after the strain increment is obtained from displacements determined by solving the structural incremental system of equations, the damage parameter is updated either through a specified damage model in the program library or through the generalized loading scheme. At this stage, the stress-strain is mathematically known and there is no need to try incrementally finding the element's stress. The latter algorithm is straight forward (which represents the second main difference) and as usual for carrying out this operation two loading cases are detected in DMGTRUSS and are clearly distinguished:

1. The element's stress level at the current increment experiences nonlinear behavior whether in tension or compression. This occurs in either of two situations: (a) reloading or loading on the nonlinear loading path or (b) unloading with sign reversal. Coding is identified by the flag $KUNLE = 0$ (Fig. 6.8). For demonstration purposes, a positive/negative zero is shown in this

figure. The positive zero indicates tensile loading captured by DMGTRUSS by the matrix LNCOD (IELEM, ISTRE) = 1 , both arguments are described in the variables glossary (Appendix IV). On the other hand the negative zero points out loading in the compression side stored by LNCOD (IELEM, ISTRE) = 2. Afterwards, a SEARCH-FIND scheme is established for multiple zone stress-strain relationships. The total strain is updated and searching process is executed till the proper zone is found, then the element's stress is calculated.

2. The element's stress level at the current increment is on the linear unloading/reloading path and the coding flag KUNLE = 1 is raised (Fig. 6.8).

6.3.7 DMGTRUSS Structure

Program DMGTRUSS consists of seven main modules as shown in Fig. 6.9:

1. Data input and initialization module: calling two subroutines DATA and INITAL.
2. Stiffness matrix and load vector module: this module formulate the structural system of equations by communications with MODTT, BMATT, INCDAT, STIFT and ASSEMB. Subroutine INCDAT calls subroutine TEMP.
3. Solution module: for equation solution through subroutines

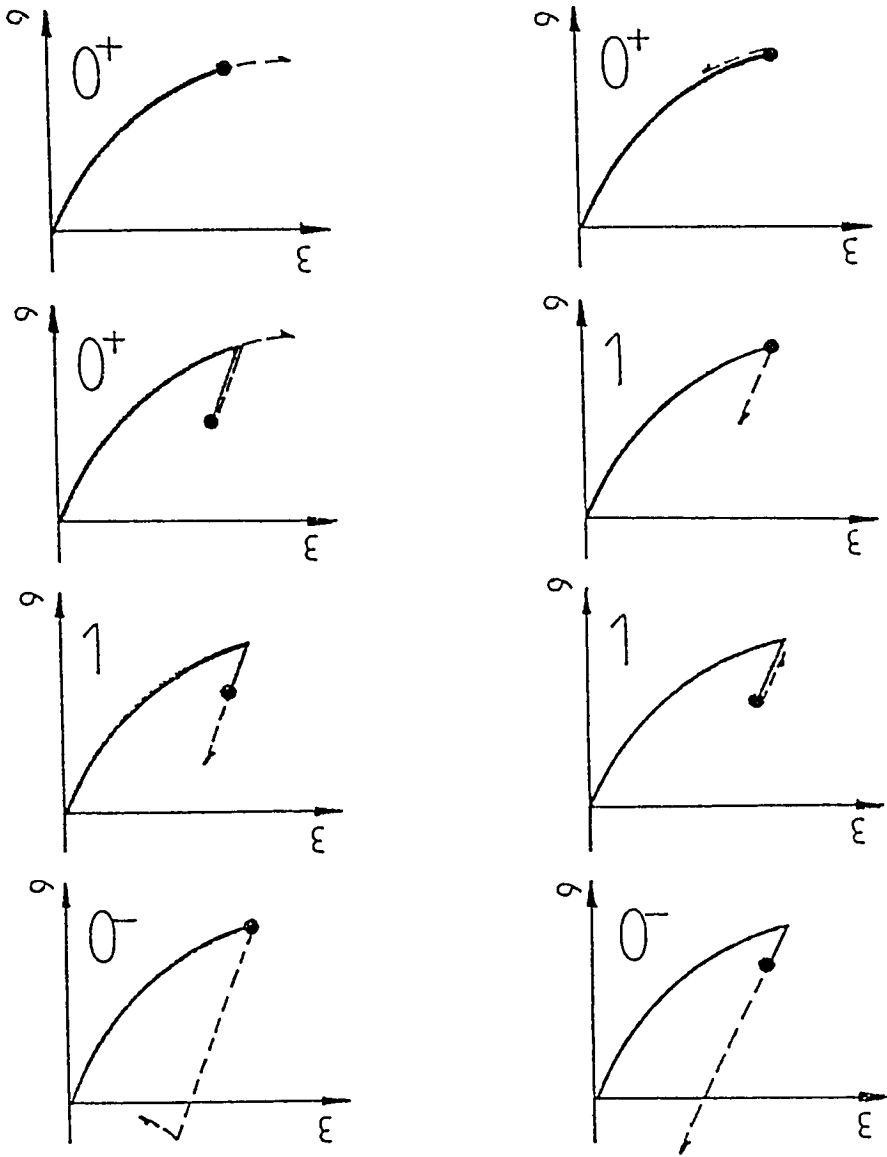


Figure 6.8 Possible loading, unloading and reloading paths

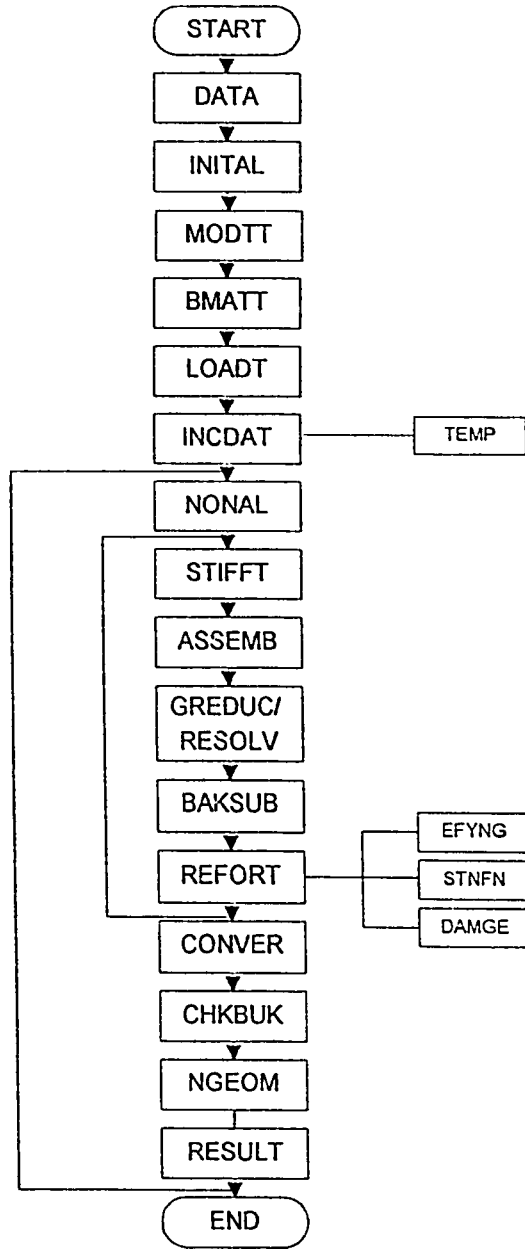


Figure 6.9 Main calls in program DMGTRUSS

GREduc, BAKSUB, and/or RESOLV.

4. Residual force and convergence module: in this module elements' stresses are computed by calling REFORT which gets assistance from Subroutines STNFN, EQYNG and DAMGE. Residual forces are calculated and convergence is monitored through subroutine CONUND.

6. Instability module: this module communicate with subroutine CHKBUK to check occurrence of instability in compression members.

6. Geometric nonlinearity module: updating the structure geometry in subroutine NGEOM.

7. Output module: output the information obtained for all nodes and members in subroutine RESULT.

Depiction of the master program and the appended subroutines requires familiarity with the variable and arrays used in the program. A glossary of variables and arrays utilized in DMGTRUSS is provided in Appendix IV.

6.3.8 DMGTRUSS Master Program and Subroutines

DMGTRUSS includes, besides the master program, 22 subroutines. The main segment controls the calling of the (18) major subroutines and is described by the Nasi-Schneiderman (N. S.) chart shown in Fig. 6.10. The function of every subroutine is given downwards.

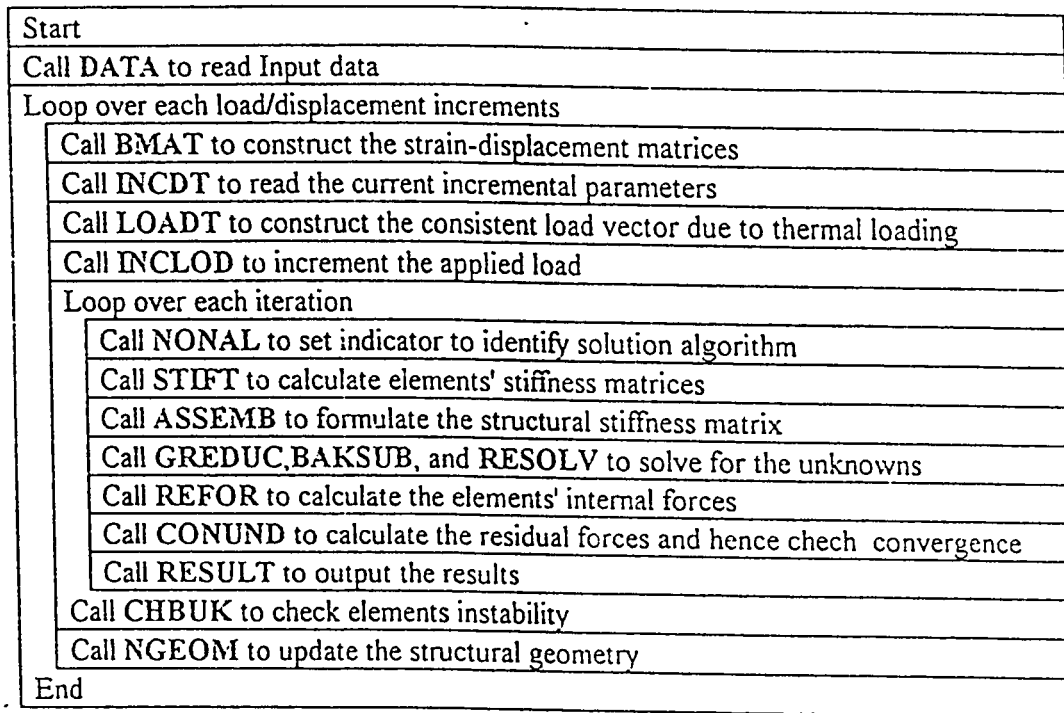


Figure 6.10 Nassi-Schneidermann chart for main calls from master DMGTRUSS

SUBROUTINE

FUNCTION

- ASSEMB* Assemble elements' stiffness matrix, ESTIF into the structural stiffness matrix, ASTIF.
- BAKSUB* Back substitution stage in Gauss elimination solution technique.
- BMATT Formulate the elements' strain-displacement matrix, BMATX and elements' length
- CHKBUK Check occurrence of buckling in compression members using Euler formula.
- CONUND* Construct the residual forces array and monitor convergence.
- DAMGE Subroutine include damage models library in which the damage parameter for loading and unloading are calculated. For some models the element's stress is calculated. Details are given ahead.
- DATA Read and write input data. Data communication are discussed forward.
- EFYNG Determine the effective linear unloading/reloading modulus, EQYNG.

* Subroutine given by Owen and Hinton, 1980.

GREduc* Gaussian reduction of the structural system of equations.

INCDAT Read and write input data for incrementations and the involved iteration.

INCLOD* Update the elements' loading arrays, ELOAD and TLOAD.

INITAL* Initialize some variables and arrays.

LOADT Construct the equivalent consistent load vector due to thermal changes.

MODTT Initialize the elements' tangential modulus matrix to initial modulus.

NGEOMT Update the structure geometry by adding the nodal displacements to the cartesian coordinates of nodal points.

NONAL* Set indicator, KRESL, to identify type of solution algorithm through NALGO.

REFORT Calculate the elements' internal forces. An illustration is made in Fig. 6.11.

RESULT Output the program results. An output file layout is shown in Data communication.

RESOLV* Resolving Gaussian reduction routine for Modified

Rewind tapes 2 and 3
Initialize element's internal loads vector, ELOAD
Loop over all elements
Find the element's material I.D. number
Read BMATX
Store element's nodal displacements from XDISP into ELDIS
Loop over stress components
Define variables KUNLE, STRAN, STNCU, DA, DT, KGASH
Calculate element's axial strain
Correct strain for thermal effects
Determine the initial load condition
Update the total strain
Call EFYNG to find the unloading modulus, EQYNG
Check for nonlinear elastic unloading
Check for sign reversal
Calculate element stresses for nonlinear unloading/reloading
Call DAMGE if a specific damage model is used
Calculate stresses for loading in case of multiple-zone stress-strain relationships by SEARCH-FIND technique
Correct total load matrix TLOAD for temperature effects in form of change in tangent modulus
Update DMATX on tape 2
Compute element's stress resultant.

Figure 6.11 Nassi-Schneidermann chart for main calls from subroutine REFORT

Newton-Raphson solution techniques.

- STIFT Construct the stiffness matrix of element by element, ESTIF, and store it in Tape 1.
- STNFN Evaluate the tangent modulus coefficient DIVFN.
- TEMP Calculate the elastic modulus degradation due to thermal effects.

6.3.9 Damage Models Library

DMGTRUSS damage library includes eight models among which are the canonical elasto-plastic damage model for both concrete and steel. Different combination of models can be used for the same material by using $IDMGS = 2$. If $IDMGS = 1$ is used, the same damage model is assumed to be valid for the material in both tension and compression. The model number is input in Subroutine DATA and goes directly to PROPS (NMATS, NPROPS, NSTRE). In case that $NPROS = 3$, the input integer indicates the damage model in tension whereas for $NPROS = 4$, indicates the model in compression. Depending on the stress status, the value of LNCOD (NELEM) changes. The model number corresponding to the current LNCOD (NELEM) is named under the index IDMGE. The models library are as follows:

IDMGE Damage model

- 1 Linear elastic-Perfectly brittle scalar model (Lemaitre, 1985).
- 2 Hognstad parabola by Krajcinovic and Silva (1982) scalar statistical damage model for brittle materials
- 3 Mazars' scalar model (1984) for concrete.
- 4 Loland's scalar model (1981) for concrete.
- 5 Isotropic ductile scalar model (Lemaitre, 1985).
- 6 Krajcinovic and Fanella (1981) directed damage model for brittle materials.
- 7 Canonical uniaxial model for concrete in both tension and compression.
- 8 Canonical uniaxial model for steel.

The relevant damage parameter for each model is input in the array PROPD (NMATS, NLDCN, NPROD, NSTRE). The damage parameters for each model and its storage according to the value of NPROD are illustrated in Appendix V. Evaluation of the damage parameter in the threshold-critical range assigned by each model is carried out in Subroutine DAMGE. The provided library can be easily extended to include other damage models.

6.3.10 Load Reversal and Hysteresis Loop

Although the cyclic behavior of materials is assumed linear (canonical model and also in the general nonlinear material), the hysteresis loop is captured on the average when load reversal is allowed. In order to provide such a characteristic for materials exhibiting permanent deformations, the origin of the stress-strain curve should be flexible to change position on load reversal. Fig. 6.12 illustrates a typical load reversal (compression to tension of concrete then tension to compression) for which the hysteresis loop is formed. A study of this phenomenon is carried out through DMGTRUSS in Chapter 6 for reinforced concrete.

6.3.11 Data Communication

Because of the uniaxial nature of the considered element, the variables are considerably few and no pre- or post-processing is considered. Communication is meant by the preparation input and output data files. All read statements are free formatted to facilitate data accessibility. User instructions for Program DMGTRUSS are set forth in APPENDIX V. In addition, a sample input file for DMGTRUSS is given as an example.

6.3.12 Thermal Loading and Thermal Degradation

The consistent nodal forces due to thermal loading depend on the tangential modulus as shown in Appendix I. As the material stiffness is

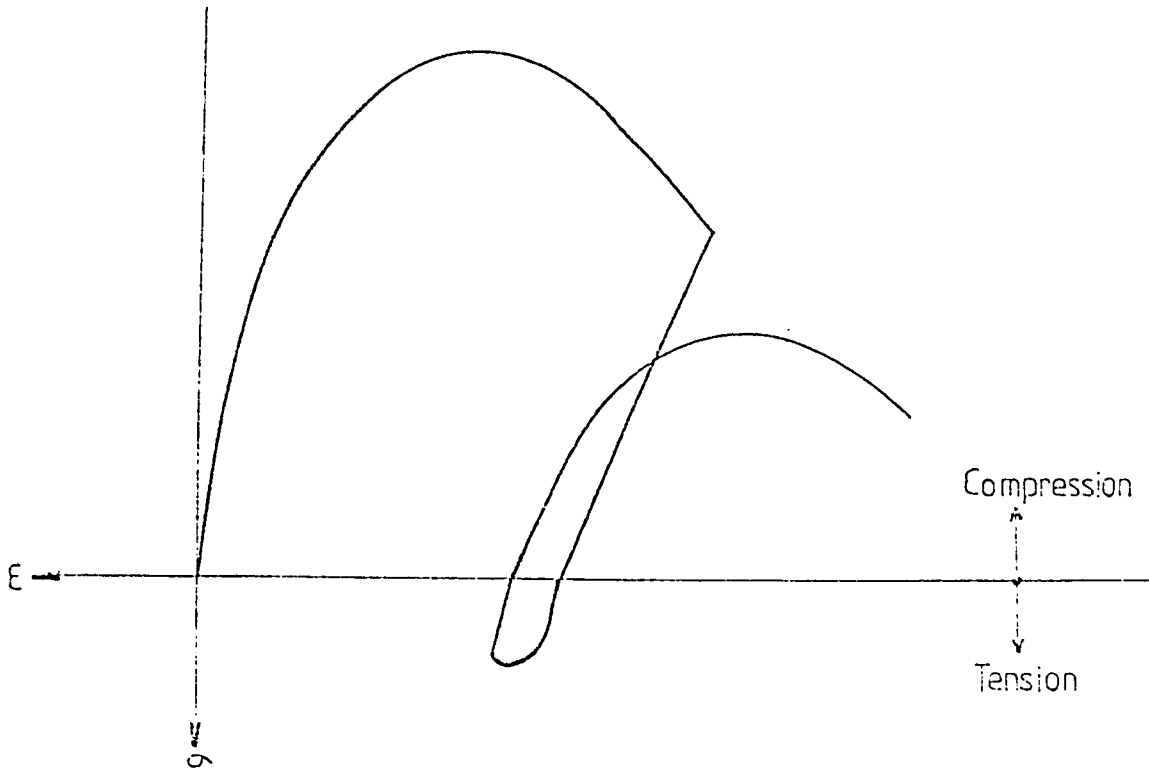


Figure 6.12 Typical stress-strain curve exhibiting unloading with sign reversal in DMGTRUSS

altered throughout the damage process, the equivalent nodal forces change as well. Despite neglecting this effect which tends to reduce the thermal forces, it should be taken into account. This requires updating the loading arrays in each iteration for elements exhibiting thermal changes. The latter task is carried out in Subroutine REFORT. The mission is carried out by recalculating the additional loads induced by the difference in stiffness.

Since the thermally induced loads are sensitive to the material stiffness, abrupt changes in load application conditions (e.g. from loading to unloading and vice versa) are advised to be incremented gradually to avoid increased execution time. Application of thermal loading solely is achieved by LDCSE = 2 while for combined thermal and applied nodal forces by LDCSE = 3.

Initial strains and shrinkage strains can be treated in a similar way as for temperature loading. A fictitious thermal change for an assumed value of the coefficient of thermal expansion has to be adopted.

Nonlinear material degradation due to temperature rise is taken into account in Subroutine TEMP. Calculations are executed at the start of the load/displacement increment. A damage law is used in the same form as that given in Eqn. (6.1) but with an understanding that E_0 is now the current value of the elastic modulus stored in YOUNG (NELEM).

6.3.13 DMGTRUSS Extendability to Other Applications

DMGTRUSS, as elucidated earlier, is constructed in a modular form. This facilitates the extension of the package to the following further applications:

1. Fatigue problems by adopting a subroutine taking into account the degradation (damage) due to either low or high cycle fatigue. A jump in cycles can be easily included (Lemaitre, 1992).
2. Creep and visco-plasticity applications by appending time-step algorithms with other necessary modifications (Owen and Hinton, 1980).
3. Creep-fatigue interaction by proper combination of the alluded two applications (Chaboche, 1977).
4. Dynamic problems to find the natural frequency and steady state analysis of forced/damped vibrations (Mario Baz, 1980).
5. An enhancement of instability analysis by expanding the CHKBUK subroutine.
6. Effect of rigid truss joints (Ghali, 1984).
7. A Geometric second order nonlinearity after the Lagrangian or Eulerian formulation (Owen and Hinton, 1980).
8. Analysis of axisymmetric membrane element for thin disks (Owen and Hinton, 1980).

6.4 COMPUTER PROGRAM "DMGPLSTS"

DMGPLSTS is a nonlinear finite element, FORTRAN 77 software package for analysing two-dimensional plane stress problems. The canonical damage model is employed to describe the material nonlinearity. Infinitesimal strain theory is used. Several elements are allowed to provide flexibility of modelling concrete and steel components. In the case of concrete continuum elements are used while for steel boom elements are developed. Interestingly, thickness of continuum elements may be reduced to the extent that interface elements or sheath elements may be reproduced. The finite element formulation as well as description of the main features of DMGPLSTS are summarized hereafter.

6.4.1 Finite element Formulation for Concrete

6.4.1.1 Proportionality of Loading

Inasmuch as the characteristic equations of the canonical model are expressed, for concrete, in the principal space in both incremental and total forms, a considerable reduction in the execution time may be afforded if two separate subroutines are developed for each case correspondingly. The first case represents nonproportional loading for which the principal axes are rotating and the biaxiality ratio is varying during the progress of loading. The biaxiality ratio is determined based on

data from previous iteration of the current load increment. Incremental equations should be employed in such situations. The other situation takes place for proportional loading for which the directions of the principal axes are fixed for conditions not associated with unloading with sign reversal. In this case adopting secant algorithms utilizing the total form equations is allowed.

In comparison with other nonlinear schemes, the present algorithm is much more sophisticated since softening and stiffness degradation are presented and the various stress paths are accounted for. In elastoplasticity, the unloading and reloading are regarded the same and their condition are distinguished from loading using scalar function which represents the yield surface in associative models. In other certain nonlinear elastic models, cases of loading and unloading/reloading are judged through the increase or decrease of the first and/or second stress invariants. In contrast, nonlinearity is thoroughly investigated through loading, reloading and unloading in a more realistic approach.

6.4.1.2 Displacement Model

The program gives the flexibility to use four-noded quadrilaterals, 6-noded elements, 8-noded Serendipity elements and 9-noded Lagrangian elements. Isoparametric formulation is employed since both the geometry and displacements are expressed by the same shape functions.

$$\{\bar{\varphi}\} = [N] \{\varphi\} , \quad (6.25)$$

$$\{\varphi\} = \begin{Bmatrix} u \\ v \end{Bmatrix} \quad (6.26)$$

$$[N] = \begin{bmatrix} N_1 & 0 & N_2 & 0 & \dots & N_n & 0 \\ 0 & N_1 & 0 & N_2 & \dots & 0 & N_n \end{bmatrix} \quad (6.27)$$

$$\{\bar{\varphi}\} = \left[u_1 \quad v_1 \quad u_2 \quad v_2 \quad \dots \quad u_n \quad v_n \right]^T \quad (6.28)$$

where,

$[N]$ the interpolation matrix,

$\{\varphi\}$ the displacement vector,

$\{\bar{\varphi}\}$ the nodal displacement vector,

u the displacement of any point inside the element in the X-axis direction whose nodal values are u_i , $i= 1, n$,

v the displacement of any point inside the element in the Y-axis direction whose nodal values are u_i , $i= 1, n$,

N_i the interpolation function corresponding to the node i , $i= 1, n$.

The interpolation functions are usually expressed in terms of the natural coordinates ξ and η to facilitate numerical integration and their

forms for each node of the selected elements are listed in Table 6.1. For the isoparametric representation, the coordinates of any general point inside the element can be interpolated using the same shape functions and consequently,

$$\begin{Bmatrix} X \\ Y \end{Bmatrix} = \begin{bmatrix} N_1 & 0 & N_2 & 0 & \dots & N_n & 0 \\ 0 & N_1 & 0 & N_2 & \dots & 0 & N_n \end{bmatrix} \begin{Bmatrix} X_1 \\ Y_1 \\ X_2 \\ Y_2 \\ \cdot \\ \cdot \\ \cdot \\ X_n \\ Y_n \end{Bmatrix} \quad (6.29)$$


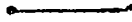






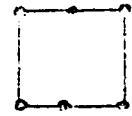


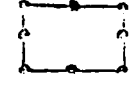

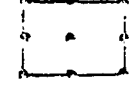
in which X_i and Y_i are the coordinates of the i th node, $(i=1,n)$.

6.4.1.3 Strain-Displacement Relationship

The infinitesimal strain vector, $\{\epsilon\}$, for two dimensional elements can be expressed in the X-Y space as,

$$\{\epsilon\} = \begin{Bmatrix} \epsilon_x \\ \epsilon_y \\ \gamma_{xy} \end{Bmatrix} = \begin{Bmatrix} \frac{\partial u}{\partial x} \\ \frac{\partial v}{\partial y} \\ \frac{\partial u}{\partial y} + \frac{\partial v}{\partial x} \end{Bmatrix} \quad (6.30)$$

Table 6.1 Properties of the elements developed in DMGPLSTS.

Element I. D. number	Number of nodes per element	Material type	Numerical integration rule	Element illustration in X-Y system	Element mapping in natural space
2	2	steel	n_p		
3	3	steel	n_p		
5	4	interface	$n_p \times 1$		
6	4	concrete	$n_p \times n_p$		
7	6	interface	$n_p \times 1$		
8	6	concrete	$n_p \times n_p$		
11	8	concrete	$n_p \times n_p$		
12	9	concrete	$n_p \times n_p$		

* n_p is the number of sampling points for one-dimensional integration rule

Substituting Eqn. (6.25) into (6.30), yields

$$\{\epsilon\} = [B] \{\bar{\varphi}\} \quad (6.31)$$

where $[B]$ is the strain displacement matrix which may be easily proved to be equal to

$$[B] = \begin{bmatrix} [B_1] & [B_2] & [B_3] & \dots & [B_n] \end{bmatrix} \quad (6.32)$$

where the submatrices $[B_i]$ are give as

$$[B_i] = \begin{bmatrix} \frac{\partial N_i}{\partial x} & 0 \\ 0 & \frac{\partial N_i}{\partial y} \\ \frac{\partial N_i}{\partial y} & \frac{\partial N_i}{\partial x} \end{bmatrix} \quad (6.33)$$

The infinitesimal strain-nodal displacement matrix $[B]$ is constant and consequently the incremental form can be written as

$$\{d\epsilon\} = [B] \{d\bar{\varphi}\} \quad (6.34)$$

where,

$\{d\epsilon\}$ the incremental strain vector,

$\{d\bar{\varphi}\}$ the incremental nodal displacement.

The elements of the $[B]$ matrix are composed of the cartesian derivatives of the interpolation functions. Using the chain rule, one gets

$$\frac{\partial N_i}{\partial \xi} = \frac{\partial N_i}{\partial x} \frac{\partial x}{\partial \xi} + \frac{\partial N_i}{\partial y} \frac{\partial y}{\partial \xi} \quad (6.35)$$

and

$$\frac{\partial N_i}{\partial \eta} = \frac{\partial N_i}{\partial x} \frac{\partial x}{\partial \eta} + \frac{\partial N_i}{\partial y} \frac{\partial y}{\partial \eta} \quad (6.36)$$

Arranging in a matrix form

$$\begin{pmatrix} \frac{\partial N_i}{\partial \xi} \\ \frac{\partial N_i}{\partial \eta} \end{pmatrix} = \begin{bmatrix} \frac{\partial x}{\partial \xi} & \frac{\partial y}{\partial \xi} \\ \frac{\partial x}{\partial \eta} & \frac{\partial y}{\partial \eta} \end{bmatrix} \begin{pmatrix} \frac{\partial N_i}{\partial x} \\ \frac{\partial N_i}{\partial y} \end{pmatrix} \quad (6.37)$$

$$= [J] \begin{pmatrix} \frac{\partial N_i}{\partial x} \\ \frac{\partial N_i}{\partial y} \end{pmatrix} \quad (6.38)$$

where $[J]$ is the Jacobian of the coordinate transformation and is given by:

$$[J] = \begin{vmatrix} \frac{\partial x}{\partial \xi} & \frac{\partial y}{\partial \xi} \\ \frac{\partial x}{\partial \eta} & \frac{\partial y}{\partial \eta} \end{vmatrix} \quad (6.39)$$

$$= \begin{vmatrix} \sum_{i=1}^n \frac{\partial N_i}{\partial \xi} x_i & \sum_{i=1}^n \frac{\partial N_i}{\partial \xi} y_i \\ \sum_{i=1}^n \frac{\partial N_i}{\partial \eta} x_i & \sum_{i=1}^n \frac{\partial N_i}{\partial \eta} y_i \end{vmatrix} \quad (6.40)$$

The cartesian derivatives are obtained by inverting Eqn. 6.37 which

yield

$$\begin{Bmatrix} \frac{\partial N_i}{\partial x} \\ \frac{\partial N_i}{\partial y} \end{Bmatrix} = |J|^{-1} \begin{Bmatrix} \frac{\partial N_i}{\partial \xi} \\ \frac{\partial N_i}{\partial \eta} \end{Bmatrix} \quad (6.41)$$

where the inverse of the Jacobian matrix can be shown to be

$$|J|^{-1} = \begin{vmatrix} \frac{\partial \xi}{\partial x} & \frac{\partial \eta}{\partial x} \\ \frac{\partial \xi}{\partial y} & \frac{\partial \eta}{\partial y} \end{vmatrix} \quad (6.42)$$

$$= \frac{1}{|J|} \begin{vmatrix} \frac{\partial y}{\partial \eta} & -\frac{\partial y}{\partial \xi} \\ -\frac{\partial x}{\partial \eta} & \frac{\partial x}{\partial \xi} \end{vmatrix} \quad (6.43)$$

6.4.1.4 Tangential Relations

The stress-strain relation was expressed in an incremental form for general loading as

$$\{d\sigma_p\} = |C_{Pt}| \{d\epsilon_p\} \quad (6.44)$$

where,

$\{d\epsilon_p\}_{3 \times 1}$ the incremental strain vector expressed in the principal plane,

$\{d\sigma_p\}_{3 \times 1}$ the incremental stress vector expressed in the principal plane,

$\left[C_{Pt} \right]_{3 \times 3}$ the tangential modulus matrix developed in the principal plane having the on-axis orthotropic form:

$$\left[C_{Pt} \right] = \begin{bmatrix} D_{11} & D_{12} & 0.0 \\ D_{12} & D_{22} & 0.0 \\ 0.0 & 0.0 & D_{33} \end{bmatrix} \quad (6.44')$$

The tangential modulus matrix depends on the stress path, i.e. loading unloading and reloading paths. It is advantageous to express these relations in the X-Y system of axes for use in Newton-Raphson algorithms. The incremental stress-strain relation in the X-Y plane can be assumed to have the following form

$$\{d\sigma\} = \left[C_t \right] \{d\epsilon\} \quad (6.45)$$

where,

$\{d\epsilon\}_{3 \times 1}$ the incremental strain vector expressed in the X-Y plane,

$\{d\sigma\}_{3 \times 1}$ the incremental stress vector expressed in the X-Y plane.

$\left[C_t \right]_{3 \times 3}$ the tangential modulus matrix transformed to the X-Y plane. having the general off-axis orthotropic form:

$$|C_t| = \begin{vmatrix} Q_{11} & Q_{12} & Q_{16} \\ Q_{12} & Q_{22} & Q_{26} \\ Q_{16} & Q_{26} & Q_{66} \end{vmatrix} \quad (6.45')$$

Assuming the angle between the X-axis and the major principal axes to be θ , it can be shown that the stress transformation law holds as

$$\{d\sigma\} = [T_{\sigma^{-1}}] \{d\sigma_p\} \quad (6.46)$$

where,

$[T_{\sigma^{-1}}]_{3 \times 3}$ the stress transformation matrix from the principal

plane to the X-Y plane and is given by

$$[T_{\sigma^{-1}}] = \begin{vmatrix} \frac{1}{2}(1 + \cos(2\theta)) & \frac{1}{2}(1 - \cos(2\theta)) & -\sin(2\theta) \\ \frac{1}{2}(1 - \cos(2\theta)) & \frac{1}{2}(1 + \cos(2\theta)) & \sin(2\theta) \\ \frac{1}{2}\sin(2\theta) & -\frac{1}{2}\sin(2\theta) & \cos(2\theta) \end{vmatrix} \quad (6.47)$$

Similarly, the strain transformation law can be written as

$$\{d\varepsilon_p\} = [T_\varepsilon] \{d\varepsilon\} \quad (6.48)$$

where,

$[T_\varepsilon]_{3 \times 3}$ the strain transformation matrix from the X-Y plane to

the principal plane and is given by

$$\left[\mathbf{T}_t \right] = \begin{vmatrix} \frac{1}{2} (1 + \cos(2\theta)) & \frac{1}{2} (1 - \cos(2\theta)) & \frac{1}{2} \sin(2\theta) \\ \frac{1}{2} (1 - \cos(2\theta)) & \frac{1}{2} (1 + \cos(2\theta)) & -\frac{1}{2} \sin(2\theta) \\ -\sin(2\theta) & \sin(2\theta) & \cos(2\theta) \end{vmatrix} \quad (6.49)$$

Using Eqn. (6.48) in (6.44) and substituting the product in Eqn. (6.46) and comparing the result with Eqn. (6.45), the tangential moduli can be shown to reduce to

$$\left[\mathbf{C}_t \right] = \left[\mathbf{T}_{\sigma^{-1}} \right] \left[\mathbf{C}_{P_t} \right] \left[\mathbf{T}_t \right] \quad (6.50)$$

The elements of the two moduli matrices presented in (6.50) can be proved after carrying out the tensorial multiplication to have the following form (Tsai and Hahn; 1980):

$$\begin{pmatrix} Q_{11} \\ Q_{22} \\ Q_{12} \\ Q_{16} \\ Q_{26} \\ Q_{56} \end{pmatrix} = \begin{vmatrix} C^4 & S^4 & 2C^2S^2 & 4C^2S^2 \\ S^4 & C^4 & 2C^2S^2 & 4C^2S^2 \\ C^2S^2 & C^2S^2 & C^4 + S^4 & -4C^2S^2 \\ C^2S^2 & C^2S^2 & -2C^2S^2 & (C^2 - S^2)^2 \\ C^3S & -CS^3 & CS^3 - C^3S & 2(CS^3 - C^3S) \\ CS^3 & -C^3S & C^3S - CS^3 & 2(C^3S - CS^3) \end{vmatrix} \begin{pmatrix} D_{11} \\ D_{22} \\ D_{12} \\ D_{33} \end{pmatrix} \quad (6.50')$$

where C and S are the sine and cosine functions of the angle θ , respectively.

6.4.1.5 Tangential Stiffness

The tangential element stiffness matrix, $[K_t]$, is obtained by numerical integration, i.e.

$$[K_t] = \int_V [B]^T [C_t] [B] dV \quad (6.51)$$

$$= \int_{\eta=-1}^{\eta=1} \int_{\xi=-1}^{\xi=1} [B]^T [C_t] [B] |J| t d\xi d\eta \quad (6.52)$$

$$= t \sum_{i=1}^{n_p} \sum_{j=1}^{n_p} W_i W_j [B(\xi_i, \eta_j)]^T [C_t(\xi_i, \eta_j)] [B(\xi_i, \eta_j)] |J(\xi_i, \eta_j)| \quad (6.53)$$

where,

n_p the number of integration points,

(ξ_i, η_j) the position of the integration point in the natural coordinate system,

W_m the weighting factor of Gauss-Legendre integration rule at the m th sample point,

t the thickness of the element.

6.4.1.6 Residual Forces

In DMGPLSTS, a similar logic to that in DMGTRUSS is followed for calculating the internal stresses, their equivalent nodal forces and the residual forces of each element but in the principal plane. Two characteristic quantities should be determined for applying the canonical elastoplastic damage law:

- (1) the orientation of the principal plane, and
- (2) the biaxiality ratio.

For proportional loading these quantities are fixed through the whole loading history from the first instance of load application except for the case of unloading with sign reversal. In such a situation, the principal axes rotate 90 degrees, i.e. the major and minor directions switch. Inspection of the various stress paths -loading, unloading or reloading whether with linear or nonlinear behavior is detected only through the major component since the same status is expected to apply for the minor.

For nonproportional loading, the orientation of the principal plane is fixed over a certain iteration and the biaxiality ratio is evaluated based on the previous iteration.

6.4.1.7 Reduction of the Concrete Element to Interface Element

Consider the six-noded element of constant thickness t shown in Fig. (6.13). Assume for simplicity without losing the generality that the local s - n system with three fictitious nodes 1',2', and 3' going along

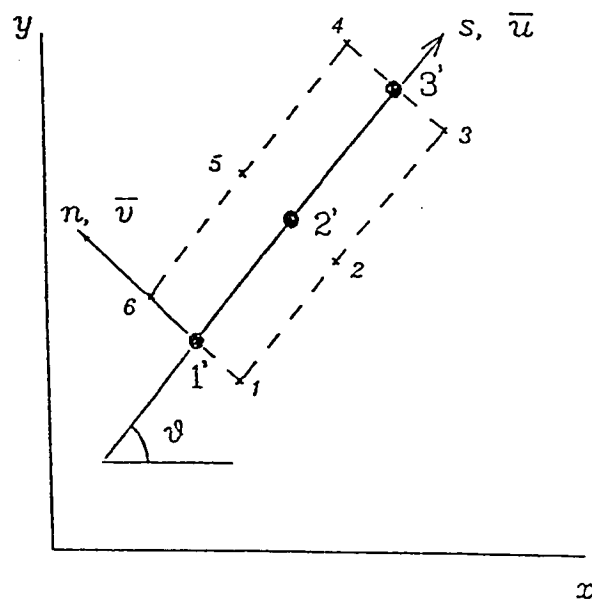


Figure 6.13 Reduction of concrete element to interface element

the s-axis. The local strain vector in the local system may be written as

$$\{e\} = \begin{Bmatrix} \epsilon_t \\ \epsilon_n \\ \gamma_{tn} \end{Bmatrix} = \begin{Bmatrix} \frac{\partial u}{\partial t} \\ \frac{\partial v}{\partial n} \\ \frac{\partial u}{\partial n} + \frac{\partial v}{\partial t} \end{Bmatrix} \quad (6.54)$$

Inasmuch as the element is linear in the n-direction, then any derivative of any arbitrary function, f , with respect to n will be just the difference of the function on the n-axis at its intercepts with the sides of the element over the thickness; i.e. for example

$$\begin{aligned} \left(\frac{\partial f}{\partial n}\right)_{\xi=1} &= \left(\frac{\Delta f}{t}\right)_{\xi=1} \\ &= \frac{1}{t} (f_{\eta=1} - f_{\eta=-1}) \\ &= \frac{1}{t} (f_6 - f_1) \end{aligned} \quad (6.55)$$

Therefore, the derivative of f with respect to n becomes

$$\begin{aligned} \left(\frac{\partial f}{\partial n}\right) &= \sum_{i=1}^3 N_i' \left(\frac{\Delta f}{t}\right)_i \\ &= \frac{1}{t} \left[N_1'(f_6 - f_1) + N_2'(f_5 - f_2) + N_3'(f_4 - f_3) \right] \end{aligned} \quad (6.56)$$

Assume the interpolation functions are expressed as the product of two functions $N_\xi \times N_\eta$. Therefore, along the side containing the nodes

1,2 and 3, where $\eta = -1$, $N_\eta = 1/2(1 - \eta)$ and along the side containing the nodes 4, 5 and 6, where $\eta = 1$, $N_\eta = 1/2(1 + \eta)$. The functions N_ξ at any of the nodes of either side will be the same as those of the fictitious nodes.

Consider a numerical integration rule of the order $1 \times n_p$ rather than the conventional rule $n_p \times n_p$. The sampling points in this case will coincide along the s -axis ($\eta = 0$), where $N_\eta = 1/2$ and $N_i = 1/2N_\xi = 1/2N'_j$, $j = 1, 3$. Thus, the derivative with respect s of the arbitrary function f will reduce to

$$\begin{aligned} \left(\frac{\partial f}{\partial s}\right) &= \sum_{i=1}^6 \frac{\partial N_i}{\partial s} f_i \\ &= \frac{1}{2} \sum_{i=1}^6 \frac{\partial N_\xi}{\partial s} f_i \\ &= \frac{dN_1'}{ds} \left(\frac{f_1 + f_6}{2}\right) + \frac{dN_2'}{ds} \left(\frac{f_2 + f_5}{2}\right) + \frac{dN_3'}{ds} \left(\frac{f_3 + f_4}{2}\right) \quad (6.57) \end{aligned}$$

Application of the integration rules given by Eqns (6.56) and (6.57) leads exactly to the same results obtained by Ziraba (1993) for the strain-displacement matrix given by Eqn. (6.54). In his work, the interface element was developed separately apart from the concrete element. Moreover, by the suggested reduction technique the matrices will be automatically obtained in the x - y system and no need to make any transformation for the stiffness calculations.

6.4.2 Finite Element Formulation for Reinforcement

6.4.2.1 Material Nonlinearity

The damage law developed in Chapter 5 is used for the reinforcing steel in DMGPLSTS. Although the program is developed for biaxial states of stress only uniaxial idealization of the material behavior is considered. This is attributable to modelling reinforcement by boom elements.

6.4.2.2 Displacement Model

The boom element considered herein is a two-dimensional isoparametric element which is composed of multiple nodes (greater than two) and internally carries only an axial stress component. Such an element is suitable for idealizing cables, prestressed tendons, and steel reinforcement. The element used in DMGTRUSS represents a special case of the more sophisticated boom element. Fig. 6.14 shows, as an example, the picture of a three-noded boom element in the X-Y plane and its mapping in the ξ plane. Choosing the S-axis going along the element, the axial displacement at any point at distance s from the origin is related to the displacement components in the X-Y plane by the relation

$$\{d\} = \{T\} \{\varphi\}, \quad (6.58)$$

where

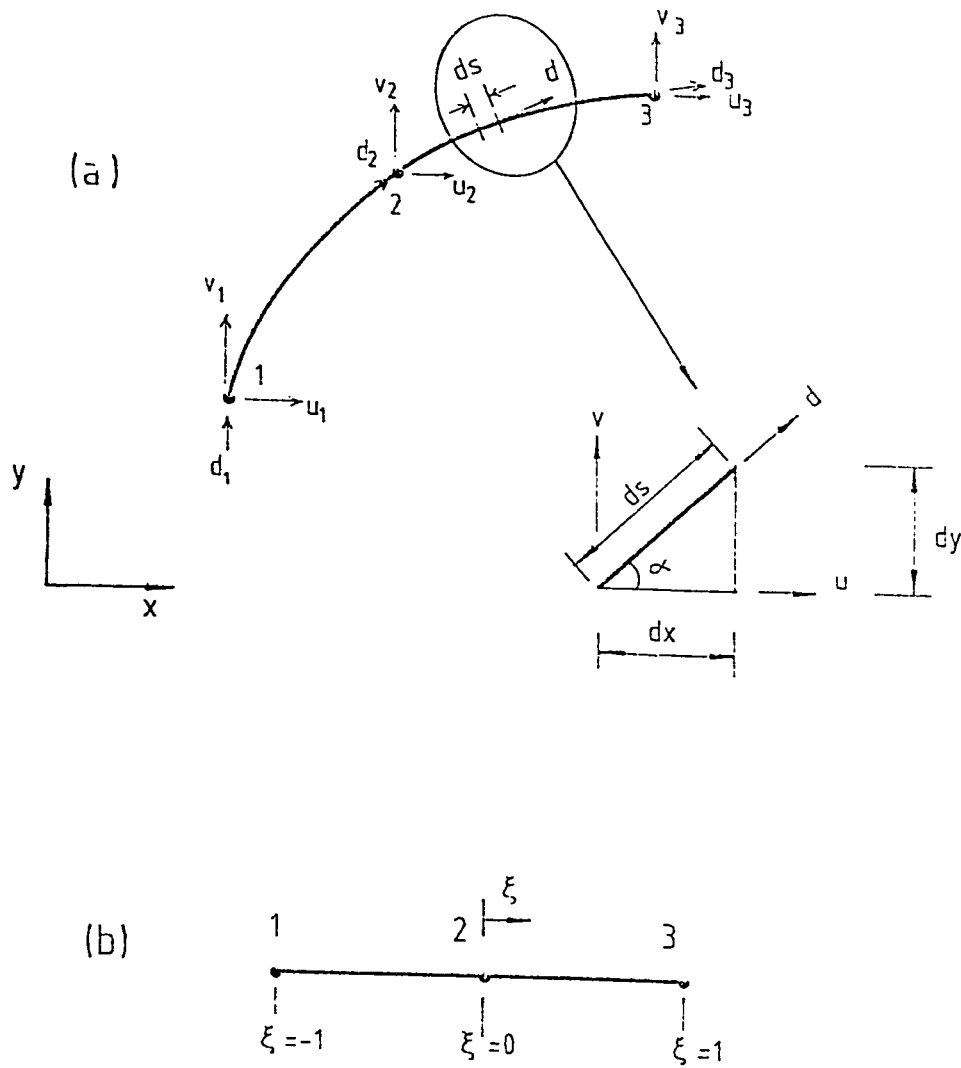


Figure 6.14 Three noded isoparametric element as an example for boom element: a) Global space and b) Local space

$\{d\}_{1 \times 1}$ The displacement vector along the S axis,

$\{\varphi\}_{2 \times 1}$ The displacement vector in the X-Y plane and is expressed as

$$\{\varphi\} = \begin{bmatrix} u & v \end{bmatrix}^T, \quad (6.59)$$

and where

$[\bar{T}]_{1 \times 2}$ is a transformation matrix from the S system to the X-Y system of axes and is given by

$$[\bar{T}] = \begin{bmatrix} C_x & C_y \end{bmatrix} \quad (6.60)$$

in which C_x and C_y are the direction cosines at the point considered.

The validity of Eqn. (6.58) can be easily checked using vector algebra by noting that

$$u = d C_x, \quad (6.61)$$

and

$$v = d C_y \quad (6.62)$$

Substituting from Eqns (6.61) and (6.62) in Eqn. (6.58) get

$$d = d (C_x^2 + C_y^2) \quad (6.63)$$

Keeping in mind that

$$C_x = \frac{\partial x}{\partial s} = \cos \alpha \quad (6.64)$$

and

$$C_y = \frac{\partial y}{\partial s} = \sin \alpha \quad (6.65)$$

Eqn. (6.63) is, thus, reduced to

$$d = d (\cos^2 \alpha + \sin^2 \alpha) \quad (6.66)$$

which represents an identity. Accordingly, the nodal displacements can be described, for the i th node, by

$$\{d_i\} = [\bar{T}_i] \{\varphi_i\}, \quad (6.67)$$

Contrary to linear elements, the transformation matrix need not constant over the element and is expressed, for the i th node, as

$$[\bar{T}_i] = \begin{bmatrix} C_{x_i} & C_{y_i} \end{bmatrix} \quad (6.68)$$

Using Eqns. (6.64) and (6.65) in Eqn. (6.68), get

$$[\bar{T}_i] = \begin{bmatrix} (\frac{\partial x}{\partial s})_i & (\frac{\partial y}{\partial s})_i \end{bmatrix} \quad (6.69)$$

For isoparametric formulation, the cartesian coordinates are expressed by

$$x = \sum_{j=1}^n N_j x_j, \quad (6.70)$$

and

$$y = \sum_{j=1}^n N_j y_j, \quad (6.71)$$

in which $N_j = N_j(\xi)$ are the interpolation functions associated with j th node, $j = 1, n$. Therefore, Eqn. (6.69) becomes

$$[\bar{T}_i] = \left[\left(\frac{\partial}{\partial s} \sum_{j=1}^n N_j x_{j,i} \right) \quad \left(\frac{\partial}{\partial s} \sum_{j=1}^n N_j y_{j,i} \right) \right] \quad (6.72)$$

which may be further reduces to

$$[\bar{T}_i] = \left[\left(\sum_{j=1}^n \frac{\partial N_j}{\partial s} x_{j,i} \right) \quad \left(\sum_{j=1}^n \frac{\partial N_j}{\partial s} y_{j,i} \right) \right] \quad (6.73)$$

Determination of the derivative $\partial(\)/\partial s$ is obtained using the Jacobian as will be shown in the next section.

Eqn. (6.67) can, now, be written in a more elaborate form as

$$\{\bar{d}\} = [T] \{\bar{\varphi}\} \quad (6.74)$$

where,

$$\{\bar{d}\} = [d_1 \quad d_2 \quad d_3 \quad \dots \quad d_n]^T, \quad (6.75)$$

$$\{\bar{\varphi}\} = [u_1 \quad v_1 \quad u_2 \quad v_2 \quad u_3 \quad v_3 \quad \dots \quad u_n \quad v_n]^T, \quad (6.76)$$

$$\begin{aligned}
 [T] = & \begin{vmatrix}
 \left| \bar{T}_1 \right|_{1 \times 2} & \left| 0 \right|_{1 \times 2} & \left| 0 \right|_{1 \times 2} & \dots & \left| 0 \right|_{1 \times 2} \\
 \left| 0 \right|_{1 \times 2} & \left| \bar{T}_2 \right|_{1 \times 2} & \left| 0 \right|_{1 \times 2} & \dots & \left| 0 \right|_{1 \times 2} \\
 \left| 0 \right|_{1 \times 2} & \left| 0 \right|_{1 \times 2} & \left| \bar{T}_3 \right|_{1 \times 2} & \dots & \left| 0 \right|_{1 \times 2} \\
 \dots & \dots & \dots & \dots & \dots \\
 \dots & \dots & \dots & \dots & \dots \\
 \dots & \dots & \dots & \dots & \dots \\
 \dots & \dots & \dots & \dots & \dots \\
 \left| 0 \right|_{1 \times 2} & \left| 0 \right|_{1 \times 2} & \left| 0 \right|_{1 \times 2} & \dots & \left| \bar{T}_n \right|_{1 \times 2}
 \end{vmatrix} & (6.77)
 \end{aligned}$$

The displacement at any point can be related to the nodal values by the interpolation functions as follows

$$\{d\} = [\bar{N}] \{\bar{d}\}, \quad (6.78)$$

where,

$$[\bar{N}] = \begin{vmatrix} N_1 & N_2 & N_3 & \dots & N_n \end{vmatrix} \quad (6.79)$$

for the S-system and

$$\{\varphi\} = [N] \{\bar{\varphi}\}, \quad (6.80)$$

where,

$$[N] = \begin{vmatrix} N_1 |I|_{2 \times 2} & N_2 |I|_{2 \times 2} & N_3 |I|_{2 \times 2} & \dots & N_n |I|_{2 \times 2} \end{vmatrix} \quad (6.81)$$

for the XY-system. Combining Eqns (6.78) and (6.74), the axial displacement is, thus, related to the nodal displacements in the X-Y plane by

$$\{d\} = [\bar{N}] [T] \{\bar{\varphi}\} \quad (6.82)$$

6.4.2.3 Strain-Displacement Relationship

The infinitesimal axial strain, $\{\epsilon\}$, for the boom element is expressed as

$$\{\epsilon\} = \left\{ \frac{\partial d}{\partial s} \right\} \quad (6.83)$$

$$= \frac{\partial}{\partial s} (|\bar{N}| [T]) \{\bar{\varphi}\} \quad (6.84)$$

which can be written in a matrix form as,

$$\{\epsilon\} = [B] \{\bar{\varphi}\} \quad (6.85)$$

This relation holds incrementally such that

$$\{d\epsilon\} = [B] \{d\bar{\varphi}\} \quad (6.86)$$

in which $[B]$ is the strain displacement matrix which may be easily proved to be equal to

$$[B] = \left[\begin{array}{cccccc} |B_1| & |B_2| & |B_3| & \dots\dots\dots & |B_n| & | \end{array} \right] \quad (6.87)$$

in which the 1×2 submatrix $|B_i|$, $i=1, n$ is given by

$$|B_i| = \left(\frac{\partial}{\partial s} (|\bar{N}| [T]) \right)_i$$

$$= \left[\begin{array}{cc} \frac{\partial N_i}{\partial s} \left(\sum_{j=1}^n \frac{\partial N_j}{\partial s} x_{j,i} \right) + N_i \left(\sum_{j=1}^n \frac{\partial^2 N_j}{\partial s^2} x_{j,i} \right) & \\ \frac{\partial N_i}{\partial s} \left(\sum_{j=1}^n \frac{\partial N_j}{\partial s} y_{j,i} \right) + N_i \left(\sum_{j=1}^n \frac{\partial^2 N_j}{\partial s^2} y_{j,i} \right) & \end{array} \right]^T$$

(6.88)

Consider now an infinitesimal element whose length is

$$ds = \sqrt{(dx)^2 + (dy)^2} \quad (6.89)$$

Since the coordinates are expressed in a parametric form in terms of ξ , the differential coordinates are

$$dx = \frac{\partial x}{\partial \xi} d\xi, \quad (6.90)$$

and

$$dy = \frac{\partial y}{\partial \xi} d\xi, \quad (6.91)$$

Using Eqns (6.90) and (6.91) in the formulae of the differential coordinates then

$$dx = \left(\sum_{j=1}^n \frac{\partial N_j}{\partial \xi} x_j \right) d\xi, \quad (6.92)$$

and

$$dy = \left(\sum_{j=1}^n \frac{\partial N_j}{\partial \xi} y_j \right) d\xi, \quad (6.93)$$

Consequently, the differential length given by Eqn. (6.89) reduces to

$$ds = \sqrt{\left(\sum_{j=1}^n \frac{\partial x}{\partial \xi} x_j \right)^2 + \left(\sum_{j=1}^n \frac{\partial y}{\partial \xi} y_j \right)^2} d\xi$$

$$= \sqrt{\left(\sum_{j=1}^n \frac{\partial N_j}{\partial \xi} x_j\right)^2 + \left(\sum_{j=1}^n \frac{\partial N_j}{\partial \xi} y_j\right)^2} d\xi \quad (6.94)$$

and the Jacobian J is, in the present case, a scalar

$$J = \frac{ds}{d\xi} = \sqrt{\left(\sum_{j=1}^n \frac{\partial N_j}{\partial \xi} x_j\right)^2 + \left(\sum_{j=1}^n \frac{\partial N_j}{\partial \xi} y_j\right)^2} \quad (6.95)$$

Therefore the natural derivative can be shown as

$$\begin{aligned} \frac{\partial(\quad)}{\partial \xi} &= \frac{\partial(\quad)}{\partial s} \frac{\partial s}{\partial \xi} \\ &= J \frac{\partial(\quad)}{\partial s} \end{aligned} \quad (6.96)$$

Inverting, the first cartesian derivative is expressed in the form

$$\begin{aligned} \frac{\partial(\quad)}{\partial s} &= \frac{\partial(\quad)}{\partial \xi} \frac{\partial \xi}{\partial s} \\ &= J^{-1} \frac{\partial(\quad)}{\partial \xi} = \frac{1}{J} \frac{\partial(\quad)}{\partial \xi} \end{aligned} \quad (6.97)$$

The second cartesian derivative is obtained from (6.97) as follows

$$\begin{aligned} \frac{\partial^2(\quad)}{\partial s^2} &= \frac{\partial}{\partial s} \left(\frac{\partial(\quad)}{\partial \xi} \frac{\partial \xi}{\partial s} \right) \\ &= \frac{1}{J} \frac{\partial}{\partial \xi} \left(\frac{1}{J} \frac{\partial(\quad)}{\partial \xi} \right) \\ &= \frac{1}{J^2} \frac{\partial^2(\quad)}{\partial \xi^2} - \frac{1}{J^3} \frac{\partial J}{\partial \xi} \frac{\partial(\quad)}{\partial \xi} \end{aligned} \quad (6.98)$$

The natural derivative of the Jacobian can be directly obtained from Eqn. (6.95) by simple differentiation which leads to

$$\frac{\partial J}{\partial \xi} = \frac{d^2 s}{d\xi^2} = \frac{1}{J} \left[\left(\sum_{j=1}^n \frac{\partial N_j}{\partial \xi} x_j \right) \left(\sum_{j=1}^n \frac{\partial^2 N_j}{\partial \xi^2} x_j \right) + \left(\sum_{j=1}^n \frac{\partial N_j}{\partial \xi} y_j \right) \left(\sum_{j=1}^n \frac{\partial^2 N_j}{\partial \xi^2} y_j \right) \right] \quad (6.99)$$

6.4.2.4 Tangential Modulus

The stress-strain relation in an incremental form can be expressed, similar to the truss element in DMGTRUSS, as

$$\{d\sigma\} = [C_t] \{dr\} \quad (6.100)$$

where,

$\{d\sigma\}$ the incremental stress vector,

$[C_t]$ the tangential modulus matrix.

The tangential modulus matrix depends on the stress path, i.e. loading unloading and reloading paths. With reference to the proposed steel uniaxial model, $[C_t]$ can be easily derived as what follows, for :

1. *loading* : $[C_t]$ can be obtained by simple differentiation and considering that the initial total modulus is equal to the initial elastic modulus, hence

$$\begin{aligned}
 |C_t| &= \frac{\{\partial\sigma\}}{\{\partial\varepsilon\}} \\
 &= \left| (1.0 - d_a) E_0 - E_0 \varepsilon \frac{\partial d_a}{\partial \varepsilon} \right| \quad (6.101)
 \end{aligned}$$

21. *linear unloading/reloading* : Since no stiffness degradation is reported, the tangential modulus is constant, therefore

$$|C_t| = E_0 \quad (6.102)$$

6.4.2.5 Tangential Stiffness

The tangential element stiffness matrix, $|K_t|$, is obtained by numerical integration, i.e.

$$|K_t| = \int_V |B|^T |C_t| |B| dV \quad (6.103)$$

$$= \int_{\xi_{i-1}}^{\xi_i} |B|^T |C_t| |B| J A d\xi \quad (6.104)$$

$$= A \sum_{i=1}^{n_p} W_i |B(\xi_i)|^T |C_t(\xi_i)| |B(\xi_i)| J(\xi_i) \quad (6.105)$$

where,

n_p the number of integration points,

ξ_i the position of the i th integration point in the natural

coordinate system,

W_i the weighting factor according to Gauss-Legendre integration rule at the i th sample point,

A the cross sectional area of the element.

6.4.2.6 Residual Forces

The same methodology utilized in DMGTRUSS is followed herein for the boom element but with minor changes. That is a particular damage model is considered and no need for the multiple zone algorithm any more. To summarize, the following steps are considered:

- (1) The incremental displacements are calculated,
- (2) The total as well as the incremental axial strains are evaluated,
- (3) Loading, linear unloading/reloading, unloading with sign reversal or reloading to the loading path are investigated.
- (4) The internal stress are calculated according to the damage rule,
- (5) The internal forces for each element are estimated.
- (6) The equivalent internal nodal forces are evaluated then the out-of-balance (residual) forces are calculated.

6.4.3 DMGPLSTS Structure

Program DMGPLSTS consists of five main modules as shown in Fig.

6.15 :

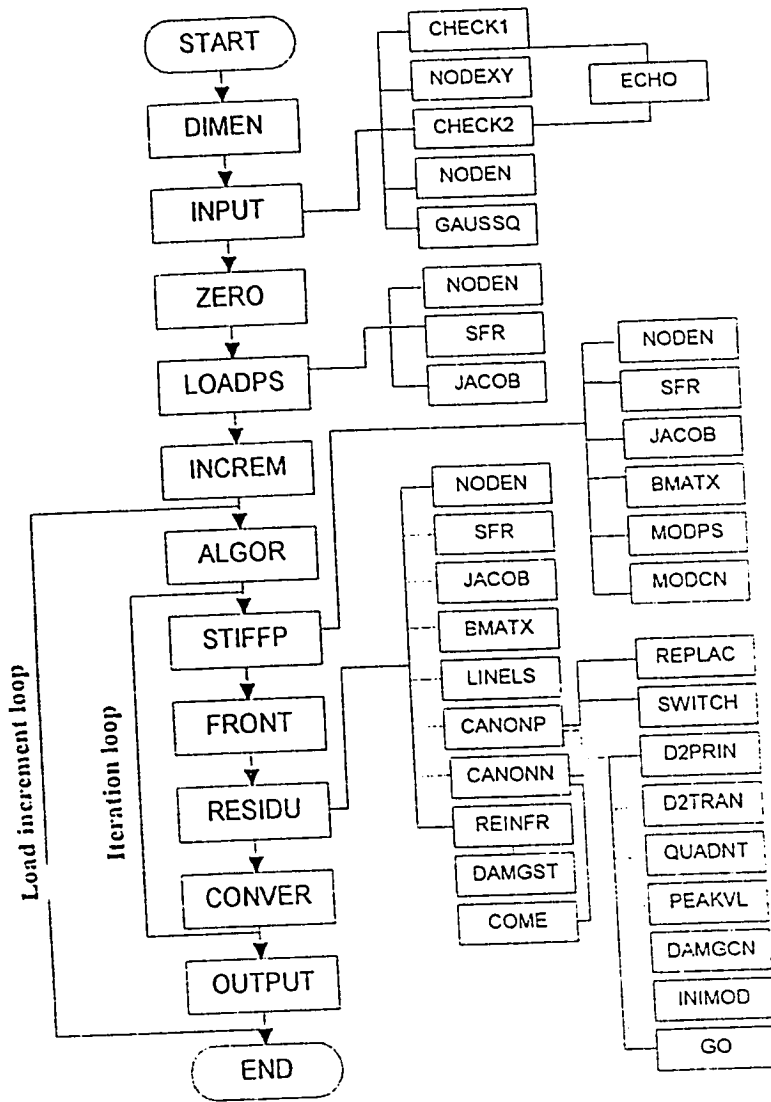


Figure 6.15 Main calls in program DMGPLSTS

1. Dynamic dimensioning, data input and initialization module : calling three subroutines DIMEN, INPUT and ZERO.
2. Stiffness and load formulation module : this module formulate the structural system of equations by communications with LOADPS, INCREM, ALGOR, STIFFP. Some of these subroutines call other modules of a lower level.
3. Solution module : for assembly to the structural level and solving the system of equations using the frontal technique in subroutine FRONT.
4. Residual force and convergence module : in this module elements' stresses are computed by calling RESIDU which gets assistance from Subroutines CANONN, CANONP and REINFR in which the residual forces are calculated and convergence is then monitored through subroutine CONUND.
5. Output module : output the information obtained for all nodes and members in subroutine OUTPUT.

Depiction of the master program and the appended subroutines requires familiarity with the variable and arrays used in the program. A glossary of variables and arrays utilized in DMGPLSTS is provided in Appendix V.

It is remarkable that the constitutive equations are formulated in two forms: (1) conventional form and (2) canonical form. In additions the moduli matrix are shown to be equivalently expressed in two

spaces: (1) the Eculidean space (X-Y space) and (2) the principal space. The possible forms and ocurrence of the moduli matrices in various planes in the program is illustrated in Fig. 6.16.

6.4.4 DMGPLSTS Master Program and Subroutines

DMGPLSTS includes, besides the master program, forty nine subroutine. The main segment controls the calling of the major subroutines (11). The function of every subroutine is given downwards.

SUBROUTINE	FUNCTION
ALGOR*	Set equation resolution index, KRESL.
BIAXL	Evaluates the biaxiality ratio for concrete elements following the canonical model.
BMATPS*	Evaluates the strain-displacement matrix
CANONN	Evaluate the internal stresses for concrete elements in the case nonproportional loading by the canonical damage model.
CANONP	Evaluate the internal stresses for concrete elements in

 * Subroutine given by Owen and Hinton, 1980.

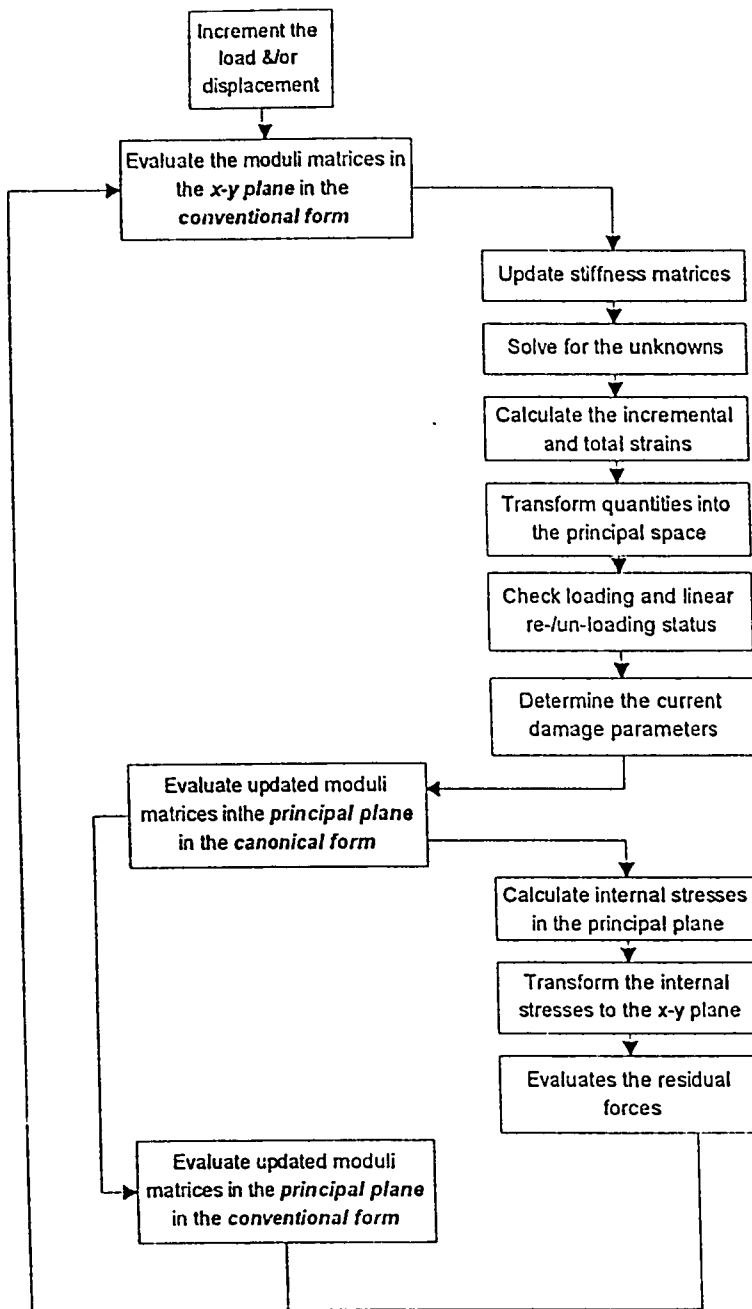


Figure 6.16 Possible forms and occurrence of moduli matrices in various planes

the case proportional loading by the canonical damage model.

- CHECK1* Check the main control data.
- CHECK2* Check nodal coordinates, elements incidences, frontwidth and data for restraint nodes.
- COME Carry out the necessary transformations for mapping from the principal space to the XY-plane.
- CONVER* Construct the residual forces array and monitor convergence of the iteration process.
- D2PRIN Determine the principal values of a plane tensor.
- D2TRAN Transform a plane tensor by rotation through an angle θ .
- DAMGCN Calculate the damage parameters for the canonical model for concrete.
- DAMGST Calculate the damage parameters for reinforcing steel.
- DBE* Multiply the stress-strain matrix by the strain-nodal displacement matrix.
- DETER Evaluate the determinate of square matrices up to 3x3 rank.
- DINTGL Calculate the differential volume for use in numerical integration.

DIMEN	Preset variables associated with dynamic dimensioning.
ECHO*	Read and write the remaining data cards on any error detection by either CHECK1 or CHECK2.
FRONT*	Undertake equation solution by the frontal technique.
GAUSSQ	Set up the Gauss-Legendre integration constants. iteration.
GO	Carry out the necessary transformations for mapping from the XY-plane to the principal plane.
INMOD	Calculate the undegraded canonical moduli.
INCREM*	Increment the applied loading and/or the prescribed displacements.
INPUT	Accept most of the input data.
JACOB	Evaluate the Jacobian matrix and the cartesian shape functions.
LINCOD	Determine stress flag: 0 for neutral, 1 for tension and 2 for compression.
LOADPS	Evaluate the consistent nodal forces for each element.
MATINV	Evaluate the inverse of a square matrix.
MODPS*	Evaluate the stress-strain matrix based on linear elastic behavior.

- NODEN** Define the number of nodes per each element type,, the number of stress components, the number of element variable and the proper numerical integration rule.
- NODEXY*** Interpolate the mid-side nodes of straight sides of 8- and 9-noded elements and the central node of the latter.
- OUTPUT** Output the program results. An output file layout is shown in Data communication.
- PEAKVL** Determine the peak functions η_{σ_i} and η_{ϵ_i} , ($i=1,2$) of any stress quadrant for a given biaxiality ratio.
- QUADNT** Determine the stress quadrant for plane stress states.
- REINFR** Evaluate the internal stresses for steel elements by the proposed uniaxial damage model.
- RESIDU** Evaluate the elements' stresses and calculates the equivalent internal nodal forces.
- REPLAC** Switch the first two records of a vector in case of unloading with sign reversal for proportional stress history.
- SFR** Evaluate the shape functions and their natural derivatives for concrete and steel elements.
- STIFFP** Evaluate the tangential stiffness matrix for each element in turn.

- SWITCH** Carry out the proper modifications in case of unloading with sign reversal for proportional stress history.
- ZERO** Initialize various arrays to zero.

6.4.5 Load Reversal and Hysteresis Loop

IN DMGPLSTS the unloading path is assumed to be linear and the residual deformations corresponding to stress free conditions can be reasonably obtained. Sign reversal of loading conditions is allowed in a similar manner as developed in DMGTRUSS. These characteristics allows for extending the program to analyse repaired structures in which the determination of the degree of damage due to preloading is of prime importance.

6.4.6 Data Communication

Pre-processing is considered herein for data manipulation. Program MEGEN2D, which was put to use by Mr. A. Shazali but with minor modifications, is used for preparing the two dimensional node generation in the cartesian coordinate system. It allows for the description of the element topology by adopting the proper connectivity and element I. D. number. User instructions for Program DMGPLSTS are set forth in APPENDIX VII. A sample input file for DMGPLSTS is given as an example.

6.4.7 DMGPLSTS Extendability to Other Applications

DMGPLSTS, as elucidated earlier, is constructed in a modular form. This facilitates extension of the package to the following further applications :

1. Model the elastoplastic damage behavior of yielding materials and those of unilateral damage behavior for which the constitutive relations are derived in Chapter 4.
2. Include more damage models for concrete and also for other materials.
3. Generalize the program to three-dimensions and also to two-dimensional plane strain and axisymmetrical cases.
4. Include damage models for interface materials to facilitate modelling of soil-structure interaction as well as various repair techniques.

CHAPTER 7

CHAPTER 7**APPLICATIONS****7.1 GENERAL**

Applications of the canonical model to boundary value problems are undertaken using the finite element programs described earlier. DMGTRUSS is employed to predict the cyclic behavior of plain concrete under reversed loading and the range of tension stiffening under uniaxial loading. Finite element predictions of reinforcing steel modelled by the proposed damage model and as elastic perfectly plastic are compared against experimental data. Reinforced concrete idealized as a bundle system is then investigated for different ratios of reinforcement under tension and compression. DMGPLSTS is utilized to predict the response of plain concrete panel subjected to several load combinations. Fundamental cases of loading applied to reinforced concrete are then studied. These include uniaxial tension, perfect bond characteristics, and pure bending. Finally, three point loading of plain concrete as well as longitudinally reinforced concrete beams are analysed in addition to the steel/concrete bond problem. The results are compared with experimental values besides the available solutions by other investigators. Finally, the predictions of the model are calibrated against code provisions for the case of reinforced concrete beams with and without shear reinforcement under three and four point loading.

7.2 FEATURES CAPTURED BY DMGTRUSS

In most of the applications two different concrete grades are used; namely Grade 28 and Grade 40. The different parameters calculated inside the program along with the corresponding formulae for these two types of concrete are listed in Table 7.1. The finite element predictions for the behavior of both plain and reinforced concrete members are given hereafter. These include the response of plain concrete components subjected to reversed loading, the range of tension stiffening of plain concrete under uniaxial loading, the uniaxial tension of the reinforcing steel then the behavior of reinforced concrete structural members to uniaxial tensile as well as compressive loading.

7.2.1 Plain Concrete Under Reversed Loading

A one meter long plain concrete member of cross section 250x250 mm of Grade 28 is subjected to reversed loading. At the first instance a tensile loading is imposed then fully unloaded. In the sequel a compressive loading is applied then fully unloaded and finally the member is again loaded in tension. The displacement of the free end of the element is incremented in order to simulate strain-controlled experiments. The global stiffness matrix is updated in every iteration of every load increment. Fig. 7.1 illustrates the response of the member to the given loading history. The results indicate that the program captures the following features:

1. The pre-peak nonlinearity as well as the post-peak softening regime.

Table 7.1 Properties of two concrete grades.

Variable	Formula	Concrete grade	
		28 MPa	40 MPa
E	$3320\sqrt{f'_c} + 6900$	24 468	27 898
f'_t	$0.324 (f'_c)^{2/3}$	2.987	3.789
ϵ_c	$\frac{n}{n-1} \frac{f'_c}{E}$	$1.845 \cdot 10^{-3}$	$2.050 \cdot 10^{-3}$
ϵ_t	$1.2 \frac{f'_t}{E}$	$1.465 \cdot 10^{-4}$	$1.630 \cdot 10^{-4}$
n	$0.0058 f'_c + 1.0$	2.623	3.333
α	$0.312 f'_t{}^2$	2.785	4.480

2. Flow stress degradation as the unloading slope is being reduced and not poling to the zero-zero point.
3. Translation of the origin of the stress-strain curve along the strain axis for both the tensile and compressive responses.
4. Reduction of the peak strength in the second tensile loading as affected by the irreversible damage experienced in the first tensile loading cycle.
5. Behavior in tension is entirely different from that in compression.
6. Moduli degradation are independent in tension and compression.
7. Residual deformations can be determined at any stress level.

7.2.2 Tension Stiffening of Plain Concrete Under Uniaxial Loading

Two vertical 150X150X1000 mm plain concrete elements of Grade 28 connected in series are restrained at both sides. An axial load is applied at the mid-point thus producing tensile stress in the upper element while compressive stress is developed in the lower element. The response is shown in Fig. 7.2 where the results are compared with the same system assuming linear elastic response. The behavior is almost identical for only a limited range of deformation which is approximately up to 5% of the peak central deflection. Another comparison is made considering only the stiffness of the lower element. It is noticed that both behaviors start to coincide with each other at deformations about 30% of the peak central deflection. This illustrates the range of tension stiffening in axial loading where the two curves become identical when

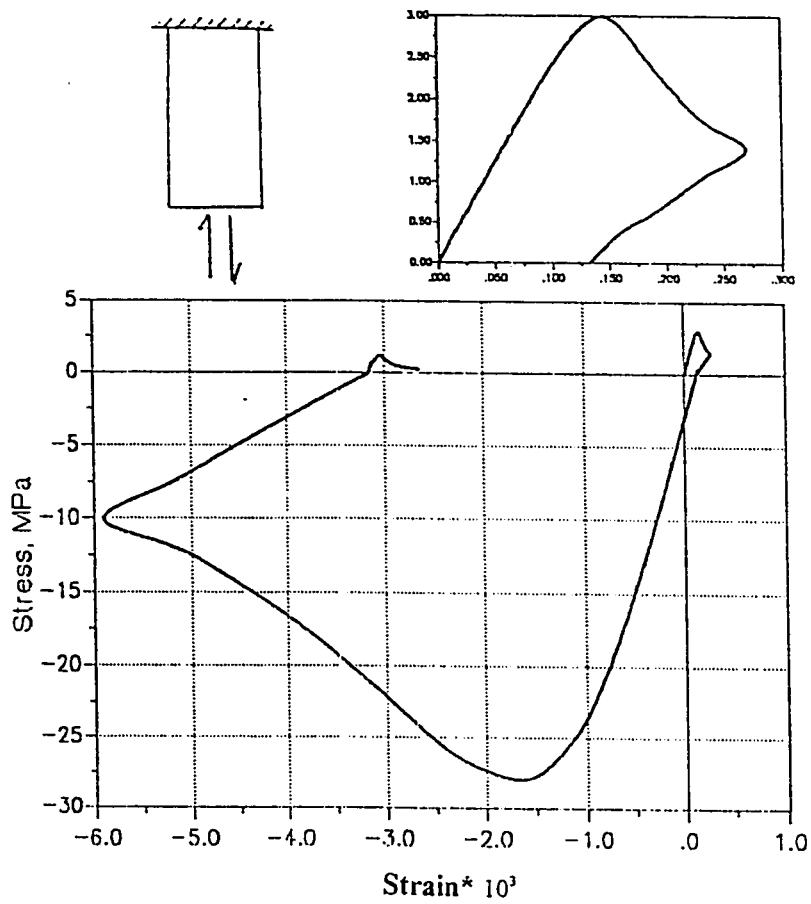


Figure 7.1 Finite element prediction for the response of plain concrete to reversed loading

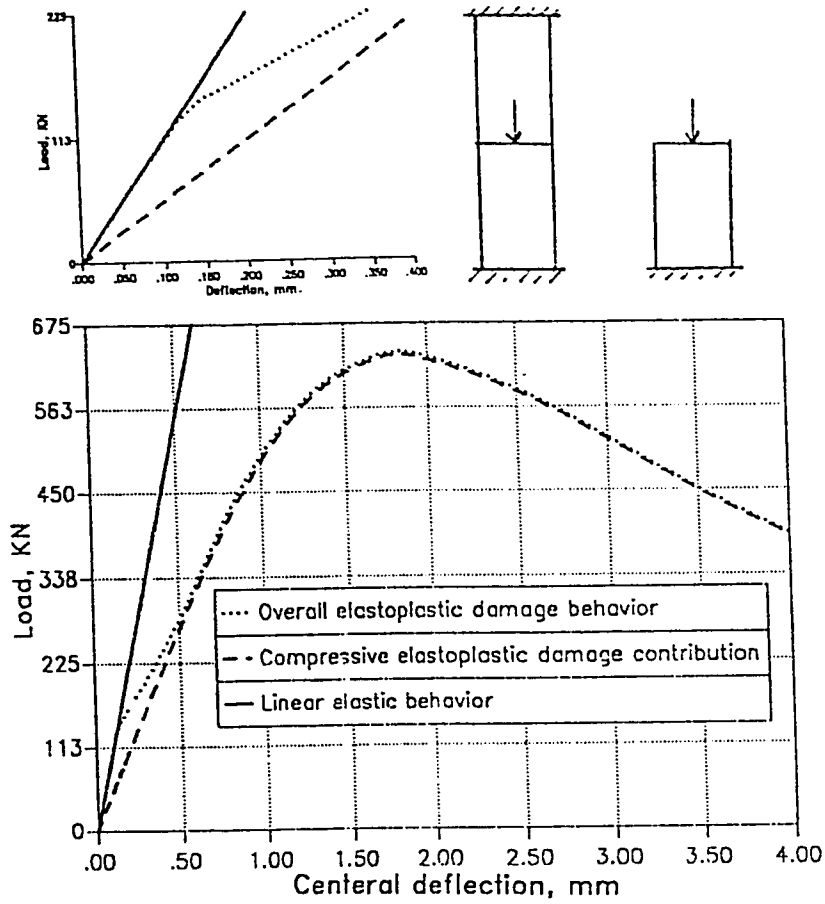


Figure 7.2 Finite element prediction for the range of tension stiffening of plain concrete subjected to axial loading

softening of the tensioned member reduces its tensile capacity to almost zero. The ultimate load P_{ult} predicted by the program is 630 KN. This load produces a compressive stress σ_{ult} in the lower element, whose cross sectional area is A, equal to

$$\sigma_{ult} = \frac{P_{ult}}{A} = \frac{630,000}{22,500} = 28\text{MPa} \quad (7.1)$$

which is the same value as the characteristic strength for the used concrete. The overall behavior in the post-peak region shows that softening of the system is picked up by the model.

7.2.3 Uniaxial Tension of Reinforcing Steel

A steel element of Grade SS41 is subjected to a uniaxial tensile force. The solution is first carried out using the proposed damage model using the material parameter α equal to unity which means that the yielding plateau is horizontal. The results are shown in close agreement with the experimental data by Kato et al. (1990) as depicted in Fig. 7.3. The response assuming linear elastic-perfectly plastic idealization is obtained by finite element solution with deflection controlled incrementation. It is clear that such an idealization is quite a crude assumption for the response at large strain levels. The same type of steel will be considered in the following applications to reinforced concrete by DMGTRUSS.

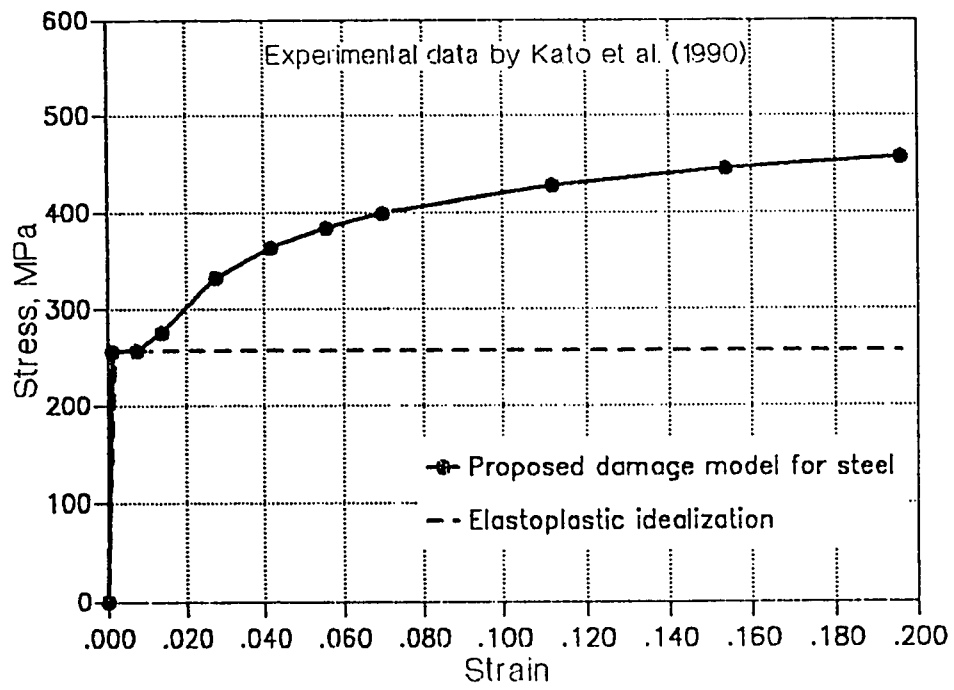


Figure 7.3 Finite element prediction of steel behavior using two idealizations

7.2.4 Tensile Loading on Reinforced Concrete

A bundle system composed of a concrete element of area A_c and a steel element of area A_s , connected in parallel, is subjected to tensile loading. Both elements are joined to the same nodal points to allow convergence at relatively high levels of deformation. The concrete element is made of Grade 40 and has the dimensions 150x150x1000 mm. The steel percentage A_s/A_c is varied in the range of 0.0 to 3.0%. For this idealization of a reinforced concrete member under tensile loading, the load-deflection curve is shown in Fig. 7.4. It is apparent that the influence of concrete softening on the total response reduces as the reinforcement ratio increases and a considerable gain in the tension carrying capacity may be achieved. For the case of plain concrete ($A_s=0.0$) the cracking load P_{cr} as predicted by the program is about 87.75 KN. This load produces a tensile stress in the concrete member equal to

$$\sigma_{cr} = \frac{P_{cr}}{A_c} = \frac{87,750}{22,500} = 3.9\text{MPa} \quad (7.2)$$

which is almost the same value of the tensile strength for the used concrete. After cracking, for all percentages of steel reinforcement, the predicted final loading carrying capacity of the system P_f tends to approach a value which produces stresses in the steel element very close to the yielding stress of the used steel σ_y .

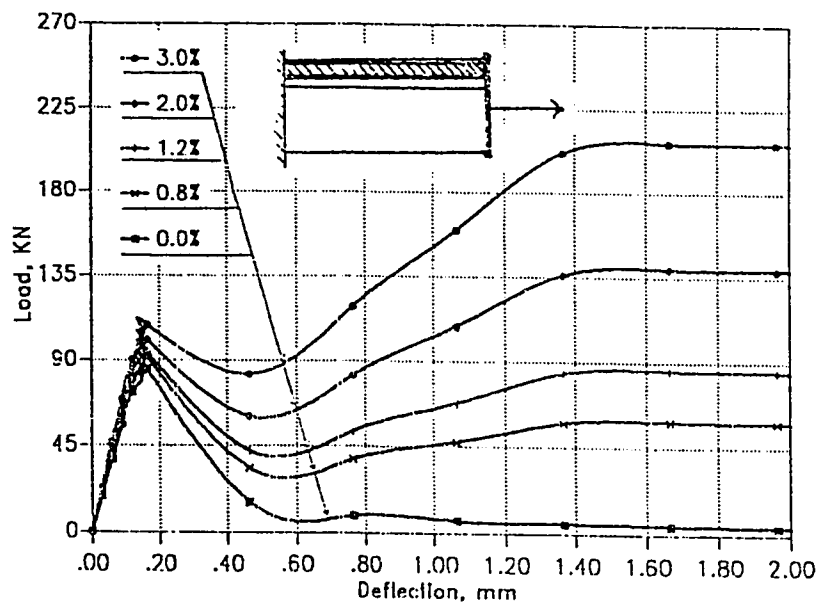


Figure 7.4 Finite element prediction for the response of reinforced concrete to uniaxial tension

7.2.5 Compressive Loading on Reinforced Concrete

A similar bundle system to that considered for tensile response of reinforced concrete is subjected to uniaxial compression. Assuming deflection controlled incrementation as before the response is plotted in Fig. 7.5 where the stress is considered as the total load per unit concrete area. It is remarkable that the trend of the behavior is mainly governed, over the whole domain, by the compressive characteristics of concrete. For the case of plain concrete ($A_s=0.0$), the ultimate load P_{ult} as predicted by the program is 900 KN. This load produces a compressive stress σ_{ult} in the concrete element, whose cross sectional area is A_c , equal to

$$\sigma_{ult} = \frac{P_{ult}}{A_c} = \frac{900,000}{22,500} = 40\text{MPa} \quad (7.3)$$

which is the same value as the characteristic strength for the used concrete.

7.3 FEATURES CAPTURED BY DMGPLSTS

Fundamental modes of loading for two dimensional structural components are investigated. These include in-plane loading of plain concrete panels under different stress paths, uniaxial tension of reinforced concrete members, perfect bond characteristics of reinforced concrete and eventually simple bending. The objective is to determine the most suitable finite element parameters for solving sophisticated

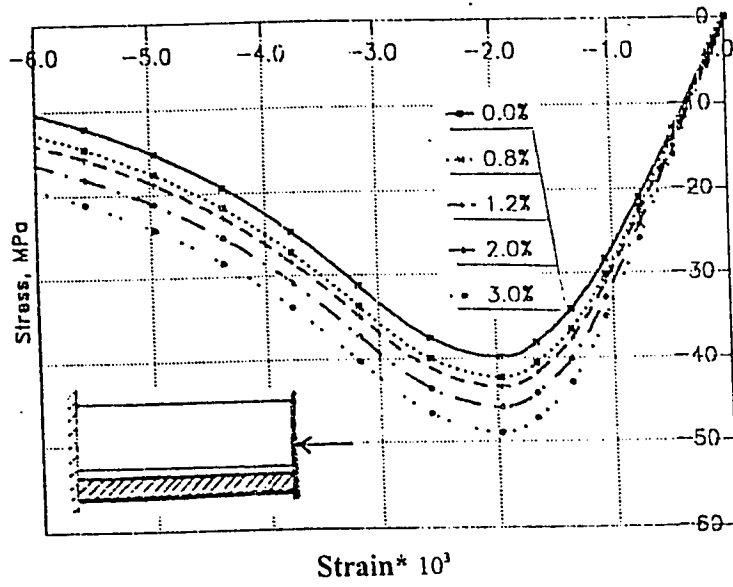
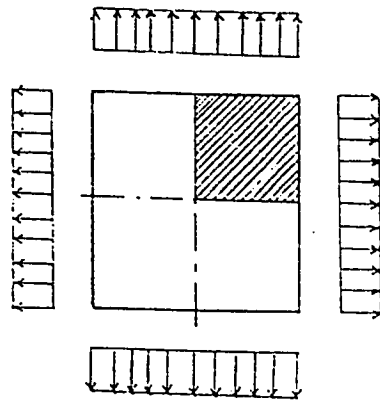


Figure 7.5 Finite element prediction for the response of reinforced concrete to uniaxial compression

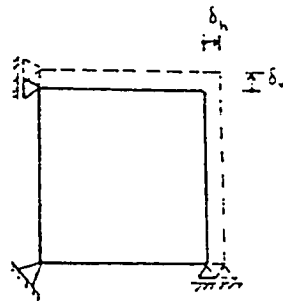
problems such as the proper nonlinear solution technique whether initial stiffness or other modified Newton-Raphson methods, the appropriate integration rule and the suitable algorithm for calculating the internal stresses and consequently the residual forces whether the proportional-secant or nonproportional-tangential algorithm. In addition, this aims at giving more understanding of the mechanical behavior of some structural problems which have not been clearly explained in the literature.

7.3.1 In-Plane Loading of Plain Concrete Panels

A unit square plain concrete panel is subjected to in-plane loading as shown in Fig. 7.6a. The grade of the concrete used is Grade 28 with Poisson's ratio of 0.18. Due to the symmetry of the problem, only one quarter of the panel is considered in the analysis as shown in Fig. 7.6b. Nodal displacements perpendicular to the axes of symmetry are restrained. To simulate strain-controlled experiments, the displacements of the two edges δ_h and δ_v are incremented in the horizontal and vertical directions, respectively. Correspondingly, uniform stresses σ_h and σ_v in the horizontal and vertical directions, respectively, are thus indirectly applied. The loading in the two directions is incremented in a proportional scheme. The algorithm developed for proportional loading using secant approach is utilized since pre-defined stress paths are followed. Several load combinations as imposed on the panel are investigated. In all cases the applied stress in a certain direction is plotted against the displacement in the associated direction, i.e. $\sigma_h - \delta_h$



(a)



(b)

Figure 7.6 Plain concrete panel considered in the analysis of the response to in-plane loading

and $\sigma_v - \delta_v$. The study cases considered herein include the following:

- (1) *Equal biaxial tension* with stress biaxiality ratio of $\beta_2 = 1$. The panel is found to withstand tensile stresses in both direction as high as the tensile strength of the concrete used. Nonlinearity of the response is quite clear with apparent softening behaviors as shown in Fig. 7.7.
- (2) *Uniaxial tension* with stress biaxiality ratio of $\beta_2 = 0$. Although the response in the vertical direction is slightly different from the corresponding in the first case in the pre-peak region, the maximum carrying capacity as well as the softening behavior are almost identical as shown in Fig. 7.8. On the other hand, the response in the horizontal direction (not plotted) coincides with the displacement axis since the applied stress in this particular direction is null.
- (3) *Equal tension-compression* such that the stress biaxiality ratio is maintained at a value of $\beta_1 = \beta_2 = -1$. The maximum absolute load carrying capacity of the panel in this case is slightly less than the tensile strength as shown in Fig. 7.9. The peak strength is about $0.92f_t'$ and the absolute displacement corresponding to the peak is about 0.61 that of the case of uni-directional tension. Strain softening in the post peak behavior can be noted in the post peak descending branch.
- (4) *Tension-compression* such that the following condition is satisfied $\sigma_v/f_t' = -\sigma_h/f_c'$ thus maintaining a stress biaxiality

ratio $\beta_1 = -0.107$. It can be noted that the peak tensile capacity is considerably reduced to almost $0.56f_t'$, while the peak compressive capacity is nearly $0.56f_c'$ as shown in Fig. 7.10. The post-peak branch is turning out to be flatter if compared with the previous cases.

(5) *Uniaxial compression* with stress biaxiality ratio of $\beta_1 = 0$. This case represents an ideal uniaxial compression in the horizontal direction as shown in Fig. 7.11. The vertical response (not plotted) is coincident with the displacement axis because the applied pressure in this particular direction is null.

(6) *Compression-compression* with stress biaxiality ratio of $\beta_1 = 1/3$. Higher load carrying capacity of about 20% in the horizontal direction is gained above the case of uniaxial compression as shown in Fig. 7.12. The optimum capacity in the vertical direction is proportional to that in the horizontal direction as attained by the stress biaxiality ratio.

(7) *Equal biaxial compression* with stress biaxiality ratio of $\beta_1 = 1$. In the current situation, the peak carrying capacity in both directions is the same and which is about 1.17 times the characteristic strength of the concrete used as shown in Fig. 7.13.

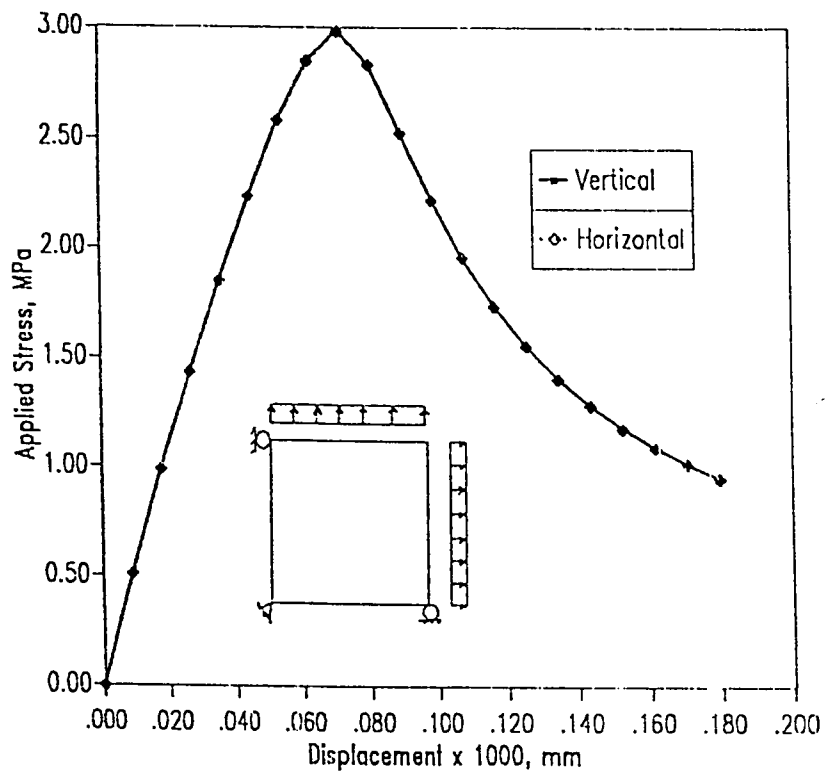


Figure 7.7 Finite element prediction for the response of plain concrete panel subjected to equal biaxial tension

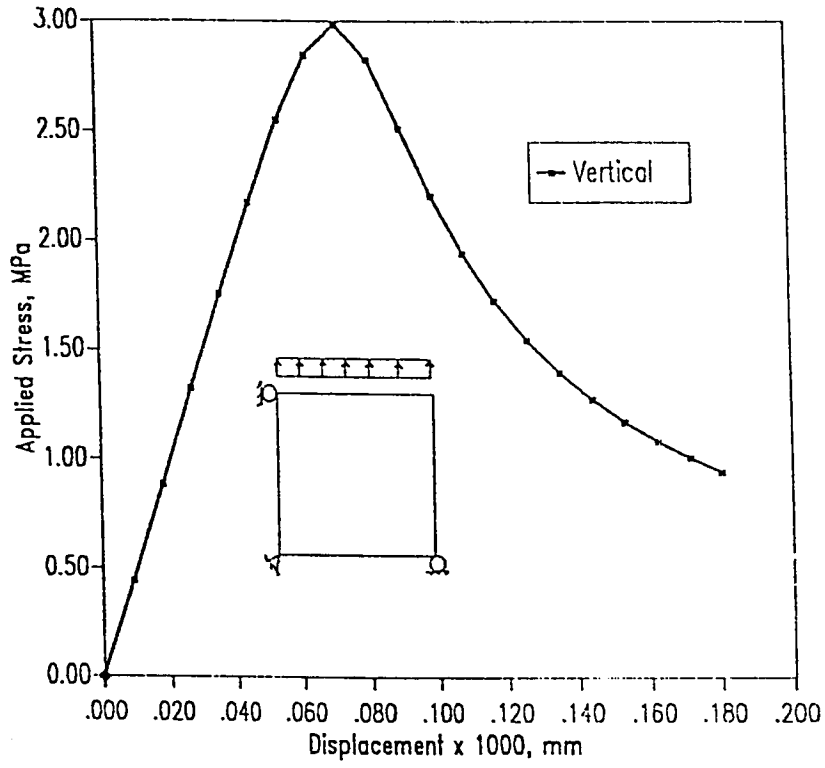


Figure 7.8 Finite element prediction for the response of plain concrete panel subjected to uniaxial tension

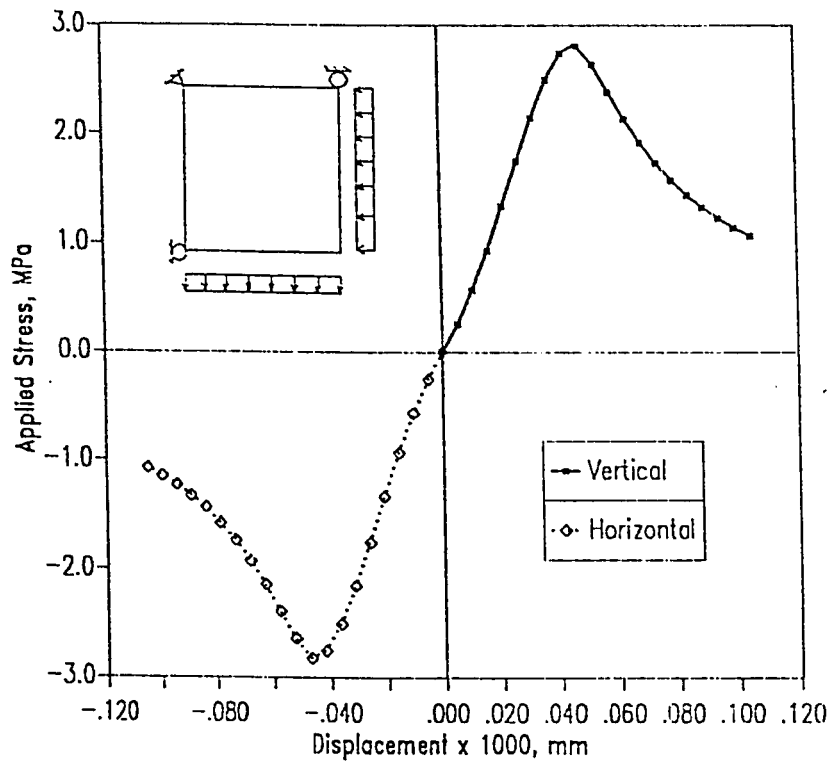


Figure 7.9 Finite element prediction for the response of plain concrete panel subjected to equal tension and compression

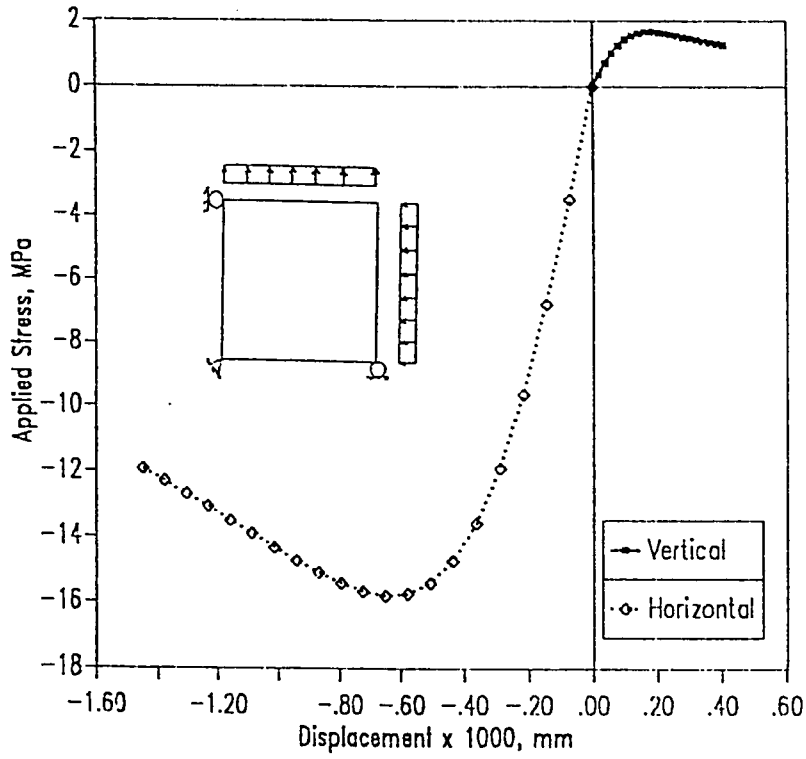


Figure 7.10 Finite element prediction for the response of plain concrete panel subjected to general tension and compression

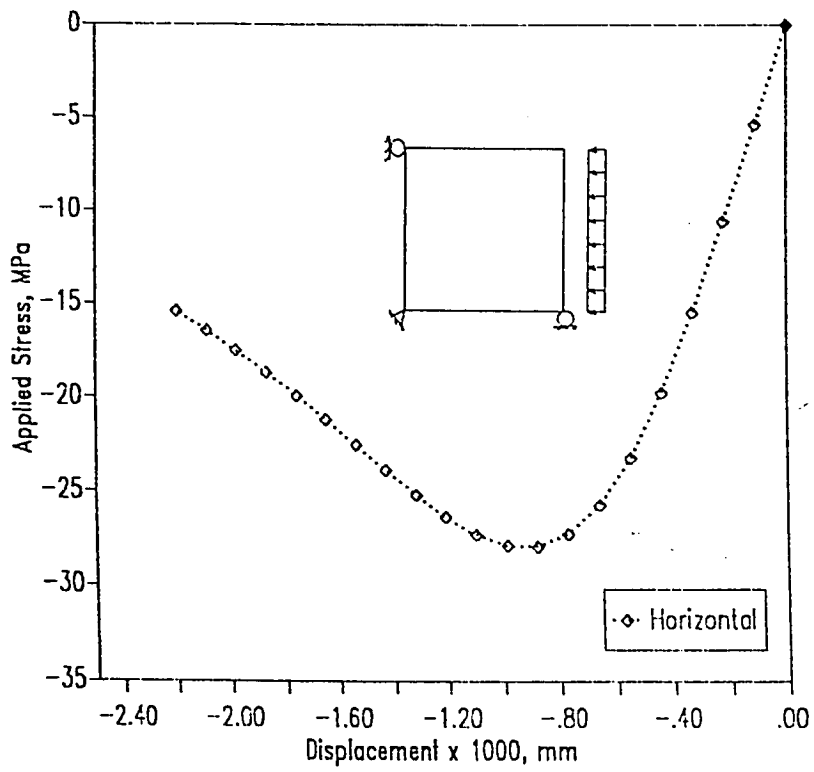


Figure 7.11 Finite element prediction for the response of plain concrete panel subjected to uniaxial compression

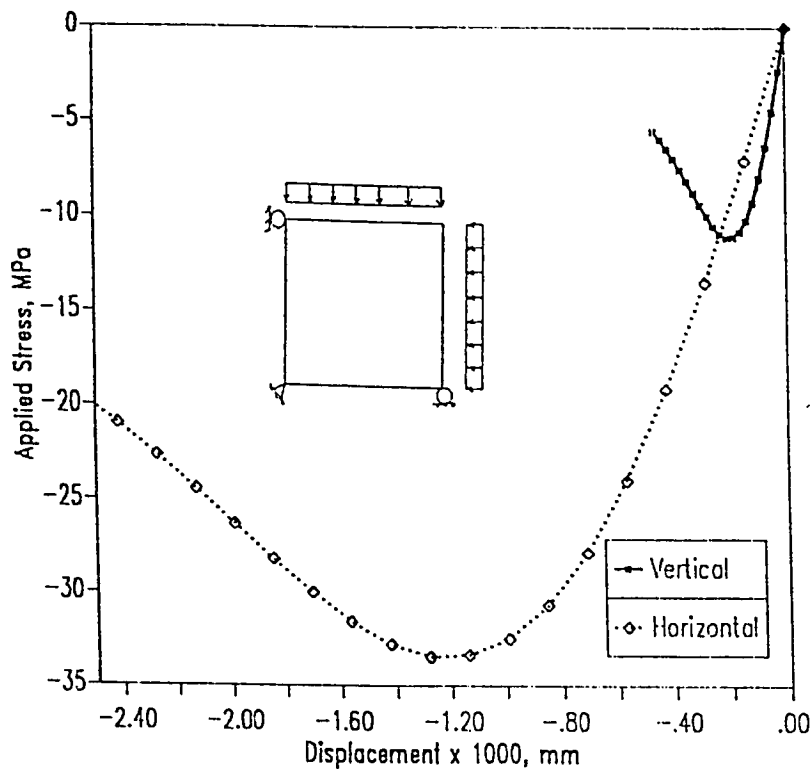


Figure 7.12 Finite element prediction for the response of plain concrete panel subjected to general biaxial compression

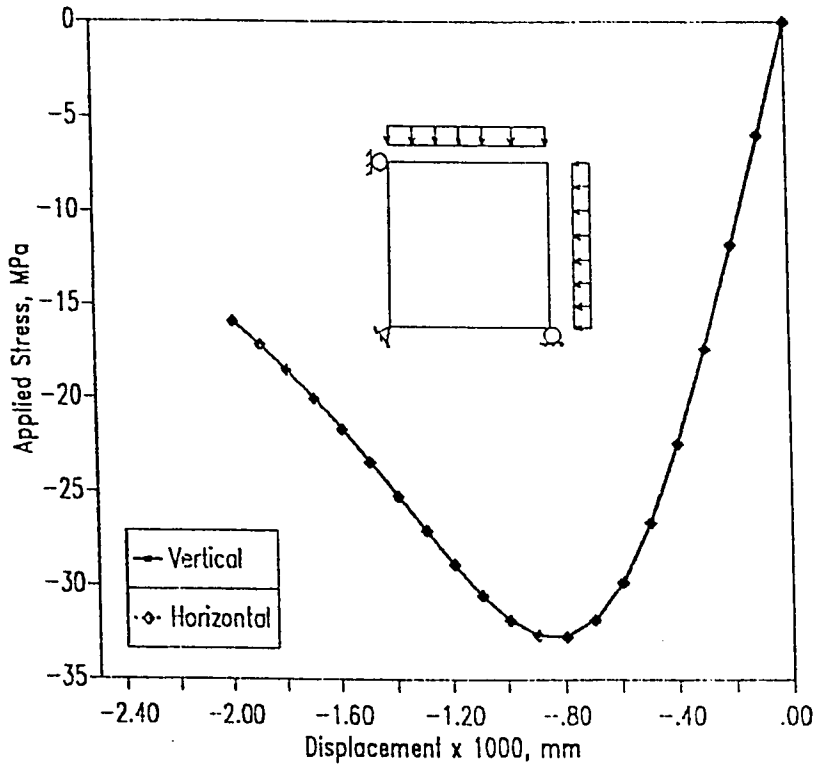


Figure 7.13 Finite element prediction for the response of plain concrete panel subjected to equal biaxial compression

7.3.2 Uniaxial Tension on Reinforced Concrete

Existence of reinforcement inside tensioned concrete members disturbs, in general, uniformity of the internal stresses at the inner material points even though the external stress field is uniform. This constitutes the basic difference from the one-dimensional idealization of the problem where the internal stresses or the strains are assumed to be uniform at all points in the cross section as in the customary practice for the design procedure of codes' provisions. In order to have more insight about this phenomenon, a concrete member of proportions $L/h=L/b=2$ is centrally reinforced with steel SS41 of an area of 4% of that of the concrete. For simplicity, the total length of the member is taken as unity. Four meshes, shown in Fig. 7.14a over one quarter of the member, are used in this investigation:

- (1) *mesh #1* : with total of nine nodes, four 4-noded concrete elements and two 2-noded steel elements.
- (2) *mesh #2* : with total of 21 node, four 8-noded concrete elements and two 3-noded steel elements.
- (3) *mesh #3* : with total of 39 node, eight 8-noded concrete elements and four 3-noded steel elements.
- (4) *mesh #4* : with total of 37 node, eight 8-noded concrete elements and two 3-noded steel elements.

Having imposed an external uniform tensile loading of magnitude of 3.2 MPa, it is found that convergence is impossible at load factor very close to one as shown in Fig. 7.15. This is due to the fact that when the concrete cracks there is no mean to direct the stress trajectories to

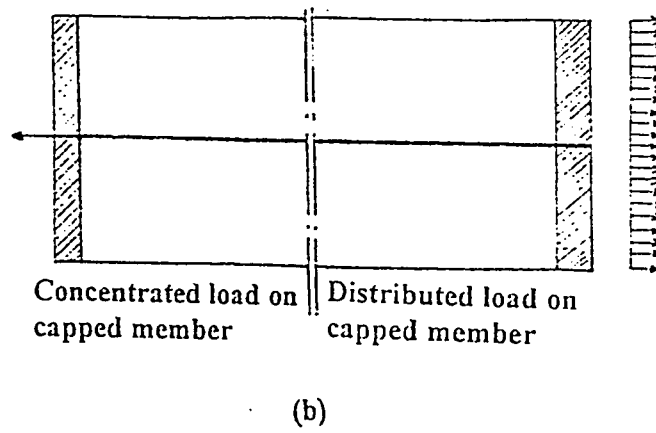
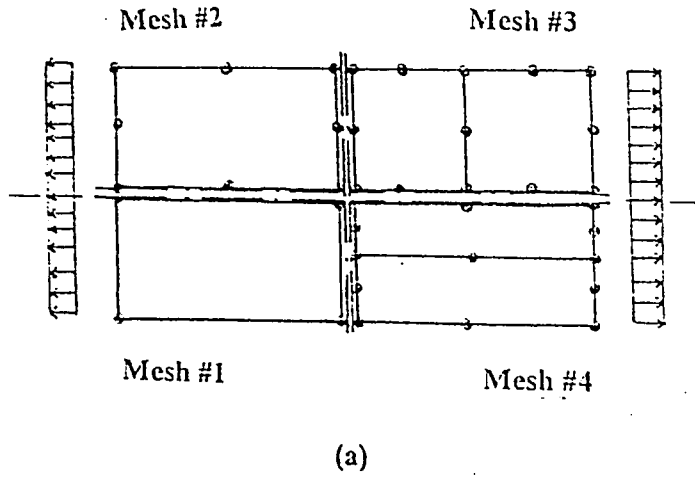


Figure 7.14 Reinforced concrete member under uniaxial tension:
 (a) mesh discretization of uncapped member, and
 (d) loading on capped member

the reinforcement in order to carry the load and thus the whole member fails. Numerically speaking, the residual forces in the concrete elements are no longer resisted since strain softening is taking place at the highly strained sampling points. Mesh #1 shows a slight difference from the other meshes utilizing 8-noded elements which give almost the same stiffness characteristics as shown in Fig. 7.15.

A closer scrutiny on the behavior of the member discretized with 8-noded elements shows uniformity of internal stresses in concrete close to the centerline of the member as shown in Fig. 7.16a. The stress distribution tends to be nonuniform close to the loaded edge as shown in Fig. 7.16b. This is believed to be attributed to the nonuniformity of the displacement distribution which is illustrated for the loaded edge in Fig. 7.16c. To investigate the stress distribution in the longitudinal direction, rather than along certain cross section, four different elevations inside the concrete from the top surface towards the centerline are considered as shown in Fig. 7.16d. It can be noticed that the internal stress in concrete is equal to the imposed tension at the loaded edges then decreases as the centerline is approached.

The internal stresses in the reinforcement increase with increasing the load increment. Mesh #1 with 4-noded elements gives almost constant stress level, if slightly departed from the loaded edge. Similar trend can be noticed for other meshes with 8-noded elements but with a drop in the stress level towards the loaded edge. This is shown for four load increments in Fig. 7.16e.

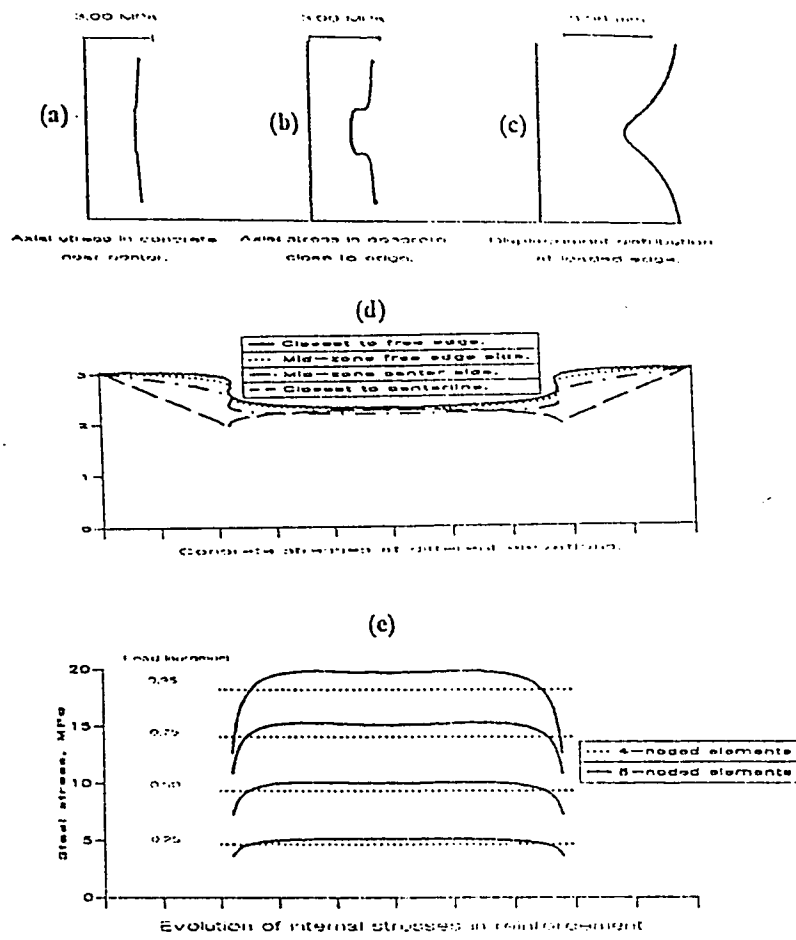


Figure 7.15 Finite element prediction for the distributions of displacement and stress in both concrete and steel for the uncapped sample

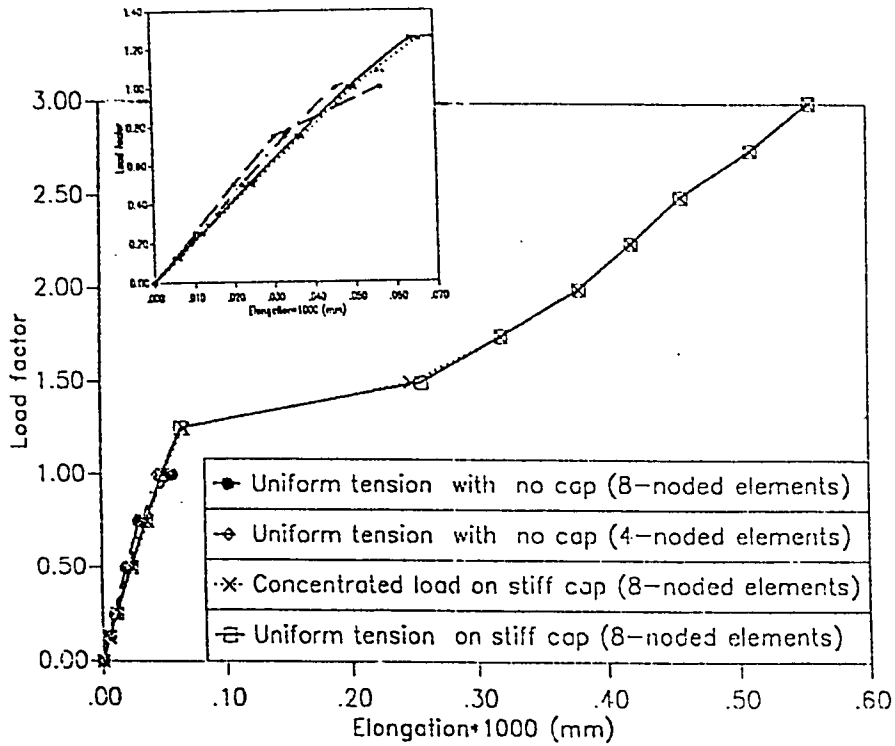


Figure 7.16 Finite element prediction for the load-elongation diagram of reinforced concrete under uniaxial tension for various cases

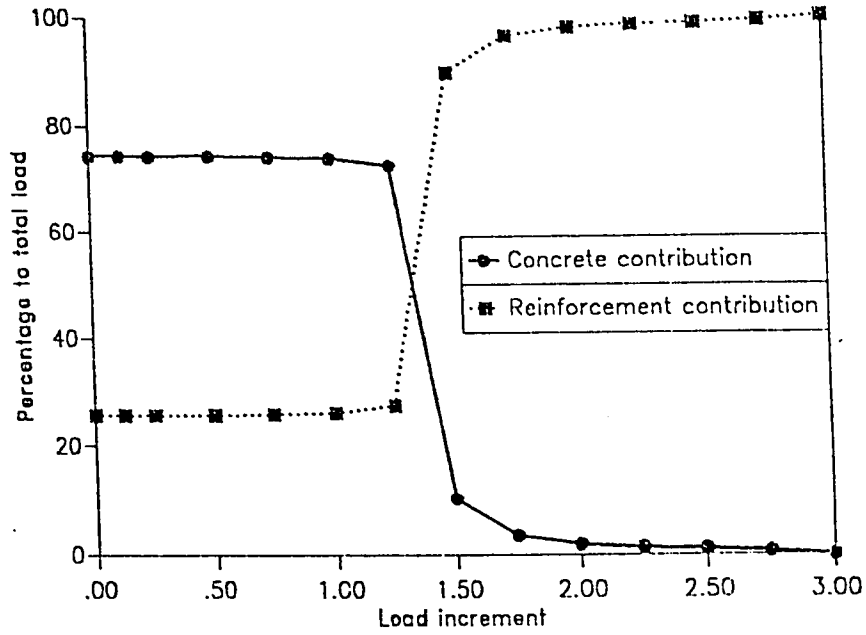


Figure 7.17 Finite element prediction for the evolution of the load carrying capacity of both concrete and steel for the capped sample

According to the existing stress status, material points close to the corners of the member approaches the tensile strength prior to other points. Consequently the damage level is higher and the cracking initiates from the upper and lower surfaces near the loaded edges then propagates towards the centerline. The overall behavior thus resembles in many aspects testing specimens with flexible plattens under stress-controlled experimentation.

In practice, as the concrete softens, most of the load tends to be carried by the reinforcement. To achieve higher loading level the member is equipped with stiff caps on the loaded edges. This is being simulated by using concrete elements of higher stiffness. Mesh #2 was used in the analysis. Two cases of loading are considered as shown in Fig. 7.14b: (1) concentrated load applied at the reinforcement level and (2) uniform external tension. In both cases, the internal stress inside the concrete along all cross sections is developed in a uniform manner and a considerably higher load carrying capacity is achieved than the case of uncapped member as shown in Fig. 7.15. This can be thought of in terms of providing sound means (cap) for translating the load to the reinforcement as the damage level in the concrete increases through uniform displacement field. This is supported by the close predictions of the two loading cases for the load-deflection diagram (Fig. 7.15). Therefore, in this manner testing with stiff plattens under strain-controlled experimentation is being simulated.

At low load levels the concrete is noticed to carry more load relative to the reinforcement. However, the concrete contribution slightly

decreases due to concrete nonlinearity in the pre-peak tensile behavior up to load increments close to unity as shown in Fig. 7.17. Due to the softening characteristics of concrete in the post-peak tensile behavior, gradual reduction of the load carrying capacity of concrete can be noticed for the capped member. As a result, the contribution of reinforcement to the overall carrying capacity builds up until all the load is completely taken by the steel at load increment of about 3.

7.3.3 Perfect Bond Characteristics of Reinforced Concrete

A specimen similar to that used for the analysis of uniaxial tension of uncapped reinforced concrete member is considered to study the characteristics of perfect bond as shown in Fig. 7.18a. A concentrated load is directly applied to the steel rebar along its axis. The two-dimensional idealization of the problem is shown in Fig. 7.18b. Only one quarter of the problem is considered in the numerical analysis due to symmetry consideration. The finite element mesh is shown in Fig. 7.18c. Twenty one 8-noded concrete elements along with six 3-noded steel elements thus constituting sixty seven nodal point are generated. The overall response is compared with the load carrying capacity of the steel rebar alone, as shown in Fig. 7.19, thus indicating the effect of tension stiffening. The load-displacement curve can be described to consist mainly of two parts. The first part represents the pre-cracking response whereas the other reflects the post-cracking behavior.

Prior to the onset of cracking the results obtained by the two algorithms appear to be identical (Fig. 7.19). The predicted cracking

load is much less than the corresponding value predicted for the same member but with stiff cap as discussed before through the analysis of uniaxial tension of reinforced concrete. This is due to the uniformity of the stress distribution inside the concrete introduced by the existence of the stiff cap and therefore the behavior of the capped and uncapped samples are entirely different.

With the virtue of the concrete/steel bond the internal stress in the reinforcement drops abruptly as one moves towards the interior of the specimen away from the vicinity of the loaded edges and then decreases gradually till reaches its least value at the centerline of the member as shown in Fig. 7.18f. At the axis of symmetry the internal stress in the reinforcement is found to be almost one quarter that of the unbonded bar (free end). The contour lines for the principal tensile stresses in concrete σ_c are drawn in Fig. 7.18e. This, of course, reflects the level of damage just before cracking. High stress concentration exists in the vicinity of the free end. At all cross sections the stress has its highest value next to the reinforcement and decreases through the concrete cover. It is interesting to point out that most of the sampling points are noted to be stressed almost uniaxially in the principal plane where the orientation of the major direction at the sampling points is depicted in Fig. 7.18d. There exists in the vicinity of the loaded edges considerable distortion which allows for development of shear stresses, in the X-Y coordinate system, in concrete (also evidenced by the high gradient of reinforcement stress). This in turn leads to inclined principal directions, implying manifestation of inclined cracks in

concrete adjacent to reinforcement that are known to occur in specimens tested in created zones of high flexural bond. Due to the relatively sharp gradient in the internal stress in concrete near the edges, the cracking load is expected to be influenced by the location of the sampling points, in this region, relative to the point of steel insert and thus affected by the mesh discretization. This is in contrast to the case of capped member where the response is independent of the mesh configuration.

As soon as the tensile level in the concrete reaches its peak strength value, a softer response of the system is noted to occur as shown in Fig. 7.19. With further loading the zone of highest stress concentration invades the concrete towards the centerline of the member leaving softened concrete at the rebar. The cracking thus starts in the concrete in the region adjacent to the rebar and propagates radially in its vicinity. This zone of high concrete shear or high gradient of reinforcement stress is noted to shift towards the interior as concrete begins the process of cracking from the loaded edge inwards. This leads to the formation of a damaged concrete zone of reduced stiffness in the surrounding of the reinforcement. This behavior, therefore, analogizes an interface layer in the bond-slip theory. Such a conclusion supports the hypothesis of pseudo-slip presented by Mazars (1984). After full cracking of concrete the entire load is eventually carried solely by the steel rebar and the tension stiffening effect is no longer influencing the response as shown in Fig. 7.19.

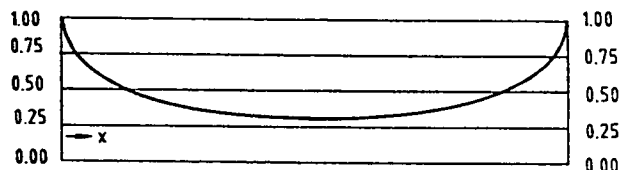
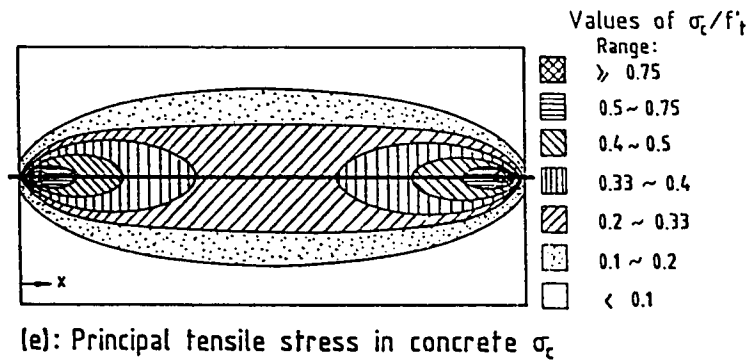
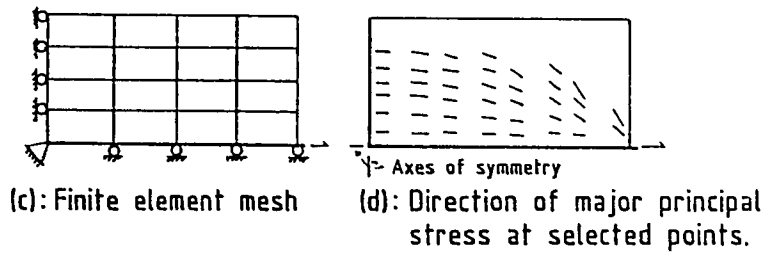
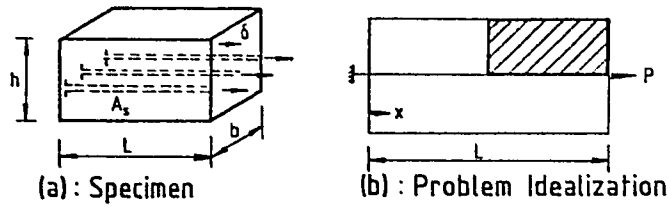


Figure 7.18 Distribution of stresses in concrete and reinforcement prior to first cracking for the bond problem

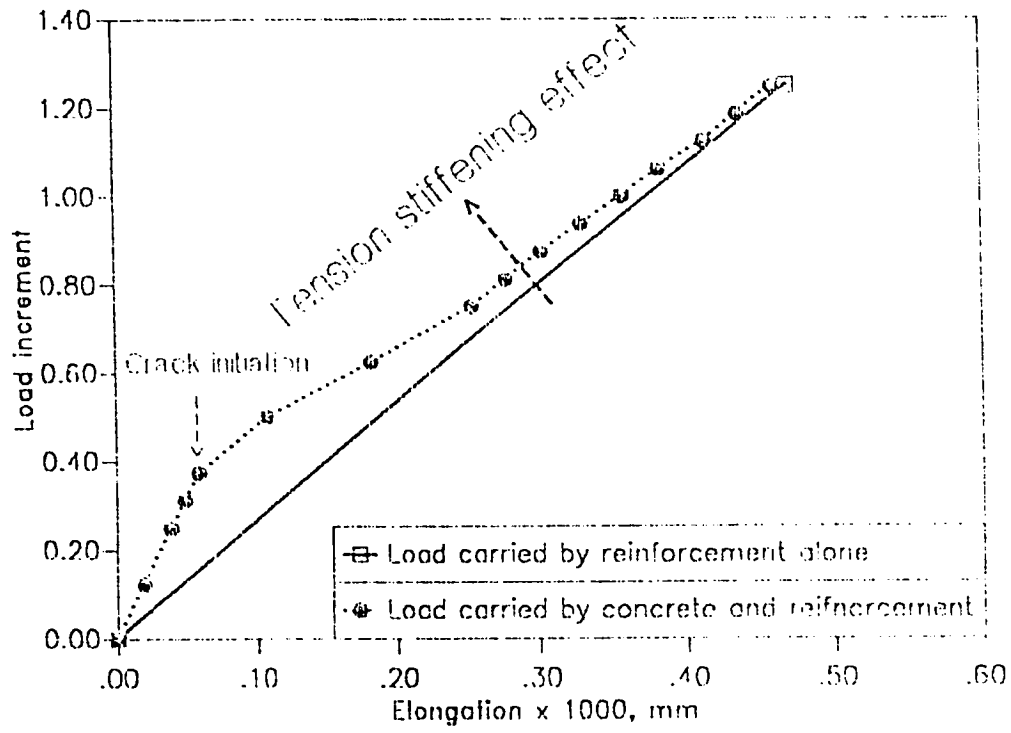


Figure 7.19 Effect of tension stiffening of concrete

7.3.4 Simple Bending

A simply supported plain concrete square panel is subjected to linearly varying stress field across the depth as shown in Fig. 7.20a. The top and bottom stresses are set equal but with negative sign to simulate the case of pure bending. Another study is conducted by providing steel reinforcement to the extremely tensioned top fiber as shown in Fig. 7.20b. Concrete grade 28 and structural steel SM50 are used as the constituent materials involved in the problem.

In the beginning a simplified single layered discretization for concrete is prepared using 4-noded element as shown in Fig. 7.20c. Various nonlinear solution techniques are tested using 2X2 and 3X3 Gauss-legendre integration rules. For 2X2 integration rule, all methods are found to yield almost the same peak external stress required to bring the internal stress at the upper sampling points to the tensile strength.

Updating stiffness in each iteration is noted to exhibit the most rapid convergence then updating the stiffness in the first and second iterations of each load increment. However, negative stiffness is sometimes encountered especially for the 3X3 rule when the stiffness is updated. Therefore, the initial stiffness technique for nonlinear solution is recommended for the more sophisticated problems. It is also noted that the 4-noded element develops unrealistic shear stresses at the sampling points although the support reactions are null and an ideal situation of pure bending exists. This necessitates the use of higher order elements for similar problems with nonuniform internal stress

field.

Serendipity and Lagrangian elements are then used for the concrete layer as shown in Fig. 7.20d. Similar to the problem of uniaxial tension of uncapped member, the carrying capacity is controlled by concrete failure where the solution for the unreinforced and reinforced members does not converge after reaching the tensile strength at the outer sampling points. Both elements are noted to provide nearly the same results without any unexpected shear stress.

The integration rule is found to affect the predictions of the nonlinear solution. Employment of 2X2 integration rule is noted to allow for imposing higher external pressure. This is due to the fact that the solution is controlled by the stress status at the sampling points. These points are located closer to the extreme fibers in the case of the 3X3 integration rule. Thus the external load required to produce the same stress level at the sampling points for the two rules is different. This is schematically shown in Fig. 7.21 for linearly imposed load which is required to bring the stress at the sampling points to the tensile strength. This leads to the recommendation that, especially for unreinforced beams where the failure is governed by this criterion, finer mesh should be used near the extreme fibers. On the other hand, for reinforced beams where the steel carries, in general, most of the internal tensile stress resultant subsequent to concrete cracking the concrete cover often governs the mesh discretization.

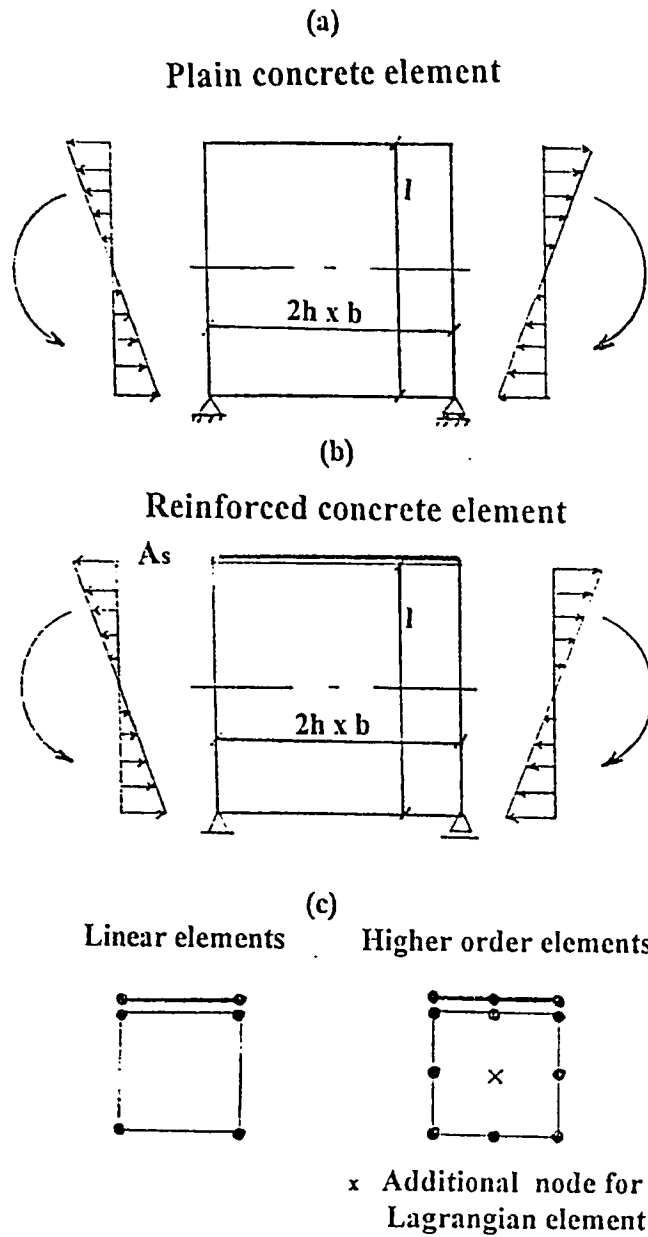


Figure 7.20 Simplified single element discretization for the bending problem: (a) plain concrete, (b) reinforced concrete, (c) Different element types used

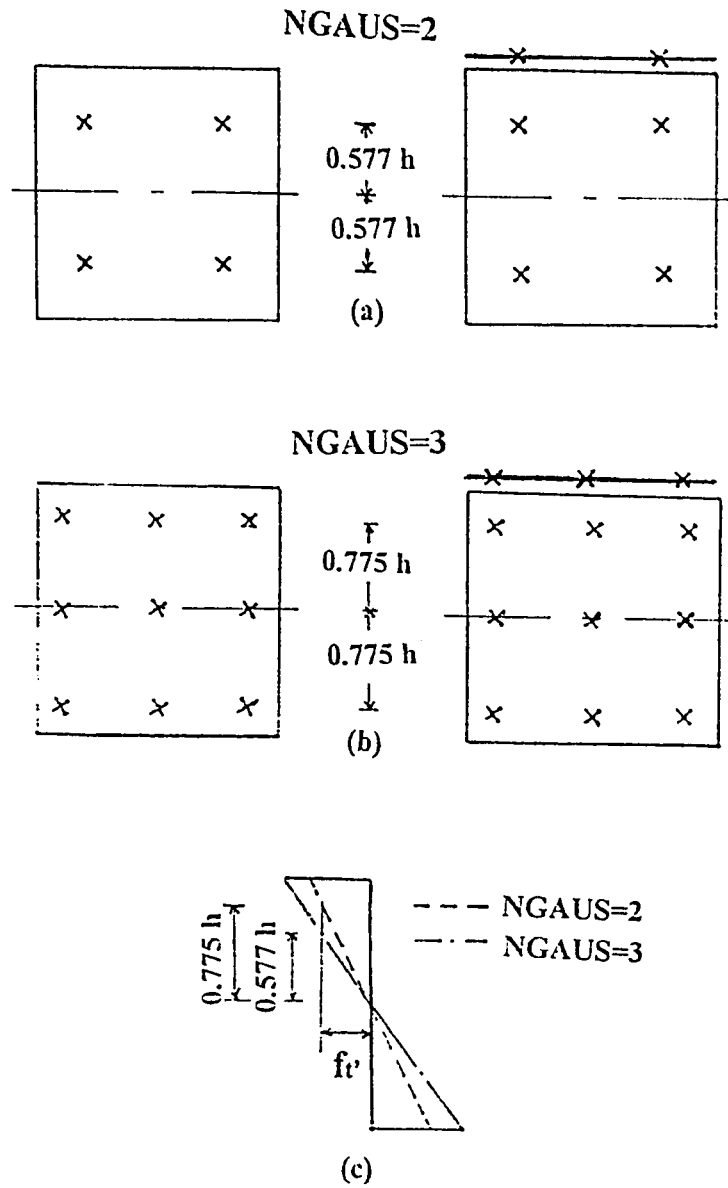


Figure 7.21 Investigating the effect of the integration rule on the cracking load: (a) 2X2 rule, (b) 3X3 rule, (c) an assumed linear stress distribution

7.4 COMPARISON WITH PREVIOUS WORK

This part represents the verification phase of the program DMGPLSTS as applied to practical structural problems. The predictions obtained from the current study is compared with the finite element solution undertaken by other investigators and in some of these problems the results are further compared against the available experimental data reported in the literature. In the following, three- as well as four-point loading of plain and reinforced concrete beams with and without shear reinforcement are analysed and the steel/concrete bond problem is finally solved.

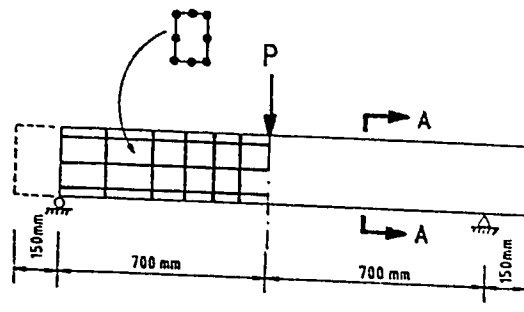
7.4.1 Plain Concrete Beams

A simply supported plain concrete beam, similar to that tested by Mazars (1984), of cross sectional dimensions of 220mm and 150 mm for the height and breadth, respectively, is considered in this investigation. The beam has a span of 1400 mm with two overhanging cantilevers of 20 mm length as schematically shown in Fig. 7.22a. The grade of the concrete used is 28 MPa and a Poisson's ratio of 0.18 is considered. Three point loading is studied where a concentrated load is imposed along the centerline of the beam. Because of the symmetry, only one half of the beam is analysed. The displacement perpendicular to the axis of symmetry is restrained. Numerical integration by 2X2 rule is employed and the initial stiffness method is used for the nonlinear solution. The problem is solved at first using linear elasticity. Similar finite element mesh to that was pointed out by Ziraba (1993) to yield

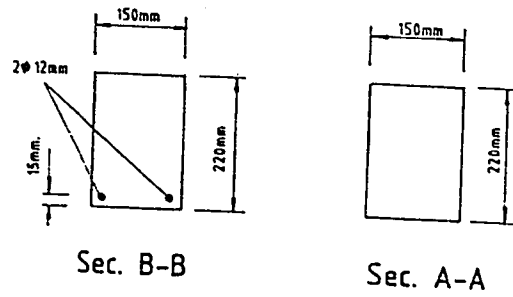
satisfactory results is used. The mesh consists of 93 nodal points and 24 8-noded concrete elements. Through the elastic solution of the problem the following three remarkable points have been noticed:

- (1) the support condition whether hinged or roller affects the results tremendously. When only half of the beam is solved taking symmetry into account, a hinged support develops high horizontal reaction which does not exist in reality.
- (2) the elevation of the point of action of the concentrated load influences the symmetry of the stress distribution along any vertical plane.
- (3) the central deflection and hence the stiffness of the system is sensitive to the elastic modulus.

With these in mind, the problem is solved considering a roller support and the load to be applied at the top fiber of centerline with similar initial modulus as that used by Mazars (1984). Nonlinear solution by the proportional-secant algorithm is carried out. The response is shown in Fig. 7.23 which appears to be in good agreement with the numerical solution as well as the experimental results of Mazars (1984). Sudden failure is predicted after relatively long linear behavior. This happens when the maximum tensile stress at the sampling points closer to the bottom fiber approaches the tensile strength of the concrete.

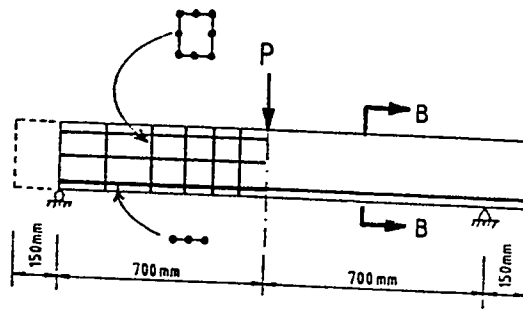


(a) Plain Concrete Beam



Sec. B-B

Sec. A-A



(b) Reinforced Concrete Beam

Figure 7.22 Three-point loading on beams considered for comparison with Mazars' work (1984): (a) plain concrete, (b) reinforced concrete

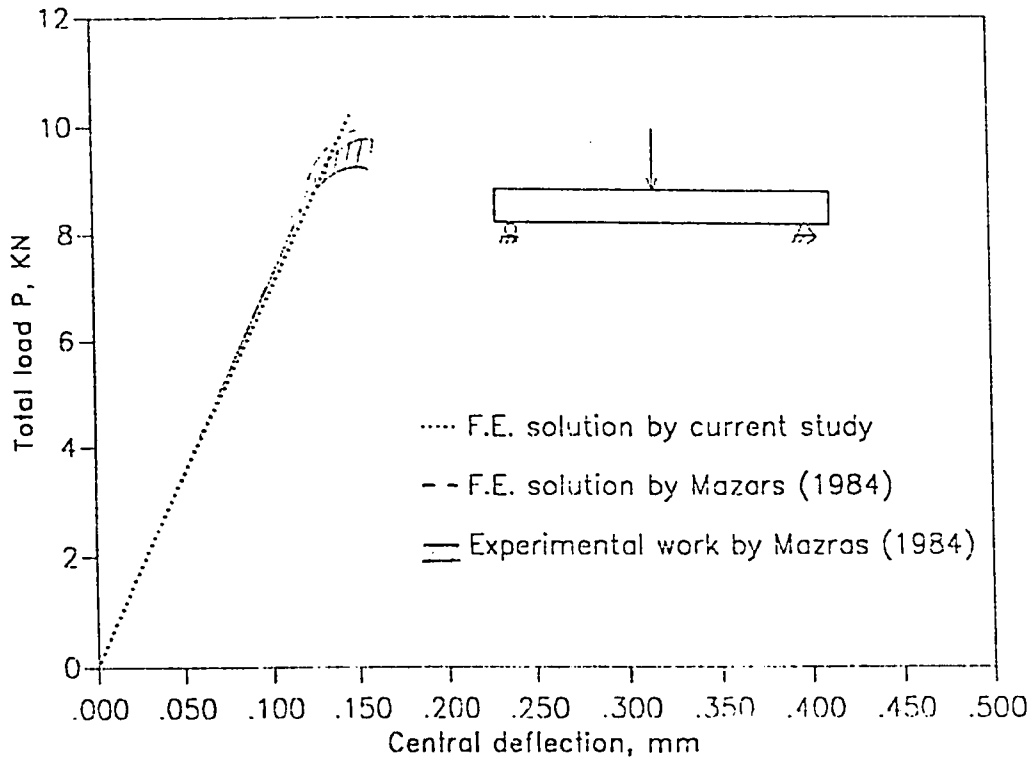


Figure 7.23 Comparison of the finite element prediction for the response of plain concrete beam with Mazars' work (1984)

7.4.2 Reinforced Concrete Beams without Shear Reinforcement

The same beam described in the analysis of three point loading of plain concrete beams is considered herein but with structural steel SS41 reinforcement of $2\phi 12$ located 15 mm above the bottom fiber of the beam as shown in Fig. 7.22b. The α factor for yielding parameters of the steel is taken as 1.15. The nonproportional-tangential algorithm along with the initial stiffness technique using 2X2 numerical integration rule is employed for the analysis. Only one half of the beam is considered due to the symmetry about the centerline of the beam. Nodal displacements normal to the axis of symmetry are restrained. The generated mesh consists of 93 nodal points and 30 8-noded concrete elements and 6 3-noded steel elements. The concentrated load is applied on the top fiber along the axis of symmetry and the deflection is monitored at the bottom fiber along the same section.

The central stiffness in the vertical direction as presented by the plot of the load-deflection is shown in Fig. 7.24. The behaviour can be described as initially quasi-linear up to load level of about 14 KN and then nonlinear. The predictions obtained from the current study are compared with the finite element calculations as well the experimental data reported by Mazars (1984). The range of experimentation illustrated in Fig. 7.24 represents a series of three mechanical testings. It is clear that the central deflection estimated by DMGPLSTS is in a very close agreement with Mazars' work (1984).

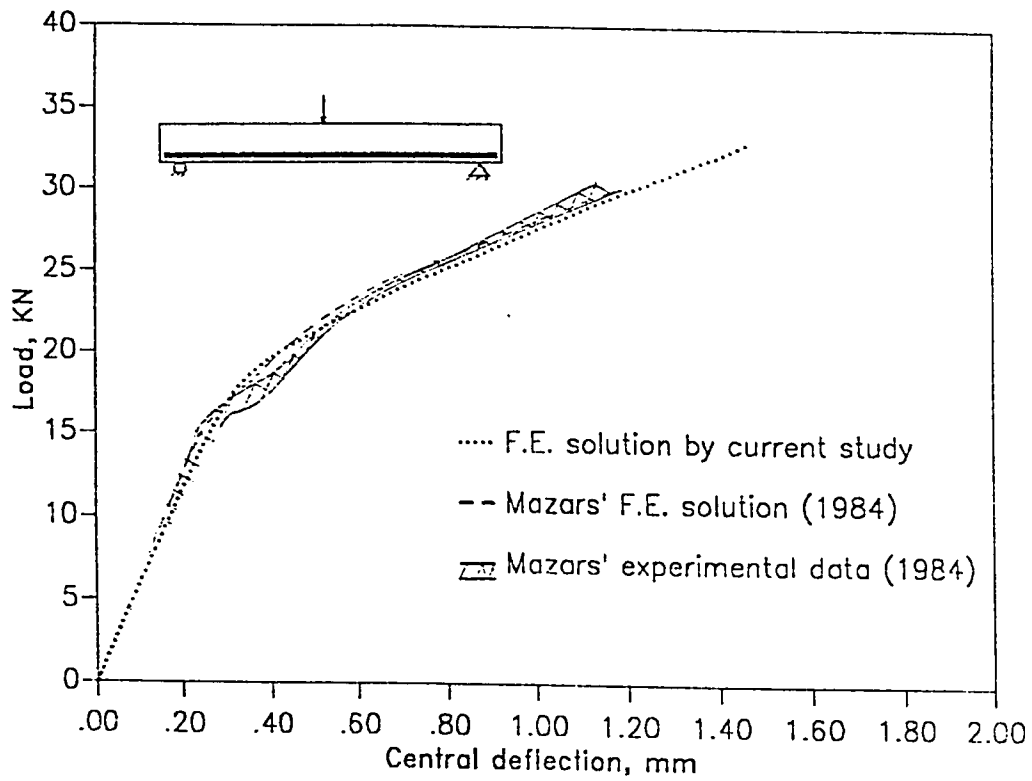


Figure 7.24 Comparison of the finite element prediction for the response of reinforced concrete beam with Mazars' work (1984)

7.4.3 Reinforced Concrete Beams with Shear Reinforcement

Four-point loading of simply supported beam with shear reinforcement over the shear span is considered. Two amounts of tension reinforcement are investigated one at a time. The first is an under-reinforced beam designated as URB1 with longitudinal main steel of $2\phi 10\text{mm}$ whereas the other is an over-reinforced beam designated as ORB1 with main steel of $4\phi 16\text{mm}$. The free span is 2250 mm out of 2400 mm total length of the beam. The shear span is one third the free span; i.e. 750 mm. The cross sectional dimensions are 100 mm X 150 mm with concrete cover of 20 mm and 31 mm for URB1 and ORB1, respectively. Compression steel serving as stirrups hanger of $2\phi 8\text{mm}$ and shear reinforcement of $\phi 6\text{mm}@70\text{mm c.c.}$ are used as sketched in Fig. 7.25a. These beams were experimentally tested to failure by Jones et al. (1982) in previous study. High strength concrete of cube strength 63.4 MPa (which is equivalent to approximately 53.89 MPa cylinder strength) is considered. Steel of diameter 10 mm has a 0.2% proof (considered herein as the yielding) stress of 530 MPa with ultimate stress of 597 MPa. On the other hand, steel of diameter 16 mm has a 0.2% proof stress of 487.5 MPa with an ultimate stress of 721 MPa. Both steel types have an elastic modulus of 200 GPa. The finite element mesh which consists of 247 nodal point with 68 8-noded concrete elements and 59 3-noded steel elements is shown in Fig. 7.25b.

The finite element solution of the under-reinforced beam URB1 is noted to be in a very close agreement with the finite element solution of Yasin Ziraba (1993) as plotted in Fig. 7.26. Both solutions show

slightly stiffer response relative to the experimental findings. However, the predicted maximum loads as characterized by steel yielding are found to be very close: 27.0 KN, 29.0 KN and 28.1 KN by the current F.E. solution, Ziraba's F.E. solution (1993) and experimentally by Jones et al. (1982), respectively. On the other hand, The ultimate load capacity calculated by the strength theory according the ACI code is estimated to be 26.83 KN (Ziraba, 1993). It is remarkable that Ziraba (1993) employed the same finite element mesh but using 9-noded lagrangian concrete elements with an additional 34 six-noded main steel/concrete interface elements, thus comprising 385 nodal points. Nonlinear fracture mechanics along with isotropic hardening plasticity was used for modelling concrete behavior in both tension and compression, respectively. Apart from the steel properties, his program required to input 7 properties for concrete and another 5 properties for the interface.

The finite element solution for the over-reinforced beam ORB1 is found to be in a very close agreement with the experimental data as illustrated in Fig. 7.26. The peak capacity of the beam is characterized by concrete crushing in the free of stirrups central region of the beam where the finite element solution failed to converge. The predicted maximum load is found to be 66.0 KN. On the other hand, the maximum experimental load was reported to be 67.5 KN. The response of the over-reinforced beam is noted to be stiffer than the under-reinforced beam. Although ORB1 sustained almost 2.5 the maximum load of URB1, over-reinforced beams are, in general, not recommended for practical use because of their sudden failure.

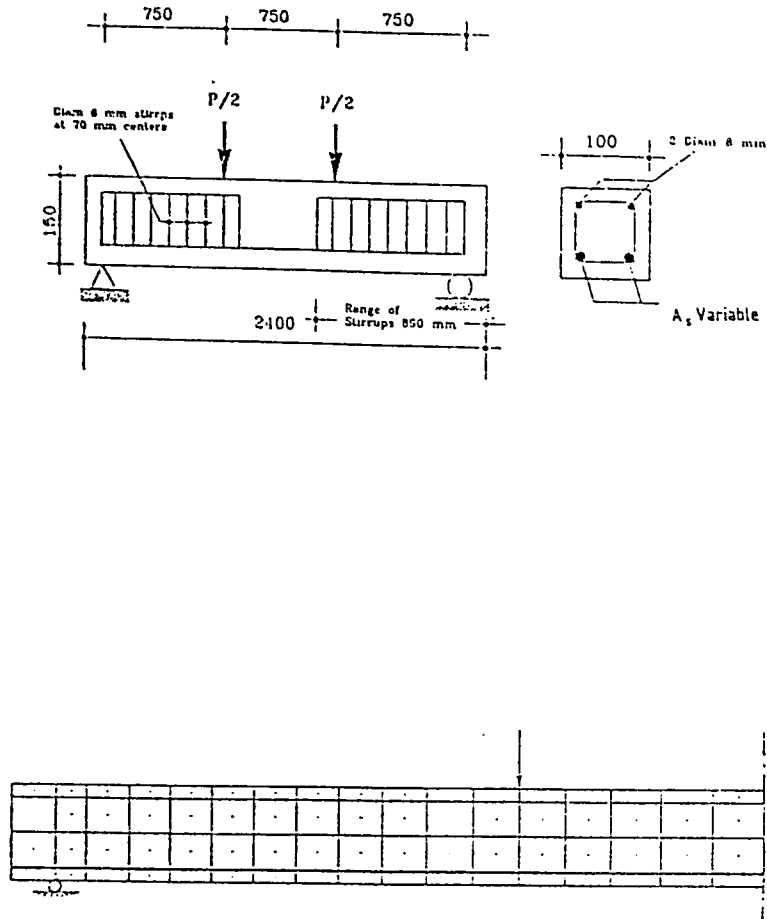


Figure 7.25 Four-point loading on beams without shear reinforcement: (a) configuration, (b) finite element mesh

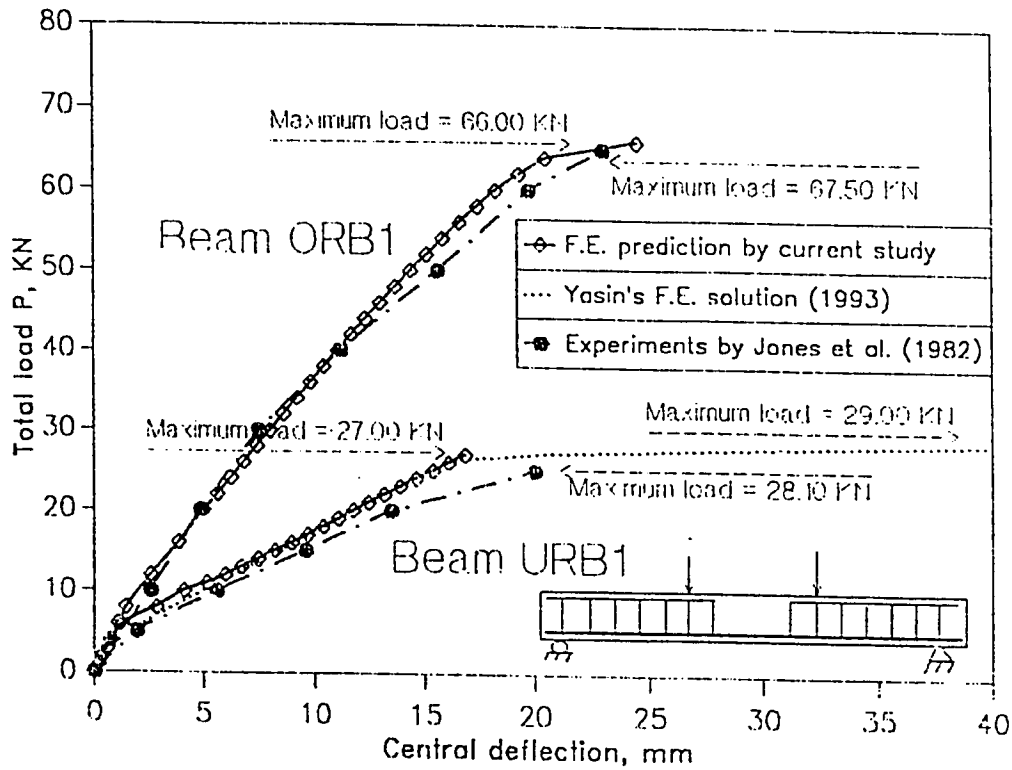


Figure 7.26 Comparison of the finite element prediction for the response of reinforced concrete beams without shear reinforcement against previous work

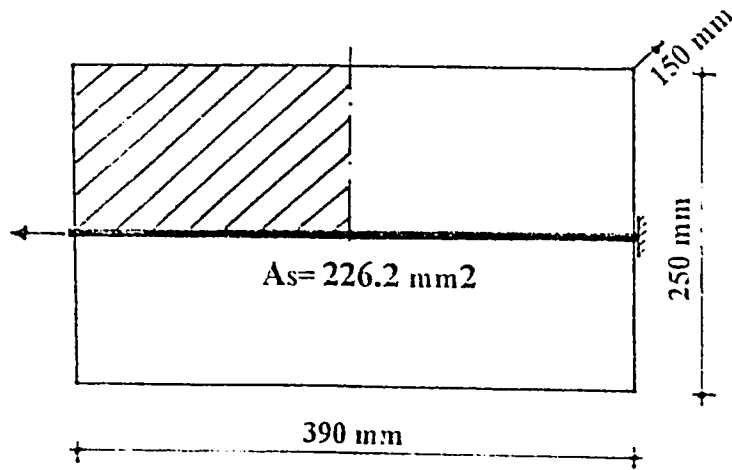
7.4.4 Steel/Concrete Bond Problem

The structural component shown in Fig. 7.27a is considered for the analysis of the problem of steel/concrete bond. The dimensions of the concrete block are 390 mm, 250mm and 150mm for the length, height and breadth, respectively. The member is reinforced by a steel layer in the middle whose area is equivalent to 2 ϕ 12 mm rebars. The concrete grade is 28 while the reinforcement type is structural steel SS41. The more general algorithm for nonproportional loading with tangential relations is utilized for the numerical solution. The finite element mesh for one quarter of the mesh is shown in Fig. 7.27b. It is a fine mesh that consists of 501 nodes and 150 8-noded concrete elements and 15 3-noded steel elements. The nonlinear solution is found to be very expensive since it necessitates long execution time especially small loading incremental intervals are needed for the convergence process. On the other hand, it is worth mentioning that Mazars' mesh (1984) consisted of 891 node with 1664 3-noded constant strain triangular elements for concrete and 26 steel elements.

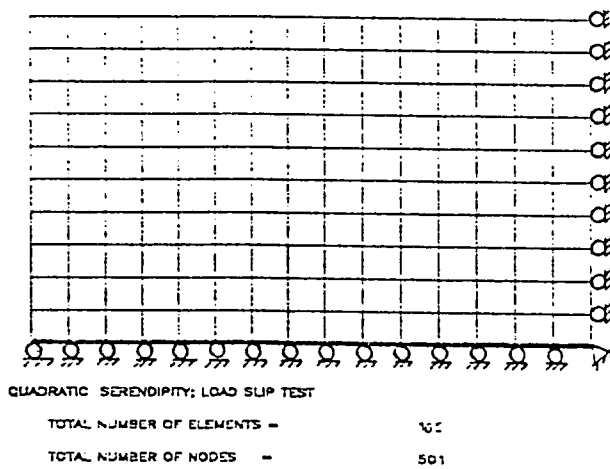
The load-extension diagram is drawn for the two finite element solutions as shown in Fig. 7.28. The predictions obtained by the canonical model, although with fewer elements, is noted to be in a very close agreement with those reported by Mazars (1984) using an extremely fine mesh. Nonlinearity of the behavior is found to commence at relatively low load levels. The trend of the curve predicted in the current study eventually gets flatter due to the steel yielding.

With respect to the cracking characteristics, a highly damaged concrete zone is formed in the surroundings to the reinforcement. The damage evolution is shown in Fig. 7.29a. It can be noted that as the load level increases the damage zone spreads towards the axis of symmetry. At high stages of loading, prior to failure, the damage zone tends to penetrate the concrete cover further at discrete locations. The corresponding damage pattern predicted by the finite element solution by Mazars (1984) is shown Fig. 7.29b. It should be kept in mind that the prediction of the crack propagation is, in general, sensitive to the mesh discretization since the internal forces are estimated at the sampling points in the finite element solution. In addition, for the comparison with Mazars' work (1984), the difference in the nature of quadratic elements employed in the current investigation and that of the linear elements used in his study should be taken into account even for elastic solutions. Moreover, for the comparison of the crack evolution predicted by two nonlinear solutions typical load increments should be considered because of the accumulation of the residual forces. However, both patterns are similar to great extent to that observed experimentally (cf. Mazars, 1984).

The evolution of the internal stresses in the reinforcement along the length of the member is plotted in Fig. 7.30 at six loading levels for the two solutions. The predictions obtained from the current study is shown in Fig. 7.30a while the corresponding by Mazars (1984) is illustrated in Fig. 7.30b. The trends of the two finite element solutions are almost the same. It can be noted that the points of the highest gradient in the internal stresses in the reinforcement shift away from



(a)



(b)

Figure 7.27 Steel/concrete bond problem considered for comparison with Mazars' work (1984): (a) Geometry, (b) Finite element mesh

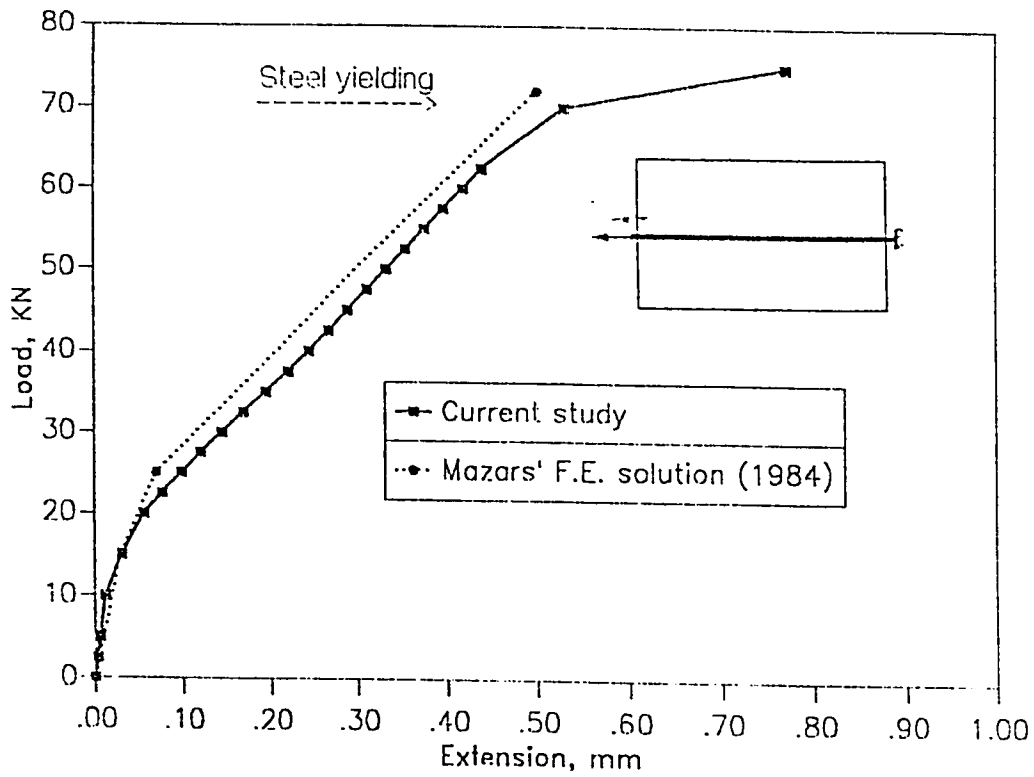


Figure 7.28 Comparison of the finite element prediction for the load-displacement characteristics in bond problem

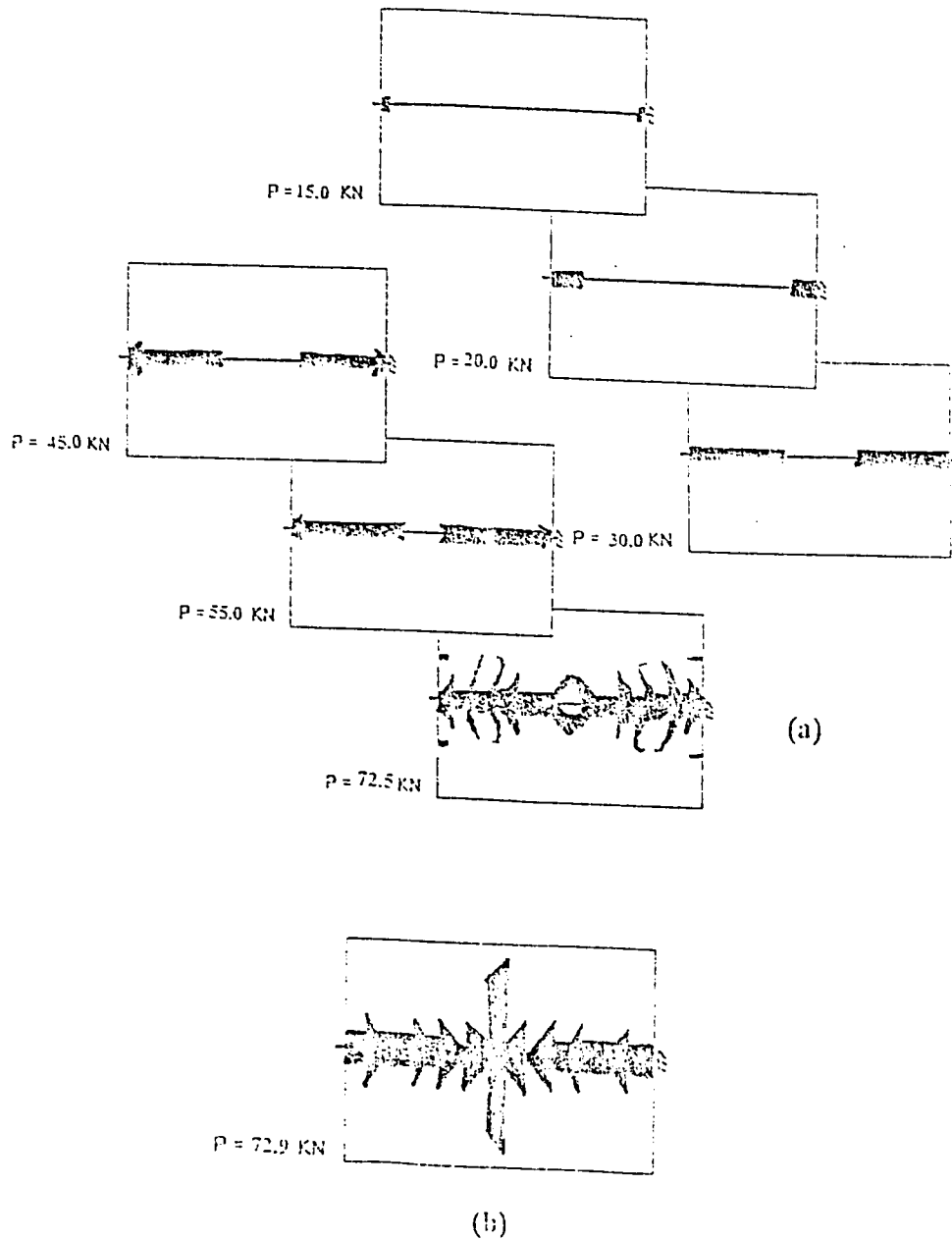
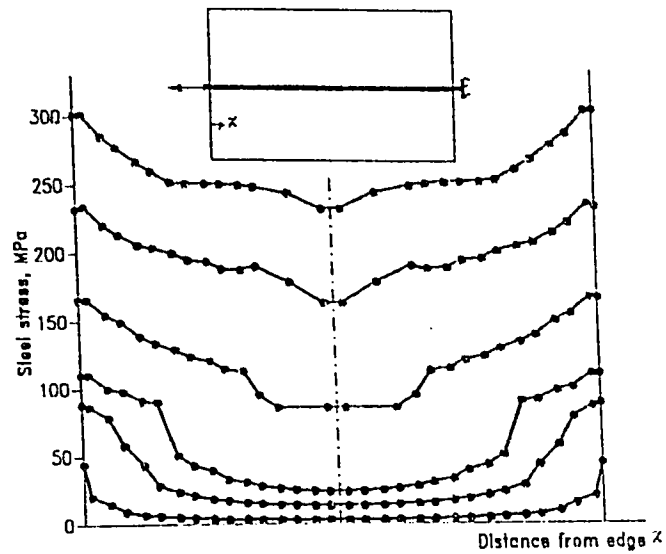
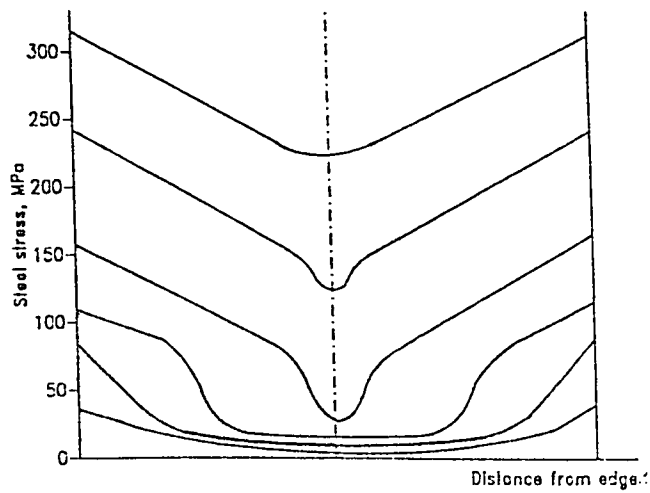


Figure 7.29 Comparison of the finite element prediction for the damage evolution in concrete: (a) current study, (b) Mazars' work (1984)



(a)



(b)

Figure 7.30 Comparison of the finite element prediction for the evolution of internal stresses in reinforcing steel: (a) current study, (b) Mazars' work (1984)

the loaded edge till reduce to a kink (drop in the internal stresses over a short distance) near the centerline of the member. The translation of these points implicitly reflects the evolution of the damage zone.

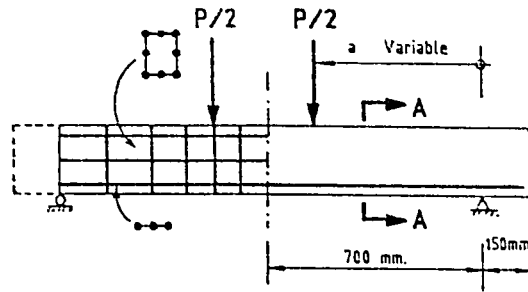
7.5 CALIBRATION AGAINST CODE PROVISIONS

This aim of this calibration is to check the rationality of the predictions of the model as applied to analyse reinforced concrete beams with and without shear reinforcement. This, of course, elaborates the ability to predict the load carrying capacity governed by various failure mechanisms. The simply supported beam considered in Mazars' work (1984) is further considered herein but with several reinforcement patterns. The main mesh established in the previous section is used but with minor modifications to provide compression steel and shear reinforcement whenever required. Concrete grade 28 and steel SS41 are considered as the constituent materials. The ACI design code (ACI 318-89 revised 1995) is selected for calibration purposes.

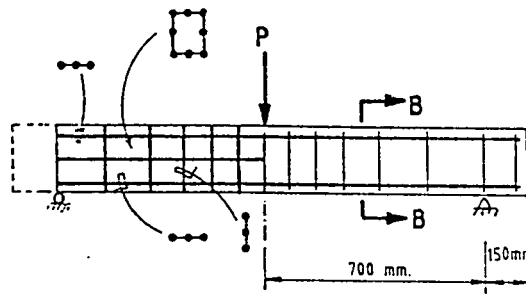
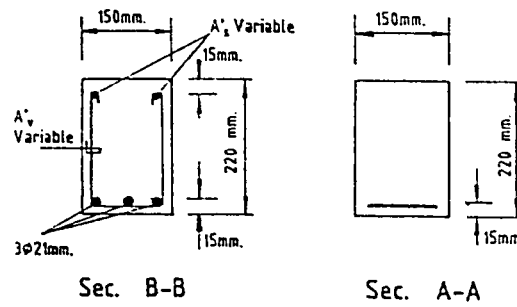
7.5.1 Reinforced Concrete Beams without Shear Reinforcement

The geometry and the finite element mesh are shown in Fig. 7.31a. Three-point loading as well as four point loading schemes are applied. In the course of the current study, the following items are evaluated:

- (1) Concrete softening.
- (2) Nonlinearity of the response.
- (3) Damage pattern.



(a) Reinforced Concrete Beam without Shear Reinforcement.



(b) Reinforced Concrete Beam with Shear Reinforcement.

Figure 7.31 Reinforced concrete beams considered for calibration against code provisions: (a) without shear reinforcement, (b) with shear reinforcement

- (4) Cracking load.
- (5) Ultimate capacity.

As in similar situations, the amount of longitudinal reinforcement and the shear span to depth ratio are the main design parameters influencing the behavior. In addition to the case of plain concrete which is frequently used, two other reinforcement ratios are used:

- (1) lightly under-reinforced concrete beam with $A_S = 226.2\text{mm}^2$ which is equivalent to 2 ϕ 12mm rebars (as used before); and
- (2) heavily under-reinforced concrete beam with the maximum permissible limit of ACI-318 $A_S = 1038.0\text{mm}^2$ which is equivalent to 3 ϕ 21mm rebars. This corresponds to reinforcement ratio $\rho_{\max} = 0.75\rho_b$ ($\rho_b = 0.046$).

The shear span, a , to depth ratio, d , to be considered are governed by the mesh discretization. Consequently, the shear span, a , takes the values of 150, 300, 400, 500, 600, 700 mm corresponding to a/d ratio of 0.73, 1.46, 1.95, 2.44, 2.93 and 3.41, respectively. The latter value indicates the case of three-point loading.

7.5.1.1 Concrete softening

Concrete softening reflects the possible effects of the testing type. Three point loading on plain concrete beams with: (1) load-controlled incrementation and (2) displacement-controlled incrementation are considered. Fig. 7.32 illustrates the slight difference in the ultimate

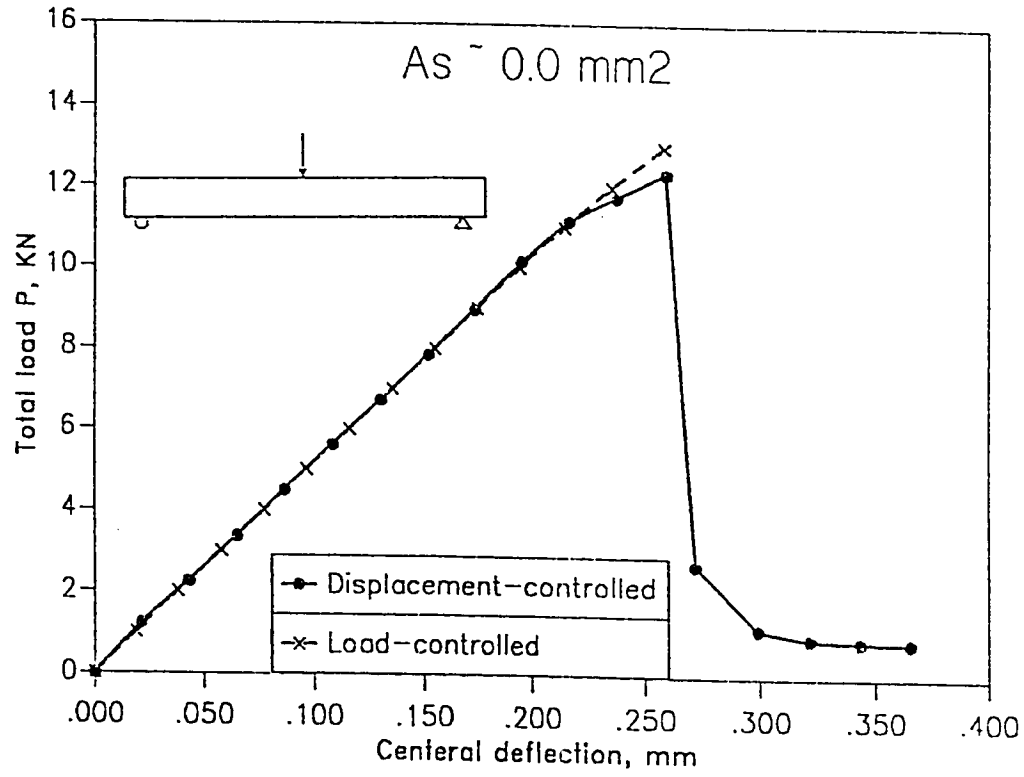


Figure 7.32 Softening characteristics of plain concrete beams

load carrying capacity as predicted by the two testing schemes. In contrast to load-controlled incrementation which failed to converge after the ultimate load, displacement-controlled incrementation has the ability to describe the behavior in post peak regime. The softening branch falls very steeply in the beginning and then goes asymptotically to the deflection axis. Although such global softening response lacks the importance for design purposes, strain softening in local sense has a considerable effect on the total behavior. Therefore, in the following analysis load-controlled incrementation is employed.

7.5.1.2 Nonlinearity of the response

As the canonical model accounts for the damage evolution from the first instance of loading, early nonlinearity of the response is expected to take place. In the case of reinforced concrete beams, deviation from the global quasi linear behavior becomes, however, more pronounced after the onset of cracking. The amount of longitudinal reinforcement has a great influence on such nonlinearity. Figure 7.33 shows, for three-point loading, the nonlinear trend of the load-central deflection for plain concrete as well as for the other cases of reinforcement. Whereas plain concrete indicates almost linear behavior, the other situations show higher stiffness associated with delayed onset of nonlinearity which is attributed to the cracking process.

The shear span to depth ratio, a/d , has, in general, a great influence on the nonlinearity of the structural response of the reinforced concrete beams. Figures 7.34 and 7.35 illustrate this effect

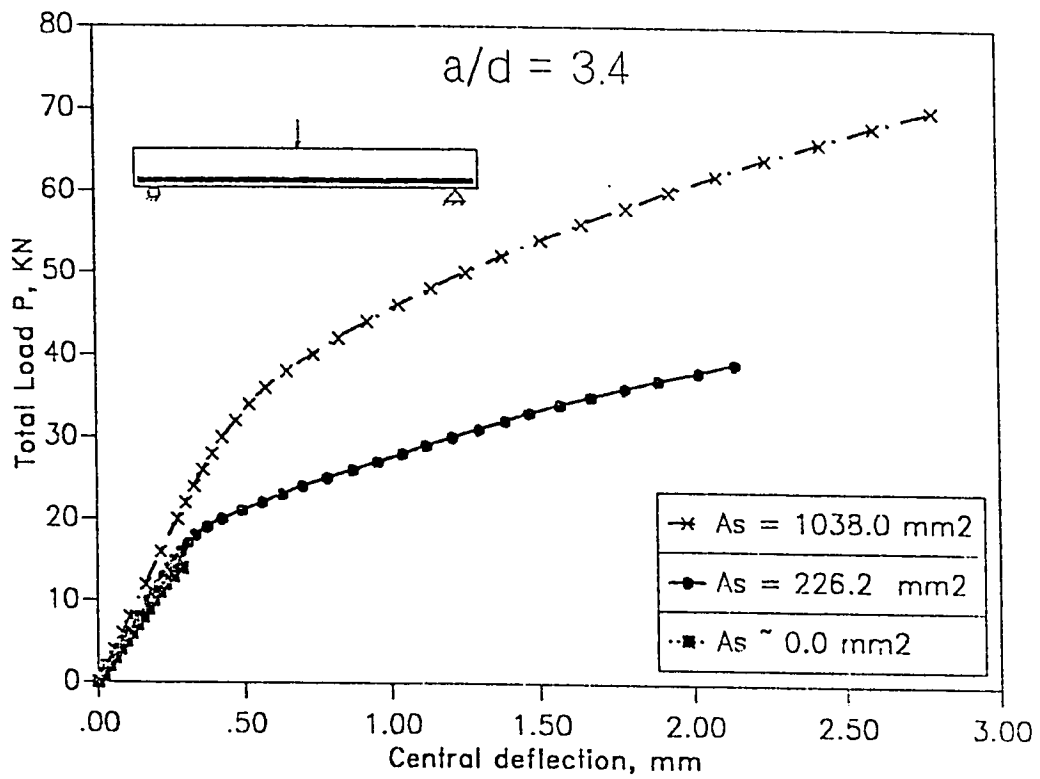


Figure 7.33 Effect of amount of main reinforcement on response nonlinearity for beams without shear reinforcement

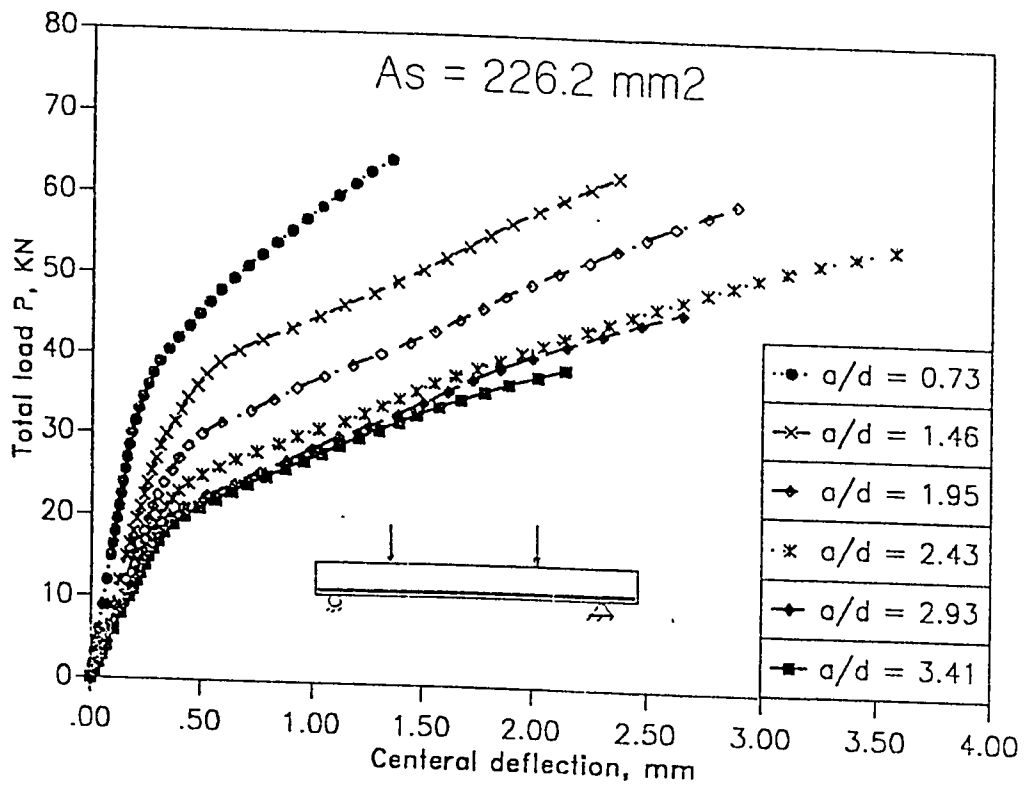


Figure 7.34 Effect of shear span to depth ratio on response nonlinearity for lightly under-reinforced concrete beams without shear reinforcement

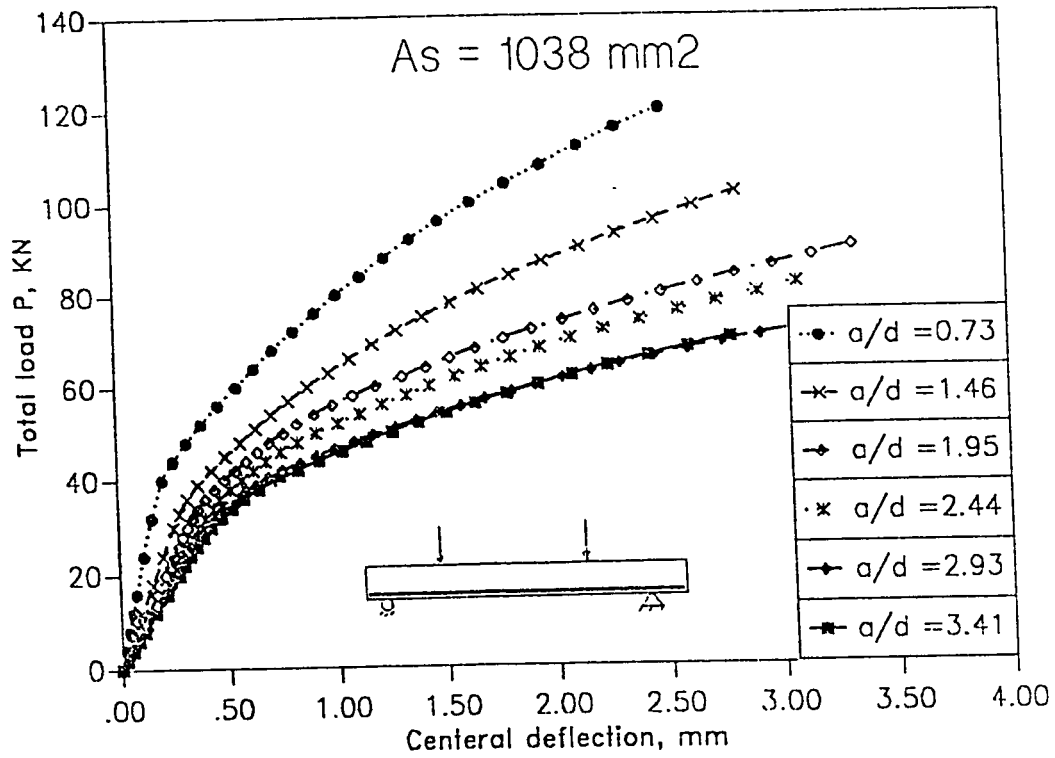


Figure 7.35 Effect of shear span to depth ratio on response nonlinearity for heavily under-reinforced concrete beams without shear reinforcement

for $A_s = 226.2\text{mm}^2$ and $A_s = 1038.0\text{mm}^2$, respectively. Nonlinearity of the response is an evident for all the studied cases. The higher the shear span to depth ratio, the softer the response. This can be justified by the fact that, for the same load value, as the load gets closer to the centerline of the beam (which means higher a/d value) the maximum bending moment increases and consequently the central deflection increases as well.

7.5.1.3 Damage pattern

The mode of failure predicted by the program is noted to be governed by:

- (1) reinforcement damage due to steel yielding; and/or
- (2) concrete damage due to shear.

Three levels of damage for concrete in both tension and compression are defined, listed in Table 7.2, as follows:

- (1) Null: for strain levels ranging from the threshold damage strain to the peak strain.
- (2) Moderate: for strain levels ranging from the peak strain up to almost the end of the steeply rising damage trend.
- (3) Severe: for strain levels ranging further to the critical damage strain.

Figures 7.36 and 7.37 illustrate the damage levels, for various shear span to depth ratio, at the cracking state and at the ultimate condition for the two cases of reinforcement; i.e. $A_s = 226.2\text{mm}^2$ and

Table 7.2 Ranges of total damage variable for different damage levels

Damage	Damage type	
Level	Tensile	Compressive
Nil	≤ 0.167	≤ 0.380
Moderate	0.167 - 0.600	0.380 - 0.768
Severe	> 0.600	> 0.768

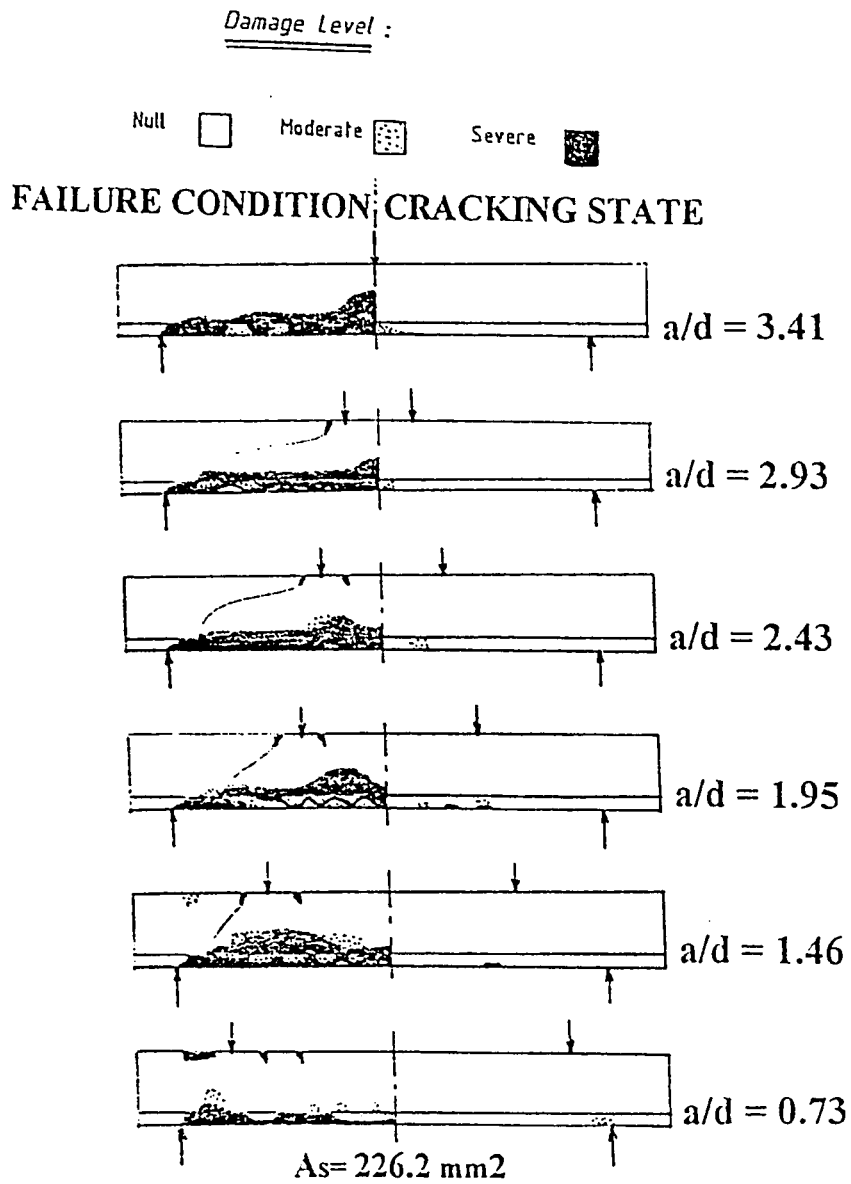


Figure 7.36 Effect of shear span to depth ratio on damage pattern for lightly under-reinforced concrete beams without shear reinforcement

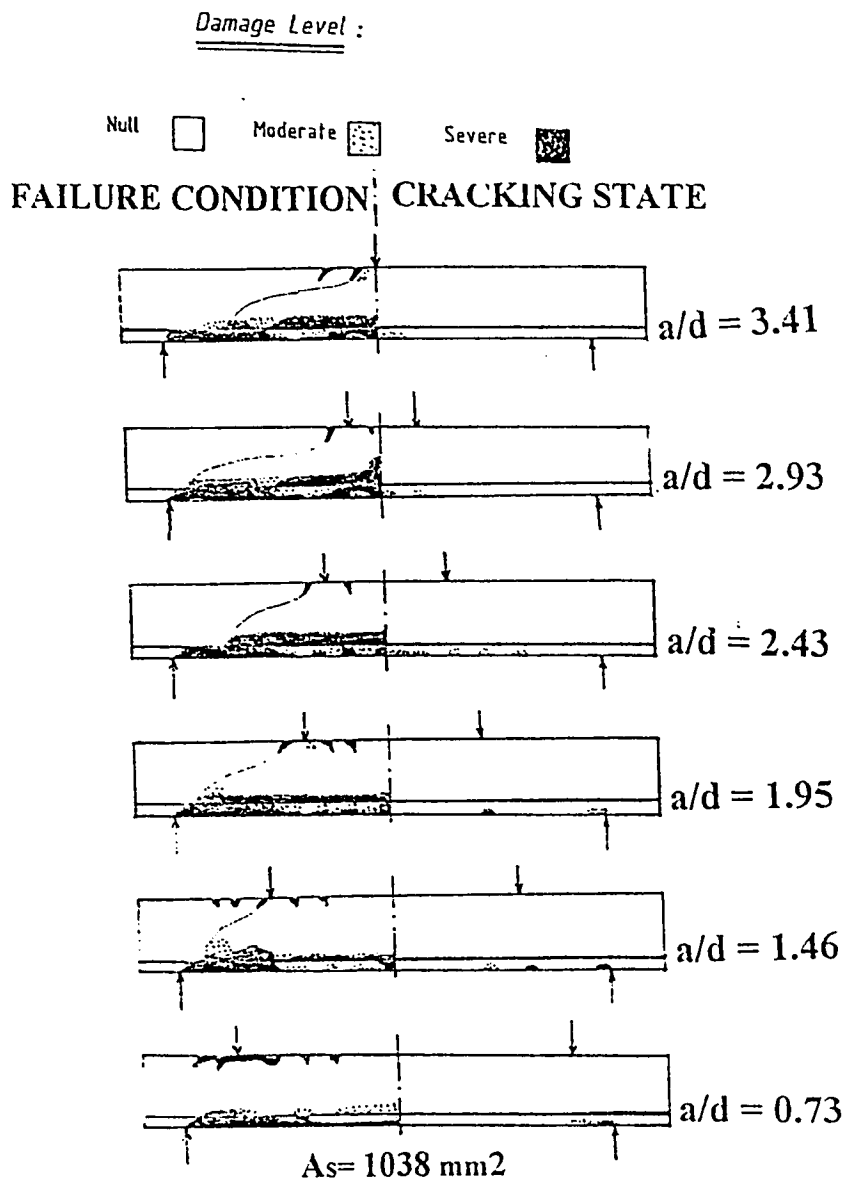


Figure 7.37 Effect of shear span to depth ratio on damage pattern for heavily under-reinforced concrete beams without shear reinforcement

$A_s = 1038.0\text{mm}^2$, respectively. From the analysis of the results obtained by the computer runs, the following observations are noted:

- (1) Except for the case of $a/d = 0.73$ in which cracking starts next to support, cracking tends to initiate between the applied load and the centerline of the beam for the case of $A_s = 226.2\text{mm}^2$, while it takes place under the applied load in the support side for the case of $A_s = 1038.0\text{mm}^2$. In all situations cracking commences in the bottom fiber of the beam.
- (2) The elevation, through the depth of the beam, of the upper bound of the zone of severe damage is higher in the case of the lightly under-reinforced beam ($A_s = 226.2\text{mm}^2$) as compared with the heavily under-reinforced beam ($A_s = 1038.0\text{mm}^2$).
- (3) The mode of failure differs according to the amount of reinforcement and to the shear span to depth ratio as sketched in Figures 7.36 and 7.37. The prominent causes of failure are summarized in Table 7.3.
- (4) Modes of failure enhanced by shear are characterized by severe damage level close to the top fiber in the proximity of the load in the support side and above the reinforcement within a horizontal distance almost equal to the depth from the support. The final cracking pattern is expected to join these two locations in almost a hyperbolic fashion.

Table 7.3 Failure modes of reinforced concrete beams without shear reinforcement

Shear span to depth ratio	Area of tensile reinforcement A_s	
	226.2 mm ²	1038.0 mm ²
0.73	Shear failure	Shear failure
1.46	Shear failure	Shear failure
1.75	Shear failure	Shear failure
2.44	Simultaneous flexural and shear failure	Shear failure
2.93	Simultaneous flexural and shear failure	Shear failure
3.41	Flexural failure	Shear failure

7.5.1.4 Cracking load

The finite element analysis indicates that the cracking load is influenced by both the amount of reinforcement as well as the shear span to depth ratio. For comparison purposes, code provisions are limited to flexural cracking and calculation of the transformed section properties are required. The calculations of concern are listed in Table 7.4 for plain concrete and other reinforcement ratios. The modulus of rupture f_r is taken as $1.25f_t'$ as implicitly specified by the ACI code. For the case of three point loading, Fig. 7.38 illustrates a comparison between the finite element predictions and the ACI cracking load as induced by flexure. It indicates that the model yields very close predictions to the ACI values although no single input about the modulus of rupture is given to the program. This is believed to be attributed to the nonlinear pre-peak behavior of concrete in tension as idealized by the canonical model where more energy can be absorbed by the beam if compared with the similar case with linear elasticity.

The ACI flexural calculations indicates that the closer is the location of the applied load to the support the higher is the cracking load. However, several influences contribute to the onset of cracking other than flexure. This is shown by the finite element predictions to be more pronounced for shear span to depth ratios less than 2.5 for the two reinforcement ratios considered as shown in Figs. 7.39 and 7.40. In such situations the cracking process is motivated by the tensile stresses in the bottom fiber close to the concentrated loads. In all cases, the higher is the amount of reinforcement, the higher is the cracking load.

Table 7.4 Properties of uncracked transformed section of reinforced concrete beams without shear reinforcement

Quantity	Area of tensile steel, A_s		
	$\sim 0.0 \text{ mm}^2$	226.2 mm^2	1038.0 mm^2
Distance of centroidal axis from bottom fiber, mm	110.00	104.65	89.60
Second moment of area $\times 10^6, \text{mm}^4$	133.10	149.87	197.00

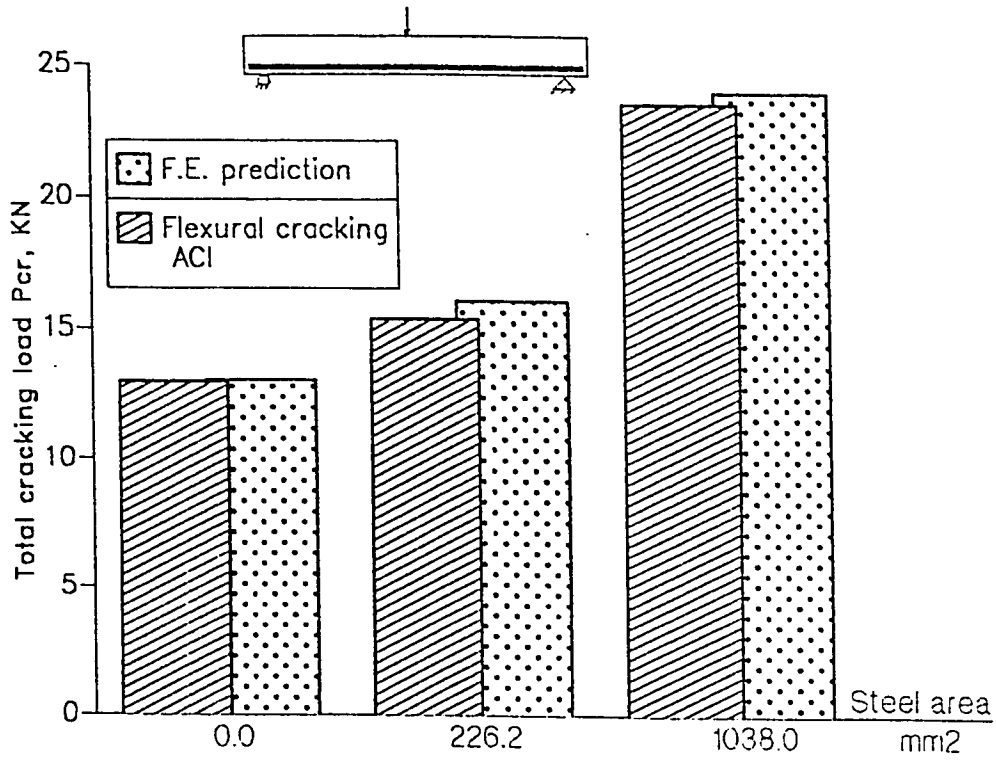


Figure 7.38 Effect of amount of main reinforcement on cracking load for beams without shear reinforcement

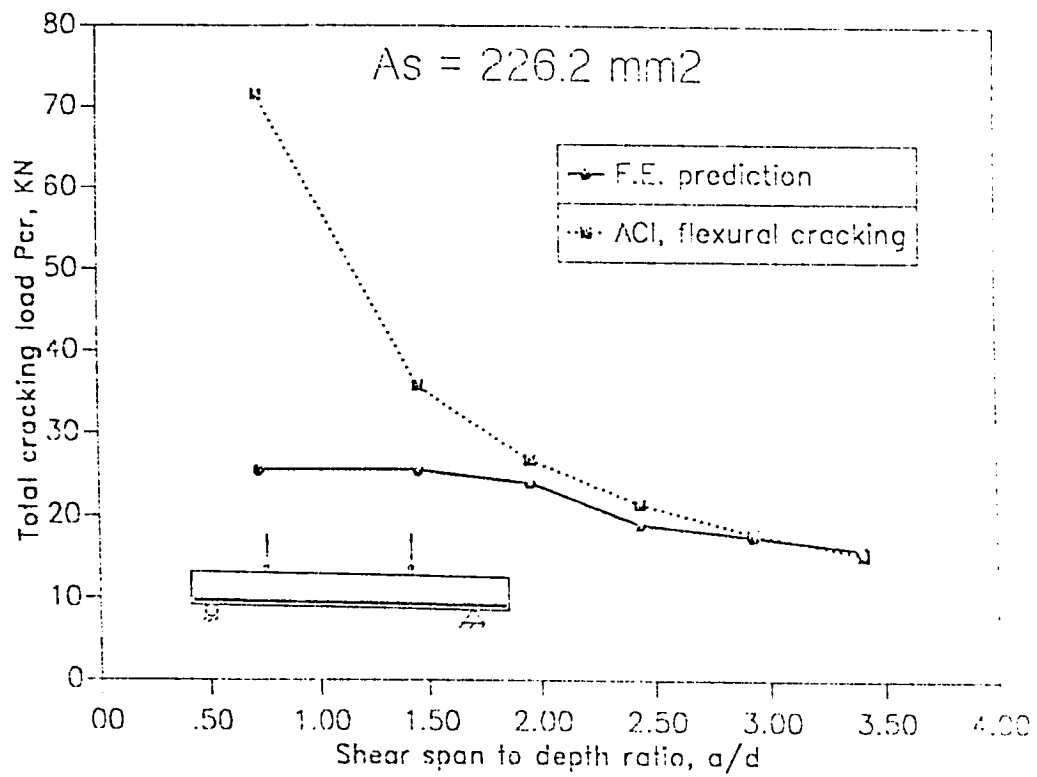


Figure 7.39 Effect of shear span to depth ratio on cracking load for lightly under-reinforced concrete beams without shear reinforcement

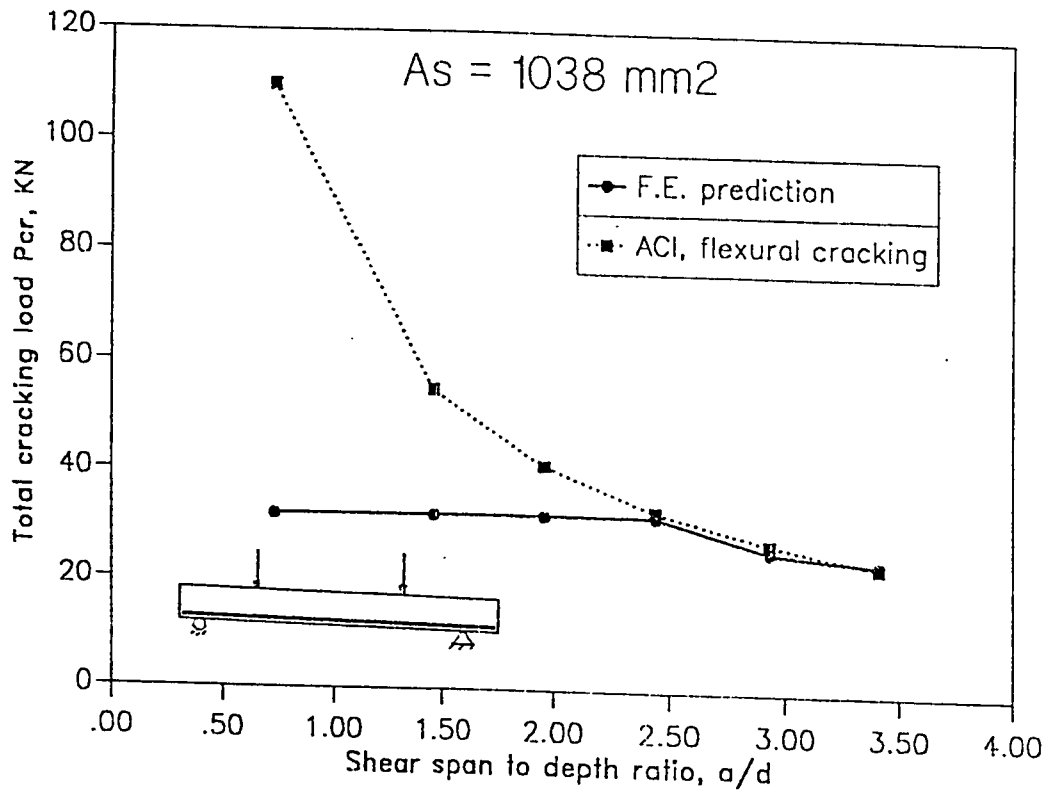


Figure 7.40 Effect of shear span to depth ratio on cracking load for heavily under-reinforced concrete beams without shear reinforcement

This is due to the higher stiffness achieved by increasing the amount of main tensile reinforcement.

7.5.1.5 Ultimate capacity

In strength design methods, the calculations are usually based on the ultimate condition then serviceability conditions are checked later. This means that the ultimate load carrying capacity of the structural component, as controlled by various collapse mechanisms, is the goal. Therefore, accurate estimation of this load is of prime importance from all practical aspects. The ACI code gives priority to failure mechanisms that are inspired by flexure and shear. For flexural calculations, the study cases represent under-reinforced beams and Whitney's rectangular stress block for concrete in compression is considered while contribution of concrete in tension is neglected. The maximum top fiber strain of concrete is taken as 0.003 whereas steel reinforcement is assumed to experience yielding. On the other hand shear calculations based on the experimental formulae of the ACI code are used (refer to the more detailed procedure of ACI-11.3.2.1).

As illustrated before, the three main failure mechanisms as depicted by the finite element results are by either:

- (1) flexure by reinforcement yielding,
- (2) shear enhanced by diagonal tension in most cases, and
- (3) simultaneous flexure and shear for two cases of a/d ratios of 1.95 and 2.44 with reinforcement of $A_s = 226.2\text{mm}^2$. This is, of

course, different from the flexural shear cracking which is considered as shear failure.

The values of the peak load predicted by the program DMGPLSTS are found to in a very close agreement with the lower bounds provided by the ACI code as shown in Figs. 7.41 and 7.42 for the cases of $A_S = 226.2\text{mm}^2$ and $A_S = 1038.0\text{mm}^2$, respectively.

7.5.2 Reinforced Concrete Beams with Shear Reinforcement

In most of the previous cases, the beam capacity is noted to be limited by the shear capacity of the section and full utilization of the reinforcement has not been achieved yet. Because in concrete practice over-reinforced beams are always recommended be avoided because of its abrupt failure by concrete crushing, the following investigation is devoted to under-reinforced beams with shear reinforcement. Reinforcement area evaluated by the maximum permissible amount is considered; i.e. heavily under-reinforced beam with $A_S = 1038.0\text{mm}^2$. In addition to the shear reinforcement, of area A_V , compression steel, of area A_S' , functioning as stirrup hanger is used with the same diameter. The amount of shear reinforcement and the spacing between stirrups are varied through out the course of this investigation to study the possible effects on the shear capacity of beams.

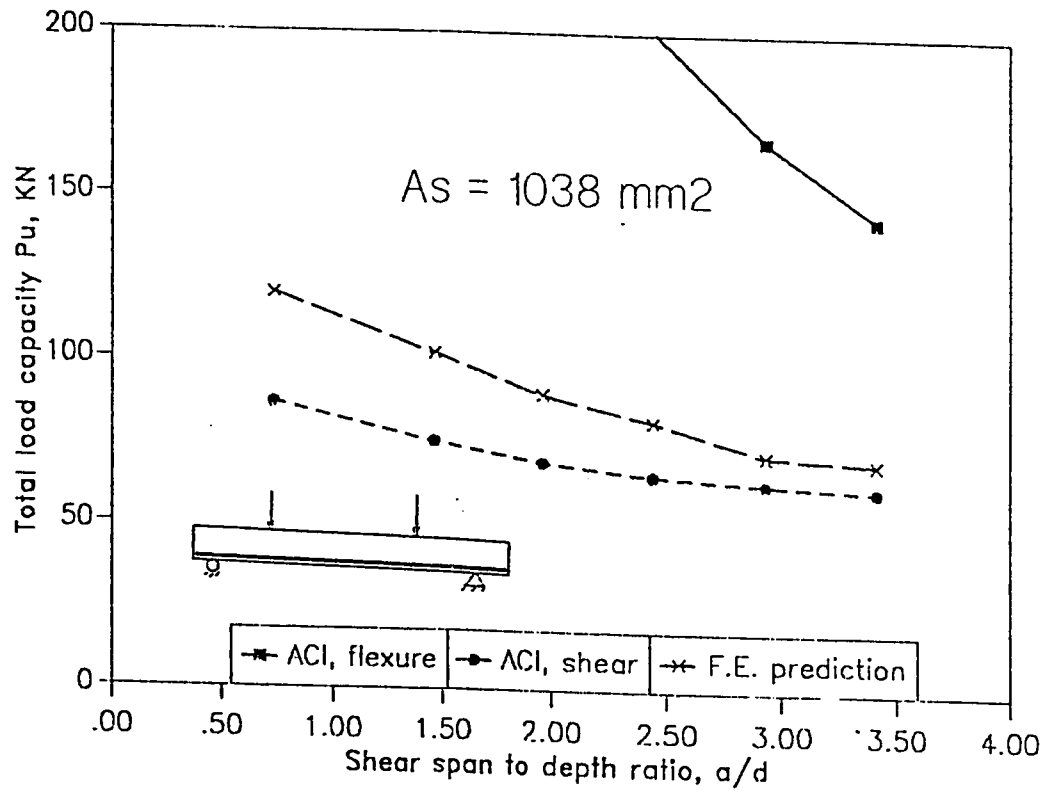


Figure 7.41 Effect of shear span to depth ratio on ultimate capacity for lightly under-reinforced concrete beams without shear reinforcement

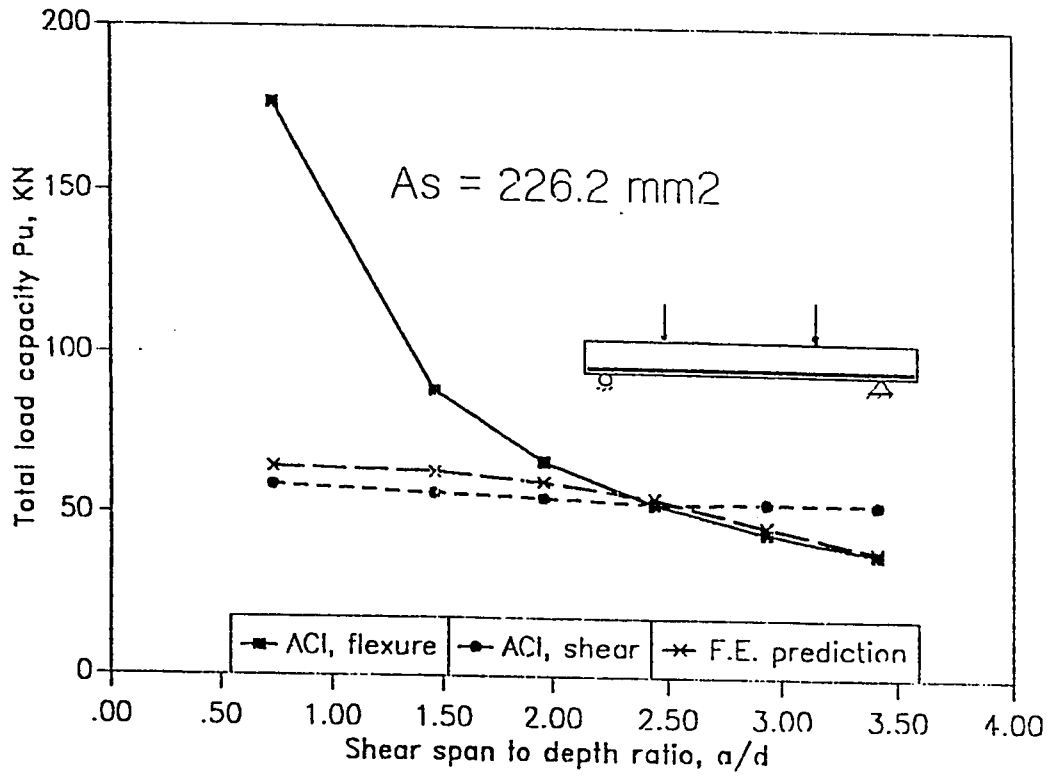


Figure 7.42 Effect of shear span to depth ratio on ultimate capacity for heavily under-reinforced concrete beams without shear reinforcement

7.5.2.1 Effect of amount of shear reinforcement

Five patterns of shear and compression steel of reinforced concrete beams subjected to three-point loading are selected as study cases:

- (1) $A_v = A_s' = 0.0$. This case was previously studied but is considered herein as a reference for comparison purposes.
- (2) $A_v = A_s' = 56.5\text{mm}^2$. This is equivalent to $\phi 6\text{mm}$ two-legged stirrup and $2\phi 6\text{mm}$ compression steel.
- (3) $A_v = A_s' = 100.5\text{mm}^2$. This is equivalent to $\phi 8\text{mm}$ two-legged stirrup and $2\phi 8\text{mm}$ compression steel.
- (4) $A_v = A_s' = 157.1\text{mm}^2$. This is equivalent to $\phi 10\text{mm}$ two-legged stirrup and $2\phi 10\text{mm}$ compression steel.
- (5) $A_v = A_s' = 226.2\text{mm}^2$. This is equivalent to $\phi 12\text{mm}$ two-legged stirrup and $2\phi 12\text{mm}$ compression steel.

The geometry and the finite element mesh are shown in Fig. 7.31b. The stirrups are arranged in the following sequence: 3 pcs @150mm c.c. starting directly from the point above the support, then the rest are spaced @100mm c.c. Incremental loading scheme is applied with almost identical steps. Emphases are given to the followings:

- i. Nonlinearity of the response.
- ii. Damage pattern.
- iii. Cracking load.
- iv. Ultimate capacity.

i. Nonlinearity of the response

The results obtained from the finite element program indicate nonlinear trend subsequent to the cracking load as shown in Fig. 7.43. The existence of the compression steel shows slightly higher stiffness. The addition of shear reinforcement is noted to increase the ductility of the beam and the ultimate load carrying capacity as well if compared with the case of the same beam but without shear reinforcement.

ii. Damage pattern

The mode of failure predicted by the program is noted to be governed by either:

- (1) tensile reinforcement damage by yielding and thus allows for the propagation of flexural cracks, or
- (2) shear reinforcement damage by yielding and thus allows for the propagation of flexural-shear cracks.

The prominent causes of failure are summarized in Table 7.5.

Figures 7.44 illustrates the tensile and compressive damage levels at ultimate condition for three particular cases considered of $A_s' = A_v = 0.0, 100.5$ and 226.2mm^2 . It is evident that the existence of shear reinforcement makes the cracking penetrates to a higher elevation and consequently the damage pattern differs from the cases analysed without shear reinforcement. It is also observed that some zones showed localized compressive moderate damage.

Table 7.5 Failure modes of reinforced concrete beams with shear reinforcement

Area of stirrups = area of compression steel, mm ²	mode of failure	damage type
0.0	Shear failure	Concrete damage
56.5	Shear failure	yielding of stirrups
100.5	Shear failure	yielding of stirrups
157.1	flexural failure	yielding of main reinforcement
226.2	flexural failure	yielding of main reinforcement

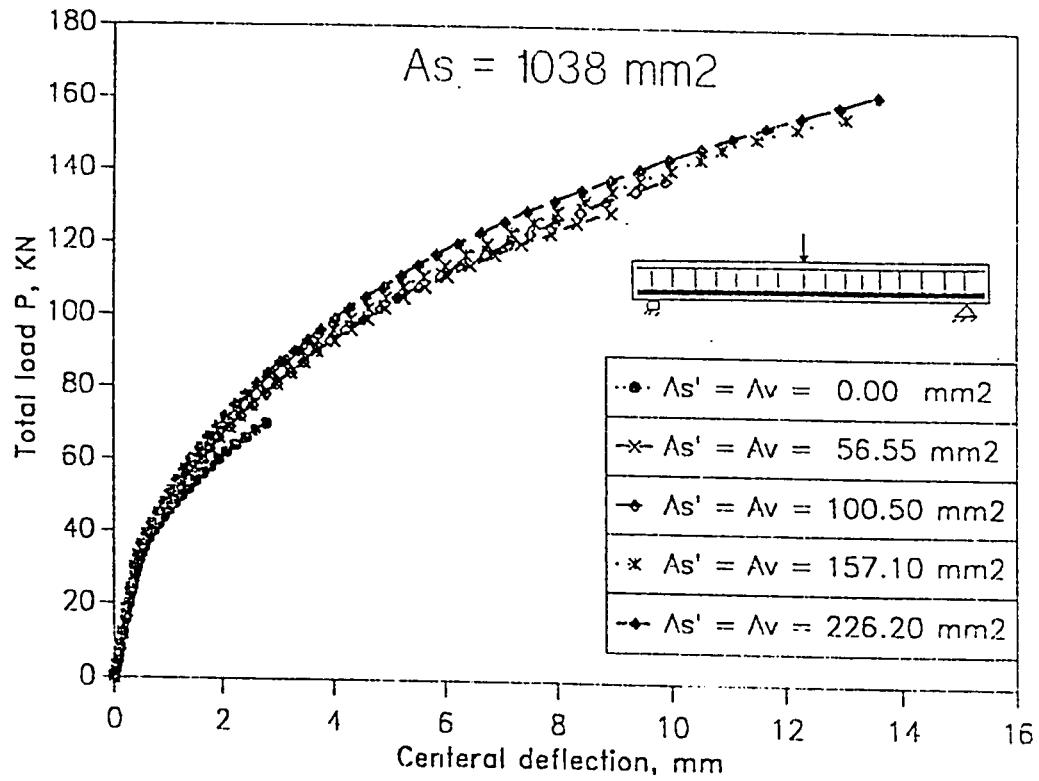


Figure 7.43 Effect of amount of shear reinforcement on response nonlinearity of heavily under-reinforced concrete beams

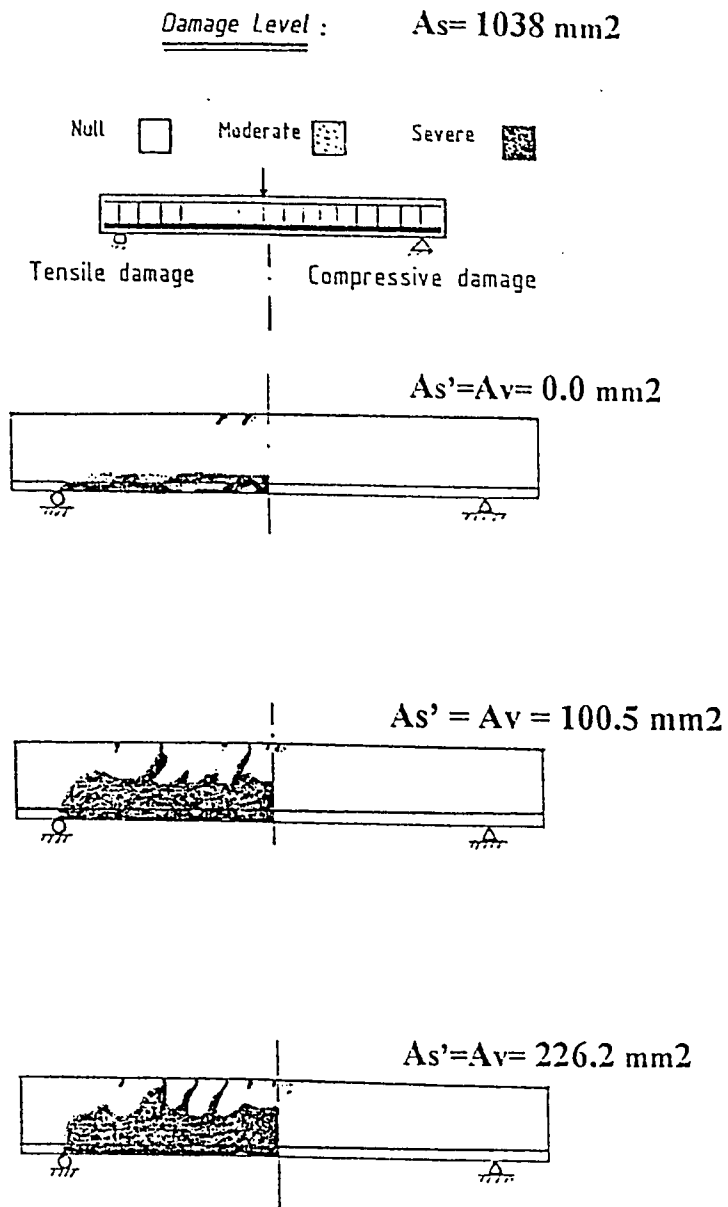


Figure 7.44 Effect of amount of shear reinforcement on damage pattern for heavily under-reinforced concrete beams

iii. Cracking load

The finite element analysis indicates that the cracking load is insensitive to the amount of compression steel and, of course, the shear reinforcement since flexural cracking is dominant for the considered case of three-point loading with $a/d=3.41$ in which the cracks are initiated near the bottom fiber closer to the centerline. The results are shown in comparison with those calculated according to the ACI code in Fig. 7.45. The cracking load, in general, is affected by the second moment of area of the transformed section along with the location of the principal centroidal axis (calculations are summarized in Table 7.6). It is found through the hand calculations that the contributions to the total second moment of area from the concrete, tension steel and compression steel are about 65%, 30% and 5%, respectively. This underscores the minimal effect of the compression steel to the cracking load which agrees quite well with the numerical results.

iv. Ultimate capacity

In flexural calculations, according to the ACI code, the contribution of the compression steel is taken into account. Its yielding at the ultimate condition is ensured to take place. However, it is found that its effect on the ultimate flexural capacity is small. On the other hand, increasing the diameter of the stirrups from 10 mm to 12 mm is noted to enhance the overall shear capacity considerably. The finite element predictions picked up these characteristics as shown in Fig. 7.46 for

Table 7.6 Properties of uncracked transformed section of reinforced concrete beams with shear reinforcement

Area of compression steel A_s' , mm^2	Distance of centroidal axis from bottom fiber, mm	Second moment of area $* 10^6$, mm^4
0.0	89.60	197.00
56.5	90.91	203.60
100.5	91.93	208.54
157.1	93.22	214.76
226.2	94.74	222.18

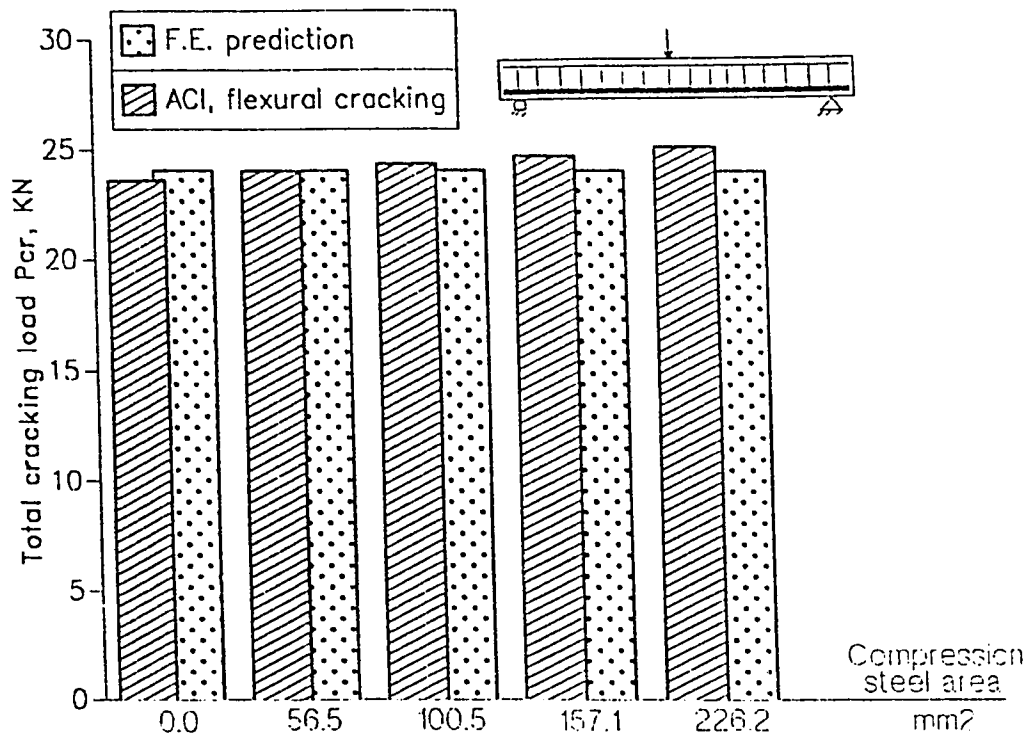


Figure 7.45 Effect of amount of shear reinforcement on cracking load for heavily under-reinforced concrete beams

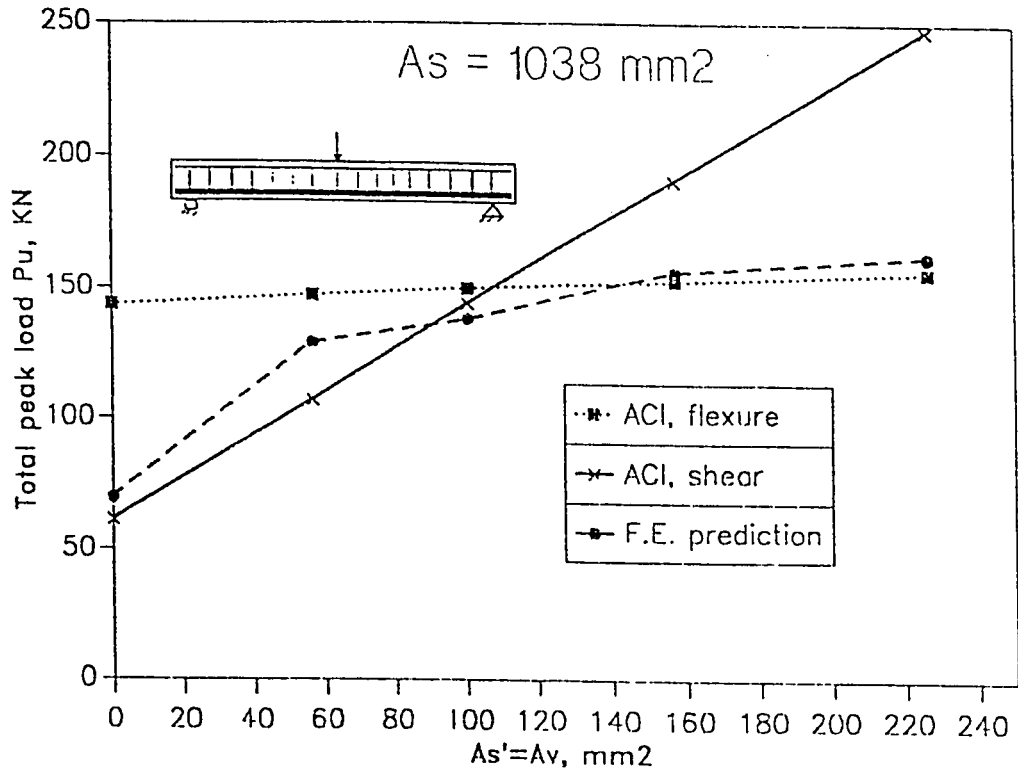


Figure 7.46 Effect of amount of shear reinforcement on ultimate capacity for heavily under-reinforced concrete beams

$A_s' = A_v$. As illustrated before, the two main failure mechanisms as depicted by the numerical results for beams with shear reinforcement are by either:

- (1) flexure by yielding of main tensile (longitudinal) reinforcement and
- (2) shear by yielding of shear reinforcement in highest strained stirrup (the first after the support)

The values of the peak load predicted by the program DMGPLSTS are found to in a very close agreement with the lower bounds provided by the ACI code as shown in Figs. 7.46. The case of the beam without shear reinforcement but with the same main steel is shown, for comparison, on the same graph in which the failure is governed by the shear capacity of concrete. These cases represents the transition of the failure mechanism from shear failure (two distinct sorts) to flexural failure.

7.5.2.2 Effect of spacing between stirrups

Four-point loading of the heavily under-reinforced beam with $2\phi 6$ mm compression steel is considered. Two-legged $\phi 6$ mm stirrups are assumed to be equally spaced over the 400 mm shear span. Such a diameter for stirrups is chosen to ensure that shear failure governed by yielding of stirrups controls as inferred from the previous article 7.5.2.1. Four different spacings are selected as study cases: $\phi 6\text{mm}@200\text{mm}$, $\phi 6\text{mm}@133\text{mm}$, $\phi 6\text{mm}@100\text{mm}$, and $\phi 6\text{mm}@80\text{mm}$. The geometry of the beam and the cross section are shown in Fig. 7.47. Emphases

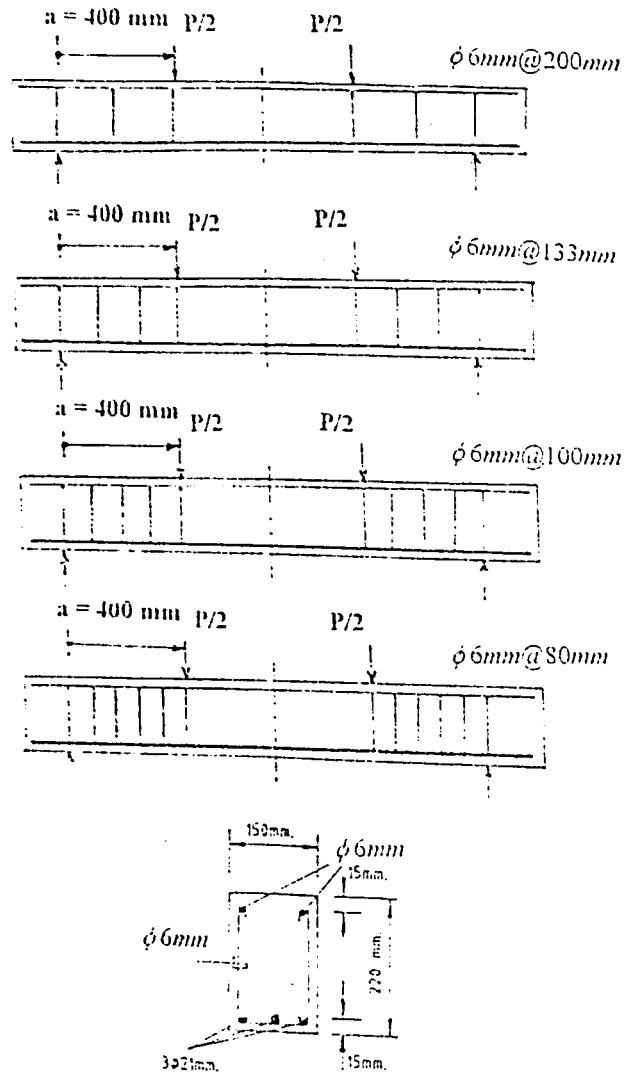


Figure 7.47 Four-point loading on heavily under-reinforced concrete beams with different spacings between stirrups

are given to the followings:

- i. Nonlinearity of the response.
- ii. Ultimate capacity.

i. Response nonlinearity

The results obtained from the finite element program indicate nonlinear trend subsequent to the cracking load as shown in Fig. 7.48. The stiffness characteristics of all cases are nearly identical. This is attributed to the fact that the main contribution to the flexural stiffness of beam comes from the second moment of area term which is independent of the shear reinforcement as formulated by the Euler-Bernoulli thin beam theory. However, closer spacing shows higher final deformation associated with higher loading capacity.

ii. Ultimate capacity

Having established the same criterion as for the ACI code, the ultimate shear capacity is determined when yielding of stirrup(s) within a projected distance equal to the depth of the beam takes place. This is noted to occur after a distance $d/2$ from the support. This is numerically observed through yielding of the first (after the support) stirrup for 200 and 133 mm spacings, first and second stirrups for 100 mm spacing, second and third stirrups for 80 mm spacing. The F.E. prediction for the ultimate capacity of the beam is shown in comparison with the ACI peak loads estimated according to the flexure and shear

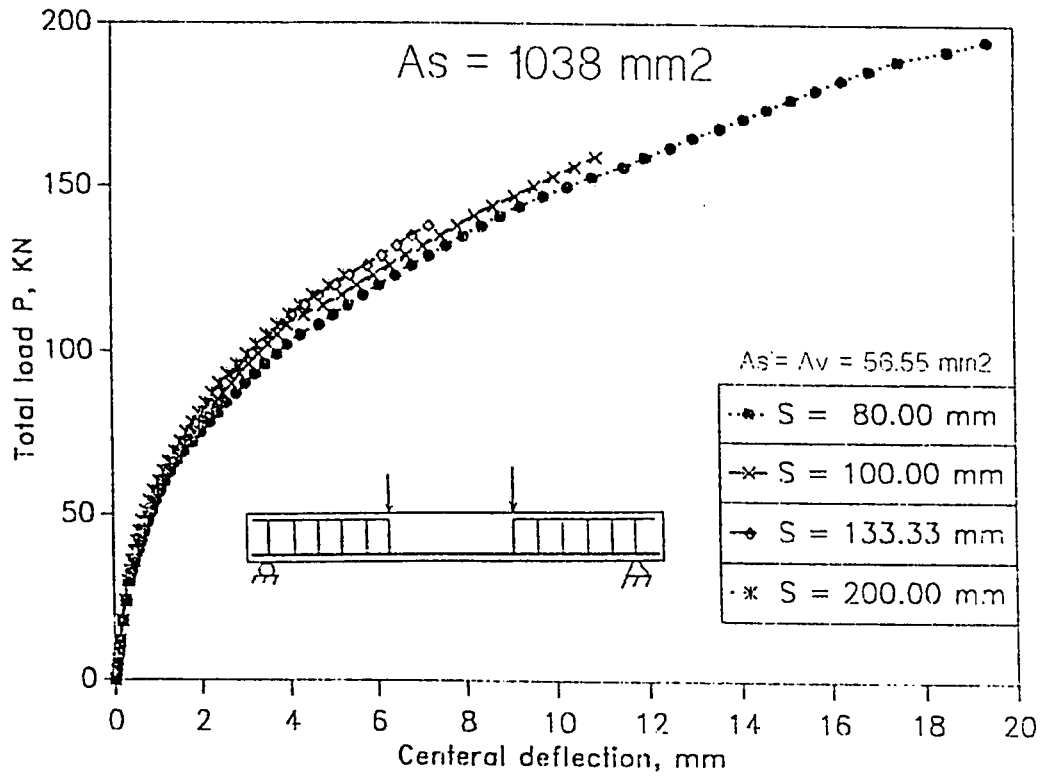


Figure 7.48 Effect of spacing between stirrups on response nonlinearity for heavily under-reinforced concrete beams

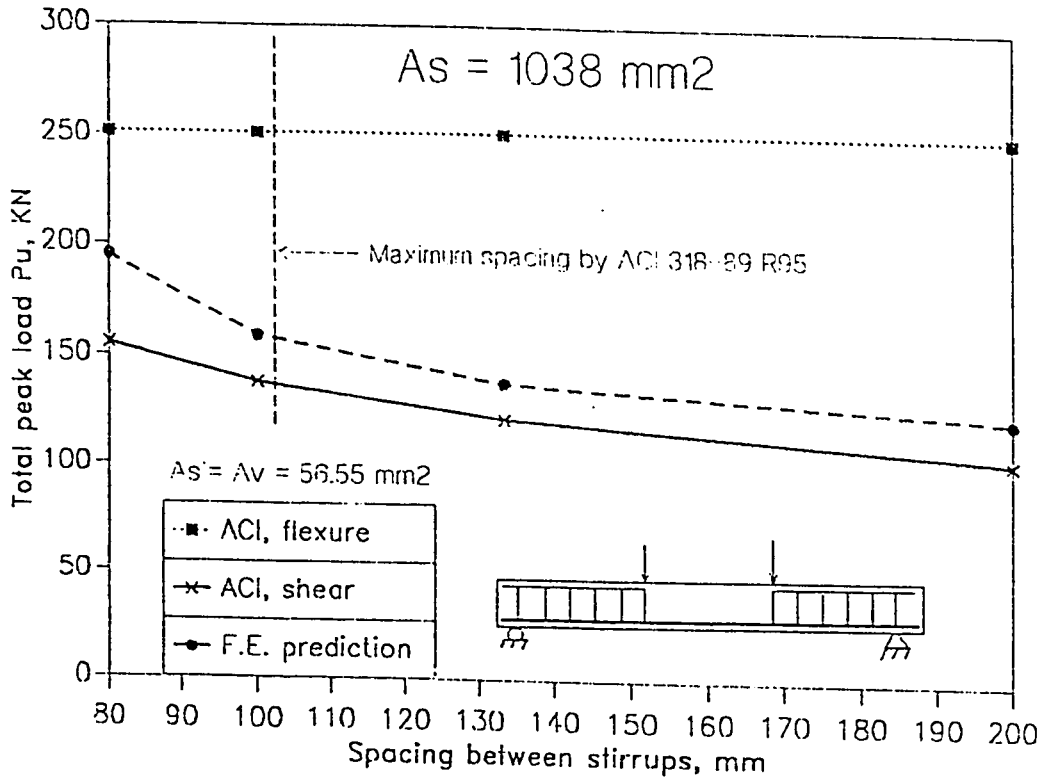


Figure 7.49 Effect of spacing between stirrups on ultimate capacity for heavily under-reinforced concrete beams

strength calculations as illustrated in Fig. 7.49. The model prediction is seen to be in a very close agreement with the controlling ACI shear capacity. The maximum spacing permitted by the ACI is drawn on the same chart. It is clear that this limitation on spacing is quite conservative for the particular beam investigated.

CHAPTER 8

CONCLUSIONS AND RECOMMENDATIONS

The conclusions drawn from the present study are:

1. The introduction of the proposed generalized concepts underlines the fundamentals of proper elastoplastic damage modelling. These include: (a) generalized damage variables, (b) generalized material degradation paths, (c) generalized decomposition of the strain tensor, (d) generalized effective stresses concept. The proposed terms are successfully applied to interpret the experimental behavior of concrete in compression and copper 99.9% in tension.

2. The utilization of the proposed concepts indicates the following:
 - (a) the overall behavior cannot be properly characterized by a single damage variable as has been the adopted practice,
 - (b) the different response phases, particularized as total-damage, elastic-damage and plastic-damage, follows constrained uncoupling. The correct expression of the decomposed Helmholtz free energy is given based on thermodynamics of irreversible changes.
 - (c) unloading along a general degraded path is allowed in contrast

to the more restrictive cases of either purely brittle or ductile paths as per existing models.

- (d) the incongruity in the assumptions postulated in some of the well-known models, such as Ju's energy-based damage model (1989) and Lemaitre's ductile damage model (1985), are revealed and corrected.

3. The generalized concepts are incorporated with different theories such as plasticity, micromechanics and unilateral damage. The governing laws are formulated and the final three-dimensional tensorial equations are derived.

4. The proposed phenomenological-micromechanical model presents a systematic procedure to provide the stress-strain relations for rock-like materials. The proposed model integrates the phenomenological aspects of damage obtained from a uniaxial cyclic tensile test with concepts of micromechanics of randomly oriented cracks derived by the self consistent method. Micromechanics is utilized for the elastic-damage phase which experiences sub-brittle behavior. Degradation of the bulk and shear moduli are established using suitable damage variables for loading and unloading. Contrary to previous models (c.f. Mazars, 1984) Poisson's ratio is assumed to be affected by the damage process taking place through the course of loading. All the parameters of the model are calibrated from a single uniaxial cyclic tensile test. Applications to concrete have shown some of the salient features of the

behavior such as strain softening, stiffness degradation, and biaxial strength envelope to be in good agreement with the experimental data.

5. In the uniaxial form of the proposed canonical model for concrete, metaphorical generalized damage variables (MGDV) are formulated in both tension and compression for an efficient unified approach. Softening is shown to be an incontestable characteristic of the stress-plastic-damage strain relationship in both tension and compression. Plastic stiffness degradation sensitivity to concrete quality is noted to be negligible. The stress-elastic damage strain curves reveal softening behavior in tension whereas a helmet-shaped knot is seen to exist in the compressive response. Comparison with existing damage models reveals the egregious simplification achieved by the proposed MGDV in predicting cyclic behavior using a single material parameter which is the compressive strength.

6. The proposed theory of dichotomy replaces the continuum by a system of orthogonal springs. This facilitates the reduction of the constitutive relations into a canonical form. The behavior of concrete is idealized as elastoplastic damage where the damage variables are identified phenomenologically from the degradation of the material moduli. The model is verified against a large number of experiments and is shown to be in a close agreement with observations. The following are proved to be some of the salient notions of the model:

a. Unilateral nature since behavior in tension and compression are

quite different.

- b. Realistic description of the stress strain curve in both of the pre-peak and post-peak regions in both tension and compression.
 - c. The cyclic behavior reasonably idealizes the stiffness degradation and the residual deformation can be determined.
 - d. The biaxial strength envelope reflects the well-documented experimental features especially in the compression-compression quadrant.
 - e. The stress free straining can be evaluated for all possible stress combinations.
 - f. The volumetric changes are plausibly predicted where early compaction followed by dilation takes place for compressive associated loading.
 - g. Reduced number of the required material parameters which can be determined from uniaxial testing.
 - h. The orthotropic nature of concrete behavior is underlined.
 - i. The degradation of the shear modulus is implicitly monitored, thus shear retention is indirectly taken into account.
7. The derived damage model for reinforcing steel allows for the nonlinear hardening features. Uniaxial tensile experiments on local steel shows that ductile behavior is exhibited.
8. Fully coupled strain-damage algorithm together with the proposed

search-find technique is found to be efficient for general uniaxial nonlinearity scheme as employed by the program DMGTRUSS. This facilitates analysing linear elastic, hyperelastic, elastic perfectly-plastic, elastic hardening, rigid perfectly-plastic and rigid hardening materials in addition to those follow particular damage behavior.

9. General finite element formulations for isoparametric and sheath elements are derived in a manner that allows their use in various related purposes.

10. Fully coupled strain-damage with proportional and nonproportional plane stress algorithms allows for material modelling on different structural scales as established in the program DMGPLSTS. Careful attention should be paid to the selection of the appropriate methodology since different results may be obtained in the post-cracking regime.

11. Practical applications to plain and reinforced concrete structural components using DMGTRUSS indicate that the program captures the pre-peak nonlinearity as well as the post-peak softening behavior of concrete, stiffness degradation, translation of the origin of the stress-strain curve along the strain axis, reduction of the peak strength in alternate cyclic loading, unilateral characteristics, and can determine the residual deformations at any stress level.

12. Predictions obtained by DMGPLSTS are shown to be in good agreement with experiments, some other models and design codes.

13. Study of plain and reinforced concrete beams with and without shear reinforcement and compression steel indicates reliable results regarding global softening, nonlinearity of the response, failure modes, prediction of the cracking load as well as the ultimate load carrying capacity as governed by concrete and/or steel damage manifested by flexural and/or shear mechanisms.

14. Study of the steel/concrete bond characteristics indicates the acceptance of the hypothesis of pseudo-slip advocated by Mazars (1984). Although perfect bond is postulated between concrete and reinforcing steel, the formation of damage zone in the vicinity of the rebars implicitly idealizes bond-slip behavior.

The damage framework presented in the current work is recommended to be generalized to multiaxial states through the proposed theory of dichotomy.

APPENDICES

APPENDIX I

FORMULATION OF THE FINITE ELEMENT EQUATIONS

The principle of virtual work states that through incremental virtual displacements; the incremental virtual work done by internal forces, $\delta (dU)$, is equal to the incremental virtual work done by external loads, $\delta (dW)$, i. e.

$$\delta (dU) = \delta (dW) \quad (I.1)$$

The virtual external work due to all sorts of forces, for an element of volume, V , and surface area, A , is given as (Chen, 1982 ; Zienkiewicz; 1978) :

$$\delta W = \{\delta(d\bar{\varphi}^*)\}^T (\{dP\} + \int_A |N|^T \{dT\} dA + \int_V |N|^T \{dX\} dV) \quad (I.2)$$

where

- $|N|$ the interpolation matrix
- $\{\delta(d\bar{\varphi}^*)\}$ the incremental virtual nodal displacements
- $\{dP\}$ the incremental concentrated nodal forces vector
- $\{dT\}$ the incremental surface traction vector
- $\{dX\}$ the incremental body forces vector

The virtual internal work can be expressed as

$$\delta U = \int_V \{\delta(\mathbf{d}\epsilon^*)\}^T \{\mathbf{d}\sigma\} dV \quad (I.3)$$

where

$\{\delta(\mathbf{d}\epsilon^*)\}$ the incremental virtual strain vector
 $\{\sigma\}$ the incremental stress

The incremental virtual strain can be related to the nodal displacements through the relation:

$$\{\delta(\mathbf{d}\epsilon^*)\} = [B] \{\delta(\mathbf{d}\bar{\varphi}^*)\}^T \quad (I.4) \text{ } \epsilon$$

in which $[B]$ is the strain-displacement matrix and depends on the element type and the chosen approximation function for the relevant degrees of freedom. Substituting Eqn. I.4 in Eqn. I.3, then equate the product to Eqn. I.2 as applied to the virtual work principal (Eqn. I.1), yields

$$\int_V [B]^T \{\mathbf{d}\sigma\} dV = \{\mathbf{d}P\} + \int_A [N]^T \{\mathbf{d}T\} dA + \int_V [N]^T \{\mathbf{d}X\} dV \quad (I.5)$$

To arrive at Eqn. I.5, the virtual displacement vector, $\{\delta(\mathbf{d}\bar{\varphi}^*)\}^T$ has been cancelled since it is arbitrary. The tangential stress-strain can be expressed in the form:

 ϵ - The same relation is applicable to incremental actual parameters

$$\{\sigma\} = [C_t] (\{d\epsilon\} - \{\alpha d\Theta\}) \quad (I.6)$$

in which, $[C_t]$ is the tangent modulus matrix, $\{d\epsilon\}$ is the incremental strain vector, $\{d\Theta\}$ is the incremental temperature vector, and α is the coefficient of thermal expansion. Substituting Eqn. I.6 in Eqn. I.5, and making use of Eqn. I.4 applied to actual, not virtual, strain-displacement relationship, it can be easily shown after simple mathematical manipulations that the reduced matrix equation is

$$[K_t] \{d\bar{\varphi}\} = \{dF\} \quad (I.7)$$

where,

$$[K_t] = \int_V [B]^T [C_t] [B] dV \quad (I.8)$$

and

$$\{dF\} = \{dP\} + \int_A [N]^T \{dT\} dA + \int_V [N]^T \{dX\} dV - \int_V [B]^t [C_t] \{\alpha d\Theta\} dV \quad (I.9)$$

Equation I.7 represents the incremental element stiffness matrix equations in terms of the tangential stiffness matrix, $[K_t]$, the incremental nodal displacement vector, $\{d\bar{\varphi}\}$, and the incremental nodal forces, $\{dF\}$. Assembly of elements' equations is required to obtain the structural stiffness matrix equations in the global system of axes.

APPENDIX II

NONLINEAR SOLUTION TECHNIQUES

Two general solution techniques were followed successfully (Anand, 1980): (1) Direct solution using either interpolative or iterative schemes, and (2) Quadratic Programming technique in which the kinematic minimum principle is used in conjunction with the Lagrangian multiplier technique. In this study, an incremental iterative finite element formulation is adopted to trace the whole structure response and to account for any possible path dependence. There have been great advances in developing efficient solution algorithms for nonlinear problems. An extensive review of most of the proposed methods is given by Abd-Alrahman (1984). Newton-Raphson method and its variants (Modified Newton-Raphson and initial Stiffness methods) are briefly described.

II.1. CALCULATION STEPS

Most of the incremental nonlinear solution procedures are combined with iteration in order to dissipate the out of plane forces $\{\psi\}$. The first step in any increment, i , is to calculate an initial estimate of the displacements, $\{\Delta\bar{q}_1^i\}$, then additional corrective displacements,

corresponding to the r^{th} iteration, $\{\delta\bar{\varphi}_R^i\}$ are obtained. The most important iteration schemes are some form of the Newton-Raphson iterative method.

II.2. NEWTON-RAPHSON METHOD

The discretized system of nonlinear equations, for any load increment i , can generally be written in the form

$$\{\psi(\{\bar{\varphi}^i\})\} = \{0\} \quad (\text{II.1})$$

where

$$\{\psi(\{\bar{\varphi}^i\})\} = \{r^i(\{\bar{\varphi}^i\})\} - \{f^i\} \quad (\text{II.2})$$

in which $\{\bar{\varphi}^i\}$ is the desired solution, $\{\psi\}$ is the gradient of the total potential energy or the out of balance residual force vector, $\{r^i\}$ is the vector of internal nodal point forces equivalent to the element stresses at the end of the load increment i and $\{f^i\}$ is the vector of externally applied nodal point loads at the considered increment.

If an approximate solution $\{\bar{\varphi}_R^i\}$ to Eqn. (II.2) is reached, an improved solution using a truncated Taylor series expansion can be obtained using the expression

$$\{\psi(\{\bar{\varphi}_{R,1}^i\})\} = \{\psi(\{\bar{\varphi}_R^i\})\} + \left\{ \frac{\partial \psi}{\partial \varphi} \right\}_{\{\bar{\varphi}_R^i\}} \{\delta\bar{\varphi}_R^i\} \quad (\text{II.3})$$

where higher order terms have been neglected. In the above equation

$$\frac{\{\partial \Psi\}}{\{\partial \bar{\varphi}\}} \Big|_{\{\bar{\varphi}_R^i\}} = [K_{tR}^i] \quad (II.4)$$

represents the tangent stiffness or Jacobean matrix at the r th iteration in the i th increment.

If the approximation $\{\bar{\varphi}_{R,1}^i\}$ is used instead of $\{\bar{\varphi}^i\}$ in Eqn. (II.1), then Eqn. (II.4) can be written as

$$\{\psi(\{\bar{\varphi}_R^i\})\} + [K_{tR}^i] \{\delta \bar{\varphi}_R^i\} = \{0\} \quad (II.5)$$

from which the iterative displacement $\{\delta \bar{\varphi}_R^i\}$ can be found as

$$\{\delta \bar{\varphi}_R^i\} = [K_{tR}^i]^{-1} \{\psi(\{\bar{\varphi}_R^i\})\} \quad (II.6)$$

The improved approximation $\{\bar{\varphi}_{R,1}^i\}$ can be computed as

$$\{\bar{\varphi}_{R,1}^i\} = \{\bar{\varphi}_R^i\} + \{\delta \bar{\varphi}_R^i\} \quad (II.7)$$

Equations (II.6) and (II.7) constitute the Newton-Raphson solution of Eqn. (II.1). The procedure using (II.6) and (II.7) continues and for each iteration a new system of linearized equations has to be solved for $\{\delta \bar{\varphi}_R^i\}$, until an appropriate termination criterion is satisfied.

II.3. MODIFIED NEWTON-RAPHSON METHOD

In the full Newton-Raphson method, the tangential stiffness matrix has to be updated and a completely new system of equations has to be solved in each iteration. This process can be highly expensive particularly if relatively small load increments have to be used. To overcome this difficulty some modifications of the full Newton-Raphson algorithm is made by updating the stiffness matrix only occasionally, e.g. once for each increment, and maintaining the same matrix for successive iterations until convergence is achieved. two possible modifications may be followed. The first includes calculation of the stiffness matrix at the beginning of each increment while the other considers the updated stiffness in the second iteration. The latter reflects the nonlinear effects induced by the current incremental load application. Of course these modifications slow down the convergence even if accelerating schemes are utilized.

II.4. INITIAL STIFFNESS METHOD

This method was first advocated by Zienkiewicz and his co-workers (Adel-Rahman, 1982) for the solution of elasto-plastic problems. The method can be thought of as a modification to the Newton-Raphson algorithm where the initial elastic stiffness is maintained throughout the entire analysis. Though the use of this method renders a particular solution to some of the problems associated with full and Modified Newton-Raphson methods, for example ill-conditioning, the convergence characteristics of the method are not encouraging particularly when

highly nonlinear problems are to be dealt with .

*APPENDIX III***CONVERGENCE CRITERIA**

In an incremental-iterative solution strategy, the solution obtained at the end of each iteration is checked to see whether it has converged within specified tolerances or whether it is diverging. The convergence tolerances must be realistic. If the convergence tolerance is too loose, inaccurate results are obtained and if the tolerance is too high, much expensive effort is spent to obtain needless accuracy.

The convergence criteria, that are usually used for nonlinear structural analysis, are based on either displacements, out of balance forces, or internal energy. In the current study, the force convergence criterion, the displacement convergence criterion or combination are found to yield satisfactory results.

III.1 FORCE CRITERION

The residual or out-of-balance forces, which are the differences between the applied forces and the equivalent internal nodal forces, are used to check equilibrium and consequently the convergence of the nonlinear solution.

Equilibrium of forces in a certain direction, j , is deemed to be

achieved if the following expression is satisfied

$$e_j = \frac{\| \psi \|_r^j}{\| f \|_r^j} \times 100 \leq (\text{TOLER})_j \quad (\text{III.1})$$

More practically, an overall (global) check for all degrees of freedom can be written in the form

$$e_f = \frac{\sum_j \| \psi \|_r^j}{\sum_j \| f \|_r^j} \times 100 \leq (\text{TOLER})_f \quad (\text{III.2})$$

In the above expressions the following notations are used:

$\| \bullet \|_r^j$ represents the Euclidean norm at iteration r for forces in direction j ,

ψ represents the out-of-balance forces,

f represents the total nodal forces,

$(\text{TOLER})_j$ a percentage value of the allowable convergence tolerance for the forces in direction, and j .

$(\text{TOLER})_f$ a percentage value of the allowable global force convergence tolerance.

III.2 DISPLACEMENT CRITERION

The incremental displacements obtained through each iteration are used to judge the overall convergence by expressing a global check over all degrees of freedom in the following form

$$e_d = \frac{\sum_j \|\delta\varphi\|_r}{\sum_j \|\varphi\|_r} \times 100 \leq (\text{TOLER})_d \quad (\text{III.3})$$

In the above expressions the following notations are used:

$\delta\varphi$ represents the incremental displacements,

φ represents the total displacements,

$(\text{TOLER})_d$ a percentage value of the allowable global displacement convergence tolerance.

APPENDIX IV

DMGTRUSS GLOSSARY

IV.1 DMGTRUSS VARIABLES

VARIABLE	DESCRIPTION
A1, B1	Material parameters in Mazars' damage model.
AE	The ratio of the elastic modulus to the total modulus.
AP	The ratio of the plastic modulus to the total modulus.
BUKST	Buckling stress in compression members after Euler's formula.
C1, C2	Material parameters used in Krajcinovic and Fanella's (1981) damage model.
C1, C3	Coefficients derived from the material parameters used in Loland's damage model.
CRDMP	Critical damage parameter.
DA	Current value of the loading damage variable.

DB	Material parameter used in Krajcinovic and Fanella's damage model, $DB = B_1 - B_3$, B_1 and B_3 are another material parameters.
DE	Current value of the unloading damage variable.
DFACT	The ratio of the final strain to the peak strain for parabolic relations.
DMATO	Uncorrected tangential modulus for thermal loading.
DMSTR	Threshold damage strain; $=\epsilon_t$ in damage models #1, #3, #4; $=\epsilon_c$ in damage models #2; $=\epsilon_{11}^0$ in damage models #6; $=\epsilon_y$ in damage models #8; and $=\epsilon_d$ in damage models #10.
DIVFN	Tangent slope coefficient at the current stress-level.
DO	Initial damage parameter used in Loland's damage model.
DP	Current value of the plastic damage variable.
EQYNG	Current linear unloading/reloading modulus.
FACTO	Current increment load/displacement factor.

FACTR	Gaussian reduction factor.
FMULT	Corrected tangential modulus for thermal loading.
FT	The tensile strength of concrete f_t' .
FUNCN	The nonlinear-damage loading function coefficient at the current stress-level.
IDMGE	Index of the current element's damage model.
IEQNS	Index of equation number.
IINCS	Current increment number.
IITER	Current iteration number.
IDMGE	Global damage indicator, IDMGE = 0; non of the built in damage models is used, IDMGE = 1; same damage model is used in tension and compression, IDMGE = 2; different damage models are used in tension and compression.
IGEOM	Global geometric nonlinearity indicator, IGEOM = 0; no geometrical nonlinearity, IGEOM = 1; structural geometry is updated after every increment.
ILINS	Global material nonlinearity indicator, ILINS = 0; linear elastic material, ILINS = 1; material has

same response in tension and compression, IINS = 2; material has different behavior in tension from compression.

ISTEP	Index for the stress pump of the current stress-strain zone.
ITEMP	Thermal loading indicator, ITEMP = 0; no temperature loading, ITEMP = 1; there is thermal changes.
IZNCU	Index for the current stress-strain zone.
LPROP	Index for the element's material number.
KRESL	Solution indicator number, KRESL = 1; compute stiffness and solve the full system, KRESL = 2; use old stiffness matrix and equation resolution need be done.
KUNLC	Unloading code of the current zone.
LDCSE	Load case indicator, LDCSE = 1; no temperature loading, LDCSE = 2; only temperature loading, LDCSE = 3; combined temperature and nodal loading.
NALGO	Solution algorithm selector.
NBOUN	Number of restrained nodes.

NCHEK	Convergence check indicator. NCHEK = 0; solution has converged, NCHEK = 1; solution is converging, NCHEK = 999; solution has diverged.
NCOLS	Number of the column in the global structural stiffness matrix and load vector.
NDIME	Number of dimensions. NDIME = 1; for one-dimensional truss, NDIME = 2; for plane truss, NDIME = 3, for space truss.
NDOFN	Number of nodal degrees of freedom in the global system; NDOFN = NDIME in DMGTRUSS.
NELEM	Number of elements.
NEVAB	Number of element variables; NEVAB = NNODE X NDOFN.
NINCS	Number of increments.
NITER	Number of iterations within an increment.
NLDCN	Number of loading conditions, NLDCN = 2; i.e. tension and compression.
NMATS	Number of different materials.
NNODE	Number of nodes per element; NNODE = 2.
NOUTP	Output type control, NOUTP = 0; print the

results on convergence, NOUTP = 1; print after first iteration and after convergence, NOUTP = 2; print after every iteration.

- NPROD** Number of properties for damage model used for each material in either tension or compression; NPROD = 5.
- NPROP** Number of properties for each material; NPROP = 16.
- NPROT** Number of parameters ample to specify nonlinear elastic degradation with temperature; NPROT = 5.
- NPROZ** Number of parameters ample to specify nonlinear-damage behavior for loading of each material in either tension or compression; NPROZ = 8.
- NROWS** Number of the row in the global structural stiffness matrix and load vector.
- NSTRE** Number of stress variables.
- NSVAB** Number of structural variables; NSVAB = NPOIN X NDOFN.
- NZONE** Number of zones sufficient to describe the material stress-strain relationship in either loading condition; maximum value is NZONE = 5.

NZONT	Number of zones sufficient to describe the material degradation with thermal effects; maximum value is NZONT = 2.
PIVOT	Diagonal term of variable currently being evaluated in equations reduction.
PO	Poisson's ratio.
PO1, POK	Coefficients related to Poisson's ratio.
PVALU	The value of RATIO in the previous iteration.
RATIO	The percentage of the residual norm.
RPARM	The material parameter R in the damage model for steel.
RPSTR	The rupture strain in the isotropic ductile damage model.
S	Exponent used in the canonical uniaxial model for concrete.
ST	The ratio of strain to the peak strain for concrete.
STEP	The value of stress pump of the current stress-strain zone.
STNCU	The current strain value with respect to the

stress-strain curve origin.

STNDF	The current strain value with respect to the initial strain of the current zone.
STNEX	The maximum strain value with respect to the stress-strain curve origin.
STNOL	The previous strain value with respect to the stress-strain curve origin.
STRAN	The incremental strain.
STRESS	The cumulative stress in SEARCH-FIND scheme.
STRSO	The ultimate strength σ_0 in the damage model for steel.
TFACTO	cumulated incremental factors.
TOLER	Tolerance for convergence.
UN	Material parameter, μ_n , in Loland's damage model.
W	Voids intensity in Krajcinovic and Fanella's (1981) damage model.
WO	The initial value of voids intensity in Krajcinovic and Fanella's (1981) damage model.

IV.2 DMGTRUSS ARRAYS

ARRAY	DESCRIPTION
ASDIS(NSVAB)	The global vector of incremental nodal displacements.
ASOLD(NSVAB)	The global vector of applied loads.
ASTIF(NEVAB,NEVAB)	The global stiffness matrix.
BMATX(NSTRE,NEVAB)	The strain-nodal displacement matrix for each element which is updated when IGEOM = 1. It is stored after its construction in Tape 3.
COORD(NPOIN)	Updated coordinates of nodal points.
CUDMP(NELEM,NLDCN,NSTRE)	Updated damage parameter for each element in either loading condition.
DL(NELEM)	Element's length which is updated if IGEOM = 1.
DMATX(NSTRE,NSTRE)	Tangential modulus matrix for each element which is updated if ILINS \neq 0. It is stored in Tape 2.

ELCOD(NDIME,NNODE)	Current coordinates of element's nodal points.
ELOAD(NELEM,NEVAB)	Applied factored nodal loads in each element.
ESTIF(NEVAB,NEVAB)	The element stiffness matrix.
ETEMP(NELEM)	The current temperature variation within every element.
ETPLD(NELEM,NEVAB)	The current temperature consistent loading within every element.
FIXED(NSVAB)	Factored prescribed variables, according to the load increment factor, in the global array.
FRESV()	Stored Gaussian reduction factors.
ICODE(NDOFN)	Fixity code for each degree of freedom at a restrained node, ICODE = 0; free degree of freedom, ICODE = 1; prescribed degree of freedom.
IFPRE(NSVAB)	Global array of fixity codes for all degrees of freedom, IFPRE = 0; free degree of freedom, IFPRE = 1; prescribed degree of freedom.

IZONE(NELEM,NSTRE) Current zone on the loading path for each stress component of every element.

LNCOD(NELEM) Current loading status, LNCOD = 1; tensile loading, LNCOD = 2; compressive loading.

LNODS(NELEM,NNODE) Element nodal connectivities.

MATNO(NELEM) Element's material identification number.

PROPD(NMATS,NLDCN,NPROD,NSTRE)
 Properties for each damage model in either loading condition of each material: DMSTR-DMSTR, DFACTO- DMSTR, A1, B1- DMSTR, FT, DO, UN- DMSTR, DB, C1, C2- DMSTR, STRSO, RPARAM- DMSTR, RPSTR, CRDMP for damage models #1-#2-#3-#4-#6-#8-#10, respectively.

PROPS(NMATS,NPROP,NSTRE)
 Properties for each material set for each stress component, for the counter IPROP= 1, NPROP take the values: 1) number of nonlinearity zones in tension, 2) number of nonlinearity zones in compression, 3) tensile damage model code, 4) compressive damage model code, 5) initial tangential modulus, 6) cross sectional area, 7) second moment of

area, 8) coefficient of thermal expansion, 9) thermal loading code ITEMP, 10) Poisson's ratio, 11) threshold elastic damage strain ϵ_{e_d} , 12-14) coefficients for degradation of elastic modulus $\sigma_0, \sigma_1, \sigma_2$, 15) mass density and 16) acceleration of gravity.

PROPT(NMATS,NZONT,NPROT)

Properties for each zone of material degradation by thermal effects, for the counter IZONT= 1, NZONT takes the values of the polynomial coefficients for the material degradation under thermal effects.

PROPZ(NMATS,NLDCN,NZONE,NPROZ,NSTRE)

Properties for each zone describing material nonlinear-damage behavior in either loading conditions. For the i th zone (counter IZONE= 1, NZONE) the properties corresponding to the counter IPROZ= 1, NPROZ are: 1) the initial strain ϵ_{o_i} , 2) the moduli multiplier ξ_i , 3-5) the polynomial coefficients $\beta_{0_i}, \beta_{1_i}, \beta_{2_i}$ for the damage variable d_{a_i} , 6) unloading code KUNLC, 7)

stress discontinuity code ISTEP, 8) initial stress discontinuity value for the zone under consideration.

PFIX(NSVAB)	Global array for prescribed values.
PLAST(NELEM,NSTRE)	Plastic strain of every stress component of each element.
RCORD(NPOIN)	Original coordinates of nodal points.
REACT(NSVAB)	Incremental reactions at prescribed nodes.
RLOAD(NSVAB)	Reference applied nodal loads.
RTEMP(NELEM)	The full range of temperature variation within every element.
RTPLD(NELEM,NEVAB)	The total temperature consistent loading within every element.
STNMN(NELEM,NSTRE)	The strain of the current stress-strain curve origin of every element.
STNMX(NELEM,NSTRE)	The maximum ever reached strain of every element.
STRES(NELEM,NSTRE)	The current stress component of every element.
STRIN(NELEM,NSTRE)	The current strain component of every

	element.
TDISP(NPOIN,NDOFN)	Nodal displacements.
TLOAD(NELEM,NEVAB)	Total applied loads at the current increment.
TREAC(NPOIN,NEVAB)	Total reactions at the prescribed nodes.
XDISP(NSVAB)	Total displacements corresponding to the structural variables.
YOUNG(NELEM)	The current elastic modulus for each element.

APPENDIX V

DMGTRUSS' INSTRUCTIONS

V.1 INPUT CARDS

The input file is composed of several cards, the description of which is given hereafter

INPUT CARD	DESCRIPTION
CARD I	Title card; one line TITLE
CARD II	Control parameters; one line: NPOIN,NELEM,NBOUN,NMATS,NDOFN,NINCS, NALGO,IGEOM,ILINS,IDMGS,ITEMP.
CARD III	Structural material parameters, NMATS blocks
CARD III.1	Control parameters: JMATS,(PROPS(JMATS,IPROP,ISTRE),IPROP=1,NPROP)
CARD III.2	Material properties for general nonlinearity:

- CARD III.2.1 Material properties for multiple tensile zones,
NTZON lines
(NTZONE=INT(PROPS(JMATS,1,ISTRE))):
(PROPZ(JMATS,1,ITZON,IZPRO,ISTRE),IZPRO=1,8)
- CARD III.2.2 Material properties for multiple compressive zones,
NCZON lines
(NCZON=INT(PROPS(JMATS,2,ISTRE))):
(PROPZ(JMATS,2,ICZON,IZPRO,ISTRE),IZPRO=1,8)
- CARD III.3 Material properties for specific damage law
(alternative to III.2):
- CARD III.3.1 Material properties for tensile damage model
number INT(PROPS(JMATS,3,ISTRE)):
(PROPD(JMATS,1,IDPRO,ISTRE),IDPRO=1,4)
- CARD III.3.2 Material properties for compressive damage model
number INT(PROPS(JMATS,4,ISTRE)):
(PROPD(JMATS,2,IDPRO,ISTRE),IDPRO=1,4)
- CARD III.4 Thermal material parameters, NTEMP lines
(NTEMP=INT(PROPS(JMATS,9,ISTRE))):
(PROPT(JMATS,JTEMP,ITPRO),ITPRO=1,8)

CARD V Elements properties: number, connectivity,
 material I.D. and temperature, NELEM lines:
 JELEM, (LNODS(JELEM, INODE), INODE=1, NNODE),
 MATNO(JELEM), RTEMP(JELEM)

CARD VI Nodal coordinates, NPOIN lines:
 JPOIN, (RCORD(JPOIN, IDIME), IDIME=1, NDIME)

CARD VII Prescribed nodal displacements, NBOUN lines:
 NODFX, (ICODE(IDOFN), VALUE(IDOFN), IDOFN=1, NDOFN)

CARD IIX Applied nodal loads, terminates when reads
 JELEM=NELEM:
 JELEM, (RLOAD(JELEM, IEVAB), IEVAB=1, NEVAB)

CARD IX Incremental/iterative control parameters, NINCS
 lines:
 LDCSE, NITER, NOUTP, FACTO, TOLER

V.2 SAMPLE INPUT FILE

A sample input file is listed in the attached sheet (P.T.O.)

APPENDIX VI

DMGPLSTS GLOSSARY

VI.1 DMGPLSTS VARIABLES

VARIABLE	DESCRIPTION
Alpha	Modified Guo and Zhang's coefficient (1987); α .
B	Modified Popovics' coefficient (1973); n .
Beta	The biaxiliaty ratio.
DMSTR	The threshold damage (yield) strain for steel, ϵ_y .
DVOLU	The differential elemental volume, = $ J \ t \ W_i \ W_j$.
EPCO	The uniaxial compressive peak strain.
EPTO	The uniaxial tensile peak strain.
ETASP	The η coordinate of the Gauss point.
EXISP	The ξ coordinate of the Gauss point.
FC	The uniaxial compressive strength.
FT	The uniaxial tensile strength.

IQUAD	The biaxial stress quadrant; =1 for biaxial tension quadrant, =2 for uniaxial tension, =3 for tension-compression quadrant, =4 for uniaxial compression, =5 for compression-compression quadrant.
KGASP	Local counter of the sampling points over each element.
KGAUS	Global counter of the sampling points over the whole structure.
LITER	Least number of iterations, in the nonlinear solution, controlled by force convergence criterion.
MTOTG	Maximum total number of sampling points over the whole structure.
NGAUI	Number of sampling points in the direction of the ξ -axis.
NGAUJ	Number of sampling points in the direction of the η -axis.
NSTRP	Number of principal stress components; =2 for plane stress and =3 for plane strain, axisymmetrical and 3-D problems.

POISS	Initial undegraded Poisson's ratio, ν_0 .
RPARAM	The material parameter R for damage model of steel.
STRSO	The ultimate strength of steel σ_0 .
THETA	The angle between the x-axis the major principal axis, θ .
THICK	The thickness or cross-sectional area of concrete and steel elements, respectively.
UYLFC	The upper yield stress multiplier coefficient α for the steel damage.
YOUNG	The initial tangential modulus.

VI.2 DMGPLSTS ARRAYS

ARRAY	DESCRIPTION
AOR(NSTRP)	The initial tangent multiplier of the total behavior in the principal plane.
BIAXL(I,MTOTG)	The biaxial characteristic quantities; I=1 for IQUAD, I=2 for BETA, and I=3 for THETA.

EOR(NSTRP)	The initial tangent multiplier of the elastic behavior in the principal plane.
DA(NSTRP)	The total damage variable in the principal plane.
DDA(NSTRP)	The differential total damage variable, $\partial d_a / \partial \epsilon$, in the principal plane.
DE(NSTRP)	The elastic damage variable in the principal plane.
EPRV(NSTRP)	The peak strain function, η_{ϵ} .
EQYNG(NSTRP)	The degraded unloading moduli in the principal space.
LETYP(NELEM)	The element type; =2 for 2-noded boom element, =3 for 3-noded boom element, =5 for 4-noded interface quadrilateral element, =6 for 4-noded quadrilateral element, =7 for 6-noded interface element, =8 for 6-noded element, =11 for 8-noded Serendipity element, =12 for 9-noded Lagrangian element.
PROPS(NMATS, NPROP)	The materials' properties array. For the counter IPROP= 1, NPROP, it takes the

values: i. *for concrete*: 1) FC, 2) POISS, 3) THICK and ii. *for steel*: 1) YOUNG, 2) DMSTR, 3) THICK, 6) STRSO, 7) RPARM, 8) UYLFC.

SIGNE(NSTRP)	The sign of the stress components; =-1 for compression and =1 for tension.
SPRV(NSTRP)	The peak stress function, η_{σ} .
STNCU(NSTRE)	The current strain in the current principal plane.
STNDF(NSTRE)	The current strain increment in the XY plane.
STNEX(NSTRE)	The maximum ever reached strain in the current principal space.
STNMN(NSTRE)	The strain ordinate corresponding to the origin of the active stress-strain curve in the XY plane.
STNMX(NSTRE)	The maximum ever reached strain ordinate in the XY plane.
STNOL(NSTRE)	The strain of the previous iteration in the current principal space.
STRAN(NSTRE)	The strain increment in the current

principal space.

STRES(NSTRE) The stress vector in the current principal space.

STRIN(NSTRE,MTOTG) The total strain ordinate in the XY plane at each sampling point.

STSDF(NSTRE) The stress increment in the current principal space.

APPENDIX VII

DMGPLSTS' INSTRUCTIONS

VII.1 INPUT CARDS

The input file is composed of several cards, the description of which is given hereafter

INPUT CARD	DESCRIPTION
CARD I	Title card; one line: TITLE
CARD II	Control parameters; one line: NPOIN,NELEM,NVFIX,NTYPE,NNOD1,NMATS, NGAUS,NALGO,NCRIT,NINCS,LSTRE,NDIME, NDOFN,IPROB
CARD III	Elements properties: number, material I.D., element type and connectivity, NELEM lines: NUMEL,MATNO(NUMEL),LETYP(NUMEL), (LNODS(NUMEL,INOD1),INOD1=1,NNOD1)

- CARD IV Nodal coordinates, NPOIN lines:
 JPOIN,(RCORD(JPOIN, IDIME), IDIME=1, NDIME)
- CARD V Prescribed nodal displacements, NVFIX lines:
 NOFIX(IVFIX), IFPRE,
 (PRESC(IVFIX, IDOFN), IDOFN=1, NDOFN)
- CARD VI Structural material parameters, NMATS blocks:
- CARD VI.1 Material number, one line:
 NUMAT
- CARD VI.2 Material properties, one line:
 (PROPS(NUMAT, IPROP), IPROP=1, NPROP)
- CARD VII Loading block and contains the following
 subcards:
- CARD VII.1 Loading title, one line:
 TITLE
- CARD VII.2 Control data for loading types, one line:
 IPLD, IGRAV, IEDGE, ITEMP, IPORE
- CARD VII.3 Nodal point loads, terminates when
 LODPT=NPOINT:

LODPT, (POINT(IDOFN), IDOFN=1, NDOFN)

CARD VII.4 Gravity loading section, one line:

THETA, GRAVY

CARD VII.5 Distributed edge loading block:

CARD VII.5.1 Number of loaded edges, one line:

NEDGE

CARD VII.5.1 Data about the loaded edge:

LDCSE, NEASS, IGTYP,
(NOPRS(IODG1), IODG1=1, NODG1)

CARD VII.5.2 Data about the loading values:

(PRESS(IODGE, IDOFN), IDOFN=1, NDOFN)
, IODGE=1, NODGE)

CARD IIX Incremental/iterative control parameters, NINCS

lines:

FACTO, TOLER, MITER, LITER, NOUTP(1), NOUTP(2)

VII.2 SAMPLE INPUT FILE

A sample input file is listed in the attached sheet (P.T.O.)

REFERENCES

REFERENCES

- Abdel-Rahman, H. H., 1982, Computational Models for the Nonlinear Analysis of Reinforced Concrete Flexural Slab System, *Ph. D. Thesis*, Depart. Civil Engng., Univ. Swansea, Swansea, U. K.
- Abdoui, B., 1982, Sur la Prevision de la Dechirure Ductile par la Theorie de l'Endommagement Associee a des Calculs de Plasticite, *These de 3eme Cycle Universite 6*.
- Ahlberg, J. E., Nilson, E. N., Walsh, J. L., 1976, *The Theory of Splines and Their Application*, Academic Press, New York.
- Akroyd, T. N., 1961, Concrete under Triaxial Stress, *Mag. Conc. Res.*, 13, 111-118.
- Andenaes, E., Gerstle, K., Ko, H. Y., 1977, Response of Mortar and Concrete to Biaxial Compression, *J. Engng Mech. Div., ASCE*, 103, EM4, 515.
- Andersson, H., 1973, A Finite Element Representation of Stable Crack Growth, *J. Mech. Phys. Solids*, 21, 337-356.
- Anquez, L., 1981, La Progression des Fissures de Fatigue en Elasto-Plasticite, *La Recherche Aerospaciale*, 6, 375-391.
- Anson, M., 1962, An Investigation into a Hypothetical Deformation and Failure Mechanism of Concrete, *Ph.D. Thesis*, Univ. of London, Nov.
- Archard, J. F., 1958, Elastic Deformation and the Laws of Friction, *Proc. R. Soc.*, A243, 190-205.
- Argyris, J. H., Faust, G., Szimmat, J., Warnke, E. P., Willam, K. J., 1974a, Recent Development in the Finite Element Analysis of Prestressed Concrete Reactor Vessels, *Nuclear Engng. and Design*, 28, 42-75.
- Argyris, J. H. 1974b, Recent Developments in the Finite Element Analysis of Prestressed Concrete Reactor Vessels, *IABSE Seminar, ISMES, Bergamo, Italy, May*.
- ASCE, 1982, State-of-the-Art on *Finite Element Analysis of Reinforced Concrete*, prepared by a Task Committee Chaired by A. Nilson, Am. Soc. of Civ. Engrs., New York.
- Aschl, H., Linse, D., Stoeckl, S., 1976, Strength and Stress Strain Behaviour of Concrete under Multiaxial Compression and Tension Loading, *ICM II, Proc. 2nd Int. Conf. Mechanical Behavior of*

- Materials*, Boston, Massachusetts, 102-117.
- Baker, A. L. L., 1959, An Analysis of Deformation and Failure Characteristics of Concrete, *Mag. Concrete*, 11, 33, 119-128.
- Baker, A. L. L., 1970, A Criterion of Concrete Failure, *Proc. Inst. Civ. Engng.*, London, Nov.
- Balmer, G. G., 1949, Shearing Strength of Concrete under High Triaxial Stress- Computation of Mohr's Envelop as a Curve, *Report, No. SP-23*, Struc. Res. Lab., Bureau of Reclamation, US Dept. of Interior.
- Bangash, Y., 1982, Reactor Pressure Vessel Design and Practice, *Progee in Nuclear Energy*, 10, 69-124.
- Bangash, Y., 1987, The Simulation of Endochronic Model in the Cracking Analysis of PCPV, *9th Int. Conf. on Structural Mech. in Reactor Technology, SMIRT*, lausanne, 4, 333-340.
- Bangash, Y., 1989, *Concrete and Concrete Structures: Numerical Modelling and Applications*, Elsevier Applied Science.
- Barnes, B. D., Diamond, S., Dolch, W. L., 1978, The Contact Zones Between Portland Cement Past and Glass Aggregate Surfaces, *Cem. Concr. Res.*, 8, 233-244.
- Bashur, F. K., and Darwin, D., 1987, Nonlinear Biaxial Low for Concrete, *J. Struct. Div., ASCE*, 104, ST1, 157.
- Bathe, K. J., and Ramaswamy, S., 1979, On Three-Dimensional Nonlinear Analysis on Concrete Structures, *Nuclear Engng. and Design*, 52, 3, 385-409.
- Bazant, Z. P., 1974, A New Approach to Inelasticity and Failure of Concrete, Sand and Rock: Endochronic Theory, *Proc. of the Soc. of Engng. Sci.*, Durham, N. C.
- Bazant, Z. P., 1976a, Instability, Ductility, and Size Effect in Strain-Softening Concrete, *J. Engng. Mech., ASCE*, 102, 331-344.
- Bazant, Z. P., and Bhat, P. D., 1976b, Endochronic Theory of Inelasticity and Failure of Concrete, *J. Engng. Mech., ASCE*, 102, 701-722.
- Bazant, Z. P., and Bhat, P. D., and Shieh, C.L., 1976c, Endochronic Theory of Inelasticity and Failure Concrete Structures, *Struct. Engng. Report No. 1976-12/259*, Northwestern Univ., Evanston, III, Dec., (available from National Technical Information Service, Springfield, Va.).

- Bazant, Z. P., and Krizek, R. J., 1976d, Endochronic Constitutive Law for Liquefaction of Sand, *J. Engng. Mech.*, ASCE, 102, 225-238.
- Bazant, Z. P., 1976e, Addendum to Report: Endochronic Theory of Inelasticity and Failure of Concrete Structures, *Struct. Engng. Rep. No. 1976-12/259* (to Oak Ridge Nat. Lab.), Northwestern Univ., Dec. (Available from Nat. Tech. Inf. Service, Springfield, Virginia); for a summary see Conf. on Finite Elements in Nonlinear Solid and Structural Mechanics, Geilo, Norway, Aug. 1977, Organized by Norwegian Inst. of Technology, Trondheim.
- Bazant, Z. P., 1978a, Endochronic Inelasticity and Incremental Plasticity, *J. Solids Structures*, 14, 691-714.
- Bazant Z. P., and Shieh, C. L., 1978b, Endochronic Model for Nonlinear Triaxial Behavior of Concrete, *Nuclear Engng. and Design*, 47, 305-315.
- Bazant Z. P., and Shieh, C. L., 1978c, Hysteretic Fracturing Endochronic Theory for Concrete, *Struct. Engng. Report No. 1978-9/640h*, Northwestern Univ., Evanston, III, Sept.
- Bazant Z. P., and Panula, L., 1978d, Statistical Stability Effects in Concrete Failure, *J. Engng. Mech.*, ASCE, 104, EM5, Proc. Paper 14074, Oct., 1195-1212.
- Bazant, Z. P., and Kim, S. S., 1979a, Plastic-Fracturing Theory for Concrete, *J. Engng. Mech.*, ASCE, 105, 429-446.
- Bazant, Z. P., and Cedolin, L., 1979b, Blunt Crack Band Propagation in Finite Element Analysis, *J. Engng Mech. Div.*, ASCE, 105, EM2, 297-315.
- Bazant, Z. P., and Cedolin, L., 1979c, Effect of Finite Element Choice in the Blunt Crack Band Analysis, *Struct. Engng. Report No. 79-740e*, Northwestern, III, (also *Computer Methods in Applied Mechanics and Engineering*, 18, 1980).
- Bazant, Z. P., 1980a, Work Inequalities for Plastic Fracturing Materials, *Int. J. Solids Structures*, 106, 873-901.
- Bazant Z. P., and Shieh, C. L., 1980b, Hysteretic Fracturing Endochronic Theory for Concrete, *J. Engng. Mech.*, ASCE, 106, 929-949.
- Bazant, Z. P., and Cedolin, L., 1980c, Fracture Mechanics of Reinforced Concrete, *J. Engng. Mech.*, ASCE, 106, EM6, 1287-1306.

- Bazant, Z. P., and Gambarova, P. G., 1980d, Rough Cracks in Reinforced Concrete, *J. Struct. Div., ASCE*, 106, St4, Paper 15330, Apr., 819,842.
- Bazant Z. P., and Tsubaki, T., 1980e, Total Strain Theory and Path-Dependence of Concrete, *J. Engng. Mech., ASCE*, 106, Em6, 1151-1173.
- Bazant, Z. P., 1981, Mathematical Modelling of Concrete and Its Experimental Basis, *Procs. of a Workshop on Constitutive Relations for Concrete*, New Mexico Engineering Research Institute, Univ. of New Mexico, Albuquerque, N. M., April 28,29.
- Bazant, Z. P., 1982a, Crack Band Model for Fracture of Geomaterials, *Proc., 4th Intern. Conf. on Numerical Methods in Geomechanics*, Edmonton, Alberta, Canada, June, Eisentein, Z., Ed., 3 (invited lectures), 1137-1152.
- Bazant, Z. P., 1982b, Rock Fracture via Stress-Strain Relations, Concrete and Geomaterials, *Report No. 82-11/665r, Northwestern Univ., Evanston, Illinois*; also *J. of Engng. Mech., ASCE*, 110 , 1015-1035.
- Bazant, Z. P., Cedolin, L., 1983a, Finite Element Modelling of Crack Band Propagation, *J. Struct. Engng, ASCE*, 109, ST2, 69-92.
- Bazant, Z. P., Oh, B. H., 1983b, Crack Band Theory for Fracture of Concrete Materials and Structures, *RILEM, Materials and Structures* 16, 155-187.
- Bazant, Z. P., 1983c, Microplane Model for Fracture of Heterogeneous Materials, *Paper presented at the 1983 ASCE Annual Convention*, Houston, Texas, Oct. 1983.
- Bazant Z. P., and Tsubaki, T., and Celep, Z., 1983d, Singular History Integral for Creep Rate of Concrete, *J. Engng. Mech., ASCE*, 109, Em3, 866.
- Bazant, Z. P., 1983e, Size Effect in Brittle Failure of Concrete Structures, *Report No. 83-2/665s*; Center for Concrete and Geomaterials, Northwestern Univ., Evanston, Illinois; also *J. of Engng. Mech, ASCE*, 110 (1984), 518-535.
- Bazant, Z. P., 1983f, Imbricate Continuum: Variation Formulation, *Report No. 83-11/428i*, Center of Concrete and Geomaterials, Northwestern Univ., Evanston, Illinois, also *J. of Engng. Mech., ASCE*, 110, No. 10, Dec. 1984.
- Bazant, Z. P., and Belytschko, 1983g, Wave Propagation in a Strain-Softening Bar: Exact Solution, *Report No. 83-10/401w*, Center of

- Concrete and Geomaterials, Northwestern Univ., Evanston, Illinois, also, *J. of Engng. Mech.*, ASCE, 105, Em2, 297-315.
- Bazant, Z. P., and Cedolin, L., 1983h, Approximate Linear Analysis of Concrete Fracture by R-Curves, *Report No. 83-7/679a*, Center of Concrete and Geomaterials, Northwestern Univ., Evanston, Illinois, also, *J. of Engng. Mech.*, ASCE, 110(1984), 1336-1355.
- Bazant, Z. P., and Oh, B. H., 1983i, Microplane Model for Fracture Analysis of Concrete Structures, *Proc. Symp. on Interaction of Nonlinear Munitions with Structures*, US Air Force Academy, Colorado Springs, May 1983, 49-55.
- Bazant, Z. P., and Oh, B. H., 1983j, Spacing of Cracks in Reinforced Concrete, *J. of Engng. Mech.*, ASCE, 109, 2266-2212.
- Bazant, Z. P., and Oh, B. H., 1983k, Model of Weak Planes for Progressive Fracture of Concrete and Rock, *Report No. 83-2/448m*, Center of Concrete and Geomaterials, Northwestern Univ., Evanston, Illinois.
- Bazant, Z. P., Pfeiffer, P., and Marchertas, A. N., 1983l, Blunt Crack Band Propagation in Finite Element Analysis for Concrete Structures, *Preprints 7yh Int. Conf. on Structural Mechanics in Reactor Technology*, Chicago, Aug.
- Bazant, Z. P., Chang, T. P., and Belytschko, T. B., 1983m, Continuum Theory for Strain Softening, *Report No. 83-11/428c*, Center of Concrete and Geomaterials, Northwestern Univ., Evanston, Illinois; also *J. of Engng. Mech.*, ASCE, 110, 12, 1666-1692, 1984.
- Bazant, Z. P., 1983n, Comment on Orthotropic Models for Concrete and Geomaterials, *J. of Engng. Mech.*, ASCE, 109, 849-865.
- Bazant, Z. P., 1984a, Mechanics of Fracture and Progressive Cracking in Concrete Structures, in *Fracture Mechanics Applied to Concrete Structures*, Sih, G. C., Ed., Martin Nijhoff Publishers, The Hague.
- Bazant, Z. P., and Gambarova, P., 1984b, Crack Shear in Concrete: Crack Band Microplane Model, *J. Struct. Div.*, ASCE, 110, 2015-2035.
- Bazant, Z. P., and Kim, J. K., 1984c, Size Effect in Shear Failure of Longitudinally Reinforced Beams *J. ACI*, 81, 456-468.
- Bazant, Z. P., 1984d, Imbricate continuum and its variational derivation, *J. Engng. Mech.*, ASCE, 110, 12, 1693-1712.

- Bazant, Z. P., 1985a, Mechanics of Distributed Cracking, *Appl. Mech. Reviews*, ASME, 39, 5, 675-705.
- Bazant, Z. P., and Oh, B. H., 1985b, Rock Fracture via Strain Softening Finite Elements, *J. Engng. Mech.*, ASCE, 110, 7, 1015-1035.
- Bazant, Z. P., 1987a, Why Damage is Nonlocal: Justification by Microcrack Array, *Mech. Res. Communication*, 14, 516, 407-419.
- Bazant, Z. P., and Pijaudier-Cabot, G., 1987b, Measurement of Characteristic Length of Non-Local Continuum, *Report No.*, 87-12/498 m, Center for Concrete and Geomaterials, Northwestern Univ., also *J. Engng. Mech.*, ASCE, 1988.
- Bazant, Z. P., and Belystschko, T. B., 1987c, Strain-Softening Continuum Damage: Localization and Size Effect, *Proc. Inter. Conf. on Constitutive Laws for Engineering Materials*, Eds., Desai et al., Tucson, Ariz., Elsevier, New York, 11-33.
- Bazant, Z. P., 1988a, Stable States and Paths for Structures with Damage and Plasticity, *J. Engng. Mech.*, ASCE, 114, 2, 2013-2034.
- Bazant, Z. P., and Pijaudier-Cabot, G., 1988b, Nonlocal Continuum Damage, Localization Instability and Convergence, *J. Appl. Mech.*, ASME, 55, 287-293.
- Bazant, Z. P., and Kazemi, M. T., 1990a, Size Effect in Fracture of Ceramics, *J. Amer. Cer. Soc.*,
- Bazant, Z. P., 1990b, Recent Progress in Damage Modelling: Nonlocality and its Microscopic Cause, *J. Amer. Cer. Soc.*,
- Bazant, Z.P., Xi, Y., and Reid, S.G., 1991a, Statistical Size Effect in Quasi-Brittle Structures: I. Is Weibull Theory Applicable?, *J. Engng. Mech.*, ASCE, 117, No. 11, pp. 2609-2622.
- Bazant, Z.P., 1991b, Why Continuum Damage is Nonlocal: Micromechanics Arguments, *J. Engng. Mech.*, ASCE, 117, No. 5, pp. 1070-1087.
- Beeby, A. W., 1991, Empiricism versus Understanding in the Successful Use of Materials in a Changing World, *Mag. Conc. Res.*, 43, 156, 141-142
- Bellamy, C. J., 1961, Strength of Concrete under Combined Stresses, *J. ACI*, 58, 367-338.
- Belytschoko, T., and Larsy, D., 1989, Localization Limiters and Numerical Strategies for strain Softening Material, in *Cracking and*

Damage Strain Localization and Size Effects, Ed. Mazars, J. and Bazant, Z.P., Elsevier Applied Science, 349-262.

- Benallal, A., 1984a, Calculs Couples Elasto-viscoplasticite-endommagement, *Conf. GAMNI, Methodes Numeriques en Fissuration et Endommagement*.
- Benallal, A., Billardon, R., and Lemaitre J., 1984b, Failure Analysis of Structure by Continuum Damage Mechanics, *Proc, ICF 6*, New Delhi, India.
- Benallal, A. Billardon R., and Marquis, D., 1984c, Prevision de l'amorçage et de la Propagation des Fissures par la Mecanique de l'endommagement Comptes Rendus, *Journées de Printemps de la S. F. M.*, Paris.
- Benallal, A. 1985, Finite Element Analysis of the Behavior and the Failure of Elasto-viscoplastic Structures, *NUMETA*, 85, Swansea, U. K.
- Benallal, A., Billardon, R., and Lemaitre J., 1991, Continuum Damage Mechanics and Local Approach to Fracture: Numerical Procedures, *Comp. Meth. Appl. Mech. Eng.*, 92, 141-155.
- Benouniche, S., 1979, Modelisation de l'Endommagement du Beton Hydraulique par Microfissuration en Compression, *These 3eme Cycle*, Universite Paris 6.
- Bensoussan, P., et al, 1985, Creep Crack Initiation and Propagation: Fracture Mechanics and Local Approach, *Post SMIRT8 Seminar*, Paris.
- Beremin, F. M., 1981a, Study of the Fracture Criteria Rupture of A508 Steel, *ICF 5, Advances in Fracture Research*, Cannes, Francois, D., ed., 809-816, Pergmon Press, Oxford.
- Beremin, F. M., 1981b, Calculation and Experiment on Axisymmetrically Cracked Tensile Bars: Prediction of Initiation, Stable Crack Growth and Instability, *SMIRT 6 Conf.*, Paris, Paper I/G, No. 2/3.
- Beremin, F. M., 1981c, Experimental and Numerical Study of the Different Stages in Ductile Rupture: Application to Crack Initiation and Stable Crack Growth, in *Three Dimensional Constitutive Relations and Ductile Fracture*, Nemat-Nasser, S., Ed., 181-205, North-Holland, London.
- Beremin, F. M., 1983, A Local criterion for Cleavage Fracture of a Nuclear Pressure Vessel Steel, *Metall. Trans.*
- Betten, J., 1981, Damage Tensor in Continuum Mechanics, *EUROMECH*

- Colloquium 147 on Damage Mechanics*, Lemaitre, J., Ed., Cachan, France.
- Billardon, R., and Lemaitre, J., 1981, Prevision de la Bifurcation des Fissures par la Theorie Mecanique de l'endommagement, *Congres AUM*, Lyon.
- Billardon R., 1983a, Mecanique de l'endommagement Appliquee au Comportement des Fissures, *Reunion de Printemps du Groupe, Fragilite-Rupture*, Lausanne.
- Billardon, R., and Lemaitre, J., 1983b, Numerical Prediction of Crack Growth Under Mixed-Mode Loading by Continuum Damage Theory, *Congres AUM*, Lyon.
- Billardon, R., and Doghri, I., 1989, Localization Bifurcation Analysis for Damage Softening Elasto-Plastic Materials, *Cracking and Damage Strain Localization and Size Effects*, Ed. Mazars, J. and Bazant, Z.P., Elsevier Applied Science.
- Blech, H. H., 1972, On Uniqueness in Ideally Elastoplastic Problems in Case of Nonassociated Flow Rules, *ASME J. Appl. Mech.*, Dec., 983-987.
- Bonder, S. R., 1981, Evolution Equations for Isotropic and Anisotropic Damage Growth, *EUROMECH Colloquium on Damage Mechanics*, Lemaitre, J., Ed., Cachan, France.
- Bonder, S. R., 1980, A Procedure for Including Damage in Constitutive Equations for Elastic-viscoplastic Work-hardening Materials, *Proc. IUTAM Conf. on Physical Non-linearities in Structural Analysis*, Hult, J., and Lemaitre, J., Eds., Springer.
- Braestrup, M. W., Nielsen, M. P., Bach, 1978, Plastic Analysis of Shear in Concrete, *ZAMM*, 58, 6, 3-14.
- Braestrup, M. W., and Nielsen, M. P., 1983, Plastic Methods of Analysis and Design, in *Handbook of Structural Concrete*, Eds. F.K. Kong, R.H. Evans, E. Cohen and F. Roll, Pitman Advanced Publishing Program, 20.
- Bresler, B., and Pister, K. S., 1957, Failure of Plain Concrete under Combined Stresses, *Trans. ASCE*, 122, 1049-1468.
- Bresler, B., and Pister, K. S., 1958, Strength of Concrete under Combined Stresses, *J. ACI*, 55, 321-345.
- British Standard CP110, 1972, Code of Practice for the Structural Use of Concrete, *Part 1, Design Materials and Workship*, BSI London,

Nov.

- Broberg, K. B., 1974a, A New Criterion for Brittle Creep Fracture, *ASME, J. Appl. Mech.*, 41.
- Broberg, K. B., 1974b, Damage Measures in Creep Deformation and Rupture, *Swedish Solid Mechanics Report*.
- Broberg, K. B., 1975, On Stable Crack Growth, *J. Mech. Phys. Solids*, 23, 215-237.
- Brooks, J. J., and Al-Samaraie, N. H., Application of the Highly Stressed Volume - Continuous Damage Model to Tensile Failure of Concrete.
- Budiansky, B., and O'Connell, R. J., 1976, Elastic Moduli of a Cracked Solid, *Int. J. Solids Structures*, 12, 81-97.
- Budiansky, B., 1959, A Reassessment of Deformation Theories of Plasticity, *J. Engng. Mech., Trans., ASME*, 26, 259-264.
- Bui, H. D., Dang Van, K., and De Langre, E., 1984, A Local Approach to Crack Growth in Creeping Materials., *Proc. 2nd Int. Conf. on Creep and Fracture of Engineering Materials and Structures*, Swansea, U. K.
- Bui, H. D., Ehrlacher, A., and Renard, D., 1984, Propagation d'une Zone Endommagee dans un Solide elastique Fragile en Mode I et en Regime Permanent, *6eme Congres Francais de Mequanique*, Lyon.
- Burt, N. J., and Dougill, J. W., 1977, Progressive Failure in Heterogeneous Medium, *J. Engng. Mech., ASCE*, 365-376.
- Buyukozturk, O., Nilson, A. H., and Slate, F. O., 1971, Stress Strain Response and Fracture of Concrete Model in Biaxial Loading, *ACI J.*, 590-599.
- Buyukozturk, O. M., and Tseng, T. M., 1984, Concrete in Biaxial Cyclic Compression, *J. Structural Engng., ASCE*, 110, 3, 18667, 461-476.
- Cailletaud, G., and Chaboche, J. L., 1982, Life Prediction in 304s by Damage Approach, *Conf. ASME-PVP*, Paper No. 82-PVP-72, Orlando, 1982, T.P. & O.N.E.R.A.
- Campbell, A. D., 1962, Strength of Concrete under Tensile and Compressive Loads, *Constructional Review*, 35, 29-37.
- Carpinteri, A., and Ingraffea, A.R., 1984, Eds., *Fracture Mechanics of*

Concrete: Material Characterization and Testing, Martinus Nijhoff Publishers, The Hague, 202.

- Carpinteri, A., DiTomasso, A. and Fanelli, M., 1986, Influence of Material Parameters and Geometry on Cohesive Crack Propagation, in *Fracture Toughness and Fracture Energy of Concrete*, Ed. F.H. Wittmann, 117-135, Elsevier, Amsterdam.
- Case, E. D., 1984, The Effect of Microcracking upon the Poisson's Ratio for Brittle Materials, *J. Mater. Sci.*, 19, 3702-3712.
- Cedolin, L., and Crutzen, Y. R. J., and Poli, S. D., 1977, Triaxial Stress-strain Relationship for Concrete, *J. Engng. Mech.*, ASCE, 103, EM3, 423.
- Cedolin, L., and Bazant, Z. P., 1980, Effect of Finite Element Choice in Blunt Crack Band Analysis, *Comp. Meth. Appl. Mech. Engng*, 24, 305-316.
- Chaboche, J. L., 1974, Une Loi Differentielle d'endommagement de Fatigue avec Cumulation Non-Lineaire, *Revue Francaise de Mecanique*, No. 50-51.
- Chaboche, J. L., 1977, Description Thermodynamique et Phenomenologique de la Viscoplasticite Cyclique avec Endommagement, *These, O.N.E.R.A.*
- Chaboche, J. L., 1979, Le Concept de Contrainte Effective Applique a l'elasticite et a la Viscoplasticite en Presence d'un Endommagement Anisotrope, *EUROMECH Colloque 115*, Grenoble Edition du CNRS 1982.
- Chaboche, J. L., 1982, Lifetime Predictions and Cumulative Damage Under High-Temperature Conditions., *Sympo. on Low-Cycle Fatigue and Life Prediction*, Firminy, France, 1980, ASTM STP 770.
- Chaboche, J. L., 1984, Anisotropic Damage in the Framework of Continuum Damage Mechanics, *Nucl Engng Design*, 79.
- Chaboche, J.L., 1990, Fracture Mechanics and Damage Mechanics: Complementarity of Approaches, 309-321.
- Chen, W. F., and Drucker, D. C., 1969, Bearing Capacity of Concrete Blocks or Rock, *Trans. ASCE*, 95, 4, 955-978.
- Chen, A. C. T., and Chen, W. F., 1975, Constitutive Relations for Concrete, *J. Engng. Mech.*, ASCE, 101, EM4, 465.
- Chen, W. F., and Suzuki, H., 1978 Constitutive Models for Concrete,

- ASCE Annual Convention, Chicago, Oct.
- Chen, W. F., and Edward, C. T., 1980, Constitutive Models for Concrete Structures, *J. of Engng. Mech.*, ASCE, 106, 1, 1-19.
- Chen, W. F., 1981, Plasticity in Reinforced Concrete, *Procs. of a Workshop on Constitutive Relations for Concrete*, New Mexico Engineering Research Institute, Univ. of New Mexico, Albuquerque, N. M., April 28-29.
- Chen, W. F., and Saleeb, A. F., 1982, *Constitutive Equations for Engineering Materials*, Vols. I & II, Wiley, New York.
- Chen, W. F., 1982, *Plasticity in Reinforced Concrete*, McGraw-Hill, New York.
- Chen, Z., and Schreyer, H. L., 1990, Failure Controlled Solution Strategies for Damage Softening with Localization, in *Micro-Mechanics of Failure of Quasi-Brittle Materials*, Shah, S. P., Swartz, S. E., and Wang, M. L., Eds., 135-145.
- Chen, E. P., and Tzou, D. Y., 1990, A Continuum Damage Model for the Quasi-Static Response of Brittle Materials, *Micro-Mechanics of Failure of Quasi-Brittle Materials*, Shah, S. P., Swartz, S. E., and Wang, M. L., Eds., 620-626.
- Chinn, J., Zimmerman, R. M., 1965, Behavior of Plain Concrete under Various High Triaxial Compression Loading Conditions, *Technical Report No. WL TR 64-163(AD468460)*, Air Force Weapon Laboratory, New Mexico, Aug.
- Chitale, A. D., and McClintock, F. A., 1971, Elastic-Plastic Mechanics of Steady Crack Growth under Anti-plane Shear, *J. Mech. Phys. Solids*, 19, 147-163.
- Chorin, et al., 1978, in Ju 1989 Continuum Damage Mechanics for Ductile Fracture. *Engng. Fract. Mech.*, 27, 547-558.
- Chow, C.L. and Wang, J., 1987a, An Anisotropic Theory of Continuum Damage Mechanics for Ductile Fracture. *Engng. Fract. Mech.*, 27, 547-558.
- Chow, C.L. and Wang, J., 1987b, An Anisotropic Continuum Damage Theory and its Application to Ductile Crack Initiation, In *Proc. ASME Winter Annual Meeting*, Edited by A.S.D. Wang and G.K. Haritos, pp. 1-9, 13-18 December 1987, Boston, MA.
- Chow, C.L. and Wang, J., 1988, A Finite Element Analysis of Continuum Mechanics for Ductile Fracture, *Int. J. Fracture*, 38, 83-102.

- Christian, J. T., and Desai, C. S., 1979, Constitutive Laws for Geologic Media, *Numerical Methods in Geotechnical Engineering*, Eds., Desai, C. S., and Christian, J. T., McGraw-Hill Book Company, 65-115.
- Christoffersen, J., and Hutchinson, J. W., 1979, A Class of Phenomenological Corner Theories of Plasticity, *J. Mech. Phys.*, 27, 465-487.
- Clapeyron, Z., 1950, *Theory of Flow and Fracture of Solids*, 2nd Edn., Nadai, A., Ed., McGraw Hill, New York.
- Clark, L. A., and Cranston, W. B., 1979, The Influence of Bar Spacing on Tension Stiffening in Reinforced Concrete Slabs, *Proc. Inter. Conf. on Concrete Slabs*, Dundee, 25-38.
- Coleman, B. D., and Gurtin, M., 1967, Thermodynamics with Internal Variables, *J. Chem. Phys.*, 47, 597-613.
- Collombet, F., 1985, Modelisation de l'Endommagement Anisotrope au Comportement du Beton sous Sollicitations Multiaxiales, *These de 3eme Cycle*, L. M. T., Universite Paris, France.
- Colson, A., and Boulabiza, M., 1992, On the Identification Models for Steel Stress-Strain Curves, *RILEM, Materials and Structures*, 25, 313-316.
- Cordebois, J. P., and Sidoroff, F., 1979, Elasticite Anisotrope Induite par l'Endommagement, (Damage Induced Elastic Anisotropy), *Mechanical Behavior of Anisotropic Solids*, Proc. EUROMECH Colloque 115 Anisotropie, Grenoble, Boehler, J. P., Ed., 761-774.
- Cordebois, J. P., and Sidoroff, F., 1982, Endommagement Anisotrope en Elasticite et Plasticite, *J. Mec. Theor. Appl.*, No. Special, 45-59.
- Cordebois, J. P., 1983, Criteres d'Instabilite Plastique et Endommagement Ductile en Grandes Deformation, *These, Paris 6*.
- Costin, L. S., 1983, A Microcrack Model for the Deformation and Failure of Brittle Rock, *J. Geophys. Res.*, 88, 9485-9492.
- Costin, L. S., 1985, Damage Mechanics in the Post Failure Regime, *Mechanics of Materials*, 4, 149-160.
- Coulomb, C. A., 1774, Essai sur une Application des Regles des Maximis et Minimis a Quelques Problemes de Statique, *Royale-Academie des Sciences*, Paris, 7.
- Crisfield, M.A., 1986, Snap-through and Snap-back Response in

- Concrete Structures and the Dangers of Under-Integration, *Int. J. Numer. Meth. Engng.*, 22, 751-768.
- Crzanowski, A. and Dusza, E., 1980, Creep Crack Propagation in a Notched Strip, *J. Mecanique Appliquee*, 4, 461-474.
- Dafalais, Y. F., 1975, On Cyclic and Anisotropic Plasticity, Ph. D. Thesis, Univ. California, Berkeley. *Int. J. Nonlinear Mech.*, 12, 327.
- Dafalias, Y. F., 1977a, Elasto-plastic Coupling within Thermodynamic Strain Space Formulation of Plasticity, *Int. J. Nonlinear Mech.*, 12, 327.
- Dafalias, Y. F., 1977b, D'riushin's Postulate and Resulting Thermodynamic Conditions on Elasto-plastic Coupling, *Int. J. Solids Structures*, 13, 239.
- Dafalias, Y. F., 1978, Restrictions on the Continuum Description of Elasto-plastic Coupling for Concrete within Thermodynamics, Eds., Chang, T. Y., and Krempl, E., *Inelastic Behavior of Pressure Vessels and Piping Components*, Series PVP-PB-028, ASME, 29.
- Dafalais, Y. F., 1981, The Concept and Application of the Bounding Surface in Plasticity Theory, *Proc. IUTAM Conf. on Physical Non-Linearities in Structural Analysis*, Eds., Hult, J., and Lemaitre, J., Springer.
- Darwin, D., and Pecknold, D. A., 1974, Inelastic Model for Cyclic Biaxial Loading of Reinforced Concrete, *Civ. Engng. Stud.*, SRS 409, Univ. of Illinois, July.
- Darwin, D., and Pecknold, D. A., 1977a, Analysis of Cyclic Loading of Plane Reinforced Concrete Structures, *J. Comp. Struct.*, 7, 134-137.
- Darwin, D., and Pecknold, D. A., 1977b, Nonlinear Biaxial Stress-Strain Law for Concrete, *J. of Eng. Mech.*, ASCE, 103, No. EM2, 229-249.
- Darwin, D., 1979, A Biaxial Stress-Strain Model for Concrete, *Proc. 3rd Engng. Mech. Div. Specialty Conf. of ASCE*, Held at Austin, Texas, Sept, 441-444.
- Davison, L., and Stevens, A. L., 1976, Thermomechanical Constitution for Spalling Elastic Bodies, *J. Appl. Phys.*, 44, 93-106.
- Davison, L., Stevens, A. L., and Kipp, M. E., 1977, Theory of Spall Damage Accumulation in Ductile Metals, *J. Mech. Phys. Solids*, 25, 11-28.

- De Borst, R., and Nanta, P., 1985, Non Orthogonal Cracks in a Smearred Finite Element Model, *Engng Comput. J.*, 2.
- De Borst, R., 1986, Non-Linear Analysis of Frictional Materials, *Ph. D Thesis*, Delft Univ. of Technology, Delft, Netherlands.
- De Koning, A. U., 1977, A Contribution to the Analysis of Quasi Static Crack Growth in Sheet Materials, *Fracture, ICF 4*, 3, Waterloo, Canada.
- De Langre, E., Bui, H. D. and Dang Van, K., 1983, Approache locale de la Fissuration dans les Milieux Viscoplastiques, *5eme Congres Francais de Mecanique*, Lyon.
- De Langre, E., 1984, Analyse de la Fissuration des Milieux Viscoplastique, Application a la theorie de l'endommagement Brutal, *These de Docteur-Ingenieur, Universite Paris 6*.
- Desyai, P., and Krishnan, S., 1964, Equation for Stress Strain Curve of Concrete, *J. ACI*, 3.
- Desai, C. S., 1971, Nonlinear Analysis Using Spline Functions, *J. Soil Mech. Found. Div., ASCE*, 97, SM10, Oct., and 98, SM9, Sept., 1972.
- Desai, C. S., and Wu, T. H., 1976, A General Function for Stress-Strain Curves, *Proc., 2nd Int. Conf. Numer. Methods Geomech.*, Blacksburg, Va., June.
- Desai, C. S., and Christian, J. T., 1979, Introduction, Numerical Methods, and Special Topics, *Numerical Methods in Geotechnical Engineering*, Eds., Desai, C. S., and Christian, J. T., McGraw-Hill Book Company, 1-64.
- Desai, C. S., and Siriwardane, 1983, *Constitutive Laws for Engineering Materials*, Prentice-Hall, Inc., Englewood Cliffs, N. J.
- Desai, C. S., and Faruque, M. O., 1984, Constitutive Model for (Geological) Materials, *J. Eng. Mech., ASCE*, 110, 9, 1391-1408.
- Devaux, J. C., and D'Escatha, Y., 1979, Numerical Study of Initiation Stable Crack Growth and Maximum Load, With a Ductile Fracture Criterion Based on the Cavity Growth, *ASTM, STP 668*, 229.
- Devaux, J. C., and Rousselier, G., Mudry, F., and Pineau, A., 1985, An Experiment Program for Validation of Global Ductile Fracture Criteria Using Axisymmetrically Cracked Bars and Compact Tension Specimens, *Eng. Fract. Mech.*, 21, 275-285.
- DiMaggio, F. L., and Sandler, I. S., 1971, Material Model for Granular

- Soils, *J. Eng. Mech.*, ASCE, 97, 3, 935-950.
- Discussions, 1989, *Cracking and Damage Strain Localization and Size Effects*, Ed. Mazars, J. and Bazant, Z.P., Elsevier Applied Science.
- Dougill, J. W., 1976, On Stable Progressively Fracturing Solids, *J. of Applied Mathematics and Physics*, 27, ZAMP, Fasc. 4, 423.
- Dougill, J. W., Lau, J. C., and Burt, N. J., 1977, Toward a Theoretical Model for Progressive Failure and Softening in Rock, Concrete and Similar Materials, *ASCE-EMD 1976*, Univ. of Waterloo Press, 335-355.
- Dougill, J. W., and Rida, M. A. M., 1980, Further Considerations of Progressively Fracturing Solids, *J. Engng Mech. Div.*, ASCE, 108, EM5, 1021.
- Dougill, J. W., 1983, Constitutive Relations for Concrete and Rock: Applications and Extensions of Elasticity and Plasticity Theory, in *Mechanics of Geomaterials: Rocks, Concretes, Soils*, Bazant, Z. P., Ed., Preprints of the William Prager Symposium, Northwestern University.
- Dragon, A., 1976, On Phenomenological Description of Rock-Like Materials with Account for Kinetics of Brittle Fracture, *Archiwum Mechaniki Stosowanej*, Warsaw, Poland, 28, No. 1, 13-30.
- Dragon, A., and Mroz, A., 1979, A Continuum Model for Plastic Brittle Behavior of Rock and Concrete, *Inter. J. Engineering Science*, 17, 121-137.
- Dragon, A., 1985a, Plasticity and Ductile Fracture Damage: Study of Void Growth in Metals, *Engng. Fract. Mech.*, 21, 875-885.
- Dragon, A. and Chihab, A., 1985b, On Finite Damage: Ductile Fracture-Damage Evolution, *Mech. Mater.*, 4, 95-106.
- Drucker, D. C., 1950, Some Implications of Work Hardening and Ideal Plasticity, *Quart. Appl. Math.*, 7, 411-418.
- Drucker, D. C., and Prager, W., 1951, A More Fundamental Approach to Plastic Stress-Strain Relation, *Proc. Natl. Cong. US Inst. Appl. Mech.*, Chicago, 487-491.
- Drucker, D. C., and Prager, W., 1952a, Soil Mechanics and Plastic Analysis or Limit Design, *Quart. Appl. Math.*, 10, 157-165.
- Drucker, D. C., Prager, W., Greenberg, H. J., 1952b, Extended Limit Design Theorems for Continuous Media, *Quart. Appl. Math.*, 9,

- 381-389.
- Drucker, D. C., Gibson, R. E., and Henkel, D. J., 1957, Soil Mechanics and Work-Hardening Theories of Plasticity, *Trans. ASCE*, 121, 338-346.
- Drucker, D. C., 1961, On Structural Concrete and the Theorems of Limit Analysis, *Int. Ass. Bridge Struct. Engng.*, 21, 49-59.
- Drucker, D. C., 1964, On the Postulate of Stability of Material in Mechanics of Continua, *J. Mechanics*, 3, 235-249.
- Dufailly, J., 1980, Modelisation Mecanique et Identification de l'Endommagement Plastique des Materiaux, *These 3eme Cycle*, Universite 6.
- Dyson, B. F., and Loveday, M. S., 1981, *IUTAM Symp. on Creep in Structures*, Leicester, U. K., 1980, Ponter, A. R. S., and Hayhurst, D. R., Eds, 406, Springer, Berlin.
- Ehler, A., and Riedel, 1980, A Finite Element Analysis of Creep Deformation in a Specimen Containing a Macroscopic Crack, in *Advances in Fracture Research*, Francois, D., et al, Eds, 2, 691-698, Pergamon Press, Oxford.
- Ehlers, R., 1985, Contribution a l'etude Thermodynamique de la Progression de Fissure et a la Mecanique de l'endommagement Brutal, *These, Universite Paris*, 6.
- Elfgran, L., 1989, Introduction, in *Report of the Technical Committee 90 - FMA Fracture Mechanics to Concrete - Application*, RILEM, Ed., L. Elfgran, Chapman and Hall, pp. 1-5.
- Elices, M., and Planas, J., 1989, Material Models, Fracture Mechanics of Concrete Structures from Theory to Application, *Report of the Technical Committee 90 - FMA Fracture Mechanics to Concrete - Application*, RILEM, Ed., L. Elfgran, Chapman and Hall, pp. 16-66.
- Elwi, A. A., and Murray, D. W., 1979, A Three-Dimensional Hypoelastic Concrete Constitutive Relationship, *J. Engng. Mech.*, ASCE, 105, EM4, 623.
- Elwi, A. A., and Murray, D. W., 1980, A Three-Dimensional Hypoelastic Concrete Constitutive Relationship, *Private Communication*.
- Ellison, E. G., and Musicco, G. G., 1981, Notch-Rupture and Crack Growth Behavior Under Creep Conditions, in *Subcritical Crack Growth due to Fatigue, Stress Corrosion and Creep*, Larsson, L.

- H., Ed., 403-448, Elivier, Amsterdam.
- Eringen, A. C., 1962, *Nonlinear Theory of Continuous Media*, McGraw-Hill Book Company, New York.
- Eringen, A. C. and Elden, D. G. B., 1972, On Nonlocal Elasticity, *Int. J. Engng. Sci.*, 10, 233-248.
- Eringen, A. C., and Ari, N., 1983, Nonlocal Stress Field at Griffith Crack, *Crist. Latt and Amorph. Mater.*, 10, 33-38
- D'Escatha, Y., and Devaux, J. C., 1979, Numerical Study of Initiation Stable Crack Growth and and Maximum Load with Ductile Criterion Based on the Growth of Holes, *Elastic Plastic Fracture*, Clarke, G. A., Ed., ASTM, STP, 668.
- Evans, R.H., and Marathe, M.S., 1968, Microcracking and Stress-Strain Curves for Concrete in Tension, *Mater. Construct.*, 12, 61-64.
- Fafitis, A., and Shah, S. P., 1984, Rheological Model for Cyclic Loading of Concrete, *J. Struct. Engng.*, ASCE, 110, 9, 2085-2102.
- Fafitis, A., and Won, Y. H., 1992, A Multiaxial Stochastic Constitutive Law for Concrete: I and II, *J. Appl. Mech.*, ASME, 59, 283-288 and 289-294.
- Faruque, M. O., 1983a, Development of a Generalized Constitutive Model and its Implementation in Soil-Structure Interaction, *Ph. D. Thesis*, Arizona Univ., Tucson, Ariz.
- Faruque, M. O., and Desai, C. S., 1983b, Implementation of a General Plasticity Model, *Proc.*, ASCE, *Eng. Mech. Div.*, *Speciality, Conf.*, Purdue Univ., West Lafayette, Indiana, May, 755-758.
- Faruque, M. O., 1987, A Cap Type Constitutive Model for Plain Concrete, *Constitutive Laws for Engineering Materials: Theory and Applications*, Eds., Desai et al., Elsevier Science Publishing Co., Inc., 395-402.
- Feenstra, P. H., De Borst, R., Rots, J. G., 1991, Numerical Study on Crack Dilatancy, Part I, II, *J. of Engng. Mech.*, ASCE, 117, 4, 733-769.
- Francois, D., Chuy, S., Benkirane, M. E., and Baron, J., 1982, Crack Propagation in Prestressed Concrete; Interaction with Reinforcement, in *Advances in Fracture Mechanics (Fracture 81)*, 4, Pergamon Press, 1507-1514.
- Francois, D., 1984, *Fracture and Damage Mechanics of Concrete*,

- Advances in Fracture Mechanics to Cementitious Composites*, NATO Advanced Research Workshop, Shah, S. P., Ed., 97-110. 1507-1514.
- Frantziskonis, G., 1986, Progressive Damage and Constitutive Behavior of Geomaterials Including Analysis and Implementation, *Ph.D. dissertation*, Dept. of Civ. Engng. Mech., Univ. of Arizona, Tucson, Arizona..1986).
- Frantziskonis, G., and Desai, C.S., 1987a, Constitutive model with Strain Softening, *Int. J. Solids Struct.*, 23, 6, 733-750.
- Frantziskonis, G., and Desai, C.S., 1987b, Analysis of a Strain Softening Constitutive model, *Int. J. Solids Struct.*, 23, 6, 751-767.
- Freudenthal, A. M., 1968, Statistical Approach to Brittle Fracture, *Fracture*, Ed., Liebowitz, H., Academic Press, 2.
- Fumagalli, E., 1975, Strength Characteristics of Concrete under Conditions of Multiaxial Compression, *Cem. Conc. Assoc.*, London, (Translation No. CU 128).
- Fung, Y. C., 1965, *Foundations of Solid Mechanics*, Prentice Hall, Inc.
- Gambarova, P. G., and Karakoc, 1983, A New Approach to the Analysis of the Confinement Role in Regularly Cracked Concrete Elements, *Trans. 7th Struct. Mech. in Reactor Tech. Conf., SMIRT*, H, 251-261.
- Gardner, N., 1969, Triaxial Behavior of Concrete, *Procs., ACI*, 66, No. 2, 136.
- Geegstra, P. N. R., 1976, A Transient Finite Element Crack Propagation Model For Nuclear Reactor Pressure Vessel, *J. Inst. Nucl. Engrs*, 17, 89-96.
- Geistefeld, H., 1977, Material Law for Concrete under Multiaxial Stress, *Trans. 4th Int. Conf. on Structural Mech. in Reactor Technology*, H5/2, San Francisco, California, Jeager, T. A., and Boley, B. A., Eds.
- Glucklich, J., 1962, On Compression Failure of Plain Concrete, *T & A M. Report*, No. 125, Univ. of Illinois, Mar.
- Gonclaves, O. J. A. and Owen, D. R. J., 1983, Numerical Analysis of Creep Brittle Rupture by Finite Element Method, *SMIRT 7*, Chicago.

- Gopalaratnam, V. S., and Shah, S. P., 1985, Softening Response of Plain Concrete in Direct Tension, *J. ACI, Proc.*, 83, 3, 310-323.
- Grady, D. E., and Kipp, M. E., 1980, Continuum Modelling of Explosive Fracture in Oil Shale, *Int. J. Rock Mech. Min. Sci. Geomech.*, 17, 147-157.
- Green, A. E., 1956, Hypoelasticity and Plasticity, *Proc. Roy. Soc. London*, A234, 46-57.
- Green, A. E., and Rivlin, R. S., 1957, The Mechanics of Nonlinear Elastic-Plastic Materials with Memory, Parts I, *Arch. Rational Mech. Anal*, 1, 1-21, 470, (Reprinted in *Ratio Rational Mech. of Mater.*, Truesdell, C., Ed., New York: Gordon and Breach, 1965).
- Green, A. E., Rivlin, R. S., and Spencer, A. J. M., 1959, The Mechanics of Nonlinear Elastic-Plastic Materials with Memory, Parts II, *Arch. Rational Mech. Anal*, 3, 82-90.
- Green, S. J., and Swanson, S. R., 1973, Static Constitutive Relations for Concrete, *Rech. Report AFWC-TR-72-2*.
- Grestle, K. H., 1981, Simple Formulation of Biaxial Concrete Behavior, *J. ACI*, 78, 1, 62-68.
- Grootenboer, 1979, Finite Element Analysis of Two Dimensional Reinforced Concrete, Taking Account of Nonlinear Physical Behavior and the Development of Discrete Cracks, *Dissertation*, Delft Univ. of Technology, Delft.
- Guo, Z., and Zhang, X., 1987, Investigation of Complete Stress-Deformation Curves for Concrete in Tension, *ACI Mat. J.*, 84, 4, 278-285.
- Gustafsson, P.J., 1985, Fracture Mechanics Studies of Non-Yielding Materials Like Concrete, *Ph.D. Dissertation*, Dept. of Civil Engng., Lundo Institute of Technology.
- Gvozdev, A. A., 1960, The Determination of the Value of the Collapse Load for Statically Indeterminate Systems Undergoing Plastic Deformatio, *Int. J. Mech. Sci*, 1, 322-333. (English Translation of Gvozdev's Article in *Sbornik Trudov Konferentsii po Plasticheskim Deformatsiyam*, Acad. of Sci., Moscow/Leningrad, 1938, 19-30). 2-15.
- Gylltoft, K., 1983, Fracture-Mechanics Models for Fatigue in Concrete Structures, *Doctoral Thesis*, No. 1983: 25D, Division of Structural Engineering, Lulea University.

- Hagmann, A. J., Christian, J. T., D'Appolonia, D. J., 1970, Stress-Strain Models for Frictional Materials,, *MIT Dept. Civ. Eng., Rep.* R70-18.
- Hagmann, A. J., 1971, Prediction of Stress and Strain under Drained Loading Conditions, *MIT Dept. Civ. Eng., Rep.* R71-3.
- Han, D. J., and Chen, W. F., 1985, A Non-uniform Hardening Plasticity Model for Concrete Material, *J. Mech.*, 4, 4, 283-302.
- Hannant, D. J., and Frederick, C. D., 1968, Failure of Concrete in Compression, *Mag. Conc. Res.*, 20, 137-144.
- Hashiguchi, K., 1989, Subloading Surface Model in Unconventional Plasticity, *Int. J. Solids Structures*, 25, 8, 917-945.
- Hayhurst, D. R., 1975, Estimates of the Creep Rupture Life Time of Structures Using the Finite Element Method, *J. Mech. Phys. Solids*, 23.
- Hayhurst, D. R., Morrison, C. J., and Brown, P. R., 1981, *Proc. IUTAM Symp. on Creep in Structures*, Leicester, U. K., 1980, Ponter, A. R. S., and Hayhurst, D. R., Eds, 564, Springer, Berlin.O
- Hayhurst, D. R., Dimmer, P. R., Morrison, C. H., 1983, The Role of Continuum Damage in Creep Crack Growth, *Report 83-4*, Univ. of Leicester, Dept. of Engng., U. K.
- Heilmann, H. G., Hilsdorf, H., and Finsterwalder, K., 1969, Strength and Deformation of Concrete under Tensile Stress, *Bulletin No. 203, Deutscher Ausschuss fur Stahlbeton*, Berlin, pp. 94.
- Hencky, H. Z., and Nadai, A., 1924a, Zur Theorie Plastischer Deformationen und des Hien durch in Material Levorgerufenen Dachspannungen, *Report 1924*, Available National Lending Library, 323-334.
- Hencky, H. Z., 1926, Zur Theorie Plastischer Deformationen und des Hien durch in Material Levorgerufenen Dachspannungen, *ZAMM*, 4, 323-334; also *Proc. 1st Int. Congr. Appl. Mech.*, Delft , 312-317, 1924.
- L'Hermite, R., Volume Changes of Concrete, *4th Int. Symposium on the Chemistry of Cement*, Washington, 659-702.
- Herrmann, G., and Kestin, J., 1989, On Thermodynamic Foundation of a Damage Theory in Elastic Solids *Cracking and Damage Strain Localization and Size Effects*, Ed. Mazars, J. and Bazant, Z.P., Elsevier Applied Science.

- Hill, R., 1948, A Theory of the Yielding and Plastic Flow of Anisotropic Metals, *Proc. Roy. Soc. London*, A164, 547-579.
- Hill, R., 1950, *The Mathematical Theory of Plasticity*, Oxford, Clarendon Press.
- Hill, R., 1964, A General Theory of Uniqueness and Stability in Elastic-plastic Solids, *J. Mech. Phys. Solids*, 6, 236-249.
- Hill, R., 1967, The Essential Structure of Constitutive Laws for Metal Composites and Polycrystals, *J. Mech. Phys. Solids*, 15, 79-95.
- Hill, R., and Rice, J. R., 1972, Constitutive Analysis of Elastic-Plastic Crystals at Arbitrary Strain, *J. Mech. Phys. Solids*, 20, 401-413.
- Hillerborg, A., Modeer, M., and Peterson, P. E., 1976, Analysis of Crack Formation and Crack Growth in Concrete by Means of Fracture Mechanics and Finite Elements, *Cem. Conc. Res.*, 6, 773-782.
- Hillerborg, A., 1979, The physical Properties of Cement Paste, *Building Materials, FK 1*, Division of Physical Materials, Univ. of Lund, Sweden.
- Hillerborg, A., 1983, Analysis of a Single Crack, in *Fracture Mechanics of Concrete*, Wittman, F. H., Ed., Elsevier Publishers, 223-249.
- Hoagland, R. G., Hahn, G. T., and Rosenfeld, A. R., 1973, Influence of Microstructure on Fracture Propagation in Rock, *Rock Mech.*, 5, 77-106.
- Hobbs, D. W., 1977, Design Stresses for Concrete Structures Subjected to Multiaxial Stresses, *Struct. Engng.*, 55, 157-164.
- Hobbs, D.W., 1983, Failure Criteria for Concrete, *Handbook of Structural Concrete*, Eds. F.K. Kong, R.H. Evans, E. Cohen and F. Roll, Pitman Advanced Publishing Program, 10.
- Hodge, P. G., and Prager, W. A., 1948, A Variational Principle for Plastic Materials with Strain Hardening, *J. Mat. Phys.*, 27, 1, 1-10.
- Hodge, P. G., Jr., 1956, Piecewise Linear Plasticity, *Proc. 9th Int. Congr. Appl. Mech.*, Brussels, 8, 65-72.
- Hognestad, E., 1951, A Study of Combined Bending and Axial Load in Reinforced Concrete Members, *Bulletin No. 339*, ment Station, Univ. of Illinois, Urbana, Illinois, 49, 22, Nov.
- Hohenemser, K., 1931, *Fliessversuche an Rohren aus Stahl bei*

- Kombinierter Zug- und Torsionbeanspruchung, *ZAMM*, 11, 15-19.
- Hohenemser, K., and Prager, W., 1932, Beitrag zur Mechanik des Bildsamen Verhaltens von Fliesstahl, *ZAMM*, 12, 1-14.
- Hordijk, D.A., 1992, Tensile and Tensile Fatigue Behavior of Concrete, *Experiments, Modelling and Analysis*, Heron, 37, 1.
- Hordijk, D.A., Van Mier, J.G.M., and Reinhardt, H.W., 1989, Material Properties, Fracture Mechanics of Concrete Structures from Theory to Application, Report of the Technical Committee 90 - FMA, *Fracture Mechanics to Concrete - Application*, RILEM, Ed. L. Elfgran, Chapman and Hall, 67-127.
- Horii, H. and Nemat-Nasser, S., 1983, Overall Moduli of Solids with Microcracks: Load Induced Anisotropy, *J. Mech. Phys. Solids*, 31, 155-171.
- Hsien, B. J., 1978, On the Uniqueness and Stability of Endochronic Plasticity Theory, *Report ANL-CT-78-51*, Argonne National Laboratory, Argonne, Illinois, III, Sept.
- Hsien, B. J., 1980, On the Uniqueness and Stability of Endochronic Theory, *Trans., ASTM, J. Appl. Mech.*, 47, 748-754.
- Hsu, T. C., Slate, F. O., Sturman, G. M., and Winter, G., 1963, Microcracking of Plain Concrete and the Shape of the Stress-Strain Curve, *J. ACI*, 60, No. 2, 209.
- Hueckel, T., 1975, On Plastic Flow of Granular Rocklike Materials with Variable Elastic Moduli, *Bull. Polish Acad. Sci.*, 23, No. 8, 405.
- Hueckel, T., 1976, Coupling of Elastic and Plastic Deformations of Bulk Solids, *Mechanics*, 11, 227.
- Hueckel, T., and Mair, G., 1977, Incremental Boundary Value Problems in the Presence of Coupling of Elastic and Plastic Deformations: A Rock Mechanics Oriented Theory, *Int. J. Solids Structures*, 13, 1.
- Hughes, B. P., and Chapman, G. P., 1966, The Complete Stress-Strain Curve for Concrete in Direct Tension, *RILEM, Materials and Structures*, 30, 95.
- Hughes, B. P., and Ash, J. E., 1970, Anisotropy and Failure Criteria for Concrete, *RILEM, Materials and Structures*, 3, 18, 371-374.
- Hult, J., 1974, Creep in Continua and Structures, *Topics in Applied Continuum Mechanics*, Springer-Verlag, Vienna.
- Hult, J., 1987, Introduction and Overview, in *Continuous Damage*

Mechanics, Theory and Applications, Eds. Krajcinovic, D., and Lemaitre, J., Springer-Verlag, Wien-New York, 1-36.

- Humphrey, D. N., and Gondhalekar, R. S., 1990, Cap Model with Transversely Isotropic Elastic Parameters, 137-140.
- Idorn, G. H., et al., 1966, Morphology of Calcium Hydroxide in Cement Paste, *Procs. of the Symposium on Structure of Portland Cement Paste and Concrete*, Highway Research Board, Washington, D. C., 154-174.
- Int. Assoc. for Bridge and Struct. Engng. *Plasticity in Reinforced Concrete, Introductory Report*, Reports of the Working Commissions, 28, Oct.
- Int. Assoc. for Bridge and Struct. Engng. *Plasticity in Reinforced Concrete, Final Report*, Reports of the Working Commissions, 29, Aug.
- Isenberg, J., and Bagge, C. F., 1972, Analysis of Steel-Lined Penetration Shafts for Deeply Buried Structures, *Proc., Symp. Appl. Finite Element Method Geotech. Eng.*, Vicksburg, Miss, Sept.
- Ishai, O., 1968, The Time Dependent Deformational Behavior of Cement Paste, Mortar and Concrete, *Procs. of the Int. Conf. on the Structure of Concrete*, Brooks, A. E., and Newman, K., Eds, Cem. Conc. Assoc., London, 345-348.
- Jaeger, J. C., and Cook, N. G. W., 1969, *Fundamentals of Rock Mechanics*, 3rd Ed., Chapman and Hall, London.
- Janson, J., and Hult, J., 1977, Fracture mechanics and Damage Mechanics, A Combined Method, *J. de Mecanique Appliquee*, 1, 69-84.
- Janson, J., 1977, Dugdale-Crack in a Material with Continuous Damage Formation, *Engng. Fract. Mech.*, 9, 891-899.
- Janson, J., 1978a, A Continuous Damage Approach to Fatigue Process, *Engng. Fract. Mech.*, 10, 651-657.
- Janson, J., 1978b, Damage Model of Crack Growth and Instability, *Engng. Fract. Mech.*, 10, 795-806.
- Janson, S., 1985, Damage, Crack Growth and Rupture in Creep, *Thesis*, Chalmers Univ. of Technology, Goteborg, Sweden.
- Jayatilaka, A. S., 1979, *Fracture of Engineering Brittle Materials*, Applied Science Publishers, London.

- Jenq, Y. S., and Shah, S. P., 1985, A Two Parameter Fracture Model for Concrete, *J. Engng. Mech.*, ASCE, 111, 10, 1227-1241.
- Johansen, K. W., 1943, *Brudlinieteorier*, Gjellerup, Copenhagen. (English Edn.: Yield Line Theory, London, Cem. Conc. Assoc., London, 1962).
- Ju, J.W., 1989a, On Energy-Based Coupled Elastoplastic Damage Theories: Constitutive Modeling and Computational Aspects." *Int. J. Solids Struct.*, 25, 7, 803-833.
- Ju, J. W., Monteiro, P. J. M., Rashed, A. I., 1989b, On Continuum Damage of Cement Paste and Mortar as Affected by Proximity and Sand Concentration, *J. Engng. Mech.*, ASCE, 115, 105-130.
- Ju, J. W., 1990, Isotropic and Anisotropic Damage Variables in Continuum Damage Mechanics *J. Engng. Mech.*, ASCE, 116, 12, 2764-2770.
- Kachanov, L. M., 1958, Time of the Rupture Process Under Creep Conditions, *Isv. Akad. Nauk S. S. R. Otd. Tekh.*, 8.
- Kachanov, L. M., 1969, *Osnovy Teorii Plastichnosti* Izdatelstvo, Nauka, Moscow. (English Edn.: *Fundamentals of the Theory of Plasticity*, Mir Publishers, Moscow, 1974).
- Kachanov, L. M., 1972, Deformation of Medium with Cracks, *Izvestia VNIIG*, Leningrad, USSR, 99, 195-210.
- Kachanov, L. M., 1980a, Crack and Damage Growth in Creep, A Combined Approach, *Int. J. Fract.*, 16.
- Kachanov, L. M., 1980b, Continuum Model of Medium with Cracks, *J. Engng. Mech.*, ASCE, 106, No. Em5, Oct. 1039-1051.
- Kachanov, L. M., 1982, A Micocrack Model of Rock Inelasticity, Parts I-III, *Mech. Mater.*, 1, 19-41, 123-129.
- Kachanov, L. M., 1984, On a Continuum Modelling of Damage, in *Application of Fracture Mechanics to Cementitious Composites*, NATO-ARW, Sept. 4-7, Northwestern Univ., U. S. A., Shah, S. P., Ed.
- Kachanov, L. M., 1987, On Modelling of Anisotropic Damage in Elastic-Brittle Materials-A Brief Review, In *Proc. ASME Winter Annual Meeting*, Wang, A. S. D., and Haritos, G. K., Eds., 99-105, Dec., Boston, M. A. Kanaun, S. K., 1983, Elastic Medium with Random Fields of Inhomogeneities, Chapter 7 in Book by Kunin: *Elastic Media with Microstructure*, 2, Springer-Verlag.

- Kaplan, M. F., 1961, Crack Propagation and Fracture of Concrete, *J. ACI*, 58, 28, 591-610.
- Karni, J., and McHenry, D., 1958, Strength of Concrete under Combined Tensile and Compressive Stresses. *J. ACI*, Apr.
- Karsan, D., Jirsa, J. O., 1969, Behavior of Concrete under Compressive Loading, *J. Struct. Div.*, 95, 2543.
- Kato, B., Aoki, H., Yamaouchi, H., 1990, Standardized Mathematical Expression for Stress-Strain Relations of Structural Steel under Monotonic and Uniaxial Tension Loading, *Mater. Struc*, 23, 42-58.
- Kestin, J., and Bataille, J., 1978, Irreversible Thermodynamics of Continua and Internal Variables, in *Continuum Models of Discrete Systems*, Provan, J. W., Ed., Univ. of Waterloo Press, Study No. 12.
- Kobayashi, A. S., 1979, Dynamic Fracture Analysis by Dynamic Finite Element Method, Generation and Propagation Analysis, in *Nonlinear and Dynamic Fracture Mechanics*, Peronne, N., and Atluri, S. N., Eds, ASME.
- Kojic, M., and Cheatham, J. B., 1974, Theory of Plasticity of Porous Media with Fluid Flow, *Soc. Pet. Engng. J.*, 257, 263.
- Koiter, W. T., 1953, Stress-Strain Relations, Uniqueness and Variational Theorems for Elastic-Plastic Materials with Singular Yield Surfaces, *Quart. Appl. Math.*, 11, 3, 350-354.
- Kotsovos M., 1974, Failure Criteria for Concrete under Generalised Stress States, *Ph. D. Thesis*, Univ. of London.
- Kotsovos M. D., and Newman, J. B., 1977, Behavior of Concrete under Multiaxial Stresses, *J. ACI*, 74, 9, 443-446.
- Kotsovos M., 1979, Effect of Stress Path on the Behavior of Concrete under Triaxial Stress States, *J. ACI*, 76, 2, 213-223.
- Kotsovos, M.D., and Cheong, H.K., 1984, Applicability of Test Specimen Results for the Description of the Behavior of Concrete in a Structure, *ACI Mat. J.*, 81, 4, 358-363.
- Krajcinovic, D., 1979, A Distributed Damage Theory of Beams in Pure Bending, *J. Appl. Mech.*, 46, 592-596.
- Krajcinovic, and Fonseka, G. U., 1981, Continuum Damage Mechanics Theory of Brittle Materials (Parts I & II), *J. Appl. Mech.*, 48, 809.

- Krajcinovic, D., 1983a, Constitutive Equations for Damage Materials, *J. Appl. Mech.*, 50, 355-360.
- Krajcinovic, D., and Selvaraj, S., 1983b, Constitutive Equations for Concrete, in *Procs. of Int. Conf. on Constitutive Laws for Engineering Materials*, Desai, C. S., Gallagher, R. H., and, Tucson, Az., Eds.
- Krajcinovic, D., 1983c, Creep of Structures-A Continuous Damage Mechanics Approach, *Procs. of 7th Int. SMIRT Conf.*, 8/4, Chicago, Ill.
- Krajcinovic, D., 1984a, Continuum Damage Mechanics, *Appl. Mech. Rev.*, 37(1).
- Krajcinovic, 1984b, Mechanics of Solids with a Progressively Deteriorating Structure, in *Application of Fracture Mechanics to Cementitious Composites*, Shah, S. P., Ed., Northwestern Univ..
- Krajcinovic, D., 1985, Constitutive Theories for Solids with Defective Microstructure, In *Damage Mechanics and Continuum Modelling*, Stubbs, N., and Krajcinovic, D. Eds., 39-56, ASCE.
- Krajcinovic, D., and Fanella, D., 1986, A Micromechanical Damage Model for Concrete, *Engng. Fract. Mech.*, 25, Nos 5/6.
- Krajcinovic, D., 1987, Micromechanical Basis of Phenomenological Models, In *Continuum Damage Mechanics: Theory and Application*, Krajcinovic, D., and Lemaitre, J., Eds., Springer.
- Krajcinovic, D., and Summarac, D., 1989, A Mesomechanical Model for Brittle Deformation Processes, Parts, I and II, *J. Appl. Mech.*, ASME, 56, 51-62.
- Krajcinovic, D., Basista, M., and Sumarac, D., 1991, Micromechanically Inspired Phenomenological Damage Model, ASME, *J. Appl. Mech.*, 58, 305-310.
- Kranz, R. L., 1979, Crack Growth and Development During Creep of Barre Granite, *Int. J. of Rock Mech. Min. Sci. Geomech.*, Abstr., 16, 23.
- Kremple, K., 1980, Inelastic Constitutive Equations and Phenomenological Laws of Damage Accumulation for Structural Metal, *Proc. IUTAM Symp. on Physical Non-linearities in Structural Analysis*, Hult, J., and Lemaitre, J., Eds, Springer, Berlin.
- Krieg, R. D., 1975, A Practical Two Surface Plasticity Theory, *J. APPL. MECH.*, ASME, 42, 641-646.

- Kroner, E., 1962, Dislocation: A New Concept in the Continuum Theory of Plasticity, *J. of Mathematics and Physics*, 42, 27-37.
- Kroner, 1968, *Mechanics of Generalized Continua*, Springer-Verlag, Heidelberg, Germany.
- Krumhansl, J. A., 1968, Some Considerations of the Relations between Solid State Physics and Generalized Continuum Mechanics, *Mechanics of Generalized Continua*, Kroner, Ed., Springer-Verlag, Heidelberg, Germany, 298-321.
- Kubo, S., Ohji, K., and Ogura, K., 1984, An Analysis of Creep Crack Propagation on the Basis of the Plastic Singular Stress Field, *Engng Fracture Mech*, 11, 315-329.
- Kunin, I. A., 1968, The Theory of Elastic Media with Microstructure and the Theory of Dislocations, *Mechanics of Generalized Continua*, Kroner, Ed., Springer-Verlag, Heidelberg, Germany, 321-328.
- Kupfer, H. B., Hilsdorf, H. K., and Rusch, H., 1969, Behavior of Concrete under Biaxial Stresses, *Proc. ACI*, 66, No. 8, 656.
- Kupfer, H. B., Gerstle, K. H., 1973, Behavior of Concrete under Biaxial Stress, *J. Engng. Mech., ASCE*, 99, EM4, 853.
- Lade, P. W., and Duncan, J. M., 1975, Elastoplastic Stress-Strain Theory for Cohesionless Soil, *J. Geotech. Eng.Div., ASCE*, 101, GT10, Oct.
- Lade, P. W., 1982, Three-Parameter Failure Criterion for Concrete, *J. Engng. Mech., ASCE*, 108, 850-863.
- Ladeveze, P., 1983, On an Anisotropic Damage Theory, *Proc. of the CNRS Int. Colloquim on Failure Criteria of Structural Media*, Villars de Lans, France. 1983.
- Ladeveze, P., and Lemaitre, J., 1984, Damage Effective Stress in Quasi Unilateral Conditions, *IUTAM Congr.*, Lyngby, Denmark.
- Lame, A., 1950, In *Theory of Flow and Fracture of Solids*, 2nd Edn., Nadai, A., Ed., McGraw Hill, New York.
- Launay, P., and Gachon H., 1970, Strain and Ultimate Strength of Concrete under Triaxial Stresses, *ACI SP-34*, 13; also *1st Int. Conf. on Structural Mech. in Reactor Technology, SMIRT*, H1/3, Berlin, Sept., 1971.
- Laws, N., 1977, A Note on Interaction Energies Associated with Cracks in Anisotropic Media, *Phil. Mag.*, 36, 367-372.

- Laws, N, and Brockenbrough, J. R., 1987, The Effect of Microcrack Systems on the Loss of Stiffness of Solids, *Int. J. Solids Structures*, 23, 9, 1247-1268.
- Lebmann, Th., 1982, On the Concept of Stress-Strain Relations in Plasticity, *Acta Mechanica*, 42, 263-275.
- Leckie, F. A., and Hayhurst, D. R., 1974, Creep Rupture of Structure, *Proc. R. Soc. A340*, 323-347.
- Leckie, F. A., and Onat, E. T., 1980, Tensorial Nature of Damage Measuring Internal Variables, *Proc. IUTAM Symp. on Physical Non-linearities in Structural Analysis*, Hult, J., and Lemaitre, J., Eds, Springer, Berlin.
- Lekhnitskii, S. G., 1963, *Theory of Elasticity of an Anisotropic Elastic Body*, Holden-Day, San Francisco, California.
- Legendre, D. and Mazar, J., 1984, Damage and Fracture Mechanics for Concrete, A Combined Approach, *ICF6*, New Delhi.
- Lemaitre, J., 1971, Evaluation of Dissipation and Damage in Metals Submitted to Dynamic Loading, *ICM 1*, Kyoto, Japan.
- Lemaitre, J., and Chaboche, 1974, A Nonlinear Model of Creep-fatigue Damage Cumulation and Interaction, *Proc. IUTAM Symp. on Mechincs of Visco-elastic Media and Bodies*, Springer, Gothenburg.
- Lemaitre, J., and Dufailly, J., 1977, Modelisation et Identification de l'endommagement Plastique de Metaux, *3eme Congres Francis de Mecanique*, Grenoble, France.
- Lemaitre, J., and Chaboche, J. L., 1978, Phenomenological Aspects of Rupture by Damage, (Aspects Phenomenologique de la Rupture par Endommagement), *J. de Mecanique Appliquee*, 2, No. 3.
- Lemaitre, J., 1979a, Damage Modelling for Prediction of Plastic or Creep Fatigue Failure in Structures, *5th Conf. on Structural Mechanics in Reactor Technology, SMIRT 5*.
- Lemaitre, J., Cordebois, J. P., and Dufailly, J., 1979b, Sur le Couplage endommagement Elasticite, *Compte-rendu a l'Academie des Sci.*, Paris, B. 391.
- Lemaitre, J., and Plumtree, A., 1979c, Application of Damage Concepts to Predict Creep-Fatigue Failures, *J. Engng. Mater. Technol.*, 101, 284-292.
- Lemaitre, J., and Mazars, J., 1980, Modelisation du Comportement et de

la Rupture du Beton, 4eme Symposium Franco-Polonais de Mecanique, Marseille.

- Lemaitre, J., Billardon, R., and Brunet, M., 1981, Numerical Approach for Non-Propagating Threshold of Fatigue Cracks, *Res. Mech., Lett.*, 1.
- Lemaitre, J., and Baptiste, D., 1982a, On Damage Criteria, *Proc. and Workshop N.S.F. on Mechanics of Damage and Fracture*, Atlanta, Georgia.
- Lemaitre, J., and Mazars, J., 1982b, Application of the Damage Theory in Nonlinear Response and Rupture of Concrete Structures, Application de la theorie de l'endommagement au Compartement non Lineaire et a la Rupture de Beton de Structure), *Annales de l'ITBTP*, 401.
- Lemaitre, J., 1984a, Evaluation of Damage by Means of Elasticity Change Measurements, .
- Lemaitre, J., 1984b, Coupled Elasto-plasticity and Damage Constitutive Equations, *Invited Lecture at FENOMECH 84*, Stuttgart (RFA), also in *Comput. Meth. Appl. Mech. Engng J.*, 1985, 51, 31-49.
- Lemaitre, J., 1984c, How to Use Damage Mechanics, *Nuclear Engineering and Design*, 80, 233-245.
- Lemaitre, J., 1985a, A Continuous Damage Mechanics Models for Ductile Fracture, *Trans. ASME, J. Engng Mater. Technol.*, 107, 1.
- Lemaitre, J., and Chaboche, J. L., 1985b, *Mecanique des Materiaux Solides*, Dunod, Ed., 532.
- Lemaitre, J., 1986a, Local Approach of Fracture, *Engng. Fract. Mech.*, 25, 5/6, 523-537.
- Lemaitre, J., 1986b, Plasticity and Damage under Random Loading, In *Proc. Tenth U.S. National Congr. of Applied Mechanics*, Edited by J.P. Lamb, pp. 125-134, 16-20 June 1986, Austin, TX, ASME.
- Lemaitre, J., 1992, *A Course on Damage Mechanics*, Springer Verlag.
- Levin, KV. H., 1971, The Relation Between Mathematical Expectation of Stress and Strain Tensors in Elastic Microhomogeneous Media, *Prikl. Mat. Mekh.*, 35, 694-701.
- Levy, M., 1870, Memoire sur les Equations Generals des Mouvements Interieur des Corps Solids Ductile au Dela des Limites ou l'Elasticite Pourrait les Ramener a leur Premier Etat, *C. R. Acad.*

Sci., Paris, 70, 1323-1325.

- Li, B., Maekawa, K., Okamura, H., 1989, Contact Density Model for Stress Transfer Across Cracks in Concrete, *J. Fac Engng. Univ. Tokyo*, 40, 1, 9-52.
- Light, M. F., Luxmoore, A., and Evans, W. T., 1976, Predication of Slow Crack Growth By a Finite Element Method, *Int. J. Fract.*, 13, 503-506.
- Lin, C. S., and Scordelis, A. C., 1975, Nonlinear Analysis of RC Shells of General Form, *J. Struct. Engng.*, ASCE, 101, ST3, 523-538.
- Link, J., 1975, Numerical Analysis Oriented Biaxial Stress-Strain Relation and Failure Criterion of Plain Concrete, *3rd Int. Conf. on Structural Mech. in Reactor Technology*, SMIRT, H1/2, London, Sept.
- Lino, M., 1973, Etude d'un Modele de Beton par la Methode de Elements Finis, *T. F. E., E. N. P. C., L. C. P. C.*, Paris.
- Lino, M., 1980, A Model for a Microcracked Material, (Un Modele de Materiau Micofissure), *Revue Francaise de Geotechnique*, No. 11, 29-41.
- Linse, D., 1973, Versuchsanlage zur Ermittlung der Dreiachsigen Festigkeit von Beton mit Ersten Versuchsergebnissen, *Cem. Conc. Res.*, 3, No. 4, 445.
- Linse, D., Aschl, H., and Stockl, S., 1975, Concrete for PCRV's: Strength of Concrete under Triaxial Loading and Creep at Elevated Temperatures, *3rd Int. Conf. on Structural Mech. in Reactor Technology*, SMIRT, H1/3, London, Sept.
- Linse, D., and Aschl, H., 1976, Tests on the Behavior of Concrete under Multiaxial Stresses, *Report*, Dept. of Reinforced Concrete, Technical Univ. of Munich.
- Liu, T. C. Y., 1971, Stress-Strain Response and Fracture of Concrete in Biaxial Compression, *Research Report No. 339*, Dept. of Structural Engng., Cornell Univ., Feb.
- Liu, T. C. Y., Nilson, A. H., and Slate, F. O., 1972a, Biaxial Stress-Strain Relations for Concrete, *J. Struct. Div.*, ASCE, 98, ST5, 1025.
- Liu, T. C. Y., Nilson, A. H., and Slate, F. O., 1972b, Stress-Strain Response and Fracture of Concrete in Uniaxial and Biaxial Compression, *Proc. ACI*, 69, No. 5, 291.

- Loland, K. E., and Gjorv, O. E., 1980a, Ductility of Concrete and Tensile Behavior, *Presented at the Annual Convention, ASCE, Florida, Oct.*
- Loland, K. E., 1980b, Continuous Damage Model for Load-Response Estimation of Concrete, *Cem. Conc. Res.*, 10, 395-402.
- Loland, K. E., 1981a, Mathematical Modelling of Deformational and Fracture Properties of Concrete Based on Principles of Damage, (Matematisk Modelling av Betongens Deformasjons-og Bruddegenskaper Basert Pa Skademekaniske Prinsipper), Univ. of Trondheim, *Rapport BML 81.101.*
- Loland, K. E., 1981b, Mathematical Modelling of Deformational and Fracture Properties of Concrete Based on Principles of Damage Mechanical Principles - Application on Concrete with and without Addition of Silica Fume, *Dr. Ing. Thesis*, Univ. of Trondheim, Norway.
- Lorrain, M., 1979, On The Application of The Damage Theory to Fracture Mechanics of Concrete *A State of The Art Report*, Civ. Engng. Dept., INSA, Toulouse, France.
- Lorrain, M., Loland, K. E., 1983, Damage Theory Applied to Concrete, in *Fracture Mechanics of Concrete*, Wittman, F. H., Ed., Chapter 4.4, Elsevier Science Publishers B. V., Amsterdam, Netherlands, 341-369.
- Lubliner, J., 1972, On the Thermodynamic Foundation of Nonlinear Solid Mechanics, *Int. J. Nonlinear Mech.*, 7, 237-254.
- Lubliner, J. 1980, On Thermodynamic Yield Criteria, *Acta Mechanica*, 37, 259-263.
- Makik, S. N., 1982, Elevated Temperature Crack Growth-State of the Art and Recommendations, *Nucl. Engng. Des.*, 72, 359-371.
- Maier, G., and Hueckel, T., 1979, Nonassociative and Coupled Flow Rules of Elastoplasticity for Rock-Like Materials, *Int. J. Rock Mech. Min. Sci. Geomech.*, 16, 77-92.
- Maier, G., Nappi, A., Papa, E, 1990, Damage Models For Masonry as a Composite Material: A Numerical Approach
- Malvern, L. E., 1969, *Introduction to the Mechanics of a Continuous Medium*, Prentice-Hall, Inc.
- Marchertas, A. S., Kulal, R. F., and Pan, Y. C., 1982, Performance of the "Blunt Crack" Approach With a General Purpose Code, in *Nonlinear Numerical Analysis of Reinforced Concrete*, Schwer, E.,

Ed., 107-123, ASME Publication H00242.

- Marigo, J. J., 1985, Modelling of Brittle and Fatigue Fracture of Concrete, In *Adv. in Fract. Res. (Fracture 81)*, 4, 1499-1506, Pergamon Press.
- Mart, P., 1980, *Zur Plastischen Berechnung von Stahlbeton*, Eidgenossische Technische Hochschule, Institut für Baustatik und Konstruktion, Zurich, Bericht Nr 104, Oct.
- Martin, J. B., 1975, *Plasticity: Fundamentals and General Results*, MIT Press, Cambridge, Mass.
- Massonet, C., and Save, M., 1963, *Calcul Plastique des Constructions, 2: Structures Spatiales*, Centre Belgo-Luxembourgeois d'Information de l'Acier, Bruxelles. (English Edn., *Plastic Analysis and Design of Plates, Shells and Disks*, North-Holland, Amsterdam, 1972).
- Mazars, J., 1980, Mechanical Damage and Fracture of Concrete Structures, in *5th Inter. Conf. on Fracture, also 1982, in Advances in Fracture Mechanics (Fracture 81)*, Francois, D., Ed., Pergamon Press, 4,1499-1506.
- Mazars, J., 1983, Probabilistic Aspects of Mechanical Damage in Concrete Structures, *Fracture Mechanics Technology Applied to Material Evaluation and Structure Design*, Martinus Nijhoff Publishers, 657-666.
- Mazars, J., 1984a, Application of the Damage Mechanics in Nonlinear Response and Rupture of Concrete Structures, (*Application de la Mecanique de l'Endommagement au Comportement Non Lineaire de la Rupture du Beton de Structure*), *These de Doctorat d'Etat*, Universite Pierre et Marie Curie, Paris 6.
- Mazars, J., and Lemaitre, J., 1984b, Application of Continuous Damage Mechanics to Strain Fracture Behavior of Concrete, *Proc. NATO Adv. Res. Workshop on Applications of Fracture Mech. on Cementitious Composites*, Evanston, Illinois.
- Mazars, J., and Legendre, D., 1984c, Damage and Fracture Mechanics for Concrete- A Combined Approach, *ICF6*, New Delhi.
- Mazars, J., 1985, A Model of a Unilateral Elastic Damageable Material and its Application to Concrete, *ICF6, Fracture Toughness and Fracture Energy of Concrete*, Ed., Wittmann, F. H., Elsevier, 1986, 61-72.
- Mazars, J., 1986a, Description of the Behavior of Composite Concretes under Complex Loading Through Continuum Damage Mechanics, In *Proc. Tenth U.S. National Congr. of Applied Mechanics*, Edited by

- J.P. Lamb, pp. 135-139, 16-20 June 1986, Austin, TX, ASME.
- Mazars, J., and Pijaudier-Cabot, G., 1986b, Continuum Damage Theory: Application to Concrete, *Int. Report No. 71-L.M.T. Cachan*, and also *J. Engng. Mech.*, ASCE, 1990.
- Mazars, J., 1986c, A Description of Micro- and Macroscale Damage of Concrete Structures *Engineering Fracture Mechanics*, 25, 5/6, 729-737.
- Mazars, J., and La Borderie, C., 1987, Comportement Oligocyclique des Beton Composites, *Int. Report No. 80-L.M.T.*, Cachan.
- Mazars, J., Pijaudier-Cabot, Clement, J. L., 1992, Analysis of Steel-Concrete Bond with Damage Mechanics: Nonlinear Behavior and Size Effect,
- Mehta, P. K., 1986, *Concrete: Structure, Properties and Materials*, Prentice-Hall, Inc.
- Mihashi, H., Izumi, M., 1977, A Stochastic Theory of Concrete Fracture, *Cement and Concrete Research*, 7, 411-422.
- Mills, L. L., and Zimmerman, R. M., 1970, Compressive Strength of Plain Concrete under Multiaxial Loading Conditions, *Proc. ACI*, 67, 802.
- Mills, L. L., and Zimmerman, R. M., 1971, Discussion of Paper, Compressive Strength of Plain Concrete under Multiaxial Loading Conditions, author's closure, *Proc. ACI*, 68, 300.
- Miller, K. J., and Kfoury, A. P., 1974, An Elastic Plastic Finite Element Analysis of Crack Tip Fields Under Biaxial Loading Conditions, *Int. J. Fracture*, 10, 393.
- Modeer, A., 1979, A Fracture Mechanics Approach to Failure Analyses of Concrete Materials, *Report Univ. of Lund*.
- Mohr, O., 1914, *Abhandlungen aus dem Geiet der Mechanik*, 2nd Edn., Wilhelm Ernst and Sohn, Berlin.
- Mroz, Z., 1963, Nonassociated Flow Rules in Plasticity, *J. de Mecanique*, Paris, France, II, 1, Mar.
- Mroz, Z, and Angellilo, M., 1982, Rate Dependent Degradation Model for Concrete and Rock, in *Numerical Models in Geomechanics*, Dungar, R., Balkema, A. A., Eds., Rotterdam.
- Muller, P., 1978, *Plastische Berechnung von Stahlbetonscheiben und Balken-Eidgenossische*, Technical Hochschule, Institut fur

- Baustatik und Konstruktion, Zurich, Bericht Nr 83 (ETH Diss. 6083), July.
- Murakami, S., and Ohno, N., 1978, Creep Damage Analysis in Thin-Walled Tubes, *Inelastic Behavior of Pressure Vessel and Piping Components*, PVP-PB-028, 55-69, ASME, New York.
- Murakami, S., 1981a, Effects of Cavity Distribution in Constitutive Equations of Creep and Creep Damage, *EUROMECH Colloquium 147 on Damage Mechanics*, Lemaitre, J., Ed., Cachan, France.
- Murakami, S., and Ohno, N., 1981b, A Continuum Theory of Creep and Creep Damage, *Proc. 3rd IUTAM Symp. on Creep in Structures*, Ponter, A.R.S., and Hayhurst, D. R., Eds, 422-444, Springer, Berlin.
- Murakami, S., 1982, Damage Mechanics Approach to Damage and Fracture of Materials, *Rairo*, 3, 1-13.
- Murakami, S., 1987, *Stress Intensity Factors Handbook*, Pergamon Press, Oxford, New York.
- Murakami, S., 1989, Mechanical Modeling of Material Damage, *J. Appl. Mech.*, ASME, 55, 280-286.
- Murrell, S. A. F., 1963, A Criterion for Brittle Fracture of Rocks and Concrete under Triaxial Stress and the Effect of Pore Pressure on the Criterion, in *Proc. 5th Rock Mechanics Symp.*, Pergamon Press, Oxford, 563-577.
- Nadai, A., 1950, *Theory of Flow and Fracture of Solids*, Vol. 1, McGraw Hill, New York.
- Naghi, P. M., Essenburg, F., and Koff W., 1958, An Experimental Study of Inertial and Subsequent Yield Surfaces in Plasticity, *J. Appl. Mech.*, 25, 201-209.
- Nasizawa, N., 1962, Strength of Concrete under Combined Tensile and Compressive Loads, *Japan Cement Engng. Assoc. Review*, May, 126-131.
- Najar, J., 1987, Continuous Damage of Brittle Solids, in *Continuous Damage Mechanics, Theory and Applications*, Eds. Krajcinovic, D., and Lemaitre, J., Springer-Verlag, Wien-New York, 233-295.
- Najar, J., 1989, Transition from Continuous Damage to Failure at Uniaxial Loading of Elastic-Brittle Materials, *Cracking and Damage Strain Localization and Size Effect*, Eds. Mazars, J. and Bazant, Z.P., Eisevier Applied Science, 150-163.

- Needleman, A., 1978, Material Rate Dependence and Mesh Sensitivity in Localization Problems, *Report of Brown Univ.*.
- Neilsen, M. K., Chen, Z. and Schreyer, H. L., 1990, A Structural Constitutive Algorithm Based on Continuum Damage Mechanics for Softening with Snapback.
- Nelissen, L. J. M., 1972, Biaxial Testing of Normal Concrete, *Heron* , 18, No. 1, 90.
- Neville, A.M., 1963, *Properties of Concrete*, Wiley, New York.
- Newman, K., and Newman, J. B., 1971, Failure Theories and Design Criteria for Plain Concrete Structure, In *Solids, Solid Mechanics*, Wiley Interscience, London, 963-995.
- Newman, J. C., 1977, Finite Element Analysis of Crack Growth Under Monotonic and Cyclic Loading, *Cyclic Stress Strain and Plastic Deformation Aspects of Fatigue Crack Growth*, ASTM STP 637, 56-80.
- Newman, J. C., 1982, Prediction of Fatigue Crack Growth Under Variable Amplitude and Spectrum Loading Using a Closure Model, *Design of Fatigue and Fracture Resistant Structures*, ASTM STP 761, 255-277.
- Newman, K., 1965, The Structure and Engineering Properties of Concrete, Theory of Arch Dams, *Procs. of an Int. Symposium*, Southampton, 1964, Editor: J.R. Rydzewski, Oxford, Pergamon Press, 683-712.
- Ngo, D., and Scordelis, A. C., 1967, Finite Element Analysis of Reinforced Concrete Structures, *J. ACI*, 64, 3 Mar.
- Nicholson, D. W., 1981, Constitutive Model for Rapidly Damaging Structural Materials, *Acta Mechanica*, 39, 195-205.
- Nielsen, M. P., 1964, Limit Analysis of Reinforced Concrete Slabs, *Acta Polytech. Scand., Civ. Engng. Bldg. Constr. Ser.*, No. 26, 167.
- Nielsen, M. P., Braestrup, M. W., Jensen, B. C., Bach, F., 1978, *Concrete Plasticity, Beam Shear-Punching Shear-Shear in Joints*, Danish Soc. for Struct. Sci. and Engng., Copenhagen, Special Publication.
- Nielsen, M. P., 1984, *Limit Analysis and Concrete Plasticity*, Prentice Hall, Inc.

- Niu, X. D., 1989, Endochronic Plastic Constitutive Equations Coupled with Isotropic Damage and Damage Evolution Models, *Europ. J. Mech.*
- Norris, D. M., Moran, B., Quinones, D. F., and Reaugh, J. E., 1978, Fundamental Study of Crack Initiation and Propagation, *EPRI Ductile Fracture Research Review Document*, Section 7.
- Ofoegbu, G. I., and Curran, J. H., 1990, An Elastic-Ductile Constitutive Model for Rock, 445-448.
- Ortiz, M., and Popov, E. P., 1982a, Plain Concrete as a Composite material, *Mech. Mater.*, 1, 139.
- Ortiz, M., Popov, E. P., 1982b, A Physical Model for the Inelasticity of Concrete, *Proc. Roy. Soc. Lond.*, A383, 101.
- Ortiz, M., 1984, A Constitutive Theory for the Inelastic Behavior of Concrete, *Report*, Division of Engineering, Brown Univ., Providence, Rhode Island 02912, Nov. 28.
- Ortiz, M., 1985, A Constitutive Theory for the Inelastic Behavior of Concrete, *Mech. of Mat.*, 4, 67-93.
- Ortiz, M., and Simo, J. C., 1986, An Analysis of a New Class of Integration Algorithms for Elastoplastic Constitutive Relations, *Int. J. Numer. Meth. Engng.*, 23, 353-366
- Ortiz, M., 1987a, A Method of Homogenization of Elastic Media, *Int. J. Engng. Sci.*, 25, 923-934
- Ortiz, M., 1987b, An Analytical Study of the Localized Failure Modes of Concrete, *Mech. Mater.*, 6, 159-174.
- Ottson, N. S., 1977a, A Failure Criteris for Concrete, *J. Engng. Mech.*, ASCE, 103, No. EM4, 527-535.
- Ottson, N. S., 1977b, Structural Failure of Thick Walled Concrete Element, *4th Int. Conf. on Structural Mechanics in Reactor Technology*, SMIRT, San Francisco, H4/3, Aug.
- Ottson, N. S., 1979, Constitutive Model for Short Time Loading of Concrete, *J. Engng. Mech.*, ASCE, 105, No. EM1, 127-141.
- Ouchterlony, F., 1983, A Distributed Damage Approach to Combined Bending and Axial Loading of Rock Meams, in *Mechanical Behavior of Materials*, Carlsson, J., and Ohlson, N. G., Ed., 2, Pergamon Press.
- Owen, D. R. H., and Hinton, E., 1980, *Finite Elements in Plasticity*,

Pineridge, Swansea.

- Owen, D.R.J., Figueiras, J.A., and Damjanic, F., 1983, Finite Element Analysis of Reinforced and Prestressed Concrete Structures Including Thermal Loading, *Computer Methods in Applied Mechanics and Engineering*, 41, 323-366.
- Pak, A. P., and Trapenznikov, L. P., 1981, Experimental Investigations Based on the Griffith-Irwin Theory Processes of the Crack Development in Concrete, in *Advances in Fracture Research (Fracture 81)*, 4, Francois, D., Ed., 1531-1539.
- Parry, R. H. G., (Ed.), 1971 Stress-Strain Behavior of Soils *Proc. Roscoe Mem. Symp. Cambridge Univ.* Foulis, G. T., and Co., London.
- Palaniswamy, R., and Shah, S. P., 1974, Fracture and Stress-Strain Relationship of Concrete under Triaxial Compression, *J. Struct. Div.*, ASCE, 100, ST5, 901.
- Patino, J. G. S., 1989, Stability and Energy Minimization in Elasticity with Damage, *Inter. J. Solids Structures*, 25, 11, 1255-1266.
- Paul, B., 1961, A Modification of the Coulomb-Mohr Theory of Fracture, *J. Appl. Mech.*, ASME, 28, 259-268.
- Petersson, P. C., 1981, Crack Growth and Development of Fracture Zones in Plain Concrete and Similar Materials, *Doctoral Dissertation*, Lund Institute of Technology, Lund, Sweden.
- Pflugger, A., 1967, Zur Plastischen Beulung von Flachentragern, *ZAMM*, 47, T209-T211.
- Pietruszczak, St., and Mroz, Z., 1981, Finite Element Analysis of Deformation of Strain-Softening Materials, *Int. J. Numer. Meth. Engng.*, 17, 327-334.
- Pijaudier-Cabot, G., 1985, Caracterisation et Modelisation du Comportement du Beton par un Essai Multiaxial Automatique, *These de 3eme Cycle*, Universite Paris 6.
- Pijaudier-Cabot, G., Bazant, Z. P., 1987a, Nonlocal Damage Theory, *J. Engng. Mech.*, ASCE, 113, 10, 1512-1533.
- Pijaudier-Cabot, G., Bazant, Z. P., 1987b, Propagation of Interacting Cracks in an Elastic Solid with Inclusions *Preliminary Report*, Northwestern Univ., Evanston, Illinois.
- Pijaudier-Cabot, G., Bazant, Z. P., and Tabbara, M., 1988, Comparison of Various Models for Strain-Softening, *Engng. Comp.*, 5, 141-150.

- Pilvin, P., 1983, Modelisation du Comportement des Assemblages de Structures a Barres, *These de IIIeme Cycle*, Universite de Paris VI.
- Podgorski, 1985, General Failure Criterion for Isotropic Media, *J. Eng. Mech.*, ASCE, 11, 188.
- Policella, H, and Culie, J. P., 1981, A Method for Predicting the Lifetime of Gas Turbine Blades, *Fatigue Engng Mater. Structures*, 4(2), 157-172.
- Popovics, S., 1973, A Numerical Approach to the Complete Stress-Strain Curve of Concrete, *Cem. Conc. Res.*, 3, pp. 583-599.
- Powers, T. C., and Brownyard, T. L., 1947, Studies of the Physical Properties of Hardened Portland Cement Paste, *J. ACI*, 977.
- Prandtl, L., 1924, Spannungsverteilung in Plastischen Korpern, *Proc. 1st Int. Congr. Appl. Mech.*, Delft, 43-54.
- Prandtl, L., and Reuss, A., 1950, *The Mathematical Theory of Plasticity*, Hill, R., Ed., Oxford Univ. Press, London.
- Prandtl, L. and Reuss, A., 1968, *Plasticity, Theory and Application*, Medelson, A., Ed. Macmillan, London.
- Rabotnov, Y. N., 1963, On the Equations of State of Creep, Progress in Applied Mechanics, *The Prager Anniversary Volume*, 307-315.
- Rabotnov, Y. N., 1968, Creep Rupture, *Proc. XII Int. Congr. in Applied Mechanics*, Stanford-Springer.
- Ramakishnan, C. V., Numerical Simulation of Dynamic Fracture, *2nd Conf. on Computer Aided Analysis and Design in Civ. Engineering*, Roorkee, 29 January-2 February.
- Ramborg, W., and Osgood, W. R., 1943, Description of Stress-Strain Curves by Three Parameters, *NACA TN 902*.
- Rankine, T., 1950, Soil Mechanics and Plastic Analysis or Limit Design, *Q. Appl. Math.*, 10.
- Read, H.E., and Hegemier, G. A., 1984, Strain Softening of Rock, Soil and Concrete - A Review Article, *Mech. Mat.*, 3, 271-294.
- Reckling, K. A., *Plastizitatstheorie und Aswendung auf Festigkeitsprobleme*, Springer-Verlag, Berlin.
- Reimann, H., 1965, Kritische Spannungszustande der Betons bei Mehrachsiger, Ruhender Kurzzeitbelastung, *Deutscher Ausschuss*

fur Stahlbeton, Heft 175, Berlin.

- Reinhardt, H.W., 1985, Plain Concrete Modeled as an Elastic Strain-Softening Material at Fracture, *Engng. Fract. Mech.*, 22, 5, 787-796.
- Resende, L., and Martin, J.B., 1984, Damage Constitutive Model for Granular Materials, *Comp. Meth. Appl. Mech. Engng.*, 42, pp. 1-18.
- Resende, L., and Martin, J.B., 1985, Formulation of Drucker-Prager Cap Model, *J. Engng. Mech., ASCE*, 111, 7, 855-881.
- Resende, L., 1987, A Damage Mechanics Constitutive Theory for the Inelastic Behavior of Concrete, *Comp. Meth. Appl. Mech. Engng.*, 60, pp. 57-93. Reuss, A., 1930, Berücksichtigung der Elastischen Formänderung in der Plastizitätslehre, *ZAMM*, 10, 266-274.
- Rice, J. R., 1968, Path Independent Integral and Approximate Analysis of Strain Concentration by Notches and Cracks, *J. Appl. Mech., ASME*, 35, 379-386.
- Rice, J. R., 1976, The localization of Plastic Deformation, *Proc. 14th IUTAM Congr.*, Delft, 207-220.
- Richart, F. E., Brandzaeg, A., and Brown, R. L., 1928, A Study of the Failure of Concrete under Combined Compressive Stresses, *Bulletin No. 185*, Engng. Experiment Station, Univ. of Illinois, 26.
- Riedel, H., 1984, A Continuum Damage Approach to Creep Crack Growth, in Fundamentals of Deformation and Fracture, *The Eshelby Memorial Symp.*, Sheffield, Miller, K. J., Ed., Cambridge Univ. Press, Cambridge.
- Riedel, H., and Wagner, W., 1981, The Growth of Microscopic Crack in Creeping Materials, *ICF6, Advances in Fracture Research*, Francois, D., Ed., 3, 683-690, Pergamon Press, Oxford.
- RILEM, 1985, Determination of the Fracture Energy of Mortar and Concrete by Means of Three-Point Bend Tests on Notched Beams, *Mater. Struct.*, 18, 285-290.
- RILEM Draft Recommendation, TC83-CUS, 1990, Fundamental Mechanical Properties of Metals, *Mater. Struct.*, 23, 35-46.
- Rivlin, A. and Erickson, J. L., 1954, Stress-Deformation Relations for Isotropic Materials, *Report*, Graduate Institute for Maths and Mechanics, Indiana Univ., Dec.; also in *J. of Rational Mech. Anal.*, 4, 323-425, 1955 (reprinted in *Rational Mech. of Materials*, Truesdell, C., Ed., New York: Gordon and Breach, 1965).

- Rivlin, R. S., 1966, The Fundamental Equations of Nonlinear Continuum Mechanics, in *Dynamics of Fluids and Plasmas*, Burgers Anniversary Volume, Pai, S. I., Ed., New York, Academic Press.
- Robinson, G. S., 1964, The Failure of Concrete under Particular Reference to the Biaxial Compressive Strength, *Ph. D. Thesis*, Univ. of London, Nov.
- Roelfstra, P. E., and Sadouki, H., 1986, Fracture Process in Numerical Concrete, in *Fracture Toughness and Fracture Energy of Concrete*, Ed., Wittmann, F. H., Elsevier.
- Rokugo, K., 1979, Energy Approach to the Failure of Concrete and Concrete Members, *Ph. D. thesis*, Univ. of Kyoto, Japan.
- Romstad, K. M., Taylor, M. A., and Herrmann, L. R., 1974, Numerical Biaxial Characterization of Concrete, *J. Engng. Mech.*, ASCE, 100, EM5, 935.
- Roscoe, K. H., Schofield, A. N., Wroth, C. P., 1958, On the Yielding of Soils *Geotechnique*, 8, 1, 25-53, Mar.
- Roscoe, K. H., Schofield, A. N., Thurairajah, A., 1963, Yielding of Soils in States Wetter than Critical, *Geotechnique*, 13, 3, 211-240, Sept.
- Rossi, P., and Richer, S., 1987, Stochastic Modelling of Concrete Cracking, *Proc. Second Inter. Conf. on the Constitutive Laws for Engineering Materials-Theory and Applications*, Tucson.
- Rots, J.G., 1985, Strain Softening Analysis of Concrete Fracture Specimens, *Proc. Int. Conf. on Fracture Mechanics of Concrete*, Elsevier, Amsterdam, 115-126.
- Rots, J.G., Nauta, P., Kusters, G.M.A., and Blaauwendraad, J., 1985, *Smeared Crack Approach and Fracture Localization in Concrete*, Heron, Delft, 30, 1, 48.
- Rots, J. G., 1988, Computational Modelling of Concrete Fracture, *Ph. D. Thesis*, Delft Univ. of Technology, Delft, Netherland.
- Rots, J.G., and de Borst, R., 1989, Analysis of Concrete Fracture in "Direct" Tension, *Int. J. Solids Structures*, 25, 12, 1381-1394.
- Rousselier, G., 1977, A Numerical Approach for Syable Crack Growth and Fracture Criteria, *Fracture 1977*, 3, 1-6.
- Rousselier, G., 1978, An Experimental and Analytical Study of Ductile Fracture and Stable Crack Growth, *Meeting on Elastic Plastic Fracture Mechanics*, OECD Nuclear Energy Agency, Daresbury,

U.K.

- Rousselier, G., 1979, Contribution a l'etude de la Rupture des Maetaux dans le Domaine de l'elasto-plasticite, These, Ecole Polytechnique et Universtie Paris 6.
- Rousselier, G., Devaux, J. C., and Mottet, G., 1985, Ductile Initiation and Crack Growth in Tensile Specimens Application of Continuum Damage Mechanics, *SMIRT8*, Brussels, Belgium.
- Rousselier, G., 1981, Finite Deformation Constitutive Relations Including Ductile Fracture Damage, *Three Dimensional Constitutive Relations and Ductile Fracture*, Nemat-Nasser, Ed., North-Holland, London.
- Rygol, J., 1983, Structural Design: National Code Specifications for Concrete and Reinforcement, *Handbook of Structural Concrete*, Eds. F.K. Kong, R.H. Evans, E. Cohen and F. Roll, Pitman Advanced Publishing Program.
- Saanouni, K., and Chaboche, J. L., 1985, Numerical Aspects of a Local Approach for Predicting Creep Crack Growth, *Colloque Tendances Actuelles en Calcul des Structures*, Bastia, Corse.
- Saanouni, K., 1984, Sur Une Approach Locale Pour la Rupture en Viscoplasticite, *Rapport GRECO*, Grandes Deformation et Endommagement. Sabnis, G. M., and Mirza, S. M., 1979, Size Effect in Model Concrete, *J. Struct. Div., ASCE*, 105, 1007-1020.
- Saenz, L. P., 1965, Equation for Stress Strain Curve of Concrete in Uniaxial and Biaxial Compression for Concrete, *J. ACI*, 61, 1229-1235.
- Sandbye, P. A., 1965, A Plastic Theory for Plain Concrete, In *Bygnings-Statistiske Meddelelser*, 36, Teknisk, Forlag, Copenhagen, 41-62.
- Sandler, I., DiMaggio, and Baladi, G. Y., 1976, Generalized Cap Model for Geotechnical Materials, *J. Geotech. Engng, ASCE*, 102, Gt7, 683-699.
- Sandler, I. S., and Rubin, D., 1979, An Algorithm and a Modular Subroutine for the Cap Model, *Int. J. Numer. Analyt. Geomech.*, 3, 173-186.
- Sandler, I. S., 1978, On the Uniqueness and Stability of Endochronic Theories of Material Behavior, *ASME J. of Appl. Mech.*, 45, 2, 263-266.
- Sandler, I. S., 1984, Strain Softening for Static and Dynamic Problems. *ASME Winter Annual Meeting, Symp. on Constitutive Equations:*

- Micro, Macro and Computational Aspects*, CEQ, New Orleans, Dec.
- Saouridis, C., and Samake, G., 1985, Caracteristion de l'endommagement et de la Fissuration de Plaques Composites en Beton Arme, *Memoire de DEA*, Laboratoire de Mecanique et Technologie, Cachan, France.
- Saouridis, C., and Mazars, J., 1989, A Multiscale Approach to Distributed Damage and Its Usefulness for Capturing Structural Size Effect, *Cracking and Damage Strain Localization and Size Effect*, Eds. Mazars, J. and Bazant, Z.P., Elsevier Applied Science.
- Saouridis, C., and Mazars, J., 1992, Prediction of the Failure and Size Effect in Concrete via a Bi-Scale Damage Approach, *Engineering Computation*, 9, 329-344.
- Scanlon, A., 1971, Time Dependent Deflections of Reinforced Concrete Slabs, *Ph.D. Thesis*, University of Alberta, Edmonton.
- Scavuzzo, R., Stankowski, T., Grestle, K. H., Ko, H. Y., 1983, Stress-Strain Curves for Concrete under Multiaxial Load Histories, *NSF CME-80-01508*, Dept. of Civ. Engng., Univer. of Colorado, Boulder.
- Schimmelpfennig, K., 1971, Ultimate Load Analysis of Prestressed Concrete Pressure Vessels Considering a General Material Law, *Paper H4/6*, 3rd Int. Conf. on Struct. Mech. in Reactor Technology, London, England, Sept.
- Schofield, A. N., and Wroth, C. P., 1968, *Critical State Soil Mechanics*, McGraw-Hill Publishing Company, Ltd., London.
- Schreyer, H.L., 1989, Formulations for Nonlocal Softening in a Finite Zone with Anisotropic Damage, *Cracking and Damage Strain Localization and Size Effect*, Eds. Mazars, J. and Bazant, Z.P., Elsevier Applied Science.
- Schapery, R. A., 1968, On a Thermodynamic Constitutive Theory and its Applications to Various Nonlinear Materials, *Proc. IUTAM Symp. East Kilbride*, June, Boley, B. A., Ed. Springer, New York.
- Schapery, R. A., 1969, Further Development of a Thermodynamic Constitutive Theory: Stress Formulation, *Rep. AA & ES 69-2 to Air Force Material Lab.(Contract F33615-67C-1412)*, School of Aeronautics and Engng. Sci., Purdue Univ., Lafayette, Indiana, Feb.
- Schickert, G., and Winkler, H., 1977, Results of Test Concerning Strength and Strain of Concrete Subjected to Multiaxial

Compressive Stresses, *Bulletin No. 277, Deutscher Ausschuss für Stahlbeton*, Berlin.

- Schleicher, F., 1925, *The Energy Limit of Elasticity*, *Zeitschrift fuer Angewandte Mathematik und Mechanik* 5, 6, 478-479.
- Schreyer, H. L., and Chen, Z., 1986, One-Dimensional Softening with Localization, *J. Appl. Mech.*, 53, 791-797.
- Schreyer, H. L., 1987, The Need for Snapback in Constitutive Algorithms, in *Computational Plasticity - Models, Software and Application*, Owen, D. R. J., Hinton, E., and Onate, E., Eds, Pineridge Press.
- Scordelis, A. C., 1972, Finite Element Analysis of Reinforced Concrete Structures, *Speciality Conf. on the Finite Element Methods in Civ. Engng*, Held at McGill Univ., Montreal, Quebec, Canada, 71-113.
- Sentler, L., 1985, A Stochastic Model of Concrete Strength, in *Memoire AIPC, IABBSE Proc.*, 88/85, 125-140.
- Sewell, M. J., 1974, A Plastic Flow Rule at a Yield Vertex, *J. Mech. Phys.*, 22, 469-490.
- Shah, S.P., and Winter, G., 1966, Response of Concrete to Repeated Loadings, RILEM, *Int. Symp. on the Effects of Repeated Loading on Materials and Structural Elements*, Mexico City, Mexico.
- Shah, S. P., and Chandra, S., 1968, Critical Stress, Volume Change and Microcracking of Concrete, *J. ACI*, 65, 770-781.
- Shah, S.P., and Chandra, S., 1970, Fracture of Concrete Subjected to Cyclic and Sustained Loading, *ACI J.*, 67, 9, 816-825.
- Shah, S.P., 1985, Ed., *Application of Fracture Mechanics to Cementitious Composites*, *NATO Advanced Science Series*, Martinus Nijhoff Publishers, Dordrecht, 714.
- Shah, S.P., and Sankar, R., 1987, Internal Cracking and Strain-Softening Response of Concrete under Uniaxial Compression, *ACI Mat. J.*, 84, 3, 200-212.
- Shih, C. F., Andrews, W. R., Delorenzi, H. G., Van Stone, R. H., Yukawa, S., and Wilkinson, J. P. D., 1978, Crack Initiation and Growth Under Fully Plastic Conditions: A Methodology for Plastic Fracture, *EPRI Ductile Fracture Research Review Document*, Section 6.
- Shockey, D. A., Curran, D. R., Seaman, L., Rosenberg, J. T., and Petersen, C. F., 1974, Failure of Rock Under High Tensile Loads,

- Int. J. Rock Mech. Sc.*, Geomech. Abstract 11, 303-317.
- Sidoroff, F., 1981, Description of Anisotropic Damage Application to Elasticity, in *IUTAM Colloquium on Physical Nonlinearities in Structural Analysis*, Springer Verlag, Berlin, 2237-244.
- Sigvaldason, O. T., 1965, Failure Characteristics of Concrete, *Ph. D. Thesis*, Univ. of London, June.
- Sih, G., 1973-1977, *Mechanics of Fracture*, Vols. I-V, Noordhoff, Leiden.
- Simo, J.C., and Ju, J.W., 1986, On Continuum Damage-Elastoplasticity at Finite Strain: A Computational Framework, *Comput. Mech.*, 23, 7, 821-840.
- Simo, J.C., and Ju, J.W., 1987a, Strain- and Stress-Based Continuum Damage Models -- I. Formulation, *J. Solids Struct.*, 23, 7, 821-840.
- Simo, J.C. and Ju, J.W. (1987b), Strain- and Stress-Based Continuum Damage Models -- I. Formulation, *J. Solids Struct.*, 23, 7, 841-869.
- Simo, J. C., Ju, J. W., Pister, K. S. and Taylor, R. L., 1988, An Assessment of the Cap Model: Consistant Return Algorithms and Rate-Dependent Extension, *J. Struct. Engng.*, ASCE, 109, 1727-1741.
- Simo, J.C., 1989, Strain Softening and Dissipation: A Unification of Approaches, *Cracking and Damage Strain Localization and Size Effect*; Eds. Mazars, J. and Bazant, Z.P., Elsevier Applied Science.
- Sinha, B. P., Gerstle, K. H., and Tulin, L. G., 1964, Stress-Strain Relations for Concrete under Cyclic Loading, *J. ACI*, 61, 2, 195-211.
- Smith, G. M., 1953, Failure of Concrete under Combined Tensile and Compressive Stresses, *J. ACI*, 50, 137-140.
- Smith, G.M., and Young, L.E., 1955, Ultimate Theory in Flexure by Exponential Function, *ACI J.*, 52, 3, 349-359.
- Srinivasan, M. G., Krajcinovic, D., Fonseka, G. U., and Valentine, R. A., 1979, The Distributed Damage Theory and its Application in *Dynamically Loaded Structures*, Abstracts, 16th Annual Meeting, Soc. of Engng. Sci., Inc., Northwestern Univ.
- Sneddon, I. N., and Lowengrub, M., 1969, *Crack Problem in the*

Classical Theory of Elasticity, John Wiley and Sons, Inc., New York.

- Spencer, A. J. M., and Rivlin, R. S., 1959a, The Theory of Matrix Polynomials and its Application to the Mechanics of Isotropic Continua, *Arch. Rational Mech. Anal.*, 2, 309-336.
- Spencer, A. J. M., and Rivlin, R. S., 1959b, Finite Integrity Bases for Five or Fewer Symmetric 3X3 Matrices, *Arch. Rational Mech. Anal.*, 2, 435-402.
- Spencer, A. J. M., and Rivlin, R. S., 1961, Further Results on the Theory of Matrix Polynomials, *Arch. Rational Mech. Anal.*, 4, 214-230.
- Spooner, D. C., and Dougill, J. W., 1975, A Quantitative Assessment of Damage Sustained in Concrete During Compressive Loading, *Mag. Conc. Res.*, 27, No. 92, 151-160.
- St. Venant, M. de, 1855, *Savants Etrangers*, 14, (A Copy of This Reference is Held at the British Museum Library, London).
- St. Venant, M. de, 1870, Sur l'Etablissement des equations des Mouvements Interieurs Operes dans les Corps Solids Ductiles au Dela des Limites ou l'Elasticite Pourrait les Rammener a leur Premier Etat, *C. R. Acad. Sci.*, Paris, 70, 473-478is Reference is Held at the British Museum Library, London).
- Stevens, D. J., and Krauthammer, T., 1989, Nonlocal continuum damage/plasticity model for impulse loaded RC beams, *J. Struct. Engrg.*, ASCE, 115, 9, 2329-2347.
- Stevens, D. J., and Liu, D., 1992, Strain-Based Constitutive Model with Mixed Evolution Rules for Concrete, *J. Engng. Mech.*, ASCE, 118, 6, 1184-1200.
- Sturman, G. M., Shah, S. P., and Winter, G., 1965, Effect of Flexural Strain Gradients on Micro-cracking and Stress-Strain Behavior of Concrete, *J. ACI*, 62, 805-822.
- Suaris, W., and Shah, S. P., 1983, Rate-Sensitive Damage Theory for Brittle Solids, *Proc. ASCE Special Conf.*, Purdue University, May.
- Suaris, W., and Shah, S. P., 1984, Rate-Sensitive Damage Theory for Brittle Solids, *J. Engng. Mech.*, ASCE, 110, 985-997.
- Suaris, W., Ouyang, C., Fernando, V., M., 1990, Damage Model for Cyclic Loading of Concrete, *J. Engng. Mech.*, ASCE, 116, 5, 1020-1035.

- Suh, N. P., 1969, A Yield Criterion for Plastic Frictional, Work Hardening Granular Materials, *Int. J. Powder Mat.*, 69.
- Suidan, M. and Schnoborich, W. C., 1973, Finite Element Analysis of Reinforced Concrete, *J. Struct. Div.*, ASCE, 99, ST10, Proc. Paper 10081, 2109-2122.
- Sumarac, D., and Krajcinovic, D., 1987, A Self-Consistent Model for Microcrack-Weakened Solids, *Mech. Mater.*, 6, 39-52.
- Taher, A. L., and Voyiadjis, G. Z., 1993, Plasticity-Damage Model for Concrete under Multiaxial Loading, *J. Engng. Mech.*, ASCE, 119, 7, 1465-1484.
- Taher, S. E.-D. F., Baluch, M. H., and Al-Gadhib, A. H., 1994a, Towards a Canonical Elastoplastic Damage Model, *Engng. Fract. Mech.*, 48, 2, 151-166.
- Tapponier, P., and Brace, W. F., 1976, Development of Stress-Induced Microcracks in Westerly Granite, *Int. J. of Rock Mech. Min. Sci.*, 13, 103-112.
- Talreja, R., 1985, A continuum mechanics characterization of damage in composite materials, *Proc. R. Soc. Lond.*, Ser. A 399, 195-216.
- Tada, H., Paris, P. C., Irwin, G. R., 1985, *The Stress Analysis of Cracks Handbook*, 2nd Ed., Paris Productions Inc., St. Louis.
- Tassoulas, J.L., 1979, Inelastic Behavior of Concrete in Compression, *M. Sc. Thesis*, Dept. of Civ. Engng., MIT, Cambridge, Mass.
- Tasuji, M. E., 1976, The Behavior of Plain Concrete Subject to Biaxial Stress, *Research Report No. 360*, Dept. of Civ. Engng., Cornell Univ., Mar.
- Tasuji, M. E., Nilson, A. H., and Slate, F. O., 1979, Biaxial Stress-Strain Relationships for Concrete, *Mag. Conc. Res.*, 31, 109, 217-224.
- Taylor, G. I., 1938, Plastic Strain in Metals, *J. Inst. Metals*, 62, 307.
- Terrien, M., 1978, Etude des Bruits Emis par la Beton au Course de la Fissuration du Mortier, du Granulat ou de Leur Interface, *Rapport de Contract*, Ecole Polytechnique, Laboratoire de Mecanique de Solides, 91128 Palaiseau, France.
- Terrien, M., 1980, Emmission Acoustique et Comportement Post-Critique d'un Beton Solicite en Traction, *Bull. de Liason des Ponts et Chaussees*, 105, 65-72.

- Timoshenko, S. P. and Goodier, J. N., 1951, *Theory of Elasticity*, 3rd Edn., McGraw-Hill Book Company.
- Torrent, R. J., 1983, The Effect of Specimen Geometry and Stress Distribution on the Tensile Strength of Concrete, *Ph. D. Thesis*, Univ. of Leeds.
- Triantafyllidis, N., and Aifantis, E., 1986, A Gradient Approach to Localization of Deformation- I. Hyperelastic Materials, *J. Elast.*, 16, 225-237.
- Torrent, R. R., and Brooks, J. J., 1985, Application of the Highly Stresses Volume Approach to Correlated Results from Different Tensile Tests of Concrete, *Mag. Conc. Res.*, 37, No. 132, 175-184.
- Tresca, H., 1864, Sur l'Ecoulement des Corps Solids Soumis a de Fort Pression, *Comp. Rend.*, 59, 754.
- Truesdell, C., 1955, Hypoelasticity, *J. Ration. Mech. Analysis*, 13, 1019-1020.
- Tsai, S. W., and Hahn, H. T., 1980, *Introduction to Composite Materials*, Technomic Inc., Pennsylvania.
- Valanis, K. C., 1971b, A Theory of Viscoplasticity Without a Yield Surface, Part I: General Theory; Part II: Application to Mechanical Behavior of Metals, *Archives of Mechanics*, 23, 517-551.
- Valanis, K. C., 1975a, On the Foundation of the Endochronic Theory of Viscoplasticity, *Archiwum Mechaniki Stosowanej (Archives of Mechanics, Warsaw)*, 27(5-6), 857-868.
- Valanis, K. C., and Wu, H. C., 1975b, Endochronic Representation of Cyclic Creep and Relaxation of Metals, *ASME J. Appl. Mech.*, 42, 67-73.
- Valanis, K. C., 1976, Some Recent Developments in the Endochronic Theory of Plasticity-The Concept of Internal Barriers, In *Constitutive Equations of Plasticity*, AMD- 21, AM. Soc. of Mech. Engrs., New York. (Presented as ASME Winter Annual Meeting, 15-32, New York, Dec. 1976).
- Valanis, K. C., 1977, On the Endochronic Foundation of Elastic-Perfectly Plastic Solids, *Proc., Soc. of Engng. Sci.*, 14th Annual Meeting, Lehigh Univ., Bethlehem, Pa., Nov., 761-763.
- Valanis, K. C., 1979, Endochronic Theory with Proper Hysteresis Loop Closure Properties, *Topical Report*, SSS-R-80-4182, System, Science and Software, San Diego, Calif., Aug.

- Valanis, K. C., 1980, Fundamental Consequences of a New Intrinsic Time Measure-Plasticity as a Limit of the Endochronic Theory, *Archives of Mechanics*, 32, 2, 171-191.
- Valanis, K. C., and Read, H. E., 1982a, A New Endochronic Plasticity Model for Soils, in *Soil Mechanics, Transient and Cyclic Loads*, Pande, G. N., and Zienkiewicz, O. C., Eds., Wiley, New York, Chapter 14.
- Valanis, K. C., and Lee, C. F., 1982b, Some Recent Developments of the Endochronic Theory with Applications, *Nuclear Engineering and Design*, 69, 327-344.
- Valanis, K. C., and Lee, C. F., 1982c, Some Development in the Endochronic Theory with Application to Cyclic Histories, in *NASA Symposium on Nonlinear Constitutive Relations for High Temperature Applications*, Univ. of Akron, Ohio, May.
- Valanis, K. C., and Fan, J., 1983, Endochronic Analysis of Cyclic Elasto-plastic Strain Fields in a Notched Plate, *ASME J. of Appl. Mech.*, 50, 4a, 789-794.
- Valanis, K. C., Lee, C. F., 1984, Endochronic Theory of Cyclic Plasticity with Applications, *J. Appl. Mech.*, 51, June, 367-374.
- Valanis, K. C., 1985, On the Uniqueness of Solution of the Initial Boundary Value Problems in Softening Materials, *J. Appl. Mech.*, 52, 949-653.
- Valanis, K. C., 1991, A Global Damage Theory and the Hyperbolicity of the Wave Problem, *J. Appl. Mech.*, 58, 311-316.
- Varanasi, S. R., 1977, Analysis of Stable and Catastrophic Crack Growth Under Rising Load, *Flow Growth and Fracture*, ASTM STP 631.
- Van Mier, J.G.M., 1984, Strain Softening of Concrete under Multiaxial Loading Conditions, *Doctoral dissertation*, Eindhoven Univ. of Technology, The Netherlands (1984).
- Verbeck, G., 1966, Pore Structure, in Significance of Tests and Properties of Cement and Concrete-Materials, *ASTM Special Technical Publication No. 169-A*, Baltimore, Md., April, 212-213.
- Vile, G. W. D., 1968, The Strength of Concrete under Short Term Static Biaxial Stress, In *The Structure of Concrete and its Behavior under Load*, Proc. Int. Conf., London, 275-288.
- Von Mises, R., 1913, *Mechanik der Festen Koerper in Plastisch*

Deformablen Zustand, Nachr. Konigl. Ges. Wiss. Gottingen, *Math. Phys.*, K1, 582-592.

- Voyiadjis, G. Z., and Kattan, P. I., 1991, Finite Simple Shear Using a Coupled Damage and Plasticity Model,
- Voyiadjis, G. Z., and Kattan, P. I., 1990, A Coupled Theory of Damage Mechanics and Finite Strain Elasto-plasticity. Part II: Damage and Finite Strain Plasticity, *Int. J. of Engng. Sci.*, 28, No. 6, 505-524.
- Voyiadjis, G. Z., and Taher, A. L., 1993, Damage Model for Concrete Using Bounding Surface Concept, *J. Engng. Mech., ASCE*, 119, 9, 1865-1884.
- Walraven, J. C., Vos, E., Reinhardt, H. W., 1979, Experiments on Shear Transfer in Cracks in Concrete, Parts I and II, *Stevin Report 5-79-3*, Delft Univ., Delft, Netherlands.
- Walraven, J. C., 1980, Aggregate Interlock: A Theoretical and Experimental Analysis, *Ph. D. Thesis*, Delft Univ. of Technology, Delft, Netherlands.
- Walraven, J. C., and Reinhardt, H. W., 1981, Theory and Experiments on the Mechanical Behavior of Cracks in Plain and Reinforced Concrete Subjected to Shear Loading, *Heron*, 26, 1a, 5-68.
- Wang, C. K., and Salmon, C. G., 1979, *Reinforced Concrete Design*, 3rd Edn., Harper and Row, Publishers.
- Wastiels, J., 1979, Behavior of Concrete under Multiaxial Stresses-A Review, *Cem. Conc. Res.*, 9, 35.
- Watanabe, O., and Atluri, S. N., 1985, A New Endochronic Approach to Computational Elastoplasticity: Example of a Cyclically Loaded Cracked Plate, *J. Appl. Mech., Trans. ASME*, 52, 857-864.
- Weibull, 1939, A Statistical Theory of the Strength of Materials, *Ing. Vet. Ak. Han.*, 151.
- Welch, P. F., 1972, Fracture of Plain Concrete, *Indian Concrete J.*, 46, 468-479.
- Willam, K. J., 1974a, Constitutive Model for the Triaxial Behavior of Concrete, *IABSE Seminar, ISMES*, Beramo, Italy, May.
- Willam, K. J., and Wanke, E. P., 1974b, Constitutive Model for the Triaxial Behavior of Concrete, *IABSE Seminar, ISMES*, Int. Assoc. for Bridge and Struct. Engng. Seminar on Concrete Structures Subjected to Triaxial Stresses, Bergamo, Italy, May.

- Willam, K., Bicanic, N., Pramono, E., Sture, S., 1986, Composite Fracture Model for Strain Softening Computations of Concrete, in *Fracture Toughness and Fracture Energy of Concrete*, Ed., Wittmann, F. H., Elsevier, Amsterdam, 146-162.
- Wu, C. H., 1974, Dual Failure Criterion for Plain Concrete, *J. Engng. Mech.*, ASCE, 100, 6, 1167-1181.
- Wu, C. H., 1985, Tension-Compression Test of a Concrete Specimen via a Structure Damage Theory, In *Damage Mechanics and Continuum Modelling*, Stubbs, N., and Krajcinovic, D., Eds., 1-12, ASCE.
- Wu, F.H. and Freund, L.B., 1984, Deformation Trapping due to Thermoplastic Instability in One-Dimensional Wave Propagation, *J. Mech. Phys. Solids*, 32, 119-132.
- Xia, S., Li., Lee, H., A Nonlocal Damage Theory, *Int. J. Fract.*, 34, 239-250.
- Yang, W. H., 1980, A Generalized von Mises Criterion for Yield and Fracture, Two Parts a,b, *J. Appl. Mech.*, 47, 297-300.
- Yakelevsky, D. Z., and Reinhardt, H. W., 1987, Response of Plain Concrete to Cyclic Tension, *J. ACI Materials*, 84, 5, M37, 365-373.
- Yazdani, S., and Schreyer, H.L., 1990, Combined Plasticity and Damage Mechanics Model for Plain Concrete, *J. Engng. Mech.*, ASCE, 116, 7, 1435-1450.
- Zaitsev, Y., and Scerbakiv, E. N., 1977, Creep Fracture of Concrete in Prestressed Concrete Members during Manufacture, *4th Int. Conf.*, Waterloo, 1977, 3-1219.
- Zienkiewicz, O. C. and Phillips, D. V., and Owen, D. R. J., 1974, Finite Element Analysis of Some Concrete Non-Linearities, Theory and Examples, *Paper III-2, ISMES*, Int. Assoc. for Bridge and Struct. Engng. Seminar on Concrete Structures Subjected to Triaxial Stresses, Bergamo, Italy, May.
- Zienkiewicz, O. C. and Pande, G. C., 1983, *Private Communication (Bangash, 1989)*.
- Zimmermann, R. W., 1991, *Compressibility of Sandstones*, Amsterdam, Elsevier.
- Ziraba, Y. N., 1993, Non-Linear Finite Element Analysis of Reinforced Concrete Beams Repaired by Plate Bonding, *Ph.D. Thesis*, Depart. Civil Engng., KFUPM, Dhahran, KSA, pp327.